

N 12-12727

**NASA CONTRACTOR  
REPORT**



**NASA CR-1830**

**NASA CR-1830**

**CASE FILE  
COPY**

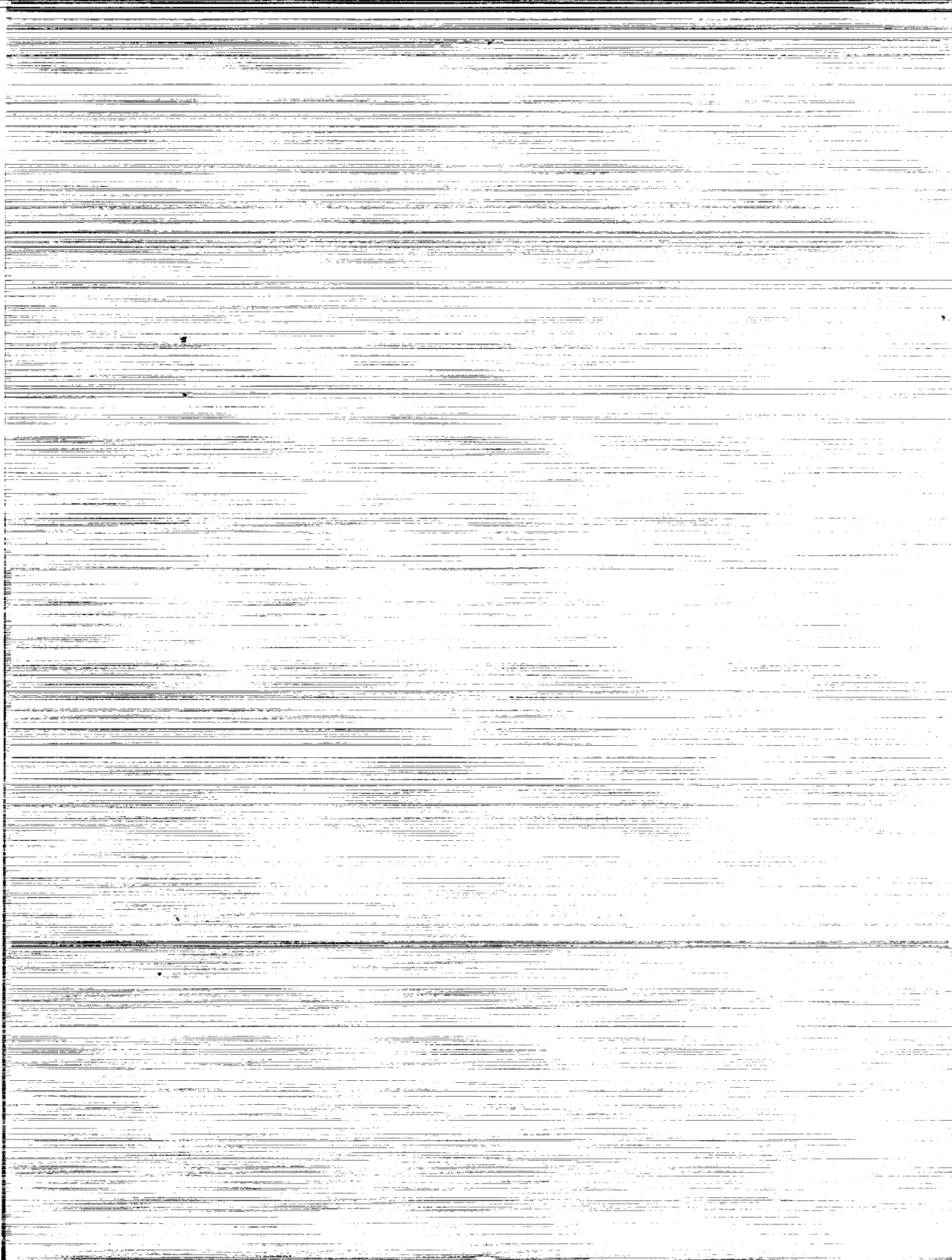
**BASIC INVESTIGATION OF  
TURBINE EROSION PHENOMENA**

*by W. D. Pouchot, R. E. Kothmann, W. K. Fentress,  
F. J. Heymann, T. C. Varljen, J. W. H. Chi, J. D. Milton,  
C. M. Glassmire, J. A. Kyslinger, and K. A. Desai*

*Prepared by*  
**WESTINGHOUSE ELECTRIC CORPORATION**  
**Pittsburgh, Pa. 15236**

*for*

**NATIONAL AERONAUTICS AND SPACE ADMINISTRATION • WASHINGTON, D. C. • NOVEMBER 1971**



1. Report No. NASA CR-1830		2. Government Accession No.		3. Recipient's Catalog No.	
4. Title and Subtitle BASIC INVESTIGATION OF TURBINE EROSION PHENOMENA				5. Report Date November 1971	
				6. Performing Organization Code	
7. Author(s) W. D. Pouchot, R. E. Kothmann, W. K. Fentress, F. J. Heymann, T. C. Varljen, J.W.H. Chi, J. D. Milton, C. M. Glassmire, J. A. Kyslinger, and K. A. Desai				8. Performing Organization Report No. WANL-TME-1977	
9. Performing Organization Name and Address Westinghouse Electric Corporation Westinghouse Astronuclear Laboratory P. O. Box 10864 Pittsburgh, Pennsylvania 15236				10. Work Unit No.	
				11. Contract or Grant No. NAS7-390	
12. Sponsoring Agency Name and Address National Aeronautics and Space Administration Washington, D. C. 20546				13. Type of Report and Period Covered Contractor Report	
				14. Sponsoring Agency Code	
15. Supplementary Notes					
16. Abstract <p>The objective of the study reported herein is to provide an analytical-empirical model of turbine erosion that fits and explains experience in both steam and metal vapor turbines. Because of the complexities involved in analyzing turbine erosion problems, in a pure scientific sense, it is obvious that this goal can be only partially realized. Therefore, emphasis is placed on providing a useful model for preliminary erosion estimates for given configurations, fluids, and flow conditions.</p> <p>The first section of this report describes the assembly of the overall erosion model, summarizes the component process models used and describes results of application of the model to several turbines. Section 2 covers detail computational procedures that may be used to follow the fluid-dynamic processes involved in erosion. Section 3 covers in detail experimental evidence and analysis thereof of the actual material removal by liquid impingement.</p>					
17. Key Words (Suggested by Author(s)) Turbine Erosion, Turbine Internal Flow, Wet Vapor Formation, Wet Vapor Collection, Drop Formation, Erosion by Drop Impact, Turbine Blade Wakes				18. Distribution Statement  Unclassified - Unlimited	
19. Security Classif. (of this report) Unclassified		20. Security Classif. (of this page) Unclassified		21. No. of Pages 377	
				22. Price* \$6.00	





## FOREWORD

The work described herein was performed under NASA Contract NAS7-390, "Basic Investigation of Turbine Erosion Phenomena." The work was done under the supervision of Mr. W. D. Pouchot of the Systems and Technology Department at the Astronuclear Laboratory of the Westinghouse Electric Corporation in Pittsburgh, Pa. Mr. L. G. Hays of the Jet Propulsion Laboratory in Pasadena, California is the NASA Program Manager. Mr. S. V. Manson of NASA Headquarters in Washington, D. C. is the NASA Technical Director.

The work reported is the result of a team effort by personnel of the Westinghouse Astronuclear Laboratory, the Westinghouse Research and Development Center, and the Westinghouse Steam Divisions. Contributors are: W. D. Pouchot, R. E. Kothmann, W. K. Fentress, F. J. Heymann, T. C. Varljen, J. W. H. Chi, J. D. Milton, C. M. Glassmire, J. A. Kyslinger and K. A. Desai.



# TABLE OF CONTENTS

<u>Section</u>		<u>Page</u>
	SECTION 1. INTRODUCTION & SUMMARY	
1.1	GENERAL	1-1
1.2	EROSION MODELS IN WET VAPOR TURBINES	1-1
1.2.1	Erosion Locations of Turbine Rotor Blades	1-2
1.2.2	Processes Involved in Erosion	1-3
1.2.3	Turbines Used for Example Calculations	1-4
1.2.4	Process Descriptions	1-6
1.3	RESULTS OF SEVERAL TURBINE EROSION ANALYSES	1-25
1.3.1	Comparative Erosion Potential of NAS5-250 Cesium Turbine and Potassium Turbine Conceptual Designs	1-25
1.3.2	Erosion Trends in Central Station Steam Turbines	1-27
1.3.3	Erosion Potential of Sunflower Mercury Turbine	1-28
1.4	CONCLUSIONS AND RECOMMENDATIONS	1-30
	APPENDICES TO SECTION 1	
A.	Row-by-Row Design Characteristics of Large Steam Turbines Used as Examples	1-31
B.	References	1-33
C.	Results of Detailed Fluid-Dynamic Analysis of Blade Passage Flows of NAS 5-250 Potassium and Cesium Turbines	1-35
	SECTION 2. FLUID-DYNAMIC COMPUTATIONAL PROCEDURES	
2.1	BACKGROUND	2-1
2.2	TURBINE PERFORMANCE WITH DETAILED HISTORY OF CONDENSATION	2-1
2.2.1	Background	2-1
2.2.2	Theory	2-1
2.2.3	Method of Solution	2-10
2.2.4	Sample Turbine Calculation Results	2-11
2.2.5	Discussion	2-13
2.2.6	Nomenclature	2-15
2.2.7	References	2-16
	APPENDICES TO SECTION 2.2	
A.	Listing of Computer Program	2-17
B.	Listing of ICEADAMS Integration Procedure	2-33
C.	List of Input Data	2-36
D.	Program Flow Chart	2-37
E.	Description of Input Control Variables	2-38
2.3	TWO-D AXISYMMETRIC FLOWS BEHIND BLADE ROWS IN WET VAPOR TURBINE	2-39
2.3.1	Background	2-39
2.3.2	Intent of Code	2-39
2.3.3	Nomenclature for Input and Output of Modified Code	2-41
2.3.4	Method for Calculation of Modified Parameters for Wet Vapor Turbines	2-44

# TABLE OF CONTENTS (CONTINUED)

<u>Section</u>		<u>Page</u>
	2.3.5 Possible Future Modifications to Code	2-47
	2.3.6 References	2-47
	APPENDICES TO SECTION 2.3	
	A. Sample Problems Illustrating Use of Code	2-47
	B. Listing of Code	2-68
	C. Control Cards for WANL CDC-6600 Computer	2-141
2.4	BLADE SURFACE VELOCITY CALCULATIONS	2-142
	2.4.1 Background	2-142
	2.4.2 Calculation of G. E. Blade	2-142
	2.4.3 Discussion	2-143
	2.4.4 Conclusions	2-146
	2.4.5 References	2-146
2.5	COLLECTION OF CONDENSATE AND MOVEMENT OF CONDENSATE ON TURBINE SURFACES	2-146
	2.5.1 Nomenclature for Section 2.5	2-146
	2.5.2 Deposition of Moisture on the Surface of Blades	2-148
	2.5.3 Movement of Moisture on Blade Surfaces	2-155
	2.5.4 Collection on Turbine Casing	2-158
	2.5.5 References	2-161
2.6	TRANSPORT OF ATOMIZED DROPS BETWEEN STATORS AND ROTORS	2-162
	2.6.1 Background	2-162
	2.6.2 Analytical Model of Atomized Drop Transport	2-162
	2.6.3 Computer Model of Atomized Drop Transport	2-165
	2.6.4 Description of the ADROP Code Package	2-169
	2.6.5 Solution of an Illustrative Problem	2-179
	2.6.6 Summary	2-182
	2.6.7 Nomenclature	2-185
	2.6.8 References	2-186
	APPENDICES TO SECTION 2.6	
	A. Calculated and Experimental Atomized Drop Velocities in Last Stage of Large Steam Turbines	2-187
	B. ADROP Code Source Program Listing	2-189
2.7	ATOMIZATION OF COLLECTED CONDENSATE	2-206
	2.7.1 Background	2-206
	2.7.2 Stator Atomization Model	2-206
	2.7.3 Conclusions	2-215
	APPENDICES TO SECTION 2.7	
	A. Primary Atomization Expressions	2-216
	B. Analysis of Contract NAS 7-391 Results	2-221
	C. References	2-225



<u>Section</u>		<u>Page</u>
	SECTION 3. TURBINE BLADE EROSION MODEL	
3.1	A SURVEY OF CLUES TO THE RELATIONSHIPS BETWEEN EROSION RATE AND IMPINGEMENT CONDITIONS	
3.1.1	General Considerations Relating to the Interpretation and Correlation of Test Data	3-1
3.1.2	Dependence on Impingement Angle	3-5
3.1.3	Dependence on Drop Size and Shape	3-8
3.1.4	Dependence on Impact Velocity	3-15
3.1.5	Dependent Parameters Other Than Rate	3-28
3.1.6	Summary and Conclusions for Section 3.1	3-30
3.2	THE VARIATION OF EROSION RATE WITH EXPOSURE TIME	3-32
3.2.1	Observed Rate-Time Patterns	3-32
3.2.2	Effect of Material Removal Mechanisms on Rate-Time Pattern	3-35
3.2.3	An Analytic Model of the Erosion Rate-Time Relationship	3-37
3.2.4	Mathematical Formulation of Model	3-43
3.3	HYDRODYNAMICS MODEL OF CORRELATION OF METAL REMOVAL RATES FROM REPETITIVE DROP IMPACT	3-47
3.3.1	Background	3-47
3.3.2	Review of Some Observations on Drop Impact Material Removal	3-47
3.3.3	Possible Reasons for Drop Size Effects	3-50
3.3.4	Correlation Model	3-53
3.3.5	Temperature Effect in Drop Impingement Material Removal	3-61
3.3.6	Summary	3-62
3.3.7	Nomenclature	3-62
3.3.8	Derivation of Expression for CEGB Apparatus Water Film Thickness	3-63
3.4	TURBINE BLADE DISSOLUTION IN LIQUID METALS	3-65
3.4.1	Background	3-65
3.4.2	Analytical Model	3-67
3.4.3	Analysis of Last Rotor of a Potassium Turbine Design	3-70
3.4.4	References	3-72
	SECTION 4. LOW SPEED CASCADE TESTS	
4.1	BACKGROUND	4-1
4.2	SYMBOLS	4-2
4.3	TEST APPARATUS & PROCEDURE	4-3
4.3.1	Blade Description	4-3
4.3.2	Test Rig	4-3
4.3.3	Instrumentation	4-5
4.3.4	Data Logging and Calculation	4-5
4.3.5	Checkout Procedure	4-5
4.3.6	Wake Traverse Tests	4-6

# TABLE OF CONTENTS (CONTINUED)

<u>Section</u>		<u>Page</u>
4.4	RESULTS & DISCUSSION	4-6
	4.4.1 Theoretical Models of Flow	4-6
	4.4.2 Test Results	4-8
4.5	SUMMARY OF RESULTS	4-12
4.6	REFERENCES	4-13

## LIST OF ILLUSTRATIONS

<u>Figure</u>		<u>Page</u>
1.2-1	Eroded Steam Turbine Blade	1-2
1.2-2	Rotor Blade Material Removal	1-3
1.2-3	WANL Turbine Blade Erosion Model	1-3
1.2-4	Yankee Steam Turbine	1-6
1.2-5	Cross Section of Six-Stage Potassium Turbine	1-6
1.2-6	Cross Section of Two-Stage Cesium Turbine	1-6
1.2-7	Thermodynamic Diagram of Vapor Turbine Expansion	1-7
1.2-8	Moisture Fracture in Divergent Portion of a Steam Nozzle	1-7
1.2-9	Pressure Data for Saturated Potassium Vapor	1-8
1.2-10	Moisture Content (Fraction of Equilibrium) as a Function of Pressure Ratio for Condensing Vapor in Two Sample Potassium Turbines	1-8
1.2-11	Steam Condensate Droplet Growth in Divergent Portion of Nozzle	1-9
1.2-12	Calculated and Experimental Turbine Moisture Collection	1-10
1.2-13	Relation of Moisture Particle Travel to Motion in Plane Normal to Axis of Rotation	1-10
1.2-14	Baker's Map of Two Phase Flow Regimes	1-13
1.2-15	Impingement on Rotating Blade	1-13
1.2-16	Wake Trough Velocity	1-14
1.2-17	Displacement of Drops to Breakup	1-14
1.2-18	Sunflower Turbine - Stage 3. Primary Drop Distance to Disruption	1-15
1.2-19	Bayshore No. 2 - Stage 7. Primary Drop Distances to Disruption	1-15

## LIST OF ILLUSTRATIONS (Continued)

<u>Figure</u>		<u>Page</u>
1.2-20	General Solutions for the Terminal Velocity of Drops Traveling along Stator Wake Axis Streamlines	1-16
1.2-21	Sunflower Turbine - Stage 3. Drop Impact Velocities Relative to the Rotor Blade	1-17
1.2-22	Bayshore No. 2 - Stage 7. Drop Impact Velocities Relative to the Rotor Blades	1-17
1.2-23	Comparison of Impact Velocities on Sunflower and Bayshore No. 2 Turbines	1-18
1.2-24	Drop Distribution Functions	1-19
1.2-25	Temperature Dependence of $\alpha$	1-21
1.2-26	Parametric Study of the Dissolution of Metals in Liquid Potassium	1-22
1.2-27	Stellite Erosion Rates - Data from CEGB; Reduced Normal Velocity ( $V_n - V_{cd}$ )	1-23
1.2-28	Correlation of CEGB Data by use of "Critical Velocity"	1-24
1.2-29	Threshold Velocity Correlation	1-25
1.3-1	Maximum Erosion Velocities at Last Rotor Blades of Central Station Steam Turbines	1-27
1.3-2	Damaging Moisture Impact Rates on Noses of Last Rotor Blades of Central Station Steam Turbines	1-27
1C-1	Potassium Sixth Stator Wake Pressure Side Velocity	1-39
1C-2	Potassium Turbine Sixth Stator Wake Suction Side Velocity	1-39
1C-3	Cesium Turbine Second Stator Wake Pressure Side Velocity	1-39
1C-4	Cesium Turbine Second Stator Wake Suction Side Velocity	1-39
1C-5	Potassium Turbine Portion Collected on Nose of Sixth Stator Blade	1-40
1C-6	Cesium Turbine Portion Collected on Nose of Second Stator Blade	1-40



# LIST OF ILLUSTRATIONS (Continued)

<u>Figure</u>		<u>Page</u>
1C-7	Potassium Turbine Portion Collected on Concave Side Sixth Stator Blade	1-40
1C-8	Cesium Turbine Portion Collected on Concave Side of Second Stator Blade	1-41
1C-9	Maximum Impact Velocities on Six-Stage Potassium Turbine	1-42
2.1-1	WANL Turbine Blade Erosion Model	2-1
2.2D-1	Flow Diagram of the Condensation Code	2-37
2.2D-2	Flow Diagram of the Sonic Flow Section of the Condensation Code	2-37
2.3-1	Axial Station Velocity Nomenclature	2-45
2.3A-1	6th Stator Blade Exit Angles	2-54
2.3A-2	6th Rotor Blade Exit Angles	2-54
2.3A-3	6th Rotor Exit Jet Velocity	2-55
2.3A-4	5th Stator Exit Static Pressure	2-55
2.4.2-1	Third Stage Nozzle Mean Section	2-142
2.4.2-2	Geometric Data for the G.E. Blade	2-143
2.4.2-3	Surface Velocities Computed for the G.E. Blade	2-143
2.5.2-1	Knudsen Number Corrections	2-149
2.5.2-2	Collection Efficiency Ninth Stage Stator Nose Yankee Turbine	2-150
2.5.2-3	Portion Collected Ninth Stage Stator Nose Yankee Turbine	2-150
2.5.2-4	Collection of Moisture on the Concave Side of the Blade	2-150
2.5.2-5	Referred Collection Efficiency on the Concave Side of the Blade	2-152
2.5.2-6	Portion Collected; Concave Side, Ninth Stator Yankee Turbine	2-153

## LIST OF ILLUSTRATIONS (Continued)

<u>Figure</u>		<u>Page</u>
2.5.2-7	Calculated and Experimental Turbine Moisture Collection	2-155
2.5.4-1	Baker's Map of Two-Phase Flow	2-159
2.5.4-2	Effect of Condensate Film Reynold's Number on Film Thickness	2-160
2.5.4-3	Effect of Vapor Reynold's Number on Film Thickness	2-160
2.6-1	Drag of Spheres and Liquid Drops	2-163
2.6-2	Analytic Solutions for the Bulk Flow Drop Impact Velocity	2-164
2.6-3	General Solutions for the Terminal Velocity of Drops Traveling along Stator Wake Axis Streamlines	2-164
2.6-4	Qualitative Representation of Vapor Wake Development Downstream of a Stator Blade Section	2-166
2.6-5	Drop Impingement Geometry	2-169
2.6A-1	Drop Velocity	2-187
2.6A-2	Secondary Drop Velocity	2-187
2.6A-3	Rotor Blade Impingement Locations	2-188
2.7-1	Drop Distribution Functions	2-213
2.7-2	Distribution of Drop Sizes in a Small Steam Turbine after Spies, Baughman, and Blake	2-213
2.7-3	Manipulation of Experimental Drop Size Distribution	2-214
2.7A-1	Average Drop Size, Primary Atomization	2-219
2.7B-1	Profile of Stator Blade 1-A	2-222
2.7B-2	Surface Velocities Computed for the Top Section of Rocketdyne Blade Shape 1-A	2-222
2.7B-3	Predicted Variation of Maximum Primary Drop Weber Numbers for the Rocketdyne Test Series with Blade Shape 1-A	2-223
2.7B-4	Variation of Drop Weber Number and Velocity with Distance along the Wake Axis Predicted for Rocketdyne Test 114A	2-223

## LIST OF ILLUSTRATIONS (Continued)

<u>Figure</u>		<u>Page</u>
2.7B-5	Variation of Drop Weber Number and Velocity with Distance along the Wake Axis Predicted for Rocketdyne Test 114B	2-223
2.7B-6	Variation of Drop Weber Number and Velocity with Distance along the Wake Axis Predicted for Rocketdyne Test 114F	2-224
2.7B-7	Variation of Drop Weber Number and Velocity with Distance along the Wake Axis Predicted for Rocketdyne Test 113L	2-224
3.1-1	Various Interpretations of Same Hypothetical Erosion Data Points	3-2
3.1-2	Definition of Incubation Period, $T_o$ , and "Steady-State" Erosion Rate, $R$	3-3
3.1-3	Hypothetical Erosion Curves	3-4
3.1-4	Rationalized Erosion Rate versus Normal Impact Velocity	3-5
3.1-5	Corrected Erosion Rate ( $E \cos \theta$ ) versus Normal Impact Velocity (From Figure 5 of Reference 11)	3-6
3.1-6	Comparison of Erosion versus Angle Curves	3-7
3.1-7	Erosion versus Velocities	3-8
3.1-8	Arrangement of Nozzles for Water-Jet Tests	3-9
3.1-9	Erosion versus Jet Size (Adapted from Reference 1)	3-9
3.1-10	Erosion Rate versus Jet Diameter	3-10
3.1-11	Effect of Drop Size on Erosion Rate	3-10
3.1-12	Effect of Drop Size on Erosion Rate (Data Cross-Plotted from Figure 3.1-11). Dotted Lines are Based on Correlation of Figure 3.1-13.	3-11
3.1-13	Correlation of Data of Figure 3.1-11 by Use of "Critical Factor" $K_c \equiv (1-10^8/V^2D)$	3-12
3.1-14	Correlation of Data of Figure 3.1-11 by Use of "Critical Velocity" $V_{cd} \equiv \sqrt{10^8/D}$	3-12

## LIST OF ILLUSTRATIONS (Continued)

<u>Figure</u>		<u>Page</u>
3.1-15	Critical Velocity versus Jet Diameter	3-13
3.1-16	Erosion-Velocity Relationships Plotted in the Manner of Fatigue Data	3-16
3.1-17	Loci of Constant Shear Stress $S$ in Semi-Infinite Solid with Belt of Uniform Pressure $P$	3-18
3.1-18	Upper and Lower Loci for Various Values of Pressure/Shear Stress Ratios	3-18
3.1-19	Area Between Surface and Lower Stress Locus	3-19
3.1-20	Impact Pressure Versus Velocity	3-22
3.1-21	Families of Hypothetical Erosion Versus Velocity Curves, According to Equations (3) through (7)	3-24
3.1-22	Erosion versus Velocity Curves, Computed from Data in Reference 2	3-25
3.1-23	The Data of Figure 3.1-7b Plotted on Semi-Log Paper	3-25
3.1-24	Data of Hobbs in Reference 36, Plotted both versus $V$ , (Curve "a"), and versus $(V-270)$ , (Curve "b")	3-26
3.1-25	Data of Figure 3.1-24a on Semi-Log Paper	3-27
3.1-26	Curves Based on the Data Points of Figures 3-1-13 and 14. Original Data from Reference 12)	3-27
3.1-27	Curves of Figure 3.1-26 on Log-Log Plot	3-27
3.1-28	Rationalized Incubation Periods at Various Drop Diameters and Velocities (Copy of Figure 7 of Reference 12)	3-29
3.1-29	Individual Curves for Different Drop Sizes, Based on Data Points of Figure 3.1-28.	3-29
3.1-30	A Comparison of Impact Failure with Failure by a Standard Fatigue Method for 304 Stainless Steel (Ripken et al, Reference 37)	3-30



## LIST OF ILLUSTRATIONS (Continued)

<u>Figure</u>		<u>Page</u>
3.2-1	Characteristic Rate-Time Curve According to Thiruvengadam	3-33
3.2-2	Characteristic Rate-Time Curve According to Plesset, Hobbs, and Pearson	3-33
3.2-3	Typical Cumulative Erosion-Time Curves from Cavitation Tests, Adapted from Figure 7 of Reference 36. (Magnetostriction Device, in Distilled Water)	3-34
3.2-4	Cumulative Cavitation Erosion-Time Curves Which Begin at Maximum Rate, Adapted from Figure 24 of Reference 52. (Rotating Disc Device at 150 ft/sec)	3-34
3.2-5	Typical Erosion Rate-Time Curve Obtained in Westinghouse Steam Division Spray Impingement Facility During 1956-1959	3-34
3.2-6	Early Loss Measurements for a Titanium (6% Al, 4% V) Alloy Tested in the Westinghouse Steam Division Facility)	3-35
3.2-7	Typical Computed Erosion Rate-Time Curves from Preliminary Statistical Model, Using Normal Distribution Functions	3-38
3.2-8	Experimental Erosion Rate-Time Curves, Computed from Cumulative Erosion Curves Given in Reference 32	3-38
3.2-9	Computed Rate-Time Curves Based on Log-Normal Distributions, Showing Effect of Varying Dispersion, $\sigma$ , with Median at Constant, $M = 1.0$	3-39
3.2-10	Computed Curves Based on Log-Normal Distributions, Showing Effect of Varying Dispersion, $\sigma$ , with Mean at Constant, $E = 1.0$	3-40
3.2-11	Effect of Higher Median Value for "Unaffected" Surface ( $M_u = 3.0$ ) than for Other Surfaces ( $M = 1.0$ ). (Compare with Figure 3.2-9. Note Difference in Vertical Scale	3-41

## LIST OF ILLUSTRATIONS (Continued)

<u>Figure</u>		<u>Page</u>
3.2-12	Examples of Computed "Surface Profile" Curves Showing the Uneroded Area as a Function of Level Below the Original Surface, At Various Values of Time: (a) - Corresponding to Figure 3.2-9 (b) - Corresponding to Figure 3.2-11 (c) - Corresponding to Figure 3.2-10	3-41
3.2-13	Computed rms Surface Roughness versus Mean Depth of Penetration (Cumulative Erosion) for Figure 3.2-12. The letters (a) (b) and (c) Correspond to the Similarly- Designated Cases in Figure 3.2-12	3-42
3.3-1	Model of Stages of Erosion After Pearson	3-48
3.3-2	CEGB 12% Chrome Incubation (Stage 1) Data	3-49
3.3-3	Stage 3 Erosion of 12% Chrome Steel (CEGB Data)	3-50
3.3-4	Configuration Diagram	3-55
3.3-5	Calculated Film Thicknesses, CEGB Apparatus	3-56
3.3-6	Threshold Velocity Correlation	3-58
3.3-7	Correlation of CEGB Data by Means of Equation 19	3-60
3.3-8	Referred Erosion Rates	3-61
3.3-9	CEGB Test Piece	3-63
3.4-1	Temperature Dependence of $\alpha$	3-70
4.3-1	Cascade Test Rig	4-4
4.4-1	Wake Velocity Profiles at Various Downstream Positions	4-9&10
4.4-2	Change in Velocity in Core of Wake with Downstream Distance, 0 Deg. Incidence; $3.4 \times 10^5$ Reynolds Number	4-11
4.4-3	Increase in Wake Mixing Loss with Downstream Distance. 0 Deg. Incidence; $3.4 \times 10^5$ Reynolds Number	4-11
4.4-4	Increase in Wake Mixing Loss with Trailing Edge Thickness. 0 Deg. Incidence; $3.4 \times 10^5$ Reynolds Number	4-12
4.4-5	Increase in Loss Coefficient with Trailing Edge Thickness. 0 Deg. Incidence; $3.4 \times 10^5$ Reynolds Number	4-12

## LIST OF TABLES

<u>Table</u>		<u>Page</u>
1.2-1	Comparative Data on Turbines Analyzed	1-5
1.2-2	Turbine Casing Flow Regime Parameters Six-Stage Potassium Turbine	1-13
1.3-1	Erosion Threshold Velocities	1-26
1.3-2	Last Rotor Blades Dissolution in a Potassium and a Cesium Turbine	1-26
1A-1	Rowe Yankee Atomic Steam Turbine Low Pressure End	1-31
1A-2	Toledo Edison Bayshore Number 2 Steam Turbine Low Pressure End	1-32
1A-3	Toledo Edison Bayshore Number 3 Steam Turbine Low Pressure End	1-32
1C-1	Condensation Results for Six-Stage Potassium Turbine	1-35
1C-2	Fog Particle Size Distribution for Six-Stage Potassium Turbine	1-35
1C-3	Condensation Results for Cesium Turbine	1-36
1C-4	Fog Particle Distribution at Exit from 1-S Cesium Turbine	1-36
1C-5	Cesium Turbine-Fluid Properties Along Height - Second Stage	1-37
1C-6	Potassium Turbine-Fluid Properties Along the Height of the Blade-Fifth and Sixth Stages	1-37
1C-7	Potassium Turbine-Calculated Boundary Layer Properties at the Trailing-Edge of the Blade	1-38
1C-8	Cesium Turbine-Calculated Boundary Layer Properties	1-38
1C-9	Potassium Turbine-Results of Blade Wake Calculation for Sixth Stator Blade, 3/4 Blade Height Position	1-39
1C-10	Cesium Turbine-Results of Blade Wake Calculation for Second Stator Blade, 3/4 Blade Height Position	1-39
1C-11	Six-Stage Potassium Turbine - Sixth Stage Moisture Inventory	1-41

# LIST OF TABLES (Continued)

<u>Table</u>		<u>Page</u>
1C-12	Two-Stage Cesium Turbine - Second Stage Moisture Inventory	1-41
1C-13	Secondary Atomization in Cesium Turbine -Suction Side Wake Streamlined at $Y/Y_o = 0.01$ Second Stator	1-41
1C-14	Secondary Atomization in Potassium Turbine - Suction Side Wake Streamlined $Y/Y_o = 0.01$ Sixth Stator	1-42
1C-15	Second Stage Rotor Drop Impingement Summary - Two Stage Cesium Turbine	1-42
2.2-1	Example Turbine Geometry for Three-Stage Potassium Turbine	2-11
2.2-2	Computer Output Summary Sheet for the Three-Stage Turbine Example	2-12
2.2-3	Nomenclature and Units for Computer Output	2-12
2.2-4	Computer Output Intermediate Summary Sheet for the Second Stator Exit	2-13
2.2-5	Nomenclature and Units for Computer Output	2-14
2.3A-1	Modified Parameters for Potassium Turbine	2-53
2.3A-2	Comparison of Potassium Turbine Data at Mean Diameter	2-54
2.4.2-1	Input	2-142
2.4.2-2	Sample of Item 4 Output	2-144
2.4.2-3	Sample of Item 5 Output	2-145
2.5.3-1	Yankee Turbine, Eighth Rotor Liquid Flow	2-156
2.5.3-2	Yankee Steam Turbine, Ninth Stator Liquid Flow	2-158
2.5.4-1	Moisture Collection on Turbine Housing Six-Stage Potassium Turbine	2-158
2.5.4-2	Moisture Collection on Turbine Housing Two-Stage Cesium Turbine	2-158



## LIST OF TABLES (Continued)

<u>Table</u>		<u>Page</u>
2.5.4-3	Estimated Condensate Film Depth on Turbine Housing Six-Stage Potassium Turbine	2-160
2.5.4-4	Estimated Condensate Film Depth on Turbine Housing Two-Stage Cesium Turbine	2-160
2.5.4-5	Mean Droplet Sizes From Sheet Atomization of Condensate on the Potassium and Cesium Turbine Housings	2-161
2.6-1	ADROP Input Namelist Definitions	2-171
2.6-2	Common Block Layout in Program ADROP	2-172
2.6-3	ADROP Input Data Cards for the Sample Program	2-180
2.6-4	ADROP Input Data Summary	2-180
2.6-5	Boundary Layer Input Data Summary	2-181
2.6-6	Detailed Boundary Layer Result Printout	2-181
2.6-7	Trailing Edge Boundary Layer Data Summary	2-183
2.6-8	Printout of Detailed Trajectory Results	2-183
2.6-9	Summary of Trajectory Results	2-183
2.6-10	Secondary Atomization Summary	2-184
2.6-11	Impact Geometry Data Summary	2-184
2.7-1	Relationship of $D_3$ , $D_{3-0}$ , $D_m$ , and $n$	2-210
2.7-2	Tabulation from Reference 2	2-214
2.7A-1	Spray Liquid Volume Distribution Versus Drop Size	2-220
2.7A-2	Data on Stator Primary Atomization	2-220
2.7B-1	Rocketdyne Test Conditions Used in the Study	2-222
2.7B-2	Trailing Edge Boundary Layer Data Obtained for the Rocketdyne Test Series	2-222
3.1-1	Erosion Rate $E$ for Different Specimen Velocities $u$ and Jet Velocities $v$	3-7
3.1-2	Drop Size Correlation Attempts for Data of Figure 3.1-11	3-11

## LIST OF TABLES (Continued)

<u>Table</u>		<u>Page</u>
3.1-3	Critical Values of $V_{cd}$ and $D_c$ Based on $(V^2D)_c = 10^8$	3-13
3.1-4	Data of Hobbs in Reference 36	3-26
3.3-1	Values of the Interface Angle $\beta$ for Which Flow First Deforms the Surface	3-51
3.3-2	Critical Pit Diameters for Capillary Water Retention	3-57
3.4-1	Experience on Material Removal by Liquid Potassium	3-66
4.3-1	Test Blade Specifications	4-4
4.3-2	List of Tests	4-7

# SECTION 1

## INTRODUCTION & SUMMARY

### 1.1 GENERAL

The objective of the study reported herein is to provide an analytical-empirical model of turbine erosion that fits and explains experience in both steam and metal vapor turbines. Because of the complexities involved in analyzing turbine erosion problems, in a pure scientific sense, it is obvious that this goal can be only partially realized. Therefore, emphasis is placed on providing a useful model for preliminary erosion estimates for given configurations, fluids, and flow conditions. In terms of the prescribed effort level, this goal was given precedence over the more interesting but less immediately fruitful goal of precise and comprehensive mathematical definition of the processes contributing to erosion.

The first section of this report describes the assembly of the overall model of erosion, summarizes the component process models used and describes results of application of the model to several turbines. The model is used to estimate erosion depths or weight losses on the rotor blades of several turbines and the results are compared qualitatively to operating experience where it exists. Section 2 covers detail computational procedures that may be used to follow the fluid-dynamic processes involved in erosion, and compares typical calculated values with experience where it was found. Section 3 covers in detail experimental evidence and analysis thereof of the actual material removal by liquid impingement, and presents theoretical models for transferring this experience to calculations of material removal in turbines. Section 4 presents results of an experimental investigation of turbine stator blade wakes and compares these results with results from use of wake analysis procedures imposed in this report.

The qualitative aspects of the model follow, to a large extent, opinions on the erosion process in wet vapor steam turbines that are widely held within the steam turbine community at the present time. In respect to the quantitative aspects, the study is indebted to excellent previous studies by Gyarmathy and Gardner. It is a refinement and extension of these two previous works (more the former than the latter) based on later experience and substantial additional component process theory and computation.

An effort has been made to make this report adequate by itself to provide calculational understanding of the erosion model and its components. However in the light of the complexities of some of these processes, knowledge of the referenced material may be required for a comprehensive understanding.

### 1.2 EROSION MODELS IN WET VAPOR TURBINES

The analytical models of processes leading to turbine blade erosion outlined herein are chiefly organized and used to examine material removal from the nose and the leading edge of a rotor blade. When erosion is a problem in a wet vapor turbine of well-ordered flow, operated at or near design condition, the attack on the leading edges of the rotor blades is generally of greatest concern to the turbine designer and the turbine user.

Other locations of erosion are observed and some are mentioned in passing. In addition, many of the processes involved in producing rotor blade leading edge erosion are not specific to that location and process models can be recast to examine other locations of erosion in turbines.

### 1.2.1 Erosion Locations of Turbine Rotor Blades

In wet vapor turbines most of the material removal by condensate is from the turbine's rotor blades. (See Figure 1.2-1.) In steam or alkali metal vapor turbines, the primary mechanism of condensation is spontaneous nucleation in the bulk vapor flow to form a fog. In the latter turbines, damage is not done directly by the fog particles in the vapor. The fog is composed of submicronic diameter particles and only a small percentage ever impinge upon a surface. The impingement of this small percentage does, however, allow concentrations of liquid to build up on the various turbine surfaces and it is this liquid that can do damage. In mercury turbines, the end result is the same but the collecting mechanism is probably different. Mercury vapor is theoretically very slow to undergo spontaneous nucleation and there is probably no fog formation in most mercury turbines. Damaging liquid does seem to collect readily, however, by direct condensation on the turbine surfaces so that the locations and kinds of damage experienced are similar to those in fog turbines.

Principal locations of material removal from rotor blades are illustrated in Figure 1.2-2. This figure shows forward and aft views of a shrouded turbine blade and points out four types of material removal by liquid that are likely to occur on the rotors of wet vapor turbines.

In turbines, such as steam and mercury, where chemical dissolution of blade material does not occur to any extent, the material removal mechanism is largely that of mechanical removal by the force of liquid impingement as at locations (1) and (2) or by cavitation induced by the circulating eddies as at (4). In potassium vapor turbines the impingement removal can be compounded by dissolution effects either directly in the impingement areas or by rivulets, as illustrated at location (3). These rivulets can occur at other locations on the rotor blades as well as the trailing edge. They are nearly radial lines because the centrifugal force component on the liquid deposited on the rotors is much higher than the vapor shear force.

Most of the liquid collects initially on the rotor and stator blades as they represent the bulk

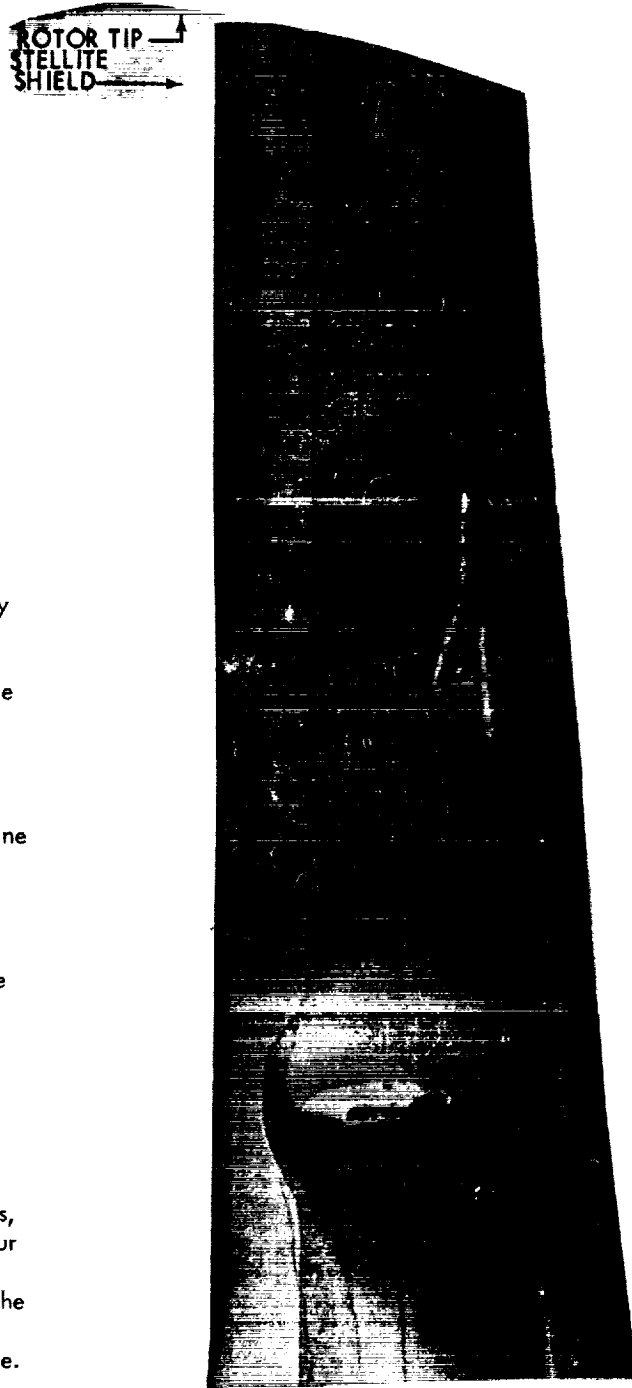


Figure 1.2-1 Eroded Steam Turbine Blade

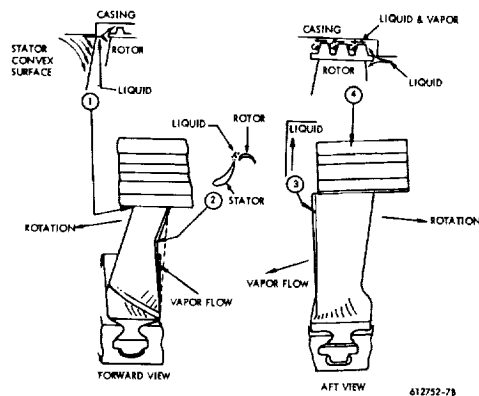


Figure 1.2-2 Rotor Blade Material Removal

of the turbine surface exposed to the main flow. As illustrated, damage can be done by casing and shroud liquid as well as liquid from or on the blades.

Liquid reaches the turbine casing primarily by being slung from the turbine rotors. It reaches the casing, secondarily, under urging of the vapor secondary flow from the pressure (concave) surface over the casing to the suction (convex) surface of the stator vanes. Other mechanisms, of less importance, are impingement and condensation from the bulk flow.

The casing-collected liquid, in addition to causing damage to shrouds and seals as indicated in Figure 1.2-2, tends to flow down over the stators on the convex side, as illustrated at location (1). This casing-collected liquid augments the liquid discharged from the stators that impacts the leading edges of the rotor blades. Since the highest normal impact velocities of collected liquid are with the leading edge of the rotor blades, increases in this liquid supply rate are obviously undesirable.

The classic means of controlling the damage that can be caused by the casing-collected liquid, as used by the steam turbine industry, is to remove this liquid periodically through suitable ports in the casing.

Even if all the casing liquid is removed, liquid which collects on the stator rotor blades of a given stage can cause material removal damage. The stator collected liquid can discharge

from the stator blade trailing edges into the path of the rotor blades, causing rotor blade edge damage as at location (2) in Figure 1.2-2. The rotor blade collected liquid can run up the rotor blades, causing dissolution damage as indicated in the figure at location (3). In principle, this stator discharged liquid can be removed, as is done in the steam turbine industry, with casing-collected liquid. However, control of damage from stator discharged liquid without removal is the prevalent practice for steam turbines.

### 1.2.2 Processes Involved in Erosion

While erosion of rotor blading in turbines is a local phenomenon, numerical calculations of amounts of erosion either on a relative or absolute basis involve a nearly complete fluid-dynamic history of the turbine flow plus an accounting to the actual material removal phenomenon. A flow diagram of the analytical steps used in the erosion model is given in Figure 1.2-3.

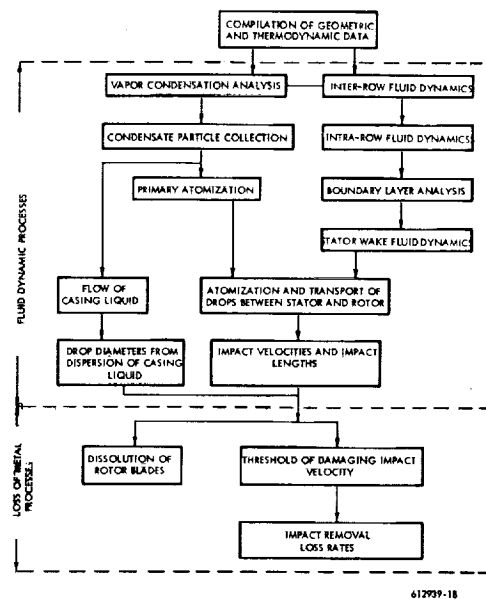


Figure 1.2-3 WANL Turbine Blade Erosion Model

In this section, procedures are discussed in outline, and characteristics calculated or experimental values of the various variables in turbines are given by example. Detail calculational procedures are given in Sections 2 and 3.

Detail methods for analyzing the material removal interaction of liquid with rotor blades is covered in Section 3. Caution in the use of the results from application of Section 3 methods is advised. The suggested procedures are based on reasonable hypotheses and are not established theory or practice.

Detailed methods by which the fluid-dynamic history may be traced are given in Section 2. The methods of fluid-dynamic analysis as given in Section 2 are generally based on widely accepted theoretical schemes. However, the actual implementation of the theories in a numerical sense in the computer codes and other computational procedures set forth in Section 2 assume that a highly efficient axial flow turbine of well-ordered flow in radial equilibrium is being analyzed for erosion. Further, these methods are basically ordered in terms of the flow path as the aerodynamic designer sees it before compromise with the mechanical design.

Most of the computer solutions of Section 2 require the insertion of a physical turbine geometry. The effective fluid-dynamic geometry rather than the real geometry should be used as input to these computer programs if possible. An attempt has been made in the bulk flow programs to adjust to a real geometry and less than ideal flow, but this range of adjustment is quite limited.

The bulk of the analysis carried out during this program was on turbines utilizing either steam or potassium vapors as the working fluids. As a result, the assemblage of analytical models proposed

for carrying out an erosion analysis are most applicable to turbines using these readily fog forming low molecular weight working fluids.

The flow regime in high efficiency steam and potassium turbines is generally subsonic. Some analysis was carried out on the Sunflower mercury turbine and a cesium turbine conceptual design. Both these turbines have supersonic stator exit flow but the flow relative to the rotors is subsonic. The bulk flow analysis programs in Section 2 provide for calculations with supersonic stator flow but not for supersonic flow relative to the rotors. The local flow analysis procedures for boundary layers, wakes, and atomization are based on subsonic information and theory without correction for Mach number effects.

The computer programs cannot be treated as "black boxes" nor should the non-computerized procedures be treated as "cookbook" recipes. The erosion analyst will have to use a considerable amount of individual discretion with all the recommended procedures for good results.

### 1.2.3 Turbines Used for Example Calculations

A great many different turbines were analyzed with respect to erosion or erosion related processes during the course of this program. Calculations concerning these various turbines are scattered throughout the remainder of this section and Sections 2 and 3 as examples. Some overall characteristics and operating conditions of these turbines as used here are tabulated below. Further details on the various turbine designs created under government contract may be found in the references cited as a part of the brief descriptions given herein. Further details about the three large central station steam turbines sometimes used as examples may be found in Appendix A to this section.

TABLE 1.2-1  
COMPARATIVE DATA ON TURBINES ANALYZED

	(Rowe Yankee Atomic) Steam Turbine Low Pressure End (Fig. 1.2-4 and Appendix A)	(Toledo Edison Boylehore No. 2) Steam Turbine Low Pressure End (Appendix A)	(Toledo Edison Boylehore No. 3) Steam Turbine Low Pressure End (Appendix A)	NASA Contract NAS 5-1143 Two Stage Potassium Test Turbine (1)	NASA Contract NAS 3-4520 Three-Stage Potassium Test Turbine (2)	NASA Contract NAS 5-250 Six-Stage Potassium Turbine Conceptual Design (Fig. 1.2-5)	NASA Contract NAS 5-250 Cesium Turbine Conceptual Design (Figure 1.2-6) (3)	(Sunflower) Mercury Turbine (4 and 5)	NASA Contract NAS 7-3911 Small Steam Test Turbine (6)	NASA Contract NAS 3-10934 KTA Turbine Design* (7)
INLET PRESSURE (Pia)	59.2	48.56	60.097	38.2	30.82	178.6	411.0	240	Variable -10 psia Z3	173.0
EXIT PRESSURE (Pia)	0.88	0.491	0.491	11.9	3.92	16.9	35.2	7	Variable -3 psia 10	5.44
INLET SUPERHEAT $t_F$		301	327					~200		71
INLET MOISTURE (Percent)	<1			<1	<1	0	q		Variable 0.4-1.4	
EXIT MOISTURE (Percent)	15.2	7.71	8.36	8.5	14	15.4	16.7	3	Variable Unknown	11.3
NUMBER OF STAGES	9	7	6	2	3	6	2	3	2	10
FLOW RATE (Lb/sec.)	252	80.04	98.4	2.64	1.956	5.76	19.3	0.23	Variable 0.119 0.270	1.988
RPM	1800	3600	3600	19,200	18,250	24,000	24,000	40,000		19,208
TIP DIAMETER OF LAST ROTOR (inches)	157.5	100.34	114.00	9.65	10.83	9.10	7.73	2.042		7.67
LAST ROTOR BLADE HEIGHT (inches)	40.0	25.17	28.47	0.837	1.58	2.25	1.99	0.242		1.57

\* Analysis carried out under subcontract to Contract NAS-3-10934

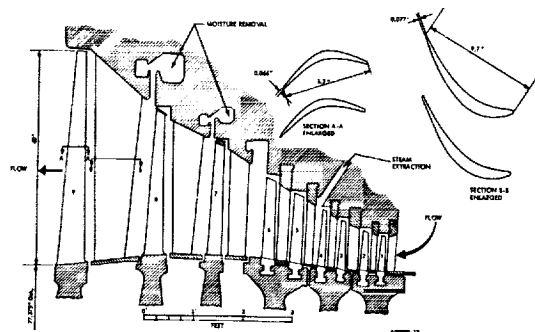


Figure 1.2-4 Yankee Steam Turbine

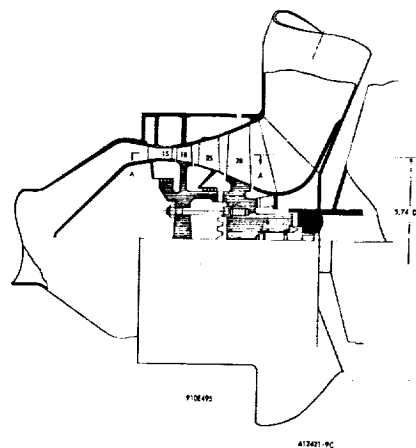
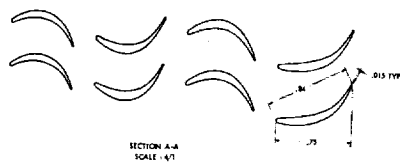
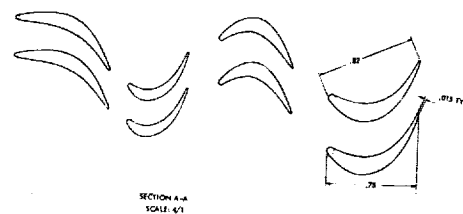


Figure 1.2-6 Cross Section of Two-Stage Cesium Turbine

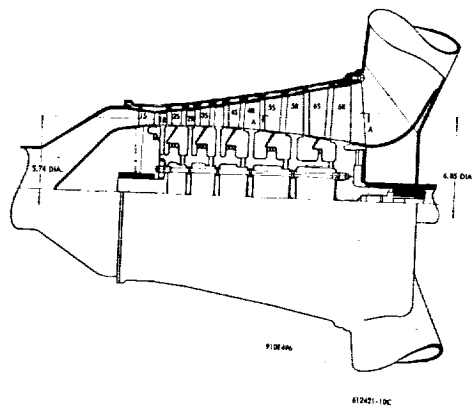


Figure 1.2-5 Cross Section of Six-Stage Potassium Turbine

#### 1.2.4 Process Descriptions

##### 1.2.4.1 Condensation

##### Nomenclature

P	Pressure
r	Fog particle radius
T	Temperature
Y	Moisture content of flow

##### Subscripts

Crit	Critical size for thermodynamic stability
IN	Nozzle inlet
L1, L2	Fog particle group





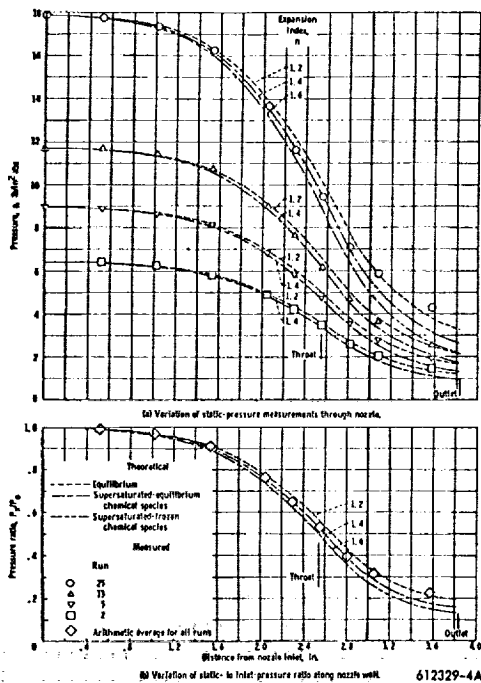


Figure 1.2-9 Pressure Data for Saturated Potassium Vapor

ilibrium expansion ( $n=1.2$ ). A potassium experiment similar to that of Goldman and Nosek is reported by Rossbach (10). Gyarmathy (11) has analyzed Rossbach's data and finds a degree of supersaturation in potassium similar to that evidenced by the Goldman and Nosek data.

Nucleation theory due to Katz, Saltzburg, and Reiss (13) coupled with vapor properties (after Ewing, et al) (14) and the energy, continuity, and momentum relations have been programmed for computer (See Section 2) in a form that can follow the expansion and nucleation process in detail as it proceeds through a turbine. Results of such calculations, for a three-stage potassium turbine and a six-stage potassium turbine, are shown in Figure 1.2-10 in the region of transition from supersaturated to thermodynamic equilibrium expansion. Also shown are points taken from the Goldman and Nosek results intersected, the expansion line,  $n=1.2$ , corresponds to 95 percent of full thermodynamic equilibrium.

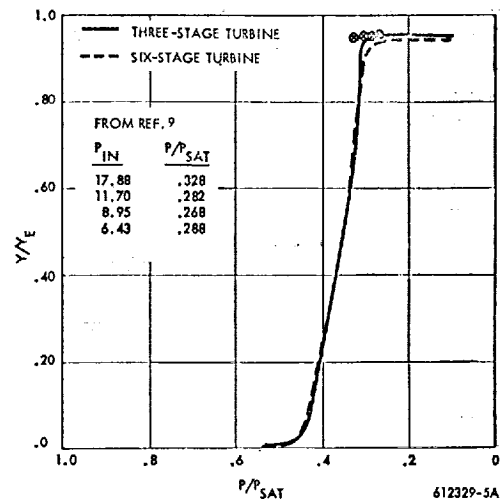


Figure 1.2-10 Moisture Content (Fraction of Equilibrium) as a Function of Pressure Ratio for Condensing Vapor in Two Sample Potassium Turbines

In examining Figure 1.2-10 it will be noted that there is little if any difference in the condensation expansion characteristics between the two turbines, even though the rate of expansion was much higher in the three-stage turbine than in the six. It will also be noted that the calculated pressure ratio for 95 percent of full thermodynamic equilibrium is in good agreement with the Goldman and Nosek results. Also, there is not much spread with pressure ratio for 95 percent of full equilibrium among the experimental results, even though the inlet pressures in the tests varied between approximately 18 psia and 6 psia. Examination of the original Goldman and Nosek publication also shows no consistent variation in condensation pressure ratio with inlet pressure conditions.

The original spontaneous nucleation creates sufficient surface area to allow further condensation to occur with minimal supersaturation. As originally formed, the condensation nuclei are extremely small (0.01 micron diameter) and are of relatively uniform size because of the short time period involved. The nuclei grow quite rapidly to about 0.2 micron diameter as the supersaturation potential created by the expansion in advance of spontaneous condensation is exhausted. Thereafter, a slower growth takes

place as the droplets progress through the turbine. This sequence of events is shown in Figure 1.2-11 by a calculated history of the formation of condensation particles during the expansion of steam in a convergent-divergent nozzle.

The final condensate particle sizes exhausting from turbines examined during this program are on the order of 0.5 micron diameter. The calculated supersaturation in equivalent moisture to initiate spontaneous condensation in turbines is around 2.5 percent in steam, 7.5 percent in potassium, and 4.5 percent in cesium. No spontaneous condensation occurred during expansion calculations on the Sunflower mercury turbine.

#### 1.2.4.2 Collection of Condensate Particles

Because of their small size\*, the condensate particles are essentially locked to the vapor flow and most of them remain with the steam of their birth until turbine exit.\*\* However, a small percentage of the condensate fog collects on surfaces because of the curvature of the flow passages and rotation of the moving blades. By calculation, the percentage collected per turbine row even in the wettest rows is on the order of 5 percent or less of the total fog present; generally, it is less.\*\*\* The collected moisture causes the erosion. The fog particles cause no erosion since they follow the vapor flow as it slices cleanly over the blading surfaces.

\* The particles are so tiny that the ratio of their diameters to the mean free molecular path places them in the slip-flow regime in most turbine flow streams.

\*\* Normal secondary flows at hub and tip will modify this picture somewhat. There is also a negligible drift on the particles relative to the vapor in a radial direction due to the turbine centrifugal field.

\*\*\* This calculation is in qualitative agreement with the observation that moisture removal devices in central-station-type steam turbines rarely remove as much as 25 percent of the total moisture present even though moisture is removed at a number of spots lengthwise along the turbine.

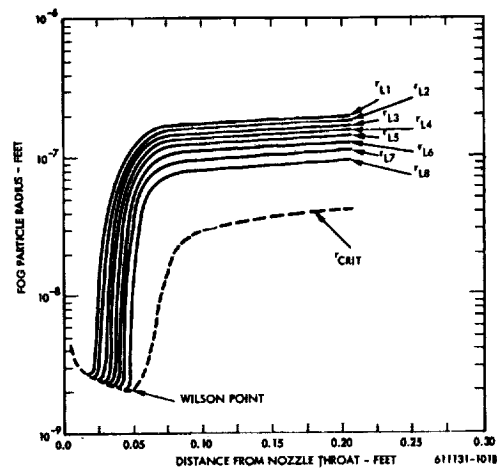


Figure 1.2-11 Steam Condensate Droplet Growth in Divergent Portion of Nozzle

It is hypothesized that the major mechanism in collection of these particles is by inertial impaction on the nose and concave surfaces of the turbine blades. Solutions for the equations governing measured collection by turbine blades by inertial impaction are given in Section 2.

The basis for using the inertial impaction hypothesis is that calculated collection using this assumption agrees reasonably well with measured collection in a steam turbine as reported by Smith<sup>(16)</sup>. Smith's tests were run on a four-stage machine with the water extraction between the third and fourth stages. The theoretical amount of moisture present at the exit of the third stage was varied by changing the amount of superheat in the vapor at the turbine inlet. Smith's data are shown as X-s in Figure 1.2-12. This is a plot of theoretical moisture against the portion of the theoretical moisture collected. Superimposed on this figure is a curve representing a theoretical calculation of the portion of moisture that would be collected by the Yankee steam turbine ninth stage stator if the turbine was operated to provide the varying amounts of theoretical moisture. In addition, the conditions and geometry are also adjusted to make the Wilson Point (at some location ahead of the ninth stator) occur at a value of  $(1/P) dP/dt$  of 1100/sec, where  $P$  is the static pressure and  $dP/dt$  is the rate of change of this pressure with time at the Wilson Point.

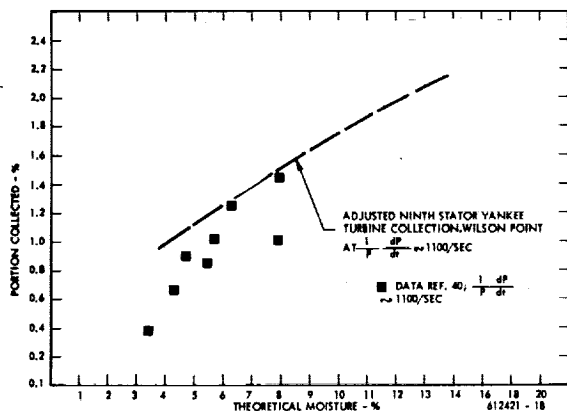


Figure 1.2-12 Calculated and Experimental Turbine Moisture Collection

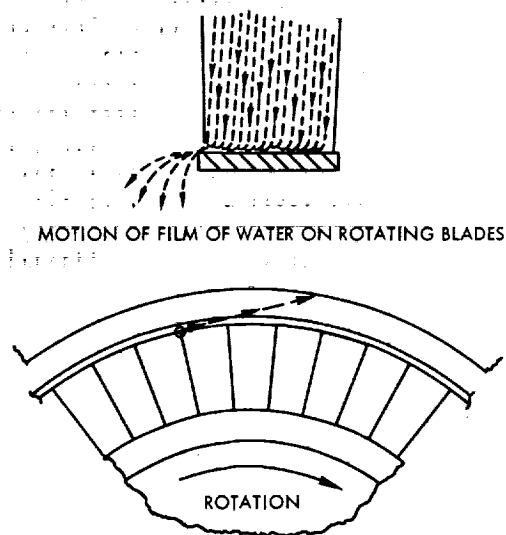


Figure 1.2-13 Relation of Moisture Particle Travel to Motion in Plane Normal to Axis of Rotation

If a line were drawn through Smith's data, it would be steeper than the theoretical line. However, the calculations are for collection on a single turbine row, whereas Smith's data represent collection on a varying number of turbine rows and fractions thereof. That is, the Wilson Point in Smith's turbine is moving toward the front end of the turbine as the amount of theoretical moisture available at the third stage exit rises. Therefore, the collecting surface area subject to the condensing region is increasing. The moisture collected at the drain port between third and fourth stages probably represents that collected on less than one row for 3 percent theoretical moisture, and on up to two or more rows for 8 percent theoretical moisture. This explains why the slope of the data points is substantially greater than the slope of the calculated line. If the drain ports in Smith's experimental turbine are catching nearly all of the moisture collected on the blades, and as the blade sections, spacing, and amount of turning of the experimental turbine rows are quite similar to that of the ninth stator of the Yankee turbine, then the theories of condensate spontaneous nucleation and deposition (taken together) somewhat over-estimate the actual amounts of moisture being collected in steam turbines.\*

The calculated portion of the condensate particles caught by a given blade row in a small turbine is substantially greater than in a large turbine. For example, the last stator row of the NAS 3-8520 Three-Stage Potassium Test Turbine is estimated to collect 7 percent of the condensate particles in vapor of an 88.6 percent average quality; whereas by Figure 1.2-12, the Yankee Steam Turbine would collect only 2.3 percent in vapor of the same quality. The higher flow accelerations in the smaller turbine relative to the larger are the principal reasons for the difference.

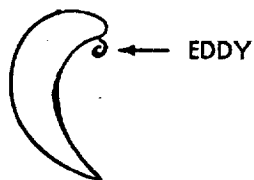
#### 1.2.4.3 Movement of Collected Moisture

The small percentage of fog particles collected form rivulets, films, and drops on the blading surfaces.

\* The conclusion is still justified even though the basic comparison is between "apples" and "oranges" because the calculated single row moisture collection is greater than the measured multiple row moisture collection.

On the rotating blading, the predominant force over most of the blading surface is that of the centrifugal field of the blades. Under this force, the liquid collected on the rotors flows nearly radially outwards\* and is thrown from the tips of the blades. The particle flow leaving the blade tips is essentially in the tangential direction, and the initial flow velocity is approximately the same as the peripheral speed of the blade. The tangential distance of travel in large steam turbines is often on the order of 5 inches. In models of cesium and potassium space turbines the tangential distances of travel may be as low as 5/32 inch.

A radial groove or grooves has been found to occur on the pressure surfaces just aft of the nose of the rotor blades in the NASA-G. E. two-and three-stage potassium test turbines after 1000 or 2000 hours operation (21, 22). This can be taken as evidence of a strong liquid rivulet in this location. In the two-stage test turbine the presence of this



rivulet was ascribed<sup>(21)</sup> to a local flow separation eddy caused by negative flow incidence entering the rotor blades. During the course of this program, a number of surface velocity and boundary layer analyses of axial flow turbine blading were carried out (by the methods in Sections 2.4 and 2.5). In all cases, even at zero flow incidence, there was sufficient diffusion of the flow at the outer edge of the boundary layer just aft of the blade nose on the pressure surface to cause a local region of flow separation. This region of flow separation is quite local. The liquid atomization and trajectory analysis code (ADROP)

\* This is not so near the leading edge of a rotary blade as may be seen by examining the markings on the eroded blade of Figure 1.2-1. Results of an analytical study of moisture movement near the leading edges of rotor blades may be found in Gardner<sup>(20)</sup>.

developed under this program (Section 2.5) cannot handle a separated flow regime and the computations relating to atomized droplets discharged from the trailing edges of stator vanes must be started downstream of this local pressure surface flow separation to obtain droplet information from the code.

Due to the high peripheral velocity of the turbine rotor blade tips, the liquid flung from the tips is well atomized. An estimate of the characteristics of the spray discharged from the tips of the third rotor of the NAS 3-8520 Three-Stage Potassium Test Turbine has been made assuming that the discharge is similar to that from an underfed disc atomizer. These estimates give:

Maximum Drop Diameter -  $76 \pm 33$  microns

Mass Mean Drop Diameter -  $46 \pm 23$  microns

These drops are still large compared to the fog particles. Most of these atomized drops proceed in an almost undisturbed trajectory to impact the turbine casing at a very shallow angle. Even with a 5-inch path length, the time of flight is only about one-half millisecond at 800 ft/sec tip velocity. This time is too short for the vapor drag forces to produce any appreciable deceleration or acceleration of most of the flung liquid. A small percentage of the liquid is undoubtedly in the form of small drops (of sufficiently high surface to mass ratio) that are turned into the succeeding stator by the vapor stream. However, such drops will slice cleanly along the stators and cause no damage. For these reasons erosion at the inlet of stators\* is seldom encountered in practice where moisture impinging on the casing is removed through suitable slots.\*\*

\* Erosion at the exit of stators is sometimes observed and assumed to be caused by drops rebounding from the rotor blades.

\*\* In steam turbines it is the practice to have a vapor flow into the slots. This tends to prevent any liquid splashes from returning to the main stream.

It is desirable not to have to incorporate internal moisture removal into alkali metal space turbines. If moisture removal slots are not incorporated, the liquid flung from the tips of the rotors will accumulate and run along the casing toward turbine discharge under the drag of the vapor flow. If unshrouded rotors are used and if the liquid remains on the casing as a film, it might not do much harm to turbine blading.

An analysis of turbine casing flows for the NAS 5-250 potassium and cesium turbine designs was carried out. This analysis is reported in greater depth in Section 2. By this analysis it is found that the casing flows towards the back end of the sixth-stage potassium turbine are unstable. That is, the film of liquid develops waves. These waves will grow to sufficient height to penetrate the vapor laminar sublayer and will be torn off as drops. Some of these drops will be upwards of 400 microns in diameter. Such drops are large enough to cause impact damage to rotor blade tips (and shrouds and seal strips if such are present). Since these drops may be formed anywhere along the casing, some of them will have insufficient time to break up before impacting the rotor blade tips or shrouds.

The stability of this casing liquid has been examined in terms of Baker's (17) two-phase flow map, and the Chien and Ibele (18) criterion for transition from annular to annular-mist flow of the form

$$(Re_V) (Re_L)^{0.3} = 1.2 (10^6)$$

where

$Re_V$  is the vapor Reynolds Number

$Re_L$  is the liquid Reynolds Number

Both Reynolds numbers are based on mass velocity using the full cross-sectional area of the flow passage as constrained by the turbine blade row.

In addition, the technique of Wrobel and McManus (19) was used to estimate the wave height and its ratio to vapor laminar sublayer thickness. The degrees of casing liquid instability predicted by the three methods do not agree very closely. In addition the correlations were obtained using observations on pipe flows and their application to turbine casing flows has not been established.

The turbine casing flow regime parameters for the last two stages of the six-stage potassium turbine may be found in Table 1.2-2. The values given in Table 1.2-1 are outside the range of the Baker Plot shown in Figure 1.2-14 but a mental extrapolation of the plot indicates unstable flow. The Chien and Ibele factors are an order of magnitude greater than required to yield flow instability.

On the basis of the foregoing observations, it appears that casing moisture removal in potassium space turbines will reduce erosion.

On the stator blades, the primary force acting on the collected liquid is the drag force of the main-stream flow. Under this force the liquid flows to the rear of the stator where it collects until torn from the stator as rather large particles. In the model used it is assumed that the collected liquid follows the bulk flow streamlines and on a time average basis is uniformly distributed along a stator from hub to tip. Although the first assumption is of doubtful validity because of the secondary flows at blade hub and tip\*, the second assumption is still reasonable, since the liquid displaced from the pressure surface of a particular stator will tend to flow over the casing or rotor hub and terminate on the suction surface of the companion stator.

The liquid, which is torn from or near the back edges of stator vanes, impinges on the following rotor blades. It may remove material by the force of impingement or by chemical dissolution of the rotor blade material or by a combination of these mechanisms. Initially, relatively large drops are

\* There is an added force on the liquid stators, tending to move it from tip to hub in the form of the turbine radial pressure gradient. This force is considered to be of negligible importance.

TABLE 1.2-2

### TURBINE CASING FLOW REGIME PARAMETERS SIX-STAGE POTASSIUM TURBINE

Exit of Blade Row	$Re_v \times 10^{-5}$	$Re_L$	$G \times 10^{-4}$ lb/hr-ft <sup>2</sup>	$L$ lb/hr-ft <sup>2</sup>	$G/\lambda \times 10^{-4}$ lb/hr-ft <sup>2</sup>	$L\lambda \psi/G$ $\times 10^4$	$Re_v Re_L^{-301}$ $\times 10^{-7}$
6K-4S	5.04	33.0	3.94	13.0	4.96	2.12	2.62
6K-4R	4.94	168.	3.32	56.1	4.11	11.2	2.56
6K-5S	4.95	321.	2.72	92.3	3.74	19.4	2.56
6K-5R	4.89	491.	2.19	120.	3.33	27.6	2.52
6K-6S	4.87	834.	1.87	181.	3.04	44.6	2.51
6K-6R	4.83	897.	1.54	164.	2.64	46.0	2.48

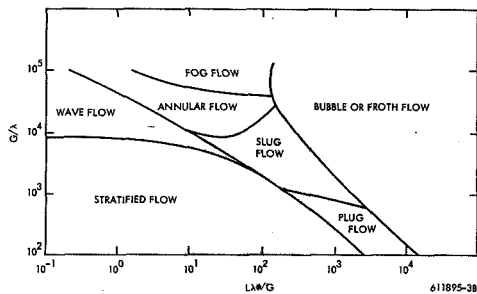


Figure 1.2-14 Baker's Map of Two Phase Flow Regimes

torn from the stators. Most of these drops undergo a breakup process and all undergo acceleration between stator and rotor. However, in the time available the drops do not attain vapor stream velocity, and because of the vector velocity difference can strike the nose and convex surfaces of the rotating blades with rather large normal velocity components. In turbines with high velocities of the liquid drops relative to the rotor blades, some of the larger drops strike with sufficient force to cause mechanical material removal by repetitive impact. This mechanical erosion of the rotor blades is confined to the nose and leading edge of the convex surfaces because of the shadow effect of companion blades. Because the blade speed is highest at the tip and hence the incident drop velocities are highest, the greatest degree of mechanical erosion occurs at the blade tips. (Dispersed casing liquid may also play a part if periodic removal is not performed.)

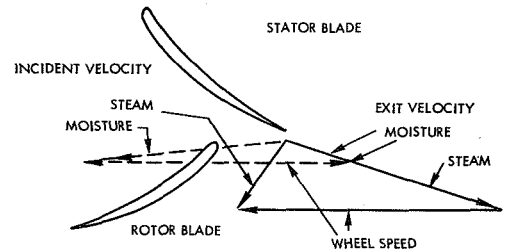


Figure 1.2-15 Impingement on Rotating Blade

As can be inferred from the preceding paragraphs, the mechanical impact intensity and the amount of mechanical erosion depend to a large degree on the extent to which the drops are accelerated and atomized in the space between the stator and rotor. In this respect the vapor density level as reflected in the vapor stream dynamic pressure is a most important parameter. The higher the pressure the more rapid the drop acceleration and the finer the atomization.

Because the vapor density levels in the potassium, cesium, and mercury turbines examined are high compared to those in a low pressure steam turbine of a central-station turbine complex, drop acceleration is much more rapid and atomized drop sizes much finer than in the low pressure steam turbine.

#### 1.2.4.4 Atomization and Trajectories of Stator Discharged Liquid

Visual observations in steam turbines (6, 23) reveal that the liquid collected on the stators is torn from the vicinity of the trailing edges of the stator vanes. Initially, this liquid is in the form of a distribution of sizes and fairly large drops. This stage of the process is called primary atomization. These large primary drops are caught up in the decaying wakes down-stream of the stators and accelerated by the vapor stream. Most of the primary drops are unstable under the aerodynamic conditions prevailing during this acceleration. Providing there is sufficient (time of flight) between stator and rotor, these unstable drops are broken down into smaller stable drops. This stage of the process is called

secondary atomization. Completion of the secondary atomization process gives a relatively stable population of drops composed of a residual of primary drops that are small enough to be stable plus the secondary drops formed from shattered primary drops. In well designed turbines, it is this stabilized population of drops that impinges upon the rotor blades and can cause erosion damage.

There are at least four different mechanisms of primary atomization and two for secondary atomization that have been observed under conditions related to those in turbines. Primary drops have been observed to be formed by (1) tearing of masses of liquid from puddles or films (2) stripping of liquid in the form of pendant drops (3) tip bursting of pendant drops and (4) the coagulation of liquid on a surface into drops. Secondary drops can be formed either through stripping or bursting of primary drops. To trace the history of all these possible processes would be a formidable, if not impossible, task. Because of this the numerical procedures for atomization estimates given in Section 2.7 involve substantial simplification through gross description of droplet classes based in large part on empirical observations or empirical correlating relations commonly used in describing gas-atomized liquid sprays. Furthermore, almost all of the empirical observations used in preparing the numerical detail of the atomization model are taken from reference material where the reported tests were made using steam vapor or air atomization of water drops. Nonetheless, it is felt that observations on steam or air atomization of water drops, particularly observations in actual turbines or turbine-like cascades, are applicable to a broader spectrum of turbine working fluids (such as the liquid metals) of low liquid-viscosity and substantial surface tension.

As a conservative assumption, it is generally assumed that the bulk of the stator discharged liquid is concentrated in the trough of the stator blade wake and atomization and trajectory calculations are carried out using trough conditions. Although there are experimental observations (24) that a considerable amount of liquid rather quickly finds its way out of the wake into the bulk stream, there is no quantitative information on this point.

The wake velocities are calculated by the semi-empirical method of Lieblein and Roudebush<sup>(25)</sup>.

Some experimental wake investigations were carried out during this program and results are reported in Section 4. If the trailing edges of the stator vanes are kept thin, the experimentally measured wake characteristics agree quite well with calculations using the Lieblein and Roudebush method. Evidence of this is given in Figure 1.2-16. It is also evident from this figure that the procedure will not give results as accurate for thicker trailing edges.

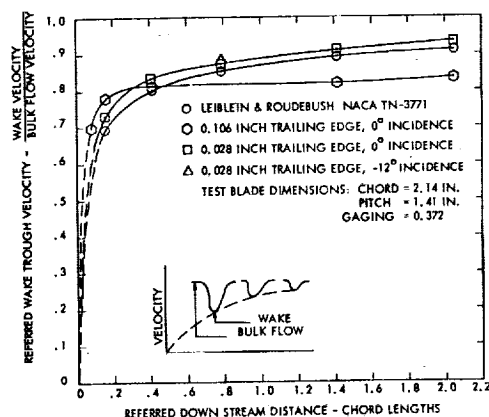


Figure 1.2-16 Wake Trough Velocity

#### Distances Required to Complete Secondary Atomization

While the equations of motion concerning breakup and drop displacement cannot be solved rigorously in closed form, a reasonable approximate solution for large drops (that do not accelerate very much before breakup) can be obtained in closed form. The results of such a solution are shown in Figure 1.2-17.

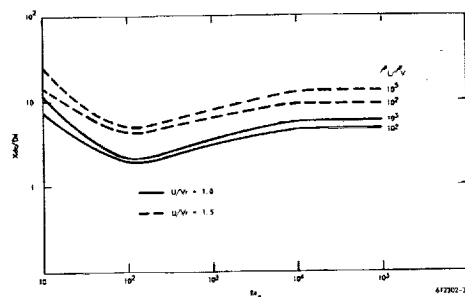


Figure 1.2-17 Displacement of Drops to Breakup



In this figure, the distance of travel before breakup ( $X_{dc}$ ) is referred to the drop diameter ( $D_d$ ) and this referred distance plotted as a function of initial drop Reynolds Number ( $Re_d$ ) based on the relative flow velocity between drop and vapor stream, drop diameter, and vapor density and viscosity. Parameters shown in this figure are  $U/V_r$  and  $\rho_L/\rho_V$

where:

$U$  is the vapor velocity relative to stator blade

$V_r$  relative velocity between drop and vapor

$\rho_L$  density of drop liquid

$\rho_V$  density of vapor

The maximum diameter primary drops discharged from stators (likely to be formed) in turbines may be assumed to have diameters about the dimension of the stator blades trailing edge thicknesses. For small potassium turbines this is about 250 microns. The initial drop Reynolds Numbers for such drops are in the order of  $10^2$  to  $10^5$ , depending upon their position in the stator blade wakes. For such drops it can be seen that the maximum breakup distance is of the order of 10 diameters. Allowing a factor of two for conservatism, the distance between stator exit and rotor inlet can be as little as 5mm (0.2 in.) along the vapor flow path with the expectation that the primary drops will be broken up before impacting the rotor blades.

The ADROP computer code of Section 2.6, uses numerical means for calculation of the distances required to complete secondary atomization. Typical results are illustrated by calculations for the Sunflower Mercury Turbine (Figure 1.2-18) and for the Toledo Edison Bayshore No. 2 Low Pressure End Steam Turbine (Figure 1.2-19). The referral distances are 2mm for Sunflower and 112 mm for Bayshore No. 2. It will be noted that there is insufficient distance between stator and rotor of the Sunflower turbine to complete secondary atomization.

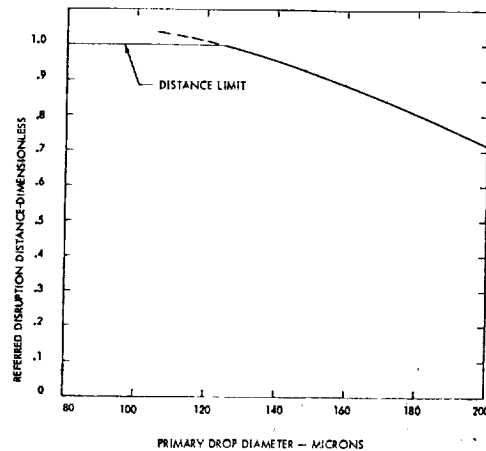


Figure 1.2-18 Sunflower Turbine - Stage 3. Primary Drop Distances to Disruption. Absolute Distances are Referred to the Maximum Possible Path Length

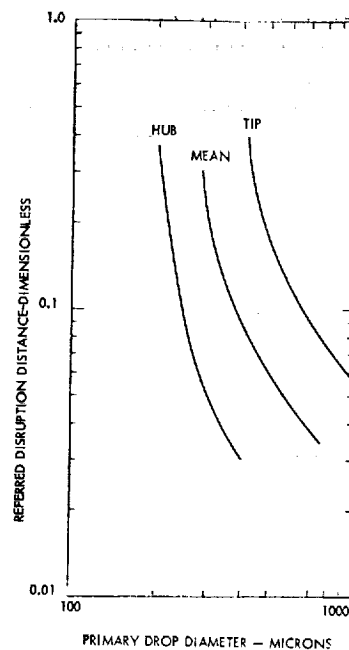


Figure 1.2-19 Bayshore No. 2 - Stage 7. Primary Drop Distances to Disruption. Absolute Distances are Referred to the Maximum Possible Path Length

### • Velocities of Stator Discharged Liquid

The history of the acceleration of the liquid discharged from turbine stator vanes is a general case of motion with a variable local velocity field within the stator wake. A closed form solution does not seem possible because of the complexity of the resulting equation of motion. For this and other reasons the ADROP computer code of Section 2.6 was created to solve the complex equation of motion. A correlation of ADROP code solutions for drops traveling along a stator blade wake axis is given in Figure 1.2-20. These solutions are plotted as a function of drop velocity ( $V_d$ ) to bulk stream velocity ratio in terms of a referred distance ( $X/C$ ) along the wake axis in blade chords ( $c$ ), with parameters of initial drop Reynolds Number ( $Re_0$ ) and  $K_d$  an initial value of an inertial parameter. Where:

$$K_d = \frac{3}{4} \frac{\rho_v}{\rho_l} \frac{C_{do}}{D_d}$$

and

$\rho_v$  vapor density

$\rho_l$  liquid density

$C_{do}$  initial drop drag coefficient

$D_d$  drop diameter — cm

Typical calculated values of  $V_d/U_o$  at the rotor inlet plane for four turbines are as follows:

	$V_d/U_o$
Sunflower, Mercury, 3rd Stator	0.05
Bayshore No. 2, Steam, 7th Stator	0.26
NAS5-250 6-Stage Potassium, 6th Stator	0.22
NAS5-250 2-Stage Cesium, 2nd Stator	0.72

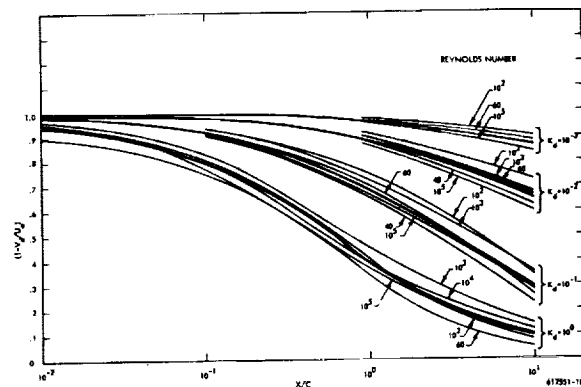


Figure 1.2-20 General Solutions for the Terminal Velocity of Drops Traveling along Stator Wake Axis Streamlines

A comparison of observed stator discharged liquid velocities in the low pressure end of a large English steam turbine and those calculated along the flow path between the 9th stator and rotor of the Yankee low pressure end, under similar conditions of jet velocity and pressure level, is given in Section 2.6, Appendix A. The observed velocities are 10 to 20 percent higher than the calculated velocities.

The velocities with which these stator discharged drops impact the rotor blades depend upon the turbine velocity triangles as illustrated by Figure 1.2-16. In all of the calculations of this program it has been assumed that the turbine is operating at design condition with zero vapor flow incidence into the rotor blades. Figures 1.2-21 and 1.2-22 give calculated values of impact velocity,  $W_d$ , with the last rotors of the Sunflower and Bayshore No. 2 turbine, respectively, as a function of drop terminal velocity,  $V_d$ . Of even more importance is the normal component,  $W_n$ , of the impact velocity for it is well established in impingement erosion experience that it is the normal component of drop impact velocities that is of primary importance. It will be noted that the normal velocities of drop impact of the Sunflower last rotor are, in general, substantially lower than the absolute velocities of impact; this is not so for the Bayshore No. 2 steam turbine. The reason is the Sunflower turbine is a relatively high hub to tip ratio impulse turbine and the inlets to the rotor blades are turned away from the direction of rotation. Bay-

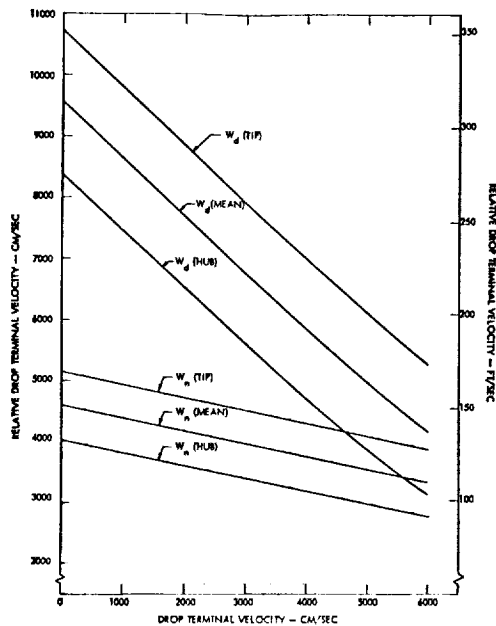


Figure 1.2-21 Sunflower Turbine - Stage 3. Drop Impact Velocities Relative to the Rotor Blade

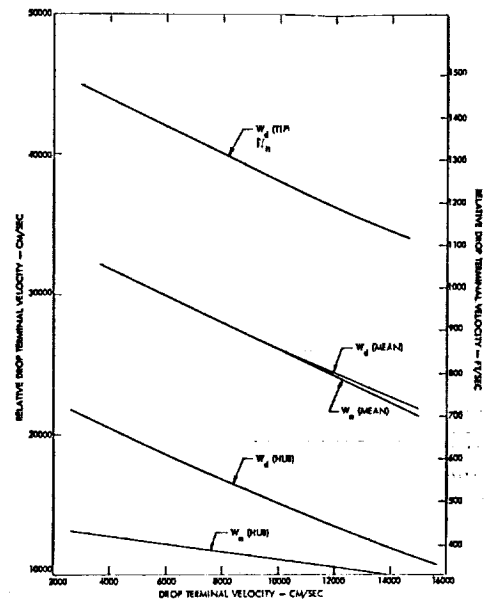


Figure 1.2-22 Bayshore No. 2 - Stage 7. Drop Impact Velocities Relative to the Rotor Blades

shore No. 2, is a relatively low hub to tip ratio turbine with a high degree of reaction at the blade tips. The inlets to the rotor blades, particularly at the tips, are turned in the direction of rotation.

The calculated drop impact normal velocities on the last rotor blades in potassium turbine designs are intermediate between those of the Sunflower and Bayshore No. 2 turbines and are in the range of 500 to 900 ft/sec. The calculated drop impact normal velocities on the last rotor blades of the NAS 5-250 two-stage cesium turbine are in the same range as those of the Sunflower turbine.

- Diameter of Drops Impinging on Turbine Rotor Blades

Two means of assessing the distribution of drop diameters impinging upon the turbine rotor blades have been investigated during this program. Both methods are discussed in Section 2.7. The first of these, of a semi-empirical nature, was used in the erosion analysis of the Yankee steam turbine low pressure end reported in Reference (26). The calculated drop diameter distribution produced is quite different from those reported by Christie (23,24) from actual observations in a large steam turbine. (See Figure 1.2-24.)

The second method is an empirical approach using an average distribution from those reported by Christie (23) applied to a calculated maximum drop

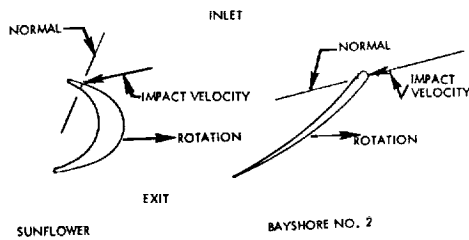


Figure 1.2-23 Comparison of Impact Velocities on Sunflower and Bayshore No. 2 Turbines

diameter of the stator discharged spray. The second method is presently preferred although it also (as discussed in Section 2.7) can yield quite inaccurate results with very small errors in determination of maximum drop diameter.

The maximum drop diameter of the stator spray is determined by use of the parametric time history of the drops in the stator wake covered in Section 2.6. It is assumed that the primary drops become entrained by a given wake streamline and the liquid represented remains with that streamline until rotor impact. The criteria for disruption of a primary drop is taken as the exceeding of a critical drop Weber Number at some point along the path between detachment from the stator to impact with the rotor. This assumes that there is time for the drop to disrupt, after the critical Weber Number has been exceeded, before it impacts the turbine rotor. All primary drops which experience a Weber Number greater than the critical are presumed to disrupt to smaller stable secondary drops.

Primary drops that experience local Weber Numbers in the wake less than the critical Weber Number are assumed stable and retain their primary configuration. The maximum size drop that will impact the rotor is the primary drop that just experiences, but does not exceed, the critical Weber Number anywhere between origin and impact with the rotor. This model uses Weber Number criteria because under local conditions at the time of break-

up of the primary drops it is believed that the ratio of dynamic pressure force to surface tension force is the single most important criterion as to whether a drop is stable or not. Unfortunately, Weber Number alone is not sufficient to allow a prediction of maximum drop diameters in sprays even when the local conditions at disruption are known with reasonable accuracy. For this reason, Westinghouse has varied the numerical value of the Weber Number that has been used in analysis of turbines from turbine to turbine.

For small turbines, 1-inch chord, 1-2 inch high blades, the critical Weber Number used has been 13. For the large low pressure ends of central station steam turbines, the value used has been Weber Number = 22. The rationale is due to Gardner<sup>(20)</sup> who apparently drew on the work of Heinze. According to Spies, et al<sup>(6)</sup>, Heinze shows that for a non-viscous fluid (the turbine working fluids are considered "non-viscous") the critical value of Weber Number is 13 for shock exposure of a drop to aerodynamic forces and this critical Weber Number increases to 22 for a steadily falling drop. This latter case is that of graduated application of aerodynamic forces to the drop. From trajectory calculations on both large and small turbines, it appears that the application of aerodynamic forces to the primary drops is quite abrupt or shock-like in the small turbine and quite gradual in the large central station steam turbine low pressure end. The selection of Weber Number = 13 for the small turbines and Weber Number = 22 are commensurate with the trajectory observations.

Since these values were selected, a considerable amount of actual observation in large steam turbines<sup>(23)</sup> and in a small steam turbine<sup>(6)</sup> built to simulate a space potassium turbine have become available. These data clearly show that from a conceptual point of view, the simplified two-valued scheme of this model is inadequate. However, in a numerical sense the selection of Weber Number = 13 for the small space turbines examined is a reasonable average value based on an analysis of the results of Spies et al<sup>(6)</sup> as given in Appendix B, Section 2.7. For a typical design such as the NAS3-GE 3-stage potassium test turbine, the procedure of Weber Number = 13 may err in estimating the maximum

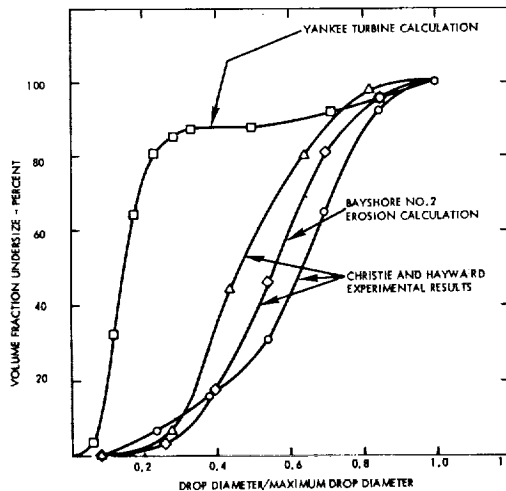


Figure 1.2-24 Drop Distribution Functions

size drop impinging on the rotor blades of that turbine by 30 microns. The maximum size drop is about 100 microns in diameter.

The selection of critical Weber Number = 22 for the low pressure ends of large central station steam turbines seems to be overly conservative in terms of steam stationary cascade tests as reported by Christie and Hayward<sup>(23)</sup> but not necessarily for actual turbines as reported by the same reference.

#### 1.2.4.5 Material Removal

The liquid that is torn from the back edges of the stator vanes and impinges on the following rotor blades may remove material by the force of impingement or by chemical dissolution of rotor blade material or by a combination of these mechanisms. In the early days of steam turbines, it was postulated that chemical effects might play a part in the observed blade erosion. While the presence of such effects has never conclusively been disproved, it is not deemed important. The observed erosion in steam turbines can be adequately explained as a physical phenomenon without recourse to chemical explanations. It is believed that this is also true of mercury turbines.

The chemical situation in alkali liquid metal turbines is not as clear. Because of the elevated operating temperatures and the nature of the fluids involved in alkali liquid metal turbine systems, all proposed structural materials have a substantial degree of solubility in the working fluid. In pure fluid systems, such as can be maintained with reasonable state-of-the-art technology with alkali metal working fluids, it is thought that dissolution of the blade materials is the main chemical possibility for material removal and that present limited quantitative data can be extrapolated to other similar systems for rough, predictive comparisons.

#### • Chemical Dissolution

The stator discharged liquid impacts the rotor blades along a relatively narrow portion of the leading edge of the convex surface and is assumed to flow in a nearly radial direction to discharge at the blade tips. It is assumed that impacted moisture forms a continuous film, and the fluid impacts uniformly along the blade impaction zone. The concern of this analysis is the chemical dissolution of the blade material associated with the flow of this film in potassium or cesium vapor turbines.

Because the film of liquid formed on the rotor blades is at most a few micrometers thick and is violently stirred by the incoming drops, it is assumed that the rate controlling step, in the dissolution process, is that of the rate of dissolution for the blade material into the liquid at the liquid-solid interface. This is different than for dissolution of solids into liquids in pipe flow. In pipe flow, the rate controlling step is often the rate of diffusion of the dissolved solute across the solvent boundary layer into the bulk flow of solvent in the pipe.

According to Epstein<sup>(27)</sup>, the rate of dissolution of a pure metal into a pure liquid solvent at the metal-liquid interface is given by

$$S = S_0 \left[ 1 - \exp \left( - \frac{\alpha A t}{V_l} \right) \right] \quad (1)$$

where

- A is the surface area in contact with the liquid -  $\text{cm}^2$
- $S_o$  is the saturation solubility of material in the solvent - dimensionless
- S is the solute concentration in the solvent at time t - dimensionless
- V is the volume of liquid in contact with the metal for time t -  $\text{cm}^3$
- t is the contact time between liquid and metal along surface A - sec
- $\alpha$  is the solution rate constant -  $\text{cm}/\text{sec}$

Under steady-state conditions, such as in a turbine operating at design, it can be shown (Section 3.4) that Epstein's equation implies that the rate of blade metal thickness removal is:

$$\dot{\delta}_m = \alpha S_o \left( \frac{\dot{m}_a}{\dot{m}_a + \rho_l k \alpha} \right) \quad (2)$$

where the added variables are:

- $\dot{m}_a$ , rate of liquid deposition per unit area per unit time -  $\text{gm}/\text{cm}^2/\text{sec}$
- $\dot{\delta}_m$ , rate of metal thickness removal -  $\text{cm}/\text{sec}$
- $\rho_l$ , liquid density -  $\text{gm}/\text{cm}^3$

The discussion so far has assumed a pure metal dissolving into a pure liquid. The latter assumption, pure liquid, is probably reasonable since turbine system operators go to some length to keep a pure liquid in the system. However, turbine blade materials are alloys composed of materials of differing solubility and probably chemical activity. In advanced high temperature Rankine cycle liquid metal systems, the turbine blade materials are likely to be refractory alloys such as TZM and TZC. These are molybdenum alloys with small amounts of titanium, carbon, and zirconium. The alloying materials such as Ti and Zr are more soluble than the base material; while present

in concentrations of only 1 to 2 percent they tend to collect at the alloy grain boundaries where they may be more readily leached from the surface than if they were uniformly mixed. In addition, if there is preferential leaching at the grain boundaries, this may so weaken the material that a considerably greater amount of material may be lost than that which simply dissolved.

At the present time, there are insufficient experimental results or theory to judge these factors adequately. Nevertheless, it is worthwhile to delineate these areas of uncertainty by the application of multiplicative correction factors to Equation (2), as:

$$\dot{\delta}_s = k_1 \dot{\delta}_m = k_1 k \alpha \alpha S_o \left( \frac{\dot{m}_a}{\dot{m}_a + \rho_l k \alpha} \right) \quad (3)$$

where

- a is the activity level of a readily dissolvable constituent of the alloy in the alloyed form relative to the constituents dissolvability in pure form -  $\text{cm}/\text{sec}$
- k is the ratio of the effective surface area from which the constituent is dissolving to the total surface area of the alloy - dimensionless
- $k_1$  is the ratio of total alloy removal rate to dissolving constituent removal rate - dimensionless
- $\dot{\delta}_s$  is the thickness removal rate for the alloy surface as a whole -  $\text{cm}/\text{sec}$

Results of a chemical dissolution examination of the sixth rotor of the NAS5-250 six-stage potassium turbine, and the second rotor of the NAS5-250 two-stage cesium turbine are reported in Section 3.0. Because of the doubtful basis for chemical dissolution

examination of the NAS5-250 turbine designs, a parametric examination of chemical dissolution is presented in this section. In both these examinations, it is assumed that:

$$k = 1/k_1 \text{ and } a \sim 1. \quad (4)$$

$$\dot{\delta}_s = a S_o \frac{\dot{m}_a}{\dot{m}_a + \rho_l k a} \quad (5)$$

Hence,

$$\delta_s = a S_o \Delta t$$

Also, it has been assumed that  $k$  (the effective surface area ratio) is equal to the ratio of dissolving constituent volume to total alloy volume.

If it is assumed that  $\dot{m}_a \gg \rho_l a$  and  $a$  is time independent, Equation (4) is readily integrated to give:

$$\delta_s = a S_o \Delta t$$

where

$\delta_s$  is the total thickness of material removed from a metal surface in time of exposure ( $\Delta t$ ) - cm

$\Delta t$  is the total time of metal surface exposure to the liquid metal - sec

With present knowledge, there are no experimental values of dissolution rate constant ( $a$ ) available on the dissolving of solid metals under turbine blade conditions into the alkali liquid metals. There are values for Fe dissolving in Na<sup>(27)</sup> and 304 SS dissolving in Li<sup>(28)</sup>, as illustrated in Figure 1.2-25 for low velocity pipe flow kind of conditions but their applicability to turbine blade dissolution is undemonstrated. However, in the dissolution examinations reported in subsequent Section 3.0, it is assumed that data for 304 SS dissolving in Li is applicable to the turbines examined (this is pure assumption).

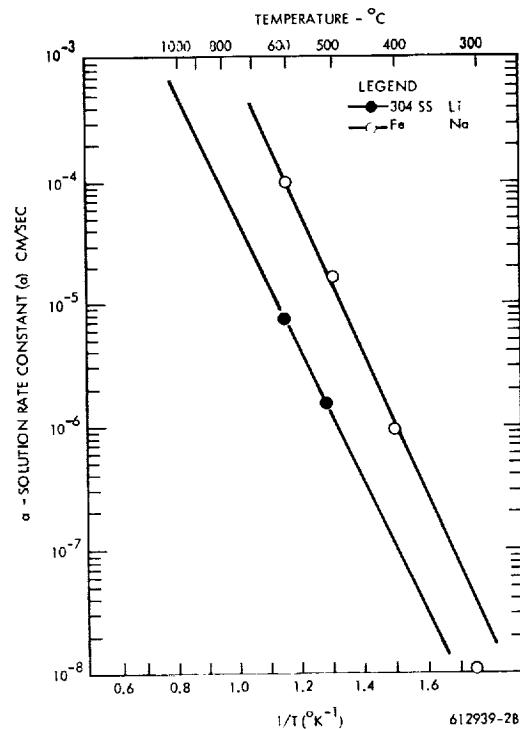


Figure 1.2-25 Temperature Dependence of  $a$

Using the saturation solubilities from Table 1.2-3, Equation 5. has been used to calculate the material thickness dissolved as a function of variation in  $a$  for Fe, Ti, Zr, Nb, and Mo dissolving in 1400°F liquid potassium. The time of exposure to liquid potassium is held constant at 10,000 hours. The results of this parametering are given in Figure 1.2-26.

#### • Mechanical Removal by Liquid Impingement

The CEGB has run experiments and published data<sup>(31,32)</sup> on the rates of removal of material by repetitive impacts of water drops on several steam turbine blading materials. This information has been analyzed and some simple correlations formed. The first set of correlations does not include the physical properties of the impinging drop fluid or of the impacted metal as variables. It may be used in the examination or prediction of erosion in steam turbines,

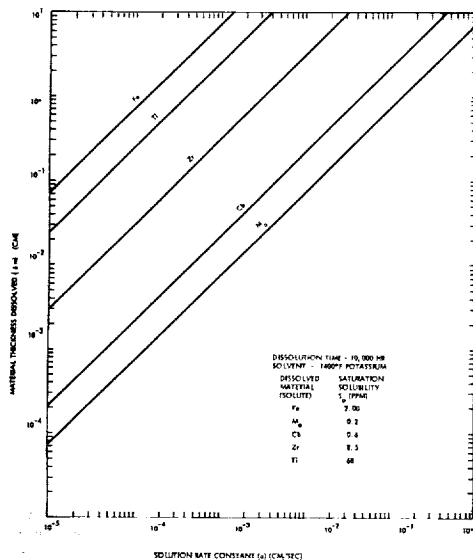


Figure 1.2-26 Parametric Study of the Dissolution of Metals in Liquid Potassium

provided, of course, the blade material or erosion shields are made from one of the materials reported upon by the CEGB. The second set of correlations attempts a broader interpretation of the CEGB steam turbine materials erosion data by factoring into the resulting correlations physical properties of fluid and metal. This is done through the use of a hypothetical mechanical erosion damage model. Neither the damage model or the resulting correlations have been checked experimentally at this time. Calculations relating to mechanical erosion of potassium, cesium, and mercury turbine blades were carried out using this second set of correlations based on the hypothetical damage model. A brief discussion of the resulting correlations follows: The study resulting in the correlations is covered in depth in Sections 3.1 and 3.3 of this report, WANL-TME-1977.

Neglecting fluid and metal properties, erosion rates are still a function of perhaps 11 or 12 independent variables. However, only three of these seem to be of first order importance, with respect to steam turbine erosion. These are (1) velocity of impact, (2) angle of impact, and (3) impacting drop size.

One of the greatest difficulties in interpreting and correlating erosion test data is not the multiplicity of the independent variables, but the identification of the dependent variable(s) for characterizing erosion. All would be well if, under given conditions, erosion proceeded at a constant rate and could be unmistakably characterized by a uniform slope of cumulative weight loss versus time curve. Since erosion rates are not constant with time, erosion can be only approximately characterized by a simplified time independent approach.

The most accepted view is that the first stage in erosion shows little or no weight loss and represents plastic deformation of the surface and initiation of fatigue cracks. This stage is followed by a second stage in which material loss appears and increases rapidly with time. This second stage merges into a third stage in which the rate of weight loss is at a maximum and relatively uniform over a period of time. This, in turn, merges into a later stage (or stages) in which the erosion rate diminishes and can or cannot tend toward another uniform value. Whatever the precise cause of this decrease in erosion rate may be, it is usually associated with rather general and severe damage to the surface, which through geometrical effects alone may result in an effective alteration of the impingement conditions.

It is assumed that the uniform rate of the third stage is the most meaningful in predicting the total erosion in the steam turbine. This assumes that the bulk of the erosion of the blades takes place during this third stage. The time periods of the first and second stages are short compared with the total operating time. Turbine designs which demonstrate severe enough erosion rates in the third stage to become fourth stage terminal cases will suffer from a lack of customer interest and disappear. In any case, from a design point of view, using a third stage rate is a conservative assumption.

CEGB<sup>(21)</sup> has measured the erosion from samples of Stellite 6 and 6B (an erosion shield material often used in steam turbines) subject to



multiple stage of erosion rates for these Stellites and other steam turbine materials in the form:

$$\frac{\Delta W_m}{\Delta W_w} = k (V_n - V_{cd})^n \sec \theta \quad (6)$$

where:

$\frac{\Delta W_m}{\Delta W_w}$  is the mass of material removed per unit mass of impinging water

$V_n$  is the component normal to the impacted surface of velocity of impact

$V_{cd}$  is a critical or threshold velocity below which erosion is negligible

$\theta$  is the angle between the impact velocity vector and the normal to the surface

$k, n$  are empirical constants

CEGB data (32) for Stellite 6 and 6B are plotted in Figure 1.2-27. The  $\sec \theta$  correction is ignored because the angles of impact at which the data were taken were always within 30 degrees of the normal to the surface. The correlation of Figure 1.2-28 thus gives the erosion in terms of two out of three of the independent variables of primary importance.

A correlation for the third independent variable, drop size, is also derived from CEGB data. This correlation uses the observation that the threshold velocity of normal impact below which erosion is negligible appears to be a regular function of drop size.

Assume that:

$$V_{cd} \propto \sqrt{\frac{1}{D}}$$

where  $D$  is the diameter of the impinging drops. As shown in Figure 1.2-28, the correlations are good.

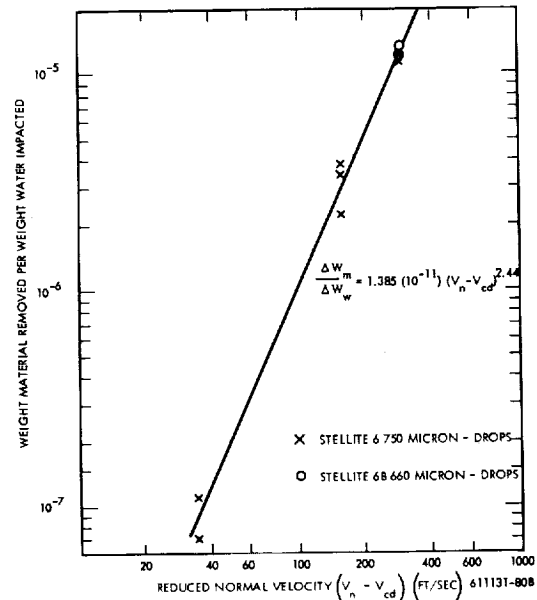


Figure 1.2-27 Stellite Erosion Rates - Data from CEGB; Reduced Normal Velocity  $(V_m - V_{cd})$

The data of Figure 1.2-28 were taken using a stainless steel. Since there is insufficient spread to attempt a similar correlation in drop sizes in the data reported for the Stellites, it is assumed that the form for the Stellites would be approximately the same as for stainless steel with a different empirical constant relating the proportionality between  $V_{cd}$  and  $D^{-1/2}$ . This yields the expression:

$$V_{cd} = \sqrt{1155/D}$$

where:

$D$  = drop diameter, ft

$V_{cd}$  = threshold velocity, ft/sec

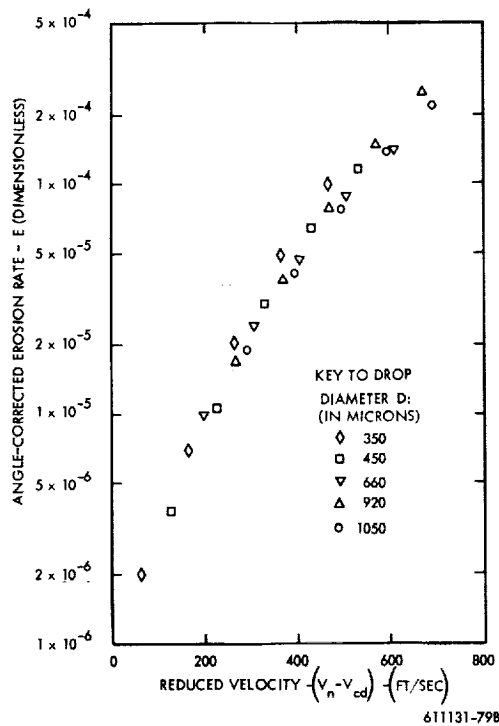


Figure 1.2-28 Correlation of CEBG Data by use of "Critical Velocity"

The foregoing expression used in conjunction with Figure 1.2-27 is then arithmetically sufficient to calculate material removal rates from Stellite 6B in steam turbines, if the states of the impacting fluid are known.

To our knowledge there are no data giving structural material removal rates by repetitive impact of drops of alkali metals or mercury that are quantitatively useful in terms of the impingement of stator-collected liquid on the rotor blades of metal vapor turbines. Therefore, correlating functions of the CEBG steam-water data have been extended to include the physical properties of liquids and a structural material strength by use of a hypothetical impact and damage model.

The basis of the model is hydrodynamic. It assumes that in multiple impact tests of the type reported by the CEBG (and in turbines subject to multiple impact damage) that the impacted material is covered by a thin liquid layer. It presumes that this layer accounts for the changes in threshold velocity that cause erosion (on a given structural material) observed as a function of impacting drop diameter and accounts for the increases in rate of material removal with an increase in velocity above a threshold velocity. The liquid layer may accomplish this through the protective nature of a film overlaying the surface and/or by providing a lubricated surface whereby the liquid outflow from the impact can occur more readily. This latter action will allow an earlier release of the impact pressure on a wet surface than on a dry surface. The model treats the eroded material as a black box characterized by its Vickers Hardness, but does not answer the question as to why, relative to their Vickers Hardness, cobalt and titanium base alloys are generally more erosion resistant than iron or nickel base alloys, and these in turn are more resistant than cemented carbides.<sup>(33)</sup> The erosion rates used here are the maximum rates of erosion observed in what is normally called the third stage of erosion when erosion is depicted as a four-stage process.

The equations developed are as follows:

$$\frac{m_m}{m_l} = \left( \frac{\epsilon}{17} \right) \left( \frac{\rho_m}{\rho_l} \right) \left( \frac{\rho_l U_n^2}{2 S} \right) \left( \frac{U_n}{C_o} \right)^2 \left( 1 - \frac{U_{cd}}{U_n} \right)$$

$$U_{cd} = K \left( \frac{S}{\rho_l C_o} \right) \left( \frac{\delta_{cd}}{D} \right)^n$$

For the particular CEBG apparatus the correlating film thickness  $\delta$  is given by:

$$\delta = \sqrt{\frac{3 \mu D_s}{4 \pi \rho_l U_s}}$$

where

- $C_o$  is the acoustic velocity in undisturbed drop liquid - ft/sec
- $D_s$  is the effective diameter of the erosion sample, assumed equal to blade height for small space turbines examined - ft
- $D$  is the impinging drop diameter - ft
- $m_m$  is the mass material eroded - slugs
- $m$  is the mass of liquid impinged - slugs
- $U_n$  is the normal velocity of drop impact - ft/sec
- $U_w$  is the blade or erosion sample average peripheral velocity - ft/sec
- $U_{cd}$  is the threshold velocity of normal impact to cause erosion - ft/sec
- $S$  is the material hardness as measured by the Vicker's Diamond Point method. (Note: Vicker's Hardness, VPN or DPN, is normally given in  $\text{kg/mm}^2$ . For use in these equations it should be converted to the system of units being used. In the case of Figure 1.2-29, the units are  $\rho$  in slugs/ft<sup>3</sup>,  $C$  in ft/sec,  $\delta$  in ft,  $d$  in ft,  $U_{cd}$  in ft/sec, and VPN in  $\text{kg/mm}^2$ .)
- $\delta$  is the depth of the liquid layer over the eroded material - ft
- $\epsilon$  is the effectiveness of impingement process - dimensionless
- $\rho_l$  is the density of the undisturbed liquid - slugs/ft<sup>3</sup>
- $\rho_m$  is the density of the eroded material prior to erosion - slugs/ft<sup>3</sup>
- $\mu$  is the viscosity of the undisturbed liquid - lb-sec/ft<sup>2</sup>

Based on the CEGB data<sup>(32)</sup> for iron and nickel base alloys,  $\epsilon \sim 0.45$ ; for cobalt base alloys of the stellite type  $\epsilon \sim 0.12$ . The threshold velocity correlation for the same materials is given in Figure 1.2-29.

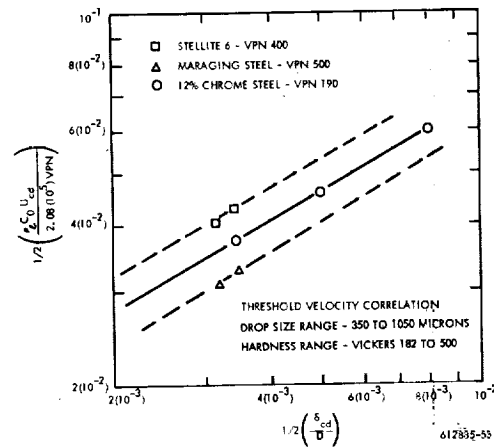


Figure 1.2-29 Threshold Velocity Correlation

### 1.3 RESULTS OF SEVERAL TURBINE EROSION ANALYSES

#### 1.3.1 Comparative Erosion Potential of NAS5-250 Cesium Turbine and Potassium Turbine Conceptual Designs

The two wet vapor turbine conceptual designs were originally created under contract NAS5-250. These turbines are (1) a two-stage turbine for cesium working fluid and (2) a six-stage turbine for potassium working fluid. Both turbines were designed to produce about 1 MW shaft output at 24,000 rpm when exhausting to a 1420°F temperature condenser. Discussion of the original design criteria and design implementation is in Reference 3. Cross-sectional views of the turbines are shown in Figures 1.2-5 and 1.2-6; and information on design operating conditions is given in Paragraph 1.2.3. The com-

parative erosion analysis is confined to the last rotors of the two turbines since vapor moisture content is highest at the back end of the turbines.

### 1.3.1.1 Potential for Mechanical Removal from Last Rotor Blades

The conditions of impact on the last rotors were estimated by the methods outlined in Section 1.2.0. The results of these various fluid-dynamic calculations for the two turbines are given in Appendix 1C.

To use the Section 1.2.4.5 correlation of CEGB material removal data, the thickness of the liquid films on the nose and leading edges of the rotor blades must be estimated. Undoubtedly, these films of liquid are not uniform over the surface of the region of maximum impingement but vary from essentially a residual film thickness up to rivulets. For purposes of these calculations, it is assumed that the film is essentially a residual film. (This is a conservative assumption since the thinner the film, the lower the threshold velocity for mechanical material removal.) This is the basis of the film thickness calculation used in establishing the correlation of the CEGB data. By analogy with the correlation calculation

$$\delta = \sqrt{\frac{3 \mu h}{4 \pi \rho_l U_w}}$$

where

$h$  is the blade height from hub to tip-ft

$U_w$  is the blade tip velocity - ft/sec

and

$\rho_l$  and  $\delta$  are as previously defined.

For the turbines examined the film flow using the thicknesses calculated from the foregoing equation is less than 20 percent of the total flow rate of impacting moisture. Table 1.3-1 gives the threshold velocities and film thicknesses calculated

for the potassium turbine sixth rotor blade tips and the cesium turbine second rotor blade tips. It is assumed that the material of the blades has a VPN = 260. This is a characteristic value for TZM, which is often mentioned as a candidate structural material for alkali metal vapor turbine blades. The values are for the drops of maximum diameter calculated to hit these rotors. Also given are the expected maximum impact velocities of these drops with the rotor blades.

TABLE 1.3-1

EROSION THRESHOLD VELOCITIES

	Sixth Rotor Potassium Turbine	Second Rotor Cesium Turbine
Drop Diameter, micron	100.	5.
Film Thickness, micron	2.9	1.95
Threshold Velocity, ft/sec	1400.	>4000.
Maximum Normal Impact Velocity, ft/sec	800.	338.

From Table 1.3-2, it can be seen that for both turbines the calculated threshold velocity to cause mechanical damage is substantially above the estimated maximum normal impact velocities of the largest drops. Therefore, it is concluded that mechanical erosion damage to the rotor blades of these turbines is not likely to be a problem. The margin for error in this statement is considerably greater for the cesium turbine than it is for the potassium turbine.

TABLE 1.3-2

LAST ROTOR BLADES DISSOLUTION  
IN A POTASSIUM AND A CESIUM TURBINE

	NAS 5-250 Potassium Turbine Sixth Rotor	NAS 5-250 Cesium Turbine Second Rotor
Bulk Fluid Temperature - °K	1060°K	1045°K
Solution Rate Constant (a) - (cm/sec)	1.1 (10 <sup>-4</sup> )	0.95 (10 <sup>-4</sup> )
Deposition Rate on Rotor Blade Noses (ho)-gm/cm <sup>2</sup> /sec	0.079	0.098
Rotor Blade Material	TZM	TZM
Average Solubility of Ti and Zr, ppm	63.	63.
Volume Fraction Ti & Zr (k)	0.0124	0.0124
Density of Liquid - gm/cm <sup>3</sup>	0.698	1.415
$k a \rho_l$ - gm/cm <sup>2</sup> /sec	9 (10 <sup>-7</sup> )	1.67 (10 <sup>-6</sup> )
$\delta$ (based on Ti & Zr) mils/1000 hour	9.6	8.5
Average Solubility of Mo, ppm	0.2	0.2
Volume Fraction Mo (k)	0.987	0.987
$k a \rho_l$ - gm/cm <sup>2</sup> /sec	7.1 (10 <sup>-5</sup> )	1.33 (10 <sup>-4</sup> )
$\delta$ (based on Mo) mils/1000 hour	0.03	0.027

### 1.3.1.2 Potential for Rotor Blade Dissolution

The chemical dissolution of material from the last rotor blades of the two NAS5-250 turbines has been calculated using Equation 4 and Figure 1.2-25 of Section 1.2.4.5. This method assumes that the rate of material loss is controlled by the rate at which material can cross the solid-liquid interface and that if selective leaching of the more soluble alloy constituents occurs, erosion surface regression will be at the rate set by selective leaching along grain boundaries. Other assumptions are (1) blade material is TZM, (2) the dissolution rate constant,  $\alpha$ , is the same as that of 304SS into lithium as given by Figure 1.2-25 for both cesium and potassium, and (3) the solubility of the alloy constituents is the same in cesium as potassium. Substantiation of these assumptions has not been demonstrated.

The results of these calculations are shown in Table 1.3-2. In this table there are two sets of thickness removal ( $\delta$ ) values. The first set assumes that the soluble trace constituents, Ti and Zr, leach preferentially at grain boundaries, and the weakened structure resulting is immediately broken off by the impinging liquid to the depth of trace element removal. The second set assumes that the trace elements are held in place by the principal constituent molybdenum, and that the rate of surface regression is controlled by the rate of dissolution of molybdenum. The 300 fold difference between  $\delta$  values for the two sets is unfortunately indicative of the uncertainty in absolute dissolution rates in potassium or cesium turbines on a calculation basis.

### 1.3.2 Erosion Trends in Central Station Steam Turbines

The low pressure ends of present day central station steam turbines are designed so that some stator discharged drops impact the rotor blades near the tips at velocities sufficient to cause erosion damage. This is particularly true of the last rotor blades. There is considerable economic incentive to use higher and higher tip speeds in these low pressure ends. For this reason it has been of interest to estimate the probable change of erosion in central station turbines last rotor blades with increase in tip speed.

The results of such an investigation are shown in Figures 1.3-1 and 1.3-2. This is a generalized investigation using a stylized turbine and is not intended as design information. To produce these two curves, estimates of moisture collection, drop diameters, and impact velocities of the drops hitting

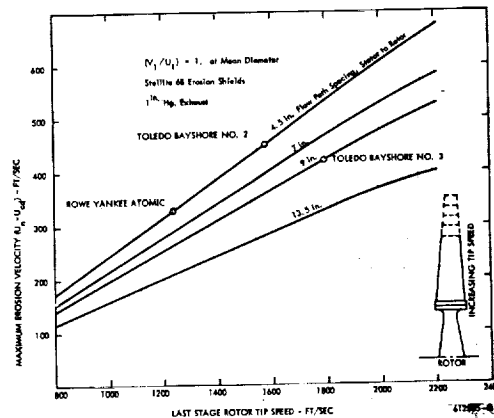


Figure 1.3-1 Maximum Erosion Velocities at Last Rotor Blades of Central Station Steam Turbines

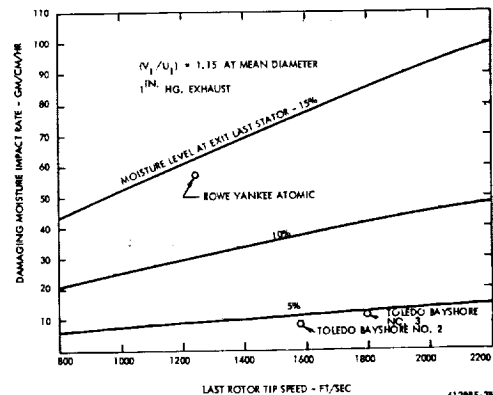


Figure 1.3-2 Damaging Moisture Impact Rates on Noses of Last Rotor Blades of Central Station Steam Turbines

the last rotor blades were made using the methods of Section 1.2. In addition, it has been assumed that the threshold velocity for stage 3 erosion moves in a regular way with drop diameter and film thickness as correlated in Section 1.2.4.5, even though the absolute velocities of drop impingement in the postulated turbines are substantially higher than in the CEGB tests and the impinging drops are on the whole substantially smaller in diameter.

Figure 1.3-1 is a plot of maximum erosion velocity versus last rotor tip speed with parameters of the spacing between stator and rotor along the path of the vapor flow. The turbines are all designed to have a mean diameter ratio of stator spouting velocity to a rotor blade speed of 1.0. The maximum erosion velocity is defined as the maximum normal impact velocity of the maximum diameter drop discharged from the stators minus the calculated stage 3 erosion threshold velocity for the maximum diameter drop.

Figure 1.3-2 is a plot of damaging moisture impact rate per unit of blade length versus last rotor tip speed with parameters of the bulk flow moisture level at the exit of the last stator. The damaging moisture is that fraction of the stator collected and discharged moisture contained in drops of sufficient diameter to have a calculated stage 3 threshold velocity below the normal impact velocity of these drops on the rotor blade at the tip. Also, it is assumed that only that moisture directly collected by the stator row is available for discharge from the stators. All moisture collected by the upstream rows of the turbine has been removed at the moisture removal parts prior to the inlet of the last stator row.

In these two curves are plotted three points representing actual steam turbines in service. While these are actual turbines, the points are still calculations and not measurements. These turbines are not identical to the stylized study turbines but are close enough for discussion purposes. All three turbines experience an acceptable level of last rotor blade erosion damage. The field reports on these turbines are qualitative in nature. It appears that Toledo Bayshore No. 3 has the lowest erosion rates of the three. Probably the Rowe Yankee Atomic Turbine has the highest rates of the three. This is consistent with Figures 1.3-1 and 1.3-2.

Toledo Bayshore No. 2 and No. 3 turbines have substantially lower damaging moisture impact rates than does Rowe Yankee Atomic. This should be more than enough to compensate for the higher maximum erosion velocities calculated for Toledo Bayshore No. 2 and No. 3 versus Rowe Yankee Atomic. A reduction in erosion rate between Toledo Bayshore No. 2 and No. 3 can be accounted for by a decrease in maximum erosion velocity through greater stator to rotor spacing along the flow path direction.

It can be said, on the basis of Figures 1.3-1 and 1.3-2, that if very wet vapor turbines for nuclear power plants of the Yankee Atomic type are to operate at last rotor blade tip speeds of the order of 2000 ft/sec that: (1) the flow path spacing between last stator and rotor will have to be increased substantially, or (2) almost all the moisture directly collected on the last stator blades will have to be removed before it can discharge into the path of the rotor blade tips, or (3) a more erosion resistant material than Stellite 6B will have to be employed, or (4) some way of providing better atomization of stator discharged liquid will have to be found.

### 1.3.3 Erosion Potential of Sunflower Mercury Turbine

The Sunflower turbine is a small mercury vapor turbine developed by TRW for NASA as a part of the Sunflower space power plant. A brief tabulation of design point parameters for the Sunflower turbine is given in Section 1.2.3.

In the overall study, the Sunflower turbine examination was the most interesting of all. The model of erosion created during the study is largely based on experimental information on the behavior of water and water vapor in apparatus of appropriate size for large central station steam turbines. The Sunflower turbine operating experience afforded an opportunity to check the reasonableness of the model in terms of a very tiny turbine operated on a vapor and liquid with physical properties quite different from those of water.

The most interesting observation made during the Sunflower analysis arose out of the size of the turbine. The nominal stator to rotor axial spacing in this turbine is only 0.6 mm (or 2mm along the path of flight of the stator discharged liquid). In addition the axial spacing tolerance band for these turbines is  $\pm 0.3$  mm, or from turbine to turbine the axial spacing could vary from 0.3 mm to 0.9 mm. From the analysis this is a significant variation. As illustrated in Figure 1.2-18 at the nominal axial spacing of 0.6 mm, there is not, on a calculated basis, sufficient time for all the third stator discharged primary drops that are unstable (those  $> 90$  microns) to breakup before reaching the rotor inlet plane. If the axial spacing is reduced to 0.3 mm (0.5 referred disruption distance) the maximum diameter drop impacting the third rotor will more than double in size.

As shown in Figure 1.2-18, at the nominal 0.6 mm axial spacing all drops with diameters greater than about 120 microns will break up into small drops. An erosion threshold velocity calculation for the Sunflower last (third) rotor blade tips has been carried out using this 120 micron drop diameter. The calculation used the threshold velocity correlation of Figure 1.2-28. The presumed liquid film thickness at the rotor blade tips was calculated in the same manner as the erosion comparison of the NAS5-250 potassium and cesium turbine designs.

The result is given in the following table and is compared to the ADROP code calculated maximum normal impact velocity. The Sunflower rotor blade material is Ph 15-7 M. A handbook value of hardness for this material has been used in the calculation.

SUNFLOWER TURBINE MAXIMUM DIAMETER DROP  
EROSION THRESHOLD VELOCITY

Maximum Drop Diameter, microns	120.
Film Thickness, microns	3.9
Threshold Velocity of Normal Impact (to cause erosion,) cm/sec; V <sub>PN</sub> = 500 (RC = 48)	5320.
Maximum Normal Impact Velocity, cm/sec	4980.

As can be seen the threshold velocity and the maximum normal impact velocity of the largest and slowest (highest rotor impact velocity) drops predicted to impact the Sunflower turbine last stage rotor blades are about the same. This indicates that little erosion was to be expected in the Sunflower turbine if the axial spacing between stator and rotor was equal to or greater than the nominal value of 0.6 mm.

The experimental observations with respect to erosion of the Sunflower turbines indicates a marginal situation in agreement with the model calculations. For example, a photograph <sup>(35)</sup> of the third (last) rotor blades of Sunflower CSUI-3 indicates average erosion depths on the blades leading edges as great as 1/64 inch and one blade appears to be cut back at the tip by as much as 1/32 inch. This was after only 2,348 hours of operation. On the other hand, visual observation <sup>(4)</sup> of the third stage rotor blades of Sunflower CSUI-3A after 4,329 hours of operation did not reveal erosion.

TRW <sup>(35)</sup> ascribed the improvement between CSUI-3 and CSUI-3A to (1) reductions in boiler-carryover and reductions in inlet nozzle plenum condensation and (2) redesign of the third stage nozzle to reduce mismatch. The third stage nozzle exit area of CSUI-3 is reported to have been 25 percent oversize. This oversize nozzle would lead to flow separation. In terms of the erosion model one can view this as an effective increase in the trailing edge thickness of the stator vanes. Because the nominal stator to rotor axial spacing in this turbine is only 0.6 mm, only a few mils increase in the stator effective trailing edge thickness is required to cause a dead space extending to the rotor inlet. Such a dead space will prevent secondary breakup of stator discharged drops. As a result, drops considerably larger than the 120 microns predicted here would impact the rotor blades. In addition the rotor on CSUI-3 might have been as close to the stator as 0.3 mm. Even without flow separation this tight spacing would have largely suppressed the secondary atomization process.

It seems possible that if the axial spacing had been a millimeter longer, the erosion of the CSUI-3 third rotor blades could have been as negligible as it was on CSUI-3A.

## 1.4 CONCLUSIONS AND RECOMMENDATIONS

An analytical model has been constructed that follows, step-by-step, the history of the condensation, collection, movement, impingement, and material removal by moisture in wet vapor turbines. The equations of the model are sufficiently detailed to allow calculation of numerical values of the erosion of turbine rotor blades.

The model has been used to examine the erosion in steam, mercury, and potassium turbines on which there is operating experience. With respect to steam and mercury turbines, where the primary mechanism of material removal is mechanical, the estimated erosion can be considered to be in agreement with observed erosion. For steam and mercury turbines, the overall model appears to be adequate for at least order of magnitude turbine erosion estimation in absolute terms and to be quite accurate where relative comparisons between turbines are concerned. With respect to potassium turbines, where it appears likely that the primary mechanism of material removal is chemical dissolution, the material removal calculation step in the erosion model is uncertain by, at least, two orders of magnitude. Unfortunately, the experimental results from operation of different potassium turbines are equally ambiguous.

Cesium vapor turbines will be less prone than potassium vapor turbines to material removal by the mechanical aspects of impingement erosion. However, in neither cesium nor potassium turbines should the purely mechanical aspects be of any great concern provided the liquid flowing along the turbine's casings is removed periodically. There should be little difference in blade erosion by chemical dissolution between cesium and potassium turbines designed for equivalent duty.

Three general rules in wet vapor turbine design that should be followed to minimize blade erosion are: (1) the turbine aerodynamic design should give well ordered flow with no gross separation in any of the turbine passages; even small local separations such as those associated with trailing edges of blades should be minimized, (2) the spacing between the stator and rotor rows of a turbine must be large enough to permit the complete atomization of stator discharged liquid, and (3) build-up of liquid flowing along the turbine casing should be minimized by periodic removal of this liquid.

It is recommended that further experiments in atomization of liquids from turbine stators be conducted. These experiments should be aimed at characterizing the total sprays so produced rather than in an examination of the detail processes as such.

It is recommended that additional experiments on material removal rates by liquid drop impact be done. The experimental information should be obtained under widely varying but carefully controlled and accurately reported velocities, angle of impingement, liquid and target temperatures, and impinging drop diameters for selected candidate turbine blade materials and comparison working fluids. Tests using the alkali liquid metals as the impinging fluid are particularly recommended. These investigations should be more oriented toward obtaining empirical engineering information of quantitative use to the turbine designer, rather than to a fundamental understanding of the complex material removal processes.



# APPENDIX 1A

## ROW-BY-ROW DESIGN CHARACTERISTICS OF LARGE STEAM TURBINES USED AS EXAMPLES

TABLE 1A-1  
 ROWE YANKEE ATOMIC STEAM TURBINE  
 LOW PRESSURE END

ROW NUMBER	YANKEE STEAM TURBINE ROW BY MEAN DIAMETER DATA *																		INLET
	9th ROTOR	9th STATOR	8th ROTOR	8th STATOR	7th ROTOR	7th STATOR	6th ROTOR	6th STATOR	5th ROTOR	5th STATOR	4th ROTOR	4th STATOR	3rd ROTOR	3rd STATOR	2nd ROTOR	2nd STATOR	1st ROTOR	1st STATOR	
EFFECTIVE BLADE HEIGHT, (inches)	40.00	37.44	27.23	24.46	21.01	19.47	15.07	14.04	12.77	11.81	10.57	9.98	9.15	8.47	7.42	6.84	6.49	6.30	7.55
EFFECTIVE MEAN DIAMETER (inches)	117.50	118.40	110.64	109.41	106.01	104.78	100.13	98.54	96.77	95.25	93.50	92.51	91.35	90.27	89.28	88.64	88.35	88.10	89.35
AVERAGE GAUGING	0.600	0.421	0.433	0.341	0.341	0.279	0.330	0.291	0.270	0.266	0.300	0.286	0.278	0.274	0.277	0.268	0.248	0.231	---
EXIT FLOW ANGLE (degrees)	37.0	25.0	25.6	20.0	20.0	16.2	19.2	16.9	15.7	15.4	17.5	16.6	16.1	15.9	16.1	15.5	14.4	13.4	---
STATIC PRESSURE, (psia)	0.88	1.515	2.313	3.411	5.072	6.573	8.745	10.695	13.331	16.367	19.386	22.748	26.473	30.521	34.832	39.679	45.345	51.931	59.2
MOISTURE CONTENT	0.132	0.140	0.130	0.120	0.108	0.100	0.0911	0.0846	0.0768	0.0693	0.0630	0.0560	0.0500	0.0440	0.0380	0.0310	0.0240	0.0170	0.0100
TEMPERATURE OF, (Cpft)	97.5	115.9	131.5	146.5	162.8	174.1	187.0	196.4	207.1	217.5	226.3	234.9	243.2	251.3	259.0	266.8	274.9	283.4	292.0
SPECIFIC VOLUME, (Cpft)	318.9	194.5	131.9	92.6	64.7	51.19	39.59	32.03	27.11	22.56	19.39	16.81	14.68	12.93	11.50	10.25	9.11	8.08	---
JET VELOCITY, (ft/sec)	1133.	1057.	1016.	1026.	857.0	905.7	779.8	811.5	800.0	744.2	727.3	709.7	700.6	686.5	692.7	699.0	705.4	689.1	---
MEAN WHEEL SPEED (rpm **)	922.8	929.9	849.0	859.3	832.6	823.0	786.4	773.9	760.0	748.1	734.4	726.6	717.5	709.0	701.2	696.2	693.9	692.0	---
TIP WHEEL SPEED, (ft/sec)	1237.0	1224.0	1082.8	1051.4	997.6	975.9	904.8	884.2	860.3	840.8	817.9	805.0	789.3	775.5	759.5	749.9	744.9	741.4	---
INLET FLOW ANGLE TO NEXT ROW, (degrees)	90.0	86.27	83.92	73.32	95.34	79.52	97.74	89.62	87.36	98.72	100.5	103.1	103.1	104.8	100.94	97.2	93.7	97.8	90.0
INLET VELOCITY TO NEXT ROW (degrees)	690.	456.	432.	378.	297.	266.	265.	242.	222.	203.	224.	210.	202.	196.	198.	192.	180.	165.	---
BLADE REYNOLDS NO. x 10 <sup>-5</sup> ***	1.5	5.9	2.2	7.9	3.4	8.2	5.7	6.1	7.6	6.4	5.3	6.3	5.2	11.6	8.4	8.2	9.5	14.7	---
STEAM FLOW (gph x 10 <sup>-3</sup> )	801.1	801.1	801.1	801.1	801.1	801.1	801.1	801.1	801.1	801.1	804.9	804.9	804.9	804.9	804.9	804.9	804.9	804.9	804.9
CENTRIFUGAL FORCE, G's, MEAN DIAMETER TIP DIAMETER	5400.	7220.	1.9	1.7	1.1	0.6	0.5	0.5	0.5	0.5	0.5	0.5	0.5	0.5	0.5	0.5	4050.	0.5	---
AXIAL SPACE STATOR EXIT TO ROTOR INLET (inches)	0.066	0.077	0.065	0.063	0.060	0.055	0.045	0.015	0.045	0.015	0.038	0.0125	0.037	0.010	0.038	0.010	0.033	0.010	---
TRAILING EDGE THICKNESS (inches)	12% Chromium Steel	Yes	Yes	Yes	Yes	Yes	Yes	Yes	Yes	Yes	Yes	Yes	Yes	Yes	Yes	Yes	Yes	Yes	No
BLADING MATERIAL	Yes	Yes	Yes	Yes	Yes	Yes	Yes	Yes	Yes	Yes	Yes	Yes	Yes	Yes	Yes	Yes	Yes	Yes	No
STELLITE SHIELDS	Yes	Yes	Yes	Yes	Yes	Yes	Yes	Yes	Yes	Yes	Yes	Yes	Yes	Yes	Yes	Yes	Yes	Yes	No

\* Generally, values are for exit of blade rows  
 \*\* Stator blade "wheel speed" is that speed equivalent to a rotor of the same diameter  
 \*\*\* Reynolds Number based on the blade chord and exit velocity

**TABLE 1A-2**  
**TOLEDO EDISON BAYSHORE NUMBER 2 STEAM TURBINE LOW PRESSURE END**  
 BAYSHORE UNIT NO. 2

ROW NO - MEAN DIAMETER SECTION	7th ROTOR	7th STATOR	6th ROTOR	6th STATOR	5th ROTOR	5th STATOR	4th ROTOR	4th STATOR	3rd ROTOR	3rd STATOR	2nd ROTOR	2nd STATOR	1st ROTOR	1st STATOR	INLET
INLET EDGE RADIUS, (Inches)	0.075	0.100	0.105	0.068	0.225	0.256	0.135	0.0966	0.130	0.077	0.201	0.1509	0.1509	0.1509	
EXIT EDGE RADIUS, (Inches)	0.025	0.031	0.035	0.032	0.027	0.032	0.021	0.005	0.016	0.005	0.016	0.005	0.005	0.005	
BLADE WIDTH, (Inches)	2.993	4.5	2.265	3.816	1.618	3.077	1.213	1.25	1.25	1.0	1.0	0.75	0.75	0.75	
AXIAL SPACE, (Inches)	1.5	3.3	1.0	1.0	0.8	0.9	0.6	0.438	0.438	0.438	0.438	0.438	0.438	0.438	
NO. OF BLADES PER ROW	120	72	122	78	154	70	169	130	138	148	146	204	215	242	
MAXIMUM THICKNESS (Inches)	0.371	0.762	0.340	0.630	0.341	0.882	0.412	0.5432	0.331	0.435	0.510	0.382	0.382	0.382	
CHORD LENGTH (Inches)	3.82	6.23	2.82	5.017	2.000	3.80	1.60	1.70	1.40	1.35	1.35	1.0	1.0	1.0	
BLADE SECTION	T5-8906	S-894	T-6246	S-845	T-388-a	S-420-a	T-477-a	6620	T-475	6600-a	5600 c1	5580-a	5580-a	5580-a	
BLADE WIDTH (ft) (Axial)	0.2494	0.375	0.18875	0.318	0.1348	0.25642	0.10108	0.10417	0.10417	0.08333	0.08333	0.0625	0.0625	0.0625	
PITCH (Inches)	1.968	3.243	1.765	2.705	1.289	2.804	1.115	1.424	1.318	1.209	1.200	0.8471	0.7969	0.7024	

**TABLE 1A-3**  
**TOLEDO EDISON BAYSHORE NUMBER 3 STEAM TURBINE LOW PRESSURE END**  
 BAYSHORE UNIT NO. 3  
 FULL LOAD  
 MEAN DIAMETER CALCULATION

ROW NO.	6th ROTOR	6th STATOR	5th ROTOR	5th STATOR	4th ROTOR	4th STATOR	3rd ROTOR	3rd STATOR	2nd ROTOR	2nd STATOR	1st ROTOR	1st STATOR	INLET
TIP DIAMETER	114.00	109.828											
EFFECTIVE MEAN DIAMETER	85.526	84.170	75.354	73.663	68.578	67.080	66.099	65.134	64.650	63.973	63.668	63.293	
AVERAGE GAUGING (percent)	46.4	29.44	33.60	24.2	33.0	32.6	31.0	30.2	29.5	28.5	26.6	25.2	
EXIT FLOW ANGLE (degree)	33°06'	17°10'	19°38'	14°0'	19°16'	19°02'	18°04'	17°35'	17°09'	16°34'	15°26'	14°30'	
EXIT STATIC PRESS, (psia)	0.491	1.457	2.632	4.468	7.386	10.430	14.168	18.645	24.140	30.792	39.128	48.596	60.097
MOISTURE CONTENT	0.0886	0.0477	0.241	0.0013	0.0	0.0	0.0	0.0	0.0	0.0	0.0	0.0	0.0
TEMPERATURE °F	79	114.7	136.4	157.5	227.9	282.6	334.7	383.4	431.6	479.3	528.2	574.3	621.6
SPECIFIC VOLUME (cf/lb)	597.9	222.8	130.9	81.6	55.1	42.1	33.2	26.8	21.8	18.0	14.9	12.57	
JET VELOCITY (fps)	1708.2	1376.2	1335.4	1346.9	1193.9	1133.8	1121.4	1108.1	1108.1	1105.6	1078.5	1056.9	
MEAN WHEEL SPEED (fps)	1343.46	1322.16	1183.7	1157.1	1077.2	1053.7	1038.3	1023.1	1015.5	1004.9	1000.1	994.2	
TIP WHEEL SPEED (fps)	1792												
INLET FLOW ANGLE	91°	80.6°	65.3°	82.8°	86.5°	18.1°	84.9°	90.01°	80.6°	82.4°	84.1°	90.0°	
INLET VELOCITY NEXT ROW (fps)	936	407	453	361	394	374	374	339	332	316	292	265	
STEAM FLOW (pph)	311181	311181	318932	318932	333607	333607	333607	333607	354364	354364	354364	354364	354364
EFFECTIVE BLADE (height -inches)	28.474	25.658	15.474	13.663	8.538	7.080	6.040	5.134	4.591	3.973	3.609	3.293	
LEADING EDGE RADIUS (Inches)	0.075	0.125	0.075	0.075									
EXIT EDGE RADIUS (Inches)	0.030	0.030	0.0225	0.025									
BLADE WIDTH (Inches)	3.50	5.00	2.414	3.560									
AXIAL SPACE (Inches)	2.5												
NUMBER OF BLADES PER ROW	120	78	120	80									
MAXIMUM THICKNESS (Inches)	0.377	0.852	0.423	0.585									
CORD LENGTH (Inches)	4.395			5.560									

## APPENDIX 1B

### REFERENCES

1. Rossbach, R.S. and G. C. Wesling, General Electric Co., "Two-Stage Potassium Test Turbine," NASA Contractor Report NASA CR-922, Feb. 1968, Vol. I, Fluid Dynamic Design and Performance, Contract NAS5-1143
2. Rossbach, R. J., G. C. Wesling, and W. F. Lemond, General Electric Co., "Three-Stage Potassium Test Turbine," NASA Contractor Report NASA CR-72749, Final Design - Volume I - Fluid Design, Contract NAS3-8520
3. Blinn, H. O., et al, "Space Power Plant Study," Final Report, NASA Contract NAS5-250, Westinghouse Electric Corp., Astronuclear Laboratory, Report WANL-PR(B)-009, December 31, 1963
4. Thompson - Ramo - Wooldridge Inc., "Sunflower Turboalternator CSU1-3A, 4329 - Hour Test Summary Report," NASA CR-169, April 1965, Contract NAS5-462
5. Szanca, E. M., "Sunflower I Turbine Design Report," Thompson - Ramo - Wooldridge Inc., ER 4368, May 1, 1961, Project 512-108131-08
6. Spies, R., J. R. Baughman, J. E. T. Blake, "Investigation of Variables in Turbine Erosion, Influence of Aerodynamic and Geometric Parameters," Rocketdyne Div. North American Rockwell Corp. R-7650, Dec. 1968, Contract NAS7-391
7. A1 Research Mfg. Co., "Potassium Turboalternator Preliminary Design Study, " Phase II Presentation, APS-5312-R, Jan. 21, 1969, Contract NAS3-10934
8. Gyarmathy, G., "Bases for a Theory for Wet Steam Turbines," Juris - Verlag, Zurich 1962
9. Goldman, L. J. and S. M. Nosek, "Experimental Nozzle Expansion and Flow Characteristics of Potassium Vapor," NASA TND-3209
10. Rossbach, R.J., "Critical Flow of Potassium Vapor Through Instrumented Converging-Diverging Nozzle," ASME Preprint 65-GTP-22, presented at the Gas Turbine Conference and Product Show, Washington D. C., Feb. 28 - Mar. 4, 1965
11. Gyarmathy, G., "Summary of Turbine Erosion Meeting Held at the Jet Propulsion Laboratory," Dec. 29 - 30, 1966 (Ed. L. G. Hays), Section II, p. 145-157, JPL Tech Memo 33-354, June 15, 1967
12. Gyarmathy, G. and H. Meyer, "Spontaneous Condensation Phenomena - Parts I and II," CEEB Information Services, C. E. Trans. 4160
13. Katz, J. L., H. Saltsburg and H. Reiss, "Nucleation in Associated Vapors," North American Aviation Science Center, SCPP-65-32, May 18, 1965
14. Ewing, C. T. et al, "High Temperature Properties of Potassium," U. S. Naval Research Laboratory, Report NRL 6233, September 24, 1965
15. Linhardt, Hans D., "Potassium Erosion Experiments," from "Summary of Turbine Erosion Meeting Held at the Jet Propulsion Laboratory, Dec. 29 - 30, 1966," (Ed. L. G. Hays) Section 9, p. 115-127, JPL Tech Memo 33-354, June 15, 1967
16. Smith, A. "The Influence of Moisture on the Efficiency of a One-Third Scale Model Low Pressure Steam Turbine," Institution of Mechanical Engineers, Thermodynamics and Fluid Mechanics Convention, Paper 10, Liverpool (Gr. Brit.), April 13-15, 1966
17. Baker, O., "Simultaneous Flow of Oil and Gas," The Oil and Gas Journal, July 1954, pp 185-195

18. Chien S. and W. Ibele, "Pressure Drop and Liquid Film Thickness of Two-Phase Annular and Annular Mist Flows," Trans. ASME, J. Heat Transfer Paper No. 62-WA-170, 1962
19. Wrobel, J. R. and McManus, H.N., "An Analytical Study of Film Depth, Wave Height, and Pressure Drop in Annular Two-Phase Flow," Developments in Mechanics, Vol. 1, Proc. 7th Midwest Mech. Conf.; Sept. 6-8, 1961, Plenum Press Inc.
20. Gardner, G. C., "Events Leading to Erosion in the Steam Turbine," Proc. Inst Mech Engrs, 178, Pt 1, No. 23, pp 593 to 623, 1963-1964
21. Zimmerman, W. F. and R. J. Rossbach, "Limited Impact Erosion and Metal Losses in Two-Stage Potassium Turbines," Section 3, "Summary of Turbine Erosion Meeting Held at the Jet Propulsion Laboratory Dec. 29-30, 1966" (Ed. L. G. Hays), JPL Tech Memo 33-354, June 15, 1967
22. Rossbach, R. J., loc cit: Three-Stage Potassium Test Turbine Review Meeting, General Electric Co., Evandale, Ohio, Oct. 15, 1968
23. Christie, D. G., and G. W. Hayward, "Observation of Events Leading to the Formation of Water Drops which Cause Turbine Blade Erosion," Phil. Trans. Roy Soc London, Series A, No. 1110, Vol. 260, pg. 183-192, 28 July 1966
24. Christie, D. G., "Experimental Investigations of Internal Flow in Turbines," Section 12 "Summary of Turbine Erosion Meeting Held at the Jet Propulsion Laboratory Dec. 29-30, 1966" (Ed. L. G. Hays), JPL Tech. Memo 33-354, June 15, 1967
25. Lieblein, S. and W. H. Roudebush, "Low-Speed Wake Characteristics of Two-Dimensional Cascade and Isolated Airfoil Sections," NACA-TN-3771, October 1956
26. Pouchot, W. D., W. K. Fentress and R. E. Kothmann, "Analytical Investigation of Turbine Erosion Phenomena," Section 2, "Summary of Turbine Erosion Meeting Held at the Jet Propulsion Laboratory December 29-30, 1966" (Ed. L. G. Hays), JPL Tech Memo 33-354, June 15, 1967
27. Epstein, L. F., "Static and Dynamic Corrosion and Mass Transfer in Liquid Metal Systems," Chem. Engr. Prog. Sym. Series, Vol. 53, No. 20, p. 67 (1952)
28. Gill, W. N., et al., "Mass Transfer in Liquid Lithium System," A. I. CHE. Jour., Vol. 6, No. 1, p. 139 (1960)
29. Swisher, J. H., "Solubility of Fe, Ni, and Co in Liquid Potassium and the Effect of Oxygen Gettering Agents," CONF-650411, AEC-NASA Liquid Metals Information Meeting, p. 43, April 1965
30. Ginell, W. S. and R. J. Teitel, "Determination of the Solubility of Transition Elements in Molten Potassium," Douglas Aircraft, SM48883, 1965
31. Baker, D.W.C., K. H. Jolliffe, and D. Pearson, "The Resistance of Materials to Impact Erosion Damage," Phil. Trans. Roy Soc London, Series A, No. 1110, Vol. 260, pp 193-203, 28 July 1966
32. Pearson, D. "A Summary of the M. E. L. Experimental Data on Erosion," Marchwood Engineering Laboratories, CEGB, RDD/M/ MIB, Job No. 30023, Nov. 1964
33. Smith, Allen, R. P. Kent, and R. L. Armstrong, "Erosion of Steam Turbine Blade Shield Materials," ASTM Special Technical Publication No. 408, March 1967
34. Brun, R. J., W. Lewis, P. J. Perkins, and J. S. Serafini, NACA Report 1215, 1955
35. Winder C., "Turbine Erosion During Mercury Rankine Turbo-Alternator Endurance Tests," Summary of Turbine Erosion Meeting Held at the Jet Propulsion Laboratory, Dec. 29-30, 1966, (Ed. L. G. Hays,) JPL Tech Memo 33-354, Section 8, June 15, 1967

## APPENDIX 1C

### RESULTS OF DETAILED FLUID-DYNAMIC ANALYSIS OF BLADE PASSAGE FLOWS OF NASS-250 POTASSIUM AND CESIUM TURBINES

#### 1.0 CONDENSATION

##### 1.1 Potassium Turbine

The results of the condensation performance calculations for the six-stage potassium turbine are shown in Table 1C-1. In this case the inlet vapor is superheated and remains superheated through the first stator row. The Wilson point occurs just before the exit of the third rotor blade row at approximately 7.3 percent moisture content. The expansion rate  $\frac{1}{P} \frac{dP}{dt} = \dot{P}$  at the Wilson point is approximately 5000/sec. P is pressure and t is time. The expansion process approaches full thermodynamic equilibrium in the fourth stator row and remains in equilibrium through the fifth stator. These calculations were, therefore, terminated at the fifth stator row.

The rapid expansion at the Wilson point produces relatively small droplet sizes as shown in Table 1C-2. The mean droplet radius at the exit of 5-R and 6-S are estimated on the basis of equilibrium condensation to be 0.238 and 0.243 microns, respectively. In this turbine there is no appreciable difference in mass flow rate between the condensing and equilibrium flow calculations. The condensation calculation is sensitive to the values of liquid surface tension used. A calculation for this turbine, using a 25 percent increase in surface tension values, shifted the point of initial condensation to the fifth rotor row.

TABLE 1C-1

CONDENSATION RESULTS FOR SIX-STAGE  
POTASSIUM TURBINE

	Static Pressure (lb/in <sup>2</sup> )	Static Temperature (°R)	Axial Velocity (ft/sec)	Equilibrium Moisture (lb/lb)	Condensed Moisture (lb/lb)
Inlet	171	2543	358	Superheated	-
1-S	144	2442	404	Superheated	-
1-R	121.5	2348	417	0.014	0
2-S	102.7	2261	415	0.029	0
2-R	86.2	2176	413	0.046	0
3-S	72.2	2093	417	0.058	0
3-R	59.0	2017	409	0.073	0.001
4-S	47.0	2093	443	0.086	0.079
4-R	36.8	2037	460	0.105	0.100
5-S*	28.5	1977	466	0.125	0.120

The results of the present calculations can be compared in a qualitative manner with the results of Goldman and Nosek, <sup>(9)</sup> in which saturated potassium vapor was expanded in a convergent-divergent nozzle. Although their results are somewhat inconclusive, it appears that condensation occurred when the ratio of pressure to initial saturation pressure was between 0.31 and 0.33 at an axial distance of about 3 inches from the nozzle inlet. In the present calculations, condensation was predicted at a pressure to initial saturation pressure ratio of 0.4. The axial distance from the inlet was about 3.5 inches. The somewhat earlier condensation, in terms of pressure ratio, in the turbine as compared to the supersonic nozzle is to be expected because of the lower expansion rate.

The droplet size results can be compared with those obtained by Linhardt. <sup>(15)</sup> His analysis predicts a droplet radius of 0.05 microns for 10 percent exit moisture in his test No. 4. Test Numbers 2, 3, and 4 had the same stagnation condition and the same nozzle except for length. With critical flow in the nozzle, the conditions at the condensation point would be unchanged due to the additional length of the nozzle. Thus, for the same conditions at the Wilson point, the droplet radius at the nozzle exit would be expected to be proportional to  $(y_e)^{1/3}$ , where  $y_e$  is the moisture fraction at the nozzle exit. Viewed in this way, the results of Linhardt's Test No. 3 corrected to 10 percent moisture would give a radius of 0.06 micron; Test No. 2 would give a 0.26

TABLE 1C-2

FOG PARTICLE SIZE DISTRIBUTION FOR SIX-STAGE  
POTASSIUM TURBINE

Group	Number (drops/lb)	Radius (microns)			
		3-R	4-S	4-R	5-S
1	$2.7 \times 10^{11}$	0.186	0.297	0.31	0.32
2	$5.2 \times 10^{11}$	0.173	0.288	0.30	0.31
3	$1.6 \times 10^{12}$	0.157	0.277	0.29	0.30
4	$3.7 \times 10^{12}$	0.142	0.267	0.28	0.29
5	$7.3 \times 10^{12}$	0.127	0.257	0.27	0.28
6	$2.2 \times 10^{13}$	0.110	0.246	0.26	0.27
7	$5.8 \times 10^{13}$	0.089	0.235	0.25	0.26
8	$1.5 \times 10^{14}$	0.066	0.222	0.236	0.247
9	$3.9 \times 10^{14}$	0.040	0.209	0.224	0.235
10	$1.3 \times 10^{15}$	0.0015	0.189	0.206	0.218
Mean Radius		0.065	0.200	0.215	0.229

N total =  $1.92 \times 10^{15}$ /lb

\* Calculations discontinued.

micron radius. The present calculations fall between these limits, but again are not directly comparable due to differences in the expansion rate and initial conditions.

## 1.2 Cesium Turbine

The results of the condensation calculations for the cesium turbine are given in Tables 1C-3 and 1C-4. The Wilson point occurs just before the exit of the first stator. The equivalent moisture at the Wilson point is approximately 0.046, and the expansion rate  $P$  is  $1.9 \times 10^4/\text{sec}$ .

TABLE 1C-3

### CONDENSATION RESULTS FOR CESIUM TURBINE

	P (lb/in. <sup>2</sup> )	T (°F)	Velocity Relative to Blade (ft/sec)	$y_e$ Equilibrium Moisture (lb/lb)	$y$ Condensed Moisture
Stagnation	411.	2440	0	200°F superheat	-----
Static Inlet	399.	2415	216.5	177°F superheat	-----
Exit 1 - S	171.5	1822	1147.	0.045	0.021
0.024 inch into 1 - R	176.	1878	592	0.043	0.039

TABLE 1C-4

### FOG PARTICLE DISTRIBUTION AT EXIT FROM 1-S CESIUM TURBINE

Group	N (drops/lb)	Drop Radius (microns)
1	$3.4 \times 10^{10}$	0.089
2	$1.2 \times 10^{11}$	0.087
3	$3.6 \times 10^{11}$	0.085
4	$1.7 \times 10^{11}$	0.082
5	$6.2 \times 10^{12}$	0.079
6	$1.9 \times 10^{13}$	0.076
7	$6.5 \times 10^{13}$	0.072
8	$2.1 \times 10^{14}$	0.068
9	$7.7 \times 10^{14}$	0.063
10	$4.5 \times 10^{15}$	0.055
11	$7.1 \times 10^{15}$	0.048

$N_{\text{total}} = 1.27 \times 10^{16}/\text{lb}$   
Mean Radius = 0.052 micron

It is seen that the drops are quite small due to the rapid expansion. The drop size is also relatively uniform and will become more uniform as the condensation proceeds. The thermodynamic description of the flow used resulted in critical flow occurring at approximately 1000 ft/sec, a slightly lower value than results for equilibrium flow. The mean droplet radii at the exit of 1-R and 2-S are estimated to 0.089 and 0.097 microns.

## 2.0 AXISYMMETRIC FLOW DOWNSTREAM OF THE BLADE ROWS

The fluid conditions such as pressure, temperature, density, velocity, and angle of flow with respect to blade height for the last or latter stages of the two turbines are given in Tables 1C-5 and 1C-6. Table 1C-5 covers the last stage of the two-stage cesium turbine. Table 1C-6 covers the fifth and sixth stages of the six-stage potassium turbine.

It will be noted in Table 1C-5 that there is recompression in the second-stage rotor of the cesium turbine at the hub of the blade. The pressure level at the inlet to the rotor hub is 26.74 psia and increases to 34.99 psia at the exit. In the turbine erosion analysis, the flow disorder (flow separation at the trailing edge of the rotor blade at the hub) is of no concern since there are no stages downstream of the second stage in the cesium turbine.

However, this same recompression at the hub was present in the fifth stage of the original conceptual design of the potassium turbine as set forth in Contract NAS 5-250. (This is not to be taken as a criticism of the work under Contract NAS 5-250. The designs were more than adequate as representative descriptions of potassium and cesium turbines for the nuclear Rankine cycle power system studies conducted.) Since our calculations indicate that there will be collected moisture as early as the fourth stage of the potassium turbine, the original design has been modified to increase the hub-to-tip ratios in the latter stages. This gives a slight fluid expansion at the hub, as will be noted in Table 1C-6. Elimination of flow separation in the fifth stage is necessary to protect the sixth stage from erosion difficulties.

TABLE 1C-5  
CESIUM TURBINE-FLUID PROPERTIES ALONG HEIGHT - SECOND STAGE

ROW APPROX. SECTION	Second Rotor Exit					Second Rotor Inlet*					Second Stator Exit					Sixth Stator Inlet				
	h	1/4	m	3/4	r	h	1/4	m	3/4	r	h	1/4	m	3/4	r	h	1/4	m	3/4	r
DIAMETER (inches)	3.71	4.87	5.74	6.61	7.77	4.34	5.14	5.74	6.34	7.14	4.34	5.14	5.74	6.34	7.14					
Gauging	0.5281	0.4652	0.4248	0.3905	0.3526	---	---	---	---	---	0.3834	0.3834	0.3834	0.3834	0.3834					
EXIT FLOW ANGLE (degrees)	31.88	27.72	25.01	22.98	20.65	24.25	20.67	19.42	18.79	18.50	29.42	25.45	24.00	23.24	22.85					
STATIC PRESSURE (psia)			34.99			26.74	37.14	44.10	50.23	57.12	27.94	37.60	44.10	49.87	56.42			82.2		
TEMPERATURE (°F)			1420.										1477.					1640.		
SPECIFIC VOLUME (cft/lb)	3.338	3.321	3.314	3.311	3.310	4.139	3.138	2.716	2.434	2.184	3.988	3.106	2.716	2.448	2.206					
JET VELOCITY (ft/s)	490.7	554.2	605.6	658.2	726.7	1136.3	1002.2	920.2	852.0	776.1	1119.7	996.7	920.7							
AXIAL VELOCITY (ft/s)	259.1	257.8	257.3	257.0	257.0	466.7	353.8	306.2	274.4	246.2	550.1	428.4	374.5							
WHEEL SPEED (ft/s)	388.1	509.8	601.1	692.4	814.1	454.5	528.3	601.1	663.9	747.7	454.5	528.3	601.1							
INLET FLOW ANGLE TO NEXT ROW (degrees)	83.72	94.28	101.6	108.6	117.2	38.74	41.54	48.89	62.54	92.72	46.57	49.87	57.35							
INLET VELOCITY TO NEXT ROW (ft/s)	260.7	258.5	262.6	271.2	288.9	745.7	533.5	406.4	309.3	246.5	737.5	560.7	444.8							

\* Discharge characteristics of unbladed axial gap between stator blade trailing edges and rotor blade leading edges.

TABLE 1C-6  
POTASSIUM TURBINE-FLUID PROPERTIES ALONG THE HEIGHT OF THE BLADE-FIFTH AND SIXTH STAGES

ROW APPROX. SECTION	Sixth Rotor Exit					Sixth Rotor Inlet*					Sixth Stator Exit					Sixth Stator Inlet				
	h	1/4	m	3/4	r	h	1/4	m	3/4	r	h	1/4	m	3/4	r	h	1/4	m	3/4	r
DIAMETER (inches)	4.54	5.70	6.85	8.00	9.16	4.82	5.82	6.82	7.82	8.82	4.75	5.75	6.75	7.75	8.75					
Gauging	0.6396	0.5694	0.5154	0.4698	0.4308	0.4488	0.4782	0.5091	0.5394	0.5684	0.4737	0.5046	0.5363	0.5673	0.5965					
EXIT FLOW ANGLE (degrees)	39.77	34.71	31.02	28.02	25.52	26.67	28.57	30.60	32.64	34.64	28.28	30.30	32.43	34.57	36.67					
STATIC PRESSURE (psia)			16.90			17.37	18.74	19.69	20.35	20.83	17.43	18.79	19.69	20.33	20.80			22.04		
TEMPERATURE (°F)			1422.										1454.					1477.		
SPECIFIC VOLUME (cft/lb)	23.81	23.79	23.79	23.81	23.81	23.19	21.70	20.81	20.23	19.82	23.13	21.67	20.81	20.25	19.85					
JET VELOCITY (ft/s)	637.8	715.8	790.6	867.6	946.8	1025.9	900.6	811.7	744.5	692.5	1021.0	898.3	811.7	746.5	696.2					
AXIAL VELOCITY (ft/s)	407.9	407.5	407.5	407.6	407.9	460.4	430.7	413.2	401.6	393.6	483.7	453.3	435.3	435.3	415.3					
WHEEL SPEED (ft/s)	475.4	596.9	717.3	837.8	959.2	504.8	609.5	714.2	818.9	923.6	497.4	602.1	706.9	811.6	916.3					
INLET FLOW ANGLE TO NEXT ROW (degrees)	87.94	91.13	95.58	100.06	104.40	48.17	67.16	92.15	115.56	131.96	50.29	69.06	92.86	114.93	130.72					
INLET VELOCITY TO NEXT ROW (ft/s)	408.2	407.6	409.4	414.0	421.1	617.8	467.4	413.5	445.2	529.3	628.8	485.3	435.9	407.0	548.					

ROW APPROX. SECTION	Fifth Rotor Exit					Fifth Rotor Inlet*					Fifth Stator Exit					Fifth Stator Inlet				
	h	1/4	m	3/4	r	h	1/4	m	3/4	r	h	1/4	m	3/4	r	h	1/4	m	3/4	r
DIAMETER (inches)	5.02	5.84	6.66	7.47	8.29	5.11	5.81	6.51	7.21	7.91	5.09	5.79	6.49	7.19	7.89					
Gauging	0.4841	0.4625	0.4438	0.4266	0.4104	0.3875	0.3950	0.4059	0.4189	0.4330	0.4032	0.4109	0.4223	0.4356	0.4500					
EXIT FLOW ANGLE (degrees)	28.95	27.55	26.35	25.25	24.23	22.80	23.23	23.95	24.77	25.67	25.78	24.26	24.97	25.82	26.74					
STATIC PRESSURE (psia)			22.04			24.57	26.78	28.51	29.89	31.01	24.62	26.81	28.51	29.87	30.97			37.04		
TEMPERATURE (°F)			1477.										1534.					1592.		
SPECIFIC VOLUME (cft/lb)	18.77	18.75	18.73	18.73	18.72	17.81	15.80	14.98	14.38	13.94	16.95	15.79	14.98	14.39	13.95					
JET VELOCITY (ft/s)	949.5	992.5	1033.5	1074.8	1117.2	1280.7	1167.2	1076.5	1001.6	929.0	1278.0	1160.0	1076.5	1002.6	940.9					
AXIAL VELOCITY (ft/s)	459.7	459.0	458.7	458.5	458.5	496.3	461.0	437.0	419.6	406.6	515.3	479.1	456.5	436.7	423.4					
WHEEL SPEED (ft/s)	525.7	611.6	697.4	782.3	868.1	535.1	608.4	681.7	755.0	828.3	533.3	606.6	680.0	753.7	826.6					
INLET FLOW ANGLE TO NEXT ROW (degrees)	56.45	59.68	63.44	67.52	71.79	37.56	44.82	55.34	69.80	87.46	391.01	46.39	56.94	71.14	88.15					
INLET VELOCITY TO NEXT ROW (ft/s)	551.5	531.8	512.7	496.2	482.7	814.2	653.9	531.2	477.1	407.0	818.7	661.7	542.3	461.5	422.6					

\* Discharge characteristics of unbladed axial gap between stator blade trailing edges and rotor blade leading edges.

### 3.0 VAPOR BOUNDARY LAYER ON SURFACES OF BLADES

Calculated values for the potassium turbine are shown in Table 1C-7 for the boundary layer thickness and form factor at the trailing edge of the sixth stator blade row, 3/4 blade height position. Values are also shown for the Reynolds No. based on chord length, the momentum thickness, the skin friction coefficient, and the shearing stress. These quantities are local blade surface values for the trailing edge position and are based on conventional turbulent boundary layer relationships.

Similar calculations performed on the second stator blade row of the cesium turbine are tabulated in Table 1C-8. The Reynolds No. and shearing stress ( $\tau$ ) are much higher in the cesium turbine due in large part to the high vapor density, roughly twelve times that in the back end of the potassium turbine. The low boundary layer thickness in the cesium turbine, approximately half the thickness in the potassium turbine, is associated with the high Reynolds Number 4.

TABLE 1C-7  
POTASSIUM TURBINE-CALCULATED BOUNDARY LAYER PROPERTIES AT THE TRAILING-EDGE OF THE BLADE

	Sixth Stator Blade at 3/4 height position		Total
	Pressure Side	Suction Side	
$\theta/\ell$	0.0009096	0.0050094	0.0059190
H	1.300	1.825	
$\delta^*/\ell$	0.0011895	0.0091422	0.103247
$\delta/\ell$	0.009066	0.31303	0.40369
$\delta$ (in.)	0.006981	0.024103	0.031084
n	6.666	2.424	
$R_{\theta\theta}$	162.	892.	
$C_f$	0.0083	0.00233	
$\tau$ (ppsf)	3.57	1.00	

where  $R_{\theta\theta} = V\ell/\mu$ ;  $n = 2/(H-1)$ ;  $R_{\theta\theta} = V\ell/\mu$ ; and  $C_f = \frac{\tau}{\frac{1}{2}\rho V^2} = 2 \times 0.123 \times 10^{-0.689H} \times R_{\theta\theta}^{-0.268}$  and  $\frac{\tau}{\frac{1}{2}\rho V^2}$

Here,  $\theta$ ,  $\delta^*$  and  $\delta$  are the momentum thickness, displacement thickness, and full thickness of the boundary layer at the trailing edge of the blade and  $\ell$  is the projected chord length of the blade.

### 4.0 DOWNSTREAM WAKES

Calculated results for the sixth stator blade of the potassium turbine and for the second stator blade of the cesium turbine are shown in Tables 1C-9 and 1C-10. As shown, the wake properties quickly change downstream of the trailing edge, where there is little change beyond  $0.20x/\ell$ . Note also that while the wake thickness ( $\delta$ ) continues to increase

TABLE 1C-8  
CESIUM TURBINE-CALCULATED BOUNDARY LAYER PROPERTIES

	Sixth Stator Blade at 3/4 height position		Total
	Pressure Side	Suction Side	
$\theta/\ell$	0.0004357	0.0025562	0.0029919
H	1.315	1.665	
$\delta^*/\ell$	0.0005729	0.0042561	0.0048290
$\delta/\ell$	0.0042105	0.0170562	0.0212667
$\delta$ (in.)	0.00296	0.01199	0.01495
n	6.349	3.008	
$R_{\theta\theta}$	470.	2750.	
$C_f$	0.00606	0.00220	
$\tau$ (ppsf)	28.2	11.3	

where  $R_{\theta\theta} = V\ell/\mu$ ;  $n = 2/(H-1)$ ;  $R_{\theta\theta} = V\ell/\mu$ ;  $C_f = \frac{\tau}{\frac{1}{2}\rho V^2} = 2 \times 0.123 \times 10^{-0.678H} \times R_{\theta\theta}^{-0.268}$  and  $\frac{\tau}{\frac{1}{2}\rho V^2}$

$\theta$ ,  $\delta^*$  and  $\delta$  are the momentum thickness, displacement thickness of the boundary layer at the trailing edge of the blade,  $\ell$  is the projected chord length of the blade.

All values are point values for the trailing edge position; e.g.,  $C_f$  is the local skin friction coefficient at the trailing edge position.

beyond  $2x/\ell$ , the velocity within the wake,  $V(y)$ , is nearly the same as that of the free stream since

$$V(y) = V(x) \left( \frac{y}{\delta} \right)^{1/n}$$

where

$$\left( n = \frac{2}{H-1} \right) \gg 1$$

Thus, the downstream flow is roughly axisymmetric from about 20 percent of the chord length distance downstream of the blade by this model of the process. The low wake thickness of the cesium turbine, about half that of the potassium turbine, is associated with the high vapor density, high Reynolds No., and low boundary layer thickness at the blade trailing edge.

Wake calculation results are also shown in Figures 1C-1 through 1C-4 in slightly different form. These curves give the wake velocity with respect to the distance, and normal to the distance, along the streamline downstream of the blades. These curves are used to estimate the atomization and acceleration of the moisture particles in the interval (both time and distance) between the stator and rotor. To compensate for the finite trailing edge thickness in these calculations, the trailing edge wake is treated mathematically as a dead space 4.8 trailing edge thicknesses in length, joined to a zero trailing edge thickness wake at a discontinuity and represented by a vertical line on the curves.



TABLE 1C-9

POTASSIUM TURBINE-RESULTS OF BLADE WAKE  
CALCULATION FOR SIXTH STATOR BLADE,  
3/4 BLADE HEIGHT POSITION

$x/z$	H	$\frac{\hat{\theta}}{\theta}$	$\alpha^\circ$	$\theta$ (inches)	$\frac{n}{2}$ H-T	$\frac{\delta}{n} - (1+n)(2+n)$ (inches)	$V(x)$ (ft/sec)	$V(y)$ (ft/sec)
Pressure Side								
0. (t.e.)	1.300	0.00250	36.1	0.000700	6.66	0.00698	767.	$V(y) = V(x) \sqrt{y/z} / n$
0.039	1.169	0.00251	34.9	0.000702	11.82	0.01059	755.	
0.078	1.130	0.00251	34.6	0.000702	15.40	0.01305	749.	
0.156	1.095	0.00251	34.6	0.000702	21.0	0.01700	746.5	
0.234	1.078	0.00251	34.6	0.000702	25.6	0.0202	746.5	
0.312	1.067	0.00251	34.6	0.000702	29.8	0.0231	746.5	
0.394(rot. inl.)	1.060	0.00251	34.6	0.000702	33.3	0.0256	746.5	
Suction Side								
0. (t.e.)	1.825	0.01380	36.1	0.00386	2.424	0.0241	767.	$V(y) = V(x) \sqrt{y/z} / n$
0.039	1.390	0.01393	34.9	0.00391	5.13	0.0332	755.	
0.078	1.285	0.1393	34.6	0.00391	7.01	0.0403	749.	
0.156	1.202	0.1393	34.6	0.00391	9.90	0.0503	746.5	
0.234	1.162	0.1393	34.6	0.00391	12.32	0.0606	746.5	
0.312	1.140	0.1393	34.6	0.00391	14.30	0.0680	746.5	
0.394(rot. inl.)	1.122	0.1393	34.6	0.00391	16.40	0.0764	746.5	

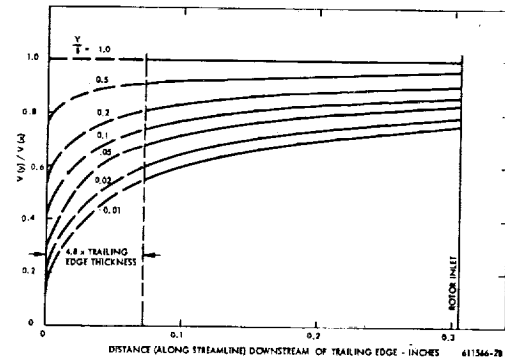
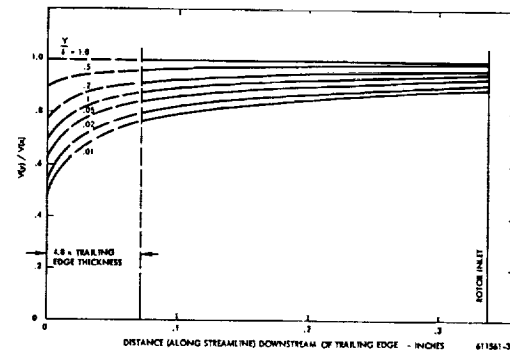
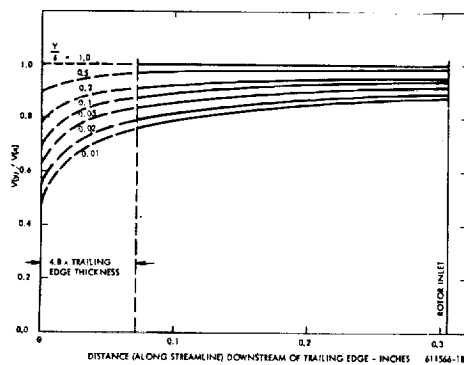
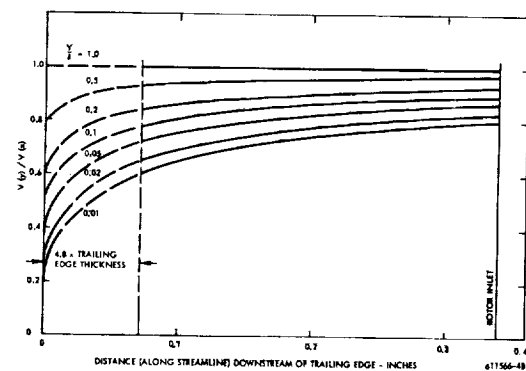
Figure 1C-2 Potassium Turbine Sixth Stator Wake  
Suction Side Velocity

TABLE 1C-10

CESIUM TURBINE-RESULTS OF BLADE WAKE  
CALCULATION FOR SECOND STATOR  
BLADE, 3/4 BLADE HEIGHT POSITION

$x/z$	H	$\frac{\theta}{\theta_0}$	$\alpha^\circ$	$\theta$ (inches)	$\frac{n}{2}$ H-T	$\frac{\delta}{n}$ $-(1+n)(2+n)$ (inches)	$V(x)$ (ft/sec)	$V(y)$ (ft/sec)
Pressure Side								
0. (t.e.)	1.315	0.002142	25.9	0.0003063	6.35	0.00296	876.	$V(y) = V(x) \sqrt{y/z} / n$
0.0426	1.171	0.002160	23.8	0.0003089	11.70	0.00460	863.	
0.0854	1.128	0.002160	23.2	0.0003089	15.62	0.00576	856.	
0.171	1.093	0.002160	23.2	0.0003089	21.50	0.00759	856.	
0.256	1.078	0.002160	23.2	0.0003089	25.65	0.00888	856.	
0.342	1.066	0.002160	23.2	0.0003089	30.30	0.01030	856.	
0.480(rot.inl.)	1.055	0.002160	23.2	0.0003089	36.35	0.01217	856.	
Suction Side								
0. (t.e.)	1.665	0.01253	25.9	0.001792	3.01	0.01199	876.	$V(y) = V(x) \sqrt{y/z} / n$
0.0426	1.320	0.01270	23.8	0.001816	6.25	0.01738	863.	
0.0854	1.238	0.01270	23.2	0.001816	8.40	0.02112	856.	
0.171	1.169	0.01270	23.2	0.001816	11.83	0.02725	856.	
0.256	1.138	0.01270	23.2	0.001816	14.50	0.03202	856.	
0.342	1.117	0.01270	23.2	0.001816	17.10	0.03669	856.	
0.480(rot.inl.)	1.097	0.01270	23.2	0.001816	20.63	0.04304	856.	

Figure 1C-3 Cesium Turbine Second Stator Wake  
Pressure Side VelocityFigure 1C-1 Potassium Sixth Stator Wake Pressure  
Side VelocityFigure 1C-4 Cesium Turbine Second Stator Wake  
Suction Side Velocity

## 5.0 DEPOSITION OF MOISTURE ON THE SURFACE OF BLADES

### 5.1 Inlet Edge Deposition

The calculated portion of drops collected on the nose of the sixth stator blade row of the potassium turbine is given parametrically in Figure 1C-5. Two methods of calculation are used that do not agree. In the summary of collected moisture for the two turbines the curve used is that generated from Gyarmathy's data, (8) because his data gives reasonable agreement with steam turbine collection information presented by Smith, et al. (16)

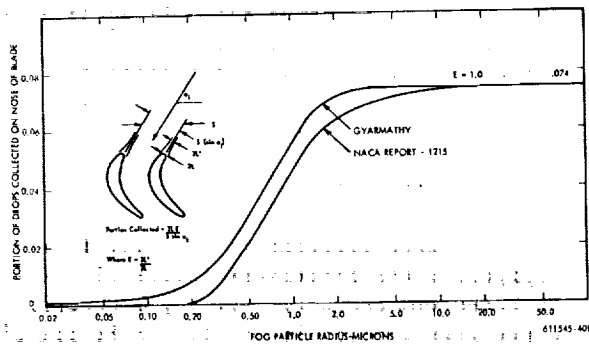


Figure 1C-5 Potassium Turbine Portion Collected on Nose of Sixth Stator Blade

For a 0.48 micron radius fog particle, the NACA (34) curve gives 2 percent collection on the inlet edge compared to 2.8 percent collection by the Gyarmathy curve. Also, by the NACA curve, fog particles of less than 0.2 micron radius are not collected.

Similar calculations performed for the second stator blade of the cesium turbine are shown in Figure 1C-6. Similar to the potassium turbine results, fog particles of less than 0.2 micron are not collected according to the NACA curve, but by the Gyarmathy curve 1 percent of the fog particles are collected for the 0.2 micron radius size.

In the cesium calculation, Figure 1C-6, there is a greater difference with respect to the NACA curve and the Gyarmathy curve than in the potassium calculation, Figure 1C-5. This is due to the fact that the NACA data account for the change in Stokes' Law drag with Reynolds No. while the Gyarmathy curve does not. As the Reynolds No. is higher in the cesium turbine, a larger difference is shown by the curves.

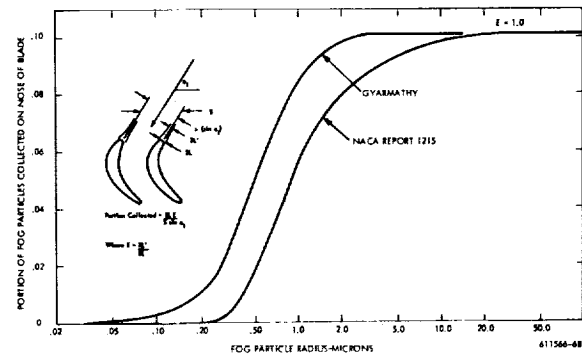


Figure 1C-6 Cesium Turbine Portion Collected on Nose of Second Stator Blade

### 5.2 Concave Surface Deposition

The calculated results for concave surface deposition on the sixth stators of the potassium turbine are shown parametrically in Figure 1C-7. Similar results for the second stators of the cesium turbine are shown in Figure 1C-8. These figures give the portion of the moisture present in the bulk flow that is collected as a function of condensate particle radius. As shown by the curve sketches, the portion collected is specified by the inlet width of the band ( $\epsilon$ ), within which all particles impinge on the blade with respect to the blade pitch. The band width cannot exceed the space between blades (pitch minus inlet edge blockage) which accounts for the breaks in the curves. For equal condensate particle radii, a somewhat higher portion of moisture will be collected by the cesium turbine than by the potassium turbine.

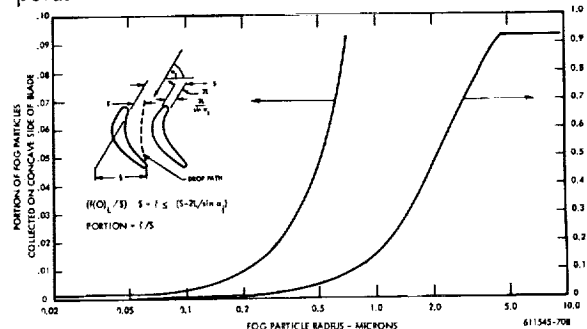


Figure 1C-7 Potassium Turbine Portion Collected on Concave Side Sixth Stator Blade

### 5.3 Quantity of Damaging Moisture Impacting Last Row Rotor Blades

As a first approximation, it will be assumed that the only potentially damaging moisture that will

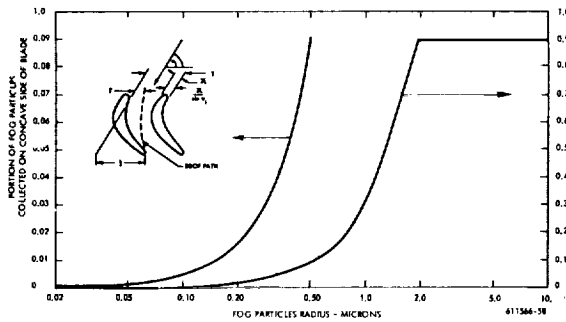


Figure 1C-8 Cesium Turbine Portion Collected on Concave Side of Second Stator Blade

impact the last rotor blades of these turbines is that collected by the last stator. The calculated amount of moisture collected by the sixth stator blades and subsequently impacting the sixth rotor blades of the six-stage potassium turbine is given in Table 1C-11. Similar information is given for the last (second) stage of the cesium turbine in Table 1C-12.

TABLE 1C-11

SIX-STAGE POTASSIUM TURBINE - SIXTH STAGE MOISTURE INVENTORY

Flow (Vapor Plus Liquid)	9100 kg/hr
Bulk Moisture Sixth Stator	14.3%
Bulk Moisture, Average Fog Particle Radius	0.24 micron
Portion of Bulk Moisture Collected, Sixth Stator	2.6%
Collected Moisture Impacting Sixth Rotor	34 kg/hr
Average Local Rate of Impact of Collected Moisture	167 gm/cm <sup>2</sup> /hr
Average Local Collected Moisture Impact Rate/10,000 Hours	1670 kg/cm

TABLE 1C-12

TWO-STAGE CESIUM TURBINE - SECOND STAGE MOISTURE INVENTORY

Flow (Vapor Plus Liquid)	31,500 kg/hr
Average Bulk Moisture, Second Stator	12.8%
Bulk Moisture, Average Fog Particle Radius	0.093 micron
Collected Moisture Impact Rate, Second Stator	26.2 kg/hr
Collected Moisture Impact Rate	294 gm/cm <sup>2</sup> /hr
Local Collected Moisture Impact Rate/10,000 Hours	2940 kg/cm

It is useful to compare these results with those calculated for the Yankee Atomic Plant steam turbine, where the calculated average local moisture impact rate per 10,000 hours was 802 kg/cm for the last stage of the low pressure turbine.

## 6.0 STATOR BLADES COLLECTED MOISTURE ATOMIZATION AND TRAJECTORIES

The moisture potentially damaging to the rotor blades collects from the bulk stream, runs to the aft edge, departs this edge as primary drops, and is caught up in the wake of the stators where additional atomization takes place and acceleration is to a fraction of bulk stream velocity.

### 6.1 Atomization

The primary drops that have the best chance to survive the passage between stator and rotor are those deep in the suction side wake. Given in Table 1C-13 are the time of flight, the initial Weber Number, the time to droplet destruction, and the mass mean diameter of the resulting secondary drops for a range of primary drops departing the second stator of the cesium turbine. Information about the primary drops leaving the sixth stage of the potassium turbine is given in Table 1C-14.

It can be concluded from these results that no drops greater than 5 microns in diameter will reach the second rotor and most, if not all, of the drops will be under 3 microns in diameter. In the case of the potassium turbine a few drops reaching the sixth rotor could be as large as 100 microns in diameter.

TABLE 1C-13

SECONDARY ATOMIZATION IN CESIUM TURBINE - SUCTION SIDE WAKE STREAMLINED AT  $Y/Y_0 = 0.01$  SECOND STATOR

Primary Drop Diameter (microns)	Time of Flight (μ sec)	Weber Number (max.)	Time to Complete Droplet Destruction (μ sec)	Mass Mean Diameter of Secondary Drops (microns)	Remarks
2	43	10	---	---	No disruption
5	58	24	1.3	0.490	"
10	67	49	2.5	0.533	Disruption
25	82	122	6.6	0.600	"
50	99	244	13.0	0.658	"
100	120	488	26.2	0.721	"
200	148	976	52.2	0.822	"
300	161	1464	78.4	0.880	"
400 (max)	173	1952	104.6	0.922	"

However, most, if not all of the drops will be under 60 microns in diameter. The average mass mean diameter drop calculated for the atomized liquid of the sixth stator of the potassium turbine is 40 microns.

TABLE 1C-14

SECONDARY ATOMIZATION IN POTASSIUM  
TURBINE - SUCTION SIDE WAKE STREAM-  
LINED  $Y/Y_0 = 0.01$  SIXTH STATOR

Primary Drop Diameter (microns)	Time of Flight ( $\mu$ sec)	Weber Number (max.)	Time to Complete Droplet Destruction ( $\mu$ sec)	Mass Mean Diameter of Secondary Drops (microns)	Remarks
10	98	2.2	6.6	-----	No disruption
20	118	4.4	13.	-----	"
50	149	11.1	32.	-----	"
75	165	15.2	48.	-----	(?)
100	179	22.2	64.	-----	(?)
200	212	44.4	128	-----	Disruption
400 (max)	255	88.4	256	-----	"

\*  $Y$  is the distance measured from the wake centerline;  $Y_0$  is the width of the wake.

### 7.0 DROP IMPACT VELOCITIES RELATIVE TO THE ROTOR BLADES

Table 1C-15 summarizes impingement results on the second stage rotor blades of the cesium turbine for drop diameters of 0, 2, and 5 microns. Two representative wake positions ( $Y/Y_0$ ) and blade heights were investigated for the suction and pressure sides of the second stators. The values given in Table 1C-15 are at the rotor inlet;  $V_d$  is drop velocity relative to the preceding stators, and  $W_d$  is the velocity relative to the rotor blades. In this turbine, the velocity  $W_d$  somewhere on the radius of the rotor blade nose is a normal velocity of impact. As can be seen the maximum normal drop impact velocities are quite low and cover only a narrow range of velocities. This is because the drops are accelerated to a very substantial fraction of the stator discharge vapor velocities.

TABLE 1C-15

SECOND STAGE ROTOR DROP IMPINGEMENT  
SUMMARY - TWO STAGE CESIUM TURBINE

Wake Position $Y/Y_0$	Drop Diameter (microns)	3/4 Blade Height		Blade Tip	
		$V_d$ (fps)	$W_d$ (fps)	$V_d$ (fps)	$W_d$ (fps)
Suction 0.01	0	685	273	632	296
	2	665	268	614	300
	5	560	267	517	338
Suction 0.2	0	796	321	735	294
	2	780	313	720	292
	5	665	268	614	300
Pressure 0.01	0	753	299	695	291
	2	740	293	683	291
	5	625	263	576	311
Pressure 0.2	0	822	338	758	299
	2	810	330	747	296
	5	700	278	646	293

Figure 1C-9 shows maximum impact velocities of drops colliding with the nose of the blades of the sixth rotor of the six-stage potassium turbine for representative drop diameters of 25, 50, and 75 microns. The impact velocities are plotted as a function of blade height fraction where the height fraction is 0 at the hub and 1.0 at the blade tips. As for the cesium turbine, somewhere on the nose these impacts are normal to the blade surface. In the potassium turbine, these maximum velocities occur for drops accelerated along the wake streamline at  $Y/Y_0 = 0.01$  of the suction side of the sixth-stator wake.

For comparison purposes the maximum impact velocities calculated for 400-micron diameter drops impacting the ninth rotor of the low pressure end of the Yankee Atomic Plant steam turbine are also shown in Figure 1C-9. A 400-micron diameter drop is about the largest expected to impact the ninth rotor of the Yankee turbine. As can be seen, the maximum drop diameters and impact velocities are much larger in the steam turbine than in either of the alkali metal vapor turbines.

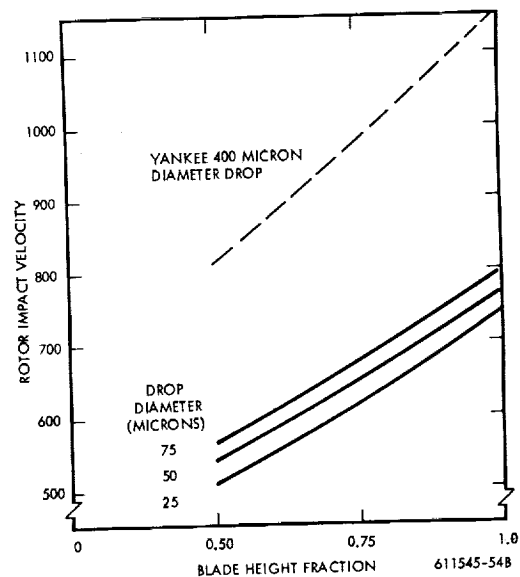


Figure 1C-9 Maximum Impact Velocities on Six -  
Stage Potassium Turbine

# SECTION 2

## FLUID - DYNAMIC COMPUTATIONAL PROCEDURES

### 2.1 BACKGROUND

As reported elsewhere in this report, while erosion in wet vapor turbines takes place locally, the conditions leading to the erosion involve the total thermodynamic and fluid-dynamic history of the working fluid from the time it enters the turbine. The many processes that require analysis are given, again, in block diagram form in Figure 2.1-1. This Section 2 gives an account of the basis of analysis and analytical procedures used in examining the detail fluid-dynamic process leading to the erosion. The processes covered in this Section 2 are indicated in Figure 2.1-1.

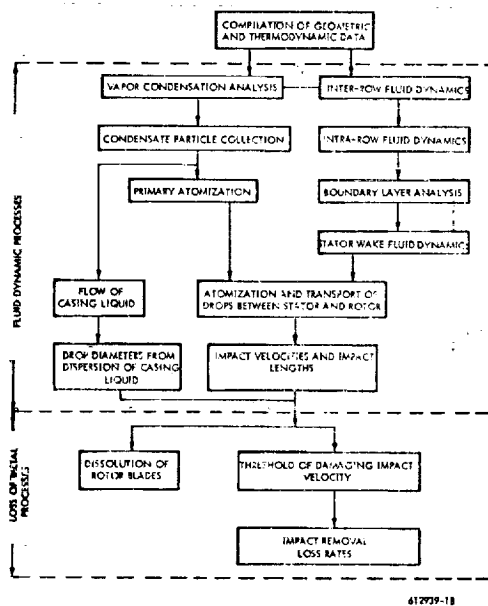


Figure 2.1-1 WANL Turbine Blade Erosion Model

### 2.2 TURBINE PERFORMANCE WITH DETAILED HISTORY OF CONDENSATION\* (NUDROP Condensation Code)

#### 2.2.1 Background

The purpose of this condensation study is to analytically predict the condensation point in wet vapor turbines and to determine the drop size distribution, including effects of molecular association on the condensation and flow processes. The approach is similar to that first developed by Oswatitch<sup>(1)</sup> and improved by others.<sup>(2,3)</sup> The method consists of simultaneous solution of the continuity, energy, momentum, and state equations written for the turbine geometry, including a description of nucleation and growth processes to determine moisture content and drop size. The present study provides the thermodynamic description of the flow process by using the virial equation of state and enthalpy relations derived by Ewing, et al.<sup>(4)</sup>

The numerical solution is by an ALGOL computer code which has been used on a Burroughs B-5500 computer.

#### 2.2.2 Theory

##### • Nucleation\*

The nucleation theory due to Katz, Saltzburg, and Reiss<sup>(5)</sup> is used to describe the nucleation

\* R. E. Kothmann, Supervisor, Power & Propulsion, Westinghouse Research Laboratories, Churchill Borough, Pa.

The change in moisture due to growth of a particular group of drops is

$$\frac{dy_i}{dz} = 4\pi \rho_L N_{ri} r_i^2 \frac{dr_i}{dz} \quad (24)$$

The total rate of change of moisture fraction, including surface condensation and atomized drops originating by surface condensation, is

$$\frac{dy}{dz} = \frac{dy_N}{dz} + \sum_{\text{all groups}} \frac{dy_i}{dz} + \frac{dy_b}{dz} + \frac{dy_{bo}}{dz} + \frac{dy_{abo}}{dz} \quad (25)$$

The liquid temperature is taken as the weighted average of the drop temperature of the various groups, or

$$T_L = \frac{1}{y} \sum_{\text{all groups}} y_i T_{ri} = T + \frac{\Delta T}{y} \sum_{\text{all groups}} \left(1 - \frac{r_{crit}}{r_i}\right) y_i \quad (26)$$

The energy equation includes the rate of change of liquid temperature. Rather than by differentiating Eq. 26, the rate of change is obtained from the present and previous values of liquid temperature obtained in the integration process. This approximation is justified since the moisture energy change is small compared to the total energy change.

#### • State Equations

From the work of Ewing, et al, (4, 7) it appears that an accurate equation of state can be obtained either by use of the virial equation or by an association model. The virial equation of state was chosen since it is generally available for use in obtaining the thermodynamic properties of wet vapors. In the case of cesium and potassium the state equations (References 4 and 7) fit the experimental PVT data with an average deviation of + 0.26 percent. The virial equation of state has the form

$$\frac{PV}{RT} = 1 + \frac{B}{V} + \frac{C}{V^2} + \frac{D}{V^3} + \frac{E}{V^4} \quad (27)$$

where B, C, D and E are functions of temperature only. These functions have the form

$$\log_{10} |B| = B_1 + B_2/T + \log_{10} T, B < 0 \quad (28)$$

$$\log_{10} C = C_1 + C_2/T + C_3/T^2 \quad (29)$$

$$\log_{10} |D| = D_1 + D_2/T, D < 0 \quad (30)$$

and

$$E = E_1 = \text{Constant} \quad (31)$$

where  $B_1, B_2, C_1, C_2, C_3, D_1$  and  $D_2$  are constants for a particular vapor. It is convenient to express the equation of state in terms of the compressibility, which gives

$$Z_c = 1 + \frac{B}{V} + \frac{C}{V^2} + \frac{D}{V^3} + \frac{E}{V^4} \quad (32)$$

#### • Property Equations

The various physical and thermodynamic properties required in the flow and nucleation calculations are computed from the following equations.

The saturation pressure equation developed in References 4 and 7 has the form

$$\log_{10} P_s = a_1 + a_2/T + a_3 \log_{10} T \quad (33)$$

where  $a_1, a_2$  and  $a_3$  are constants for a given metal vapor. By rewriting this equation for the saturation temperature corresponding to the vapor pressure P, subtracting the two equations and linearizing, the following approximate relation between supercooling, supersaturation pressure ratio, and temperature can be obtained:

$$\Delta T = \frac{-\Lambda_o T}{\Lambda_o - a_3 + \frac{a_2}{T \log_{10} e}} \quad (34)$$

Surface tension of the liquid is correlated by an equation of the form:

$$\sigma = \sigma_o \left(1 - \frac{T}{T_c}\right)^{1.25} \quad (35)$$

The liquid density at saturation pressure is correlated in References 4 and 7 by

$$\rho_L = \rho_0 - \rho_1 (T-460) - \rho_2 (T-460)^2 \quad (36)$$

The enthalpy of the vapor derived from the virial equation of state in References 4 and 7 is

$$h_g = h_g^0 - \frac{R_0 T}{M J} \left\{ \frac{1}{V} \left[ B - T \left( \frac{dB}{dT} \right) \right] - \frac{1}{V^2} \left[ C - \frac{T}{2} \left( \frac{dC}{dT} \right) \right] - \frac{1}{V^3} \left[ D - \frac{T}{3} \left( \frac{dD}{dT} \right) \right] + \frac{1}{V^4} \left[ E - \frac{T}{4} \left( \frac{dE}{dT} \right) \right] \right\} \quad (37)$$

where

$$h_g^0 = h_{g0} - h_{g1} T - h_{g2} \exp(-h_{g3}/T) \quad (38)$$

with  $h_{g0}$ ,  $h_{g1}$ ,  $h_{g2}$ , and  $h_{g3}$  constants.

For calculating the enthalpy of vaporization the enthalpy of saturated liquid is expressed (4,7) by

$$h_L = h_{L0} + h_{L1} T + h_{L2} T^2 + h_{L3} T^3 \quad (39)$$

The enthalpy of vaporization of the super-saturated vapor is obtained by

$$h_{fg} = h_g - h_L \quad (40)$$

The specific volume of the vapor mixture is approximated by

$$v_m \cong x_v = \frac{x V}{M} \quad (41)$$

The specific heat at constant pressure is given in References 4 and 7 by

$$C_{pv} = C_{pv}^0 - \frac{R}{M J} \left( 1 - X_{C1} + \frac{T X_{C2}}{V} \right)$$

where

$$X_{C1} = \frac{\left( \frac{Z_c}{V} + T \frac{\partial Z_c}{\partial T} \right)^2}{\left( 1 + \frac{2B}{V} + \frac{3C}{V^2} + \frac{4D}{V^3} + \frac{5E}{V^4} \right)} \quad (42)$$

$$X_{C2} = \left\{ \left( T \frac{d^2 B}{dT^2} + \frac{2dD}{dT} \right) + \frac{1}{2V} \left( T \frac{d^2 C}{dT^2} + \frac{2dE}{dT} \right) + \frac{1}{3V^2} \left( T \frac{d^2 D}{dT^2} + \frac{2dE}{dT} \right) \right\} \quad (43)$$

$$C_{pv}^0 = C_{po} + C_{pi} \exp(-C_{p2}/T) \quad (44)$$

## • Association

The discussion of association is in terms of a method which successfully handled the association of cesium and potassium vapors. The molecular compositions of cesium and potassium are deduced from PVT data in References 4 and 7. The data indicate that potassium vapor consists primarily of monomer, dimer, and tetramer species, whereas cesium probably also contains species of still higher order. The molecular species reactions are represented by a series of independent equilibria of the type

$$iK = k_i \quad (46)$$

and the equilibrium constants are defined by

$$k_i = \frac{N_i}{N_1^i \left( \frac{P}{P_a} \right)^{i-1}} \quad (47)$$

Of the total vapor molecules, the fraction  $N_1$  exists as a monomer, and the remainder  $1 - N_1$  is assumed to exist as a dimer. The partial pressure of the monomer is the mole fraction  $N_1$  times the mixture pressure, or

$$P_1 = N_1 P \quad (48)$$

The association is evaluated at both actual pressure and saturation pressure to obtain the ratio of partial pressure required in the nucleation expressions. The equilibrium constants  $k_2$  and  $k_4$  are expressed as functions of temperature in References 4 and 7 as follows:

$$\log_{10}(k_2) = k_{20} + k_{21}/T \quad (49)$$

and

$$\log_{10}(k_4) = k_{40} + k_{41}/T \quad (50)$$

The apparent equilibrium constant of dimerization  $\bar{k}_2$ , when all association is taken to be dimerization, can be expressed as a power series in terms of pressure and the true equilibrium constants:

$$\bar{k}_2 = k_2 + \frac{2k_3 P}{P_a} + \frac{3k_4 P^2}{P_a^2} - \frac{2k_2 k_4 P^3}{P_a^3} + \dots \quad (51)$$

Then, the fraction of total atoms which remains as the monomer  $\bar{N}_1$  is obtained from

$$\bar{N}_2 = \frac{\bar{N}_2}{(\bar{N}_1)^2 \left(\frac{P}{P_a}\right)} \quad (52)$$

where

$$\bar{N}_2 = 1 - \bar{N}_1 \quad (53)$$

Solution for  $\bar{N}_1$  from these two equations gives

$$\bar{N}_1 = \frac{-1 - \sqrt{1 - \frac{4 P \bar{K}_2}{P_a}}}{\left(\frac{2 P \bar{K}_2}{P_a}\right)} \quad (54)$$

#### • Flow Equations

The flow through the turbine is described by one-dimensional flow equations. The flow is assumed to have uniform velocity and pressure across the flow area; thus curvature of flow path and radial pressure gradients due to rotation have been neglected. The description is intended to describe the mean diameter flow conditions. The differential form of the continuity, energy, and state equations are as follows:

$$\frac{1}{A} \frac{dA}{dz} + \frac{1}{W} \frac{dW}{dz} - \frac{1}{v} \frac{dv}{dz} + \frac{1}{x} \frac{dx}{dz} = 0, \quad (55)$$

$$\frac{W^2}{Jg} \left( \frac{1}{W} \frac{dW}{dz} \right) + x \frac{d}{dz} \left( h_g(v, T) \right) - h_{fg} \frac{dy}{dz} + y C_{pL} \frac{dT_L}{dz} = 0, \quad (56)$$

and

$$\frac{1}{P} \frac{dP}{dz} + \left( 1 - \frac{V}{Z_c} \frac{\partial Z_c}{\partial V} \right) \left( \frac{1}{v} \frac{dv}{dz} \right) - \left( 1 + \frac{T}{Z_c} \frac{\partial Z_c}{\partial T} \right) \left( \frac{1}{T} \frac{dT}{dz} \right) = 0 \quad (57)$$

It should be noted that the enthalpy change cannot be described by the form  $C_p dT$  since enthalpy is pressure or volume dependent due to association reactions. The extra terms in the state equation arise from the use of the virial equations of state where the compressibility  $Z_c$  is a function of  $T$  and  $V$ . For an ideal gas,  $Z_c = 1$  and the partial derivatives of  $Z_c$  are zero.

The momentum equation for a stream tube can be written as

$$\frac{W}{g} \frac{dW}{dz} = -v_m \frac{dP}{dz} - v_m F \quad (58)$$

where  $F$  is the friction force per unit volume of the flowing mixture. For an isentropic flow the change in enthalpy is  $dh = v_m dP$ . If it is assumed that irreversibilities (friction losses) are proportional to isentropic enthalpy change, the expression

$$-v_m F = (1 - \eta_p) \frac{dh_s}{dz} = (1 - \eta_p) \left( v_m \frac{dP}{dz} \right)$$

is obtained, and the momentum equation becomes

$$\frac{W}{g} \frac{dW}{dz} = -\eta_p v_m \frac{dP}{dz} \quad (59)$$

For a given value of  $\eta_p$  the description is that of a constant local condition expansion process; namely, for each increment in isentropic enthalpy drop, the fraction  $(1 - \eta_p)$  appears as a friction loss which is converted to heating of the flow, and the remaining fraction  $\eta_p$  is the net gain in kinetic energy.

In the solution of the flow equations the quantities  $P$ ,  $T$ ,  $v$ , and  $W$  are treated as dependent variables with other quantities as independent variables. Simultaneous algebraic solution of the flow equations for the changes in  $P$ ,  $T$ ,  $v$ , and  $W$  gives the following:

$$\frac{1}{W} \frac{dW}{dz} = \frac{\Delta W}{\Delta_o} \quad (60)$$

$$\frac{1}{v} \frac{dv}{dz} = \frac{1}{W} \frac{dW}{dz} + \frac{1}{A} \frac{dA}{dz} + \frac{1}{x} \frac{dx}{dz} \quad (61)$$

$$\frac{1}{P} \frac{dP}{dz} = - \left( \frac{W^2}{g} \right) \left( \frac{1}{W} \frac{dW}{dz} \right) / (P \times v \eta_p) \quad (62)$$

and

$$\frac{1}{T} \frac{dT}{dz} = \frac{\frac{1}{P} \frac{dP}{dz} + \left( 1 - \frac{V}{Z_c} \frac{\partial Z_c}{\partial V} \right) \left( \frac{1}{v} \frac{dv}{dz} \right)}{\left( 1 + \frac{T}{Z_c} \frac{\partial Z_c}{\partial T} \right)} \quad (63)$$

where

$$\Delta_o = P \times v \eta_p \left[ \frac{W^2}{Jg} \left( 1 + \frac{T}{Z_c} \frac{\partial Z_c}{\partial T} \right) + x \phi \right] - \frac{W^2}{g} \times T \frac{\partial}{\partial T} \left( h_g(v, T) \right) \quad (64)$$

$$\phi = T \left( 1 - \frac{V}{Z_c} \frac{\partial Z_c}{\partial V} \right) \frac{\partial}{\partial T} \left( h_g(v, T) \right) + v \left( 1 + \frac{T}{Z_c} \frac{\partial Z_c}{\partial T} \right) \frac{\partial}{\partial V} \left( h_g(v, T) \right) \quad (65)$$

and

$$\Delta_w = P \times v \eta_p \left[ \left( 1 + \frac{T}{Z_c} \frac{\partial Z_c}{\partial T} \right) \left( h_{fg} \frac{dy}{dz} - y C_{pL} \frac{dT_L}{dz} \right) - \phi \left( \frac{1}{A} \frac{dA}{dz} + \frac{1}{x} \frac{dx}{dz} \right) \right] \quad (66)$$



### • Turbine Description

The turbine geometry is required to compute the flow cross-sectional area. The passage for each blade row is described as the annular area between concentric truncated cones, with modification to account for blade thickness and blade angles. The axial cross-sectional area is

$$A_a = \frac{\pi}{4} (d_2^2 - d_1^2) \left(1 - \frac{t_b}{t_{bs}}\right) \quad (67)$$

The diameters and blade thicknesses are given by

$$d_1 = d_{1i} + (d_{1o} - d_{1i}) z/L \quad (68)$$

$$d_2 = d_{2i} + (d_{2o} - d_{2i}) z/L \quad (69)$$

and

$$t_b = t_{bi} + (t_{bm} - t_{bi}) \left(1 - \frac{z}{L}\right) \frac{4z}{L} \quad (70)$$

The blade shape is assumed to have a parabolic contour so that the local angle is

$$\cot \beta = \cot \beta_1 + (\cot \beta_o - \cot \beta_1) z/L \quad (71)$$

and the local gauging is

$$\sin \beta = \frac{1}{\sqrt{1 + \cot^2 \beta}} \quad (72)$$

The cross-sectional area normal to the local flow direction is

$$A = A_a \sin \beta \quad (73)$$

The flow velocity relative to the blade is

$$w = U_a / \sin \beta \quad (74)$$

The changes in area with axial position are obtained by differentiating the above expressions.

### • Approximation Method for Supersonic Exit Velocities

Special techniques are required to continue stepwise numerical integration of the flow equations through the transition from subsonic to supersonic

flow due to the singularity in the flow equations at the critical point. An approximate method is derived which permits computation to proceed for flow through the throat of a convergent-divergent passage. Briefly, the method is to continue the numerical calculation until the critical point approaches some arbitrary amount, say  $W = 0.95 C_{crit}$ . At this point special equations are employed to obtain the flow properties at the critical point and at some point just past the throat where the flow is supersonic. The stepwise integration can then be continued.

The following assumptions are made to extrapolate the flow variables from the subsonic to the supersonic state.

- 1) The enthalpy change of the condensate is neglected.
- 2) The value of  $\eta_p$  is maintained at the original value for the particular nozzle.
- 3) The condensation can be calculated from the supercooling at the beginning and end points.
- 4) Certain vapor properties during the extrapolation are defined by their effective values at the starting point of the extrapolation.

The flow equations described in a previous section can be integrated in a manner similar to the case of isentropic expansion of an ideal gas except that condensation terms are also included.

The critical point occurs when the denominator of the solution for  $\frac{dw}{dz}$  is equal to zero, namely when  $\Delta_o = 0$ , as defined by Eq. 64. Rearranging the expression for  $\Delta_o$  and setting  $\Delta_o = 0$  to find the critical speed gives

$$P_x^2 v_{\eta p} \left(1 - \frac{W^2}{C_{crit}^2}\right) = 0 \quad (75)$$

where

$$C_{crit}^2 = \frac{R_o \gamma_{\eta} gT}{M} \quad (76)$$

and

$$y_{\eta} = \frac{Mx}{R_o} \left[ \frac{V_z \frac{\partial h_g(V, T)}{\partial T} + \frac{VT_z}{T} \frac{\partial h_g(V, T)}{\partial V}}{\frac{T}{P v \eta_p} \frac{\partial h_g(V, T)}{\partial T} - \frac{T_z}{J}} \right] \quad (77)$$

Thus, the critical point is reached when  $W = C_{crit}$ , where  $C_{crit}$  is defined by Eq. 76 and where  $y_{\eta}$  is assumed to be a constant calculated from the properties at the initial state point of the extrapolation. The symbols  $V_z$  and  $T_z$  are defined by equations 80 and 81.

For smooth flow transition through the critical point, the numerator in the solution for  $\frac{dw}{dz}$  must be zero simultaneously with  $\Delta_o = 0$ . This requires that  $\Delta_w = 0$ , which from Eq. 66 is found to occur when

$$\frac{1}{A} \frac{dA}{dz} - \left( \frac{T_z h_{fg}}{\phi} - \frac{1}{x} \right) \frac{dy}{dz} = 0 \quad (78)$$

Since  $dy$  is positive during an expansion and the term in parentheses is also positive for  $x$  near 1, the critical point must occur at a location where  $dA$  is positive, that is at some point past the throat of the passage. For the present work the assumption is made that the critical point occurs at the throat, so that the minimum area is taken as  $A^*$ .

The flow equations will now be integrated by defining a number of pseudo properties which are held constant during the extrapolation. From the first assumption (page 2-7) above, the term  $dT_L$  is set equal to zero in the energy equation 56.  $\frac{dT_L}{dz}$  Eliminating  $dP$  and  $\frac{dW}{dz}$  from the momentum, energy, and state equations 56, 57, and 59 gives

$$\frac{1}{T} \frac{dT}{dz} + \left( \frac{\phi V - V_z}{\phi T - T_z} \right) \frac{1}{v} \frac{dv}{dz} + \left( \frac{J h_{fg}}{P v \eta_p (\phi T - T_z)} \right) \frac{1}{x} \frac{dx}{dz} = 0 \quad (79)$$

where

$$V_z = \left( 1 - \frac{V}{Z_c} \frac{\partial Z_c}{\partial V} \right) \quad (80)$$

\*Complex conjugate of  $A = A^*$

$$T_z = \left( 1 + \frac{T}{Z_c} \frac{\partial Z_c}{\partial T} \right) \quad (81)$$

$$\phi_V = \frac{V J \frac{\partial h_g(V, T)}{\partial V}}{P v \eta_p} \quad (82)$$

and

$$\phi_T = \frac{J T \frac{\partial h_g(V, T)}{\partial T}}{P v \eta_p} \quad (83)$$

Defining

$$k_{\eta} - 1 = \frac{\phi_V + V_z}{\phi_T - T_z} \quad (84)$$

and

$$\lambda_{\eta} = \frac{J h_{fg}}{P v \eta_p (\phi_T - T_z)} \quad (85)$$

and assuming  $k_{\eta}$  and  $\lambda_{\eta}$  are constant during the extrapolation of their initial values, Eq. 79 can be integrated to give

$$\frac{v}{v_1} = \left[ \frac{T}{T_1} \left( \frac{x}{x_1} \right)^{\lambda_{\eta}} \right]^{\frac{1}{1 - k_{\eta}}} \quad (86)$$

where the subscript 1 refers to values at the starting point of the extrapolation.

Also assuming  $T_z$  and  $V_z$  are constant during the extrapolation, the state equation 57 can be integrated to give

$$\frac{P}{P_1} = \left( \frac{T}{T_1} \right)^{T_z} \left( \frac{v}{v_1} \right)^{-V_z} \quad (87)$$

Integration of continuity equation 60 gives

$$\frac{A}{A_1} = \frac{\left( \frac{v}{v_1} \right) \left( \frac{x}{x_1} \right)}{\left( \frac{W}{W_1} \right)} \quad (88)$$

Substituting the expression for  $\frac{1}{v} \frac{dv}{dz}$  from Eq. 79 into the energy equation 56 yields

$$\frac{W}{J g} \frac{dW}{dz} + C_{\eta} \frac{1}{T} \frac{dT}{dz} + h_{\eta} \frac{dx}{dz} = 0 \quad (89)$$

where

$$C_\eta = x \left[ T \frac{\partial h_g(V, T)}{\partial T} - \frac{V}{(k_\eta - 1)} \frac{\partial h_g(V, T)}{\partial V} \right] \quad (90)$$

and

$$h_\eta = h_{fg} - \frac{\lambda_\eta}{k_\eta - 1} \left( V \frac{\partial h_g(V, T)}{\partial V} \right) \quad (91)$$

By assuming the values of  $C_\eta$ , and  $h_\eta$  to be constant at their initial values, Eq. 89 can be integrated to give

$$\frac{W^2}{2gJ} + C_\eta T + h_\eta x = \frac{W_1^2}{2gJ} + C_\eta T_1 + h_\eta x_1 \quad (92)$$

At the critical point,  $W^2 = C_{crit}^2 = C_\eta R_o g T / M$ .

Then, denoting the temperature at the critical point by  $T^*$ , the energy equation at the critical point gives

$$\frac{T^*}{T_1} = \frac{1 + \frac{W_1^2}{2gJ C_\eta T_1} + \frac{h_\eta}{C_\eta T_1} (x_1 - x^*)}{1 + \frac{\gamma_\eta R_o}{2M J C_\eta}} \quad (93)$$

Equations 86, 87 and 76 written at the critical point then give

$$\frac{v^*}{v_1} = \left[ \frac{T^*}{T_1} \left( \frac{x^*}{x_1} \right)^{\lambda_\eta} \right]^{\frac{1}{1-k_\eta}} \quad (94)$$

$$\frac{P^*}{P_1} = \left( \frac{T^*}{T_1} \right)^{\frac{\gamma_\eta}{1-k_\eta}} \left( \frac{v^*}{v_1} \right)^{-\gamma_\eta} \quad (95)$$

and

$$W^* = \sqrt{\lambda_\eta g \frac{R_o T_1}{M} \left( \frac{T^*}{T_1} \right)} \quad (96)$$

The critical area ratio can then be found from

$$\frac{A^*}{A_1} = \frac{\left( \frac{v^*}{v_1} \right) \left( \frac{x^*}{x_1} \right)}{\left( \frac{W^*}{W_1} \right)} \quad (97)$$

Provided  $x^*$  is known, Eqs. 94, 95, 96, and 97 define the conditions at the critical point in terms of those at the start of the extrapolation.

An iteration technique is required to determine  $x^*$  to complete the description of the critical point

conditions. It is assumed that the condensation rate is proportional to the supercooling rate for the drops that already exist and no new drops are formed. Let the supercooling at the start of the extrapolation be  $\Delta T_1$ , and at the critical point,  $\Delta T^*$ . The average supercooling rate is

$$\Delta \bar{T} = \frac{1}{2} (\Delta T_1 + \Delta T^*) \quad (98)$$

and the average condensation rate is

$$\left( \frac{dy}{dz} \right) = \left( \frac{dy}{dz} \right)_1 \left( \frac{\Delta \bar{T}}{\Delta T_1} \right) \quad (99)$$

Integrating and expressing the results in terms of  $x$  gives

$$x^* = x_1 - \left( \frac{dy}{dz} \right)_1 \left( \frac{\Delta \bar{T}}{\Delta T_1} \right) (z^* - z_1) \quad (100)$$

From the geometry,  $z^*$  is known as the location of  $A_{min}$ . A value of  $\Delta T^*$  is assumed and  $x^*$  is calculated. Then  $T^*$ ,  $v^*$ , and  $P^*$  are calculated and the value of  $\Delta T^*$  is found from Eqs. 33 and 34. When  $\Delta T^*$  matches the assumed value, the critical point is specified. Then, it is necessary to compare the value of  $A^*$  with the actual minimum area  $A_{min}$ . If  $A^*$  and  $A_{min}$  are not within a specified tolerance, the inlet velocity is corrected and calculations begin anew at the turbine inlet. When  $A^*$  and  $A_{min}$  agree, the extrapolation is continued to a point past the throat in the case of a convergent-divergent passage, or the extrapolation ends at the throat for a convergent passage. Let  $A_2$  be the area at this point to which the extrapolation takes place. The Mach number at this position is estimated by approximate expression to start the iteration, or

$$M_2 = \sqrt{\frac{2(A_2 - A_{min})}{A_{min}(3 - k_\eta)}} \quad (101)$$

Then  $x_2$  is found from

$$x_2 = x^* - \left( \frac{dy}{dz} \right) (z_2 - z^*) \quad (102)$$

The values of  $T_2$ ,  $v_2$ ,  $P_2$ ,  $W_2$  and  $A_2$  are then found with Eqs. 93, 94, 95, 96, and 97 rewritten in terms of conditions at position 2. Thus,

$$\frac{T_2}{T_1} = \frac{1 + \frac{W_1^2}{2gJ C_\eta T_1} + \frac{h_\eta}{C_\eta T_1} (x_1 - x_2)}{1 + \frac{M_2^2 (\gamma_\eta R_o)}{2M J C_\eta}} \quad (103)$$

$$\frac{v_2}{v_1} = \left[ \frac{T_2}{T_1} \left( \frac{x_2}{x_1} \right)^{\lambda \eta} \right]^{\frac{1}{1-k_\eta}} \quad (104)$$

$$\frac{P_2}{P_1} = \left( \frac{T_2}{T_1} \right)^{\gamma_z} \left( \frac{v_2}{v_1} \right)^{-\gamma_z} \quad (105)$$

$$\frac{W_2}{W_1} = \sqrt{\gamma_\eta g \frac{R_o T_1}{M} \left( \frac{T_2}{T_1} \right)} \quad (106)$$

and

$$\frac{A_2}{A_1} = \frac{\left( \frac{v_2}{v_1} \right) \left( \frac{x_2}{x_1} \right)}{\left( \frac{W_2}{W_1} \right)} \quad (107)$$

If  $A_2$  does not agree with the desired value,  $M_2$  is corrected until  $A_2$  converges. These properties are then used as inputs to continue the stepwise integration process. Each type of moisture, including surface condensate, is assumed to increase in the same proportion during the extrapolation, and these new values are also required as inputs for continuing stepwise integration.

#### • Expansion from Stagnation to Static Inlet Conditions

The inlet to the turbine is specified by the stagnation temperature  $T_o$ , and the axial velocity  $U_{ao}$  at the first stator inlet. In the case where the inlet is supersaturated, the inlet temperature  $T_o$  is obtained from its value corresponding to the equilibrium state as  $P_s$  and  $T_s$  and moisture fraction  $y$  by using the relationship:

$$T_o = T_s - \frac{y h_{fg}}{C_{pv}} \quad (108)$$

The expansion from stagnation to static conditions at the inlet is evaluated by the same technique used in the extrapolation. The values of  $C_\eta$  and  $k_\eta$  are evaluated at the inlet stagnation state, which is analogous to state point 1 in the extrapolation. The static temperature is obtained from

$$T = T_o - \frac{U_{ao}^2}{2gJ C_\eta \sin^2 \beta_1} \quad (109)$$

The specific volume is obtained from

$$v = v_o \left( \frac{T}{T_o} \right)^{\frac{1}{1-k_\eta}} \quad (110)$$

and the pressure from the state equation using the values of  $v$  and  $T$  to evaluate the compressibility.

#### 2.2.3 Method of Solution

The numerical solution to the problem consists of integrating the continuity, energy, state, and momentum equations 60, 61, 62, and 63 for the area change obtained from the turbine geometry and the rate of change of condensate as determined by the nucleation and growth expressions. A stepwise integration is performed using the ICEADAMS integration procedure listed in Appendix B. Basically, the order of calculation is as follows. Knowing the properties  $T$ ,  $P$ ,  $v$ , and the velocity  $W$  at a point, the property equations are used to calculate

$$Z_c, \frac{\partial Z_c}{\partial T}, \frac{\partial Z_c}{\partial v}, C_{pv}, h_g, \frac{\partial h_g}{\partial v}, \frac{\partial h_g}{\partial T}, h_{fg}, \rho_L, \sigma_L, P_s, \Lambda_o, \Delta T, T_s, r, \text{ and } T_{rec}$$

The association expressions are then used to obtain  $k_L', P_1, P_{1s}$ , and  $\Lambda_1$ . The turbine description gives  $dA$ . The nucleation expression gives  $\dot{J}$  and  $\frac{dN_i}{dz}$  for the group of droplets being formed at the present value of  $z$ . The droplet growth and surface condensation expressions are evaluated to obtain  $\frac{dr_{Li}}{dz}$ ,  $\frac{dT_L}{dz}$ , and  $\frac{dy}{dz}$ . These calculations then provide the required data to calculate  $\frac{dT}{dz}$ ,  $\frac{dP}{dz}$ ,  $\frac{dv}{dz}$ , and

$\frac{dW}{dz}$  which are used to obtain the new values at the end of the integration step. This brief description is intended only as an overall view of the calculation routine.

A listing of the computer code is given in Appendix A. The list of input quantities is given in Appendix C in the order required by the code. A flow chart for the code, showing the major control and logic, is provided in Appendix D. The correspondence between the code symbols and the text symbols is given in the nomenclature. Appendix E gives a description of the function and use of the control variables not included in the text.

## 2.2.4 Sample Turbine Calculation Results

The computer code was run for a three-stage potassium turbine. The numerical input data used are listed in Appendix C, except for the turbine geometry description which is presented in Table 2.2-1. The stagnation inlet state is defined by  $T = 2010^\circ\text{R}$ ,  $P_o = 30.2 \text{ psia} = 4349 \text{ lb/ft}^2$ , and  $x = 0.99$ . The inlet is assumed to be supersaturated, and the inlet temperature corrected for moisture content by Eq. 108 is  $T = 1982.9^\circ\text{R}$ . The summary of calculation results provided by the computer printout is shown in Table 2.2-2, and the output nomenclature when the mean radius is in feet and units are given in Table 2.2-3. A typical printout is shown in Table 2.2-4 for the conditions at the exit of the second stator with corresponding nomenclature and units given in Table 2.2-5.

The value of  $y_e$  calculated by the computer program requires correction due to variable specific heat between supercooled and saturated state points. The value of  $y_e$  is obtained from

$$y_e = y + \frac{\Delta T C_{pv}}{h_{fg}}$$

where  $y_e$  is the equivalent moisture, and  $C_{pv}$  is the specific heat at the supersaturated state. The correction to be applied is

$$y'_e = y + \frac{(y_e - y)}{2} \left[ 1 + \frac{(C_{pv})_{\text{sat}}}{C_{pv}} \right]$$

The value of  $C_{pv}$  is obtained from the computer printout and  $(C_{pv})_{\text{sat}}$  may be obtained from any suitable source of thermodynamic property values for the specific turbine fluid. For this particular example, see Reference 4. In Table 2.2-2, the value of  $C_{pv}$  is 0.36 Btu/lb- $^\circ\text{R}$ , and  $(C_{pv})_{\text{sat}}$  is found to be 0.28. Thus, the corrected equilibrium moisture content is 0.102 and the tabulated value is 0.105. The correction is larger when greater supercooling exists. The correction required on the value of  $y_e$  does not affect any other calculations in the program.

TABLE 2.2-1

### EXAMPLE TURBINE GEOMETRY FOR THREE-STAGE POTASSIUM TURBINE

Row	1	2	3	4	5	6
Inlet Mean Diameter (in.)	7.693	8.080	8.17	8.68	8.80	9.22
Inlet Blade Height (in.)	0.605	0.772	0.66	1.076	1.04	1.59
Outlet Mean Diameter (in.)	8.08	8.17	8.68	8.80	9.22	9.31
Outlet Blade Height (in.)	0.772	0.66	1.076	1.04	1.59	1.53
Expansion Efficiency (%)	0.95	0.80	0.95	0.80	0.90	0.80
Axial Length (ft)	0.1166	0.081	0.0955	0.0903	0.101	0.0983
Inlet Angle (degrees)	90	26.41	124.72	30.19	121.32	47.70
Outlet Angle (in.)	14.5	154.65	16.70	152.14	21.55	146.95
Blade Pitch (in.)	0.653	0.41	0.572	0.455	0.641	0.557
Edge Blade Thickness (in.)	0.012	0.0125	0.012	0.012	0.012	0.012
Blade Velocity (ft/sec)	0	641	0	689	0	734
Maximum Blade Thickness (in.)	0.12	0.166	0.100	0.154	0.120	0.125

The Wilson point occurred at  $z/L \cong 0.63$  inch in the second stator row at a corrected equivalent moisture content of 7.4 percent. The expansion rate at the Wilson point was approximately  $P = 2500/\text{sec}$ .

The Wilson point occurred at a supersaturation pressure ratio of 2.32. With all other parameters fixed, the classical nucleation theory would predict a critical supersaturation ratio of about 2.13. In the present case this will shift the Wilson point slightly within the second stator.

The turbine geometry used has a diffuser-type section in the first part of the second rotor, causing the flow to return to the saturation state. The condensation zone in which nuclei growth occurred was located in this portion of the second rotor and the flow remained near the saturated state throughout the remainder of the turbine.

The results of the present calculations can be compared in a qualitative manner with the results of Goldman and Nosek<sup>(8)</sup> in which saturated potassium vapor was expanded in a convergent-divergent nozzle. Although their results are somewhat inconclusive, it appears that condensation occurred when the ratio of pressure to initial saturation pressure was between 0.31 and 0.33 at an axial distance of about 3 inches from the nozzle inlet. In the present example, condensation is predicted at a pressure/inlet saturation pressure ratio of 0.324.

TABLE 2.2-2  
COMPUTER OUTPUT SUMMARY SHEET FOR  
THE THREE-STAGE TURBINE EXAMPLE

SUMMARY OF RESULTS OF CONDENSATION CALCULATIONS										
RØW	T	P	VV	W	UA	YE	YS	Y	RMEAN	NTOTAL
0	1970.7	4324.7	16.03	333.4	333.4	0.00000	0.00000	0.00000	0.0000E+00	0.0000E+00
1	1786.4	2765.9	22.19	1375.5	343.3	0.06189	0.00000	0.00000	0.0000E+00	0.0000E+00
2	1731.1	2336.8	25.28	1056.7	452.4	0.07921	0.00000	0.00000	9.9317E-08	1.4163E+12
3	1685.1	1360.9	44.28	1484.4	426.6	0.10519	0.00000	0.06805	9.9459E-07	4.2736E+14
4	1712.8	1114.3	56.52	1146.3	533.9	0.11004	0.00000	0.10182	1.1401E-06	4.2736E+14
5	1666.5	784.0	79.06	1232.3	452.6	0.13338	0.00000	0.12930	1.2300E-06	4.2736E+14
6	1601.4	554.1	107.95	1146.7	624.0	0.15442	0.00000	0.14664	1.2762E-06	4.2736E+14

TABLE 2.2-3  
NOMENCLATURE AND UNITS FOR COMPUTER  
OUTPUT

Title	Code Symbol	Text Symbol	Units
RØW	S	Blade row index	---
T	T	T	°R
P	P	P	lb/ft <sup>2</sup>
VV	VV	U	ft <sup>3</sup> /lb
W	W	W	ft/sec
UA	UA	U <sub>a</sub>	ft/sec
YE	YEQUILIB	y <sub>e</sub>	---
YS	YSURFACE	y <sub>b</sub> + y <sub>bo</sub> + y <sub>abs</sub>	---
Y	YSUM	y	---
RMEAN	RMEAN	$\tau = \left( \frac{3y}{4 \pi \Sigma N_{rl}} \right)^{1/3}$	ft
NTOTAL	NTOTAL	$\Sigma N_{rl}$	lb <sup>-1</sup>

An earlier condensation in terms of pressure ratio, in the turbine as compared to the supersonic nozzle, is expected due to the lower expansion rate.

According to Linhardt, condensation in his tests occurred upstream of the nozzle throat. This would imply a ratio of condensation point pressure to inlet saturation pressure ratio greater than 0.5. This is contrary to the Goldman and Nosek experiment and theoretical calculation.

The droplet size results can be compared with results obtained by Linhardt<sup>(9)</sup>. His analysis of his experiment predicts a droplet radius of 0.05 microns for 10 percent exit moisture in his test No. 4. His tests 2, 3 and 4 had the same stagnation condition and the same nozzle except for length. With critical flow in the nozzle, the conditions at the condensation point would be unchanged due to the additional length of the nozzle. Thus, for the same conditions at the Wilson point the droplet radius at the nozzle exit is expected to be proportional to (y<sub>e</sub>)<sup>1/3</sup>, where y<sub>e</sub> is the moisture fraction at the nozzle exit.

COMPUTER OUTPUT INTERMEDIATE SUMMARY  
SHEET FOR THE SECOND STATOR EXIT

Viewed in this way, the results of Linhardt's test 3 corrected to 10 percent moisture would give a radius of 0.06 microns while Linhardt's test 2 would give a 0.26 micron radius. The present calculations indicate a mean radius of 0.35 microns at 10 percent moisture. The larger size is consistent with the lower expansion rate.

The results obtained by the condensation code have been in general agreement with the limited experimental data available for comparison. The

The computer code performance has been satisfactory for subsonic turbine analysis. On occasion, choking flow conditions have been encountered in turbines designed for subsonic flow. This difficulty is due to the relatively simple blade profile and blade thickness expressions which are not general enough to give the same flow area as an actual blade when the actual blade thickness is used in

TABLE 2.2-5  
NOMENCLATURE AND UNITS FOR COMPUTER  
OUTPUT

Title	Code Symbol	Text Symbol	Units
COUNT	COUNT	Steps since last output	---
STEP SIZE H	H	Step size	ft
Z	Z	$z$	ft
P	P	$P$	lb/ft <sup>2</sup>
T	T	$T$	°R
SP. VEL. -V	VV	$v$	ft <sup>3</sup> /16
w	W	$W$	ft/sec
U-AXIAL	UA	$U_a$	ft/sec
Z-COMPRESS	ZC	$Z_c$	---
DP	DP	$dP/dx$	lb/ft <sup>3</sup>
DT	DT	$dT/dx$	°R/ft
DV	DVV	$dV/dx$	ft <sup>2</sup> /lb
DW	DW	$dW/dx$	1/sec
-DP/DT/P	PDPT	$1/P \cdot dP/dt$	1/sec
AREAA	AREAA	$A_a$	in. <sup>2</sup>
DA/A	DA	$1/A \cdot dA/dx$	---
DELTA T	DELTA T	$\Delta T$	°R
TLIQUID	TLIQUID	$T_L$	°R
LAMBDA 0	LAMBDA 0	$\Lambda_0$	---
LAMBDA 1	LAMBDA 1	$\Lambda_1$	---
JDPT	JDPT	$\bar{T}$	1/ft <sup>3</sup> sec
RCRITICAL	RCRIT	$r_{crit}$	ft
DN/DZ	NEU	$\bar{T} \cdot v/U_a$	1/16 ft
K2	K2	$k_2$	1/atom
K4	K4	$k_4$	1/atom <sup>3</sup>
K2 PRIME	K2 PRIME	$k_2$	1/atom
HFG	HFG	$h_g$	Btu/lb
CPV0	CPV0	$C_{pv}$	Btu/lb °R
CPV	CPV	$C_{pv}$	Btu/lb °R
SIGMA	SIGMA	$\sigma$	lb/ft
TOTAL MOISTURE	YSUM	$y$	---
PARTIAL M	PI	$P_i$	lb/ft <sup>2</sup>
QUALITY	X	$x$	---
MEAN RADIUS	RMEAN	$\bar{r} = \left( \frac{3y}{4\pi \rho_L \sum N_{ri}} \right)^{1/3}$	ft
TOTAL DROPS	NTOTAL	$N_{ri}$	1/lb
K2 PRIME SAT	K2PRIMES	$k_2$ at saturation	1/atom
SINBETA	SINB	$\sin \beta$	---
Y - EQUILIB	YEQUILIB	$y_e$	---
HG	HG	$h_g$	Btu/lb
HL	HL	$h_L$	Btu/lb
HFG	HFG	$h_{fg}$	Btu/lb
DELØ	DELØ	$\Delta_o$	Btu ft/lb
DELW	DELW	$\Delta_w$	Btu/lb
I - M*2	DELØS	$1-W^2/c_{crit}^2$	---
YB = YBLADE	YB	$y_b$	---
YBØ = Y CASE	YBØ	$y_{bo}$	---
YABS =	YABS	$y_{abo}$	---
YATØMIZED			
YSURFACE	YSURFACE	$y_b \cdot y_{bo} \cdot y_{bo}$	---
NATØMIZE	NATØMIZE	Number of atomized drops	1/lb
GROUP	I	Index denoting group	---
MOISTURE	Y [I]	$y_i$	---
NUMBER	NL [I]	$N_{ri}$	1/lb
RADIUS	RL [I]	$r_i$	ft
DMØISTURE	DY [I]	$dy_i/dx$	1/ft
DNUMBER	DNL [I]	$dN_{ri}/dx$	1/ft - lb
DRADIUS	DRLD [I]	$dr_i/dx$	---

the expressions. This difficulty is overcome by decreasing the blade thickness. The blade heights used should also correspond to the actual flow areas.

In the present version of the program, the inlet angles to blade rows are modified to line up with the relative velocity vector at the inlet to the blade row. The incidence angle effect could be approximated by assuming that an additional blade row exists between each actual blade row to provide the expansion or compression effect of non-zero incidence.

The code has a provision for extrapolating through the critical point from subsonic to supersonic flow. After one such extrapolation, subsequent blade thicknesses must be modified to accommodate the flow, since no provision for shock waves is included. The code has a provision for automatically adjusting blade thickness; however, the code did not converge in the case of a cesium turbine analysis.

The subsonic-supersonic transition worked smoothly when the correct blade thickness was supplied as input. Careful description of the flow areas at the throat and exit of a supersonic blade row is required to obtain a desired exit velocity since an increase in Mach number from 1.00 to approximately 1.10 will occur for a change in the exit-to-throat area ratio from 1.00 to 1.01.

In summary, the code has performed satisfactorily for subsonic turbines but requires careful input to obtain desired area ratios for turbines having supersonic flow.



## 2.2.6 Nomenclature

Test Symbol	Code Symbol	Definition - Units
A	-	Flow cross-sectional area, (ft <sup>2</sup> )
A <sub>a</sub>	AREA	Axial cross-sectional area, (ft <sup>2</sup> )
A <sub>1</sub> , A <sub>2</sub>	A1, A2	Flow cross-sectional area at points 1 and 2, (ft <sup>2</sup> )
A <sub>min</sub>	AMIN	Minimum flow cross section, (ft <sup>2</sup> )
A <sub>cr</sub>	-	Critical minimum flow cross section, (ft <sup>2</sup> )
a <sub>1</sub> , a <sub>2</sub> , a <sub>3</sub>	APS, APS1, APS2	Constants describing saturation pressure, (ft <sup>3</sup> /lb mole)
B, B <sub>1</sub> , B <sub>2</sub>	B, B1, B2	Constants in virial equation of state, (ft <sup>3</sup> /lb mole), (-), (°R)
C, C <sub>1</sub> , C <sub>2</sub> , C <sub>3</sub>	C, C1, C2, C3	Constants in virial equation of state, (ft <sup>3</sup> /lb mole) <sup>2</sup> , (-), (°R), (°R <sup>2</sup> )
C <sub>crit</sub>	CCRIT	Critical speed of mixture, (ft/sec)
C <sub>pl</sub>	CPL	Specific heat of liquid, (Btu/lb °R)
C <sub>pv</sub>	CPV	Specific heat of vapor, (Btu/lb °R)
C <sub>p</sub>	CPV	Temperature dependent term in expression for C <sub>p</sub> , (Btu/lb °R)
C <sub>p0</sub> , C <sub>p1</sub> , C <sub>p2</sub>	ACP0, ACP1, ACP2	Constants defining C <sub>p0</sub> as a function of T, (Btu/lb °R), (Btu/lb °R), (°R)
C <sub>e</sub>	CETA	Effective specific heat (Btu/lb °R)
D, D <sub>1</sub> , D <sub>2</sub>	D, D1, D2	Constants in virial equation of state, (ft <sup>3</sup> /lb mole) <sup>3</sup> , (-), (°R)
d <sub>1</sub> , d <sub>11</sub> , d <sub>10</sub>	DIA1, DIA11, DIA10	Hub passage diameter, at stage inlet, at stage outlet, (ft)
d <sub>2</sub> , d <sub>21</sub> , d <sub>20</sub>	DIA2, DIA21, DIA20	Tip passage diameter, at stage inlet, at stage outlet, (ft)
E, E <sub>1</sub>	E, E1	Constants in virial equation of state (ft <sup>3</sup> /lb mole) <sup>4</sup>
F	-	Friction force per unit volume of flow, (lb/ft <sup>3</sup> )
g	G	Acceleration of gravity, (ft/sec <sup>2</sup> )
h <sub>abs</sub>	HABS	Heat transfer coefficient, atomized moisture, (Btu/sec ft <sup>2</sup> °R)
h <sub>amb</sub>	HAMB	Heat transfer coefficient, cooling to ambient, (Btu/sec ft <sup>2</sup> °R)
h <sub>b</sub>	HB	Heat transfer coefficient on blade surface, (Btu/sec ft <sup>2</sup> °R)
h <sub>c</sub>	-	Heat transfer coefficient, (Btu/ft <sup>2</sup> °R)
h <sub>fg</sub>	HFG	Latent heat of vaporization, (Btu/lb)
h <sub>g</sub>	HG	Enthalpy of vapor, (Btu/lb)
h <sub>g0</sub>	HG0	Enthalpy of monomer species, (Btu/lb)
h <sub>g0</sub> , h <sub>g1</sub> , h <sub>g2</sub>	AHG, AHG1, AHG2, AHG3	Constants defining temperature dependence of h <sub>g</sub> , (Btu/lb), (°R Btu/lb), (Btu/lb), (°R)
h <sub>l</sub>	HL	Enthalpy of saturated liquid, (Btu/lb)
h <sub>l0</sub> , h <sub>l1</sub> , h <sub>l2</sub>	AHL, AHL1, AHL2, AHL3	Constants defining temperature dependence of h <sub>l</sub> , (Btu/lb), (Btu/lb °R), (Btu/lb °R), (Btu/lb °R <sup>2</sup> )
h <sub>g</sub>	HETA	Effective heat of vaporization, see Eq. 91, (Btu/lb °R)
J	J	Mechanical equivalent of heat, (ft-lb/Btu)
J <sub>DOT</sub>	JDOT	Nucleation rate, (1/ft <sup>3</sup> sec)
K	-	Chemical symbol for potassium
K <sub>1</sub>	K2, K4	Equilibrium constants for species I = 2, 4 (ftm) <sup>1-2</sup>
k <sub>1</sub> , k <sub>2</sub> , k <sub>3</sub>	AK2, AK21, AK4, AK41	Constants defining temperature dependence of k <sub>i</sub> , (-), (°R), (-), (°R)
k <sub>2</sub>	K2PRIME	Apparent equilibrium constant, (ftm) <sup>-1</sup>
k <sub>v</sub>	KV	Vapor thermal conductivity (Btu/sec ft °R)
k <sub>p</sub>	KETA	Effective polytropic exponent, (-)
L	-	Length along chord, (ft)
L	LENGTH	Axial length of blade row, (ft)
M	-	Mass flow rate, (lb/sec)
M	M	Molecular weight of monomer vapor, (lb/lb mole)
M <sub>2</sub>	M2	Mach number at point 2, (-)
N <sub>0</sub>	N0	Avogadro's number, (molecules/lb mole)
N <sub>1</sub>	-	Molal concentration of species 1, (-)
N <sub>1</sub>	N1PRIME	Apparent molal concentration of species 1, (-)
N <sub>1</sub>	NL [1]	Droplets per pound in group 1, (1/lb)
P	P	Static pressure, (lb/ft <sup>2</sup> )
P <sub>0</sub>	PATM	Atmospheric pressure conversion constant, (lb/ft <sup>2</sup> /atm)
P <sub>1</sub>	-	Partial pressure of species 1, (lb/ft <sup>2</sup> )
P <sub>eff</sub>	PEFF	Pressure term in nucleation equation, (lb/ft <sup>2</sup> )
P	PDOT	Expansion rate defined by 1/P dP/dT, (1/sec)
P <sub>0</sub>	P0	Inlet stagnation pressure, (lb/ft <sup>2</sup> )
P <sub>1</sub>	P1S	Partial pressure of monomer at saturation pressure corresponding to vapor temperature, (lb/ft <sup>2</sup> )
Pr	PRANDTL	Prandtl number, (-)

## Nomenclature (Continued)

P <sub>s</sub>	PS	Saturation pressure at vapor temperature, (lb/ft <sup>2</sup> )
Q	-	Heat transfer rate to blade surface, (Btu/sec)
R <sub>0</sub>	RO	Universal gas constant, (ft-lb/lb mole °R)
r	RECF	Recovery factor, (-)
r	RMEAN	Radius of mean droplet, (ft)
r <sub>abs</sub>	RABS	Atomized drop radius, (ft)
r <sub>crit</sub>	RCRIT	Critical radius, (ft)
r <sub>1</sub>	RL [1]	Droplet radius of group 1, (ft)
s	-	Perimeter of flow passage, (ft)
T	T	Vapor temperature, (°R)
T <sub>amb</sub>	TAMB	Ambient temperature, (°R)
T <sub>c</sub>	TC	Critical vapor temperature, (°R)
T <sub>L</sub>	TL	Condensate temperature, (°R)
T <sub>o</sub>	TEMP0	Inlet stagnation temperature, (°R)
T <sub>rec</sub>	TREC	Adiabatic recovery temperature, (°R)
T <sub>rl</sub>	-	Temperature of droplets in group 1, (°R)
T <sub>s</sub>	TSAT	Saturation temperature at pressure P, (°R)
T <sub>z</sub>	TZ	Parameter, see Eq. 81, (-)
T*	-	Temperature at critical point, (°R)
T <sub>1</sub> , T <sub>2</sub>	OLDT, T2	Temperature at point 1, 2, (°R)
ΔT, ΔT*, ΔT <sub>1</sub>	DELTA T, DELTAT*, DELTAT1	Supercooling, at critical point, at point 1, average during extrapolation, (°R)
t	-	Time, (sec)
t <sub>b</sub> , t <sub>bl</sub> , t <sub>bm</sub>	THICKB, THICKBL, THICKBM	Blade thickness, at stage inlet, maximum blade thickness, (ft)
t <sub>bs</sub>	BLADESPACE	Blade spacing at mean diameter, (ft)
t <sub>f</sub>	-	Thickness of flow channel, (ft)
U <sub>o</sub> , U <sub>ao</sub>	UA, UA0	Axial velocity of vapor, at inlet, (ft/sec)
v <sub>v</sub> , v <sub>m</sub>	VV, -	Specific volume of vapor, of mixture (ft <sup>3</sup> /lb)
v*	-	Specific volume of vapor at critical point (ft <sup>3</sup> /lb)
v <sub>1</sub> , v <sub>2</sub> , v <sub>o</sub>	OLDVV, V2 -	Specific volume of vapor at point 1, 2, at inlet stagnation (ft <sup>3</sup> /lb)
v	V	Molal specific volume of vapor, (ft <sup>3</sup> /lb mole)
v <sub>z</sub>	VZ	Parameter, see Eq. 80, (-)
W, W <sub>1</sub> , W <sub>2</sub>	W, OLDW, W2	Stream velocity relative to blade, at point 1, 2 (ft/sec)
w <sub>crit</sub>	-	Weight of critical size droplet, (lb)
x <sub>1</sub> , x <sub>1</sub> , x <sub>2</sub> , x*	X, OLDX, X2, XSTAR	Vapor quality, at point 1, at point 2, at critical point, (lb/lb)
x <sub>C1</sub> , x <sub>C2</sub>	XC1, XC2	Abbreviations, see Eqs. 43 and 44, (-), (ft <sup>3</sup> /lb mole)
y	YSUM	Moisture fraction, (-)
y <sub>abs</sub>	YABS	Moisture fraction atomized from blade, (-)
y <sub>b</sub> , y <sub>bo</sub>	YB, YB0	Moisture fraction on blades, casing, (-)
y <sub>b</sub>	-	Rate of condensate formation on blades, (lb/sec)
y <sub>e</sub> , y <sub>e</sub>	YEQUILB, -	Equivalent equilibrium moisture, corrected value, (-)
y <sub>1</sub>	MY [1]	Moisture fraction of group 1, (-)
y <sub>N</sub>	-	Moisture fraction due to formation of stable droplets, (-)
Z <sub>1</sub>	Z1	Parameter in nucleation expression, (-)
Z <sub>c</sub>	ZC	Compressibility, (-)
z <sub>1</sub> , z <sub>1</sub> , z <sub>2</sub> , z*	Z, OLDZ, Z2, ZMIN	Axial coordinate, at point 1, at point 2, at critical point, (ft)
α, β, β <sub>o</sub>	BETA, BETAI, BETA0	Blade angle, at inlet, at exit, (degrees)
γ <sub>e</sub>	GETA	Effective specific heat ratio, (-)
δ <sub>o</sub>	DEL0	Abbreviation, see Eq. 64, (Btu ft/lb)
δ <sub>w</sub>	DELW	Abbreviation, see Eq. 66 (Btu/lb)
η <sub>p</sub>	ETAP	Local expansion efficiency, (-)
λ <sub>o</sub> , λ <sub>1</sub>	LAMBDA0, LAMBDA1	Logarithmic supersaturation pressure ratio, for monomer, (-)
λ <sub>e</sub>	LETA	Exponent in extrapolation, see Eq. 85, (-)
ν <sub>v</sub>	NEUV	Kinematic viscosity of vapor, (ft <sup>2</sup> /sec)
μ	-	Absolute viscosity, (lb/ft-sec)
ρ <sub>L</sub>	RH0L	Density of saturated liquid, (lb/ft <sup>3</sup> )
ρ <sub>L0</sub> , ρ <sub>L1</sub> , ρ <sub>L2</sub>	ARH0, ARH01, ARH02	Constants defining temperature dependence of ρ <sub>L</sub> , (lb/ft <sup>3</sup> ), (lb/ft <sup>3</sup> °R), (lb/ft <sup>3</sup> °R <sup>2</sup> )
σ	SIGMA	Surface tension, (lb/ft)
σ <sub>0</sub>	SIGMA0	Constant in surface tension correlation, (lb/ft)
φ	PHI0	Abbreviation, see Eq. 65, (Btu/lb)
φ <sub>1</sub>	PHI1	Abbreviation, see Eq. 83, (-)
φ <sub>v</sub>	PHIV	Abbreviation, see Eq. 82, (-)

## 2.2.7 References

1. Oswatitsch, K., and Z. Angew, Math. U. Mech., Vol. 22, pp. 1-14 (1942).
2. Hill, P. G., H. Witing, and E. P. Demetri, "Condensation of Metal Vapors During Rapid Expansion," Trans. ASME (Heat Transfer), Vol. 85, Part C, pp. 303 to 314, November 1963.
3. Gyarmathy, G., "The Basis for a Theory of the Wet Steam Turbine," Juris-Verlag Zurich, 1962.
4. Ewing, C. E. et al, "High Temperature Properties of Potassium," U. S. Naval Research Laboratory, Report NRL 6233, September 24, 1965.
5. Katz, J. L., H. Saltsburg, and H. Reiss, "Nucleation in Associated Vapors," North American Aviation Science Center, SCPP-65-32, May 18, 1965.
6. Eckert, E. R. G., and R. M. Drake, Jr., Heat and Mass Transfer, McGraw-Hill, New York, N. Y., 1959, pp. 211, 257-260.
7. Ewing, C. T., et al, "High Temperature Properties of Cesium," U. S. Naval Research Laboratory, NRL 6246, Sept. 24, 1965.
8. Goldman, L. J., and S. M. Nosek, "Experimental Nozzle Expansion and Flow Characteristics of Potassium Vapor," NASA TN D-3209.
9. Linhardt, H. D., "Potassium Condensate Droplet Size Determination," Aeronutronic Division, Philco Corporation, U-3709, August 1, 1966.

# APPENDIX 2.2A

## LISTING OF COMPUTER PROGRAM

09:17:23 THURSDAY, SEPTEMBER 28, 1967

```

BEGIN
COMMENT      STUDY OF CONDENSATION OF ASSOCIATING VAPORS IN TURBINES;
FILE OUT PRINT 4(2, 15);
FILE IN READER(2, 10);
REAL ARRAY ROTOR, DIAMI, HEIGHTI, DIAMO, HEIGHTO, BETAIN, BETAOUT,
  BSPACE, ETAPI, LI, UB, THICKBOI, THICKBMAXI(0:18);
REAL ARRAY QLOF, QLOCASE(0:154);
INTEGER COUNT, EQNS, GROUPS, GROUPMAX, GROUPO, GROUPPRINT, I, S,
  STAGES, N, N2;
REAL ARRAY JS, MY, DTL, ORLO, DNL, DMY, RL, RLD, RLO, WR, NL(0:25);
BOOLEAN WILSON, WILSONO, RESTART;
LABEL LABELV, EXIT, SKIPV;
LABEL NEWSTAGE;
BOOLEAN EXTRAPOLATED;
REAL ARRAY ASAVE(0:100);
REAL ARRAY F(0:154);
INTEGER ARRAY CASE(0:25);
COMMENT DECLARATIONS;
LABEL ENTERICE, INITIAL;
LABEL LABELICE;
LABEL CHECKSTAR;
REAL ARRAY DT, DP, UVV, DW, DUA, DYE, DYS, DY, ORMEAN, ONT(0:18);
REAL ACPO, ACP1, ACP2, AREAA, AHFG, AHFG1, ARHO, ARHO1, ARHO2, AK2,
  AK21, AK4, AK41, B, B1, B2, BDOT, BDDOT, BPRIME, BPPRIME,
  BLADESPACE, APS, APS1, APS2, BETAI, C, C1, C2, C3, CPL, CPV, CPVO,
  COTB, COTBT, COTBO, CDDT, CDDOT, CPRIME, CPPRIME, CNSB, CALLCD,
  JOLU, D, D1, D2, DDOT, DDDOT, DA, DIA2, DIA2I, DIA2O, DIA1, DIA1I,
  DIA1O, DAREAA, DBETAOZ, DELQ, DTLIO, DPRIME, DPPRIME, DZDT, DZOV,
  DELTAT, DYSUM, DELW, DW, DP, DT, DVV, CALLC, HMIN, HMAX, DELOS, DMF,
  PHIV, PHIT, PHIP, KETA, CETA, PHIG, GETA, CCRITSQ, OLOW, OLOVV,
  OLOP, OLOT, OLOZ, OLODELQ, OLODHGV, OLODPVN, OLODHGDT, OLOVZ,
  OLOTZ, OLOX, OLOV, OLDAREA, AMIN, ZMIN, PP, OLOGROUPS, TSTART,
  VSTARV, WSTARV, ASTARA, ERHORA, M2, T2, W2, VV2, A2, Z2, ZF, TSAT,
  PRANDTL, RECF, TR, TAMR, HAMR, SOA, REYNOLDS, HR, DYB, DYBO, RABS,
  YABS, DYABS, HABS, YB, YBO, YSURFACE, NATOMIZE, TF, SOAO, E, E1, G,
  GAMMA, H, HFG, J, JDOT, JCRIT, JINC, HG, HGO, HL, DHGDT,
  DHGUV, YEQUILIB, AHG, AHG1, AHG2, AHG3, AHL, AHL1, AHL2, AHL3, LETA,
  HETA, TD, TDS, DYDZ, XSTAR, PSTARP, ERRDT, PHIO, AA1, X2, OLOHFG,
  OLOUYDZ, OLODELTAT, SUSPEND, NOSURF, JO1, JO2, KV, K2, K4, K2PRIME,
  K2PRIMES, LENGTHB, LNPA, LAMDAO, LAMDA1, M, ML, MACH, NO, NEU,
  NEUV, NEFF, NIPRIME, NIPRIMES, NTOTAL, P, P1, PI, PS, POOT, PATM,
  PIS, PEFF, PXVN, PO, RELB, ABSB, PHI, RO, RI, RHOL, RCRIT, SINR,
  SIGMA, SIGMAO, TB, TBP, T, TZ, THICKB, THICKBO, THICKBMAX, TC, SMP,
  TLSUM, TL, TEMPO, TLOLD, UA, V, VV, VM, W, W2G, X, XC1, XC2, XCPVT,
  UAO, YSUMN, DYSUMN, YTOTAL, YSUM, BETAO, VZ, ETAP, RMEAN, ZCE, Z,
  ZO, Z1, ZC, GAMAJ;
FORMAT
  FEXTRA1(X25,"EXTRAPOLATION OUTPUT"/X15,"OLD",X25,"NEW"/X3,"Z",
    X11,E14.7,X14,E14.7/X3,"P",X11,E14.7,X14,E14.7/X3,"T",X11,E14.7,
    X14,E14.7/X3,"W",X11,E14.7,X14,E14.7/X3,"X",X11,E14.7,X14,E14.7/
    X3,"DELTAT",X6,E14.7,X14,E14.7/X3,"VV",X10,E14.7,X14,E14.7/))
LIST LEXTRA1(OLDZ, Z, OLOP, P, OLOT, T, OLOW, W, OLOX, X, OLODELTAT,
  DELTAT, OLOVV, VV);
FORMAT
  FTHICK("NEW THICKNESS = ",E14.7/))
LIST LEXTRAKETA, CETA, TSTART, VSTARV, WSTARV, ASTARA, CCRITSQ,
  GETA, A2, ZC, S);

```

```

FORMAT
  FEXTRA(X1,X8,"KETA",X8,"CETA",X8,"T*/T",X8,"V*/V",X8,"W*/W",X8,
    "A*/A",X2,"W-CRIT*2" //X1,7E12.4//X1,X8,"GETA",X10,"A2",X10,"ZC",
    ,X11,"S"/X1,4E12.4//);
FORMAT
  FEXTRA2(X10,
    "ATTEMPTED EXTRAPOLATION-MINIMUM AREA DOES NOT MATCH, RETURN TO INLET"
    //X10,"OLDZ WAS ",F15.5," OLDW WAS",F15.5//);
FORMAT
  FGEOM(X15," TURBINE GEOMETRY TABULATION"///"ROW",X3,"DIA.-IN",
    " HEIGHT-IN",X2,"DIA.-OUT",X2,"HEIGHT-O",X3,"ETAP",X3,"LENGTH",
    X1,"BETA-IN",X1,"BETAOUT",X1,"BLADESPACE",X3,"THICKBO UB",X1,
    "THICKBMAX"/(13,4F10.4,F7.3,F9.4,F8.2,F8.2,F11.4,F10.4,14,F10.4/
    /));
LIST GEOM(FOR S+ 1 STEP 1 UNTIL STAGES DO(S, DIAMI(S), HEIGHTI(S),
  DIAMO(S), HEIGHTO(S), ETAPI(S), LI(S), BETAIN(S), BETAOUT(S),
  BSPACE(S), THICKBOI(S), UB(S), THICKBMAXI(S)));
FORMAT
  FSUMY(X20,"SUMMARY OF RESULTS OF CONDENSATION CALCULATIONS"///
    "ROW",X7,"T",X7,"P",X6,"VV",X7,"W",X6,"UA",X7,"YE",X7,"YS",X8,
    "Y",X7,"RMEAN",X6,"NTOTAL"/(13,2F8.1,F8.2,2F8.1,3F9.5,2E12.4//)
    /);
LIST LSUMY(FOR S+ 0 STEP 1 UNTIL STAGES DO(S, OT(S), OP(S), OVV(S),
  OW(S), OUA(S), OYE(S), OYS(S), OY(S), ORMEAN(S), ONT(S)));
LIST LADAM(W, CALLC, HMAX, HMIN, RELB, ABSB);
LIST LMAIN1(UAO, TEMPO, PO, LENGTHB);
LIST LMAIN2(M, RO, KV, NEUV, JCRT, JINC, J, UB(S));
LIST LMAIN3(B1, B2, C1, C2, C3, D1, D2, E1);
LIST LMAIN4(ACPO, ACP1, ACP2, ARHO, ARH1, ARH2);
LIST LMAIN5(CPL, APS, APS1, APS2, AK2, AK21, AK4, AK41);
LIST LMAIN5A(AHG, AHG1, AHG2, AHG3, AHL, AHL1, AHL2, AHL3);
LIST LMAIN6(DIA1I, DIA1O, DIA2I, DIA2O, BETA1, BETA2, BLADESPACE,
  THICKBO);
LIST LMAIN6A(STAGES, FOR S+ 1 STEP 1 UNTIL STAGES DO(ROTOR(S), DIAMI
  (S), HEIGHTI(S), DIAMO(S), HEIGHTO(S), ETAPI(S), LI(S), UB(S),
  BETAIN(S), BETAOUT(S), BSPACE(S), THICKBOI(S), THICKBMAXI(S)));
LIST LMAIN7(THICKBMAX, PATM, TC, SMP, SIGMAO, ETAP, GROUPMAX);
LIST LMAIN7A(PATM, TC, SMP, SIGMAO, GROUPMAX);
LIST LMAIN8(OME, ERRORA, ERRDT, AA1, SUSPEND, NOSURF);
LIST LMAIN9(S, P, T, VV, UA, W);
LIST LMAIN11(TAMB, HAMB, RABS);
FORMAT
  FA2("A2=",E14.7);
LIST LRESTART(GROUPS, FOR I+ 1 STEP 1 UNTIL GROUPS DO(RLO(I), NL(I),
  , YSUM, TLOLD, VV);
FORMAT
  FMAIN1(X3,X26,"INPUT CONSTANTS AND PARAMETERS"//X3,X9,"UAO",X7,
    "TEMPO",X10,"PO",X6,"LENGTHB"/X3,4E12.4//);
FMAIN2(X3,X11,"M",X10,"RO",X10,"KV",X8,"NEUV",X3,"J-CRITICAL",X2,
    "JINCREMENT",X11,"J",X10,"UB"/X3,4E12.4//);
FMAIN3(X3,X10,"B1",X10,"B2",X10,"C1",X10,"C2",X10,"C3",X10,"D1",
    X10,"D2",X10,"E1"/X3,4E12.4//);
FMAIN4(X3,X8,"ACPO",X8,"ACP1",X8,"ACP2",X6,"ARHO",X7,"ARH1",X7,
    "ARH2"/X3,4E12.4//);
FMAIN5(X3,X9,"CPL",X9,"APS",X8,"APS1",X8,"APS2",X9,"AK2",X8,
    "AK21",X9,"AK4",X8,"AK41"/X3,4E12.4//);
FMAIN5A(X3,X9,"AHG",X8,"AHG1",X8,"AHG2",X8,"AHG3",X9,"AHL",X8,
    "AHL1",X8,"AHL2",X8,"AHL3"/X3,4E12.4//);
FMAIN6(X3,X7,"DIA1I",X7,"DIA1O",X7,"DIA2I",X7,"DIA2O",X7,"BETA1",
    X7,"BETA2",X2,"BLADESPACE",X5,"THICKBO"/X3,4E12.4//);
FMAIN9(X3,X9,"OME",X6,"ERRORA",X7,"ERRDT",X9,"AA1",X5,"SUSPEND",
    X6,"NOSURF"/X3,4E12.4//);
FMAIN10(X5,"XSTAR=",F12.6,X5,"DELTATSTAR=",F12.5,X2,"DYDZ=",F14.5
    /);
FMAIN11(X3,X4,"TAMBIENT",X4,"HAMBIENT",X8,"RABS"/X3,4E12.4//);
FMAIN7(X3,X3,"THICKBMAX",X8,"PATM",X10,"TC",X9,"SMP",X6,"SIGMAO",
    X8,"ETAP",X4,"GROUPMAX"/X3,7E12.4//);

```

```

FORMAT
FHESTART(X8,"GROUPS",X13,"I",X12,"RL",X12,"NL",X6,"MOISTURE",X7,
"TLIQUID",X12,"VV"/2J14,5E14.5/(X15,I14,2E14.7//));
FORMAT
FADAM(X25,"ICE-ADAMS PARAMETERS"/X5,X13,"H",X9,"CALLC",X10,
"HMAX",X6,"HMIN",X10,"RELR",X10,"ARSB"/X5,6F14.8//);
FORMAT
FAREA("AMIN=",E12.4,"ZMIN=",E12.4,"AEXIT=",E12.4);
FORMAT
FSTG(X5,X12,"PP",X12,"VV",X13,"T",X10,"CETA",X10,"GETA",X10,
"KETA",X6,"PHIP"/X5,7E14.5//);
FORMAT
FMAIN9(X15,"STATIC PROPERTIES AT INLET OF BLADE ROW NO.",I2//X1,
X11,"P",X11,"T",X10,"VV",X10,"UA",X11,"WW"/X1,5E12.4);
SS 8 ICEADAMS
COMMENT BEGIN ICE-ADAMS;
PROCEDURE BOXA(Z, Y, DY);
VALUE Z;
REAL Z;
ARRAY Y, DY[*];
BEGIN
LABEL LABELC, LABELG, SKIPGSTART, SKIPGROUPS, VANISH, GSTART;
COMMENT BEGIN Y TRANSLATION;
FOR N= 1 STEP 1 UNTIL GROUPMAX DO
BEGIN
N2= N+GROUPMAX;
NL[N]= Y[N];
RLD[N]= Y[N2];
END;
W= Y[EQNS-3];
P= Y[EQNS-2];
T= Y[EQNS-1];
VV= Y[EQNS];
COMMENT TURBINE DESCRIPTION;
DIA1= DIA1I+(DIA1O-DIA1I)*Z/LENGTHB;
DIA2= DIA2I+(DIA2O-DIA2I)*Z/LENGTHB;
THICKB, THICKBO, (THICKHMAX-THICKRO)*(1-Z/LENGTHB)*4*Z/LENGTHB;
AREAA= PI*(DIA2+2-DIA1+2)*(1-THICKB/BLADESPACE)/4;
DAREAA= 2*(DIA2*(DIA2O-DIA2I)-DIA1*(DIA1O-DIA1I))/(LENGTHB*(DIA2+
2-DIA1+2))-4*(THICKHMAX-THICKRO)*(1-2*Z/LENGTHB)/(LENGTHB*(
BLADESPACE-THICKH));
COTB= COTRI+(COTRO-COTBI)*Z/LENGTHB;
SINB= 1/SQRT(1+COTB+2);
DRETADZ=(SINB+2*(COTBO-COTBI)/LENGTHB)*COTB*(-1);
COMMENT ***** CALC AXIAL VELOCITY;
UA= W*SINB;
DA= DAREAA+DRETADZ;
COMMENT V IS FT*3/LH-MOLE;
V= VV*M;
COMMENT CALC Z AND CPV;
B=-EXP((B1+B2/T)/ML*LN(T));
C= EXP((C1+(C2+C3/T)/T)/ML);
D=-EXP((D1+D2/T)/ML);
E= E1;
BDDOT=((1-(B2)/(ML*T))/T);
CDDOT=((C2+2*C3/T)/(ML*T+2));
DDDOT=-D2/(T+2*ML);
BDDOT+((2*B2)/(ML*T)-1)/T+2;
CDDOT+((2*C2+6*C3/T)/(ML*T+3));
DDDOT+(2*D2)/(ML*T+3);
BPRIME= B*BDDOT;
BPPRIME= B*(BDDOT+2*BDDOT);
CPRIME= C*CDDOT;
CPPRIME= C*(CDDOT+2*CDDOT);
DPRIME= D*DDDOT;
DPPRIME= D*(DDDOT+2*DDDOT);
ZC= 1+(((E/V+D)/V+C)/V+B)/V;
DZDT=(((DPRIME)/V+CPPRIME)/V+BPRIME)/V;
DZDV=(((4*E/V+3*D)/V+2*C)/V+B)/V+2;

```

00000000

```

CPVO+ ACP0+ACP1*EXP(-ACP2/T)
XC1+(ZC+T*UZDT)*2/((5*E/V+4*D)/V+3*C)/V+2*R)/V+1)
XC2+((T*DPPRIME+2*DPRIME)/(3*V)+CPRIME+T*CPPRIME/2)/V+2*RPRIME+T*
  BPPRIME)
CPV+ CPVO-(R0/(M*J))*(1-XC1+T*XC2/V)
HGO+ AHG+AHG1*T+AHG2*EXP(-AHG3/T)
DHG00T+ AHG1+AHG2*AHG3*EXP(-AHG3/T)/T+2
DHGDV+(R0*T/V)*(UZDV+T*((DPRIME/V+CPRIME)/V+BPRIME)/V+2)/J
DHGDT+ DHG00T+(R0*T/M)*(UZDT+(ZC-1)/T-2*((DPRIME/(3*V)+CPRIME/2)/
  V+BPRIME)/V-T*((DPPRIME/(3*V)+CPPRIME/2)/V+BPPRIME)/V)/J
COMMENT CALC RHOL,HFG,AND SIGMA
HG+ HGO+(R0*T/M)*(ZC-1)-T*((DPRIME/(3*V)+CPRIME/2)/V+BPRIME)/V)/J
HL+ AHL+AHL1*T+AHL2*T+2+AHL3*T+3
HFG+(HG-HL)
RHOL+ ARH0+ARH01*T+ARH02*T+2
SIGMA+ SIGMA0*(1-T/TC)*SMP
COMMENT CALC SATURATION PRESSURE AND T
PS+ EXP((APS+APS1/T)/ML+APS2*LN(T)+LNPA)
LAMBDA0+ LN(P/PS)
DELTAT+ LAMBDA0*T/(APS2-LAMBDA0-APS1/(ML*T))
COMMENT CALC OF ASSOCIATION AT P AND T
K2+ EXP((AK2+AK21/T)/ML)
K4+ EXP((AK4+AK41/T)/ML)
K2PRIME+ K2+K4*(P/PATM)*2*(3-2*K2*P/PATM)
N1PRIME+(SQRT(1+4*P*K2PRIME/PATM)-1)/(2*P*K2PRIME/PATM)
P1+ P*N1PRIME
COMMENT CALC OF ASSOCIATION AT PS AND T
K2PRIMES+ K2+K4*(PS/PATM)*2*(3-2*K2*PS/PATM)
N1PRIMES+(SQRT(1+4*PS*K2PRIMES/PATM)-1)/(2*PS*K2PRIMES/PATM)
P1S+ PS*N1PRIMES
LAMBDA1+ LN(P1/P1S)
COMMENT SURFACE CONDENSATION
PRANDTL+ NEUV*CPV/(KV*G*V)
TSAT+ T+DELTAT
RECF+ PRANDTL*(1/3)
TR+ T+RECF*x*2/(2*G*J*CPV)+NOSURF*TSAT
IF TSAT>TR THEN
  BEGIN
    TF+(BLADESPACE-THICKB)/12
    SOA+ 2/(TF*SINH)
    SOAU+ 12/BLADESPACE
    REYNOLDS+ 2*TF*x/NEUV
    HB+ 0.023*KV*REYNOLDS*0.8*PRANDTL*0.4/(2*TF)
    DYB+ SOA*HB*VV*(TSAT-TR)/(HFG*UA)
    DYB0+(SOA*HB*VV/(HFG*UA))*((TSAT-TR+HAMB*(TSAT-TAMB))/HB)
  END
ELSE
  DYB+ DYB0+ 0
IF DELTAT>0 THEN
  BEGIN
    HABS+ KV/(HABS+2.39*NEUV/SQRT(G*R0*T/M))
    DYABS+ 3*YABS*DELTAT*HABS/(RAHS*RHOL*HFG*UA)
  END
COMMENT WHEN P1/P1S < 0 VAPOR IS SUPERHEATED
IF LAMBDA1<0 THEN
  IF CASE[1]=0 THEN
    GO TO SKIPGROUPS
  ELSE
    BEGIN
      RCRIT+ 0
      GO TO LABELC
    END

```

```

COMMENT      CALC OF NUCLEATION RATE,
NEFF= NO;
PEFF= P1+2*(P-P1)*SQRT(2);
RCRIT= 2*SIGMAXM/(RHOL*RO*T*LAMBDA1);
Z0= NEFF*SQRT(2*G*SIGMAXM/PI)/(RHOL*(RO*T)+2);
Z1= 16*PI*NO*(SIGMAXM/(RO*T))+3/(3*RHOL+2*M);
JDOT= P*PEFF*Z0*EXP(-Z1*0.5/LAMBDA1+2)*EXP(-Z1*0.5/LAMBDA1+2);
IF CASE[1]=0 THEN
  GO TO SKIPGROUPS;
NEU= JDOT*VVX/UA;
LABELC:
COMMENT      CALC OF DROP GROWTH AND NUMBER;
IF GROUPS<2 THEN
  GO TO GSTART;
FOR I= 1 STEP 1 UNTIL GROUPS-1 DO
  BEGIN
    RI= RL[I]+ RLO[I]+RLD[I];
    IF LAMBDA1<0.1 THEN
      GO TO LABELG;
    IF RI<0.5*RCRIT THEN
      BEGIN
        NL[I]= DRLO[I]+ RLD[I]+ RLO[I]+ 0;
        GO TO VANISH;
      END;
    IF RI>0 THEN
      BEGIN
        DTL[I]=(1-RCRIT/RI)*DELTA1;
        DRLO[I]= KX*DTL[I]/((1+2.38*NEUV/(RI*SQRT(G*RO*T/M)))
          *(UA*RHOL*RI*HFG));
      END;
    DNL[I]= 0;
    WR[I]= 4*PI*RHOL*RI+3/3;
    MY[I]= WR[I]*NL[I];
    DMY[I]= 4*PI*RHOL*RI+2*DRLO[I]*NL[I];
  END;
GSTART: I= GROUPS;
IF CASE[I]=0 THEN
  DRLO[I]= DMY[I]+ DNL[I]+ 0;
ELSE
  BEGIN
    DRLO[I]= 0;
    DNL[I]= NEU;
    RL[I]= RLO[I]+RLD[I];
    WR[I]= 4*PI*RHOL*RI+3/3;
    DMY[I]= WR[I]*DNL[I];
    MY[I]= WR[I]*NL[I];
  END;
SKIPGSTART: FOR I= GROUPS+1 STEP 1 UNTIL GROUPMAX DO
  DRLO[I]= DMY[I]+ DNL[I]+ 0;
YSUM= DYSUM+ TLSUM+ DYSUMN+ YSUMN+ 0;
FOR I= 1 STEP 1 UNTIL GROUPS DO
  BEGIN
    DYSUMN= DYSUMN+DMY[I];
    YSUMN= YSUMN+MY[I];
    TLSUM= TLSUM+MY[I]*DTL[I];
  END;
SKIPGROUPS: DYSUM= DYSUMN+DYB+DYBO+DYARS;
YSUM= YSUMN+YB+YBO+YABS;

TL= IF YSUM=0 THEN T ELSE T+TLSUM/YSUM;
DTLIQ=(TL-TLOLD)/H;
X= 1-YSUM;

```

```

COMMENT      FLOW EQUATIONS;
TZ= 1+T*NDZDT/ZC;
VZ= 1-V*NDZDV/ZC;
PXVN= PXX*VV*ETAP;
XCPVT= X*CPV*TX;
W2G= W*2/G;
DELO= PXVN*(W2G*TZ/J+X*TX*VZ*DHGDT+TZ*X*V*DHGDV)-W2G*X*TX*DHGDT;
DELOS= DELO/(PXVN*(X*TX*VZ*DHGDT+TZ*X*V*DHGDV));
IF DELOS<DME AND Z<ZMIN*LENGTHR THEN
  GO TO CHECKSTAR;
DELM= PXVN*((HFG*OYSUM-YSUM*CPL*DTLIQ)*TZ+(-DA-OYSUM/X)*(X*TX*VZ*
  DHGDT+X*TX*V*DHGDV));
DW=(DELM/DELO)*W;
DVV= VV*(DW/W+DAREAA+DBETADZ+OYSUM/X);
DP=-P*(W2G/PXVN)*DW/W;
DT= TX*(DP/P+VZ*DVV/VV)/TZ;
COMMENT      BEGIN INVERSE Y TRANSLATION;
FOR N= 1 STEP 1 UNTIL GROUPMAX DO
  BEGIN
    N2= N+GROUPMAX;
    Y[N]= NL[N];
    Y[N2]= RL[N];
    DY[N]= ONL[N];
    DY[N2]= ORL[N];
  END;
  Y(EQNS-3)= W;
  DY(EQNS-3)= DW;
  Y(EQNS-2)= P;
  DY(EQNS-2)= DP;
  Y(EQNS-1)= T;
  DY(EQNS-1)= DT;
  Y(EQNS)= VV;
  DY(EQNS)= DVV;
COMMENT      END INVERSE TRANSLATION;
END BOXA;
PROCEDURE BOXB(Z, Y, DY);
VALUE Z;
REAL Z;
ARRAY Y, DY[*];
BEGIN
  LABEL ALLSAME;
  IF JDOT<JCRT AND CASE[1]=0 THEN

    GO TO ALLSAME;
  IF WILSONO THEN
    WILSON= IF JDOT>JCRT AND JDOT>JO2 AND JDOT>JO1 AND JDOT>JOLO
      THEN FALSE ELSE TRUE
  ELSE
    WILSON= IF JDOT<JOLO AND JDOT<JO1 AND JDOT<JO2 THEN TRUE ELSE
      FALSE;
  IF WILSONO THEN
    BEGIN
      IF WILSON THEN
        GO TO ALLSAME
      ELSE
        BEGIN
          I= GROUPS;
          CASE[I]= 1;
          JS[I]= JDOT;
          RLO[I]= JCRT;
          GO TO ALLSAME;
        END;
    END;

```



```

      END
    ELSE
      IF WILSON THEN
        BEGIN
          GROUPS+ GROUPS+1;
          GO TO ALLSAME;
        END;
      I+ GROUPS;
      IF JOUT>JS[I]*JINC THEN
        BEGIN
          GROUPS+ GROUPS+1;
          I+ GROUPS;
          CASE[I]+ 1;
          JS[I]+ JOUT;
          RLQ[I]+ RCHIT;
        END;
      ALLSAME: IF GROUPS>GROUPMAX THEN
        GROUPS+ GROUPMAX;
        YB+ YB+H*DYB;
        YBQ+ YBQ+H*DYBQ;
        YABS+ YABS+H*DYABS;
        YSURFACE+ YB+YBQ+YABS;
        NATOMIZE+ 3*YABS/(4*PI*RHOL*RABS+3);
        JQ2+ JQ1;
        JU1+ JQ1;
        WILSOND+ WILSON;
        JQ1D+ JQ1;
        TLOLD+ TL;
        COUNT+ COUNT+1;
        OLDW+ W;
        OLDVV+ VV;
        OLDOP+ P;
        OLDOT+ T;
        OLDZ+ Z;
        OLDELLOS+ DELOS;
        OLDDHGOV+ DHGOV;
        OLDPXVN+ PXVN;
        OLDDHGD+ DHGD;
        OLDDVZ+ VZ;
        OLDDTZ+ TZ;
        OLDGX+ X;
        OLDDV+ V;
        OLDDAREA+ AREA*XSINB;
        OLDDDELTA+ DELTA;
        OLDDHFG+ HFG;
        OLDDYDZ+ 0;
        FOR I+ 1 STEP 1 UNTIL GROUPS-1 DO
          OLDDYDZ+ OLDDYDZ+DMY[I];
        END BOXB;
        PROCEDURE BOXC(Z, Y, DY);
        VALUE Z;
        REAL Z;
        ARRAY Y, DY(+);
        BEGIN
          FORMAT
            FC1(X5,X13,"P",X13,"T",X3,"SP. VOL.-V",X13,"W",X7,"U-AXIAL",X3
              ,"Z-COMPRESS"/X5,6E14,5//);
          FORMAT
            FC2(X5,X12,"DP",X12,"UT",X12,"DV",X12,"DW",X4,"-(UP/DT)/P",X10
              ,"ARFAA",X9,"DA/A"/X5,7E14,5//);
          FORMAT
            FC3(X5,X8,"DELTA",X7,"TLIQUID",X7,"LAMBDA0",X7,"LAMBDA1",X10,
              "JOUT",X5,"RCRITICAL",X9,"DN/DZ"/X5,7E14,5//);

```

```

FORMAT
FC4(X5,X12,"K2",X12,"K4",X7,"K2PRIME",X11,"HFG",X10,"CPV0",X11
,"CPV",X9,"SIGMA"/X5,7E14.5//);
FORMAT
FC5(X5,"TOTAL MOISTURE",X4,"PARTIAL P1",X7,"QUALITY",X3,
"MEAN RADIUS",X3,"TOTAL DROPS",X3,"K2PRIME SAT",X7,"SINBETA"/
X5,7E14.5//);
FORMAT
FC5A(X5,X5,"Y=EQUILIB",X12,"HG",X12,"HL",X11,"HFG",X10,"DELO",
X10,"DELW",X9,"1-M*2"/X5,7E14.5//);
FORMAT
FC0(X5,X9,"COUNT",X3,"STEP SIZE H",X13,"Z"/X5,114,2E14.7//);
FORMAT
FC6(X5,X9,"GROUP",X6,"MOISTURE",X9,"NUMBER",X8,"RADIUS",X5,
"DMOISTURE",X7,"DNUMBER",X7,"DRADIUS"/X5,114,6E14.7//);
FORMAT
FC7(X5,X4,"YB=Y BLADE",X4,"YB0=Y CASE",X1,"YABS=YATOMIZED",X5,
"YSURFACE",X6,"NATOMIZE"/X5,5E14.5//);
LIST LC7(YB, YB0, YABS, YSURFACE, NATOMIZE);
LIST LC6(FOR I= 1 STEP 1 UNTIL GROUPPRINT DO(I, MY(I), NL(I), RL(
I), DM(I), DNL(I), DR(L(I)));
COMMENT CALCULATE PDOT,NTOTAL,MEANRADIUS;
GROUPPRINT= IF GROUPS<GROUPMAX THEN GROUPS+1 ELSE GROUPMAX;
YEQUILIB= YSUM+CPV*DELTAT/HFG;
PDOT=-(DP/P)*UA;
NTOTAL= YTOTAL+ 0;
FOR I= 1 STEP 1 UNTIL GROUPS=1 DO
BEGIN
NTOTAL= NTOTAL+NL(I);
YTOTAL= YTOTAL+MY(I);
END;
IF NTOTAL>0 THEN
RMEAN=(3*YTOTAL/(4*PI*RHOL*NTOTAL))*0.3333333;
WRITE(PRINT,PAGE);
WRITE(PRINT,FC0,COUNT,H,Z);
WRITE(PRINT,FC1,P,T,VV,W,UA,ZC);
WRITE(PRINT,FC2,DP,DT,DVV,DW,PDOT,AREAA,DA);
WRITE(PRINT,FC3,DELTAT,TL,LAMBDAO,LAMBDA1,JDOT,RCRIT,NEU);
WRITE(PRINT,FC4,K2,K4,K2PRIME,HFG,CPV0,CPV,SIGMA);
WRITE(PRINT,FC5,YSUM,P1,X,RMEAN,NTOTAL,K2PRIME,SINB);
WRITE(PRINT,FC5A,YEQUILIB,HG,HL,HFG,DELO,DELW,DELOS);
WRITE(PRINT,FC7,LC7);
WRITE(PRINT,FC6,LC6);
COUNT= 0;
CALLC= IF LENGTHB-Z<CALLC THEN(LENGTHB-Z) ELSE CALLC;
IF Z>LENGTHB THEN
BEGIN
YABS= YSURFACE;
YB= YB0+ 0;
DT(S)= T;
DP(S)= P;
DVV(S)= VV;
DM(S)= W;
QUA(S)= UA;
OYE(S)= YEQUILIB;
OYS(S)= YSURFACE;
OY(S)= YSUM;
ORMEAN(S)= RMEAN;
ONT(S)= NTOTAL;

```

```

      IF GROUPS>0 THEN
        FOR I= 1 STEP 1 UNTIL GROUPS DO
          RLD[I]= RL[I];
        COSB= COS(HTAO*PI/180);
        IF ROTQR[S]=0 THEN
          PHI= ARCTAN((WXCOSB-UB[S+1])/UA)*180/PI
        ELSE
          PHI= ARCTAN((WXCOSB+UB[S])/UA)*180/PI;
        BETAI= 90-PHI;
        S= S+1;
        IF S>STAGES THEN
          GO TO EXIT;
        BETAIN[S]= BETAI;
        GO TO NEWSTAGE;
      END;
END H0XC;
PROCEDURE H0XD(Z, Y, DY);
VALUE Z;
REAL Z;
ARRAY Y, DY[*];
BEGIN
  FORMAT
    F01(X5,"FAILED AT Z=",E15.5,X5,"H=",E15.5);
  FORMAT
    F02(//X5,X13,"P",X13,"T",X12,"VV",X13,"W",X7,"U-AXIAL",X6,
      "MACH",X3,"Z-COMPRESS"/X5,7E14.5//);
  FORMAT
    F03(X5,X12,"DP",X12,"DT",X11,"DVV",X12,"DW",X10,"DFLU",X10,
      "DELW",X10,"YSUM"/X5,7E14.5//);
  FORMAT
    F04(X5,"TL= ",E14.4,X5,"TLOLD= ",E14.4//);
  WRITE(PRINT, F01, Z, H);
  WRITE(PRINT, F02, P, T, VV, W, UA, MACH, ZC);
  WRITE(PRINT, F03, DP, DT, DVV, DW, DFLU, DELW, YSUM);
  WRITE(PRINT, F04, TL, TLOLD);
  GO TO EXIT;
END H0XD;
COMMENT MAIN PROGRAM ;

G= 32.17;
NO= 2.732E+26;
PI= 3.141592653;
ML= 0.434294482;
J= 778;
RO= 1545;
PATM= 2116.8;
READ(READER,/, H, CALLC, HMAX, HMIN, RELB, ABSB, DME, ERRORA, ERROT,
  AA1, RESTART, WILSOND, EXTRAPOLATED, SUSPEND, NOSURF, JCRIT, JINC,
  GROUPMAX, B1, B2, C1, C2, C3, D1, D2, E1, AK2, AK21, AK4, AK41,
  ACP0, ACP1, ACP2, ARH0, ARH01, ARH02, AHG, AHG1, AHG2, AHG3, AHL,
  AHL1, AHL2, AHL3, APS, APS1, APS2, M, TC, SIGMA0, SMP, CPL, KV,
  NEUV, TAMB, HAMB, RABS, UAD, PO, TEMPO);
READ(READER,/, LMAIN6A);
IF RESTART THEN
  READ(READER,/, LRESTART);
CLOSE(READER, RELEASE);
WRITE(PRINT(PAGE));
WRITE(PRINT, FGEOM, GEOM);
WRITE(PRINT(PAGE));
CALLCO= CALLC;
JS[0]= JCRIT/JINC;
LNPA= LN(PATM);
INITIAL: P= PO;
T= TEMPO;
UA= UAD;

```

```

COMMENT CALCULATE INITIAL SPECIFIC VOLUME;
IF RESTART THEN
  GO TO SKIPV;
ETAP= ETAPI(1);
K2= EXP((AK2+AK21/T)/ML);
K4= EXP((AK4+AK41/T)/ML);
K2PRIME= K2+K4*(P/PATM)*2*(3-2*K2*P/PATM);
N1PRIME=(SQRT(1+4*P*K2PRIME/PATM)-1)/(2*P*K2PRIME/PATM);
ZC= 1/(2-N1PRIME);
VV= ZC*RO*T/(P*M);
LABELV: V= VV*M;
B=EXP((B1+B2/T)/ML+LN(T));
C= EXP((C1+(C2+C3/T)/T)/ML);
D=EXP((D1+D2/T)/ML);
E= E1;
ZCE= 1+((E/V+D)/(V+C)/(V+B)/V);
IF ABS(ZCE-ZC)>0.0005 THEN
  BEGIN
    ZC= ZCE;
    VV= ZC*RO*T/(P*M);
    GO TO LABELV;
  END;
W= UAO/SIN(RETAIN(1)*PI/180);
VV= V/M;
X= 1-YSUM;
BDDT=(1-B2/(ML*T))/T;
BDDDT=((2*B2)/(ML*T)-1)/T+2;
CDDT=(C2+2*C3/T)/(ML*T+2);
CDDDT=(2*C2+6*C3/T)/(ML*T+3);
UDDT=-D2/(T+2*ML);
ODDT=(2*D2)/(ML*T+3);
BPRIME= B*BDDT;
BPPRIME= B*(BDDT+2+BDDDT);
CPRIME= C*CDDT;
CPPRIME= C*(CDDT+2+CDDDT);
DPRIME= D*ODDT;
UPPRIME= D*(ODDT+2+UDDT);
DZDT=((UPRIME)/(V+CPRIME)/(V+BPRIME)/V);
DZDV=-(((4*E/V+3*D)/(V+2*C)/(V+B)/V+2);
DHGDDT= AHG1+AHG2*AHG3*EXP(-AHG3/T)/T+2;
DHGDV=(RO*T/4)*(DZDV+T*((DPRIME)/(V+CPRIME)/(V+BPRIME)/V+2)/J);
DHGDT= DHGDDT+(RO*T/4)*(DZDT+(ZC-1)/T-2*((DPRIME)/(3*V)+CPRIME/2)/V+
  BPRIME)/V-T*((DPRIME)/(3*V)+CPPRIME/2)/V+BPPRIME)/V)/J;
PXVN= P*X*VV*ETAP;
TZ= 1+T*DZDT/ZC;
VZ= 1-V*UZDV/ZC;
PHIV= X*V*DHGDV*J/(PXVN);
PHIT=(T*X*DHGDT*J)/PXVN;
PHIP=(PHIV*TZ+PHIT*VZ)/(PHIV+VZ);
KETA= 1+(PHIV+VZ)/(PHIT-TZ);
CETA= X*DHGDT-X*V*DHGDV/((KETA-1)*T);
PHIG= X*(DHGDT*VZ+V*DHGDV*TZ/T);
GETA=(PHIG*M/RO)/(T*X*DHGDT/PXVN-TZ/J);
T= TEMPO-W*2/(2*G*J*CETA);
VV= VV*(T/TEMPO)*(1/(1-KETA));
V= VV*M;
PP= PD*(T/TEMPO)*PHIP;
B=EXP((B1+B2/T)/ML+LN(T));
C= EXP((C1+(C2+C3/T)/T)/ML);
D=EXP((D1+D2/T)/ML);
E= E1;
ZC= 1+((E/V+D)/(V+C)/(V+B)/V);
P= ZC*RO*T/(M*VV);
WRITE(PRINT, FSTG, PP, VV, T, CETA, GETA, KETA, PHIP);

```

```

SKIPV: S+ 0;
OT(S)+ T;
OP(S)+ P;
OVV(S)+ VV;
OW(S)+ W;
OUA(S)+ UA;
OYE(S)+ YEQUILIR;
OYS(S)+ YSURFACE;
OY(S)+ YSUM;
ORMEAN(S)+ RMEAN;
ONT(S)+ NTOTAL;
S+ 1;
BETAI+ BETAIN(1);
FOR I+ 1 STEP 1 UNTIL GROUPMAX DO
  BEGIN
    N2+ GROUPMAX+I;
    CASE(1)+ 0;
    F(N2)+ F(1)+ 0;
  END;
IF RESTART THEN
  FOR I+ 1 STEP 1 UNTIL GROUPS DO
    CASE(1)+ 1;
  IF RESTART THEN
    FOR I+ 1 STEP 1 UNTIL GROUPS DO
      BEGIN
        F(1)+ NL(1);
        N2+ I+GROUPMAX;
        F(N2)+ RLO(1);
        RLN(1)+ 0;
      END;
    GROUPD+ GROUPS;
  NEWSTAGE: Z+ 0;
  DIA1+ DIAMI(S)-HEIGHTI(S);
  DIA10+ DIAMO(S)-HEIGHTO(S);
  DIA2+ DIAMI(S)+HEIGHTI(S);
  DIA20+ DIAMO(S)+HEIGHTO(S);
  BETAU+ HETAOUT(S);
  BLADESPACE+ BSPACE(S);
  THICKRO+ THICKBOI(S);
  LENGTHB+ LI(S);
  ETAP+ ETAPI(S);
  THICKBMAX+ THI RMAXI(S);
  WRITE(PRINT(PAGE));
  WRITE(PRINT, FADAM, LADAM);
  WRITE(PRINT, FMAIN1, LMAIN1);
  WRITE(PRINT, FMAIN2, LMAIN2);
  WRITE(PRINT, FMAIN3, LMAIN3);
  WRITE(PRINT, FMAIN4, LMAIN4);
  WRITE(PRINT, FMAIN5, LMAIN5);
  WRITE(PRINT, FMAIN5A, LMAIN5A);
  WRITE(PRINT, FMAIN6, LMAIN6);
  WRITE(PRINT, FMAIN7, LMAIN7);
  WRITE(PRINT, FMAIN8, LMAIN8);
  WRITE(PRINT, FMAIN11, LMAIN11);
COMMENT CALC OF CONSTANTS AND INITIAL CONDITIONS;
SINB+ SIN(K2+ PI*BETAQ/180);
COTBU+ COS(K2)/SINB;
SINB+ SIN(K2+ PI*BETAI/180);
COTBI+ COS(K2)/SINB;
W+ UA/SINB;
EGNS+ 4+2*GROUPMAX;
FOR I+ 0 STEP 1 UNTIL 100 DO

```

```

BEGIN
  ZF= 1/100;
  DIA1= DIA1I+(DIA1D-DIA1I)*ZF;
  DIA2= DIA2I+(DIA2D-DIA2I)*ZF;
  THICKB= THICKB0+(THICKBMAX-THICKB0)*(1-ZF)*4*ZF;
  AREAA= PI*(DIA2*2-DIA1*2)*(1-THICKB/BLADESPACE)/4;
  COTB= COTBI+(COTB0-COTBI)*ZF;
  SINB= 1/SQRT(1+COTB*2);
  ASAVE(I)= AREAA*SINB;
  IF ZF=0 THEN
    AMIN= AREAA*SINB;
  IF AMIN>AREAA*SINB THEN
    BEGIN
      AMIN= AREAA*SINB;
      ZMIN= ZF;
    END;
  END;
  WRITE(PRINT, FAREA, AMIN, ZMIN, ASAVE(100));
  COMMENT INITIALIZATION BEGINS;
  ENTERICE: WRITE(PRINT(PAGE));
  WRITE(PRINT, FMAIN9, LMAIN9);
  FOR I= 1 STEP 1 UNTIL GROUPMAX DO
    BEGIN
      N2= GROUPMAX+I;
      OLDCASE(I)= CASE(I);
      F(N2)= RL(I);
      RLO(I)= 0;
      FI(I)= NL(I);
    END;
    F(EQNS=3)= W;
    F(EQNS=2)= P;
    F(EQNS=1)= T;
    F(EQNS)= VV;
    FOR I= 1 STEP 1 UNTIL EQNS DO
      OLOF(I)= FI(I);
      OLDGROUPS= GROUPS;
  LABELICE: CALLC= IF LENGTHB-Z<CALLC THEN(LENGTHB-Z) ELSE CALLC;
  ICEADAMS(EQNS, Z, H, CALLC, HMAX, HMIN, RELR, ARSH, F, BOXA, BOXB,
    BOXC, BOXD);
  CHECKSTAR;
  COMMENT THIS SECTION CHECKS AND CORRECTS INLET OR EXTRAPOLATES PAST
    THE THROAT TO SUPERSONIC CONDITION;
  BEGIN
    REAL MUMMY;
    LABEL M2CHANGE, REXS, SKIPZ, ADJUSTGEOMETRY, A2CHANGE;
    PHIV= OLOX*OLDV*OLDHGDV/J/OLDPXVN;
    PHIT= OLOT*OLDX*OLDHGDV/J/OLDPXVN;
    PHIP=(PHIV*OLDTZ+PHIT*OLDVZ)/(PHIV+OLDVZ);
    KETA= 1+(PHIV+OLDVZ)/(PHIT-OLDTZ);
    CETA= OLOX*OLDHGDV-OLDX*OLDV*OLDHGDV/((KETA-1)*OLDT);
    PHIG= OLOX*(OLDHGDV*OLDVZ+OLDV*OLDHGDV*OLDTZ/OLDT);
    GETA=(PHIG*M/RO)/(OLDT*OLDX*OLDHGDV/OLDPXVN-OLDTZ/J);
    CCRITSQ= G*GETA*H0*OLDT/M;
    PHIO= OLOT*OLDVZ*OLDHGDV+OLDV*OLDTZ*OLDHGDV;
    LETA= J*OLDHFG*OLDX/(OLDPXVN*(PHIT-OLDTZ));
    HETA= OLDHFG-LETA*OLDV*OLDHGDV/(KETA-1);
    TD= OLDDELTA;
  REXS: DYDZ=(OLDYDZ*TD/OLDDELTA)*XSUSPEND;
    XSTAR= OLOX-DYDZ*(ZMIN*LENGTHB-OLDZ);
    TSTART=(1+OLDW*2/(2*G*J*CETA*OLDT)+HETA*(OLDX-XSTAR)/(CETA*OLDT))
      /(1+RO*GETA/(2*G*J*CETA));
    VSTARV=(TSTART*(XSTAR/OLDX)+LETA)*(1/(1-KETA));
    PSTARP=(TSTART)*OLDTZ*VSTARV*(-OLDVZ);

```

```

WSTARW+ SQRT(CCRITSQ*XTSTART)/OLDW;
ASTARA+ VSTARV*XTSTAR/(WSTARW*OLDX);
T+ OLDT*XTSTART;
PS+ EXP((APS+APS1/T)/ML+APS2*LN(T)+LNPA);
LAMBDA0+ LN(PSTAR*OLDP/PS);
DELTAT+ LAMBDA0*T/(APS2-LAMBDA0-APS1/(ML*T));
TDS+(OLDDDELTAT+DELTAT)/2;
IF ABS((TDS-TD)/OLDDDELTAT)>ERRDT THEN
  BEGIN
    TD+ TDS;
    GO TO REXS;
  END;
WRITE(PRINT,PAGE);
WRITE(PRINT, FMAIN10, XSTAR, DELTAT, OLDDYDZ);
IF EXTRAPOLATED THEN
  GO TO ADJUSTGEOMETRY;
IF ABS(ASTARA-AMIN/OLDAREA)>ERRORA THEN
  BEGIN
    UAO+ UAO*AMIN/(ASTARA*OLDAREA);
    WRITE(PRINT, FEXTRA2, OLDZ, OLDW);
    GROUPS+ 0;
    FOR I+ 1 STEP 1 UNTIL GROUPMAX DO
      RL(I)+ CASE(I)+ NL(I)+ 0;
    WILSON+ FALSE;
    GO TO INITIAL;
  END;
EXTRAPOLATED+ TRUE;
OLDAREA+ AMIN/ASTARA;
IF ZMIN<0.98 AND ASAVE(100)/AMIN>1.01 THEN
  BEGIN
    A2+(1+AA1)*AMIN;
    FOR I+ 100*ZMIN STEP 1 UNTIL 100 DO
      IF ASAVE(I)-A2>0 THEN
        BEGIN
          Z2+((I-(ASAVE(I)-A2)/(ASAVE(I)-ASAVE(I-1)))/100)*
            LENGTHB;
          X2+ XSTAR-SUSPEND*(DYDZ*(1-ZMIN)*LENGTHB)*DELTAT/
            OLODELTAT;
          M2+ SQRT(2*(AA1)/(3-KETA))+1;
          GO TO M2CHANGE;
        END;
      END;
    M2+ IF ASAVE(100)>AMIN THEN 1+SQRT(2*(ASAVE(100)/AMIN-1)/(3-
      KETA)) ELSE 1;
    Z2+ LENGTHB;
    X2+ SUSPEND*OLDYDZ*(1-ZMIN)*LENGTHB*DELTAT/OLODELTAT+XSTAR;
    M2CHANGE: T2+ OLDT*(1+OLDW*2/(2*GX*J*OLDT*CETA)+HETA*(OLDX-X2)/(CETA*
      OLDT))/(1+GETA*RO*M2*2/(2*M*J*CETA));
    M2+ M2*SQRT(GETA*RO*GX*T2/4);
    VV2+ OLDVV*((T2/OLDT)*(X2/OLDX)+LETA)*(1/(1-KETA));
    A2+ OLDAREA*OLDW*VV2*X2/(OLDVV*OLDX*M2);
    WRITE(PRINT, FA2, A2);
    IF ZMIN<0.98 AND ASAVE(100)/AMIN>1.01 THEN
      BEGIN
        IF (A2-AMIN*(1+AA1))/A2>ERRORA THEN
          BEGIN
            M2+ 1+(M2-1)*SQRT(AMIN*AA1/(A2-AMIN))*0.99;
            GO TO M2CHANGE;
          END;
        FOR I+ 100*ZMIN STEP 1 UNTIL 100 DO
          BEGIN
            IF ASAVE(I)-A2>0 THEN

```

```

      BEGIN
        Z2=((I-(ASAVE[I]-A2))/(ASAVE[I]-ASAVE[I-1]))/100
        )*LENGTHB;
        GO TO SKIPZ;
      END
    ELSE
      Z2= LENGTHB;
    END;
SKIPZ:  Z= Z2;
        T= T2;
        W= W2;
        VV= VV2;
        V= M*VV;
        B=-EXP((B1+B2/T)/ML+LN(T));
        C= EXP((C1+(C2+C3/T)/T)/ML);
        D=-EXP((D1+D2/T)/ML);
        E= E1;
        ZC= 1+(((E/V+D)/V+C)/V+B)/V;
        P= ZC*R0*T/V;
        PS= EXP((APS+APS1/T)/ML+APS2*LN(T)+LNPA);
        LAMBDAA= LN(P/PS);
        DELTAT= LAMBDAA*T/(APS2-LAMBDAA-APS1/(T*ML));
        X= X2;
        YSUM= 1-X2;
        IF OLDX<1 THEN
          BEGIN
            FOR I= 1 STEP 1 UNTIL GROUPS-1 DO
              RL[I]= RL[I]*((1-X2)/(1-OLDX))*(1/3);
              YB= YB*(1-X2)/(1-OLDX);
              YB= YB*(1-X2)/(1-OLDX);
              YABS= YABS*(1-X2)/(1-OLDX);
            END;
            TLSUM= 0;
            FOR I= 1 STEP 1 UNTIL GROUPS-1 DO
              BEGIN
                MY[I]= NL[I]*4*PI*RHQ*RL[I]*2*(RL[I]-RCRIT)*DELTAT/3
                ;
                TLSUM= TLSUM+MY[I];
              END;
            TLOLD= TL= IF YSUM=0 THEN T ELSE T+TLSUM/YSUM;
            WRITE(PRINT,PAGE);
            WRITE(PRINT, FEXTRA1, LEXTRA1);
            WRITE(PRINT, FEXTRA, LEXTRA);
            GO TO ENTERICE;
          END;
        SINB= COS(PI*BETA0/180)/COTB0;
        Z= 0;
        T= T2;
        W= W2;
        VV= VV2;
        V= M*VV;
        B=-EXP((B1+B2/T)/ML+LN(T));
        C= EXP((C1+(C2+C3/T)/T)/ML);
        D=-EXP((D1+D2/T)/ML);
        E= E1;
        ZC= 1+(((E/V+D)/V+C)/V+B)/V;
        P= ZC*R0*T/V;
        PS= EXP((APS+APS1/T)/ML+APS2*LN(T)+LNPA);
        LAMBDAA= LN(P/PS);
        DELTAT= LAMBDAA*T/(APS2-LAMBDAA-APS1/(T*ML));
        X= X2;
        YSUM= 1-X2;
        IF OLDX<1 THEN

```



```

BEGIN
  FOR I= 1 STEP 1 UNTIL GROUPS=1 DO
    RL(I)= RL(I)*((1-X2)/(1-OLDX))*(1/3);
    YABS= YSURFACE+ YSURFACE*(1-X2)/(1-OLDX);
    YB= YB0+ 0;
  END;
  UA= HXSINB;
  OT(S)= T;
  OP(S)= P;
  OV(S)= VV;
  OW(S)= W;
  OUA(S)= UA;
  OYE(S)= YEQUILIB;
  OYS(S)= YSURFACE;
  OY(S)= YSUM;
  ORMEAN(S)= RMEAN;
  ONT(S)= NTOTAL;
  COSB= COS(SETAO*PI/180);
  IF ROTOR(S)=0 THEN
    PHI= ARCTAN((WxCOSB-UB(S+1))/(WXSINB))*180/PI
  ELSE
    PHI= ARCTAN((WxCOSB+UB(S))/(WXSINB))*180/PI;
    BETAI= 90-PHI;
    S= S+1;
    WRITE(PRINT,PAGE);
    WRITE(PRINT, FEXTRA1, LEXTRA1);
    WRITE(PRINT, FEXTRA, LEXTRA);
    IF S>STAGES THEN
      GO TO EXIT;
    BETAIN(S)= BETAI;
    TLSUM= 0;
    FOR I= 1 STEP 1 UNTIL GROUPS=1 DO
      BEGIN
        MY(I)= NL(I)*4*PI*HOL*RL(I)+2*(RL(I)-RCRIT)*DELTA/3;
        TLSUM= TLSUM+MY(I);
      END;
    TLOD= TL+ IF YSUM=0 THEN T ELSE T+TLSUM/YSUM;
    GO TO NEXTSTAGE;
  ADJUSTGEOMETRY: IF ABS(AMIN/OLDAREA-ASTAR)>ERRORA THEN
    BEGIN
      TB=(THICKBMAX-THICKB0)*ZMIN*(1-ZMIN)*4+THICKB0;
      TBP= TB-0.7*(ASTAR*OLDAREA/AMIN-1)*(BLADESPACE-TB);
      THICKBMAX= THICKB0+((TBP-THICKB0)/(ZMIN*(1-ZMIN)))/4;
      WRITE(PRINT, FTHICK, THICKBMAX);
      IF THICKBMAX<0 THEN
        BEGIN
          GO TO EXIT;
        END;
      FOR I= 1 STEP 1 UNTIL EGNS DO
        F(I)= OLDF(I);
      GROUPS= OLDGROUPS;
      FOR I= 1 STEP 1 UNTIL GROUPMAX DO
        CASE(I)= OLDCASE(I);
      Z= 0;
      GO TO LABELICE;
    END
  ELSE
    BEGIN
      M2= IF ASAVE[100]>AMIN THEN 1+SQRT(2*((ASAVE[100]/AMIN-1))/(3-KETA)) ELSE 1;
      Z2= LENGTH;
      X2=-SUSPEND*OLDYD/(1-ZMIN)*LENGTH*DELTA/OLDDELTA+YSTAR;
    A2CHANGE: T2= OLDOT*(1+OLDW+2/(2*GX*J*OLDT*CETA))+HETA*(OLDX-X2)/(CETA*
      OLDOT)/(1+GETA*RO*2+2/(2*GX*J*CETA));

```

```

W2+ M2*SQRT(GETA*RO*G*T2/M);
VV2+ OLDVV*((T2/OLDT)*(X2/OLDX)+LETA)*(1/(1-KETA));
OLDAREA+ AMIN/ASTARA;
A2+ OLDAREA*OLDW*VV2*X2/(OLDVV*OLDX*W2);
WRITE(PRINT, FA2, A2);
IF(A2-ASAVE(100))/A2>ERRORA THEN
  BEGIN
    M2+ 1+(M2-1)*SQRT((ASAVE(100)-AMIN)/(A2-AMIN))*0.9951
    GO TO A2CHANGE;
  END;
SINB+ COS(PI*BETA0/180)/COTB0;
Z+ 0;
T+ T2;
W+ W2;
VV+ VV2;
V+ M*VV;
B+ EXP((B1+B2/T)/ML+LN(T));
C+ EXP((C1+(C2+C3/T)/T)/ML);
D+ EXP((D1+D2/T)/ML);
E+ E1;
ZC+ 1+(((E/V+D)/V+C)/V+B)/V;
P+ ZC*RO*T/V;
PS+ EXP((APS+APS1/T)/ML+APS2*LN(T)+LNPA);
LAMBDA0+ LN(P/PS);
DELTAT+ LAMBDA0*T/(APS2-LAMBDA0-APS1/(T*ML));
X+ X2;
YSUM+ 1-X2;
IF OLDX<1 THEN
  BEGIN
    FOR I+ 1 STEP 1 UNTIL GROUPS DO
      RL[I]+ RL[I]*((1-X2)/(1-OLDX))*(1/3);
      YABS+ YSURFACE+ YSURFACE*(1-X2)/(1-OLDX);
      YB+ YB0+ 0;
    END;
    UA+ W*SINB;
    YEQUILIB+ YSUM+CPV*DELTAT/HFG;
    OT[S]+ T;
    OP[S]+ P;
    OVV[S]+ VV;
    OW[S]+ W;
    OUA[S]+ UA;
    OYE[S]+ YEQUILIB;
    OYS[S]+ YSURFACE;
    OY[S]+ YSUM;
    ORMEAN[S]+ RMEAN;
    ONT[S]+ NTOTAL;
    COSB+ COS(BETA0*PI/180);
    IF ROTOR[S]=0 THEN
      PHI+ ARCTAN((W*COSB-UB[S+1])/(W*SINB))*180/PI
    ELSE
      PHI+ ARCTAN((W*COSB+UB[S])/(W*SINB))*180/PI;
    BETA1+ 90-PHI;
    S+ S+1;
    TLSUM+ 0;
    FOR I+ 1 STEP 1 UNTIL GROUPS-1 DO
      BEGIN
        MY[I]+ NL[I]*4*PI*RHOL*RL[I]+2*(RL[I]-RCRIT)*DELTAT/3
        ;
        TLSUM+ TLSUM+MY[I];
      END;
  END;

```

```

      TLOLD= TL+ IF YSUM=0 THEN T ELSE T+TLSUM/YSUM;
      WRITE(PRINT, FEXTRA1, LEXTRA1);
      WRITE(PRINT, FEXTRA, LEXTRA);
      IF S>STAGES THEN
        GO TO EXIT;
      BETAIN(S)= BETAI;
      GO TO NEWSTAGE;
    END;
  END;
EXIT: WRITE(PRINT(PAGE));
      WRITE(PRINT, FGEOM, GEOM);
      WRITE(PRINT(PAGE));
      WRITE(PRINT, FSUMY, LSUMY);
END.

```

## APPENDIX 2.2B

### LISTING OF ICEADAMS INTEGRATION PROCEDURE

```

PROCEDURE ICEADAMS(N,T,H,CALLC,HMAX,HMIN,RELB,ABSB,XO,
  BOXA,BOXB,BOXC,BOXD);
  COMMENT
  N=NO. OF EQUATIONS,
  T=INDEPENDENT VARIABLE, SET IT=INITIAL T WHEN ICEADAMS IS FIRST CALLED,
  H=STEP SIZE, SET IT = SUGGESTED STEP SIZE WHEN ICEADAMS FIRST CALLED,
  CALLC= CHANGE IN T BETWEEN CALLS ON BOXC,
  HMAX=MAXIMUM STEP SIZE ACCEPTABLE,
  HMIN=MINIMUM STEP SIZE ACCEPTABLE,
  RELB=MAXIMUM ACCEPTABLE RELATIVE ERROR,
  ABSB=MAXIMUM ACCEPTABLE ERROR,
  XO=VECTOR OF INITIAL VALUES OF DEPENDENT VARIABLES,
  BOXA(T,X,F)=PROCEDURE GIVING THE XDUT VECTOR, IN F, WHEN CALLED WITH THE
    CURRENT VALUES OF THE VECTOR X OF DEPENDENT VARIABLES AND THE
    INDEPENDENT VARIABLE T,
  BOXB(T,X,F)=PROCEDURE CALLED AFTER EACH SUCCESSFUL INTEGRATION STEP,
  BOXC(T,X,F)=PROCEDURE CALLED AFTER T HAS INCREASED BY "CALLC" SINCE
    BEGINNING OF ICEADAMS OR SINCE BOXC WAS LAST CALLED,
  BOXD(T,X,F)=PROCEDURE CALLED WHEN SUCCESSFUL INTEGRATION STEP CANNOT BE
    MADE WITHOUT REDUCING STEP SIZE BELOW HMIN;
  COMMENT ADAMS SOLVES A SYSTEM OF FIRST ORDER DIFFERENTIAL EQUATIONS BY A
    4TH ORDER ADAMS P-C METHOD. STARTING IS BY RUNGE-KUTTA;
  COMMENT
  NEI AND GEIL J
  VALUE RELB,ABSB,HMIN,N;
  INTEGER N;
  REAL T,H,CALLC,RELB,ABSB,HMAX;
  REAL HMIN;
  ARRAY XO(*);
  PROCEDURE BOXA,BOXB,BOXC,BOXD;
  BEGIN
    INTEGER I,J,A,K;
    REAL ABSTEST,BOUND,D1,D2,FACTOR,LB,RELTEST,ITEMP;
    LABEL S11,S22,S33,S44,S55,S66,RETN;
    ARRAY X,K,F(0:15,0:N),E,XP(0:N);
    COMMENT SET UP INITIAL VALUES;
    FOR I=1 STEP 1 UNTIL N DO
      X(I,1)=XO(I);
      BOUND=T+CALLC = .01*HMIN;
      RELTEST=14.2*RELB;

```

```

ARSTEST*14.2*ARSH;
FACIOR=RELR/ABSE;
LR=RETEST/200;
H*2.0*H;
COMMENT RUNGA-KUTTA STARTING METHOD;
S11:A*2;
B*2;
S22:FOR J=A STEP 1 UNTIL B DO
BEGIN
  BOXA(T,X(J-1,*),F(J-1,*));
  FOR I=1 STEP 1 UNTIL N DO
  BEGIN
    K(1,I)+H*F(J-1,I);
    X(J,I)+X(J-1,I)+0.5*K(1,I) END;
    TTEMP=T+0.5*H;
    BOXA(TTEMP,X(J,*),F(J,*));
    FOR I=1 STEP 1 UNTIL N DO
    BEGIN
      K(2,I)+H*F(J,I);
      X(J,I)+X(J-1,I)+0.5*K(2,I) END;
      BOXA(TTEMP,X(J,*),F(J,*));
      FOR I=1 STEP 1 UNTIL N DO BEGIN
        K(3,I)+H*F(J,I);
        X(J,I)+X(J-1,I)+K(3,I) END;
        T+T*H;
        BOXA(T,X(J,*),F(J,*));
        FOR I=1 STEP 1 UNTIL N DO BEGIN
          K(4,I)+H*F(J,I);
          X(J,I)+X(J-1,I)+0.16666667*(K(1,I)+2.0*(K(2,I)+K(3,I))+K(4,I));
        END; END;
        IF B = 2 THEN BEGIN
          S33:
          FOR I=1 STEP 1 UNTIL N DO X(I)+X(2,I);
          COMMENT X(I)=DOUBLE INTERVAL RESULT TO BE USED IN ERROR ANALYSIS;
          T+T*H;
          H*0.5*H;
          IF H<HMIN THEN BOXA(T,X(1,*),F(1,*));
          H*3;
          GO TO S22 END;
          IF B = 3 THEN BEGIN
            COMMENT IS ACCURACY CRITERION MET;
            J*3;
            S44:FOR I=1 STEP 1 UNTIL N DO BEGIN
              E(I)+ABS(X(I)-X(J,I));
              IF E(I) < ABS(X(J,I))*RELTEST THEN
                E(I)+E(I)/ABS(X(J,I)) ELSE
                IF E(I) < ARSTEST THEN
                  E(I)+E(I)*FACTOR ELSE
                  BEGIN T+T*H;
                    IF J = 5 THEN BEGIN FOR I=1 STEP 1 UNTIL N DO X(1,I)+X(4,I);
                      GO TO S11 END;
                      GO TO S33 END;
                    END;
                    IF J = 5 THEN GO TO S66;
                    A*4; B*4;
                    GO TO S22 END;
                    COMMENT SHOULD ANY OF THE STARTING VALUES BE PRINTED OUT;
                    T+T-3.0*H;
                    FOR J=2,3,4 DO BEGIN
                      T+T*H;
                      BOXA(T,X(J,*),F(J,*));
                      IF T>BOUND THEN BEGIN
                        BOXA(T,X(J,*),F(J,*));
                        BOUND*BOUND+CALLC END;

```

```

END;
COMMENT BEGIN ALAMS METHOD;
S55;
H(XA(T,X(4,*),F(4,*)));
FOR I=1 STEP 1 UNTIL N DO
XP(I)+X(4,I)+0.04166667*H*(55.0*X(4,I)-
59.0*X(3,I)+37.0*X(2,I)-9.0*X(1,I));
T=T+H;
H(XA(T,XP,F(5,*)));
FOR I=1 STEP 1 UNTIL N DO
X(5,I)+X(4,I)+0.04166667*H*(9.0*X(5,I)+19*X(4,I)-5*X(3,I)+F(2,I));
J=5; GO S44;
S66;
FOR I=1 STEP 1 UNTIL N DO BEGIN X(4,I)+X(5,I);
FOR J=2 STEP 1 UNTIL 5 DO F(J,I)+F(J,I) END;
H(XB(T,X(4,*),F(4,*)));
IF T2 BOUND THEN BEGIN
H(XC(T,X(4,*),F(4,*)));
BOUND=BOUND+CALLC END;
COMMENT TEST WHETHER INTERVAL CAN BE DOUBLED;
FOR I=1 STEP 1 UNTIL 1 DO BEGIN
IF L(I) > LR THEN GO S55 END;
IF CALLC<(D1+2*H) OR (BOUND-T)<C1 OR D1>HMAX THEN GO TO S55;
FOR I=1 STEP 1 UNTIL N DO X(1,I)+X(4,I);
H=4.0*H;
GO S11;
RETURN END OF ICEADAMS ;

```

1600214

2620217

2620219

1600216

2620223

1600218

2620225

2620301

1600220

1600222

1600224

1600307

# APPENDIX 2.2C

## LIST OF INPUT DATA

LIST OF INPUT DATA			Numerical Values*	
Code Symbol	Text Symbol or Description	Unit	Perman	Calcm**
H	Step size		(0.0005)	
CALLC	Interval between output		(0.010)	
HMAX	Max. step size		(0.0005)	
HMIN	Min. step size		(0.00001)	
RELB	Integration error allowed		(0.0001)	
ABSB	Integration error allowed		(0.0001)	
DME	(1-W/C <sub>st</sub> ) to start extrapolation		(0.05)	
ERRORA	*A		(0.002)	
ERRDT	*T		(0.01)	
AA1	(A <sub>2</sub> -A <sub>1</sub> )/A <sub>min</sub>		(0.005)	
WILSON	Control variable		(0)	
EXTRAPOLATED	Control variable		(0)	
SUSPEND	Control variable		(0)	
NOISURF	Control variable		(0)	
JCRIT	Control variable		(0)	
JNC	Control variable		(1,0)	
GROUPMAX	Max. number of groups allowed		(5.0 x 10 <sup>15</sup> )	
B1			(1.5)	
B2			-3.6787	-3.62
C1			4890.7	4000.0
C2			0.5873	3.351
C3			4385.7	-531.5
D1			0.0	1.0825 x 10 <sup>7</sup>
D2			1.4595	4.1856
E1			7863.8	880.0
E2			0.0	6 x 10 <sup>5</sup>
E3			-3.8411	-3.6561
AK2			5312.5	4570.0
AK4			-10.145	-9.05
AK1			13745.0	8400.0
ACPO			0.127	0.03761
ACP1			2.888	1.3099
ACP2			28070.0	25633.0
ARH0			32.768	124.18
ARH20			-0.0074975	-0.01597
ARH20			-5.255 x 10 <sup>-7</sup>	-1.6855 x 10 <sup>-6</sup>
ARH2			998.95	232.18
ARH			0.127	0.037261
ARH1			24836.0	2480.0
ARH2			39575.0	31290.0
ARH3			-10.29	-2.6769
AHL			0.2271	0.06683
AHL1			-3.245 x 10 <sup>-5</sup>	0.
AHL2			7.741 x 10 <sup>-9</sup>	0.
AHL3			6.1276	5.873
APS	*1			

LIST OF INPUT DATA (CONTINUED)			Numerical Values*	
Code Symbol	Text Symbol or Description	Unit	Perman	Calcm**
AP51	*2		-8128.8	-7040.7
AP52	*3		-0.53299	-0.5329
M	*4		39.1	132.91
TC	*5		4310	3700
SIGMAP	*6		(7.84 x 10 <sup>-3</sup> )	(5.75 x 10 <sup>-3</sup> )
SMP	*7		(1.25)	(1.25)
CPL	*8		0.190	0.5683
KV	*9		(2.22 x 10 <sup>-3</sup> )	(0.9 x 10 <sup>-3</sup> )
NEUV	*10		(2.14 x 10 <sup>-3</sup> )	(2.31 x 10 <sup>-3</sup> )
TAMB	*11		(560)	(560)
HAMB	*12		(10.0)	(10.0)
RAIS	*13		(1.64 x 10 <sup>-3</sup> )	(1.64 x 10 <sup>-3</sup> )
UAG	*14		(333)	(333)
Ueo	*15		(4403)	(4403)
Po	*16		(1982.9)	(1982.9)
STAGES	*17		(6)	(6)
Following				
ROTOR	Control variable		0 for stator row	1 for rotor row
DIAM1	Inlet mean diameter, (in.)			
HEIGHT1	Inlet blade height, (in.)			
DIAM2	Outlet mean diameter, (in.)			
HEIGHT2	Outlet blade height, (in.)			
ETA1	*18			
U1	*19			
U2	*20			
BETA1	*21			
BETA2	*22			
BSPACE	*23			
THICKBOT	*24			
THICKMAX	*25			
Following				
GROUPS	Number of droplet size groups			
RLD 1	*26			
RLD 2	*27			
RLD 3	*28			
RLD 4	*29			
RLD 5	*30			
RLD 6	*31			
RLD 7	*32			
RLD 8	*33			
RLD 9	*34			
RLD 10	*35			
RLD 11	*36			
RLD 12	*37			
RLD 13	*38			
RLD 14	*39			
RLD 15	*40			
RLD 16	*41			
RLD 17	*42			
RLD 18	*43			
RLD 19	*44			
RLD 20	*45			
RLD 21	*46			
RLD 22	*47			
RLD 23	*48			
RLD 24	*49			
RLD 25	*50			
RLD 26	*51			
RLD 27	*52			
RLD 28	*53			
RLD 29	*54			
RLD 30	*55			
RLD 31	*56			
RLD 32	*57			
RLD 33	*58			
RLD 34	*59			
RLD 35	*60			
RLD 36	*61			
RLD 37	*62			
RLD 38	*63			
RLD 39	*64			
RLD 40	*65			
RLD 41	*66			
RLD 42	*67			
RLD 43	*68			
RLD 44	*69			
RLD 45	*70			
RLD 46	*71			
RLD 47	*72			
RLD 48	*73			
RLD 49	*74			
RLD 50	*75			
RLD 51	*76			
RLD 52	*77			
RLD 53	*78			
RLD 54	*79			
RLD 55	*80			
RLD 56	*81			
RLD 57	*82			
RLD 58	*83			
RLD 59	*84			
RLD 60	*85			
RLD 61	*86			
RLD 62	*87			
RLD 63	*88			
RLD 64	*89			
RLD 65	*90			
RLD 66	*91			
RLD 67	*92			
RLD 68	*93			
RLD 69	*94			
RLD 70	*95			
RLD 71	*96			
RLD 72	*97			
RLD 73	*98			
RLD 74	*99			
RLD 75	*100			
RLD 76	*101			
RLD 77	*102			
RLD 78	*103			
RLD 79	*104			
RLD 80	*105			
RLD 81	*106			
RLD 82	*107			
RLD 83	*108			
RLD 84	*109			
RLD 85	*110			
RLD 86	*111			
RLD 87	*112			
RLD 88	*113			
RLD 89	*114			
RLD 90	*115			
RLD 91	*116			
RLD 92	*117			
RLD 93	*118			
RLD 94	*119			
RLD 95	*120			
RLD 96	*121			
RLD 97	*122			
RLD 98	*123			
RLD 99	*124			
RLD 100	*125			
RLD 101	*126			
RLD 102	*127			
RLD 103	*128			
RLD 104	*129			
RLD 105	*130			
RLD 106	*131			
RLD 107	*132			
RLD 108	*133			
RLD 109	*134			
RLD 110	*135			
RLD 111	*136			
RLD 112	*137			
RLD 113	*138			
RLD 114	*139			
RLD 115	*140			
RLD 116	*141			
RLD 117	*142			
RLD 118	*143			
RLD 119	*144			
RLD 120	*145			
RLD 121	*146			
RLD 122	*147			
RLD 123	*148			
RLD 124	*149			
RLD 125	*150			
RLD 126	*151			
RLD 127	*152			
RLD 128	*153			
RLD 129	*154			
RLD 130	*155			
RLD 131	*156			
RLD 132	*157			
RLD 133	*158			
RLD 134	*159			
RLD 135	*160			
RLD 136	*161			
RLD 137	*162			
RLD 138	*163			
RLD 139	*164			
RLD 140	*165			
RLD 141	*166			
RLD 142	*167			
RLD 143	*168			
RLD 144	*169			
RLD 145	*170			
RLD 146	*171			
RLD 147	*172			
RLD 148	*173			
RLD 149	*174			
RLD 150	*175			
RLD 151	*176			
RLD 152	*177			
RLD 153	*178			
RLD 154	*179			
RLD 155	*180			
RLD 156	*181			
RLD 157	*182			
RLD 158	*183			
RLD 159	*184			
RLD 160	*185			
RLD 161	*186			
RLD 162	*187			
RLD 163	*188			
RLD 164	*189			
RLD 165	*190			
RLD 166	*191			
RLD 167	*192			
RLD 168	*193			
RLD 169	*194			
RLD 170	*195			
RLD 171	*196			
RLD 172	*197			
RLD 173	*198			
RLD 174	*199			
RLD 175	*200			
RLD 176	*201			
RLD 177	*202			
RLD 178	*203			
RLD 179	*204			
RLD 180	*205			
RLD 181	*206			
RLD 182	*207			
RLD 183	*208			
RLD 184	*209			
RLD 185	*210			
RLD 186	*211			
RLD 187	*212			
RLD 188	*213			
RLD 189	*214			
RLD 190	*215			
RLD 191	*216			
RLD 192	*217			
RLD 193	*218			
RLD 194	*219			
RLD 195	*220			
RLD 196	*221			
RLD 197	*222			
RLD 198	*223			
RLD 199	*224			
RLD 200	*225			
RLD 201	*226			
RLD 202	*227			
RLD 203	*228			
RLD 204	*229			
RLD 205	*230			
RLD 206	*231			
RLD 207	*232			
RLD 208	*233			
RLD 209	*234			
RLD 210	*235			
RLD 211	*236			
RLD 212	*237			
RLD 213	*238			
RLD 214	*239			
RLD 215	*240			
RLD 216	*241			
RLD 217	*242			
RLD 218	*243			
RLD 219	*244			
RLD 220	*245			
RLD 221	*246			
RLD 222	*247			
RLD 223	*248			
RLD 224	*249			
RLD 225	*250			
RLD 226	*251			
RLD 227	*252			
RLD 228	*253			
RLD 229	*254			
RLD 230	*255			
RLD 231	*256			
RLD 232	*257			
RLD 233	*258			
RLD 234	*259			
RLD 235	*260			
RLD 236	*261			
RLD 237	*262			
RLD 238	*263			
RLD 239	*264			
RLD 240	*265			
RLD 241	*266			
RLD 242	*267		</	

### PROGRAM FLOW CHART

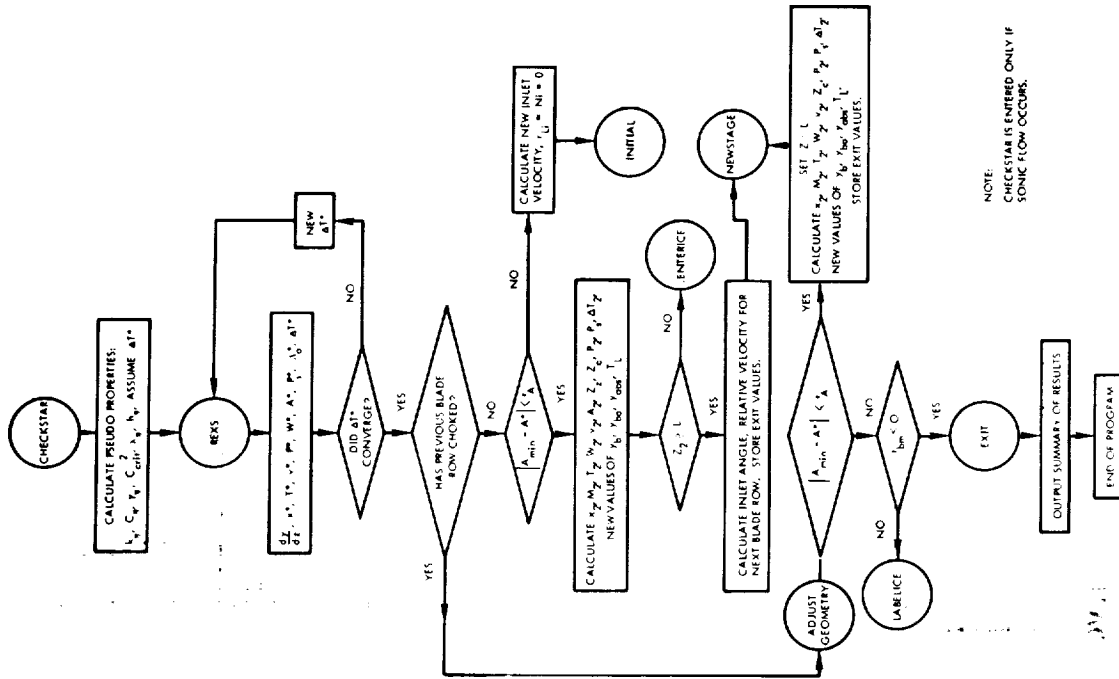


**Figure 2.2D-2 Flow Diagram of the Sonic Flow Section of the Condensation Code**

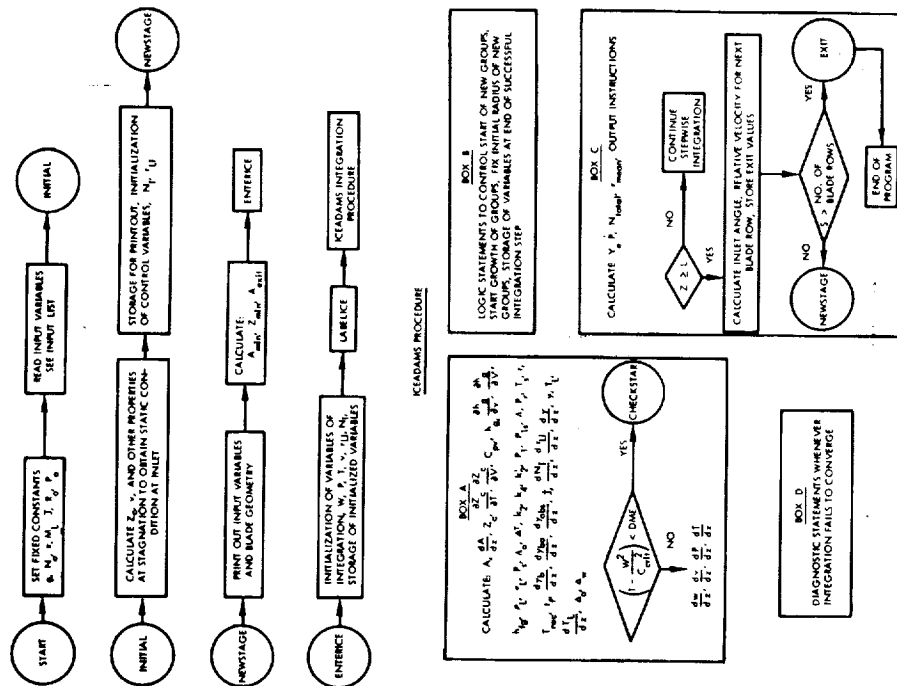


Figure 2.2D-1 Flow Diagram of the Condensation Code

## APPENDIX 2.2.E

### DESCRIPTION OF INPUT CONTROL VARIABLES

The use of the following control variables in the computer code is as follows:

AA1	The extrapolation from subsonic to supersonic flow in the first blade row having critical flow is from area $A_1$ to area $A_2$ where $A_2 = A_{\min} (1 + AA1)$ .
DME	Defines the minimum value of $(1 - W^2/C_{\text{crit}}^2)$ which is allowed before extrapolation is initiated.
EERDT	Maximum allowable difference between assumed and calculated $\Delta T$ .
ERRØRA	Maximum allowable value of $(A^* - A_{\min})/A_{\min}$ which permits extrapolation to occur.
EXTRAPØ-LATED	Input of TRUE means a previous blade row has critical flow, and requires the program to adjust blade thickness to accommodate the flow.
GRØUP MAX	The maximum number of droplet groups permitted. (Code limits GRØUPMAX to maximum value of 25.)
JCRIT	The value of $j$ must exceed the value of JCRIT before the counting or growth of drops is begun, except that surface condensation may occur independently.

RESTART	Input of TRUE permits input of additional data necessary to continue calculation from a prior run. For example, an error was contained in the data for blade row 4. Calculations could be continued from the results at exit of blade row 3 used as input for Blade row 4. Input of FALSE causes inlet properties to be treated as stagnation conditions.
SUSPEND	Input of 0.0 freezes the amount of condensate during extrapolation. Input of 1.0 causes condensation to occur during extrapolation at a rate proportional to $\Delta T$ .
WILSØNØ	Input of TRUE when restarting after the Wilson point has occurred in a previous blade row. Otherwise, input is FALSE.
JINC	A new group of droplets is initiated each time $j$ increases by the factor JINC.
NØSURF	Input of 1.0 causes all surface condensation to be neglected. Input of 0.0 causes surface condensation to be included.



## 2.3 TWO-D AXISYMMETRIC FLOWS BEHIND BLADE ROWS IN WET VAPOR TURBINE\*

### 2.3.1 Background

This report is designed to be used in conjunction with NASA CR-710 (Reference 1) to give the user sufficient information to allow utilization of the NASA Performance Computer Code for Axial Flow Turbines as modified at WANL. The modified code is written entirely in FORTRAN IV for the CDC 6600 computer. But the code should be capable of being used with appropriate control cards on any computer having at least 32 K of core storage.

The following sections of the report give: the applicability and modifications made from the original code, definitions of the input and output nomenclature, a method for making the code input applicable for wet vapor turbines, suggestions for further possible future modifications, three sample problems illustrating the usage of the code, a FORTRAN listing of the entire code, and control cards showing proper deck setup. No attempt is made to discuss the method of calculation of turbine performance or to give computer flow diagrams since these topics are adequately covered in Reference (1). The modifications made to the code do not significantly change the original program logic or capability. These modifications for the most part were necessary to enable the code to accurately calculate wet vapor turbine performance. Ideal gas turbines can still be analyzed as well as air breathing fossil fuel burning turbines for which the code was originally designed.

### 2.3.2 Intent of Code

#### • Applicability of Code and Limiting Assumptions

The principal purpose of the original code as written by E. E. Flagg<sup>(1)</sup> is to provide a complete performance map of axial flow turbines suitable for use in air breathing fossil fuel fired jet engines. In the process of accomplishing this end, the code calculates the two-dimensional bulk flow conditions fore and aft of the turbine rows.

---

\*by James D. Milton, Doctoral Candidate-Nuclear Engineering, University of Cincinnati

### 1. Description and Scope of Modified Code

- a) Axial flow turbines.
- b) Up to 8 stages.
- c) Up to 6 radial sectors (although only 5 are usually used for reasons of symmetry).
- d) Each sector is a quasi-one-dimensional element with the properties at the radial centers of these sectors being joined, utilizing simple radial equilibrium at the stator and rotor exits.
- e) Semi-perfect gas properties (gas constant and specific heat ratio) are assumed and are input at the entrance and exit of each blade row. Provision is also made to simulate changes in gas flow rates at the entrance and exit of each blade row. Energy balance effects are simulated by changing the values of the gas constant and specific heat ratio.
- f) The turbine geometry may be either input as a passage distributed area (SPA and RPA)\* or as effective exit vector flow angles (SDEA and RDEA). The assumption that the effective exit flow angles are approximately equal to the design blade exit angles is usually valid. Mandatory inputs are the diameters of the root (DR) and tip (DT) for the entrance and exit of each blade row and the stator and rotor design inlet angles (SDIA and RDIA) for each of the radial sectors.
- g) Even though there are two subroutines (LOSS 1 and LOSS 2) which are capable of calculating losses by a total pressure loss coefficient method, the values for the coefficients of the series expansion are not generally known. (See page 11 of NASA CR-710.) The standard method is to input the values of optimum recovery coefficients for stator and rotor (SREC and RREC) together with exponents to be used in the event of both negative and positive (EXPN and EXPP) incidence. (See page 10 of NASA CR-710 for equations used.)

---

\* Nomenclature defined in Section 2.3.3 of this report.

h) Separate cases may be run for various turbine speeds by merely changing the RPM and indicating that is a change case (STGCH = 0.0).

i) The FORTRAN IV code calculates a performance map for the case of a given turbine at a particular RPM by in effect varying the exit back pressure. The output for each "iteration" (i.e., value of back pressure) gives flow rates, velocities, flow angles, temperatures, pressures, densities, Mach numbers, efficiencies, and work done both for an overall stage output and also row-by-row output for each of the radial sectors. An exact choke point is found during the calculation of the performance map and the turbine back-pressure is effectively further reduced until the discharge annulus area is choked at the pitchline sector (assuming AACs = 1.0). A single performance point can be obtained by simply setting all pressure ratio increments (DELC, DELL, and DELA) to zero. This is the usual case when fixed operating conditions are known at design.

j) The gas flow at the entrance to the first stator is assumed to have uniform radial temperature, pressure, and velocity. The flow is further assumed to be exactly aligned with the turbine axial direction (i.e., no tangential velocity component).

#### • Modifications to Code

As stated previously, as originally programmed the code was principally intended for analysis of JP-4 burning, air breathing jet engines. Internal to the code is a subroutine for calculating the thermodynamic properties of reacted JP-4-air mixtures. It also had a capability to input thermodynamic properties which was extended as required by the method used in determining the performance of wet vapor turbines. It was decided that the thermodynamic properties fore and aft of each blade row would be inputted in terms of representative values for the particular working fluid and its state. The variables to be input would be the ratio of specific heats at constant pressure to that at constant volume and Boyles and Charles law gas constant. The internals of the program are then used to calculate effective specific heat and various other effective

thermodynamic properties.

The following modifications were made in the code:

1) Wherever the Boyles and Charles gas law constant RG appeared in the code, it was replaced by a two-dimensional variable RV (I,K) with proper choice of axial blade position I and stage number K to correspond to the location in the turbine for which the calculation is being performed.

2) A change was made in the input NAMELIST format to allow reading in of a variable RV. Also a modification was made to read in reference values for the gas constant, temperature, pressure, and specific heat ratio all at standard sea level conditions. Formerly the code contained these values for air internally in a DATA statement. But since gases other than air will be used, it was thought useful to include a capability for inputting these values for each case rather than requiring a recompilation whenever a different working fluid was used.

3) The output was expanded to print out the values for the flow,  $\gamma$  (ratio of specific heats), gas constant, and RWG (the ratio of the flow at a particular station to turbine inlet flow). To insure that these variables were being properly handled within the code, decreasing values of  $\gamma$ , RV, and RWG were fed in. The output was found to be consistent after a slight change in the logic.

4) Since values for  $\gamma$  and RV are now fed in for all cases, the subroutines to calculate  $\gamma$ , RG, and  $C_p$ , are superfluous since they would never be called upon. If by inadvertently omitting the inputting of  $\gamma$  and/or RV and subsequently a subroutine for calculating its value is entered, then an error message was added which would print out the words "SUBROUTINE ( ) HAS BEEN CALLED UPON" followed by a string of asterisks so that attention would be immediately drawn to the error. The ( ) is filled in by the name of the subroutine being called. After the error message is printed out, the calculation is allowed to proceed using properties for air, water and JP-4 fuel.

5) On page 193 of NASA CR-170 the statement:

$$21 \text{ PTP}(I, K + 1) = \text{PTBAR}(K) * ( ( \text{TTRA}(I, K) / \text{TTBAR}(K) ) ** E 3 \quad \text{ST2A 153}$$

was found to be incorrect and should read:

$$21 \text{ PTP}(I, K + 1) = \text{PTBAR}(K) * (\text{TT2A}(I, K) / \text{TTBAR}(K)) ** E 3$$

6) On page 208 of NASA CR-710 the statement:

$$\text{ASOH} = \text{SQRT}(\text{GAM}(I, K) * G * \text{RG} * \text{STTSO}(L)) \quad \text{INST 175}$$

was found to be incorrect and should read:

$$\text{ASOH} = \text{SQRT}(\text{GAM}(I, K) * G * \text{RG} * \text{STTSO}(L))$$

7) Any cards from the original code which had to be removed rather than modified were denoted by a comment card with the words "CARD DELETED" followed by a string of asterisks.

8) As an aid in debugging a computer run, an option was added to allow the printout of when entry or exit was made from each subroutine. This enables the user to examine the program logic as an aid in determining where discrepancies occur. This option is not recommended for other than debugging runs since a large amount of output results.

### 2.3.3 Nomenclature for Input and Output of Modified Code

#### • Input Definitions \*

1) "TRUE" or "FALSE" card depending on whether or not a listing of when an entrance and exit is made from each subroutine is desired. This card is input only once per case.

2) Two heading cards of 60 characters each inputted only once per case.

3) Constants input once per case:

Code Name	Definition	Units
STAGE **	Stage identification number	---
STGCH	Flag indicating whether following data is for the basic case (1.0) or for a change case (0.0)	---
TTIN	Turbine inlet total temperature	°R
PTIN	Turbine inlet total pressure	psia
WAIR	Water to air ratio (not used in modified code); should be input as 0.0	---
FAIR	Fuel to air ratio (not used in modified code); should be input as 0.0	---
PTPS	Pitchline pressure ratio (total to static) across first stator for 0 <sup>th</sup> calculation. This ratio is incremented by DELC, DELL, or DELA for next calculation	---
DELC	First try at increment to PTPS	---
DELL	Increment to PTPS after first stator has critical flow and also when choke iteration is complete	---
DELA	Increment to PTPS when last rotor is choked	---
STG	Number of stages in turbine (8 maximum)	---
SECT	Number of radial sectors (6 maximum)	---
EXPN	Exponent of cosine term for negative incidence used in calculating an inlet recovery factor (see page 10 of Reference 1)	---
EXPP	Exponent of cosine term for positive incidence used in calculating an inlet recovery factor (see page 10 of Reference 1)	---
PAF	Profile averaging fork (either 0.0, 1.0, or 2.0); gives the next stage inlet conditions for either: uniform (0.0) at the average value of the preceding stage, or the radial sector profiles (1.0) of pressure and temperature of the preceding stage, or a third option which keeps the exit total temperature radial profile and "smooths" (2.0) the exit total pressure profile from the preceding stage	---
SLI	Stage loss indicator (0.0 means that recovery, efficiency, and flow coefficients are input for each stage; 1.0 means that they are input only once and are assumed constant throughout the turbine)	---
AACS	Discharge annulus area choke stop which is the maximum limit for the turbine exit axial Mach number at the pitchline sector. This code will continue to decrease the back pressure until this limit is reached (assuming DELC, DELL, and DELA ≠ 0.0)	---
RPM	Turbine speed	RPM
VCTD	Vector diagram interstage output (either 0.0 for overall stage performance output only or 1.0 for row-by-row sector performance in addition to overall stage output printout)	---
RSL	Gas constant at sea level standard conditions	ft lb/lb °R
TSL	Standard temperature at sea level = 518.688	°R
PSL	Standard pressure at sea level = 14.696	psia
GAMSL	Specific heat ratio at sea level standard conditions	---
ENDSTG	0.0 if more stage data to follow; 1.0 if last stage data has been read in	---
ENDJOB	0.0 if more cases to follow; 1.0 if all data for all cases has been input	---
PCNH	Percent station height distribution (example: if 5 equal (in height) radial sectors were desired, then PCNH = 0.2, 0.2, 0.2, 0.2)	---

\* Refer to Standard Option Input Sheet (page 11).

\*\* Must be input every time new stage data is read in.

4) Axial station input for each stage  
(stations 0, 1, 1A, 2, and 2A)

Code Name	Definition	Units
RG	Gas constant	ft lb/lb °R
GAMG	Specific heat ratio	---
DR	Diameter of root or hub of turbine	in
DT	Diameter of tip of turbine	in
RWG	Ratio of station flow to turbine inlet flow	---

5) Stator radial distributions for each stage (hub to tip sectors)

Code Name	Definition	Units
SDIA	Stator design inlet angle	(° from axis)
SDEA	Stator effective exit flow angle — should not be input if SPA is input	(° from axis)
SREC	Stator optimum recovery coefficient ( $\eta_{r, opt}$ )	---
SETA	Stator efficiency coefficient ( $\eta_s$ )	---
SCF	Stator flow coefficient ( $C_{fs}$ )	---
SPA	Stator passage area per unit height — should not be input if SDEA is input	in <sup>2</sup> /in
SESTH *	Stator ratio of exit blade height to throat height	---

6) Rotor radial distributions for each stage (hub to tip sectors)

Code Name	Definition	Units
RDIA	Rotor design inlet angle	(° from axis)
RDEA	Rotor effective exit flow angle — should not be input if RPA is input	(° from axis)
RREC	Rotor optimum recovery coefficient ( $\eta_{r, opt}$ )	---
RETA	Rotor efficiency coefficient ( $\eta_r$ )	---
RCF	Rotor flow coefficient ( $C_{fr}$ )	---
RPA	Rotor passage area per unit height — should not be input if RDEA is input	in <sup>2</sup> /in
RTF	Rotor test factor used to represent the non-uniform work extraction due to blade end effects	---
RERTH *	Rotor ratio of exit blade height to throat height	---

\* Only a single value is input.

WANL MODIFIED  
TURBINE COMPUTER PROGRAM  
STANDARD OPTION  
INPUT SHEET

Start All Input Cards in Column 2

Subroutine Entry and Exit Listing Option (TRUE or FALSE)

Name (Comment Information)

Title (Comment Information)

\$DATAIN STAGE = ,  
STGCH= ,  
TTIN= , PTIN= , WAIR= , FAIR= ,  
PTPS= , DELC= , DELL= , DELA= ,  
STG= , SECT= , EXPN= , EXPP= ,  
PAF= , SLI= , AAC= , RPM= ,  
VCTD= , RSL= , TSL= , PSL= ,  
GAMSL= , ENDSTG= , ENDJØB= ,

INLET RADIAL PROFILE

PCNH(1)= ,  
AXIAL STATIONS  
STA. 0 STA. 1 STA. 1A STA. 2 STA. 2A  
RG(1)= , , , , ,  
GAMG(1)= , , , , ,  
DR(1)= , , , , ,  
DT(1)= , , , , ,  
RWG(1)= , , , , ,

STATOR RADIAL DISTRIBUTIONS

ROOT	PITCH	TIP
SDIA(1)=		
SDEA(1)=		
SREC(1)=		
SETA(1)=		
SCF(1)=		
SPA(1)=		
SESTH=		

ROTOR RADIAL DISTRIBUTIONS

ROOT	PITCH	TIP
RDIA(1)=		
RDEA(1)=		
RREC(1)=		
RETA(1)=		
RCF(1)=		
RPA(1)=		
RTF(1)=		
RERTH=		

ENDSTG= , ENDSTG=1.0 IF LAST CASE  
ENDJØB= \$ ENDJØB=1.0 IF LAST STAGE

• Output Definitions

1) Station Nomenclature

The axial station numbers (0, 1, 1A, 2, and 2A) following a parameter refer to the following designations:

Station Number	0	1	1A	2	2A
Definition	Stator Inlet	Stator Exit	Rotor Inlet	Rotor Exit	Next Stage Stator Inlet

Also see Figure 2.3-1 for further clarification of terminology.

In the stage and overall performance output printout several parameters are given in terms of the equivalent parameter referenced to standard sea level conditions. This provides a common basis for comparison of performance maps for different turbine cases.

## 2) Stage Performance Parameters

Symbol	Definition	Units
TTBAR 0	Stage average inlet total temperature	$^{\circ}\text{R}$
PTBAR 0	Stage average inlet total pressure	psia
WG 0	Stage inlet total weight flow	lb/sec
DEL H	Stage enthalpy drop (energy output)	BTU/lb
WRT/P	Stage corrected weight flow function	$(\text{lb/sec}) (^{\circ}\text{R}/\text{psia})^{1/2}$
DH/TTBAR0	Stage energy function	$\text{BTU/lb } ^{\circ}\text{R}$
N/RT	Stage corrected speed	$\text{RPM}/(^{\circ}\text{R})^{1/2}$
ETA TT	Stage total to total efficiency	---
ETA TS	Stage total to static efficiency	---
ETA AT	Stage total to axial total efficiency	---
PT0/PS1	Stator total to static pressure ratio at pitchline	---
PTBAR0/PTBAR2	Stage average total to total pressure ratio	---
ITBAR0/PS2	Stage average total to pitchline static pressure ratio	---
PTR2/PS2	Rotor exit relative total to static pressure ratio at pitchline	---
TTBAR2/TTBAR0	Stage average total to total temperature ratio	---
TTT1A/TTBAR0	Rotor inlet pitchline relative total to stage inlet average total temperature ratio	---
WG 1	Stator exit total weight flow	lb/sec
PS 1A	Rotor inlet static pressure at pitchline	psia
TTR 1A	Rotor inlet relative total temperature at pitchline	$^{\circ}\text{R}$
PTR 1A	Rotor inlet relative total pressure at pitchline	psia
WG 1A	Rotor inlet total weight flow	lb/sec
PS 2	Rotor exit static pressure at pitchline	psia
TTBAR 2	Stage exit average total temperature	$^{\circ}\text{R}$
PTBAR 2	Stage exit average total pressure	psia
WG 2	Rotor exit total weight flow	lb/sec
WG 2A	Next stage stator inlet total weight flow	lb/sec
UP/VI	Wheel speed to isentropic velocity ratio at pitchline	---
UR/VI	Root wheel speed to pitchline isentropic velocity ratio	---
PSI P	Kinetic energy loading parameter at pitchline	---
PSI R	Kinetic energy loading parameter at root	---
RX P	Reaction ratio at pitchline	---
RX R	Reaction ratio at root	---
ALPHA 0	Stator inlet gas angle at pitchline	$^{\circ}$
I STATOR	Stator inlet incidence angle at pitchline	$^{\circ}$
BETA 1A	Rotor inlet gas angle at pitchline	$^{\circ}$

Symbol	Definition	Units
I R ØTOR	Rotor inlet incidence angle at pitchline	$^{\circ}$
ALPHA 2A	Next stage stator inlet gas angle at pitchline	$^{\circ}$
DBETA R	Rotor root turning angle	$^{\circ}$
M 1	Stator exit Mach number at pitchline	---
M1 RT	Stator exit Mach number at root	---
MR 1A	Rotor inlet relative Mach number at pitchline	---
MR1A RT	Rotor inlet relative Mach number at root	---
MR 2	Rotor exit relative Mach number at pitchline	---
MR2 TIP	Rotor exit relative Mach number at tip	---
E/TH CR	Stage equivalent energy, corrected to standard inlet critical conditions	BTU/lb
N/RTH CR	Stage equivalent speed, corrected to standard inlet critical conditions	RPM
WRTHCRE/D	Stage equivalent flow, correct to standard inlet critical conditions	lb/sec

## 3) Overall Turbine Performance Parameters

Symbol	Definition	Units
PSI P	Overall kinetic energy loading parameter at pitchline	---
PSI R	Overall kinetic energy loading parameter at root	---
DEL H	Overall enthalpy drop (energy output)	BTU/lb
WRT/P	Turbine inlet corrected weight flow function	$(\text{lb/sec}) (^{\circ}\text{R}/\text{psia})^{1/2}$
N/RT	Turbine inlet corrected speed	$\text{RPM}/(^{\circ}\text{R})^{1/2}$
DELH/TTIN	Overall energy function	BTU/lb $^{\circ}\text{R}$
PT0/PTBAR2	Overall average total pressure ratio	---
PT0/PS2	Overall total to static pressure ratio at pitchline	---
PT0/PAT2A	Overall total to axial total pressure ratio at pitchline	---
ETA TT	Overall total to total efficiency	---
ETA TS	Overall total to static efficiency	---
ETA TAT	Overall total to axial total efficiency	---
WNE/60D	Turbine inlet equivalent flow-speed parameter	$\text{lb/sec}^2$
N/RTH CR	Turbine inlet equivalent speed, corrected to standard inlet critical conditions	RPM
E/TH CR	Overall equivalent energy, corrected to standard inlet critical conditions	BTU/lb

## 4) Inter-Stage Radial Sector Performance Parameters

Symbol	Definition	Units
DIAM 0	Diameter of mid-points of radial sectors at stator inlet	in
TT 0	Total temperature at stator inlet	$^{\circ}\text{R}$
PT 0	Total pressure at stator inlet	psia
ALPHA 0	Gas angle (with respect to axial direction) at stator inlet	$^{\circ}$
I STATØR	Incidence angle at stator inlet	$^{\circ}$
V 0	Gas velocity (composed of tangential and axial components) at stator inlet	ft/sec
VU 0	Tangential gas velocity at stator inlet	ft/sec
VZ 0	Axial gas velocity at stator inlet	ft/sec

Symbol	Definition	Units
TS 0	Static temperature at stator inlet	$^{\circ}\text{R}$
PS 0	Static pressure at stator inlet	psia
DENS 0	Static density at stator inlet	$\text{lb}/\text{ft}^3$
M 0	Mach number at stator inlet	---
CP 0	Specific heat at constant pressure at stator inlet	$\text{BTU}/\text{lb } ^{\circ}\text{R}$
RG 0	Gas constant at stator inlet	$\text{ft } \text{lb}/\text{lb } ^{\circ}\text{R}$
GAMG 0	Ratio of specific heats at stator inlet	---
RWG 0	Ratio of station flow to turbine inlet flow (by definition this must be 1.0 at the first stator inlet of turbine)	---
WG 0	Weight flow at stator inlet	$\text{lb}/\text{sec}$
DIAM 1	Diameter of mid-points of radial sectors at stator exit	in
ALPHA 1	Gas angle (with respect to axial direction) at stator exit	$^{\circ}$
DEL A	Gas turning angle ( $\alpha_0 + \alpha_1$ )	$^{\circ}$
V 1	Gas velocity (composed of tangential and axial components) at stator exit	$\text{ft}/\text{sec}$
VU 1	Tangential gas velocity at stator exit	$\text{ft}/\text{sec}$
VZ 1	Axial gas velocity at stator exit	$\text{ft}/\text{sec}$
TS 1	Static temperature at stator exit	$^{\circ}\text{R}$
PS 1	Static pressure at stator exit	psia
DENS 1	Static density at stator exit	$\text{lb}/\text{ft}^3$
M 1	Mach number at stator exit	---
ZWI INC	Zweifel parameter, incompressible	---
CP 5	Stator pressure coefficient, incompressible	---
CP 1	Specific heat at constant pressure at stator exit	$\text{BTU}/\text{lb } ^{\circ}\text{R}$
RG 1	Gas constant at stator exit	$\text{ft } \text{lb}/\text{lb } ^{\circ}\text{R}$
GAMG 1	Ratio of specific heats at stator exit	---
RWG 1	Ratio of stator exit flow to turbine inlet flow	---
WG 1	Weight flow at stator exit	$\text{lb}/\text{sec}$
DIAM 1A	Diameter of mid-points of radial sectors at root inlet	in
PTR 1A	Relative total pressure at rotor inlet	psia
TTR 1A	Relative total temperature at rotor inlet	$^{\circ}\text{R}$
BETA 1A	Relative gas angle at rotor inlet	$^{\circ}$
I RDTOR	Incidence angle at rotor inlet	$^{\circ}$
R 1A	Relative gas velocity at rotor inlet	$\text{ft}/\text{sec}$
RU 1A	Relative gas tangential velocity at rotor inlet	$\text{ft}/\text{sec}$
MR 1A	Relative Mach number at rotor inlet	---
U 1A	Wheel speed at rotor inlet	$\text{ft}/\text{sec}$
PS 1A	Static pressure at rotor inlet	psia
TS 1A	Static temperature at rotor inlet	$^{\circ}\text{R}$
CP 1A	Specific heat at constant pressure at rotor inlet	$\text{BTU}/\text{lb } ^{\circ}\text{R}$
RG 1A	Gas constant at rotor inlet	$\text{ft } \text{lb}/\text{lb } ^{\circ}\text{R}$
GAMG 1A	Ratio of specific heats at rotor inlet	---
RWG 1A	Ratio of rotor inlet flow to turbine inlet flow	---
WG 1A	Weight flow at rotor inlet	$\text{lb}/\text{sec}$
DIAM 2	Diameters of mid-points of radial sectors at rotor exit	in
PTR 2	Relative total pressure at rotor exit	psia
TTR 2	Relative total temperature at rotor exit	$^{\circ}\text{R}$
BETA 2	Relative gas angle at rotor exit	$^{\circ}$
DBETA	Gas turning angle ( $\beta_{1A} + \beta_2$ )	$^{\circ}$
R 2	Relative gas velocity at rotor exit	$\text{ft}/\text{sec}$

Symbol	Definition	Units
RU 2	Relative tangential gas velocity at rotor exit	$\text{ft}/\text{sec}$
MR 2	Relative Mach number at rotor exit	---
U 2	Wheel speed at rotor exit	$\text{ft}/\text{sec}$
RX	Reaction	---
DELH	Enthalpy drop (energy output)	$\text{BTU}/\text{lb}$
PSI P	Kinetic energy loading parameter	---
ETA TT	Total to total efficiency	---
ETA TS	Total to static efficiency	---
ETA AT	Total to axial total efficiency	---
ZWI INC	Zweifel parameter, incompressible	---
CP R	Rotor pressure coefficient, incompressible	---
PS 2	Static pressure at rotor exit	psia
TS 2	Static temperature at rotor exit	$^{\circ}\text{R}$
CP 2	Specific heat at constant pressure at rotor exit	$\text{BTU}/\text{lb } ^{\circ}\text{R}$
RG 2	Gas constant at rotor exit	$\text{ft } \text{lb}/\text{lb } ^{\circ}\text{R}$
GAMG 2	Ratio of specific heats at rotor exit	---
RWG 2	Ratio of rotor exit flow to turbine inlet flow	---
WG 2	Weight flow at rotor exit	$\text{lb}/\text{sec}$
PT 2A	Total pressure at inlet to next stator	psia
TT 2A	Total temperature at inlet to next stator	$^{\circ}\text{R}$
V 2A	Gas velocity (composed of tangential and axial components) at inlet to next stator	$\text{ft}/\text{sec}$
VU 2A	Tangential gas velocity at inlet to next stator	$\text{ft}/\text{sec}$
ALPHA 2A	Gas angle (with respect to axial direction) at inlet to next stator	$^{\circ}$
MF 2A	Axial Mach number at inlet to next stator	---
VZ 2A	Axial gas velocity at inlet to next stator	$\text{ft}/\text{sec}$
TS 2A	Static temperature at inlet to next stator	$^{\circ}\text{R}$
PS 2A	Static pressure at inlet to next stator	psia
DENS 2A	Static density at inlet to next stator	$\text{lb}/\text{ft}^3$
M 2A	Mach number at inlet to next stator	---
CP 2A	Specific heat at constant pressure at inlet to next stator	$\text{BTU}/\text{lb } ^{\circ}\text{R}$
RG 2A	Gas constant at inlet to next stator	$\text{ft } \text{lb}/\text{lb } ^{\circ}\text{R}$
GAMG 2A	Ratio of specific heats at inlet to next stator	---
RWG 2A	Ratio of flow at inlet to next stator to turbine inlet flow	---
WG 2A	Weight flow at inlet to next stator	$\text{lb}/\text{sec}$

### 2.3.4 Method for Calculation of Modified Parameters for Wet Vapor Turbines

#### • Assumptions Used and Development of Equations for Modified Parameters

In wet vapor turbines since there exists two distinct phases (gas and liquid), the usual ideal thermodynamic relationships which are valid for gas turbines are not directly applicable. The approach used to determine the performance of wet vapor turbines involved making a minimum of changes in the code but required modifying the input data

appropriately to closely simulate the thermodynamic processes of a turbine operating within the saturation dome of a T-S (temperature entropy) diagram. The following method was derived and gives good agreement with the results from the WSD 2-D code as run by Fentress (2).

In order to arrive at a consistent set of relatively simple relationships, the following assumptions were made:

1) The inlet hub and tip diameters for a given blade row are assumed equal to the exit hub and tip diameters from the preceding blade row. The same assumption holds true for the modified  $\gamma^*$ ,  $\eta^*$ , and  $R^*$ . The superscript \* indicates that it is a modified value for specific heat ratio, blade efficiency, and gas constant.

2) All inefficiencies are assumed to be lumped into the single blade efficiency parameter  $\eta^*$ . This includes such items as incidence and exit losses and flow coefficients. Consequently  $EXPP = EXPN = 0.0$ ,  $SREC = RREC = 1.0$ ,  $SCF = RCF = 1.0$ ,  $RTF = 1.0$ , and  $SESTH = RERTH = 1.0$ . The definitions of these computer code terms may be found in Section 2.3.3.

3) The exit gas flow angle from each blade row is taken to be equal to the exit blade angle. Therefore, actual blade exit angles (SDEA and RDEA) are input rather than distributed passage areas (SPA and RPA).

4) Since all energy changes are accounted for in the calculation of the modified parameters, there is no need to take into consideration the decrease in the gas flow rate due to condensation effects. Consequently  $RWG = 1.0$ .

5) Radial variations in  $\gamma^*$ ,  $\eta^*$ , and  $R^*$  are assumed to be negligible.

In applying the following formulae to determine the modified values of  $R^*$ ,  $\gamma^*$ , and  $\eta^*$ , care must be exercised to obtain the proper relative velocity either entering or leaving a blade row. See Figure 2.3-1 for clarification of the station terminology used in the example potassium turbine.

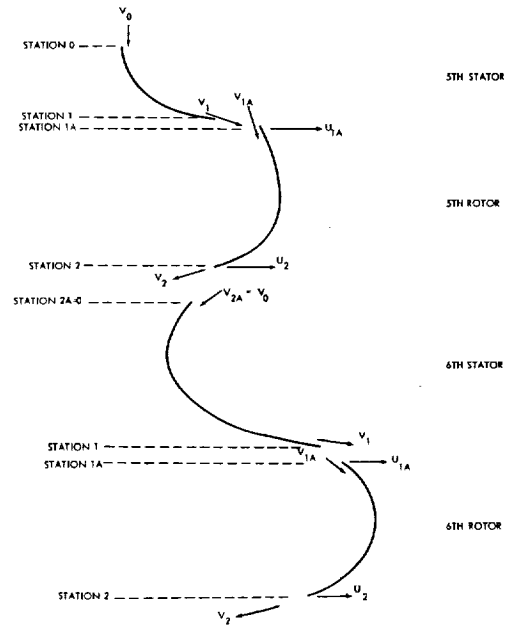


Figure 2.3-1 Axial Station Velocity Nomenclature

The initial values for static temperatures, pressures, specific volumes, and velocities are obtained from previous 1-D calculations. Definitions of the nomenclature used are given in Section 2.3.4.2

#### FIFTH STAGE

$$R_0^* = \frac{144 P_{S0} v_{S0}}{T_{S0}} \quad (1)$$

$$\gamma_0^* = \frac{1}{1 - \frac{2 g R_0^* (T_{T0} - T_{S0})}{V_0^2}} \quad (2)$$

$$P_{T0}^* = P_{S0} \left( \frac{T_{T0}}{T_{S0}} \right)^{\frac{\gamma_0^*}{\gamma_0^* - 1}} \quad (3)$$

$$PTPS = \frac{P_{T0}^*}{P_{S1}} \quad (4)$$

$$R_1^* = \frac{144 P_{S1} v_{S1}}{T_{S1}} \quad (5)$$

$$\gamma_1^* = \frac{1}{1 - \frac{2gR_1^*(T_{T0} - T_{S1})}{V_1^2}} \quad (6)$$

$$\eta_1^* = \frac{T_{T0} - T_{S1}}{T_{T0} \left[ 1 - \left( \frac{P_{S1}}{P_{T0}^*} \right) \frac{\gamma_1^* - 1}{\gamma_1^*} \right]} \quad (7)$$

$$D_{R1A}^* = D_{R1} \quad (8)$$

$$D_{T1A}^* = D_{T1} \quad (9)$$

$$R_{1A}^* = R_1^* \quad (10)$$

$$\gamma_{1A}^* = \gamma_1^* \quad (11)$$

$$R_2^* = \frac{144 P_{S2} V_{S2}}{T_{S2}} \quad (12)$$

$$T_{T2g} = T_{S1A} + \frac{(\gamma_{1A}^* - 1)(V_{1A}^2 + U_2^2 - U_{1A}^2)}{2g \gamma_{1A}^* R_{1A}^*} \quad (13)$$

$$P_{T2g} = P_{S1A} \left[ 1 + \frac{(\gamma_{1A}^* - 1)(V_{1A}^2 + U_2^2 - U_{1A}^2)}{2g \gamma_{1A}^* R_{1A}^* T_{S1A}} \right]^{\frac{\gamma_{1A}^*}{\gamma_{1A}^* - 1}} \quad (14)$$

$$\gamma_2^* = \frac{1}{1 - \frac{2gR_2^*(T_{T2g} - T_{S2})}{V_2^2}} \quad (15)$$

$$\eta_2^* = \frac{T_{T2g} - T_{S2}}{T_{T2g} \left[ \left( 1 - \frac{P_{S2}}{P_{T2g}^*} \right) \frac{\gamma_2^* - 1}{\gamma_2^*} \right]} \quad (16)$$

$$D_{R2A}^* = D_{R2} \quad (17)$$

$$D_{T2A}^* = D_{T2} \quad (18)$$

$$R_{2A}^* = R_2^* \quad (19)$$

$$\gamma_{2A}^* = \gamma_2^* \quad (20)$$

$$D_{R0}^* = D_{R2A}^* \quad (21)$$

$$D_{T0}^* = D_{T2A}^* \quad (22)$$

$$R_0^* = R_{2A}^* \quad (23)$$

$$\gamma_0^* = \gamma_{2A}^* \quad (24)$$

$$R_1^* = \frac{144 P_{S1} V_{S1}}{T_{S1}} \quad (25)$$

$$T_{T0g} = T_{S2A} + \frac{\frac{V_{2A}^2}{2g \gamma_{2A}^* R_{2A}^*}}{\frac{\gamma_{2A}^*}{\gamma_{2A}^* - 1}} \quad (26)$$

$$P_{T0g} = P_{S2A} \left( \frac{T_{T0g}}{T_{S2A}} \right)^{\frac{\gamma_{2A}^*}{\gamma_{2A}^* - 1}} \quad (27)$$

$$\gamma_1^* = \frac{1}{1 - \frac{2gR_1^*(T_{T0g} - T_{S1})}{V_1^2}} \quad (28)$$

$$\eta_1^* = \frac{T_{T0g} - T_{S1}}{T_{T0g} \left[ 1 - \left( \frac{P_{S1}}{P_{T0g}^*} \right) \frac{\gamma_1^* - 1}{\gamma_1^*} \right]} \quad (29)$$

The remainder of the expressions for the modified parameters for the rest of the sixth stage are the same as those in Equations (8) through (20). For turbines with more than two stages, the same relationships are repeated for each succeeding stage. Since there is a significant amount of hand calculations involved in obtaining the modified parameters, a small computer program could be written to punch out these values in a format compatible with the input to the modified NASA turbine code.



## ● Nomenclature Used in Calculation of Modified Parameters

Symbol	Definition	Units
$D_R$	Root diameter	in
$D_T$	Tip diameter	in
$g$	Gravitational acceleration (32.2)	ft/sec <sup>2</sup>
$P_S$	Static pressure	psia
$P_T$	Total pressure	psia
PTPS	Total-to-static pressure ratio across first stator	---
$R$	Gas constant	ft <sup>2</sup> /°R
$T_S$	Static temperature	°R
$T_T$	Total temperature	°R
$U$	Wheel speed	ft/sec
$V$	Gas velocity	ft/sec
$v_S$	Specific volume	ft <sup>3</sup> /lb
$\gamma$	Ratio of specific heats	---
$\eta$	Overall effective blade efficiency	---

### 2.3.5 POSSIBLE FUTURE MODIFICATIONS TO CODE

1) With the advent of the CDC 6600 computer and its 65 K core (as compared to the IBM 7094 and its core of 32 K), it is possible to expand the maximum number of radial sectors to greater than 6 and the maximum number of stages to exceed 8. Of course computer run times would be longer and a different method of printing out data would have to be used.

2) The code could be changed so as to iterate to a desired exit pressure condition automatically by comparing the average turbine exit total pressure with that desired. If the difference between the exit total pressures were not within some given tolerance, the first stator pressure ratio PTPS would be adjusted accordingly.

3) Non-uniform turbine inlet radial distributions in pressure, temperature, and velocity could be achieved by inputting such quantities. The assumption in the code as presently programmed is that the inlet radial distributions are uniform.

### 2.3.6 REFERENCES

1. E. E. Flagg, "Analytical Procedure and Computer Program for Determining the Off-Design Performance of Axial Flow Turbines," NASA CR-710, February 1967.
2. Westinghouse Electric Corporation, Astronuclear Laboratory, Report WANL-PR (DD)-017, January 1967, Contract NAS 7-390.

## APPENDICES TO SECTION 2.3

### APPENDIX 2.3 A

#### SAMPLE PROBLEMS ILLUSTRATING USE OF CODE

#### 2.3 A-1 NASA Reference Two-Stage Gas Turbine (5 Radial Sectors)

##### 1. Comparison of Results

The sample problem given in NASA CR-710 was run both on the IBM 7094 (II) and CDC 6600 computer. The data output from both machines was in exact agreement to at least the sixth significant figure. The minor discrepancies noted were thought to be due to the difference in the number

of significant places carried in the respective machines. It was found that the sample problem data output given in NASA CR-710 did not exactly correspond to that report's data input. When the data input was appropriately changed, the subsequent output was in substantial agreement (at least to the fourth significant place) with that given in NASA CR-710. No explanation can be given at this time as to why there was not agreement to at least the sixth place. But it is felt that the agreement is more than adequate to satisfy engineering criteria.

## 2. Data Input

TUBINE COMPTER PROGRAM  
NASA TWO STAGE REFERENCE TURBINE

1.00 5041 -8 DEG. LOSS PROFILE .98 .946. .977 .90.

SDATAIN

STGCR=	1.000					
ITIN=	700.000	PTIN=	17.140	WAIR=	0.000	FAIR= 0.000
PTPS=	1.600	DELC=	0.000	DELL=	0.000	DELA= 0.000
STG=	2.000	SECT=	5.000	EXPN=	3.000	EXPP= 3.000
PAF=	0.000	SLI=	0.000	AACS=	1.000	RPM= 5041.000
VCTD=	1.000	RSL=	53.350	TSL=	518.608	PSL= 14.696
GAMSL=	1.600	ENDSTG=	0.000	ENDJOB=	0.000	

INLET RADIAL PROFILES

PCNH=	.200	.200	.200	.200	.200	0.000
-------	------	------	------	------	------	-------

STANDARD OPTION  
AXIAL STATIONS

STAGE=	1					
	STA. 0	STA. 1	STA. 1A	STA. 2	STA. 2A	
RG=	53.350	53.350	53.350	53.350	53.350	0.000
GAMG=	1.400	1.400	1.400	1.400	1.400	0.000
DR=	19.110	19.110	18.969	18.406	18.265	0.000
DT=	28.000	28.000	28.141	28.704	28.845	0.000
RWG=	1.000	1.000	1.000	1.000	1.000	0.000

STATOR RADIAL DISTRIBUTIONS

	ROOT		PITCH		TIP	
SDIA=	0.000	0.000	0.000	0.000	0.000	0.000
SDEA=	0.000	0.000	0.000	0.000	0.000	0.000
SPEC=	1.000	1.000	1.000	1.000	1.000	0.000
SEIA=	.970	.980	.980	.980	.970	0.000
SCF=	.977	.977	.977	.977	.977	0.000
SPA=	22.140	26.035	30.135	34.194	38.499	0.000
SESTH=	1.000					

ROTOR RADIAL DISTRIBUTIONS

RDIA=	50.600	44.900	38.100	30.200	20.900	0.000
RDEA=	0.000	0.000	0.000	0.000	0.000	0.000
RREC=	1.000	1.000	1.000	1.000	1.000	0.000
RETA=	.919	.946	.946	.946	.919	0.000
RCF=	.950	.950	.950	.950	.950	0.000
RPA=	33.408	36.352	38.976	41.280	43.008	0.000
RTF=	1.000	1.000	1.000	1.000	1.000	0.000
REPTH=	1.010					

STANDARD OPTION  
AXIAL STATIONS

STAGE=	2					
	STA. 0	STA. 1	STA. 1A	STA. 2	STA. 2A	
RG=	53.350	53.350	53.350	53.350	53.350	0.000
GAMG=	1.400	1.400	1.400	1.400	1.400	0.000
DR=	18.265	17.814	17.673	17.110	17.110	0.000
DT=	28.845	29.296	29.437	30.000	30.000	0.000
RWG=	1.000	1.000	1.000	1.000	1.000	0.000

STATOR RADIAL DISTRIBUTIONS						
	ROOT		PITCH		TIP	
SDIA=	25.000	22.400	20.200	18.300	16.600	0.000
SDEA=	0.000	0.000	0.000	0.000	0.000	0.000
SREC=	1.000	1.000	1.000	1.000	1.000	0.000
SETA=	.970	.980	.980	.980	.970	0.000
SCF=	.925	.925	.925	.925	.925	0.000
SPA=	30.420	36.855	43.485	50.765	58.240	0.000

SESTH= 1.010

ROTOR RADIAL DISTRIBUTIONS						
RDIA=	36.600	26.900	16.100	4.600	-6.700	0.000
RDEA=	0.000	0.000	0.000	0.000	0.000	0.000
RREC=	1.000	1.000	1.000	1.000	1.000	0.000
RETA=	.919	.946	.946	.946	.919	0.000
RCF=	.900	.900	.900	.900	.900	0.000
RPA=	43.350	48.150	52.350	55.750	58.550	0.000
RTF=	1.000	1.000	1.000	1.000	1.000	0.000

REPTH= 1.010

### 3. Listing of Data Output

NASA TURBINE COMPUTER PROGRAM  
 NASA TWO STAGE REFERENCE TURBINE  
 1.00 5041 -R DEG. LOSS PROFILE .93 .946. .977 .90,  
 CASE 1. 0  
 STAGE PERFORMANCE

	STAGE 1	STAGE 2	STAGE 3	STAGE 4
TTBAR 0	700.0	608.5		
PTBAR 0	17.140	10.120		
WG 0	43.612	43.612		
CEL P	21.960	11.370		
WRI/P	67.320	106.303		
DH/TTBAR0	.03137	.01864		
N/R1	190.532	204.358		
ETA T1	.93545	.93026		
E1A TS	.82312	.74101		
E1A AT	.92064	.92176		
PT0/PS1	1.600	1.327		
PTBAR0/PTBAR2	1.694	1.358		
PTBAR0/PS2	1.840	1.475		
PTR2/PS2	1.340	1.216		
TTBAR2/TTBAR0	.86926	.92212		
TTA1A/TTBAR0	.91710	.94753		
WG 1	43.612	43.612		
PS 1A	10.770	7.659		
TTR 1A	642.0	576.8		
PTR 1A	12.470	8.343		
WG 1A	43.612	43.612		
PS 2	9.314	6.860		
TTBAR 2	608.5	561.1		
PTBAR 2	10.120	7.452		
WG 2	43.612	43.612		
WG 2A	43.612	43.612		
UP/VI	.44821	.59095		
UR/VI	.35559	.43632		
PS1 P	1.02409	.53026		
PS1 R	1.62705	.97270		
RX P	.21420	.26054		
RX R	-.08793	-.07253		
ALPHA 0	0.000	20.327		
I STATOR	0.000	.127		
RETA 1A	46.336	15.343		
I ROTOR	8.236	-.757		

### 3. Output Data (continued)

ALPHA 2A	20.327	-9.259
DELTA R	116.216	86.338
M 1	.83798	.64215
M1 RT	1.01118	.78439
MR 1A	.47064	.35156
MR1A RT	.69181	.50438
MR 2	.64048	.52017
MR2 TIP	.69787	.61846
E/TH CR	16.272	9.652
N/RTM CR	4339.3	4654.2
WRTMCR/C	43.440	68.554

PSI P	.77717	OVERALL PERFORMANCE	PSI W	1.32335	DEL H	33.33064
WRT/P	67.31951	N/RT	190.53189	DELH/TTIN	.04761	
PT0/PT0AR2	2.24991	PT0/PS2	2.49847	PT0/PAT2A	2.30903	
ETA TT	.93700	ETA TS	.86213	ETA TAT	.93477	
WNE/60C	3141.641	N/RTM CR	4339.329	E/TH CR	24.69720	

NASA TURBINE COMPUTER PROGRAM  
 NASA TWO STAGE REFERENCE TURBINE  
 1.00 5041 -B DEG. LOSS PKCFIL .98 .946, .977 .90,  
 CASE 1, 0  
 INTER-STAGE PERFORMANCE

STA 0 STATOR INLET			STAGE 1.			
DIAM 0	19.999	21.777	23.555	25.333	27.111	
TT 0	700.0	700.0	700.0	700.0	700.0	
PT 0	17.140	17.140	17.140	17.140	17.140	
ALPHA 0	0.000	0.000	0.000	0.000	0.000	
I STATOR	0.000	0.000	0.000	0.000	0.000	
V 0	299.463	299.463	299.463	299.463	299.463	
VU 0	0.000	0.000	0.000	0.000	0.000	
VZ 0	299.463	299.463	299.463	299.463	299.463	
TS 0	692.5	692.5	692.5	692.5	692.5	
PS 0	16.509	16.509	16.509	16.509	16.509	
DENS 0	.06434	.06434	.06434	.06434	.06434	
M 0	.23213	.23213	.23213	.23213	.23213	
CP 0	.23996	.23996	.23996	.23996	.23996	
RG 0	53.350	53.350	53.350	53.350	53.350	
GAMG 0	1.40000	1.40000	1.40000	1.40000	1.40000	
RWG 0	1.00000	1.00000	1.00000	1.00000	1.00000	
WG 0	6.58435	7.70666	8.80273	9.78081	10.73712	43.61168 TOTAL FLOW
STA 1 STATOR EXIT						
DIAM 1	19.999	21.777	23.555	25.333	27.111	
ALPHA 1	69.539	67.940	66.303	64.911	63.359	
DEL A	69.539	67.940	66.303	64.911	63.359	
V 1	1147.472	1080.202	1017.726	954.148	895.217	
VU 1	1075.549	1001.125	931.914	864.123	800.175	
VZ 1	401.291	405.692	404.026	404.586	401.413	
TS 1	590.3	602.9	613.8	624.2	633.3	
PS 1	9.252	10.046	10.712	11.379	11.936	
DENS 1	.04230	.04498	.04711	.04920	.05087	
M 1	.96384	.89743	.83798	.77904	.72567	
ZWI INC	-.65502	-.69615	-.73603	-.77804	-.80159	
CP 1	.93195	.92314	.91342	.90150	.88810	
CP 1	.23996	.23996	.23996	.23996	.23996	
RG 1	53.350	53.350	53.350	53.350	53.350	
GAMG 1	1.40000	1.40000	1.40000	1.40000	1.40000	
RWG 1	1.00000	1.00000	1.00000	1.00000	1.00000	
WG 1	6.58435	7.70666	8.80273	9.78081	10.73712	43.61168 TOTAL FLOW

### 3. Output Data (continued)

NASA TURBINE COMPUTER PROGRAM  
 NASA TWO STAGE REFERENCE TURBINE  
 1.00 5041 -8 DEG. LOSS PROFILE .98 .946, .977 .90,  
 CASE 1, 0  
 INTER-STAGE PERFORMANCE

STA 1A	ROTOR INLET	STAGE 1.				
DIAW 1A	19.888	21.721	23.555	25.389	27.224	
PTW 1A	11.944	12.251	12.478	12.778	13.083	
ITW 1A	637.2	639.2	642.0	645.8	650.4	
RETA 1A	58.685	53.188	48.336	37.984	27.212	
1 ROTOR	8.085	8.288	8.236	7.764	6.312	
R 1A	754.102	656.463	572.034	493.769	433.126	
RU 1A	644.243	525.969	413.810	303.751	198.059	
WR 1A	633.40	545.64	470.64	402.74	350.68	
U 1A	437.407	477.755	516.104	558.452	598.801	
PS 1A	9.225	10.067	10.770	11.461	12.035	
TS 1A	589.8	603.3	614.7	625.5	634.8	
CP 1A	.23996	.23996	.23996	.23996	.23996	
RG 1A	53.350	53.350	53.350	53.350	53.350	
GAMG 1A	1.40000	1.40000	1.40000	1.40000	1.40000	
RWG 1A	1.00000	1.00000	1.00000	1.00000	1.00000	
WG 1A	6.58435	7.70666	8.80273	9.74081	10.73712	43.61168 TOTAL FLOW
STA 2	ROTOR EXIT					
DIAW 2	19.436	21.495	23.555	25.615	27.674	
PTW 2	11.947	12.225	12.478	12.810	13.154	
ITW 2	636.5	638.8	642.0	644.3	651.4	
RETA 2	57.531	58.629	59.379	60.258	60.964	
UBETA 2	116.218	111.817	105.715	98.223	88.175	
R 2	700.060	738.948	764.765	797.556	818.486	
RU 2	590.630	630.922	658.123	692.496	715.611	
WR 2	585.12	618.84	640.48	664.793	684.11	
U 2	477.500	472.802	516.104	563.406	608.708	
RX	-.00402	.11699	.61420	.30756	.38245	
DELH	21.683	22.134	24.182	22.137	21.658	
PSI P	2.90236	2.45376	2.06895	1.76143	1.48743	
ETA TT	.91412	.94184	.94518	.94752	.92554	
ETA TS	.80596	.82681	.83127	.83236	.81639	
ETA AT	.89419	.92233	.92980	.92438	.91677	
ZWI INC	-1.85326	-1.61317	-1.42033	-1.24554	-1.09099	
CP R	-.16035	.20957	.44051	.61671	.71997	
PS 2	9.277	9.295	9.314	9.330	9.342	
TS 2	595.7	593.3	593.3	593.3	595.7	
CP 2	.23996	.23996	.23996	.23996	.23996	
RG 2	53.350	53.350	53.350	53.350	53.350	
GAMG 2	1.40000	1.40000	1.40000	1.40000	1.40000	
RWG 2	1.00000	1.00000	1.00000	1.00000	1.00000	
WG 2	6.89415	7.85826	8.73519	9.64391	10.45615	43.61166 TOTAL FLOW
WT 2A	10.061	10.112	10.122	10.148	10.138	
TT 2A	609.6	607.7	607.6	607.7	609.7	
V 2A	402.148	404.590	403.078	404.007	398.169	
VU 2A	164.083	158.536	140.019	128.806	106.469	
ALPHA 2A	24.080	22.949	20.327	18.592	15.509	
MF 2A	.30674	.31338	.31636	.32046	.32044	
VZ 2A	367.151	374.409	377.978	382.924	383.670	
TS 2A	596.2	594.0	594.0	594.2	596.5	
PS 2A	9.304	9.334	9.355	9.376	9.391	
DEFS 2A	.04213	.04241	.04251	.04259	.04249	
M 2A	.33598	.34032	.33736	.33811	.33255	
CP 2A	.23996	.23996	.23996	.23996	.23996	
RG 2A	53.350	53.350	53.350	53.350	53.350	
GAMG 2A	1.40000	1.40000	1.40000	1.40000	1.40000	
RWG 2A	1.00000	1.00000	1.00000	1.00000	1.00000	
WG 2A	6.89415	7.85826	8.73519	9.64391	10.45615	43.61166 TOTAL FLOW

### 3. Output Data (continued)

NASA TURBINE COMPUTER PROGRAM  
 NASA TWO STAGE REFERENCE TURBINE  
 1.00 5041 -8 DEG. LOSS PROFILE .98 .946 .977 .90,  
 CASE 1, 0  
 INTER-STAGE PERFORMANCE

STA 0	STATOR INLET	STAGE 2.				
DIAM 0	19.323	21.439	23.555	25.671	27.787	
TT 0	608.5	608.5	608.5	608.5	608.5	
PT 0	10.120	10.120	10.120	10.120	10.120	
ALPHA 0	24.080	22.949	20.327	18.592	15.509	
I STATOR	-.920	.549	.127	.292	-1.090	
V 0	402.148	406.590	403.078	404.607	398.169	
VU 0	164.083	158.536	140.019	128.806	106.469	
VZ 0	367.151	374.409	377.978	382.924	363.670	
TS 0	596.2	594.0	594.0	594.2	596.5	
PS 0	9.304	9.334	9.355	9.376	9.391	
DENS 0	.04213	.04241	.04251	.04250	.04249	
M 0	.33598	.34032	.33736	.33811	.33255	
CP 0	.23996	.23996	.23996	.23996	.23996	
RG 0	53.350	53.350	53.350	53.350	53.350	
GAMG 0	1.40000	1.40000	1.40000	1.40000	1.40000	
RWG 0	1.00000	1.00000	1.00000	1.00000	1.00000	
WG 0	6.89815	7.85826	8.73519	9.64391	10.45615	43.61166 TOTAL FLOW

STA 1	STATOR EXIT	STAGE 2.				
DIAM 1	18.962	21.259	23.555	25.851	28.148	
ALPHA 1	61.651	59.301	57.068	54.670	52.236	
DEL A	85.731	82.250	77.395	73.262	67.744	
V 1	852.196	795.576	740.339	695.126	650.709	
VU 1	749.990	684.085	626.415	567.111	514.398	
VZ 1	404.665	406.168	405.742	401.978	398.519	
TS 1	548.0	555.8	562.1	568.3	573.2	
PS 1	6.934	7.321	7.624	7.926	8.158	
DENS 1	.03415	.03556	.03661	.03765	.03841	
M 1	.74259	.68839	.64215	.59484	.55441	
ZWI INC	-1.03734	-1.09864	-1.13154	-1.14854	-1.17646	
CP S	.77731	.73881	.70832	.68221	.65558	
CP 1	.23996	.23996	.23996	.23996	.23996	
RG 1	53.350	53.350	53.350	53.350	53.350	
GAMG 1	1.40000	1.40000	1.40000	1.40000	1.40000	
RWG 1	1.00000	1.00000	1.00000	1.00000	1.00000	
WG 1	6.56380	7.69027	8.76394	9.79979	10.79323	43.61164 TOTAL FLOW

STA 1A	ROTOR INLET	STAGE 2.				
DIAM 1A	18.849	21.202	23.555	25.908	28.261	
PTR 1A	7.993	8.161	8.343	8.600	8.871	
TTR 1A	570.7	573.3	576.8	581.8	587.6	
BETA 1A	40.535	28.960	15.343	-5.585	-15.815	
I ROTOR	3.935	2.060	-.757	-5.185	-9.115	
R 1A	522.702	457.435	404.333	389.963	400.905	
RU 1A	339.876	219.552	108.311	-3.979	-109.261	
MR 1A	.45573	.39220	.35196	.33344	.34128	
U 1A	414.602	464.353	518.104	569.855	621.606	
PS 1A	6.930	7.341	7.659	7.970	8.209	
TS 1A	548.0	556.2	562.9	569.2	574.3	
CP 1A	.23996	.23996	.23996	.23996	.23996	
RG 1A	53.350	53.350	53.350	53.350	53.350	
GAMG 1A	1.40000	1.40000	1.40000	1.40000	1.40000	
RWG 1A	1.00000	1.00000	1.00000	1.00000	1.00000	
WG 1A	6.56380	7.69027	8.76394	9.79979	10.79323	43.61164 TOTAL FLOW

NASA TURBINE COMPUTER PROGRAM  
NASA TWO STAGE REFERENCE TURBINE  
1.00 5041 -8 DEG. LOSS PROFILE .98 .946. .977 .90.  
CASE 1. 0  
INTER-STAGE PERFORMANCE

STA 2	WCTOR EXIT				
DIAW 2	18.399	20.977	23.555	26.133	28.711
PIR 2	7.950	8.142	8.343	8.625	8.926
TTW 2	570.0	573.0	576.8	582.3	588.7
RETA 2	45.803	47.980	49.600	51.528	52.888
URETA	46.334	48.440	49.943	50.944	52.072
D 2	510.818	554.390	597.132	646.661	635.002
PI 2	366.232	414.834	454.736	506.279	546.256
PH 2	.44500	.44703	.52077	.56377	.59605
I 2	404.645	461.399	516.104	574.808	631.513
RX	.32767	.16069	.26054	.36780	.43067
DELTA	11.872	11.918	11.852	11.307	10.570
PSI P	1.77102	1.38865	1.08674	.86417	.67406
ETA TT	.92495	.94980	.94776	.94026	.89652
ETA TS	.77200	.77551	.75903	.73739	.69018
ETA AT	.92268	.94655	.94164	.93302	.88571
Z+I INC	-1.83575	-1.49053	-1.21766	-.96425	-.75608
CL F	-.04411	.34059	.53009	.63634	.65747
PS 2	6.855	6.857	6.860	6.863	6.867
TS 2	547.3	547.0	547.1	547.5	549.6
CP 2	.23996	.23996	.23996	.23996	.23996
RG 2	53.350	53.350	53.350	53.350	53.350
GANG 2	1.40000	1.40000	1.40000	1.40000	1.40000
RWG 2	1.00000	1.00000	1.00000	1.00000	1.00000
WG 2	6.21734	7.46046	8.67619	10.00385	11.25376
PT 2A	7.334	7.349	7.439	7.491	7.537
TT 2A	559.0	558.8	559.9	561.4	564.4
V 2A	358.174	376.670	394.171	408.102	422.019
VU 2A	-36.463	-46.565	-63.368	-64.529	-85.256
ALPHA 2A	-6.165	-7.101	-9.299	-9.667	-11.655
MF 2A	.31022	.32601	.33752	.35074	.35964
VZ 2A	356.102	373.780	387.017	402.308	413.318
TS 2A	546.3	547.0	547.1	547.5	549.6
PS 2A	6.855	6.857	6.860	6.863	6.867
DENS 2A	.03374	.03384	.03384	.03384	.03372
M 2A	.31702	.32853	.34202	.36579	.36721
CP 2A	.23996	.23996	.23996	.23996	.23996
RG 2A	53.350	53.350	53.350	53.350	53.350
GANG 2A	1.40000	1.40000	1.40000	1.40000	1.40000
RWG 2A	1.00000	1.00000	1.00000	1.00000	1.00000
RG 2A	6.21734	7.46046	8.67619	10.00385	11.25376
					43.61162 TOTAL FLOW

### 2.3 A-2 Wet-Vapor Potassium Turbine\*(5 Radial Sectors)

#### 1. Calculation of Modified Parameters

Using the equations given in Section 2.3.4, the values for the modified parameters (given in Table 2.3 A-1) were calculated by hand and used as data input to the modified NASA turbine code. Only the 5th and 6th stages are analyzed and correspond to stages 1 and 2 in the output listing.

#### 2. Comparison of Results from Modified NASA Code and WSD Code

Table 2.3A-2 shows a comparison of the results between the 1-D and 2-D codes from WSD and the NASA code using the modified parameters. The total-to-static pressure ratio (PTPS) across the first stator was adjusted until the turbine exit conditions were identical to those obtained in

\*Described in Reference (2).

the Steam Division codes. The modified parameters were assumed to remain constant during the small changes in PTPS. Unfortunately, a completely consistent set of input data was impossible to be obtained from either Table I or Table II of Reference (2) or

TABLE 2.3A-1

#### MODIFIED PARAMETERS FOR POTASSIUM TURBINE

Station	D <sub>2</sub> *	D <sub>1</sub> *	R*	γ*	η*	
0	5.29	7.51	31.158	1.1825	---	P <sub>T0</sub> = 38.828; PTPS = 1.3619
1	5.15	7.83	30.842	1.1437	0.92577	
1A	5.15	7.83	30.842	1.1437	---	
2	5.04	8.28	30.689	1.16607	0.81662	
2A	5.04	8.28	30.689	1.16607	---	
0	5.04	8.28	30.689	1.16607	---	
1	4.88	8.62	30.828	1.1447	0.94752	
1A	4.88	8.62	30.828	1.1447	---	
2	4.60	9.10	30.763	1.1637	0.8155	
2A	4.60	9.10	30.763	1.1637	---	

**TABLE 2.3A-2**  
**COMPARISON OF POTASSIUM TURBINE DATA AT MEAN DIAMETER**

BLADE ROW EXIT CONDITIONS	Fourth Stator			Fifth Stator			Fifth Rotor			Sixth Stator			Sixth Rotor		
	Q1-D Code (1)	NASA Code (2)	% Difference	Q1-D Code (1)	NASA Code (2)	% Difference	Q1-D Code (1)	NASA Code (2)	% Difference	Q1-D Code (1)	NASA Code (2)	% Difference	Q1-D Code (1)	NASA Code (2)	% Difference
BLADE HEIGHT (inch)	1.11	1.11 *	0.0	1.34	1.34 *	0.0	1.62	1.62 *	0.0	1.87	1.87 *	0.0	2.25	2.25 *	0.0
MEAN DIAMETER (inch)	6.40	6.40 *	0.0	6.49	6.49 *	0.0	6.66	6.66 *	0.0	6.75	6.75 *	0.0	6.85	6.85 *	0.0
FLOW ANGLE (degree)	64.37	--	--	64.37(65.03)	65.03*	+1.03(0.0)	64.37(63.65)	63.65*	-1.12(0.0)	57.32(57.57)	57.57*	+0.436(0.0)	60.30(58.98)	58.98*	-2.19(0.0)
STATIC PRESSURE (psia)	37.00	--	--	28.51	28.198	-1.09	22.04	21.963	-0.349	19.69	19.495	-0.950	16.90	16.892	-0.047
STATIC TEMPERATURE (°R)	2052	--	--	1994	1991.9	-0.105	1937	1936.7	-0.015	1914	1911.9	-0.110	1882	1882.0	0.0
FLOW RATE (lb/sec)	5.76	--	--	5.76	5.75951	0.0	5.76	5.75951	0.0	5.76	5.75951	0.0	5.76	5.75951	0.0
JET VELOCITY (ft/sec)	1034	--	--	1049(1076.5)	1091.3	+4.03(+1.37)	1075(1033.5)	1028.4	-4.33(-0.496)	815 (811.7)	823.0	+0.982(1.39)	822(790.6)	779.9	-4.77(-1.35)
GAMMA	1.211	1.1825*	--	1.203	1.1437*	--	1.196	1.6607*	--	1.195	1.1447*	--	1.194	1.1637	--
GAS CONSTANT (ft <sup>2</sup> /°R)	31.51	31.158*	--	31.23	30.842*	--	30.93	30.689*	--	30.80	30.826*	--	30.65	30.763*	--
EFFICIENCY COEFFICIENT FOR BLADE ROW	--	--	--	--	0.92577	--	--	0.81662*	--	--	0.94752*	--	--	0.8155	--

(1) From Reference (2)

(2) Using modified NASA Code (5 radial sectors)

Terms in parentheses are from Q2-D code. See Reference (2)  
Flow angles are with respect to axial direction

\* Indicates NASA code input data.

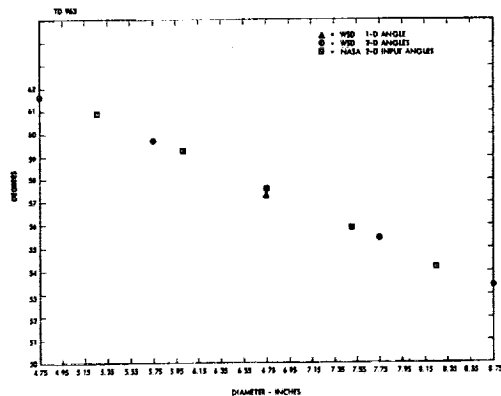


**Figure 2.3A-1 6th Stator Blade Exit Angles**

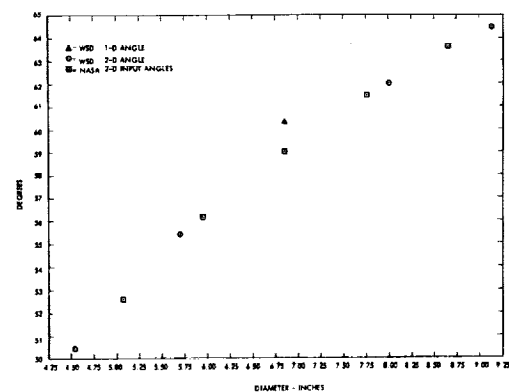


**Figure 2.3A-2 6th Rotor Blade Exit Angles**



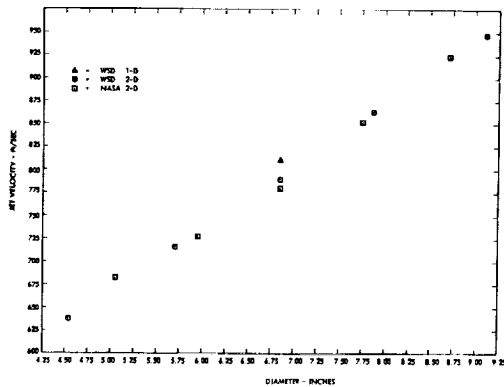


Figure 2.3A-3 6th Rotor Exit Jet Velocity

a combination of the two. The difference in the 2-D blade angle distribution from that used in the 1-D calculation is most likely the primary reason that the jet velocities at the mean diameters are not in better agreement.

Figures 2.3A-1 and 2.3A-2 show the slight differences in the angles used in WSD 2-D calculations and those used as input to the NASA code 2-D analysis. Figure 2.3A-3 shows the good agreement between the turbine exit jet

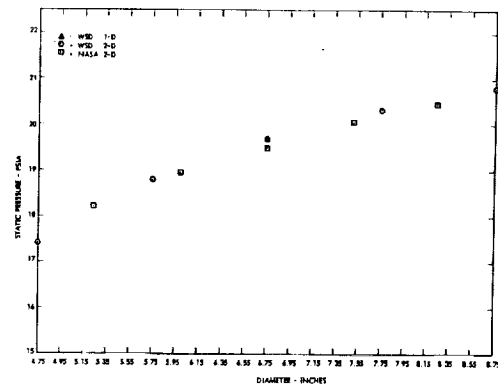


Figure 2.3A-4 5th Stator Exit Static Pressure

velocities as calculated by both codes. In Figure 2.3A-4 there is also good agreement with the static pressure distributions from the 5th stator exit.

It is therefore concluded that if one performs a hand solution (or uses an appropriate computer code) for a 1-D turbine analysis, then this method of using modified  $\gamma$ ,  $R$ , and  $\eta$  parameters with the NASA code will give a valid and thermodynamically consistent two-dimensional analysis of a turbine operating in the wet vapor region.

### 3. Data Input

```

TURBINE COMPUTER PROGRAM
TWO STAGE POTASSIUM TURBINE
FIVE RADIAL SECTIONS
$DATAIN
STGCM= 1.000
TTIN= 2067.300 PTIN= 30.828 WATR= 0.000 FAIR= 0.000
PTPS= 1.377 DELC= 0.000 DELL= 0.000 DELA= 0.000
STG= 2.000 SECT= 5.000 EXPA= 0.000 EXFP= 0.000
PAF= 1.000 SLI= 0.000 AAC= 1.000 RPM= 2400.000
VCTR= 1.000 WSL= 37.600 TSL= 100.000 PSL= 11.200
GAPSL= 1.618 EAUSTG= 0.000 ENDJUR= 0.000

INLET RADIAL PROFILES
PCNH= .200 .200 .200 .200 .200 0.000

STANDARD OPTION
AXIAL STATIONS
STAGE= 1
STA. 0 STA. 1 STA. 1A STA. 2 STA. 2A
PG= 31.158 30.842 30.842 30.689 30.689 0.000
GANG= 1.182 1.144 1.144 1.166 1.166 0.000
DH= 5.290 5.150 5.150 5.040 5.040 0.000
DT= 7.510 7.830 7.830 8.280 8.280 0.000
RWG= 1.000 1.000 1.000 1.000 1.000 0.000

STATOR RADIAL DISTRIBUTIONS
ROOT PITCH TIP
SDIA= 0.000 0.000 0.000 0.000 0.000 0.000
SDEA= 66.100 65.000 65.000 64.350 63.650 0.000
SREC= 1.000 1.000 1.000 1.000 1.000 0.000
SETA= .926 .926 .926 .926 .926 0.000
SCF= 1.000 1.000 1.000 1.000 1.000 0.000
SPA= 0.000 0.000 0.000 0.000 0.000 0.000
SESTH= 1.000

```

ROTOR RADIAL DISTRIBUTIONS						
ROIA=	48.850	41.500	33.060	22.000	8.500	0.000
ROEA=	61.600	62.650	63.650	64.550	65.350	0.000
RPEC=	1.000	1.000	1.000	1.000	1.000	0.000
RETA=	.817	.817	.817	.817	.817	0.000
RCE=	1.000	1.000	1.000	1.000	1.000	0.000
RPA=	0.000	0.000	0.000	0.000	0.000	0.000
RTF=	1.000	1.000	1.000	1.000	1.000	0.000
PERT=	1.000					

STANDARD OPTION							
AXIAL STATIONS							
STAGE=	2	STA. 0	STA. 1	STA. 1A	STA. 2	STA. 2A	
RG=		30.6P9	30.42R	30.820	30.7-3	30.763	0.000
GANG=		1.166	1.145	1.145	1.164	1.164	0.000
DR=		5.040	4.880	4.880	4.600	4.600	0.000
DT=		8.2P0	8.620	8.620	9.100	9.100	0.000
HWG=		1.000	1.000	1.000	1.000	1.000	0.000

STATOR RADIAL DISTRIBUTIONS						
	ROOT		PITCH		TIP	
SOIA=	32.300	29.700	26.540	23.400	20.000	0.000
SDEA=	60.900	59.250	57.570	55.450	54.150	0.000
SREC=	1.000	1.000	1.000	1.000	1.000	0.000
SETA=	.948	.948	.948	.948	.948	0.000
SCF=	1.000	1.000	1.000	1.000	1.000	0.000
SPA=	0.000	0.000	0.000	0.000	0.000	0.000
SEST=	1.000					

ROTOR RADIAL DISTRIBUTIONS						
ROIA=	32.000	16.000	-2.850	-20.500	-35.000	0.000
ROEA=	52.600	56.100	58.980	61.450	63.600	0.000
RPEC=	1.000	1.000	1.000	1.000	1.000	0.000
RETA=	.816	.816	.816	.816	.816	0.000
RCE=	1.000	1.000	1.000	1.000	1.000	0.000
RPA=	0.000	0.000	0.000	0.000	0.000	0.000
RTF=	1.000	1.000	1.000	1.000	1.000	0.000
PERT=	1.000					

#### 4. Output Data

NASA TURBINE COMPUTER PROGRAM  
TWO STAGE POTASSIUM TURBINE  
FIVE RADIAL SECTORS

	CASE 2. 0 STAGE PERFORMANCE			
	STAGE 1	STAGE 2	STAGE 3	STAGE 4
TYBAR 0	2067.3	1955.8		
PTBAR 0	38.623	23.524		
WG 0	5.758	5.758		
DEL H	32.071	17.954		
WRT/P	6.743	10.825		
DM/TTBAR0	.01590	.00918		
N/R1	527.549	542.687		
ETA TT	.82986	.82761		
ETA TS	.73329	.71650		
ETA AT	.80877	.82531		
PT0/PS1	1.377	1.205		
PTBAR0/PTBAR2	1.651	1.331		
PTBAR0/PS2	1.768	1.353		
PTR2/PS2	1.396	1.219		
TTBAR2/TTBAR0	.94606	.96900		
TTT1A/TTT3R0	.97296	.94389		
WG 1	5.758	5.758		
PS 1A	26.190	19.445		
TTR 1A	2011.4	1924.3		
PTD 1A	30.472	20.520		
WG 1A	5.758	5.758		
PS 2	21.963	10.892		
TTRAR 2	1955.8	1895.2		
PTBAR 2	23.524	17.676		
WG 2	5.758	5.758		
WG 2A	5.758	5.758		
UP/VI	.45953	.63693		
UR/VI	.35610	.44398		
PS1 P	.86799	.44324		
PS1 R	1.44550	.91223		
RX P	.42914	.42908		

#### 4. Output Data (continued)

RX R	.20904	.12460
ALPHA 0	0.000	26.147
I STATOR	0.000	-.393
BETA 1A	33.910	-1.554
I ROTOR	.850	1.276
ALPHA 2A	26.147	-6.951
OBETA R	109.973	64.948
M 1	.72584	.55860
M1 RT	.86583	.70312
MR 1A	.36920	.29968
MR1A RT	.55090	.42459
MR 2	.68866	.52969

NASA TURBINE COMPUTER PROGRAM  
TWO STAGE POTASSIUM TURBINE  
FIVE RADIAL SECTORS

CASE 2. 0 STAGE PERFORMANCE			
STAGE 1	STAGE 2	STAGE 3	STAGE 4
MR2 TIP	.75376	.65843	
E/TH CR	39.397	23.242	
N/PTH CR	26274.6	27306.5	
WRTHCRC/D	1.806	2.853	

OVERALL PERFORMANCE			
PSI P	.64847	PSI H	1.19809
PT/P	6.74307	N/HT	527.84874
PT0/PTRAF2	2.19659	PT0/PS2	2.29857
ETA TT	.83219	ETA TS	.78924
WNE/60C	791.002	N/PTH CR	26274.585
		DEL H	50.82549
		DELH/TTIN	.02459
		PTG/PAT2A	2.20133
		ETA TAT	.83138
		E/TH CR	60.91617

NASA TURBINE COMPUTER PROGRAM  
TWO STAGE POTASSIUM TURBINE  
FIVE RADIAL SECTORS

CASE 2. 0  
INTER-STAGE PERFORMANCE

STA 1A ROTOR INLET		STAGE 1.					
DIAM 1A	5.418	5.954	6.490	7.026	7.562		
PTR 1A	29.654	30.037	30.472	31.095	31.763		
TTR 1A	2006.4	2008.6	2011.4	2015.7	2020.5		
BETA 1A	48.373	42.053	33.910	22.748	9.389		
I ROTOR	-.477	.553	.850	.748	.889		
R 1A	754.950	644.729	555.112	479.687	433.031		
RU 1A	564.315	431.849	309.689	185.482	70.616		
MR 1A	.50486	.42985	.36920	.31830	.28681		
U 1A	567.371	623.501	679.631	735.760	791.890		
PS 1A	25.666	27.044	28.198	29.351	30.308		
TS 1A	1970.3	1982.3	1991.9	2001.2	2008.6		
CP 1A	.31545	.31545	.31545	.31545	.31545		
RG 1A	30.842	30.842	30.842	30.842	30.842		
GAMG 1A	1.14370	1.14370	1.14370	1.14370	1.14370		
RG 1A	1.00000	1.00000	1.00000	1.00000	1.00000		
WG 1A	.96621	1.06158	1.15544	1.24444	1.33073	5.75839 TOTAL FLOW	
STA 2 ROTOR EXIT							
DIAM 2	5.364	6.012	6.660	7.308	7.956		
PTR 2	29.607	30.095	30.660	31.441	32.298		
TTR 2	2006.0	2009.1	2013.0	2018.6	2024.8		
BETA 2	61.600	62.650	63.650	64.550	65.350		
OBETA	109.973	104.703	97.560	87.298	74.739		
R 2	982.663	1002.932	1028.350	1063.272	1100.654		
RU 2	864.397	890.820	921.504	960.092	1000.536		
MR 2	.65812	.67166	.68866	.71198	.73700		
U 2	561.716	629.575	691.433	765.291	833.150		
RX	.27374	.35918	.42914	.49716	.55252		
DELH	32.437	32.851	33.097	33.027	32.852		
PSI P	2.54805	2.09519	1.74763	1.44741	1.24504		

#### 4. Output Data (continued)

ETA TT	.82775	.83218	.83334	.83074	.82585
ETA TS	.71574	.72958	.73822	.73985	.73811
ETA AT	.79117	.80466	.81300	.81534	.81449
ZWI INC	-1.34588	-1.19694	-1.06034	-.92090	-.81566
CP R	.40976	.58675	.70861	.79647	.84527
PS 2	21.823	21.907	21.963	22.019	22.058
TS 2	1936.3	1936.5	1936.7	1937.0	1937.4
CP 2	.27692	.27692	.27692	.27692	.27692
RG 2	30.689	30.689	30.689	30.689	30.689

NASA TURBINE COMPUTER PROGRAM  
TWO STAGE POTASSIUM TURBINE  
FIVE RADIAL SECTORS  
CASE 2. 0  
INTER-STAGE PERFORMANCE

STA 0	STATOR INLET		STAGE 1.		
DIAM 0	5.512	5.956	6.400	6.844	7.288
TT 0	2067.3	2067.3	2067.3	2067.3	2067.3
PT 0	38.828	38.828	38.828	38.828	38.828
ALPHA 0	0.000	0.000	0.000	0.000	0.000
I STATOR	0.000	0.000	0.000	0.000	0.000
V 0	447.396	447.396	447.396	447.396	447.396
VU 0	0.000	0.000	0.000	0.000	0.000
VZ 0	447.396	447.396	447.396	447.396	447.396
TS 0	2051.9	2051.9	2051.9	2051.9	2051.9
PS 0	36.991	36.991	36.991	36.991	36.991
DENS 0	.08332	.08332	.08332	.08332	.08332
M 0	.28686	.28686	.28686	.28686	.28686
CP 0	.25944	.25944	.25944	.25944	.25944
RG 0	31.158	31.158	31.158	31.158	31.158
GANG 0	1.18250	1.18250	1.18250	1.18250	1.18250
RWG 0	1.00000	1.00000	1.00000	1.00000	1.00000
WG 0	.96621	1.06158	1.15544	1.24444	1.33073
					5.75839 TOTAL FLOW
STA 1	STATOR EXIT				
DIAM 1	5.418	5.954	6.400	7.026	7.562
ALPHA 1	66.100	65.600	65.030	64.350	63.650
DEL A	66.100	65.600	65.030	64.350	63.650
V 1	1237.625	1158.855	1091.327	1021.851	962.546
VU 1	1131.606	1055.350	985.319	921.253	862.536
VZ 1	501.495	478.729	460.698	442.375	427.230
TS 1	1970.3	1982.3	1991.9	2001.2	2008.6
PS 1	25.666	27.044	28.198	29.351	30.308
DENS 1	.06082	.06370	.06609	.06848	.07045
M 1	.82778	.77262	.72584	.67812	.63751
ZWI INC	-.74081	-.75242	-.76537	-.77843	-.79547
CP 1	.86926	.85045	.83194	.81343	.79596
CP 1	.31545	.31545	.31545	.31545	.31545
RG 1	30.842	30.842	30.842	30.842	30.842
GANG 1	1.14370	1.14370	1.14370	1.14370	1.14370
RWG 1	1.00000	1.00000	1.00000	1.00000	1.00000
WG 1	.96621	1.06158	1.15544	1.24444	1.33073
					5.75839 TOTAL FLOW
STA 2					
GANG 2	1.16607	1.16607	1.16607	1.16607	1.16607
RWG 2	1.00000	1.00000	1.00000	1.00000	1.00000
WG 2	.93714	1.03939	1.14342	1.25898	1.37946
					5.75839 TOTAL FLOW
PT 2A	23.455	23.560	23.492	23.480	23.473
TT 2A	1957.3	1955.9	1955.0	1955.3	1955.9
V 2A	556.829	529.680	505.471	496.706	488.699
VU 2A	302.681	261.246	224.071	194.801	167.386
ALPHA 2A	32.428	29.552	26.147	23.491	20.630
MF 2A	.31302	.30858	.30566	.30596	.30742
VZ 2A	467.379	460.772	456.437	456.913	459.139
TS 2A	1936.3	1936.5	1936.7	1937.0	1937.4
PS 2A	21.823	21.907	21.963	22.019	22.058
DENS 2A	.05288	.05308	.05321	.05334	.05342
M 2A	.37293	.35473	.34051	.32760	.32721
CP 2A	.27692	.27692	.27692	.27692	.27692
RG 2A	30.689	30.689	30.689	30.689	30.689
GANG 2A	1.16607	1.16607	1.16607	1.16607	1.16607
RWG 2A	1.00000	1.00000	1.00000	1.00000	1.00000
WG 2A	.93714	1.03939	1.14342	1.25898	1.37946
					5.75839 TOTAL FLOW

#### 4. Output Data (continued)

NASA TURBINE COMPUTER PROGRAM  
TWO STAGE POTASSIUM TURBINE  
FIVE RADIAL SECTORS  
CASE 2, 0  
INTER-STAGE PERFORMANCE

STA 0	STATOR INLET		STAGE 2.		
DIAM 0	5.364	6.012	6.660	7.308	7.956
TT 0	1957.3	1955.9	1955.0	1965.3	1955.9
PT 0	23.655	23.566	23.492	23.480	23.473
ALPHA 0	32.928	29.552	26.147	23.091	20.030
I STATOR	.628	-.144	-.393	-.309	.030
V 0	556.829	529.680	508.471	496.706	488.699
VU 0	302.681	261.246	224.071	194.801	167.386
VZ 0	467.379	460.772	456.437	456.913	459.139
TS 0	1936.3	1936.5	1936.7	1937.0	1937.4
PS 0	21.823	21.907	21.963	22.019	22.058
DENS 0	.05288	.05302	.05321	.05334	.05342
M 0	.37293	.35473	.34051	.33260	.32721
CP 0	.27692	.27692	.27692	.27692	.27692
RG 0	30.689	30.689	30.689	30.689	30.689
GAMG 0	1.16607	1.16607	1.16607	1.16607	1.16607
RWG 0	1.00000	1.00000	1.00000	1.00000	1.00000
WG 0	.93714	1.03939	1.14342	1.25898	1.37946
					5.75839 TOTAL FLOW
STA 1	STATOR EXIT				
DIAM 1	5.254	6.002	6.750	7.498	8.246
ALPHA 1	60.900	59.250	57.570	55.850	54.150
DEL A	93.828	88.802	83.717	78.941	74.180
V 1	972.507	889.612	823.007	758.647	707.705
VU 1	849.749	764.538	694.656	627.834	573.632
VZ 1	472.965	454.853	441.353	425.875	414.479
TS 1	1897.0	1905.4	1911.9	1918.6	1923.9
PS 1	18.215	18.945	19.495	20.045	20.459
DENS 1	.04485	.04644	.04763	.04880	.04967
M 1	.66265	.60483	.55860	.51402	.47883
ZWI INC	-1.15624	-1.17526	-1.18763	-1.19784	-1.19952
CP S	.67216	.64549	.61830	.57133	.52315
CP 1	.31340	.31340	.31340	.31340	.31340
RG 1	30.828	30.828	30.828	30.828	30.828
GAMG 1	1.14470	1.14470	1.14470	1.14470	1.14470
RWG 1	1.00000	1.00000	1.00000	1.00000	1.00000
WG 1	.90940	1.03454	1.15778	1.27150	1.38518
					5.75840 TOTAL FLOW

4. Output Data (continued)

NASA TURBINE COMPUTER PROGRAM  
TWO STAGE POTASSIUM TURBINE  
MEAN DIAMETER CALCULATION  
CASE 3. 0  
INTER-STAGE PERFORMANCE

STA 0	STATOR INLET		STAGE 1.
DIAM 0	5.290	6.400	7.510
TT 0	2067.3	2067.3	2067.3
PT 0	38.828	38.828	38.828
ALPHA 0	0.000	0.000	0.000
I STATOR	0.000	0.000	0.000
V 0	447.396	447.396	447.396
VU 0	0.000	0.000	0.000
VZ 0	447.396	447.396	447.396
TS 0	2051.9	2051.9	2051.9
PS 0	36.991	36.991	36.991
DENS 0	.08332	.08332	.08332
M 0	.28686	.28686	.28686
CP 0	.25944	.25944	.25944
RG 0	31.158	31.158	31.158
GAMG 0	1.18250	1.18250	1.18250
RWG 0	1.00000	1.00000	1.00000
STA 1	STATOR EXIT		
DIAM 1	5.150	6.490	7.830
ALPHA 1	69.720	65.030	60.672
UEL A	69.720	65.030	60.672
V 1	1329.131	1091.327	940.563
VU 1	1246.734	989.319	820.011
VZ 1	460.698	460.698	460.698
TS 1	1955.5	1991.9	2011.3
PS 1	24.344	28.198	30.458
DENS 1	.05812	.06609	.07070
M 1	.89220	.72584	.62254
ZWI INC	-.65026	-.76537	-.85406
CP S	.88670	.83194	.77374
CP 1	.31545	.31545	.31545
RG 1	30.842	30.842	30.842
GAMG 1	1.14370	1.14370	1.14370
RWG 1	1.00000	1.00000	1.00000

### 2.3A-3 Wet-Vapor Potassium Turbine \* (Mean Diameter Calculation)

#### 1. Comparison of Results

The same modified parameters given in Table 2.3A-1 are used in the one radial sector (mean diameter) calculation. The results are in good agreement with the 5 radial sector calculation as can be seen by comparing the calculated parameters at the

mean diameter. In the single sector case the hub and tip values are calculated assuming a free vortex distribution.\*\* There is a slight inconsistency in the results in that  $P_g$ ,  $T_g$ ,  $P$ , and  $M$  for station 0 of the second stage are not identical to those at station 2A of the first stage. The discrepancies are small and thought not to be significant. At this time there is no explanation for this anomaly. The output format for the mean diameter case is slightly different from that using 5 radial sectors.

#### 2. Data Input

```

                                TURBINE COMPUTER PROGRAM
                                TWO STAGE POTASSIUM TURBINE
                                MEAN DIAMETER CALCULATION
SDATAIN
  STGCH= 1.000
  TTIN= 2067.300  PTIN= 38.828  WAIR= 0.000  FAIR= 0.000
  PTPS= 1.377  DELC= 0.000  DELL= 0.000  DELA= 0.000
  STG= 2.000  SECT= 1.000  EXPN= 0.000  EXPP= 0.000
  PAF= 1.000  SLI= 0.000  AACs= 1.000  RPM= 24000.000
  VCTD= 1.000  HSL= 37.600  TSL= 1000.000  PSL= 11.200
  GAMSL= 1.618  ENDSTG= 0.000  ENDJOB= 0.000

                                INLET RADIAL PROFILES
  PCNH= 1.000  0.000  0.000  0.000  0.000  0.000

```

\*Described in Westinghouse Electric Corporation,  
Astronuclear Laboratory Report WANL-PR(DD)-017,  
January 1967, Contract NAS 7-390.

\*\* Assumes a constant axial velocity component

## 2. Data Input (continued)

STANDARD OPTION						
AXIAL STATIONS						
STAGE= 1	STA. 0	STA. 1	STA.1A	STA. 2	STA.2A	
RG=	31.158	30.842	30.842	30.689	30.689	0.000
GAMG=	1.182	1.144	1.144	1.166	1.166	0.000
DR=	5.290	5.150	5.150	5.040	5.040	0.000
DT=	7.510	7.830	7.830	8.280	8.280	0.000
RWG=	1.000	1.000	1.000	1.000	1.000	0.000

STATOR RADIAL DISTRIBUTIONS						
	ROOT	PITCH			TIP	
SDIA=	0.000	0.000	0.000	0.000	0.000	0.000
SDEA=	65.030	0.000	0.000	0.000	0.000	0.000
SREC=	1.000	0.000	0.000	0.000	0.000	0.000
SETA=	.926	0.000	0.000	0.000	0.000	0.000
SCF=	1.000	0.000	0.000	0.000	0.000	0.000
SPA=	0.000	0.000	0.000	0.000	0.000	0.000
SESTH=	1.000					

ROTOR RADIAL DISTRIBUTIONS						
ROIA=	33.060	0.000	0.000	0.000	0.000	0.000
RDEA=	63.650	0.000	0.000	0.000	0.000	0.000
RREC=	1.000	0.000	0.000	0.000	0.000	0.000
RETA=	.817	0.000	0.000	0.000	0.000	0.000
RCF=	1.000	0.000	0.000	0.000	0.000	0.000
RPA=	0.000	0.000	0.000	0.000	0.000	0.000
RTF=	1.000	0.000	0.000	0.000	0.000	0.000
PERTH=	1.000					

STANDARD OPTION						
AXIAL STATIONS						
STAGE= 2	STA. 0	STA. 1	STA.1A	STA. 2	STA.2A	
RG=	30.689	30.828	30.828	30.763	30.763	0.000
GAMG=	1.166	1.145	1.145	1.164	1.164	0.000
DR=	5.040	4.880	4.880	4.600	4.600	0.000
DT=	8.280	8.620	8.620	9.100	9.100	0.000
RWG=	1.000	1.000	1.000	1.000	1.000	0.000

STATOR RADIAL DISTRIBUTIONS						
	ROOT	PITCH			TIP	
SDIA=	26.540	0.000	0.000	0.000	0.000	0.000
SDEA=	57.570	0.000	0.000	0.000	0.000	0.000
SREC=	1.000	0.000	0.000	0.000	0.000	0.000
SETA=	.948	0.000	0.000	0.000	0.000	0.000
SCF=	1.000	0.000	0.000	0.000	0.000	0.000
SPA=	0.000	0.000	0.000	0.000	0.000	0.000
SESTH=	1.000					

ROTOR RADIAL DISTRIBUTIONS						
ROIA=	-2.860	0.000	0.000	0.000	0.000	0.000
RDEA=	58.980	0.000	0.000	0.000	0.000	0.000
RREC=	1.000	0.000	0.000	0.000	0.000	0.000
RETA=	.816	0.000	0.000	0.000	0.000	0.000
RCF=	1.000	0.000	0.000	0.000	0.000	0.000
RPA=	0.000	0.000	0.000	0.000	0.000	0.000
RTF=	1.000	0.000	0.000	0.000	0.000	0.000
PERTH=	1.000					



### 3. Listing of Data Output

#### NASA TURBINE COMPUTER PROGRAM TWO STAGE POTASSIUM TURBINE MEAN DIAMETER CALCULATION

CASE 3. 0					
STAGE PERFORMANCE					
	STAGE 1	STAGE 2	STAGE 3	STAGE 4	
TTBAR 0	2067.3	1952.6			
PTBAR 0	38.828	23.187			
WG 0	5.777	5.777			
DEL P	33.818	19.562			
WRT/P	6.765	11.710			
OH/TTBAR0	.01636	.01002			
N/RT	527.849	543.133			
ETA TT	.83062	.83613			
ETA TS	.73030	.72533			
ETA AT	.80615	.83602			
PT0/PS1	1.377	1.212			
PTBAR0/PTBAR2	1.675	1.362			
PTBAR0/PS2	1.803	1.430			
PTH2/PS2	1.423	1.248			
TTBAR2/TTBAR0	.94451	.96618			
TTT1A/TTBAR0	.97296	.98377			
WG 1	5.777	5.777			
PS 1A	28.199	19.126			
YTR 1A	2011.4	1920.9			
PTR 1A	30.472	20.164			
WG 1A	5.777	5.777			
PS 2	21.540	16.219			
TTBAR 2	1952.6	1886.5			
PTBAR 2	23.187	17.022			
WG 2	5.777	5.777			
WG 2A	5.777	5.777			
UP/VI	.45217	.61276			
UR/VI	.35039	.42713			
PSI P	.89299	.48294			
PSI R	1.48713	.94352			
RX P	.44730	.45539			
RX R	.18072	.10147			
ALPHA 0	0.000	28.042			
I STATOR	0.000	1.502			
RETA 1A	33.910	-.209			
I ROTOR	.850	2.651			
ALPHA 2A	28.042	-1.642			
ORETA R	97.560	58.771			
M 1	.72584	.56766			
M1 RT	.89220	.73450			
MR 1A	.36920	.30442			
MR1A RT	.56669	.44181			
MR 2	.70879	.56012			
MR2 TIP	.78183	.70431			
E/TH CR	40.532	25.366			
N/RT CR	26274.6	27329.0			
WRT/CR/D	1.812	2.942			
OVERALL PERFORMANCE					
PSI P	.68107	PSI R	1.25831	DEL H	53.38050
WRT/P	6.76508	N/RT	527.84874	DELM/TTIN	.02582
PT0/PTBAR2	2.28102	PT0/PS2	2.39404	PT0/PAT2A	2.28112
ETA TT	.83611	ETA TS	.79231	ETA TAT	.83607
WNE/600	793.584	N/RT CR	26274.585	E/TH CR	63.97818

### 3. Output Data (continued)

NASA TURBINE COMPUTER PROGRAM  
TWO STAGE POTASSIUM TURBINE  
FIVE RADIAL SECTIONS

CASE 2. 0  
INTER-STAGE PERFORMANCE

STAGE 1		STAGE 2		STAGE 3		STAGE 4		STAGE 5		TOTAL FLOW	
STA 1A	ROTOR INLET										
DIAM 1A	5.254	6.002	6.750	7.496	8.246						
PT 1A	19.788	20.105	20.520	21.156	21.871						
TT 1A	1917.0	1919.8	1924.3	1931.7	1940.2						
RETA 1A	32.348	16.648	-1.584	-20.279	-34.969						
1 ROTOR	-4.452	.648	1.276	.221	.031						
R 1A	559.866	474.753	441.522	454.016	505.793						
RU 1A	299.552	136.010	-12.202	-157.354	-289.886						
WR 1A	.38147	.32277	.29968	.30762	.34222						
U 1A	550.197	628.527	706.458	785.188	863.518						
PS 1A	18.215	18.945	19.495	20.045	20.459						
TS 1A	1897.0	1905.4	1911.9	1918.6	1923.9						
CP 1A	.31340	.31340	.31340	.31340	.31340						
RG 1A	30.428	30.428	30.428	30.428	30.428						
GAMG 1A	1.14470	1.14470	1.14470	1.14470	1.14470						
RWG 1A	1.00000	1.00000	1.00000	1.00000	1.00000						
WG 1A	.90940	1.03454	1.15778	1.27150	1.38518	5.75040					

STAGE 2		STAGE 3		STAGE 4		STAGE 5		STAGE 6		TOTAL FLOW	
STA 2	ROTOR EXIT										
DIAM 2	5.050	5.950	6.850	7.750	8.650						
PT 2	19.669	20.069	20.600	21.390	22.300						
TT 2	1915.5	1919.4	1925.2	1934.4	1945.0						
RETA 2	52.600	56.100	58.980	61.450	63.600						
DRETA	84.948	72.748	57.396	41.171	28.631						
R 2	482.758	726.616	779.865	851.208	924.085						
RU 2	542.393	603.100	666.334	747.701	827.713						
WR 2	.46369	.49354	.52969	.57800	.62726						
U 2	528.434	623.082	717.330	811.577	905.825						
RX	.22043	.33974	.42908	.51389	.57638						
DELK	18.960	18.696	18.208	17.619	16.959						
PSI P	1.63020	1.19519	.69898	.69187	.54219						
EIA TT	.85797	.85186	.83888	.81776	.79218						
EIA TS	.74297	.74135	.72943	.70720	.68159						
EIA AT	.85783	.85155	.83705	.81470	.78772						
ZWI INC	-1.43231	-1.11191	-.86859	-.67083	-.51999						
CP R	.32764	.57310	.67947	.71551	.70041						
PS 2	16.889	16.889	16.892	16.895	16.899						
TS 2	1882.4	1881.8	1882.0	1882.9	1884.3						
CP 2	.28103	.28103	.28103	.28103	.28103						
RG 2	30.763	30.763	30.763	30.763	30.763						
GAMG 2	1.16370	1.16370	1.16370	1.16370	1.16370						
RWG 2	1.00000	1.00000	1.00000	1.00000	1.00000						
WG 2	.86346	.99454	1.13553	1.30005	1.46480	5.75839					
PT 2A	17.685	17.650	17.650	17.679	17.708						
TT 2A	1893.3	1892.7	1893.6	1895.8	1898.6						
V 2A	414.913	405.754	404.869	411.799	418.240						
VU 2A	13.559	-19.982	-48.996	-63.877	-78.112						
ALPHA 2A	1.873	-2.823	-6.951	-8.924	-10.764						
MF 2A	.28163	.27527	.27297	.27624	.27890						
VZ 2A	414.691	405.267	401.894	406.814	410.881						
TS 2A	1882.4	1881.8	1882.0	1882.9	1884.3						
PS 2A	16.889	16.889	16.892	16.895	16.899						
DENS 2A	.04200	.04201	.04201	.04200	.04198						
M 2A	.28178	.27561	.27499	.27963	.28390						
CP 2A	.28103	.28103	.28103	.28103	.28103						
RG 2A	30.763	30.763	30.763	30.763	30.763						
GAMG 2A	1.16370	1.16370	1.16370	1.16370	1.16370						
RWG 2A	1.00000	1.00000	1.00000	1.00000	1.00000						
WG 2A	.86346	.99454	1.13553	1.30005	1.46480	5.75839					

### 3. Output Data (continued)

NASA TURBINE COMPUTER PROGRAM  
TWO STAGE POTASSIUM TURBINE  
MEAN DIAMETER CALCULATION  
CASE 3, 0  
INTER-STAGE PERFORMANCE

STA 1A	ROTOR INLET		STAGE 1.
DIAM 1A	5.150	6.490	7.830
PIR 1A	29.190	30.472	32.116
TIR 1A	2000.6	2011.4	2024.7
BETA 1A	56.927	33.910	.007
I ROTOR	.291	.850	1.473
R 1A	844.214	555.112	460.698
RU 1A	707.428	308.689	.056
MR 1A	.56669	.36920	.30493
U 1A	539.306	679.631	819.955
PS 1A	24.344	28.198	30.458
TS 1A	1955.5	1991.9	2011.3
CP 1A	.31545	.31545	.31545
RG 1A	30.842	30.842	30.842
GAMG 1A	1.14370	1.14370	1.14370
RWG 1A	1.00000	1.00000	1.00000
STA 2	ROTOR EXIT		
DIAM 2	5.040	6.660	8.280
BETA 2	61.327	63.650	66.283
OBETA	118.254	97.560	66.290
R 2	977.999	1057.223	1166.653
RU 2	858.070	947.377	1068.121
MR 2	.65625	.70879	.78183
U 2	527.787	697.433	867.079
RX	.21685	.44730	.57436
DELH	33.818	33.818	33.818
PST P	2.97392	1.78568	1.18905
ETA TT	.83062	.83062	.83062
ETA TS	.73030	.73030	.73030
ETA AT	.80615	.80615	.80615
ZWI INC	-1.54897	-1.06034	-.73654
CP R	.25488	.72431	.84406
PS 2	21.278	21.540	21.664
TS 2	1929.0	1932.4	1933.9
CP 2	.27692	.27692	.27692
RG 2	30.689	30.689	30.689
GAMG 2	1.16607	1.16607	1.16607
RWG 2	1.00000	1.00000	1.00000
PT 2A	23.187	23.187	23.187
TT 2A	1952.6	1952.6	1952.6
V 2A	573.834	531.667	510.506
VU 2A	330.283	249.944	201.042
ALPHA 2A	35.140	28.042	23.192
MF 2A	.31487	.31460	.31447
VZ 2A	469.253	469.253	469.253
TS 2A	1929.0	1932.4	1933.9
PS 2A	21.278	21.540	21.664
DENS 2A	.05176	.05230	.05256
M 2A	.38505	.35644	.34212
CP 2A	.27692	.27692	.27692
RG 2A	30.689	30.689	30.689
GAMG 2A	1.16607	1.16607	1.16607
RWG 2A	1.00000	1.00000	1.00000

### 3. Output Data (continued)

NASA TURBINE COMPUTER PROGRAM  
TWO STAGE POTASSIUM TURBINE  
MEAN DIAMETER CALCULATION  
CASE 3. 0  
INTER-STAGE PERFORMANCE

STA 0	STATOR INLET		STAGE 2.
DIAM 0	5.040	6.660	8.280
TT 0	1952.6	1952.6	1952.6
PT 0	23.187	23.187	23.187
ALPHA 0	35.140	24.042	23.192
I STATOR	1.715	1.502	1.305
V 0	573.834	531.667	510.506
VU 0	330.283	249.944	201.042
VZ 0	469.253	469.253	469.253
TS 0	1928.8	1932.4	1933.8
PS 0	21.266	21.540	21.652
DENS 0	.05173	.05230	.05254
M 0	.38506	.35644	.34213
CP 0	.27692	.27692	.27692
RG 0	30.689	30.689	30.689
GAMG 0	1.16607	1.16607	1.16607
RWG 0	1.00000	1.00000	1.00000
STA 1	STATOR EXIT		
DIAM 1	4.880	6.750	8.620
ALPHA 1	65.329	57.570	50.945
DEL A	100.469	85.612	74.137
V 1	1073.451	835.528	711.146
VU 1	975.465	705.225	552.235
VZ 1	448.068	448.068	448.068
TS 1	1879.2	1908.1	1920.4
PS 1	16.948	14.126	20.120
DENS 1	.04213	.04682	.04894
M 1	.73490	.56766	.48161
ZWI INC	-1.00388	-1.21163	-1.31870
CP S	.71424	.59569	.48467
CP 1	.31340	.31340	.31340
RG 1	30.828	30.828	30.828
GAMG 1	1.14470	1.14470	1.14470
RWG 1	1.00000	1.00000	1.00000

### 3. Output Data (continued)

NASA TURBINE COMPUTER PROGRAM  
TWO STAGE POTASSIUM TURBINE  
MEAN DIAMETER CALCULATION  
CASE 3. 0  
INTER-STAGE PERFORMANCE

STA 1A	ROTOR INLET		STAGE 2.
DIAH 1A	4.880	6.750	8.620
PTR 1A	18.936	20.164	21.894
YTR 1A	1905.7	1920.9	1941.0
BETA 1A	46.027	-2.209	-38.030
I ROTOR	.940	2.651	2.043
R 1A	645.339	448.071	568.840
RU 1A	464.433	-1.633	-350.448
MR 1A	.44181	.30442	.38524
U 1A	511.032	706.858	902.504
PS 1A	16.948	19.126	20.120
TS 1A	1879.2	1908.1	1920.4
CP 1A	.31340	.31340	.31340
RG 1A	30.828	30.828	30.828
GANG 1A	1.14470	1.14470	1.14470
RWG 1A	1.00000	1.00000	1.00000
STA 2	ROTOR EXIT		
DIAH 2	4.600	6.850	9.100
BETA 2	47.552	58.960	65.806
DBETA	93.579	58.771	27.776
R 2	628.292	822.853	1034.685
RU 2	463.610	705.175	943.709
MR 2	.42768	.56012	.70431
U 2	481.710	717.330	952.949
RX	.12058	.45539	.59732
DELH	19.562	19.562	19.562
PSI P	1.90611	.96502	.56053
ETA TT	.83613	.83613	.83613
ETA TS	.72533	.72533	.72533
ETA AT	.83602	.83602	.83602
ZWI INC	-1.94035	-.88134	-.48493
CP R	-.05500	.70348	.69775
PS 2	16.218	16.219	16.219
TS 2	1873.7	1873.7	1873.7
CP 2	.28103	.28103	.28103
RG 2	30.763	30.763	30.763
GANG 2	1.16370	1.16370	1.16370
RWG 2	1.00000	1.00000	1.00000
PT 2A	17.022	17.022	17.022
TT 2A	1886.5	1886.5	1886.5
V 2A	424.434	424.222	424.146
VU 2A	-18.101	-12.155	-9.150
ALPHA 2A	-2.444	-1.642	-1.236
MF 2A	.28865	.28865	.28865
VZ 2A	424.047	424.047	424.047
TS 2A	1873.7	1873.7	1873.7
PS 2A	16.218	16.219	16.219
DENS 2A	.04052	.04052	.04052
M 2A	.28892	.28877	.28872
CP 2A	.28103	.28103	.28103
RG 2A	30.763	30.763	30.763
GANG 2A	1.16370	1.16370	1.16370
RWG 2A	1.00000	1.00000	1.00000

# APPENDIX 2.3B LISTING OF CODE

The asterisks in the identification columns (73-80) indicate that the card has been changed from the original listing given in NASA CR-710. Most of the changes are in format statements so as to make the output nomenclature agree with the names of program variables used in the computer code.

```

PROGRAM JIM(INPUT,OUTPUT,TAPE5=INPUT,TAPE6=OUTPUT)
CNTCP
C NASA TURBINE PROGRAM
C
REAL MFSTOP
LOGICAL PREVER,SFFLAG
COMMON SFFLAG
COMMON /SNTCP/G,AJ,PRFC,ICASE,PREVER,MFSTOP,JUMP,LOPIN,ISCASE,
1KN,GAMF,IP,SCHIT,PTRN,ISECT,KSTG,WTOL,RHOTOL,PRITOL,TRLOOP,LSTG,
2LBRC,IBRC,ICHOKE,ISORH,CHOKE,PTOPSI(6,8),PTRSZ(6,8),TRDING,SC,RC,
3DELPR,PASS,IPC,LOPC,ISS
C
COMMON /SINPUT/ RSL,TSL,PSL,GAMSL,
1PTPS,PTIN,TTIN,WAIR,FAIR,DELC,DELL,DELA,AACS,VCTD,STG,SECT,EXPN,
2EXPP,EXPRES, RPM,PAF,SL1,STGCH,FNDJOR,NAME(10),TITLE(10),PCNH(6),
3RV(6,8),GAM(6,8),DR(6,8),DT(6,8),RWG(6,8),ALPHAS(6,8),ALPHA1(6,8),
4ETAS(6,8),ETAS(6,8),CFS(6,8),AND0(6,8),BETA1(6,8),BETA2(6,8),ETARNTCP
5R(6,8),ETAR(6,8),CFR(6,8),TFR(6,8),ANDCR(6,8),OMEGAS(6,8),AS0(6,8),NTCP
6,ASMP0(6,8),ACHN0(6,8),A1(6,8),A2(6,8),A3(6,8),A4(6,8),A5(6,8),A6(NTCP
76,8),OMEGAR(6,8),BSIA(6,8),RSMPIA(6,8),BCHMIA(6,8),B1(6,8),B2(6,8),NTCP
8,B3(6,8),B4(6,8),B5(6,8),B6(6,8),SESTH1(8),RERTH1(8)
C
REAL MR2,M2,MF2
COMMON /SFLOW2/TS2(6,8),CP2(8),R2(6,8),RHOS2(6,8),BET2E(6,8),RU2(6,8),
1,8),VU2(6,8),DPUR2(6,8),VZ2(6,8),MR2(6,8),MF2(6,8),M2(6,8)
C
DIMENSION CS(8),CR(8)
C
CALL SLITE(0)
WAIR=0.0
FAIR=0.0
PTPS=1.02
DELC=0.0
DELL=0.0
DELA=0.0
EXPN=2.0
EXPP=2.0
EXPRES=0.0
RV(1,1)=0.0
PAF=0.0
SLI=0.0
AACS=1.0
SECT=1.0
VCTD=0.0
WTOL=1.E-04
RHOTOL=1.E-04
PRITOL=1.E-06
PCNH(1)=1.0
GAM(1,1)=0.0
RWG(1,1)=1.0
ETAS(1,1)=0.0
ALPHA1(1,1)=0.0
ETAR(1,1)=0.0
BETA2(1,1)=0.0
TRLOOP=0.

```

# Listing of Code (continued)

```

TRDIAG=0.0
G=32.17405
AJ=778.161
ICASE=0
1 PREVER=.FALSE.
  READ(5,100) SHFLAG
100 FORMAT(1X,L1)
  IF (SHFLAG) WRITE(6,10000)
10000 FORMAT(1111.39H AN ENTRY HAS BEEN MADE IN MAIN PROGRAM)
  CALL INIT
  ISCASE=0
  IF (PREVER) GO TO 1
  DO 25 I=1,8
    CS(I)=0.0
25 CR(I)=0.0
  PASS=0
2 PRPC=CS(KN)
  CALL STA01
  IF (PREVER) GO TO 40
  IF (ICHOKE.NF.0) GO TO 3
  IF (SCRIT.EQ.1.) SC=SC+1.
3 CALL STA1A
  IF (PREVER) GO TO 40
  LOPIN=0
4 JUMP=0
  PRPC=CR(KN)
  CALL STA2
  CR(KN)=PRPC
  IF (PREVER) GO TO 40
  IF (1.-MF2(1,KN))24,5,5
5 IF (JUMP)4,6,20
6 CALL STA2A
  IF (PREVER) GO TO 40
  IF (KN-KSTG)7,9,9
7 KN=KN+1
  LOPIN=0
8 JUMP=0
  PRPC=CS(KN)
  CALL STA1
  CS(KN)=PRPC
  IF (PREVER) GO TO 40
  IF (JUMP)3,3,20
9 CALL OVHALL
  IF (VCTD)11,11,10
10 CALL INSTG
11 PASS=1.
  IF (TRDIAG)13,13,12
12 CALL DIAGT(0)
13 IF (1.-MFSTOP)24,24,14
14 IF (DELC)24,24,15
15 IF (DELL)17,17,16
16 IF (DELP)24,24,18
17 IF (CHOKE)24,18,24
18 ISCASE=ISCASE+1
19 JL=(ISGRH-1)*8+LSTG
  IF (SC.EQ.1.) DELPR=DELL
  PTOP51(IP,JL)=PTOP51(IP,JL)+DELPR
20 LOPIN=1
  KN=LSTG
  IBRC=LARC
  IPC=0
  IF (KN-1)21,21,22

```

```

NTCP 054
NTCP 055
NTCP 056
NTCP 057
NTCP 058
NTCP 059
*****
*****
*****
NTCP 060
NTCP 061
NTCP 062
NTCP 063
NTCP 064
NTCP 065
NTCP 066
NTCP 067
NTCP 068
NTCP 069
NTCP 070
NTCP 071
NTCP 072
NTCP 073
NTCP 074
NTCP 075
NTCP 076
NTCP 077
NTCP 078
NTCP 079
NTCP 080
NTCP 081
NTCP 082
NTCP 083
NTCP 084
NTCP 085
NTCP 086
NTCP 087
NTCP 088
NTCP 089
NTCP 090
NTCP 091
NTCP 092
NTCP 093
NTCP 094
NTCP 095
NTCP 096
NTCP 097
NTCP 098
NTCP 099
NTCP 100
NTCP 101
NTCP 102
NTCP 103
NTCP 104
NTCP 105
NTCP 106
NTCP 107
NTCP 108
NTCP 109
NTCP 110
NTCP 111

```

# Listing of Code (continued)

```

21 IF (ISORR-1)2,2,4
22 IF (ISORR-1)8,8,4
40 WRITE(6,106)
24 IF (ENDJOB-1)1,23,23
23 IF (SRFLAG) WRITE(6,20000)
20000 FORMAT(1H,40H AN EXIT HAS BEEN MADE FROM MAIN PROGRAM)
      CALL EXIT
106 FORMAT(//3X65H THE PREVIOUS CASE HAS BEEN TERMINATED DUE TO ERRORS
1- CHECK DUMP.)
      STOP
      END
      SUBROUTINE INIT
CINIT
C      SUBROUTINE FOR INITIALIZATION OF INPUT DATA
C
      REAL MFSTOP
      LOGICAL PREVER,SRFLAG
      COMMON SRFLAG
      COMMON /SNTCP/G,AJ,PRFC,ICASE,PREVER,MFSTOP,JUMP,LOPIN,ISCASE,
      JKN,GAMF,IP,SCRT,PTRN,ISECT,KSTG,WIOL,RHOTOL,PTOL,TRLOP,LSTG,
      ZLBRC,IBRC,ICHOKE,ISORR,CHOKE,PTOP1(6,8),PTRS2(6,8),JPDIA,SC,RC,
      3DELPH,PASS,IPC,LOPC,ISS
C
      COMMON /SINIT/H1(6,8),H2(6,8),DP0(6,8),DP1(6,8),DP1A(6,8),DP2(6,8),
      1,DP2A(6,8),CSALF1(6,8),ALF1(6,8),CSBET2(6,8),BET2(6,8),RADSD(6,8),
      2RADRD(6,8),ANN1(6,8),ANN2(6,8),ANN2A(6,8),ANN1A(6,8),B1A(6,8),
      3UZ(6,8),ANN0(6,8),PT0(6,8),TT0(6,8),ALPHA0(6,8),PTP(6,8)
C
      COMMON /SINPUT/ RSL,TSL,PSL,GAMSL,
      1PTPS,PTIN,T1IN,WAIR,FAIR,DELC,DELL,DELA,AACS,VCTD,STG,SECT,EXPN,
      2EXPP,EXPHE, RPM,PAF,SLI,STGCH,ENDJOB,NAME(10),TITLE(10),PCNM(6),
      3RV(6,8),GAM(6,8),DR(6,8),DT(6,8),RWG(6,8),ALPHAS(6,8),ALPHA1(6,8),
      4ETARS(6,8),ETAS(6,8),CFS(6,8),AND0(6,8),HETA(6,8),BETA2(6,8),ETARINIT
      5R(6,8),ETAR(6,8),CFR(6,8),TFR(6,8),ANDCH(6,8),OMEGAS(6,8),AS0(6,8)
      6,ASMP0(6,8),ACHN0(6,8),A1(6,8),A2(6,8),A3(6,8),A4(6,8),A5(6,8),A6(6,8),
      7A(6,8),OMEGAR(6,8),BSIA(6,8),BSMPIA(6,8),HOMNIA(6,8),B1(6,8),B2(6,8),
      8,B3(6,8),B4(6,8),B5(6,8),B6(6,8),SESTHI(8),RERTHI(8)
C
      DIMENSION F1A(6,8),H0(6,8),H2A(6,8)
C
C      READ INPUT DATA, CHECK FOR ERRORS.
C      SKIP CHANGE CASES IF BASIC CASE HAS AN ERROR
C
      IF (SRFLAG) WRITE(6,10000)
10000 FORMAT(4H AN ENTRY HAS BEEN MADE IN SUBROUTINE INIT )
      CALL INPUT
      ICASE=ICASE+1
      IF (STGCH)5,5,4
      4 IK=1
      5 CALL CHECK(I)
      GO TO(6,8),I
      6 WRITE(6,100)ICASE
      IF (STGCH)3,3,7
      7 IK=2
      GO TO 3
      8 IF (IK-2)9,3,3
      INITIALIZE INDEX REGISTERS AND FORKS
C
      9 ISECT=SECT+.0001

```

```

NTCP 112
NTCP 113
NTCP 114
NTCP 115
NTCP 116
*****
*****
*****
NTCP 118
NTCP 119
NTCP 120
NTCP 121
INIT 001
INIT 002
INIT 003
INIT 004
INIT 005
*****
*****
INIT 007
INIT 008
INIT 009
INIT 010
INIT 011
INIT 012
INIT 013
INIT 014
INIT 015
INIT 016
*****
INIT 018
*****
*****
INIT 021
INIT 022
INIT 023
INIT 024
INIT 025
INIT 026
INIT 027
INIT 028
INIT 029
INIT 030
*****
*****
INIT 031
INIT 032
INIT 033
INIT 034
INIT 035
INIT 036
INIT 037
INIT 038
INIT 039
INIT 040
INIT 041
INIT 042
INIT 043

```



Listing of Code (continued)

KSTG= STG*.0001	INIT 044
LOPC=0	INIT 045
CHOKE=0.	INIT 046
ICHOKE=0	INIT 047
ISORR=1	INIT 048
KN=1	INIT 049
LSTG=1	INIT 050
IHRC=1	INIT 051
LHRC=1	INIT 052
DELPH=DELC	INIT 053
SC=0.0	INIT 054
RC=0.0	INIT 055
PRPC=0.0	INIT 056
IPC=0	INIT 057
ISS=0	INIT 058
PTRN=0.0	INIT 059
C TEST STAGE LOSS INDICATOR	INIT 060
IF(SLI)13,13,11	INIT 061
11 DO 12 I=1,ISECT	INIT 062
DO 12 J=1,KSTG	INIT 063
ETAHS(I,J)=ETARS(I,1)	INIT 064
ETAS(I,J)=ETAS(I,1)	INIT 065
CFS(I,J)=CFS(I,1)	INIT 066
ETARR(I,J)=ETARR(I,1)	INIT 067
ETAR(I,J)=ETAR(I,1)	INIT 068
CFR(I,J)=CFR(I,1)	INIT 069
TFR(I,J)=TFR(I,1)	INIT 070
12 CONTINUE	INIT 071
C TEST FOR EQUAL SECTORS	INIT 072
13 IF(PCNH(1)-1.)16,14,14	INIT 073
14 DO 15 I=1,ISECT	INIT 074
15 PCNH(I)= 1./SECT	INIT 075
C SET UP SECTOR HEIGHT, PITCH DIAMETER, ANNULUS AREA,	INIT 076
C PITCHLINE WHEEL SPEED	INIT 077
16 DO 19 K=1,KSTG	INIT 078
SH0=DT(1,K)-DR(1,K)	INIT 079
SH1=DT(2,K)-DR(2,K)	INIT 080
SH1A=DT(3,K)-DR(3,K)	INIT 081
SH2=DT(4,K)-DR(4,K)	INIT 082
SH2A=DT(5,K)-DR(5,K)	INIT 083
DO 18 I=1,ISECT	INIT 084
H0(I,K)=.5*PCNH(I)*SH0	INIT 085
H1(I,K)=.5*PCNH(I)*SH1	INIT 086
H1A(I,K)=.5*PCNH(I)*SH1A	INIT 087
H2(I,K)=.5*PCNH(I)*SH2	INIT 088
H2A(I,K)=.5*PCNH(I)*SH2A	INIT 089
IF(I-1)20,20,17	INIT 090

Listing of Code (continued)

```

20 DP0(I,K)=DR(1,K)* H0(I,K)
DP1(I,K)=DR(2,K)* H1(I,K)
DP1A(I,K)=DW(3,K)* F1A(I,K)
DP2(I,K)=DR(4,K)* H2(I,K)
DP2A(I,K)=DR(5,K)* F2A(I,K)
GO TO 21
17 DP0(I,K)= H0(I-1,K)* H0(I,K)+CP0(I-1,K)
DP1(I,K)= H1(I-1,K)* H1(I,K)+CP1(I-1,K)
DP1A(I,K)= H1A(I-1,K)* H1A(I,K)+DP1A(I-1,K)
DP2(I,K)= H2(I-1,K)* H2(I,K)+CP2(I-1,K)
DP2A(I,K)= H2A(I-1,K)* H2A(I,K)+DP2A(I-1,K)
21 ANNO(I,K)=.0218166*DP0(I,K)*H0(I,K)
ANN1(I,K)=.0218166*DP1(I,K)*H1(I,K)
ANN1A(I,K)=DP1A(I,K)*F1A(I,K)*.0218166
ANN2(I,K)=.0218166*DP2(I,K)*H2(I,K)
ANN2A(I,K)=.0218166*DP2A(I,K)*H2A(I,K)
U1A(I,K)= 3.14159*DP1A(I,K)*RPM/720.
U2(I,K)= 3.14159*DP2(I,K)*RPM/720.
18 CONTINUE
219 CONTINUE
C21 DEFINE PITCHLINE INDEX
IT=ISECT-2*(ISECT/2)
IF(IT)22,22,23
22 IP=ISECT/2
GO TO 24
23 IP=(ISECT+1)/2
C22 CALCULATE INLET AND EXIT ANGLES IN RADIANS
24 IF (ALPHA1(1,1))25,25,27
25 SDEAF=0.
DO 26 K=1,KSTG
DO 26 I=1,ISECT
CSALF1(I,K)=AND0(I,K)*CFS(I,K)/(SESTHI(K)*3.14159*DP1(I,K)*
1SQRT(ETAS(I,K)))
26 ALF1(I,K)=ATAN2(SQRT(1.-CSALF1(I,K)*CSALF1(I,K)),CSALF1(I,K))
GO TO 31
27 DO 28 K=1,KSTG
DO 28 I=1,ISECT
ALF1(I,K)= ALPHA1(I,K)*.01745328
28 CSALF1(I,K)=COS(ALF1(I,K))
31 IF (BETA2(1,1))29,29,32
29 RDEAF=0.
DO 30 K=1,KSTG
DO 30 I=1,ISECT
CSBET2(I,K)=ANDUR(I,K)*CFR(I,K)/(RETHI(K)*3.14159*DP2(I,K)*
1SQRT(ETAH(I,K)))
30 BET2(I,K)=ATAN2(SQRT(1.-CSBET2(I,K)*CSBET2(I,K)),CSBET2(I,K))
GO TO 34

```

```

INIT 091
INIT 092
INIT 093
INIT 094
INIT 095
INIT 096
INIT 097
INIT 098
INIT 099
INIT 100
INIT 101
*****
*****
*****
*****
INIT 107
INIT 108
INIT 109
INIT 110
INIT 111
INIT 112
INIT 113
INIT 114
INIT 115
INIT 116
INIT 117
INIT 118
INIT 119
INIT 120
INIT 121
INIT 122
INIT 123
INIT 124
INIT 125
INIT 126
INIT 127
*****
INIT 129
INIT 130
INIT 131
INIT 132
INIT 133
INIT 134
INIT 135
INIT 136
INIT 137

```

Listing of Code (continued)

32 DO 33 K=1,KSTG	INIT 138
DO 33 I=1,ISECT	INIT 139
BET2(I,K)= HETA2(I,K)*.01745328	*****
33 CSBET2(I,K)=COS(BET2(I,K))	INIT 141
34 DO 35 K=1,KSTG	INIT 142
DO 35 I=1,ISECT	INIT 143
PTP(I,K)=PTIN	INIT 144
PTO(I,K)=PTIN	INIT 145
TT0(I,K)=TTIN	INIT 146
ALPHA0(I,K)=0.0	INIT 147
PTOPS1(I,K)=PTPS	INIT 148
RADSD(I,K)=ALPHAS(I,K)*.01745328	*****
35 RADRD(I,K)=HETA1(I,K)*.01745328	*****
IF(RV(1,1))36,36,37	*****
36 CALL R(PTIN,TTIN,FAIR,wAIR,RV(1,1))	*****
GAMF=0.0	INIT 153
GO TO 38	INIT 154
37 GAMF=1.0	INIT 155
38 CALL CHECK(J)	INIT 156
GO TO (39,40),J	INIT 157
39 GO TO 3	INIT 158
40 IF(SRFLAG) WRITE(6,20000)	*****
20000 FORMAT(45H AN EXIT HAS BEEN MADE FROM SUBROUTINE INIT )	*****
RETURN	*****
100 FORMAT(28X,6HCASE I5,13H HAS AN ERROR)	INIT 160
END	INIT 161

```

SUBROUTINE INPUT
CINPUT
C*****
C
REAL MFSTOP
LOGICAL PREVER,SHFLAG
COMMON SHFLAG
COMMON /SNTCP/G,AJ,PRFC,ICASE,PREVER,MFSTOP,JUMP,LOPIN,ISCASE,
1KN,GAMF,IP,SCHIT,PTHN,ISECT,KSTG,WIOL,RHOTOL,PRTOL,TRLOOP,LSTG,
2LHRC,IHRC,ICHOKE,ISURH,CHOKE,PTOPS1(6,8),PTRS2(6,8),TRDIAG,SC,RC,
3DELPH,PASS,IPC,LOPC,ISS
C
COMMON /SINPUT/ HSL,ISL,PSL,GAMSL,
1PTPS,PTIN,TTIN,WAIR,FAIR,DELC,DELL,DELA,AACS,VCTD,STG,SECT,EXPN,
2EXPP,EXPE, RPM,PAF,SLI,STGCH,FNUJOH,NAME(10),TITLE(10),PCNH(2),*****
3RV(6,8),GAM(6,8),SR(6,8),ST(6,8),SWG(6,8),ALPHAS(6,8),ALPHA1(6,8),*****
4ETAS(6,8),ETAS(6,8),CFS(6,8),ANNO(6,8),BETA1(6,8),BETA2(6,8),ETARINPT
5R(6,8),ETAR(6,8),CFR(6,8),TFR(6,8),ANDOR(6,8),OMEGAS(6,8),ASO(6,8)INPT
6,ASMP0(6,8),ACMNO(6,8),A1(6,8),A2(6,8),A3(6,8),A4(6,8),A5(6,8),A6(INPT
7,8),OMEGAR(6,8),BSIA(6,8),RSMPIA(6,8),HCMNIA(6,8),B1(6,8),B2(6,8)INPT
8,B3(6,8),B4(6,8),B5(6,8),B6(6,8),SESTH(8),RERTH(8)
C
DIMENSION X(6,8,38),Y(6,38)
C
EQUIVALENCE (X(1,1,1),RV(1,1)),(Y(1,1),RG(1))
C
COMMON HG(6),
1 GAMG(6),DR(6),UT(6),RWG(6),SDIA(6),SDEA(6),SREC(6),SETA(6),*****
2SCF(6),SPA(6),RDIA(6),RDEA(6),RREC(6),RETA(6),RCF(6),RTF(6),RPA(6)INPT
3,STPLC(6),SINR(6),SINMP(6),SINMN(6),SCPS(6),SCPC(6),SCPQ(6),SCNS(6)INPT
4,SCNC(6),SCNQ(6),RTPLC(6),RINR(6),RINMP(6),RINMN(6),RCPS(6),RCPC(6)INPT
5,RCQ(6),RCNS(6),RCNC(6),RCNQ(6)
C
NAMELIST/DATAIN/ RSL,ISL,PSL,GAMSL,
1 PTPS,PTIN,TTIN,WAIR,FAIR,DELC,DELL,DELA,AACS,VCTD*****
2,STG,SECT,STAGE,EXPN,EXPP,EXPE,RPM,PAF,SLI,ENDSTG,ENDJOB,PCNH,RG,*****
3GAMG,DR,UT,SWG,SDIA,SDEA,SREC,SETA,SCF,SPA,RDIA,RDEA,RREC,RETA,RCFINPT
4,RTF,RPA,STPLC,SINR,SINMP,SINMN,SCPS,SCPC,SCPQ,SCNS,SCNC,SCNQ,RTPLINPT
5,RINR,RINMP,RINMN,RCPS,RCPC,RCQ,RCNS,RCNC,RCNQ,SESTH,RERTH,
6WITOL,RHOTOL,PRTOL,TRLOOP,TRDIAG,STGCH
C
DATA BLANKS/66666666/
C
READ THE HEADING CARDS EVERY TIME ENTRY IS MADE
IF(SHFLAG) WRITE(6,10000)

```

Listing of Code (continued)

```

10000 FORMAT(44H AN ENTRY HAS BEEN MADE IN SUBROUTINE INPUT )
10 READ(5,6669) (NAME(I),I=1,10)
20 READ(5,6669) (TITLE(I),I=1,10)
J=0
30 DO 25 L=1,38
DO 25 I=1,6
25 Y(I,L)=BLANKS
SESTH=BLANKS
RERTH=BLANKS
READ(5,DATAIN)
40 K=STAGE+.0001
50 ISECT=SECT+.0001
60 DO 80 L=1,38
70 DO 80 I=1,6
IF (Y(I,L).NE.BLANKS) GO TO 71
Y(I,L)=0.0
GO TO 80
71 X(I,K,L)=Y(I,L)
80 CONTINUE
IF (SESTH.EQ.BLANKS) GO TO 95
90 SESTH(K)=SESTH
GO TO 96
95 SESTH=0.
96 IF (RERTH.EQ.BLANKS) GO TO 105
100 RERTH(K)=RERTH
GO TO 110
105 RERTH=0.
110 IF (K-1)120,120,130
120 WRITE(6,6670)NAME,TITLE,STGCH,TTIN,PTIN,WAIR,FAIR,PTPS,DELC,DELL,
1DELA,STG,SECT,EXPN,EXPP, PAF,S,I,AACS,RPM,VCTD,RSL,TSL,PSL,GAMSL
2,ENDSTG,ENDJOB,PCNH
J=J+1
130 WRITE(6,6671) K,RG,GANG,DR,DT,RWG,SDIA,SDEA,SREC,SETA,SCF,SPA,
1SESTH,
1RDIA,RDEA,RREC,RETA,RCF,RPA,RTF,RERTH
140 IF (OMEGAS(1,K))160,160,150
150 WRITE(6,6672)STPLC,SINR,SINMP,SINMN,SCPS,SCPC,SCPQ,SCNS,SCNC,SCNQ,
1RTPLC,RINR,RINMP,RINMN,RCPS,RCPC,RCPQ,RCNS,RCNC,RCNQ
160 J=J+1
180 AM= J-2*(J/2)
190 IF (AM)200,210,200
200 WRITE(6,6673)
210 IF (ENDSTG-1.)30,170,170
170 IF (SHFLAG) WRITE(6,20000)
20000 FORMAT(1H1,45H AN EXIT HAS BEEN MADE FROM SUBROUTINE INPUT )
RETURN
6669 FORMAT(10A6)

```

```

*****
INPT 043
INPT 044
INPT 045
*****
INPT 047
INPT 048
INPT 049
INPT 050
INPT 051
INPT 052
INPT 053
*****
INPT 055
INPT 056
INPT 057
INPT 058
INPT 059
INPT 060
INPT 061
INPT 062
INPT 063
INPT 064
INPT 065
INPT 066
INPT 067
INPT 068
INPT 069
*****
INPT 073
*****
INPT 075
*****
INPT 077
INPT 078
INPT 079
INPT 080
INPT 081
INPT 082
INPT 083
INPT 084
*****
*****
INPT 086

```

Listing of Code (continued)

```

6670 FORMAT (1H1,24X,24HTURBINE COMPUTER PROGRAM/6X,10A6/6X,10A6/2X, INPT 087
17HSCATAIN/2X,7H STGCW=F10.3/2X7H TTIN=F10.3,1X,7H PTIN=F10.3,2X,*****
16H *AIR=F10.3,2X, *****
25HFAIR=F10.3/2X,7H PIPS=F10.3,1X,7H CELC=F10.3,2X,6H DELL=F10.3,*****
32X,SHDELA=F10.3/2X,7H STG=F10.3,1X,7H SECT=F10.3,2X,6H EXPN=F10,*****
4.3,2X,5HEXPP=F10.3/2X, 7H PAF=F10.3,2X,6H SLI=*****
5F10.3,3X,5HAACS=F10.3, 2X,5H RPM=F10.3/2X,7H VCTD=F10.3,4X,4HRS*****
4=F10.3,4X,4HISL=F10.3,3X,4HPSL=F10.3/2X,7H GAMSL=F10.3,1X,7HENDSTG*****
7=F10.3,1X,7HENDJOB=F10.3//25X,21HINLET RADIAL PROFILES *****
8 /4X,5HPCNH=6(F8.3,2X)/1H1) *****
6671 FORMAT(28X,15HSTANDARD OPTION/3X,6HSTAGE=13,16X,14HAXIAL STATIONS/*****
111X,6HSTA. 04X,6HSTA. 14X,6HSTA. 1A4X,6HSTA. 23X,7H STA.2A/ *****
23X,6H RG=6(F8.3,2X)/ *****
33X,6H GAMG=6(F8.3,2X)/3X,6H DR=6(F8.3,2X)/3X,6H DT=6(F8.3,2X)/INPT 097
33X,6H RWG=6(F8.3,2X)//22X,27HSTATOR RADIAL DISTRIBUTIONS/ INPT 098
413X,4HROOT,15X,5HPITCH,16X,3HTIP/ *****
53X,6H SOIA=6(F8.3,2X)/3X,6H SOEA=6(F8.3,2X)/3X,6H SREC=6(F8.3,2X)/INPT 100
63X,6H SFTA=6(F8.3,2X)/3X,6H SCF=6(F8.3,2X)/3X,6H SPA=6(F8.3,2X)/INPT 101
73X,6HSESTH=F8.3//22X,26HROTOR RADIAL DISTRIBUTIONS/ *****
83X,6H ROIA=6(F8.3,2X)/3X,6H ROEA=6(F8.3,2X)/3X,6H RREC=6(F8.3,2X)/INPT 103
93X,6H RETA=6(F8.3,2X)/3X,6H RCF=6(F8.3,2X)/3X,6H RPA=6(F8.3,2X)/*****
13X,6H RTF=6(F8.3,2X)/3X,6HRTTH=1F8.3/) *****
6672 FORMAT(/25X,23HLOSS COEFFICIENT OPTION/22X,27HSTATOR RADIAL DISTRINPT 106
1AUTIONS/ INPT 107
23X,6HSTPLC=6(F8.3,2X)/3X,6H SINR=6(F8.3,2X)/3X,6HSINMP=6(F8.3,2X)/INPT 108
33X,6HSINMN=6(F8.3,2X)/3X,6H SCPS=6(F8.3,2X)/3X,6H SCPC=6(F8.3,2X)/INPT 109
43X,6H SCPQ=6(F8.3,2X)/3X,6H SCNS=6(F8.3,2X)/3X,6H SCNC=6(F8.3,2X)/INPT 110
53X,6H SCNQ=6(F8.3,2X)/023X,26HROTOR RADIAL DISTRIBUTIONS/ INPT 111
63X,6HRTPLC=6(F8.3,2X)/3X,6H RINR=6(F8.3,2X)/3X,6HRINMP=6(F8.3,2X)/INPT 112
73X,6HRINMN=6(F8.3,2X)/3X,6H RCPS=6(F8.3,2X)/3X,6H RCPC=6(F8.3,2X)/INPT 113
83X,6H RCPQ=6(F8.3,2X)/3X,6H RCNS=6(F8.3,2X)/3X,6H RCNC=6(F8.3,2X)/INPT 114
93X,6H RCNQ=6(F8.3,2X) INPT 115
6673 FORMAT (1H1) INPT 116
END INPT 117

```

# Listing of Code (continued)

```

SUBROUTINE STA01
CSTA01
C      ESTABLISH FIRST STATOR EXIT FLOW. ADJUST FLOWS FOR COOLING
C      AIR INJECTION BETWEEN STATIONS 0 AND 1. FIND INLET
C      MACH NUMBER AND INCIDENCE ANGLE LOSS AT STATION 0.
C      ADJUST PI, GET NEW FLOW AT STATION 1 FOR FINAL RESULT.
C
      REAL MFSTOP
      LOGICAL PREVER,SRFLAG
      COMMON SRFLAG
      COMMON /SNTCP/G,AJ,PRFC,ICASE,PREVER,MFSTOP,JUMP,LOPIN,ISCASE,
1KN,GAMF,IP,SCRIT,PTRN,ISECT,KSTG,WIOL,HOTOL,PTOL,TRLOOP,LSTG,
2LHRC,IHNC,ICHUK,ISORN,CHOKF,PTOPS1(6,8),PTRS2(6,8),TRDIAG,SC,RC,
3DELPR,PASS,IPC,LOPC,ISS
C
      COMMON /SINIT/H1(6,8),H2(6,8),DP0(6,8),DP1(6,8),DP1A(6,8),DP2(6,8),
1,DP2A(6,8),CSALF1(6,8),ALF1(6,8),CSBET2(6,8),HET2(6,8),RADSD(6,8),
2RADSD(6,8),ANN1(6,8),ANN2(6,8),ANN2A(6,8),ANN1A(6,8),U1A(6,8),
3U2(6,8),ANNO(6,8),PT0(6,8),TT0(6,8),ALPHA0(6,8),PTP(6,8)
C
      COMMON /SINPUT/ RSL,TSL,PSL,GAMSL,
1PTPS,PTIN,TTIN,WAIR,FAIR,DELC,DELL,DELA,AACS,VCTD,STG,SECT,EXPN,
2EXPP,EXPRF, RPM,PAF,SLI,STGCH,FNDJON,NAME(10),TITLE(10),PCNH(6),
3RV(6,8),GAM(6,8),DR(6,8),UT(6,8),RWG(6,8),ALPHAS(6,8),ALPHA1(6,8),
4ETAS(6,8),ETAS(6,8),CFS(6,8),ANNO(6,8),BETA1(6,8),HETA2(6,8),ETARST01
5R(6,8),ETAR(6,8),CFR(6,8),TFR(6,8),ANDCH(6,8),OMEGAS(6,8),AS0(6,8),
6,ASMP0(6,8),ACMN0(6,8),A1(6,8),A2(6,8),A3(6,8),A4(6,8),A5(6,8),A6(
76,8),OMEGAR(6,8),HSIA(6,8),RSMPIA(6,8),HCMNIA(6,8),R1(6,8),R2(6,8),
R,R3(6,8),R4(6,8),R5(6,8),R6(6,8),SESTHI(8),RERTHI(8)
C
      REAL M0
      COMMON /SSTA01/CP0(8),
18),VU0(6,8),VZ0(6,8),RHOS0(6,8),PS1(6,8),WGT1(8),TA1(8),WG1(6,8),
2CPDH1(6,8),SI(6,8), CP1(8),PHI1(6,8),TS1(6,8),V1(6,8),
3,RHOS1(6,8),ALF1E(6,8),VU1(6,8),VZ1(6,8),M0(6,8),WGT0(8),WG0(6,8)
C
      DIMENSION      TA0(8),      TT0TS0(6,8),PTOPSO(6,8),FFA0(6,8)
1),AAS0(6,8)
C
C      IF(SRFLAG) WRITE(6,10000)
10000 FORMAT(44H AN ENTRY HAS BEEN MADE IN SUBROUTINE STA01 )
      K=KN
      SCRIT=0.0
      I=IP
      ID=-1

```

Listing of Code (continued)

WGT1(K)=0.0	ST01 043
JW=1	ST01 044
IF(GAMF)2,2,3	ST01 045
2 TA1(K)=.95*TT0(IP,K)	ST01 046
CALL GAMMA(PTIN,TA1(K),FAIR,WAIR,GAM(2,K))	ST01 047
3 CALL FLOW1(I)	ST01 048
IF (PREVER) GO TO 26	ST01 049
WGT1(K)=WGT1(K)+WG1(I,K)	ST01 050
C TEST FOR TIP SECTOR	ST01 051
IF(ISECT-I)5,5,4	ST01 052
4 I=I-ID	ST01 053
IF(I)6,6,22	ST01 054
22 L=I-ID	ST01 055
PS1(I,K)=PS1(L,K)+FLOAT(ID)*DPOH(L,K)*	ST01 056
HL(I,K)+H1(L,K))/2.	ST01 057
PTOPSI(I,K)=PT0(I,K)/PS1(I,K)	ST01 058
IF (PTOPSI(I,K)-1.)27,3,3	ST01 059
27 PTRK=-1.	ST01 060
PTOPSI(I,K)= 1.0	ST01 061
GO TO 3	ST01 062
6 ID=1	ST01 063
I=IP-ID	ST01 064
GO TO 22	ST01 065
C CALCULATE STA 0 FOR INCIDENCE CORRECTION	ST01 066
5 IF (JW=1)16,16,18	ST01 067
16 IF(GAMF)7,7,17	ST01 068
7 GAM(1,K)=GAM(2,K)	ST01 069
17 EX=(GAM(1,K)-1.)/GAM(1,K)	ST01 070
EXI=1./EX	ST01 071
WGT0(K)=WGT1(K)/RWG(2,K)	ST01 072
I= IP	ST01 073
WG0(I,K)=WG1(I,K)/RWG(2,K)	ST01 074
FFA0(I,K)=WG0(I,K)*SQRT( TT0(I,K)/(144.*PT0(I,K)*	ST01 075
1ANNO(I,K))	ST01 076
19 J=1	ST01 077
8 CALL PRATIO(FFA0(I,K)*GAM(1,K)*RV(1,K),PTOPSO(I,K),PRTOL)	*****
PS0(I,K)=PTP(I,K)/PTOPSO(I,K)	ST01 079
TT0TS0(I,K)=PTOPSO(I,K)**EX	ST01 080
TS0(I,K)=TT0(I,K)/TT0TS0(I,K)	ST01 081
9 IF(GAMF) 10,10,12	ST01 082
10 TAO(K)=.5*(TT0(I,K)+TS0(I,K))	ST01 083
CALL GAMMA(PTIN,TA0(K),FAIR,WAIR,GAM(1,K))	ST01 084
EX=(GAM(1,K)-1.)/GAM(1,K)	ST01 085
EXI=1./EX	ST01 086
IF(J-1)11,11,12	ST01 087
11 J=J+1	ST01 088
GO TO 8	ST01 089



Listing of Code (continued)

```

12 CP0(K)=RV(1,K)*EXI/AJ
DO 14 I=1,ISECT
  WGO(I,K)=WG1(I,K)/RWG(2,K)
  PT0M0=PT0(I,K)
  FFA0(I,K)=WGO(I,K)*SQRT( TT0(I,K))/(144.*PT0(I,K)*
  1ANN0(I,K))
  IF(I.EQ.IP) GO TO 28
  PS0(I,K) = PS0(IP,K)
  PT0PS0(I,K) = PTP(I,K)/PS0(I,K)
28 TT0TS0(I,K)=PT0PS0(I,K)**EX
  TS0(I,K)=TT0(I,K)/TT0IS0(I,K)
13 V0(I,K)=SQRT(2.*G*AJ*CP0(K)*(TT0(I,K)-TS0(I,K)))
  AAS0(I,K)=SQRT(GAM(1,K)*G*RV(1,K)*TS0(I,K))
  M0(I,K)=V0(I,K)/AAS0(I,K)
  SI(I,K)=ALPHA0(I,K)-HADS0(I,K)
  IF(SI(I,K))24,24,20
24 EXPS=EXPX
  GO TO 21
20 EXPP=EXPP
21 PT0PS0(I,K)=(1.+EX*M0(I,K)*ETARS(I,K)*GAM(1,K)*M0(I,K)/2.
  1*(CCS(SI(I,K))*EXPS)**EXI
  PT0(I,K)=PS0(I,K)*PT0PS0(I,K)
  WGO(I,K)=WGO(I,K)*PT0(I,K)/PT0M0
  WG1(I,K)=WG1(I,K)*PT0(I,K)/PT0M0
  RHOS0(I,K)=144.*PS0(I,K)/(RV(1,K)*TS0(I,K))
  VU0(I,K)=V0(I,K)*SIN(ALPHA0(I,K))
  VZ0(I,K)=V0(I,K)*COS(ALPHA0(I,K))
14 CONTINUE
C   END OF INCIDENCE LCSS CORRECTION LOOP
  WGT1(K)=0.
  I=IP
  ID=-1
  JW=2
15 GO TO 3
18 CONTINUE
  WGT0(K)=WGT1(K)/RWG(2,K)
  IF(THLOOP.EQ.0.) GO TO 23
  WRITE(6,1000) WGT0(K)*WG1(K),(WGO(L,K),L=1,ISECT)
  WRITE(6,1001) (PT0PS0(L,K),L=1,ISECT)
  WRITE(6,1002) (WG1(L,K),L=1,ISECT)
  WRITE(6,1003) (PT0PS1(L,K),L=1,ISECT)
1000 FORMAT(2X,6H WGT0=F8.3,2X,6H WGT1=F8.3/2X,6H WGO=6F8.3)
1001 FORMAT(1X,7HPT0PS0=6F8.5)
1002 FORMAT(2X,6H WG1=6F8.3)
1003 FORMAT(1X,7HPT0PS1=6F8.5)
23 CALL CHECK (J)
  GO TO (25,26),J

```

\*\*\*\*\*  
 ST01 091  
 ST01 092  
 ST01 093  
 ST01 094  
 ST01 095  
 ST01 096  
 ST01 097  
 ST01 098  
 ST01 099  
 ST01 100  
 ST01 101  
 \*\*\*\*\*  
 ST01 103  
 ST01 104  
 ST01 105  
 ST01 106  
 ST01 107  
 ST01 108  
 ST01 109  
 ST01 110  
 ST01 111  
 ST01 112  
 ST01 113  
 \*\*\*\*\*  
 ST01 115  
 ST01 116  
 ST01 117  
 ST01 118  
 ST01 119  
 ST01 120  
 ST01 121  
 ST01 122  
 ST01 123  
 ST01 124  
 ST01 125  
 ST01 126  
 ST01 127  
 ST01 128  
 ST01 129  
 ST01 130  
 ST01 131  
 ST01 132  
 ST01 133  
 ST01 134  
 ST01 135  
 ST01 136

### Listing of Code (continued)

```

25 CALL DIAGT(1)
26 IF(SRFLAG) WRITE(6,20000)
20000 FORMAT(45H AN EXIT HAS BEEN MADE FROM SUBROUTINE STA01 )
      RETURN
      END

```

ST01 137  
\*\*\*\*\*  
\*\*\*\*\*  
\*\*\*\*\*  
ST01 139

Listing of Code (continued)

```

      SUBROUTINE FLOW1(I)
CFLOW1
C      ESTABLISH VALUES FOR STATOR EXIT FLOW
C
      REAL MFSTOP
      LOGICAL PREVER,SHFLAG
      COMMON SRFLAG
      COMMON /SNTCP/G,AJ,PRFC,ICASE,PREVER,MFSTOP,JUMP,LOPIN,ISCASE,
      1KN,GAMF,IP,SCRIT,PTRN,ISECT,KSTG,WTOL,RHOTOL,PRTOL,TRLOOP,LSTG,
      2LBRC,IHHC,ICHUKE,ISORH,CHOKE,PTOPSI(6,8),PTRS2(6,8),TRDIAG,SC,RC,
      3DELPR,PASS,IPC,LOPC,ISS
C
      COMMON /SINIT/H1(6,8),H2(6,8),DP0(6,8),DP1(6,8),DP1A(6,8),DP2(6,8),
      1,DP2A(6,8),CSALF1(6,8),ALF1(6,8),CSHET2(6,8),BET2(6,8),RADSD(6,8),
      2RADRD(6,8),ANN1(6,8),ANN2(6,8),ANN2A(6,8),ANN1A(6,8),U1A(6,8),
      3U2(6,8),ANN0(6,8),PT0(6,8),TT0(6,8),ALPHA0(6,8),PTP(6,8)
C
      COMMON /SINPUT/ HSL,TSL,PSL,GAMSL,
      1PTPS,PTIN,TTIN,WAIR,FAIR,DELC,DELL,DELA,AACS,VCTD,STG,SECT,EXPN,
      2EXPP,EXPHE, RPM,PAF,SLI,STGCH,FNDJUH,NAME(10),TITLE(10),PCNH(6),
      3RV(6,8),GAM(6,8),DR(6,8),DT(6,8),HWG(6,8),ALPHAS(6,8),ALPHA1(6,8),
      4ETARS(6,8),ETAS(6,8),CFS(6,8),ANN0(6,8),HETA1(6,8),BETA2(6,8),ETARFLW1
      5R(6,8),ETAR(6,8),CFR(6,8),TFR(6,8),ANDOR(6,8),OMEGAS(6,8),AS0(6,8),
      6,ASMP0(6,8),ACMN0(6,8),A1(6,8),A2(6,8),A3(6,8),A4(6,8),A5(6,8),A6(
      7,8),OMEGAR(6,8),BSIA(6,8),BSMPIA(6,8),HCMN1A(6,8),B1(6,8),B2(6,8),
      8,B3(6,8),B4(6,8),B5(6,8),B6(6,8),SESTHI(8),RERTHI(8)
C
      REAL M0
      COMMON /SSTA01/CP0(8),
      1,8),VU0(6,8),VZ0(6,8),RHOS0(6,8),PS1(6,8),WGT1(8),TA1(8),WG1(6,8),
      2DPDH1(6,8),SI(6,8), CP1(8),PHI1(6,8),TS1(6,8),V1(6,8),
      3,RHOS1(6,8),ALF1E(6,8),VU1(6,8),VZ1(6,8),M0(6,8),WGT0(8),WG0(6,8)
C
      DIMENSION PHI1C(8),PTFS1C(8),VIC(6,8),TS1C(6,8),RHOS1C(6,8),WG1C(
      1,8),CSALLE(6,8),SFF(6,8)
C
      IF(SRFLAG) WRITE(6,10000)
10000 FORMAT(44H AN ENTRY HAS BEEN MADE IN SUBROUTINE FLOW1 )
      K=KN
      EX=(GAM(2,K)-1.)/GAM(2,K)
C      COMPUTE ISENTROPIC STATOR TEMPERATURE RATIO
      7 PHI1(I,K)=PTOPSI(I,K)**EX
C      TEST FOR LOSS COEFFICIENT INPUT
      IF (OMEGAS(1,1))2,2,1
      1 CALL LOSS1(I,K,EX)

```

Listing of Code (continued)

2	TS1(I,K)=TT0(I,K)*(1.-ETAS(I,K)*(1.-1./PHI1(I,K)))	FLW1 043
	IF(I-IP)6,3,6	FLW1 044
3	IF(GAMF)4,4,5	FLW1 045
4	TA1(K)=.5*(TT0(I,K)+TS1(I,K))	FLW1 046
	CALL GAMMA(PT0(IP,K),TA1(K),FAIR,WAIR,GAM(2,K))	FLW1 047
5	EX=(GAM(2,K)-1.0)/GAM(2,K)	FLW1 048
	FXI=1./EX	FLW1 049
C	CRITICAL PRESSURE RATIO	FLW1 050
	CALL PHIM(EXI,ETAS(I,K),PHI1C(K),PTPS1C(K))	FLW1 051
	CP1(K)=RV(2,K)*EXI/AJ	*****
C	EXIT VELOCITY	FLW1 053
6	V1(I,K)=SQRT(2.*G*AJ*CP1(K)*(TT0(I,K)-TS1(I,K)))	FLW1 054
C	EXIT PRESSURE	FLW1 055
	PS1(I,K)=PT0(I,K)/PT0PS1(I,K)	FLW1 056
C	EXIT DENSITY	FLW1 057
	RHOS1(I,K)=144.*PS1(I,K)/(HV(2,K)*TS1(I,K))	*****
C	TEST CRITICAL PRESSURE RATIO	FLW1 059
	IF(PT0PS1(I,K)-PTPS1C(K))15, R,R	FLW1 060
C	GREATER THAN CRITICAL	FLW1 061
8	IF (IP-1) 21,9,21	FLW1 062
9	IF (PRPC)10,10,22	FLW1 063
C	PREVIOUS PITCH NONCRITICAL	FLW1 064
10	PRPC=1.	FLW1 065
	PT0PS1(I,K)=PTPS1C(K)*(1.+PRTO1)	FLW1 066
	GO TO 7	FLW1 067
21	IF (PT0PS1(I,K).LE.PT0PS1(IP,K)) GO TO 22	FLW1 068
	GO TO 12	FLW1 069
22	IF ((I.EQ.1).OR.(I.EQ.ISECT)) SCHIT=1.	FLW1 070
	GO TO 11	FLW1 071
C	PITCH ON OUTBOARD SECTION	FLW1 072
11	CONTINUE	FLW1 073
	V1C(I,K)=SQRT(2.*G*AJ*CP1(K)*TT0(I,K)*ETAS(I,K)*(PHI1C(K)	FLW1 074
	1-1.)/PHI1C(K))	FLW1 075
	TS1C(I,K)=TT0(I,K)*(1.-ETAS(I,K)*(1.-1./PHI1C(K)))	FLW1 076
	RHOS1C(I,K)=144.*PT0(I,K)/(PTPS1C(K)*TS1C(I,K)*RV(2,K))	*****
	WG1C(I,K)=RHOS1C(I,K)*V1C(I,K)*ANN1(I,K)*CSALF1(I,K)	FLW1 078
	WG1(I,K)=WG1C(I,K)	FLW1 079
13	CSAL1E(I,K)=WG1(I,K)/(RHOS1(I,K)*V1(I,K)*ANN1(I,K))	FLW1 080
C	EFFECTIVE STATION EXIT ANGLE	FLW1 081
14	ALF1E(I,K)=ATAN2(SQRT(1.-CSAL1E(I,K)*CSAL1E(I,K)),	FLW1 082
	1CSAL1E(I,K))	FLW1 083
	GO TO 16	FLW1 084
12	IF (PRPC-1.)15,15,24	FLW1 085
24	WG1(I,K)=SFF(I,K)*PT0(I,K)/SQRT(TT0(I,K))	FLW1 086
	GO TO 13	FLW1 087
C	PRESSURE RATIO LESS THAN CRITICAL OR SUPERSONIC FLOW DECREASE	FLW1 088
15	WG1(I,K)=RHOS1(I,K)*V1(I,K)*ANN1(I,K)*CSALF1(I,K)	FLW1 089

Listing of Code (continued)

CSALIE(I,K)=CSALF1(I,K)	FLW1 090
ALF1E(I,K)=ALF1(I,K)	FLW1 091
SFF(I,K)=WG1(I,K)*SQRT(TT0(I,K))/PT0(I,K)	FLW1 092
16 VU1(I,K)=V1(I,K)*SIN(ALF1E(I,K))	FLW1 093
DPDR1(I,K)=.01388889*RHOS1(I,K)*VU1(I,K)*VU1(I,K)/	*****
1(G*DP1(I,K))	FLW1 095
VZ1(I,K)=V1(I,K)*CSALIE(I,K)	FLW1 096
IF(I.LT.ISECT) GO TO 17	FLW1 097
IF(PRPC.EQ.1.) PRPC=2.	FLW1 098
17 CALL CHECK(J)	FLW1 099
GO TO (19,20),J	FLW1 100
19 CALL DIAGT(2)	FLW1 101
20 IF(SRFLAG) WRITE(6,20000)	*****
20000 FORMAT(45H AN EXIT HAS BEEN MADE FROM SUBROUTINE FLOW1 )	*****
RETURN	*****
END	FLW1 103

# Listing of Code (continued)

```

SUBROUTINE LOSS1(I,K,EX)
CLOSS1
C
C   CALCULATE EFFICIENCY
C
REAL MFSTOP
LOGICAL PREVER,SFFLAG
COMMON SRFLAG
COMMON /SNTCP/G,AJ,PRFC,ICASE,PRFVER,MFSTOP,JUMP,LOPIN,ISCASE,
1KN,GAMF,IP,SCHIT,PTRN,ISECT,KSTG,WOTOL,HOTOL,PTOL,TRLOOP,LSTG,
2LARC,IBRC,ICHOKE,ISORN,CHOKE,PTOPSL(6,8),PTRS2(6,8),TRDIAG,SC,RC,
3DELPR,PASS,IPC,LOPC,ISS
C
COMMON /SINIT/H1(6,8),H2(6,8),DP0(6,8),DP1(6,8),DP1A(6,8),DP2(6,8),
1,UP2A(6,8),CSALF1(6,8),ALF1(6,8),CSHET2(6,8),HET2(6,8),RADSD(6,8),
2RADRD(6,8),ANN1(6,8),ANN2(6,8),ANN2A(6,8),ANN1A(6,8),U1A(6,8),
3U2(6,8),ANN0(6,8),PT0(6,8),TT0(6,8),ALPHA0(6,8),PTP(6,8)
C
COMMON /SINPUT/ RSL,TSL,PSL,GAMSI,
1PTPS,PTIN,TTIN,WAIR,FAIR,DELC,DELL,DELA,AACS,VCTD,STG,SECT,EXPN,
2EXPP,EXPRE, RPM,PAF,SLI,STGCH,FNDJUR,NAME(10),TITLE(10),PCNH(6),
3RV(6,8),GAM(6,8),DR(6,8),DT(6,8),RWG(6,8),ALPHAS(6,8),ALPHA1(6,8),
4ETAHS(6,8),ETAS(6,8),CFS(6,8),ANN0(6,8),BETA1(6,8),BETA2(6,8),ETARLOS1
5R(6,8),ETAR(6,8),CFR(6,8),TFR(6,8),ANDOR(6,8),OMEGAS(6,8),ASO(6,8),
6,ASMPO(6,8),ACMNO(6,8),A1(6,8),A2(6,8),A3(6,8),A4(6,8),A5(6,8),A6(
76,8),OMEGAR(6,8),BSIA(6,8),RSMPIA(6,8),HCMNIA(6,8),R1(6,8),R2(6,8),
8,R3(6,8),H4(6,8),H5(6,8),H6(6,8),SESTHI(8),RERTHI(8)
C
REAL M0
COMMON /SSTA01/CP0(8),
18),VU0(6,8),VZ0(6,8),RHOS0(6,8),PS1(6,8),WGT1(8),TA1(8),WG1(6,8),
2DPDH1(6,8),SI(6,8),CP1(8),PHI1(6,8),TS1(6,8),V1(6,8),
3,RHOS1(6,8),ALF1E(6,8),VU1(6,8),VZ1(6,8),M0(6,8),WGT0(8),WGT0(6,8)
C
C   IF(SFFLAG) WRITE(6,10000)
10000 FORMAT(44H AN ENTRY HAS BEEN MADE IN SUBROUTINE LOSS1 )
EXPA=0.0
EXPP=0.0
ETAHS(I,K)=1.0
SI(I,K)=ALPHA0(I,K)-RADSD(I,K)
IF(SI(I,K))5,1,2
1 W01=OMEGAS(I,K)
GO TO 9
2 AS=A1(I,K)
AC=A2(I,K)

```

```

LOS1 001
LOS1 002
LOS1 003
LOS1 004
LOS1 005
LOS1 006
*****
*****
LOS1 008
LOS1 009
LOS1 010
LOS1 011
LOS1 012
LOS1 013
LOS1 014
LOS1 015
LOS1 016
LOS1 017
*****
LOS1 019
*****
LOS1 022
LOS1 023
LOS1 024
LOS1 025
LOS1 026
LOS1 027
LOS1 028
LOS1 029
LOS1 030
LOS1 031
*****
LOS1 033
LOS1 034
*****
*****
LOS1 035
LOS1 036
LOS1 037
LOS1 038
LOS1 039
LOS1 040
LOS1 041
LOS1 042
LOS1 043

```

Listing of Code (continued)

AQ=A3(I,K)	LOS1 044
IF(ASMPO(I,K)-SI(I,K))3,4,4	LOS1 045
3 WMWS=SI(I,K)/ASMPO(I,K)	LOS1 046
AR=ASMPO(I,K)/ASO(I,K)	LOS1 047
GO TO 8	LOS1 048
4 WMWS=1.0	LOS1 049
AR=SI(I,K)/ASO(I,K)	LOS1 050
GO TO 8	LOS1 051
5 AS=A4(I,K)	LOS1 052
AC=A5(I,K)	LOS1 053
AQ=A6(I,K)	LOS1 054
IF(SI(I,K)-ACMNO(I,K))6,4,4	LOS1 055
6 WMWS=SI(I,K)/ACMNO(I,K)	LOS1 056
AR=ACMNO(I,K)/ASO(I,K)	LOS1 057
8 W01=(1.+AR*AR*(AS*AR*(AC*AR*AQ)))*WMWS*OMEGAS(I,K)	LOS1 058
9 ETAS(I,K)=(1.-(1./(PTOPSI(I,K)*(1.-W01)+W01))*EX)*PHI1(I,K)/	LOS1 059
1(PHI1(I,K)-1.)	LOS1 060
CALL CHECK(J)	LOS1 061
IF(SRFLAG) WRITE(6,20000)	*****
20000 FORMAT(45H AN EXIT HAS BEEN MADE FROM SUBROUTINE LOSS1 )	*****
RETURN	LOS1 062
END	LOS1 063

Listing of Code (continued)

	SUBROUTINE R(P,T,F,W,RX)	R	001
CR		R	002
C	CALCULATE GAS CONSTANT	R	003
	WRITE (6,100)		*****
100	FORMAT (//120H SUBROUTINE R HAS BEEN CALLED UPON *****		*****
	1*****		*****
	2**,//)		*****
	RX=53.35045+(.658*F+32.433*W)/(1.+F*W)	R	004
	RETURN	R	005
	END	R	006



Listing of Code (continued)

SUBROUTINE GAMMA(P,T,F,w,GAMX)		GAMA 001
CGAMMA		GAMA 002
C		GAMA 003
C	CALCULATE SPECIFIC HEAT RATIO FOR MIXTURE	GAMA 004
	WRITE (6,100)	*****
100	FORMAT (//120H SUBROUTINE GAMMA HAS BEEN CALLED UPON *****	
1	*****	
2	*,//)	*****
	CALL CPA(P,T,F,w,CPAX)	GAMA 005
	IF (F) 2,2,1	GAMA 006
1	CALL CPF(P,T,F,w,CPFX)	GAMA 007
2	IF (w) 4,4,3	GAMA 008
3	CALL CPW(P,T,F,w,CPWX)	GAMA 009
4	CPGX=(CPAX+F*CPFX+W*CPWX)/(1.+F+W)	GAMA 010
	CALL R(P,T,F,w,RX)	GAMA 011
	GAMX=CPGX/(CPGX-RX/778.161)	GAMA 012
	RETURN	GAMA 013
	END	GAMA 014

Listing of Code (continued)

	SUBROUTINE CPA(P,T,F,w,CPAX)	CPA 001
		CPA 002
CCPA	CALCULATE SPECIFIC HEAT RATIO FOR AIR	CPA 003
C	DIMENSION	CPA 004
	1XT(7),A(7)	CPA 005
	WRITE (6,100)	*****
100	FORMAT (//120H SUBROUTINE CPA HAS BEEN CALLED UPON *****	*****
	1*****	*****
	2**,//)	CPA 006
	IF(T-100.)1.2.2	CPA 007
	1 TX=100.	CPA 008
	GO TO 5	CPA 009
	2 IF(6400.-T)3.4.4	CPA 010
	3 TX=6400.	CPA 011
	GO TO 5	CPA 012
	4 TX=T	CPA 013
	5 XT(1)=TX/1000.	CPA 014
	DO 6 I=2,7	CPA 015
	6 XT(I)=XT(I-1)*XT(1)	CPA 016
	CPAX=2.4264907E-01-2.6657395E-02*XT(1)+4.6617756E-02*XT(2)	CPA 017
	1-1.3546542E-02*XT(3)-8.4500931E-04*XT(4)+1.0303393E-03*	CPA 018
	2XT(5)-1.7159795E-04*XT(6)+9.1627911E-06*XT(7)	CPA 019
	RETURN	CPA 020
	END	

# Listing of Code (continued)

	SUBROUTINE CPF(P,T,F,*,CPFX)	CPF	001
CCPF		CPF	002
C	CALCULATE SPECIFIC HEAT RATIO FOR FUEL	CPF	003
	DIMENSION	CPF	004
	1XT(7),A(7)	CPF	005
	WRITE (6,100)	*****	
100	FORMAT (//120H SUBROUTINE CPF HAS BEEN CALLED UPON *****		
	1*****		
	2**,//)	*****	
	IF(T=400.)1,2,2	CPF	006
1	TX=400.	CPF	007
	GO TO 5	CPF	008
2	IF(3000.-T)3,4,4	CPF	009
3	TX=3000.	CPF	010
	GO TO 5	CPF	011
4	TX=T	CPF	012
5	XT(1)=TX/1000.	CPF	013
	DO 6 I=2,7	CPF	014
6	XT(I)=XT(I-1)*XT(1)	CPF	015
	CPFX=1.0625243E-01+9.5291284E-01*XT(1)-7.2605169E-01*XT(2)	CPF	016
	1+2.4481406E-01*XT(3)+5.3332162E-02*XT(4)-6.4699814E-02*XT(5)	CPF	017
	2+1.7495567E-02*XT(6)-1.6029820E-03*XT(7)	CPF	018
	RETURN	CPF	019
	END	CPF	020

Listing of Code (continued)

	SUBROUTINE CPW(P,T,F,*,CPWX)	CPW 001
CCPW		CPW 002
C	CALCULATE SPECIFIC HEAT FOR WATER VAPOR	CPW 003
	DIMENSION	CPW 004
	1XT(7),A(7)	CPW 005
	WRITE (6,100)	*****
100	FORMAT (//120H SUBROUTINE CPW HAS BEEN CALLED UPON *****	
	1*****	*****
	2*,//)	
	IF(T=400.)1,2,2	CPW 006
1	TX=400.	CPW 007
	GO TO 5	CPW 008
2	IF(3000.-T)3,4,4	CPW 009
3	TX=3000.	CPW 010
	GO TO 5	CPW 011
4	TX=T	CPW 012
5	XT(1)=TX/1000.	CPW 013
	DO 6 I=2,7	CPW 014
6	XT(I)=XT(I-1)*XT(1)	CPW 015
	CPWX=4.5728850E-01+9.7007556E-02*XT(1)+1.6536409E-01	CPW 016
	1*XT(2)-4.1138066E-02*XT(3)-2.6979575E-02*XT(4)+2.2619243E-02	CPW 017
	2*XT(5)-6.2706207E-03*XT(6)+6.2246710E-04*XT(7)	CPW 018
	RETURN	CPW 019
	END	CPW 020

Listing of Code (continued)

SUBROUTINE PRATIO(TFF,GAMX,RX,PTPS,PTHOL)	PRIO n01
CPRATIO	PRIO n02
C CALCULATE PRESSURE RATIO	PRIO n03
LOGICAL PREVER,SHFLAG	*****
COMMON SRFLAG	*****
IF(SHFLAG) WRITE(6,10000)	*****
10000 FORMAT(44H AN ENTRY HAS BEEN MADE IN SUBROUTINE PRATIO)	*****
A=GAMX/(GAMX-1.)	PRIO n04
R=2./GAMX	PRIO n05
C=(GAMX+1.)/GAMX	PRIO n06
D=TFF*SQRT(RX/(64.3481*A))	PRIO n07
PCHIT=((GAMX+1.)/2.)*A	PRIO n08
PUP=PCHIT	PRIO n09
PLOW=1.0	PRIO n10
PTRMO=0.0	PRIO n11
1 PTR=(PUP+PLOW)/2.	PRIO n12
DELFM=SQRT(1./(PTR**R)-1.)/(PTR**C)-D	PRIO n13
IF(DELFM)2,3,3	PRIO n14
2 PLOW=PTR	PRIO n15
GO TO 4	PRIO n16
3 PUP=PTR	PRIO n17
4 PRE=(PTR-PTRMO)/PTR	PRIO n18
IF (ABS(PRE)-PTHOL)6,6,5	PRIO n19
5 PTRMO=PTR	PRIO n20
GO TO 1	PRIO n21
6 IF(PCHIT-PTR)7,8,8	PRIO n22
7 PTPS=PCHIT	PRIO n23
GO TO 9	PRIO n24
8 PTPS=PTR	PRIO n25
9 CONTINUE	PRIO n26
IF(SHFLAG) WRITE(6,20000)	*****
20000 FORMAT(45H AN EXIT HAS BEEN MADE FROM SUBROUTINE PRATIO)	*****
RETURN	PRIO n27
END	PRIO n28

# Listing of Code (continued)

	SUBROUTINE CHECK(I)	CHCK 001
CCHECK		CHCK 002
C	SUBROUTINE TO CHECK SENSE LIGHTS	CHCK 003
C		CHCK 004
	REAL MFSTOP	CHCK 005
	LOGICAL PREVEN,SRFLAG	*****
	COMMON SRFLAG	*****
	COMMON /SNTCP/G,AJ,PRFC,ICASE,PREVER,MFSTOP,JUMP,LOPIN,ISCASE,	CHCK 007
	1KN,GAMF,IP,SCHIT,PTNK,ISECT,KSTG,WIUL,HMOTOL,PRYOL,TRLOOP,LSTG,	CHCK 008
	2LHRC,IHMC,ICHUKE,ISORH,CHOKE,PTOPS1(6,8),PTRS2(6,8),TRDIAG,SC,RC,	CHCK 009
	3DELPH,PASS,IPC,LOPC,ISS	CHCK 010
C		CHCK 011
	IF(SRFLAG) WRITE(6,10000)	*****
10000	FORMAT(44H AN ENTRY HAS BEEN MADE IN SUBROUTINE CHECK )	CHCK 012
	DO 1 I=1,4	CHCK 013
	CALL SLITET(I,J)	CHCK 014
	GO TO (2,1),J	CHCK 015
1	CONTINUE	CHCK 016
	J=2	*****
	IF(SRFLAG) WRITE(6,20000)	CHCK 017
	RETURN	CHCK 018
2	J=1	CHCK 019
	PREVEN=.TRUE.	*****
	IF(SRFLAG) WRITE(6,20000)	*****
20000	FORMAT(45H AN EXIT HAS BEEN MADE FROM SUBROUTINE CHECK )	CHCK 020
	RETURN	CHCK 021
	END	

# Listing of Code (continued)

```

SUBROUTINE STA1A
CSTA1A
C
    REAL MFSTOP
    LOGICAL PREVEN,SRFLAG
    COMMON SRFLAG
    COMMON /SNTCP/G,AJ,PRFC,ICASE,PRFVER,MFSTOP,JUMP,LOPIN,ISCASE,
    1KN,GAMF,IP,SCRIT,PTRN,ISECT,KSTG,WOTOL,RHOTOL,PTOL,TRLOOP,LSTG,
    2LHRC,IHHC,ICHOKE,ISORH,CHOKE,PTOPSI(6,8),PTRS2(6,8),TRDIAG,SC,RC,
    3DELPR,PASS,IPC,LOPC,ISS
C
    COMMON /SINIT/H1(6,8),H2(6,8),DP0(6,8),DP1(6,8),DP1A(6,8),DP2(6,8),
    1,DP2A(6,8),CSALF1(6,8),ALF1(6,8),CSHET2(6,8),BET2(6,8),RADSD(6,8),
    2RADRD(6,8),ANN1(6,8),ANN2(6,8),ANN2A(6,8),ANN1A(6,8),U1A(6,8),
    3U2(6,8),ANN0(6,8),PT0(6,8),TT0(6,8),ALPHA0(6,8),PTP(6,8)
C
    COMMON /SINPUT/ HSL,TSL,PSL,GAMSI,
    1PTPS,PTIN,TFIN,WAIR,FAIR,DELC,DELL,DELA,AACS,VCTD,STG,SECT,EXPN,
    2EXPP,EXPRE, RPM,PAF,SLI,STGCH,FNDJOB,NAME(10),TITLE(10),PCNH(6),
    3RV(6,8),GAM(6,8),DR(6,8),DT(6,8),RWG(6,8),ALPHAS(6,8),ALPHA1(6,8),
    4ETARS(6,8),ETAS(6,8),CFS(6,8),AND0(6,8),BETA1(6,8),BETA2(6,8),ETARSTIA
    5R(6,8),ETAR(6,8),CFR(6,8),TFR(6,8),ANDCR(6,8),OMEGAS(6,8),AS0(6,8)STIA
    6,ASMP0(6,8),ACMN0(6,8),A1(6,8),A2(6,8),A3(6,8),A4(6,8),A5(6,8),A6(STIA
    7A(6,8),OMEGAR(6,8),BSIA(6,8),BSMPIA(6,8),HCMN1A(6,8),B1(6,8),B2(6,8)STIA
    8,B3(6,8),B4(6,8),B5(6,8),B6(6,8),SESTHI(8),RERTHI(8)
C
    REAL M0
    COMMON /SSTA01/CP0(8),
    1A),VU0(6,8),VZ0(6,8),RHOS0(6,8),PS1(6,8),WGT1(8),TA1(8),WG1(6,8),
    2DPDR1(6,8),S1(6,8),
    3RHOS1(6,8),ALF1E(6,8),VU1(6,8),VZ1(6,8),M0(6,8),WGT0(8),WGO(6,8)
    REAL MR1A
    COMMON /SSTA1A/VU1A(6,8),WG1A(6,8),WGT1A(8),VZ1A(6,8),
    1PS1A(6,8),RU1A(6,8),R1A(6,8),HET1A(6,8),RI(6,8),TTR1A(6,8),PTR1A(6,8)STIA
    2,MR1A(6,8),TS1A(6,8)
C
    DETERMINE FLOW CONDITIONS RELATIVE TO ROTOR. FIND INCIDENCE
    C ANGLE RECOVERY ROTOR INLET STATIONS. OBTAIN GAS PROPERTIES.
    C ABSOLUTE TANGENTIAL COMPONENT VELOCITY ADJUSTED FOR DIAMETER
    C CHANGE TO CONSERVE ANGULAR MOMENTUM. AXIAL COMPONENT
    C VELOCITY ADJUSTED FOR WEIGHT FLOW. AREA,, AND DENSITY CHANGE
    C FROM STA 1.
C
    IF(SRFLAG) WRITE(6,10000)
    10000 FORMAT(44H AN ENTRY HAS BEEN MADE IN SUBROUTINE STA1A )
    K=KN

```

Listing of Code (continued)

	I=IP	ST1A 043
	ID=-1	ST1A 044
	TS1A(I,K)=TS1(I,K)	*****
C	RATIO OF FLOW CHANGE	ST1A 046
	WR=RWG(3,K)/RWG(2,K)	ST1A 047
C	TOTAL STATION FLOW	ST1A 048
	WGT1A(K)=WR*WGT1(K)	ST1A 049
C	ADJUST TANGENTIAL VELOCITY	ST1A 050
	13 VU1A(I,K)=VU1(I,K)*DPI(I,K)/DPIA(I,K)	ST1A 051
C	ADJUST FLOW	ST1A 052
	WG1A(I,K)=WR*WG(I,K)	ST1A 053
	RHOSTR=RHOS1(I,K)	ST1A 054
C	ADJUST AXIAL VELOCITY	ST1A 055
	1 VZ1A(I,K)=WR*VZ1(I,K)*ANN1(I,K)*RHOS1(I,K)/(ANN1A(I,K)	ST1A 056
	1*RHOSTR)	ST1A 057
	V1A=SQRT(VU1A(I,K)*VU1A(I,K)+VZ1A(I,K)*VZ1A(I,K))	ST1A 058
	IF(I-IP)2,3,2	ST1A 059
	2 EX=(GAM(3,K)-1.)/GAM(3,K)	ST1A 060
	EXI=1./EX	ST1A 061
	GO TO 4	ST1A 062
	3 IF(GAMF)12,12,2	ST1A 063
	12 TA1A=.5*(TT0(I,K)+TS1A(I,K))	*****
	CALL GAMMA(PT0(I,K),TA1A,FAIR,WAIR,GAM(3,K))	ST1A 065
	EX=(GAM(3,K)-1.)/GAM(3,K)	ST1A 066
	EXI=1./EX	ST1A 067
	4 CP1A(K)=RV(3,K)*EXI/AV	*****
	DELTS=(V1(I,K)*V1(I,K)-V1A*V1A)/(2.*G*AJ*CP1A(K))	ST1A 069
	TS1A(I,K)=TS1(I,K)+DELTS	*****
	PS1A(I,K)=PS1(I,K)*(1.+DELTS/TS1(I,K))*EXI	ST1A 071
	RHOS1A=144.*PS1A(I,K)/(RV(3,K)*TS1A(I,K))	*****
C	DENSITY ERROR	ST1A 073
	RHOE=(RHOS1A-RHOSTR)/RHOS1A	ST1A 074
	IF(ABS(RHOE)-RHOTOL)6,6,5	ST1A 075
	5 RHOSTR=RHOS1A	ST1A 076
	GO TO 1	ST1A 077
	6 RU1A(I,K)=VU1A(I,K)-U1A(I,K)	ST1A 078
	RIA(I,K)=SQRT(RU1A(I,K)*RU1A(I,K)+VZ1A(I,K)*VZ1A(I,K))	ST1A 079
	SBET1A=RU1A(I,K)/RIA(I,K)	ST1A 080
	BET1A(I,K)=ATAN2(SBET1A,SQRT(1.-SBET1A*SBET1A))	ST1A 081
	IF(OMEGAR(I,K))8,8,7	ST1A 082
	7 ETARR(I,K)=1.	ST1A 083
	EXPRES=0.0	ST1A 084
	8 MR1A(I,K)=RIA(I,K)/SQRT(GAM(3,K)*G*RV(3,K)*TS1A(I,K))	*****
	TRTS1A=1.+(GAM(3,K)-1.)*MR1A(I,K)*MR1A(I,K)/2.	ST1A 086
	IF(TRTS1A.GT.1.)GO TO 32	ST1A 087
	PREVER=.TRUE.	ST1A 088
	GO TO 17	ST1A 089



Listing of Code (continued)

```

32 TTR1A(I,K)=TS1A(I,K)*IRTS1A          *****
   RI(I,K)=BET1A(I,K)-RACRD(I,K)        ST1A 091
   IF(RI(I,K).GT.1.570796) RI(I,K)=1.570796 *****
   IF(RI(I,K).LT.-1.570796) RI(I,K)=-1.570796 *****
   IF(RI(I,K))9,9,10                    ST1A 094
9   EXPR=EXPX                            ST1A 095
   GO TO 11                              ST1A 096
10  EXPR=EXPP                            ST1A 097
11  PRPS1A  =(1.+(TRTS1A  -1.)*ETARR(I,K)*(COS(RI(I,K)))** ST1A 098
   1(EXPR))**EXI                        ST1A 099
   PTR1A(I,K)=PS1A(I,K)*PRPS1A         ST1A 100
   IF (ISECT-I)14,16,14                 ST1A 101
14  I=I+10                              ST1A 102
   IF (I)15,15,13                       ST1A 103
15  ID=1                                ST1A 104
   I=IP+ID                              ST1A 105
   GO TO 13                              ST1A 106
16  CONTINUE                            ST1A 107
   CALL CHECK(J)                        ST1A 108
   GO TO (17,18)*J                      ST1A 109
17  CALL DIAGT(3)                       ST1A 110
18  IF(SRFLAG) WRITE(6,20000)           *****
20000 FORMAT(45H AN EXIT HAS BEEN MADE FROM SUBROUTINE ST1A ) *****
   RETURN                               *****
   END                                  ST1A 112

```

### Listing of Code (continued)

```

SUBROUTINE STA2
CSTA2
C
REAL MFSTOP
LOGICAL PREVER,SHFLAG
COMMON SHFLAG
COMMON /SNTCP/G,AJ,PRFC,ICASE,PRFVER,MFSTOP,JUMP,LOPIN,ISCASE,
1KN,GAMF,IP,SCHIT,PTRN,ISECT,KSTG,WIOL,HHOTUL,PTOL,TRLOOP,LSTG,
2LHRC,IHRC,ICHOKE,ISORH,CHUKE,PTOP1(6,B),PTRS2(6,B),TRDIAG,SC,RC,
3DELPH,PASS,IPC,LOPC,ISS
C
COMMON /SINIT/H1(6,B),H2(6,B),DPn(6,B),DP1(6,B),DP1A(6,B),DP2(6,B)
1,DP2A(6,B),CSALF1(6,B),ALF1(6,B),CSHET2(6,B),HET2(6,B),RADSD(6,B),
2RADRD(6,B),ANN1(6,B),ANN2(6,B),ANN2A(6,B),ANN1A(6,B),U1A(6,B),
3U2(6,B),ANNO(6,B),PT0(6,B),TT0(6,B),ALPHA0(6,B),PTP(6,B)
C
COMMON /SINPUT/ RSL,TSL,PSL,GAMSI,
1PTPS,PTIN,TTIN,WAIR,FAIR,DELC,DEIL,DELA,AACS,VCTD,STG,SECT,EXPN,
2EXPP,EXPRE, RPM,PAF,SLI,STUCH,FNDJUH,NAME(10),TITLE(10),PCNH(6),
3RV(6,B),GAM(6,B),DR(6,B),DT(6,B),RWG(6,B),ALPHAS(6,B),ALPHA1(6,B),
4ETAHS(6,B),ETAS(6,B),CFS(6,B),ANNO(6,B),BETA1(6,B),BETA2(6,B),ETARST
5R(6,B),ETAR(6,B),CFR(6,B),TFR(6,B),ANDCH(6,B),OMEGAS(6,B),AS0(6,B)
6,ASMP0(6,B),ACMNO(6,B),A1(6,B),A2(6,B),A3(6,B),A4(6,B),A5(6,B),A6
7(6,B),OMFGAR(6,B),BSIA(6,B),RSMPIA(6,B),HCMNIA(6,B),B1(6,B),B2(6,B)
8,B3(6,B),B4(6,B),B5(6,B),B6(6,B),SESTH1(8),HERTH1(8)
C
REAL MR1A
COMMON /SSTA1A/VU1A(6,B),WG1A(6,B),WGT1A(8),VZ1A(6,B), CP1A(8),
1PS1A(6,B),RU1A(6,B),RIA(6,B),RET1A(6,B),RI(6,B),TTR1A(6,B),PTR1A
2(6,B),MH1A(6,B),TS1A(6,B)
C
COMMON /SSTA2/V2(6,B),TTR2(6,B),PTH2(6,B),WG2(6,B),WGT2(8),TA2(8),
1 PS2(6,B),PHI2(6,B)
C
REAL MR2,M2,MF2
COMMON /SFLOW2/IS2(6,B),CP2(8),R2(6,B),RHOS2(6,B),BET2E(6,B),RU2(6,B)
1(8),VU2(6,B),UPUH2(6,B),VZ2(6,B),MR2(6,B),MF2(6,B),M2(6,B)
C
DIMENSION WGT2C(8),FFA2(6,B),IS2(8)
C
C
IF(SHFLAG) WRITE(6,10000)
10000 FORMAT(44H AN ENTRY HAS BEEN MADE IN SUBROUTINE STA2 )
K=KN
J=1

```

Listing of Code (continued)

SCRIT=0.0	ST2	n43
PTRM0=1.	ST2	n44
IS2(K)=0	ST2	n45
EXI=GAM(3,K)/(GAM(3,K)-1.)	ST2	n46
WR=RWG(4,K)/RWG(3,K)	ST2	n47
DO 1 I=1,ISECT	ST2	n48
TTR2(I,K)=TTR1A(I,K)+(U2(I,K)**2 - U1A(I,K)**2)/(2.*G*AJ*CP1A(K))	ST2	n49
PTR2(I,K)=PTR1A(I,K)*(TTR2(I,K)/TTR1A(I,K))**EXI	ST2	n50
1 WGT(I,K)=WR*WG1A(I,K)	ST2	n51
WGT2(K)=WR*WGT1A(K)	ST2	n52
I=IP	ST2	n53
ID=-1	ST2	n54
WGT2C(K)=0.	ST2	n55
IF(ICH0KE)26,26,3	ST2	n56
26 IF(LOPIN)27,27,3	ST2	n57
27 IF(GAMF)2,2,16	ST2	n58
2 TA2(K)=.95*TTR2(IP,K)	ST2	n59
CALL GAMMA(PTR2(I,K),TA2(K),FAIR,WAIR,GAM(4,K))	ST2	n60
16 FFA2(I,K)=WG2(I,K)*SQRT(TTR2(I,K))/(144.*PTR2(I,K)*CSBET2(I,K)*	ST2	n61
IANN2(I,K))	ST2	n62
CALL PRATIO(FFA2(I,K),GAM(4,K),RV(4,K),PTRS2(I,K),PRTOL)	*****	
3 CALL FLOW2(I)	ST2	n64
IF (PREVER) GO TO 22	ST2	n65
WGT2C(K)=WGT2C(K)+WG2(I,K)	ST2	n66
L=1	ST2	n67
IF (PTRS2(I,K).LE.PTRS2(IP,K)) L=I	ST2	n68
IF(ISECT-I)7,7,4	ST2	n69
4 I=I-ID	ST2	n70
IF(I)5,5,6	ST2	n71
5 ID=1	ST2	n72
I=IP-ID	ST2	n73
6 L=I-ID	ST2	n74
PS2(I,K)=PS2(L,K)+FLOAT(ID)*DPDR2(L,K)*(H2(I,K)+H2(L,K)	ST2	n75
1)/2.	ST2	n76
PTRS2(I,K)=PTR2(I,K)/PS2(I,K)	ST2	n77
IF (PTRS2(I,K)-1.)19,19,3	ST2	n78
19 PTRS2(I,K) = 1.0 + PRTOL	ST2	n79
GO TO 3	ST2	n80
7 IF(IS2(K))8,8,9	ST2	n81
8 EXI=GAM(4,K)/(GAM(4,K)-1.)	ST2	n82
CALL PHIM(EXI,ETAR(L,K),PHIX,PRC0IT)	ST2	n83
PRUP=PTH2(IP,K)*PRC1I*PS2(L,K)/(PTR2(L,K)*PS2(IP,K))	ST2	n84
1*(1.+PRTOL)	ST2	n85
PRL0W=1.	ST2	n86
GO TO 10	ST2	n87
9 IS2(K)=IS2(K)+1	ST2	n88
10 L = IHRC + 1	ST2	n89

Listing of Code (continued)

IF (ICHOKE.EQ.L) PTRS2(IP,K) = PRUP	ST2 090
IF (WGT2(K)-WGT2C(K))12.15.11	ST2 091
11 PRLOW= PTRS2(IP,K)	ST2 092
GO TO 13	ST2 093
12 PRUP= PTRS2(IP,K)	ST2 094
IS2(K)=1	ST2 095
13 WE=1.-WGT2(K)/WGT2C(K)	ST2 096
J=J+1	ST2 097
IF (J-32)29.18.18	ST2 098
29 IF (ICHOKE-L) 30.31.30	ST2 099
31 SCRIT= -WE	ST2 100
GO TO 15	ST2 101
30 IF (LOPIN)14.14.15	ST2 102
14 PRE= (PTRS2(IP,K)-PTRMC)/PTRS2(IP,K)	ST2 103
IF (ABS(PRE)-PR10L)17.17.24	ST2 104
17 CONTINUE	ST2 105
IF (ABS(WE)-WTOL)15.15.23	ST2 106
24 PTRMO=PTRS2(IP,K)	ST2 107
WGT2C(K)=0.0	ST2 108
I=IP	ST2 109
ID=-1	ST2 110
IF (SCRIT)28.28.15	ST2 111
28 PTRS2(IP,K)=.5*(PRLOW+PRUP)	ST2 112
IF (PTRS2(IP,K).LE.PRCRIT) PRPC=0.0	ST2 113
GO TO 3	ST2 114
23 SCRIT= 1.	ST2 115
15 IF (TLOOP.EQ.0.) GO TO 25	ST2 116
18 WRITE(6,1000)K,PRUP,PRLOW,WE,PCRIT,J,WGT2(K),WGT2C(K),(WG2(L,K),	ST2 117
1 L=1,ISECT)	ST2 118
WRITE(6,1001) (PTRS2(L,K),L=1,ISECT)	ST2 119
1000 FORMAT(2X,2H=I4, 2X,6H PRUP=F8.5,2X,6H PRLOW=F8.5,2X,6H WE=	ST2 120
1F8.5,1X,7HPCRIT=F8.5,2X,2HJ=I4/	ST2 121
22X,6H WGT2=F8.3,2X,6HWGT2C=F8.3/	ST2 122
32X,6H WG2=6F8.3)	ST2 123
1001 FORMAT(2X,6HPTPS2=6F8.5)	ST2 124
25 CALL CHECK(J)	ST2 125
GO TO (20,21),J	ST2 126
20 CALL DIAGT(4)	ST2 127
GO TO 22	ST2 128
21 CALL LOOP	ST2 129
22 IF (SHFLAG) WRITE(6,20000)	*****
20000 FORMAT(45H AN EXIT HAS BEEN MADE FROM SUBROUTINE STA2 )	*****
RETURN	*****
END	ST2 131

Listing of Code (continued)

```

SUBROUTINE FLOW2(I)
CFLW2
C   CALCULATE ROTOR EXIT SECTOR FLOW
C
  REAL MFSTOP
  LOGICAL PREVER,SRFLAG
  COMMON SRFLAG
  COMMON /SNTCP/G,AJ,PRPC,ICASE,PREVER,MFSTOP,JUMP,LOPIN,ISCASE,
  1KN,GAMF,IP,SCRIT,PTRN,ISECT,KSTG,WOTOL,HOTOL,PTOL,TRLOOP,LSTG,
  2LRRC,IBWC,ICHUKE,ISORH,CHOKE,PTOPSI(6,8),PTRS2(6,8),TRDIAG,SC,RC,
  3DELPR,PASS,IPC,LOPC,ISS
C
  COMMON /SINIT/H1(6,8),H2(6,8),DP0(6,8),DP1(6,8),DP1A(6,8),DP2(6,8),
  1,DP2A(6,8),CSALF1(6,8),ALF1(6,8),CSHET2(6,8),BET2(6,8),RADSD(6,8),
  2RADRD(6,8),ANN1(6,8),ANN2(6,8),ANN2A(6,8),ANN1A(6,8),U1A(6,8),
  3UZ(6,8),ANNO(6,8),PT0(6,8),TT0(6,8),ALPHA0(6,8),PTP(6,8)
C
  COMMON /SINPUT/ HSL,TSL,PSL,GAMSL,
  1PTPS,PTIN,TTIN,WAIR,FAIR,DELC,DELL,DELA,AACS,VCTD,STG,SECT,EXPN,
  2EXPP,EXPRE, RPM,PAF,SLI,STGCH,FNDJOH,NAME(10),TITLE(10),PCNH(6),
  3RV(6,8),GAM(6,8),DH(6,8),DT(6,8),RWG(6,8),ALPHAS(6,8),ALPHA1(6,8),
  4ETARS(6,8),ETAS(6,8),CFS(6,8),ANNO(6,8),BETA1(6,8),BETA2(6,8),ETAR
  5R(6,8),ETAR(6,8),CFR(6,8),TFR(6,8),ANDGR(6,8),OMEGAS(6,8),AS0(6,8),
  6,ASMP0(6,8),ACMNO(6,8),A1(6,8),A2(6,8),A3(6,8),A4(6,8),A5(6,8),A6
  7(6,8),OMEGAR(6,8),BSIA(6,8),RSMPIA(6,8),HCMNIA(6,8),B1(6,8),B2(6,8),
  8,B3(6,8),H4(6,8),B5(6,8),B6(6,8),SESTH1(8),RERTH1(8)
C
  COMMON /SSTA2/V2(6,8),TTR2(6,8),PTH2(6,8),WG2(6,8),WGT2(8),TA2(8),
  1PS2(6,8),PHI2(6,8)
C
  REAL MR2,M2,MF2
  COMMON /SFLOW2/TS2(6,8),CP2(8),R2(6,8),RHOS2(6,8),BET2E(6,8),RU2(6,8),
  1,8,VU2(6,8),DPDH2(6,8),VZ2(6,8),MR2(6,8),MF2(6,8),M2(6,8)
C
  DIMENSION P1AS2C(8),PHI2C(8),R2C(6,8),TS2C(6,8),RHOS2C(6,8),WG2C(6,8),
  1,8,CBET2E(6,8),AS2(6,8),RFF(6,8)
C
  IF(SRFLAG) WRITE(6,10000)
10000 FORMAT(44H AN ENTRY HAS BEEN MADE IN SUBROUTINE FLOW2 )
  K=KN
  EX=(GAM(4,K)-1.)/GAM(4,K)
C   ISENTROPIC ROTOR RELATIVE TEMPERATURE RATIO
10 PHI2(I,K)= PTRS2(I,K)**EX
  IF(OMEGAR(1,K))2,2,1
  1 CALL LOSS2(I,K)

```

```

FLW2 001
FLW2 002
FLW2 003
FLW2 004
FLW2 005
*****
FLW2 007
*****
FLW2 009
FLW2 010
FLW2 011
FLW2 012
FLW2 013
FLW2 014
FLW2 015
FLW2 016
*****
FLW2 018
*****
FLW2 021
FLW2 022
FLW2 023
FLW2 024
FLW2 025
FLW2 026
FLW2 027
FLW2 028
FLW2 029
FLW2 030
FLW2 031
FLW2 032
FLW2 033
FLW2 034
FLW2 035
FLW2 036
FLW2 037
*****
FLW2 038
FLW2 039
FLW2 040
FLW2 041
FLW2 042

```

# Listing of Code (continued)

C	EXIT TEMPERATURES	FLW2 043
2	TS2(I,K)=TTR2(I,K)*(1.-ETAR(I,K)*(1.-1./PHI2(I,K)))	FLW2 044
	IF(I-IP)6,3,6	FLW2 045
3	IF( GAMF)4,4,5	FLW2 046
4	TA2(K)=.5*(TTN2(I,K)+TS2(I,K))	FLW2 047
	CALL GAMMA(PTH2(I,K),TA2(K),FAIR,WAIR,GAM(4,K))	FLW2 048
5	EXI=GAM(4,K)/(GAM(4,K)-1.)	FLW2 049
	EX=1./EXI	FLW2 050
C	CRITICAL PRESSURE RATIO	FLW2 051
	CALL PHIM(EXI,ETAR(I,K),PHI2C(K),PIAS2C(K))	FLW2 052
C	SPECIFIC HEAT AT CONSTANT PRESSURE	FLW2 053
	*****	
6	CP2(K)=HV(4,K)*EXI/AJ	FLW2 055
C	RELATIVE EXIT VELOCITY	FLW2 056
	R2(I,K)=SQRT(2.*G*AJ*CP2(K)*(TTR2(I,K)-TS2(I,K)))	FLW2 057
C	EXIT PRESSURE	FLW2 058
	PS2(I,K)=PTR2(I,K)/PTRS2(I,K)	FLW2 059
C	EXIT DENSITY	*****
	RHOS2(I,K)=144.*PS2(I,K)/(HV(4,K)*TS2(I,K))	FLW2 061
C	TEST CRITICAL PRESSURE RATIO	FLW2 062
	IF( PTRS2(I,K)-PIAS2C(K))15, 7,7	FLW2 063
7	IF (IP-1) 22,8,22	FLW2 064
8	IF (PHPC)9,9,18	FLW2 065
9	PHPC=1.	FLW2 066
	PTH2(I,K)=PIAS2C(K)*(1.+PRTOL)	FLW2 067
	GO TO 10	FLW2 068
22	IF (PTRS2(I,K).LE.PTRS2(IP,K)) GO TO 18	FLW2 069
	GO TO 13	FLW2 070
18	IF ((1.EQ.1).OR.(1.EQ.ISECT)) SCRT=1.	FLW2 071
	GO TO 11	FLW2 072
11	CONTINUE	FLW2 073
	R2C(I,K)=SQRT(2.*G*AJ*CP2(K)*TTR2(I,K)*ETAR(I,K)*(	FLW2 074
	1PHI2C(K)-1.)/PHI2C(K))	FLW2 075
	TS2C(I,K)=TTR2(I,K)*(1.-ETAR(I,K)*(1.-1./PHI2C(K)))	*****
	RHOS2C(I,K)=144.*PTH2(I,K)/(HV(4,K)*PIAS2C(K)*TS2C(I,K))	FLW2 077
	WG2C(I,K)=RHOS2C(I,K)*R2C(I,K)*ANN2(I,K)*CSHET2(I,K)	FLW2 078
12	WG2(I,K)=WG2C(I,K)	FLW2 079
	GO TO 14	FLW2 080
13	IF( PHPC-1.)15,15,24	FLW2 081
24	WG2(I,K)=RFF(I,K)*PTR2(I,K)/SQRT(TIHW2(I,K))	FLW2 082
	GO TO 14	FLW2 083
C	OVEREXPANSION AFTER SUPERSONIC FLOW DECREASE	FLW2 084
14	CHET2E(I,K)=WG2(I,K)/(RHOS2(I,K)*R2(I,K)*ANN2(I,K))	FLW2 085
	BET2E(I,K)=ATAN2(SQRT(1.-CHET2E(I,K)*CHET2E(I,K)),CHET2E(I,K))	FLW2 086
	GO TO 16	FLW2 087
15	WG2(I,K)=RHOS2(I,K)*R2(I,K)*ANN2(I,K)*CSHET2(I,K)	FLW2 088
	CHET2E(I,K)=CSHET2(I,K)	FLW2 089
	BET2E(I,K)=BET2(I,K)	

# Listing of Code (continued)

```

      RFF(I,K)=WG2(I,K)*SQRT(TTR2(I,K))/PTR2(I,K)          FLW2 090
16  RU2(I,K)=R2(I,K)*SIN(ΘET2E(I,K))                      FLW2 091
      VU2(I,K)=RU2(I,K)-U2(I,K)                            FLW2 092
      DPOR2(I,K)=(RHOS2(I,K)*VU2(I,K)+VU2(I,K)/(G*DP2(I,K)))*.01388889*****
      VZ2(I,K)=R2(I,K)*CBET2E(I,K)                        FLW2 094
      AS2(I,K)=SQRT(GAM(4,K)*G*HV(4,K)*TS2(I,K))          *****
      V2(I,K)=SQRT(VZ2(I,K)*VZ2(I,K)+VU2(I,K)*VU2(I,K))   FLW2 096
      M2(I,K)=V2(I,K)/AS2(I,K)                            FLW2 097
      MR2(I,K)=R2(I,K)/AS2(I,K)                          FLW2 098
      MF2(I,K)=MR2(I,K)*CHEI2E(I,K)                      FLW2 099
      IF(I.LT.ISECT) GO TO 17                             FLW2 100
      IF(PRPC.EQ.1.) PRPC=2.                               FLW2 101
17  CALL CHECK(J)                                          FLW2 102
      GO TO (19,21),J                                     FLW2 103
19  CALL DIAGT(4)                                          FLW2 104
21  IF(SHFLAG) WRITE(6,20000)                             *****
20000 FORMAT(45H AN EXIT HAS BEEN MADE FROM SUBROUTINE FLOW2 ) *****
      RETURN                                              *****
      END                                                  FLW2 106

```

Listing of Code (continued)

```

SUBROUTINE LOSS2(I,K)                                LOS2 n01
CLOSS2                                                LOS2 n02
C CALCULATE ETA R FROM QUADRATIC POLYNOMIAL          LOS2 n03
C                                                     LOS2 n04
C REAL MFSTOP                                         LOS2 n05
C LOGICAL PREVER,SRFLAG                               *****
C COMMON SRFLAG                                       *****
C COMMON /SNTCP/G,AJ,PRPC,ICASE,PREVER,MFSTOP,JUMP,LOPIN,ISCASE, LOS2 n07
1KN,GAMF,IP,SCHIT,PTNN,ISECT,KSTG,WTOL,WHOTOL,PTOL,TRLOOP,LSTG, LOS2 n08
2LBRC,IBRC,ICHOKE,ISORH,CHOKE,PTOPSI(6,8),PTRS2(6,8),TRDIAG,SC,RC, LOS2 n09
3DELPR,PASS,IPC,LOPC,ISS                             LOS2 n10
C                                                     LOS2 n11
C                                                     *****
C COMMON /SINPUT/ WSL,TSL,PSL,GAMSL,                LOS2 n13
1PTPS,PTIN,TTIN,WAIR,FAIR,UELC,DELL,DELA,AACS,VCTD,STG,SECT,EXPN, LOS2 n16
2EXPP,EXPHE, RPN,PAF,SLI,STGCH,FNUJOB,NAME(10),TITLE(10),PCNH(6), *****
3RV(6,8),GAM(6,8),DR(6,8),DT(6,8),RWG(6,8),ALPHAS(6,8),ALPHA1(6,8), *****
4ETARS(6,8),ETAS(6,8),CFS(6,8),AND0(6,8),BETA1(6,8),BETA2(6,8),ETAH LOS2 n17
5R(6,8),ETAH(6,8),CFH(6,8),TFR(6,8),ANDUR(6,8),OMEGAS(6,8),AS0(6,8) LOS2 n18
6,ASMP0(6,8),ACMNO(6,8),A1(6,8),A2(6,8),A3(6,8),A4(6,8),A5(6,8),A6( LOS2 n19
76,8),OMEGAR(6,8),BSIA(6,8),BSMPIA(6,8),BSMNIA(6,8),B1(6,8),B2(6,8) LOS2 n20
8,B3(6,8),B4(6,8),B5(6,8),B6(6,8),SESTHI(8),RENTHI(8)          LOS2 n21
C                                                     LOS2 n22
C REAL MR1A                                           LOS2 n23
C COMMON /SSTA1A/VU1A(6,8),WG1A(6,8),WGT1A(8),VZ1A(6,8), CP1A(8), LOS2 n24
1PS1A(6,8),RU1A(6,8),RIA(6,8),HET1A(6,8),RI(6,8),TTR1A(6,8),PTR1A(6,8)
2,8),MH1A(6,8),TS1A(6,8)          *****
C                                                     LOS2 n26
C COMMON /SSTA2/V2(6,8),TTR2(6,8),PTR2(6,8),WG2(6,8),WGT2(8),TA2(8), LOS2 n27
1 PS2(6,8),PHI2(6,8)          LOS2 n28
C                                                     LOS2 n29
C                                                     LOS2 n30
C                                                     *****
C IF(SRFLAG) WRITE(6,10000)                          *****
10000 FORMAT(44H AN ENTRY HAS BEEN MADE IN SUBROUTINE LOSS2 )  LOS2 n31
C ETARR(I,K)=1.0                                       LOS2 n32
C IF(HI(I,K))4,1,2                                     LOS2 n33
1 W1A2=OMEGAR(I,K)                                    LOS2 n34
C GO TO 8                                              LOS2 n35
2 AS=R1(I,K)                                           LOS2 n36
C AC=B2(I,K)                                           LOS2 n37
C AQ=B3(I,K)                                           LOS2 n38
C IF(BSMPIA(I,K)-HI(I,K))3,6,6                       LOS2 n39
3 WHWR=R1(I,K)/BSMPIA(I,K)                           LOS2 n40
C AR=BSMPIA(I,K)/BSIA(I,K)                           LOS2 n41
C GO TO 7                                              LOS2 n42
4 AS=R4(I,K)                                           LOS2 n43
C AC=B5(I,K)

```



Listing of Code (continued)

AQ=H6(I,K)	LOS2 044
IF(R1(I,K)-HCMNIA(I,K))5,6,6	LOS2 045
5 WMWR=H1(I,K)/BCMNIA(I,K)	LOS2 046
AR=HCMNIA(I,K)/BSIA(I,K)	LOS2 047
GO TO 7	LOS2 048
6 WMWR=1.0	LOS2 049
AR=RI(I,K)/HSIA(I,K)	LOS2 050
7 W1A2=OMEGAR(I,K)*(1.+AR*AR*(AS+AR*(AC+AR*AQ)))*WMWR	LOS2 051
8 EX=(GAM(3,K)-1.)/GAM(3,K)	LOS2 052
ETAH(I,K)=(1.-(1./(PTH2(I,K)*(1.-W1A2)+W1A2))*EX)*PHI2(I,K)/	LOS2 053
1(PHI2(I,K)-1.)	LOS2 054
CALL CHECK(J)	LOS2 055
IF(SRFLAG) WRITE(6,20000)	*****
20000 FORMAT(45H AN EXIT HAS BEEN MADE FROM SUBROUTINE LOSS2 )	*****
RETURN	LOS2 056
END	LOS2 057

# Listing of Code (continued)

```

SUBROUTINE LOOP                                LOOP 001
C                                                LOOP 002
C    HANDLES ALL LOGIC FOR ITERATING TO OBTAIN EXACT CHOKE POINT- LOOP 003
C    UNDERFLOW, NO CHOKE INITIAL CHOKE, CHOKE ITERATION    LOOP 004
C    SUBCRITICAL, CHOKE ITERATION SUPERCRITICAL, MULTIPLE  LOOP 005
C    CHOKE, CHOKE ITERATION COMPLETE                    LOOP 006
C                                                        LOOP 007
C                                                        LOOP 008
C    REAL MFSTOP                                         *****
C    LOGICAL PREVER, SRFLAG                             *****
C    COMMON SRFLAG
C    COMMON /SNTCP/G, AJ, PRFC, ICASE, PRFVER, MFSTOP, JUMP, LOPIN, ISCASE, LOOP 010
C    1KN, GAMF, IP, SCHIT, PTRN, ISECT, KSTG, WTOL, HHTOL, PRTO, TRLOOP, LSTG, LOOP 011
C    2LHRC, IRRC, ICHOKE, ISORH, CHOKE, PTOP1(6,8), PTRS2(6,8), TRDIAG, SC, RC, LOOP 012
C    3DELPR, PASS, IPC, LOPC, ISS                      LOOP 013
C                                                        LOOP 014
C    *****
C    COMMON /SINPUT/ RSL, TSL, PSL, GAMS1,
C    1PTPS, PTIN, TTIN, WAIR, FAIR, DELC, DELL, DELA, AACS, BLLO, STG, SECT, EXPN, LOOP 016
C    2FXPP, EXPRF, RPM, PAF, SLI, STGCH, FNDJOH, NAME(10), TITLE(10), PCNH(6), *****
C    3RV(6,8), GAM(6,8), DR(6,8), DT(6,8), RWG(6,8), ALPHAS(6,8), ALPHA1(6,8), *****
C    4ETAS(6,8), ETAS(6,8), CFS(6,8), ANNO(6,8), HETA1(6,8), HETA2(6,8), ETARLOOP 019
C    5R(6,8), ETAR(6,8), CFH(6,8), TFR(6,8), ANDCH(6,8), OMEGAS(6,8), AS0(6,8) LOOP 020
C    6, ASMP0(6,8), ACMNO(6,8), A1(6,8), A2(6,8), A3(6,8), A4(6,8), A5(6,8), A6(6,8) LOOP 021
C    7A(6,8), OMEGAR(6,8), HSIA(6,8), RSMPIA(6,8), HCMNIA(6,8), R1(6,8), R2(6,8) LOOP 022
C    8, B3(6,8), R4(6,8), B5(6,8), B6(6,8), SESTHI(8), RENTHI(8)          LOOP 023
C    9, B3(6,8), R4(6,8), B5(6,8), B6(6,8), SESTHI(8), RENTHI(8)          LOOP 024
C    *****
C    IF (SRFLAG) WRITE(6,10000)                                *****
10000 FORMAT(44H AN ENTRY HAS BEEN MADE IN SUBROUTINE LOOP )
C    IJ=A+KSTG                                                LOOP 025
C    INCREASE BLADE ROW COUNTER                                LOOP 026
C    IBRC=IBRC+1                                              LOOP 027
C    TEST NEGATIVE SECTOR PRESSURE RATIO                      LOOP 028
C    IF (PTRN)18,1,1                                          LOOP 029
C    TEST CHOKE ITERATION ON BLADE ROW                        LOOP 030
C    1 IF (ICHOKE-IBRC)3,2,3                                  LOOP 031
C    TEST INCREMENT TOLERANCE                                LOOP 032
C    2 IF (PRTO-DELPR)3,3,4                                  LOOP 033
C    TEST STATION FLOW CRITICAL                              LOOP 034
C    3 IF (SCHIT)5,5,6                                        LOOP 035
C    CHOKE ITERATION COMPLETE                                LOOP 036
C    4 ICHOKE=0                                              LOOP 037
C    IPC=IBRC                                                LOOP 038
C    ISS=IBRC                                                LOOP 039
C    ISORH=2+((IBRC/2)*2-IBRC)                                LOOP 040
C    JL=(ISORH-1)*8+KN                                       LOOP 041
C    IF (JL-IJ)22,23,23                                     LOOP 042
C    22 DELPR=DELL                                           LOOP 043

```

Listing of Code (continued)

24	LOPC=0	LOOP	n44
	CHOKE=1.	LOOP	n45
	LSTG=KN	LOOP	n46
	LBRC=IBRC-1	LOOP	n47
	GO TO 18	LOOP	n48
23	DELPR=DELA	LOOP	n49
	GO TO 24	LOOP	n50
5	IF (ICHOKE-IBRC)18,7,18	LOOP	n51
C	TEST CHOKE ITERATION LOOP	LOOP	n52
6	IF (ISS-IBRC)8,18,18	LOOP	n53
C	CHOKE ITERATION	LOOP	n54
C	ISORR = 1 FOR STATOR	LOOP	n55
C	= 2 FOR ROTOR	LOOP	n56
7	DELPR=DELPR/2.	LOOP	n57
	JL=(ISORR-1)*8+LSTG	LOOP	n58
	PTOPSI(IP,JL)=PTOPSI(IP,JL)+DELPR	LOOP	n59
	GO TO 16	LOOP	n60
C	CHOKE HAS OCCURRED	LOOP	n61
8	IF (ICHOKE)80,80,13	LOOP	n62
80	J=(IBRC-2*(KN-1)-1)*8+KN	LOOP	n63
	WRITE(6,801)IBRC,PTOPSI(IP,J)	LOOP	n64
801	FORMAT(16X10HBLADE ROW 13,8H CHOKED,4X5HPTPS=F10.5)	LOOP	n65
C	TEST SINGLE CALCULATION POINT	LOOP	n66
9	IF (DELC)18,18,10	LOOP	n67
C	TEST PREVIOUS CHOKE	LOOP	n68
10	IF (IPC)11,11,12	LOOP	n69
C	SAVE COMBINATIONS PRIOR FIRST CHOKE	LOOP	n70
11	LBRC=LBRC	LOOP	n71
	ISORRS=ISORR	LOOP	n72
	JL=(ISORR-1)*8+LSTG	LOOP	n73
	SPTPS=PTOPSI(IP,JL)-DELPR	LOOP	n74
	LSTGS=LSTG	LOOP	n75
	SDELPR=DELPR	LOOP	n76
	GO TO 13	LOOP	n77
12	JL=LSTGS+(ISORRS-1)*8	LOOP	n78
	DELNU = (PTOPSI(IP,JL)-SPTPS)/4.	LOOP	n79
	IF (DELNU,LE,0.0001) DELNU = SDELPR/4.	LOOP	n80
	DELPR = DELNU	LOOP	n81
	SDELPR = DELNU	LOOP	n82
	WRITE(6,1201)IPC,IBRC,DELPR	LOOP	n83
1201	FORMAT(6X11HBLADE ROWS 15,5H AND 15,25H, CHOKED - INCREMENT NOW	LOOP	n84
	1F10.5)	LOOP	n85
	LBRC=LBRC	LOOP	n86
	LSTG=LSTGS	LOOP	n87
	ISORR=ISORRS	LOOP	n88
	PTOPSI(IP,JL) = SPTPS + SDELPR	LOOP	n89
	LOPC=10	LOOP	n90

# Listing of Code (continued)

ICHOKE=0	LOOP 091
IPC=0	LOOP 092
ISS=0	LOOP 093
CHOKE=0.0	LOOP 094
GO TO 17	LOOP 095
C TEST PREVIOUS COMPLETE CALCULATION	LOOP 096
13 IF (PASS)15,15,14	LOOP 097
14 ICHOKE=IHRC	LOOP 098
DELPR=.5*DELPR	LOOP 099
15 JL=(ISORH-1)*8+LSTG	LOOP 100
PTOPSI(IP,JL)=PTOPSI(IP,JL)-DELPR	LOOP 101
C SET INDEX REGISTERS	LOOP 102
16 CONTINUE	LOOP 103
LOPC=LOPC+1	LOOP 104
C SET JUMP FOR CHOKE ITERATION	LOOP 105
17 JUMP=1	LOOP 106
GO TO 19	LOOP 107
C JUMP SET FOR NO CHOKE OR CHOKE COMPLETE	LOOP 108
18 JUMP=0	LOOP 109
C TEST LOOP-TRACE	LOOP 110
19 IF (THLOOP)21,21,20	LOOP 111
20 WRITE(6,2001)IHRC,LHRC,ISURR,KN,LSTG,IPC,ISS,ICHOKE,JUMP,LHRC,	LOOP 112
ISORRS,LSTGS,SPIPS,PTOPSI(IP,JL),DELPR,DELL,SCRIT,LOPC	LOOP 113
2001 FORMAT(3X12I5/3X4F10.5,F10.0,I10)	LOOP 114
21 IF(SRFLAG) WRITE(6,20000)	*****
20000 FORMAT(45H AN EXIT HAS BEEN MADE FROM SUBROUTINE LOOP )	*****
RETURN	*****
END	LOOP 116

# Listing of Code (continued)

```

SUBROUTINE STA2A
CSTA2A
C      DETERMINE INLET FLOW CONDITIONS TO ALL STATORS
C      AFTER THE FIRST STATUR
C
C      REAL MFSTOP
C      LOGICAL PHEVER,SRFLAG
C      COMMON SRFLAG
C      COMMON /SNTCP/G,AJ,PRFC,ICASE,PHEVER,MFSTOP,JUMP,LOPIN,ISCASE,
1KN,GAMF,IP,SCRIT,PTRN,ISECT,KSTG,WOTOL,RHOTOL,PTOL,TRLOOP,LSTG,
2LBRC,IHRC,IHCKE,ISORH,CHCKE,PTOP1(6,8),PTRS2(6,8),TRDIAG,SC,RC,
3DELPR,PASS,IPC,LOPC,ISS
C
C      COMMON /SINIT/H1(6,8),H2(6,8),DPn(6,8),DP1(6,8),DP1A(6,8),DP2(6,8),
1,DP2A(6,8),CSALF1(6,8),ALF1(6,8),CSBET2(6,8),BET2(6,8),RADSD(6,8),
2RADRD(6,8),ANN1(6,8),ANN2(6,8),ANN2A(6,8),ANN1A(6,8),U1A(6,8),
3U2(6,8),ANNn(6,8),PT0(6,8),TT0(6,8),ALPHA0(6,8),PTP(6,8)
C
C      COMMON /SINPUT/ HSL,ISL,PSL,GAMSI,
1PTPS,PTIN,TTIN,WAIR,FAIR,DELC,DELL,DELA,AACS,VCTD,STG,SECT,EXPN,
2EXPP,EXPRE, RPM,PAF,SLI,STGCH,FNUJOH,NAME(10),TITLE(10),PCNH(4),
3RV(6,8),GAM(6,8),DR(6,8),DT(6,8),RWG(6,8),ALPHAS(6,8),ALPHA1(6,8),
4ETARS(6,8),ETAS(6,8),CFS(6,8),ANNO(6,8),BETA1(6,8),BETA2(6,8),ETAHST2A
5R(6,8),ETAR(6,8),CFR(6,8),TFR(6,8),ANDOR(6,8),OMEGAS(6,8),ASO(6,8),
6,ASMP0(6,8),ACMNO(6,8),A1(6,8),A2(6,8),A3(6,8),A4(6,8),A5(6,8),A6(6,8),
76,8),OMEGAR(6,8),BSIA(6,8),RSMPIA(6,8),HCMNIA(6,8),R1(6,8),R2(6,8),
8,R3(6,8),R4(6,8),R5(6,8),R6(6,8),SESTH1(8),HERTHI(8)
C
C      REAL M0
C      COMMON /SSTA01/CP0(8),
18),VU0(6,8),VZ0(6,8),MHUS0(6,8),PS1(6,8),WGT1(8),TA1(8),WG1(6,8),
2DPDR1(6,8),SI(6,8), CP1(8),PHI1(6,8),TS1(6,8),V1(6,8),
3,RHOS1(6,8),ALF1E(6,8),VU1(6,8),VZ1(6,8),M0(6,8),WGT0(8),WG0(6,8)
C
C      REAL MR1A
C      COMMON /SSTA1A/VU1A(6,8),WG1A(6,8),WGT1A(8),VZ1A(6,8), CP1A(8),
1PS1A(6,8),RU1A(6,8),RIA(6,8),HET1A(6,8),RI(6,8),TTR1A(6,8),PTH1A(6,8),
2,8),MR1A(6,8),TS1A(6,8)
C
C      COMMON /SSTA2/V2(6,8),TTR2(6,8),PTH2(6,8),WG2(6,8),WGT2(8),TA2(8),
1PS2(6,8),PHI2(6,8)
C
C      REAL MR2,MZ,MF2
C      COMMON /SFLOW2/TS2(6,8),CP2(8),R2(6,8),RHUS2(6,8),HET2E(6,8),RU2(6,8),
1,8),VU2(6,8),DPDR2(6,8),VZ2(6,8),MH2(6,8),MF2(6,8),MZ(6,8)

```

Listing of Code (continued)

```

      REAL M2A,MF2A
      COMMON /SSTA2A/WG2A(6,8),WGT2A(8),VU2A(6,8),VZ2A(6,8),PS2A(6,8),
1ALF2A(6,8),TT2A(6,8),FT2A(6,8),TTHAR(8),PTBAR(8),STT0(8),SPT0(8),
2M2A(6,8),MF2A(6,8),CP2A(8),V2A(6,8),TS2A(6,8),TAS(8),PAS(8),GAMS(8)
3),CPS(8),DELMVD(6,8),HVBAR(8)
C
C      DIMENSION          TTT2A(6,8)
C
C      IF(SRFLAG) WRITE(6,10000)
10000 FORMAT(44H AN ENTRY HAS BEEN MADE IN SUBROUTINE STA2A )
      K=KN
      ID=-1
      I=IP
      TS2A(I,K)=TS2(I,K)
      WR=HWG(5,K)/RWG(4,K)
      SUMT=0.0
      SUMLT=0.0
      SUMLP=0.0
      WGT2A(K)=WR*WGT2(K)
12 VU2A(I,K)=VU2(I,K)*DP2(I,K)/DP2A(I,K)
      WG2A(I,K)=WR*WG2(I,K)
      RHOSTH=RHOS2(I,K)
1 VZ2A(I,K)=WR*VZ2(I,K)*ANN2(I,K)*RHOS2(I,K)/(ANN2A(I,K)*RHOSTR)
      V2A(I,K)=SQRT(VU2A(I,K)*VU2A(I,K)+VZ2A(I,K)*VZ2A(I,K))
      IF(I-IP)4,2,4
2 IF( GAMF)3,3,4
3 TA2A =.5*(TTR2(I,K)+TS2A(I,K))
      CALL GAMMA(PTH2(IP,K),TA2A ,FATR,WAJR,GAM(5,K))
4 EX=(GAM(5,K)-1.)/GAM(5,K)
      EXI=1./EX
      CP2A(K)=HV(5,K)*EXI/AJ
      DELTS=(V2(I,K)*V2(I,K)-V2A(I,K)*V2A(I,K))/(2.*G*AJ*CP2A(K))
      TS2A(I,K)=TS2(I,K)+DELTS
      IF(TS2A(I,K).GT.0.) GO TO 32
      PREVER = .TRUE.
      MFSTOP = 2.
      GO TO 30
32 PS2A(I,K)=PS2(I,K)*(1.+DELTS/TS2(I,K))*EXI
      RHOS2A =1+.5*PS2A(I,K)/(RV(5,K)*TS2A(I,K))
      IF(ABS(RHOSTH-RHOS2A )-1.E-07)6,6,5
5 RHOSTH=RHOS2A
      GO TO 1
6 SALF2A =VU2A(I,K)/V2A(I,K)
      ALF2A(I,K)=ATAN2(SALF2A ,SQRT(1.-SALF2A *SALF2A ))
11 IF (I-IP)28,24,28

```

```

ST2A 046
ST2A 047
ST2A 048
ST2A 049
ST2A 050
*****
ST2A 052
ST2A 053
ST2A 054
ST2A 055
*****
ST2A 056
ST2A 057
ST2A 058
ST2A 059
ST2A 060
ST2A 061
ST2A 062
ST2A 063
ST2A 064
ST2A 065
ST2A 066
ST2A 067
ST2A 068
ST2A 069
ST2A 070
ST2A 071
ST2A 072
ST2A 073
ST2A 074
*****
ST2A 076
ST2A 077
ST2A 078
ST2A 079
ST2A 080
ST2A 081
ST2A 082
*****
ST2A 084
ST2A 085
ST2A 086
ST2A 087
ST2A 088
ST2A 089

```

Listing of Code (continued)

24 IF (GAMF) 25,25,26	ST2A 090
25 TAS(K)=.5*(TA1(K)+TA2(K))	ST2A 091
PAS(K)=.5*(PT0(IP,K)+PT2A(IP,K))	ST2A 092
CALL GAMMA(PAS(K),TAS(K),FAIR,WAIR,GAMS(K))	ST2A 093
GO TO 27	ST2A 094
26 GAMS(K)=.5*(GAM(2,K)+GAM(4,K))	ST2A 095
27 E4=GAMS(K)/(GAMS(K)+1.)	ST2A 096
RVBAR(K)=.5*(HV(2,K)+HV(4,K))	*****
CPS(K)=RVBAR(K)*E4/AJ	*****
28 DELHVD(I,K)=(U1A(I,K)*VU1A(I,K)+U2(I,K)*VU2(I,K))/AJ/G	ST2A 098
M2A(I,K)=V2A(I,K)/SQRT(GAM(5,K)*G*RV(5,K)*TS2A(I,K))	*****
DELT=TFR(I,K)*DELHVD(I,K)/CPS(K)	ST2A 100
TT2A(I,K)=TTO(I,K)-DELT	ST2A 101
TTTS2A(I,K)=1.+(M2A(I,K)*M2A(I,K)*(GAM(5,K)-1.)/2.)	ST2A 102
PTPS2A = (TTTS2A(I,K))*EXI	ST2A 103
PT2A(I,K)=PS2A(I,K)*PTPS2A	ST2A 104
MF2A(I,K)=M2A(I,K)*COS(ALF2A(I,K))	ST2A 105
IF (ISECT-I) 13,15,13	ST2A 106
13 I=I-ID	ST2A 107
IF (I) 14,14,12	ST2A 108
14 ID=1	ST2A 109
I=IP-ID	ST2A 110
GO TO 12	ST2A 111
15 CONTINUE	ST2A 112
DO 16 I=1,ISECT	ST2A 113
RW=WG2A(I,K)/WG12A(K)	ST2A 114
TR=TT2A(I,K)/TT2A(IP,K)	ST2A 115
PR=PT2A(I,K)/PT2A(IP,K)	ST2A 116
SUMT=SUMT+RW*TR	ST2A 117
SUMLT=SUMLT+RW*ALOG(TR)	ST2A 118
16 SUMLP=SUMLP+RW*ALOG(PR)	ST2A 119
E3=GAM(5,K)/(GAM(5,K)+1.)	ST2A 120
TTBAR(K)=TT2A(IP,K)*GLMT	ST2A 121
PTBAR(K)=PT2A(IP,K)*EXP(SUMLP+E3*(ALOG(SUMT)-SUMLT))	ST2A 122
IF (K-KSTG) 17,18,18	ST2A 123
17 STTO(K+1)=TTBAR(K)	ST2A 124
SPTO(K+1)=PTBAR(K)	ST2A 125
DO 23 I=1,ISECT	ST2A 126
29 SI(I,K+1)=ALF2A(I,K)-RADSD(I,K+1)	ST2A 127
IF(SI(I,K+1).GT. 1.570796) SI(I,K+1)= 1.570796	*****
IF(SI(I,K+1).LT.-1.570796) SI(I,K+1)=-1.570796	*****
IF(OMEGAS(I,K)) 8,8,7	ST2A 130
7 ETARS(I,K+1)=1.0	ST2A 131
EXPSI=0.	ST2A 132
GO TO 117	ST2A 133
8 IF(SI(I,K+1)) 9,9,10	ST2A 134
9 EXPSI=EXPN	ST2A 135

Listing of Code (continued)

GO TO 117	ST2A 136
10 EXPSI=EXPP	ST2A 137
117 IF (PAF-1.)19,20,21	ST2A 138
C UNIFORM PROFILES	ST2A 139
19 PTP(I,K+1)=PTBAH(K)	ST2A 140
PTO(I,K+1)= PTP(I,K+1)	ST2A 141
1*(1.+(TTTS2A(I,K)-1.)*ETAHS(I,K+1))*(COS(SI(I,K+1))**EXPSI)**EXI	ST2A 142
2/(TTTS2A(I,K))**EXI	ST2A 143
TT0(I,K+1)=TTBAH(K)	ST2A 144
GO TO 23	ST2A 145
C SAVE PROFILES	ST2A 146
20 PTP(I,K+1)=PT2A(I,K)	ST2A 147
PT0(I,K+1)= PTP(I,K+1)	ST2A 148
1*(1.+(TTTS2A(I,K)-1.)*ETAHS(I,K+1))*(COS(SI(I,K+1))**EXPSI)**EXI	ST2A 149
2/(TTTS2A(I,K))**EXI	ST2A 150
GO TO 22	ST2A 151
C SMOOTH PRESSURE PROFILES	ST2A 152
21 PTP(I,K+1)=PTBAH(K)*(IT2A(I,K)/TTHAR(K))**E3	*****
PT0(I,K+1)= PTP(I,K+1)	ST2A 154
1*(1.+(TTTS2A(I,K)-1.)*ETAHS(I,K+1))*(COS(SI(I,K+1))**EXPSI)**EXI	ST2A 155
2/(TTTS2A(I,K))**EXI	ST2A 156
22 TT0(I,K+1)=TT2A(I,K)	ST2A 157
23 CONTINUE	ST2A 158
18 MFSTOP=MF2A(IP,K)/AACS	ST2A 159
CALL CHECK(J)	ST2A 160
GO TO (30,31)*J	ST2A 161
30 CALL DIAGT(5)	ST2A 162
31 IF(SRFLAG) WRITE(6,20000)	*****
20000 FORMAT(45H AN EXIT HAS BEEN MADE FROM SUBROUTINE STA2A )	*****
RETURN	*****
END	ST2A 164



Listing of Code (continued)

```

SUBROUTINE STA1                                ST1 001
CSTA1                                          ST1 002
C    SATISFY CONTINUITY OF FLOW AT EXIT OF ALL STATORS ST1 003
C    AFTER THE FIRST STATOR                  ST1 004
C                                          ST1 005
C    REAL MFSTOP                              ST1 006
C    LOGICAL PREVER,SRFLAG                    *****
C    COMMON SRFLAG                            *****
C    COMMON /SNTCP/G,AJ,PRFC,ICASE,PREVER,MFSTOP,JUMP,LOPIN,ISCASE, ST1 008
C    1KN,GAMF,IP,SCHIT,PTRN,ISECT,KSTG,WIOL,HHOTOL,PTOL,TRLOOP,LSTG, *****
C    2LHRC,IHRC,ICHOKE,ISORH,CHOKE,PTOPSI(6,8),PTRS2(6,8),TRDIAG,SC,RC, ST1 010
C    3DELPH,PASS,IPC,LOPC,ISS                ST1 011
C                                          ST1 012
C    COMMON /SINIT/H1(6,8),H2(6,8),DP0(6,8),DP1(6,8),DP1A(6,8),DP2(6,8) ST1 013
C    1,DP2A(6,8),CSALF1(6,8),ALF1(6,8),CSHET2(6,8),HET2(6,8),RADSD(6,8), ST1 014
C    2RADHD(6,8),ANN1(6,8),ANN2(6,8),ANN2A(6,8),ANN1A(6,8),U1A(6,8), ST1 015
C    3U2(6,8),ANN0(6,8),PT0(6,8),TT0(6,8),ALPHA0(6,8),PTP(6,8) ST1 016
C                                          ST1 017
C    COMMON /SINPUT/ RSL,TSL,PSL,GAMSI, *****
C    1PTPS,PTIN,TTIN,WAIR,FAIR,DELC,DEI,DELA,AACS,VCTD,STG,SECT,EXPN, ST1 019
C    2EXPP,EXPPE, RPM,PAF,SLI,STGCH,FNDJOB,NAME(10),TITLE(10),PCNM(6), *****
C    3RV(6,8),GAM(6,8),DR(6,8),DT(6,8),RWG(6,8),ALPHAS(6,8),ALPHA1(6,8), *****
C    4ETARS(6,8),ETAS(6,8),CFS(6,8),AND0(6,8),BETA1(6,8),BETA2(6,8),ETARST1 022
C    5R(6,8),ETAR(6,8),CFH(6,8),TFR(6,8),ANDOH(6,8),OMEGAS(6,8),AS0(6,8) ST1 023
C    6,ASMP0(6,8),ACMNO(6,8),A1(6,8),A2(6,8),A3(6,8),A4(6,8),A5(6,8),A6( ST1 024
C    76,8),OMEGAR(6,8),RSIA(6,8),RSMPIA(6,8),BCMNI(6,8),B1(6,8),B2(6,8) ST1 025
C    8,B3(6,8),B4(6,8),B5(6,8),B6(6,8),SESTHI(8),RERTHI(8) ST1 026
C                                          ST1 027
C    REAL M0                                  ST1 028
C    COMMON /SSTA01/CP0(8), P50(6,8),V0(6,8),TS0(6,8) ST1 029
C    1R,VU0(6,8),VZ0(6,8),MHOS0(6,8),PS1(6,8),WGT1(8),TA1(8),WG1(6,8), ST1 030
C    2 DPH1(6,8),SI(6,8), CP1(8),PHI1(6,8),TS1(6,8),V1(6,8) ST1 031
C    3,RHCS1(6,8),ALF1E(6,8),VU1(6,8),VZ1(6,8),M0(6,8),WGT0(8),WG0(6,8) *****
C                                          ST1 033
C    REAL M2A,MF2A                          ST1 034
C    COMMON /SSTA2A/WG2A(6,8),WGT2A(8),VU2A(6,8),VZ2A(6,8),PS2A(6,8), ST1 035
C    1ALF2A(6,8),TT2A(6,8),FT2A(6,8),TTBAR(8),PTBAR(8),STT0(8),SPT0(8), ST1 036
C    2M2A(6,8),MF2A(6,8),CP2A(8),V2A(6,8),TS2A(6,8),TAS(8),PAS(8),GAMS(8) ST1 037
C    3,CPS(8),DELMVD(6,8),MVHAR(8) *****
C                                          ST1 039
C    DIMENSION WGTIC(8),LC1(8),FFA1(6,8) ST1 040
C                                          ST1 041
C                                          ST1 042
C    IF(SRFLAG) WRITE(6,10000) *****
10000 FORMAT(44H AN ENTRY HAS BEEN MADE IN SUBROUTINE STA1 ) *****
      K=KN

```

Listing of Code (continued)

J=1	ST1 043
SCRIT=0.0	ST1 044
PTRM0=1.	ST1 045
WR1=HWG(1,K)/HWG(5,K-1)	*****
WR=HWG(2,K)/HWG(5,K-1)	ST1 046
DO 1 I=1,ISECT	ST1 047
WG0(I,K)=WR1*WG2A(I,K-1)	*****
WG1(I,K)=WR*WG2A(I,K-1)	ST1 048
ALPHA0(I,K)=ALF2A(I,K-1)	ST1 049
PS0(I,K)=PS2A(I,K-1)	ST1 050
V0(I,K)=V2A(I,K-1)	ST1 051
TS0(I,K)=TS2A(I,K-1)	ST1 052
VU0(I,K)=VU2A(I,K-1)	ST1 053
VZ0(I,K)=VZ2A(I,K-1)	ST1 054
M0(I,K)=M2A(I,K-1)	ST1 055
1 CONTINUE	*****
CP0(K)=CP2A(K-1)	*****
WGT0(K)=WR1*WGT2A(K-1)	*****
WGT1(K)=WR*WGT2A(K-1)	*****
I=IP	ST1 057
ID=-1	ST1 058
WGTIC(K)=0.0	ST1 059
LC1(K)=0	ST1 060
IF(ICHOKL)17,17,16	ST1 061
17 IF(LOPIN)18,18,16	ST1 062
18 IF(GAMF)2,2,3	ST1 063
2 TA1(K)=.95*TT0(IP,K)	ST1 064
CALL GAMMA(PT0(IP,K),TA1(K),FAIR,WAIR,GAM(2,K))	ST1 065
3 FFA1(I,K)=WG1(I,K)*SQRT(TT0(I,K))/(144.*PT0(I,K)*ANN1(I,K)	ST1 066
1*CSALF1(I,K))	ST1 067
CALL PRATIO(FFA1(I,K),GAM(2,K),RV(2,K),PT0PS1(I,K),PRTOL)	*****
16 CALL FLOW(I)	ST1 069
IF (PHEVER) GO TO 25	ST1 070
WGTIC(K)=WGTIC(K)+WG1(I,K)	ST1 071
L=1	ST1 072
IF (PT0PS1(I,K).LE.PTGPS1(IP,K)) L=I	ST1 073
IF (ISECT-I)7,7,4	ST1 074
4 I=I-ID	ST1 075
IF(I)5,5,6	ST1 076
5 ID=1	ST1 077
I=IP-ID	ST1 078
6 L=I-ID	ST1 079
PS1(I,K)=PS1(L,K)+FLOAT(ID)*DPDR1(L,K)*(H1(I,K)+H1(L,K))/2.	ST1 080
PT0PS1(I,K)=PT0(I,K)/PS1(I,K)	ST1 081
GO TO 16	ST1 082
7 IF(LC1(K))8,8,9	ST1 083
8 LC1(K)=1	ST1 084

Listing of Code (continued)

EX=GAM(2,K)/(GAM(2,K)-1.)	ST1	085
CALL PHIM(EX,ETAS(L,K),PHIX,PRCRIT)	ST1	086
PRUP=PTOPSI(IP,K)*PRCRIT/PTOPSI(L,K)	ST1	087
1*(1.+PRTUL)	ST1	088
PRL0W=1.0	ST1	089
GO TO 10	ST1	090
9 LC1(K)=LC1(K)+1	ST1	091
10 L = IIRC + 1	ST1	092
IF(ICHOKE.EQ.L) PTOPSI(IP,K) = PRUP	ST1	093
IF(WGT1(K)-WGT1C(K))14,15,11	ST1	094
11 PRL0W=PTOPSI(IP,K)	ST1	095
GO TO 13	ST1	096
12 PRUP=PTOPSI(IP,K)	ST1	097
13 WE=1.-WGT1(K)/WGT1C(K)	ST1	098
J=J+1	ST1	099
IF(J-32)29,22,22	ST1	100
29 IF(ICHOKE-L) 30,31,30	ST1	101
31 SCRIT= -WE	ST1	102
GO TO 15	ST1	103
30 IF(LOPIN)14,14,15	ST1	104
14 PRE=(PTOPSI(IP,K)-PTRMO)/PTOPSI(IP,K)	ST1	105
IF (ABS(PRE)-PRTUL)21,21,27	ST1	106
21 CONTINUE	ST1	107
IF (ABS(WE)-WTOL)15,15,20	ST1	108
27 PTRMO=PTOPSI(IP,K)	ST1	109
WGT1C(K)=0.0	ST1	110
I=IP	ST1	111
ID=-1	ST1	112
IF (SCRIT)19,19,15	ST1	113
19 PTOPSI(IP,K)=.5*(PRL0W+PRUP)	ST1	114
IF (PTOPSI(IP,K),LE,PRCRIT) PRPC=0.	ST1	115
GO TO 16	ST1	116
20 SCRIT= 1.	ST1	117
15 IF(THLOOP.EQ.0.) GO TO 28	ST1	118
22 WRITE(6,1000)K,PRUP,PRL0W,WE,PRCRIT,J,WGT1(K),WGT1C(K),(WGT1(L,K),	ST1	119
1 L=1,ISECT)	ST1	120
WRITE(6,1001)(PTOPSI(L,K),L=1,ISFCT)	ST1	121
1000 FORMAT(2X,2HK=14, 2X,6H PRUP=F8.5,2X,6HPRL0W=F8.5,2X,6H WE=	ST1	122
1F8.5,1X,7HPRCRIT=F8.5,2X,2HJ=14/	ST1	123
22X,6H WGT1=F8.3,2X,6HWGT1C=F8.3/	ST1	124
32X,6H WGT1=6F8.3)	ST1	125
1001 FORMAT(1X,7HPTOPSI=6F8.5)	ST1	126
28 CALL CHECK(J)	ST1	127
GO TO (23,24),J	ST1	128
23 CALL DIAGT(2)	ST1	129
GO TO 25	ST1	130
24 CALL LOOP	ST1	131

Listing of Code (continued)

```
      25 IF(SHFLAG) WRITE(6,20000)
20000 FORMAT(45H AN EXIT HAS BEEN MADE FROM SUBROUTINE STA1 )
      RETURN
      END
```

\*\*\*\*\*  
\*\*\*\*\*  
\*\*\*\*\*  
ST1 133

Listing of Code (continued)

```

SUBROUTINE OVRALL
COVRALL
C PURPOSE IS TO CALCULATE STAGE PERFORMANCE VALUES
C AFTER FLOW ITERATION IS COMPLETED THROUGH THE LAST STAGE
C
REAL MFSTOP
LOGICAL PREVER,SRFLAG
COMMON SRFLAG
COMMON /SNTCP/G,AJ,PRFC,ICASE,PREVER,MFSTOP,JUMP,LOPIN,ISCASE,
1KN,GAMF,IP,SCHIT,PTRN,ISECT,KSTG,WTOI,RHOTOL,PTOL,TRLOOP,LSTG,
2LBRG,IBWC,ICHOKE,ISORR,CHOKE,PTOPSI(6,8),PTRS2(6,8),TRDIAG,SC,RC,
3DELPR,PASS,IPC,LOPC,ISS
C
COMMON /SINIT/H1(6,8),H2(6,8),DP0(6,8),DP1(6,8),DP1A(6,8),DP2(6,8),
1,DP2A(6,8),CSALF1(6,8),ALF1(6,8),CSHET2(6,8),HET2(6,8),RADSD(6,8),
2RADRD(6,8),ANN1(6,8),ANN2(6,8),ANN2A(6,8),ANN1A(6,8),U1A(6,8),
3U2(6,8),ANN0(6,8),PT0(6,8),TT0(6,8),ALPHA0(6,8),PTP(6,8)
C
COMMON /SINPUT/ RSL,TSL,PSL,GAMSL,
1PTPS,PTIN,TTIN,WAIR,FAIR,DELC,DELL,DELA,AACS,VCTD,STG,SECT,EXPN,
2EXPP,EXPHE, RPM,PAF,SLI,STGCH,FNDJOR,NAME(10),TITLE(10),PCNH(8),
3RV(6,8),GAM(6,8),DR(6,8),UT(6,8),RWG(6,8),ALPHAS(6,8),ALPHA1(6,8),
4ETARS(6,8),ETAS(6,8),CFS(6,8),ANNO(6,8),BETA1(6,8),BETA2(6,8),ETAROVLL
5R(6,8),ETAR(6,8),CFR(6,8),TFR(6,8),ANDCR(6,8),OMEGAS(6,8),ASO(6,8)
6,ASMP0(6,8),ACMN0(6,8),A1(6,8),A2(6,8),A3(6,8),A4(6,8),A5(6,8),A6(
7A,8),OMEGAR(6,8),BS1A(6,8),RSMPIA(6,8),HCMN1A(6,8),B1(6,8),B2(6,8),
8B3(6,8),H4(6,8),B5(6,8),H6(6,8),SESTHI(8),RERTHI(8)
C
REAL M0
COMMON /SSTA01/CP0(8),
18),VU0(6,8),VZ0(6,8),MHOS0(6,8),PS1(6,8),WGT1(8),TA1(8),WG1(6,8),
2DPD01(6,8),SI(6,8),CP1(8),PHI1(6,8),TS1(6,8),V1(6,8),
3,RHOS1(6,8),ALF1E(6,8),VU1(6,8),VZ1(6,8),M0(6,8),WGT0(8),WG0(6,8)
C
REAL MR1A
COMMON /SSTA1A/VU1A(6,8),WG1A(6,8),WGT1A(8),VZ1A(6,8),CP1A(8),
1PS1A(6,8),RU1A(6,8),R1A(6,8),RET1A(6,8),RI(6,8),TTR1A(6,8),PTR1A(6,8),
2,8),MH1A(6,8),TS1A(6,8)
COMMON /SSTA2/V2(6,8),TTR2(6,8),PTR2(6,8),WG2(6,8),WGT2(8),TA2(8),
1PS2(6,8),PHI2(6,8)
C
REAL MR2,M2,MF2
COMMON /SFLW2/TS2(6,8),CP2(8),R2(6,8),MHOS2(6,8),BET2E(6,8),RU2(6,8),
1,8),VU2(6,8),DPDR2(6,8),VZ2(6,8),MR2(6,8),MF2(6,8),M2(6,8)
C
REAL M2A,MF2A

```

# Listing of Code (continued)

```

COMMON /SSTA2A/WGZA(6,8),WGTZA(8),VUZA(6,8),VZ2A(6,8),PS2A(6,8), OVLL 046
1ALF2A(6,8),TT2A(6,8),PT2A(6,8),TTBAR(8),PTBAR(8),STT0(8),SPT0(8), OVLL 047
2M2A(6,8),MF2A(6,8),CP2A(8),VZA(6,8),TS2A(6,8),TAS(8),PAS(8),GAMS(8)OVLL 048
3),CPS(8),DELHVD(6,8),HVBAR(8) *****
C OVLL 050
COMMON /SOVRAL/DELHT(6,8),DELHTI(6,8),DELHSI(6,8),DEHATI(6,8), OVLL 051
1ETATT(6,8),ETATS(6,8),ETATAT(6,8) OVLL 052
C OVLL 053
REAL MIS(8),MIRS(8),MH1AR(8),MR2T(8) OVLL 054
DIMENSION SA0(8),SIS(8),SB1A(8),SIR(8),SAZ(8),THCR(8),EPSI(8),DELTOVLL 055
1(8),SETATT(8),SETATS(8),SETAAT(8),SWRTP(8),SNRT(8),SDHT(8),SETHC(8)OVLL 056
2),SNRTHC(8),SWRTED(8),SPTPT2(8),SPTPS2(8),ST2TT0(8),STRIT0(8),UPS(OVLL 057
3A),UPUPS(8),URS(8),URLRS(8),VIS(8),UPVIS(8),URVIS(8),PSIPS(8),PSIROVLL 058
4S(8),RXP(8),RXR(8),DBETAR(8),DELHTS(8),DEHTIS(8),DEHSIS(8),DHATIS(OVLL 059
5A),PAT2A(6,8) *****
C OVLL 061
C ***** CARD DELETED ***** *****
C OVLL 063
C OVLL 064
C *****
IF(SHFLAG) WRITE(6,10000) *****
10000 FORMAT(44H AN ENTRY HAS BEEN MADE IN SUBROUTINE OVRALL) *****
STT0(1)=TTIN OVLL 065
SPT0(1)=PTIN OVLL 066
*****
RGO=0.0 OVLL 067
TAO=0.0 OVLL 068
PAO=0.0 OVLL 069
GAMC=0.0 OVLL 070
OUUPU=0.0 OVLL 071
OURUH=0.0 OVLL 072
ODELHT=0.0 OVLL 073
5 E1=GAMSL/(GAMSL-1.) OVLL 074
DO 17 K=1,KSTG *****
RGO=RGO+HVBAR(K) OVLL 075
IF (GAMF)1,1,2 OVLL 076
1 TAO=TAO+TAS(K) OVLL 077
PAO=PAO+PAS(K) OVLL 078
GO TO 3 OVLL 079
2 GAMO=GAMO+GAMS(K) OVLL 080
3 E2=GAM(1,K)/(GAM(1,K)-1.) OVLL 081
E3=GAM(5,K)/(GAM(5,K)-1.) OVLL 082
E4=GAMS(K)/(GAMS(K)-1.) OVLL 083
E5=1./E4 OVLL 084
DELHTS(K)=0.0 OVLL 085
DEHTIS(K)=0.0 OVLL 086
DEHSIS(K)=0.0 OVLL 087
DHATIS(K)=0.0 OVLL 088
DO 6 I=1,ISECT

```

Listing of Code (continued)

```

RW=GT2A(I,K)/GT2A(K)
DELHT(I,K)=DELHVN(I,K)*TFR(I,K)
DELHTI(I,K)=CPS(K)*TT0(I,K)*(1.-(PT2A(I,K)/PTP(I,K))*E5)
ETATT(I,K)=DELHT(I,K)/DELHTI(I,K)
DELHSI(I,K)=CPS(K)*TT0(I,K)*(1.-(PS2A(I,K)/PTP(I,K))*E5)
ETATS(I,K)=DELHT(I,K)/DELHSI(I,K)
PAT2A(I,K)=PS2A(I,K)*(1.+(GAM(5,K)-1.)*MF2A(I,K)*MF2A(I,K)
1/2.)*E3
DEHATI(I,K)=CPS(K)*TT0(I,K)*(1.-(PAT2A(I,K)/PTP(I,K))*E5)
ETATAT(I,K)=DELHT(I,K)/DEHATI(I,K)
DELHTS(K)=DELHTS(K)+R*DELHT(I,K)
DEHTIS(K)=DEHTIS(K)+R*DELHTI(I,K)
DEHSIS(K)=DEHSIS(K)+R*DELHSI(I,K)
DHATIS(K)=DHATIS(K)+R*DEHATI(I,K)
6 CONTINUE
13 SA0(K)=ALPHA0(IP,K)*57.2958
SIS(K)=SI(IP,K)*57.2958
SB1A(K)=HET1A(IP,K)*57.2958
SIR(K)=RI(IP,K)*57.2958
SA2(K)=ALF2A(IP,K)*57.2958
THCR(K)=GAM(1,K)*(GAMSL+1.)*RV(1,K)*STT0(K)/
1(GAMSL*(GAM(1,K)+1.)*SL*TSL)
EPSI(K)=GAMSL*(GAM(1,K)+1.)/2.)*E2/(GAM(1,K)*((GAMSL
1+1.)/2.)*E1)
DELT(K)=SPT0(K)/PSL
SETATT(K)=DELHTS(K)/DEHTIS(K)
SETATS(K)=DELHTS(K)/DEHSIS(K)
SETAAT(K)=DELHTS(K)/DHATIS(K)
C ***** CARD DELETED*****
SWRT(K)=WGT0(K)*SQRT(STT0(K))/SPT0(K)
SNRT(K)=HPM/SQRT(STT0(K))
SDHT(K)=DELHTS(K)/STT0(K)
SETHC(K)=DELHTS(K)/THCR(K)
RTHCH=SUMT(THCR(K))
SNRTHC(K)=HPM/RTHCH
SWRTED(K)=WGT0(K)*RTHCH*EPSI(K)/DELT(K)
SPTPT2(K)=SPT0(K)/PTBAR(K)
SPTPS2(K)=SPT0(K)/PS2(IP,K)
ST2TT0(K)=TTBAR(K)/STT0(K)
STRIT0(K)=TTR1A(IP,K)/STT0(K)
UPS(K)=.5*(U1A(IP,K)+U2(IP,K))
UPUPS(K)=UPS(K)*UPS(K)
OUPUP=OUPUP+UPUPS(K)
URS(K)=.5*(U1A(1,K)*DH(3,K)/DPIA(1,K)+U2(1,K)*UR(4,K)/DP2(1,K))
URURS(K)=URS(K)*URS(K)
OURUR=OURUR+URURS(K)
ODELHT=ODELHT+DELHTS(K)

```

OVLL 089  
 OVLL 090  
 OVLL 091  
 OVLL 092  
 OVLL 093  
 OVLL 094  
 OVLL 095  
 OVLL 096  
 OVLL 097  
 OVLL 098  
 OVLL 099  
 OVLL 100  
 OVLL 101  
 OVLL 102  
 OVLL 103  
 OVLL 104  
 OVLL 105  
 OVLL 106  
 OVLL 107  
 OVLL 108  
 \*\*\*\*\*  
 OVLL 109  
 OVLL 110  
 OVLL 111  
 OVLL 112  
 OVLL 113  
 OVLL 114  
 OVLL 115  
 \*\*\*\*\*  
 OVLL 117  
 OVLL 118  
 OVLL 119  
 OVLL 120  
 OVLL 121  
 OVLL 122  
 OVLL 123  
 OVLL 124  
 OVLL 125  
 OVLL 126  
 OVLL 127  
 OVLL 128  
 OVLL 129  
 OVLL 130  
 OVLL 131  
 OVLL 132  
 OVLL 133  
 OVLL 134

# Listing of Code (continued)

IF (DELHSL(IP,K))14,14,15	OVLL 135
14 VIS(K)=1.	OVLL 136
GO TO 16	OVLL 137
15 VIS(K)=SQRT(2.*G*AJ*DELHSL(IP,K))	OVLL 138
16 UPVIS(K)=UPS(K)/VIS(K)	OVLL 139
URVIS(K)=URS(K)/VIS(K)	OVLL 140
PSIPS(K)=G*AJ*DELHSL(K)/(2.*UPUPS(K))	OVLL 141
PSIRS(K)=G*AJ*DELHSL(K)/(2.*URURS(K))	OVLL 142
RXP(K)=1.-(1.-(PS1(IP,K)/PTP(IP,K))*E5)/(1.-(PS2(IP,K)/	OVLL 143
PTP(IP,K))*E5)	OVLL 144
VUIR=VUI(1,K)*DP1(1,K)/DR(2,K)	OVLL 145
VIR=SQRT(VUIR**2+VZ1(1,K)**2)	OVLL 146
PHIR=1./(1.-VIR**2/(2.*G*AJ*CP1(K)*TT0(1,K)*ETAS(1,K)))	OVLL 147
PTPSIR=PHIR**GAM(2,K)/(GAM(2,K)-1.)*PTP(1,K)/PT0(1,K)	OVLL 148
RXR(K)=1.-(1.-(1./PTPSIR))*E5)/(1.-(PS2(1,K)/PTP(1,K))*E5)	OVLL 149
DBETAR(K)=(HET1A(1,K)*BET2E(1,K))*57.2958	OVLL 150
MIS(K)=V1(IP,K)/SQRT(GAM(2,K)*G*RV(2,K)*TS1(IP,K))	*****
TS1R=TT0(1,K)-VIR**2/(2.*G*AJ*CP1(K))	OVLL 152
MIRS(K)=VIR/SQRT(GAM(2,K)*G*RV(2,K)*TS1R)	*****
VUIAR=VUIA(1,K)*DP1A(1,K)/DR(3,K)	OVLL 154
V1AR=SQRT(VUIAR**2+VZ1A(1,K)**2)	OVLL 155
TS1AR=TT0(1,K)-V1AR**2/(2.*G*AJ*CP1A(K))	OVLL 156
RU1AR=VUIAR-V1A(1,K)*CR(3,K)/DP1A(1,K)	OVLL 157
R1AR=SQRT(RU1AR**2+VZ1A(1,K)**2)	OVLL 158
MR1AR(K)=R1AR/SQRT(GAM(3,K)*G*RV(3,K)*TS1AR)	*****
VU2T=VU2(ISECT,K)*DP2(ISECT,K)/DT(4,K)	OVLL 160
V2T=SQRT(VU2T**2+VZ2(ISECT,K)**2)	OVLL 161
TS2T=TS2(ISECT,K)*(V2(ISECT,K)**2-V2T**2)/(2.*G*AJ*CP2(K))	OVLL 162
RU2T=VU2T+U2(ISECT,K)*DT(4,K)/DP2(ISECT,K)	OVLL 163
R2T=SQRT(RU2T**2+VZ2(ISECT,K)**2)	OVLL 164
MR2T(K)=R2T/SQRT(GAM(4,K)*G*RV(4,K)*TS2T)	*****
17 CONTINUE	OVLL 166
IF (GAMF)4,4,7	OVLL 167
4 TAO=TAO/STG	OVLL 168
PAO=PAO/STG	OVLL 169
CALL GAMMA(PAU,TAO,FAIR,WAIR,GAMO)	OVLL 170
GO TO 8	OVLL 171
7 GAMO=GAMO/STG	OVLL 172
8 EO=(GAMO-1.)/GAMO	OVLL 173
RG0=RG0/STG	*****
CPO=RG0/EO/AJ	*****
K=KSTG	OVLL 175
ODEHTI = 0.	OVLL 176
ODEHSI = 0.	OVLL 177
ODHATI = 0.	OVLL 178
DO 9 I=1,ISECT	OVLL 179
RW=G2A(I,K)/WGT2A(K)	OVLL 180



Listing of Code (continued)

```

ODEHTI = CP0*TT0(I,1)*(1.-(PT2A(I,K)/PTP(I,1))*EO)*RW*ODEHTI      OVLL 181
ODEHSI = CP0*TT0(I,1)*(1.-(PS2A(I,K)/PTP(I,1))*EO)*RW*ODEHSI      OVLL 182
9 ODHATI = CP0*TT0(I,1)*(1.-(PAT2A(I,K)/PTP(I,1))*EO)*RW*ODHATI    OVLL 183
OPSIP=G*AJ*ODELHT/(2.*OUPUP)                                       OVLL 184
OPSIH=G*AJ*ODELHT/(2.*OURUR)                                       OVLL 185
OWRTP=SWRTP(1)                                                      OVLL 186
OWNED=SWRTED(1)*SNRTHC(1)/60.                                       OVLL 187
ONRTHC=SNRTHC(1)                                                    OVLL 188
ONRT=SNRT(1)                                                         OVLL 189
ODHT=ODELHT/TTIN                                                    OVLL 190
OPT0T2=PTIN/PTAR(KSTG)                                              OVLL 191
OPT0S2=PTIN/PS2(IP,KSIG)                                           OVLL 192
OPTAT2=PTIN/PAT2A(IP,KSTG)                                         OVLL 193
OETATI=ODELHT/ODEHTI                                               OVLL 194
OETATS=ODELHT/ODEHSI                                               OVLL 195
OETAAT=ODELHT/ODHATI                                               OVLL 196
OETHC=ODELHT/THCH(1)                                               OVLL 197
C                                                                    OVLL 198
C          PRINT OUT FOR STAGE PERFORMANCE                          OVLL 199
I=1                                                                    OVLL 200
WRITE(6,1000)NAME,TITLE,ICASE,ISCASE                                OVLL 201
1000 FORMAT(1H1,21X,29MNASA TURBINE COMPUTER PROGRAM /6X,10A6/    OVLL 202
1 6X,10A6/ 30X,6HCASE 13.1H,.13/28X,1/HSTAGE PERFORMANCE /19X    *****
27HSTAGE 1,6X,7HSTAGE 2,6X,7HSTAGE 3,6X,7HSTAGE 4/ )             OVLL 204
IF (KSTG-4)19,19,18                                                OVLL 205
18 KS=4                                                              OVLL 206
GO TO 20                                                            OVLL 207
19 KS=KSTG                                                           OVLL 208
20 WRITE(6,1001)(ST10(K),K=1,KS)                                    OVLL 209
1001 FORMAT(2X,12H      T10AH 02X,F10.1,3X,F10.1,3X,F10.1,3X,F10.1) *****
WRITE(6,1002)(SPT0(K),K=1,KS)                                       OVLL 211
1002 FORMAT(2X,12H      PT0AH 02X,F10.3,3X,F10.3,3X,F10.3,3X,F10.3) *****
WRITE(6,1003)(WGT0(K),K=1,KS)                                       *****
1003 FORMAT(2X,12H      WGT 02X,F10.3,3X,F10.3,3X,F10.3,3X,F10.3) *****
WRITE(6,1004)(DELHTS(K),K=1,KS)                                       OVLL 215
1004 FORMAT(2X,12H      DEL H2X,F10.3,3X,F10.3,3X,F10.3,3X,F10.3) *****
WRITE(6,1005)(SWRTP(K),K=1,KS)                                       OVLL 217
1005 FORMAT(2X,12H      WRT/P2X,F10.3,3X,F10.3,3X,F10.3,3X,F10.3) *****
WRITE(6,1006)(SDHT(K),K=1,KS)                                       OVLL 219
1006 FORMAT(2X,12H      DH/TTEAH02X,F10.5,3X,F10.5,3X,F10.5,3X,F10.5) *****
WRITE(6,1007)(SNRT(K),K=1,KS)                                       OVLL 221
1007 FORMAT(2X,12H      N/RT2X,F10.3,3X,F10.3,3X,F10.3,3X,F10.3) *****
WRITE(6,1008)(SETATT(K),K=1,KS)                                       OVLL 223
1008 FORMAT(2X,12H      ETA TT2X,F10.5,3X,F10.5,3X,F10.5,3X,F10.5) *****
WRITE(6,1009)(SETATS(K),K=1,KS)                                       OVLL 225
1009 FORMAT(2X,12H      ETA TS2X,F10.5,3X,F10.5,3X,F10.5,3X,F10.5) *****
WRITE(6,1010)(SETAAT(K),K=1,KS)                                       OVLL 227

```

Listing of Code (continued)

```

1010 FORMAT(2X,12H      F1A AT2X,F10.5,3X,F10.5,3X,F10.5,3X,F10.5)      *****
      WRITE(6,1011) (PT0PS1(IP,K),K=I,KS)      OVLL 229
1011 FORMAT(2X,12H      PT0/PS12X,F10.3,3X,F10.3,3X,F10.3,3X,F10.3)      *****
      WRITE(6,1012) (SPTPT2(K),K=I,KS)      OVLL 231
1012 FORMAT(1X,13HPTBAR0/PTBAR2,2X,F10.3,3X,F10.3,3X,F10.3,3X,F10.3)      *****
      WRITE(6,1013) (SPTPS2(K),K=I,KS)      OVLL 233
1013 FORMAT(2X,12H      PTBAR0/PS22X,F10.3,3X,F10.3,3X,F10.3,3X,F10.3)      *****
      WRITE(6,1014) (PTRS2(JF,K),K=I,KS)      OVLL 235
1014 FORMAT(2X,12H      PTW2/PS22X,F10.3,3X,F10.3,3X,F10.3,3X,F10.3)      *****
      WRITE(6,1015) (ST2TT0(K),K=I,KS)      OVLL 237
1015 FORMAT(1X,13HTTHAR2/TTHAR02X,F10.5,3X,F10.5,3X,F10.5,3X,F10.5)      *****
      WRITE(6,1016) (STRTT0(K),K=I,KS)      OVLL 239
1016 FORMAT(2X,12HTTH14/TTHAW02X,F10.5,3X,F10.5,3X,F10.5,3X,F10.5)      *****
      WRITE(6,2003) (WGT1(K),K=I,KS)      *****
2003 FORMAT(2X,12H      WG 12X,F10.3,3X,F10.3,3X,F10.3,3X,F10.3)      *****
      WRITE(6,1017) (PS1A(IP,K),K=I,KS)      *****
1017 FORMAT(2X,12H      PS 1A2X,F10.3,3X,F10.3,3X,F10.3,3X,F10.3)      *****
      WRITE(6,1018) (TTR1A(IP,K),K=I,KS)      OVLL 243
1018 FORMAT(2X,12H      TTH 1A2X,F10.1,3X,F10.1,3X,F10.1,3X,F10.1)      *****
      WRITE(6,1019) (PTR1A(IP,K),K=I,KS)      OVLL 245
1019 FORMAT(2X,12H      PTH 1A2X,F10.3,3X,F10.3,3X,F10.3,3X,F10.3)      *****
      WRITE(6,3003) (WGT1A(K),K=I,KS)      *****
3003 FORMAT(2X,12H      WG 1A2X,F10.3,3X,F10.3,3X,F10.3,3X,F10.3)      *****
      WRITE(6,1020) (PS2(IP,K),K=I,KS)      OVLL 247
1020 FORMAT(2X,12H      PS 22X,F10.3,3X,F10.3,3X,F10.3,3X,F10.3)      *****
      WRITE(6,1021) (TTHAR(K),K=I,KS)      OVLL 249
1021 FORMAT(2X,12H      TTBAW 22X,F10.1,3X,F10.1,3X,F10.1,3X,F10.1)      *****
      WRITE(6,1022) (PTBAR(K),K=I,KS)      OVLL 251
1022 FORMAT(2X,12H      PTHAR 22X,F10.3,3X,F10.3,3X,F10.3,3X,F10.3)      *****
      WRITE(6,4003) (WGT2(K),K=I,KS)      *****
4003 FORMAT(2X,12H      WG 22X,F10.3,3X,F10.3,3X,F10.3,3X,F10.3)      *****
      WRITE(6,5003) (WGT2A(K),K=I,KS)      *****
5003 FORMAT(2X,12H      WG 2A2X,F10.3,3X,F10.3,3X,F10.3,3X,F10.3)      *****
      WRITE(6,1023) (UPVIS(K),K=I,KS)      OVLL 253
1023 FORMAT(2X,12H      UP/V12X,F10.5,3X,F10.5,3X,F10.5,3X,F10.5)      *****
      WRITE(6,1024) (URVIS(K),K=I,KS)      OVLL 255
1024 FORMAT(2X,12H      UH/V12X,F10.5,3X,F10.5,3X,F10.5,3X,F10.5)      *****
      WRITE(6,1025) (PSIPS(K),K=I,KS)      OVLL 257
1025 FORMAT(2X,12H      PSI P2X,F10.5,3X,F10.5,3X,F10.5,3X,F10.5)      *****
      WRITE(6,1026) (PSIRS(K),K=I,KS)      OVLL 259
1026 FORMAT(2X,12H      PSI R2X,F10.5,3X,F10.5,3X,F10.5,3X,F10.5)      *****
      WRITE(6,1027) (RXP(K),K=I,KS)      OVLL 261
1027 FORMAT(2X,12H      RX P2X,F10.5,3X,F10.5,3X,F10.5,3X,F10.5)      *****
      WRITE(6,1028) (RXR(K),K=I,KS)      OVLL 263
1028 FORMAT(2X,12H      RX R2X,F10.5,3X,F10.5,3X,F10.5,3X,F10.5)      *****
      WRITE(6,1029) (SA0(K),K=I,KS)      OVLL 265
1029 FORMAT(2X,12H      ALPHA 02X,F10.3,3X,F10.3,3X,F10.3,3X,F10.3)      *****

```

Listing of Code (continued)

```

WRITE(6,1030) (SIS(K),K=1,KS)
1030 FORMAT(2X,12H      I STATOR2X,F10.3,3X,F10.3,3X,F10.3,3X,F10.3)
WRITE(6,1031) (SH1A(K),K=1,KS)
1031 FORMAT(2X,12H      BETA 1A2X,F10.3,3X,F10.3,3X,F10.3,3X,F10.3)
WRITE(6,1032) (SIR(K),K=1,KS)
1032 FORMAT(2X,12H      I RCTOR2X,F10.3,3X,F10.3,3X,F10.3,3X,F10.3)
WRITE(6,1033) (SA2(K),K=1,KS)
1033 FORMAT(2X,12H      ALPHA 2A2X,F10.3,3X,F10.3,3X,F10.3,3X,F10.3)
WRITE(6,1034) (DBETAR(K),K=1,KS)
1034 FORMAT(2X,12H      DHEIA R2X,F10.3,3X,F10.3,3X,F10.3,3X,F10.3)
WRITE(6,1035) (MIS(K),K=1,KS)
1035 FORMAT(2X,12H      M 12X,F10.5,3X,F10.5,3X,F10.5,3X,F10.5)
WRITE(6,1036) (MIRS(K),K=1,KS)
1036 FORMAT(2X,12H      M1 RT2X,F10.5,3X,F10.5,3X,F10.5,3X,F10.5)
WRITE(6,1037) (MR1A(IP,K),K=1,KS)
1037 FORMAT(2X,12H      M1 1A2X,F10.5,3X,F10.5,3X,F10.5,3X,F10.5)
WRITE(6,1038) (MR1AR(K),K=1,KS)
1038 FORMAT(2X,12H      MR1A RT2X,F10.5,3X,F10.5,3X,F10.5,3X,F10.5)
WRITE(6,1039) (MR2(IP,K),K=1,KS)
1039 FORMAT(2X,12H      M2 22X,F10.5,3X,F10.5,3X,F10.5,3X,F10.5)
WRITE(6,1040) (MR2T(K),K=1,KS)
1040 FORMAT(2X,12H      MR2 TIP2X,F10.5,3X,F10.5,3X,F10.5,3X,F10.5)
WRITE(6,1041) (SETHC(K),K=1,KS)
1041 FORMAT(2X,12H      E/TH CR2X,F10.3,3X,F10.3,3X,F10.3,3X,F10.3)
WRITE(6,1042) (SNRTHC(K),K=1,KS)
1042 FORMAT(2X,12H      N/RT CR2X,F10.1,3X,F10.1,3X,F10.1,3X,F10.1)
WRITE(6,1043) (SWRTED(K),K=1,KS)
1043 FORMAT(2X,12H      WRTHCHE/D2X,F10.3,3X,F10.3,3X,F10.3,3X,F10.3)
IF (KSTG=KS) 22,22,21
21 WRITE(6,1045) NAME, TITLE, I CASE, I SCASE
1045 FORMAT(1H1,21X,29H NASA TURBINE COMPUTER PROGRAM /6X,10A6/
1 6X,10A6/ 30X,6HCASE 13,1H,,13/28X,17HSTAGE PERFORMANCE /19X
27HSTAGE 5,6X,7HSTAGE 6,6X,7HSTAGE 7,6X,7HSTAGE 8/ )
I=5
KS=KSTG
GO TO 20
22 WRITE(6,1044) OPSIP, OPSIH, ODELHT, OWRTIP, CNRT, ODHT, OPTOT2,
10PT0S2, OPTAT2, OETATT, CETATS, OETAAT, OWNED, ONRTHC, OETHC
1044 FORMAT(//31X,19H OVERALL PERFORMANCE/7X,9HPSI P
1F10.5, 5X,10HPSI R F10.5, 5X,9HDEL F F10.5/7X,9HWRT/P
2F10.5, 5X,10HN/RT F10.5, 5X,9HDELH/TTINF10.5/7X,10HPT0/PTBAR2
3F9.5, 5X,10HPT0/PS2 F10.5, 5X,9HPT0/PAT2AF10.5/7X,9HETA TT
4F10.5, 5X,10HETA TS F10.5, 5X,9HETA TAT F10.5/7X,9HWNE/60D
5F10.3, 5X,10HN/RTM CR F10.3, 5X,9HE/TH CR F10.5/)
IF (SRFLAG) WRITE(6,20000)
20000 FORMAT(1H1,45H AN EXIT HAS BEEN MADE FROM SUBROUTINE OVRALL)
RETURN

```

```

OVLL 267
*****
OVLL 269
*****
OVLL 271
*****
OVLL 273
*****
OVLL 275
*****
OVLL 277
*****
OVLL 279
*****
OVLL 281
*****
OVLL 283
*****
OVLL 285
*****
OVLL 287
*****
OVLL 289
*****
OVLL 291
*****
OVLL 293
*****
OVLL 295
*****
OVLL 296
*****
OVLL 297
*****
OVLL 299
*****
OVLL 300
*****
OVLL 301
*****
OVLL 302
*****
OVLL 303
*****
OVLL 304
*****
*****
*****
*****
*****
*****
*****
*****
*****
OVLL 311

```

Listing of Code (continued)

END

OVLL 312

# Listing of Code (continued)

```

SUBROUTINE DIAGT(M)
CDIAGT
C
REAL MFSTOP
LOGICAL PREVER,SRFLAG
COMMON SRFLAG
COMMON /SNTCP/G,AJ,PRFC,ICASE,PREVER,MFSTOP,JUMP,LOPIN,ISCASE,
1KN,GAMF,IP,SCHIT,PTHR,ISECT,KSTG,WIOL,MMOTOL,PRYOL,TRLOOP,LSTG,
2LHHC,IHHC,ICHUKE,ISORH,CHUKE,PTOPSL(6,B),PTHS2(6,B),TRDIAG,SC,WC,
3DELPH,PASS,IPC,LUPC,ISS
C
COMMON /SINIT/H1(6,B),H2(6,B),DPN(6,B),UP1(6,B),DP1A(6,B),DP2(6,B),
1,DP2A(6,B),CSALF1(6,B),ALF1(6,B),CSHET2(6,B),BET2(6,B),RADSD(6,B),
2RADHD(6,B),ANN1(6,B),ANN2(6,B),ANN2A(6,B),ANN1A(6,B),U1A(6,B),
3U2(6,B),ANNO(6,B),PT0(6,B),TT0(6,B),ALPHA0(6,B),PTP(6,B)
C
COMMON /SINPUT/ HSL,TSL,PSL,GAMSI,
1PTPS,PTIN,TTIN,WAIR,FAIR,DELC,DELL,DELA,AACS,VCTD,STG,SECT,EXPN,
2EXPP,EXPE, WPM,PAF,SLT,STGCH,FNDJUH,NAME(10),TITLE(10),PCNH(6),
3RV(6,B),GAM(6,B),DR(6,B),UT(6,B),RWG(6,B),ALPHAS(6,B),ALPHA1(6,B),
4ETARS(6,B),FTAS(6,B),CFS(6,B),ANNO(6,B),BETA1(6,B),BETA2(6,B),ETARDIGT
5R(6,B),ETAR(6,B),CFR(6,B),TFR(6,B),ANDUH(6,B),OMEGAS(6,B),AS0(6,B),
6,ASVP0(6,B),ACMNO(6,B),A1(6,B),A2(6,B),A3(6,B),A4(6,B),A5(6,B),A6(
76,B),OMEGAR(6,B),BSIA(6,B),HSMP1A(6,B),HCMN1A(6,B),R1(6,B),B2(6,B),
8,R3(6,B),R4(6,B),R5(6,B),R6(6,B),SESTHI(8),HERTHI(8)
C
REAL MN
COMMON /SSTA01/CP0(8),
1R),VU0(6,B),VZ0(6,B),MHOS0(6,B),PS1(6,B),WGT1(8),TA1(8),WG1(6,B),
2
3,RHOS1(6,B),ALF1E(6,B),VU1(6,B),VZ1(6,B),M0(6,B),WGT0(8),WG0(6,B)
C
REAL MR1A
COMMON /SSTA1A/VU1A(6,B),WG1A(6,B),WGT1A(8),VZ1A(6,B),
1PS1A(6,B),RU1A(6,B),R1A(6,B),HET1A(6,B),RI(6,B),TTN1A(6,B),PTR1A(
2,B),MR1A(6,B),TS1A(6,B)
C
COMMON /SSTA2/VZ2(6,B),TTR2(6,B),PTR2(6,B),WG2(6,B),WGT2(8),TA2(8),
1
PS2(6,B),PHI2(6,B)
C
REAL MR2,M2,MF2
COMMON /SFLW2/TS2(6,B),CP2(8),R2(6,B),MHOS2(6,B),BET2E(6,B),RU2(
1,B),VU2(6,B),UPUH2(6,B),VZ2(6,B),MR2(6,B),MF2(6,B),M2(6,B)
C
REAL M2A,MF2A
COMMON /SSTA2A/WG2A(6,B),WGT2A(8),VU2A(6,B),VZ2A(6,B),PS2A(6,B),

```

Listing of Code (continued)

```

1ALF2A(6,8),TT2A(6,8),PT2A(6,8),TTBAR(A),PTBAR(8),STT0(8),SPT0(8), DIGT 046
2M2A(6,8),MF2A(6,8),CP2A(8),V2A(6,8),TS2A(6,8),TAS(8),PAS(8),GAMS(8)DIGT 047
3),CPS(8),DELMVD(6,8),HVBAR(A) *****
C DIGT 049
IF(SHFLAG) WRITE(6,10000) *****
10000 FORMAT(44H AN ENTRY HAS BEEN MADE IN SUBROUTINE DIAGT ) *****
WRITE(6,1000)NAME,TITLE DIGT 050
1000 FORMAT(1H1,5X,10A6/6X,10A6/20X,20HNASA TURBINE COMPUTER PROGRAM/ DIGT 051
131X,10HDIAGNOSTIC) DIGT 052
IF (M.EQ.0) GO TO 10 DIGT 053
GO TO (10,19,11,12,13),M DIGT 054
10 DO 14 K=1,KN DIGT 055
WRITE(6,1001)K,CP0(K),GAM(1,K) DIGT 056
1001 FORMAT(9X,1HK,15,9X,3F10.3,9X,5HGAMMA,F10.5) DIGT 057
WRITE(6,1002) (PTP(I,K),I=1,ISECT) DIGT 058
1002 FORMAT(3X,6H PTP,6F10.3) DIGT 059
WRITE(6,1003) (PT0(I,K),I=1,ISECT) DIGT 060
1003 FORMAT(3X,6H PT0,6F10.3) DIGT 061
WRITE(6,1004) (PS0(I,K),I=1,ISECT) DIGT 062
1004 FORMAT(3X,6H PS0,6F10.3) DIGT 063
WRITE(6,1005) (TT0(I,K),I=1,ISECT) DIGT 064
1005 FORMAT(3X,6H TT0,6F10.1) DIGT 065
WRITE(6,1006) (TS0(I,K),I=1,ISECT) DIGT 066
1006 FORMAT(3X,6H TS0,6F10.1) DIGT 067
WRITE(6,1007) (V0(I,K),I=1,ISECT) DIGT 068
1007 FORMAT(3X,6H V0,6F10.3) DIGT 069
WRITE(6,1008) (ALPHA0(I,K),I=1,ISECT) DIGT 070
1008 FORMAT(3X,6H ALPHA0,6F10.3) DIGT 071
14 WRITE(6,1009) (SI(I,K),I=1,ISECT) DIGT 072
IF (M.EQ.0) GO TO 19 DIGT 073
GO TO 14 DIGT 074
19 DO 20 K=1,KN DIGT 075
1009 FORMAT(3X,6H SI,6F10.3) DIGT 076
WRITE(6,1010) K,CP1(K),GAM(2,K) DIGT 077
1010 FORMAT(9X,1HK,15,9X,3F10.3,9X,5HGAMMA,F10.5) DIGT 078
WRITE(6,1011) (PS1(I,K),I=1,ISECT) DIGT 079
1011 FORMAT(3X,6H PS1,6F10.3) DIGT 080
WRITE(6,1012) (OPDH1(I,K),I=1,ISECT) DIGT 081
1012 FORMAT(3X,6H OPDH1,6F10.5) DIGT 082
WRITE(6,1013) (TS1(I,K),I=1,ISECT) DIGT 083
1013 FORMAT(3X,6H TS1,6F10.1) DIGT 084
WRITE(6,1014) (WGL(I,K),I=1,ISECT) DIGT 085
1014 FORMAT(3X,6H WGL,6F10.3) DIGT 086
WRITE(6,1015) (V1(I,K),I=1,ISECT) DIGT 087
1015 FORMAT(3X,6H V1,6F10.3) DIGT 088
WRITE(6,1016) (ALF1E(I,K),I=1,ISECT) DIGT 089
1016 FORMAT(3X,6H ALF1E,6F10.3) DIGT 090

```

# Listing of Code (continued)

20	WRITE(6,1017) (ALF1(I,K),I=1,ISECT)	DIGT 091
1017	FORMAT(3X,6H ALF1,6F10.3)	DIGT 092
	IF (M.EQ.0) GO TO 11	DIGT 093
	GO TO 1H	DIGT 094
11	DO 15 K=1,KN	DIGT 095
	WRITE(6,1018) K,CP1A(K),GAM(3,K)	DIGT 096
1018	FORMAT(9X,1HK,15,9X,4F10.3,8X,5HGAMMA,F10.5)	DIGT 097
	WRITE(6,1019) (PTH1A(I,K),I=1,ISECT)	DIGT 098
1019	FORMAT(3X,6H PTH1A,6F10.3)	DIGT 099
	WRITE(6,1020) (PS1A(I,K),I=1,ISECT)	DIGT 100
1020	FORMAT(3X,6H PS1A,6F10.3)	DIGT 101
	WRITE(6,1021) (TTR1A(I,K),I=1,ISECT)	DIGT 102
1021	FORMAT(3X,6H TTR1A,6F10.1)	DIGT 103
	WRITE(6,1022) (WG1A(I,K),I=1,ISECT)	DIGT 104
1022	FORMAT(3X,6H WG1A,6F10.3)	DIGT 105
	WRITE(6,1023) (H1A(I,K),I=1,ISECT)	DIGT 106
1023	FORMAT(3X,6H H1A,6F10.3)	DIGT 107
	WRITE(6,1024) (HET1A(I,K),I=1,ISECT)	DIGT 108
1024	FORMAT(3X,6H HET1A,6F10.3)	DIGT 109
15	WRITE(6,1025) (R1(I,K),I=1,ISECT)	DIGT 110
1025	FORMAT(3X,6H R1,6F10.3)	DIGT 111
	IF (M.EQ.0) GO TO 12	DIGT 112
	GO TO 1H	DIGT 113
12	DO 16 K=1,KN	DIGT 114
	WRITE(6,1026) K,CP2(K),GAM(3,K)	DIGT 115
1026	FORMAT(9X,1HK,15,9X,3F10.3,9X,5HGAMMA,F10.5)	DIGT 116
	WRITE(6,1027) (PTH2(I,K),I=1,ISECT)	DIGT 117
1027	FORMAT(3X,6H PTH2,6F10.3)	DIGT 118
	WRITE(6,1028) (PS2(I,K),I=1,ISECT)	DIGT 119
1028	FORMAT(3X,6H PS2,6F10.3)	DIGT 120
	WRITE(6,1029) (DPDR2(I,K),I=1,ISECT)	DIGT 121
1029	FORMAT(3X,6H DPDR2,6F10.5)	DIGT 122
	WRITE(6,1030) (TTR2(I,K),I=1,ISECT)	DIGT 123
1030	FORMAT(3X,6H TTR2,6F10.1)	DIGT 124
	WRITE(6,1031) (TS2(I,K),I=1,ISECT)	DIGT 125
1031	FORMAT(3X,6H TS2,6F10.1)	DIGT 126
	WRITE(6,1032) (WG2(I,K),I=1,ISECT)	DIGT 127
1032	FORMAT(3X,6H WG2,6F10.3)	DIGT 128
	WRITE(6,1033) (H2(I,K),I=1,ISECT)	DIGT 129
1033	FORMAT(3X,6H H2,6F10.3)	DIGT 130
	WRITE(6,1034) (HET2E(I,K),I=1,ISECT)	DIGT 131
1034	FORMAT(3X,6H HET2E,6F10.3)	DIGT 132
16	WRITE(6,1035) (HET2(I,K),I=1,ISECT)	DIGT 133
1035	FORMAT(3X,6H HET2,6F10.3)	DIGT 134
	IF (M.EQ.0) GO TO 13	DIGT 135
	GO TO 1H	DIGT 136
13	DO 17 K=1,KN	DIGT 137

Listing of Code (continued)

L=K+1	DIGT 138
WRITE(6,1036) K, CP2A(K), GAM(5,K)	DIGT 139
1036 FORMAT(9X,1HK,15,9X,4F,CP2A,F10.3,9X,5HGAMMA,F10.5)	DIGT 140
WRITE(6,1037) (PT2A(I,K),I=1,ISECT)	DIGT 141
1037 FORMAT(3X,6H PT2A,6F10.3)	DIGT 142
WRITE(6,1038) (PS2A(I,K),I=1,ISECT)	DIGT 143
1038 FORMAT(3X,6H PS2A,6F10.3)	DIGT 144
WRITE(6,1039) (TT2A(I,K),I=1,ISECT)	DIGT 145
1039 FORMAT(3X,6H TT2A,6F10.1)	DIGT 146
WRITE(6,1040) (TS2A(I,K),I=1,ISECT)	DIGT 147
1040 FORMAT(3X,6H TS2A,6F10.1)	DIGT 148
WRITE(6,1041) (WG2A(I,K),I=1,ISECT)	DIGT 149
1041 FORMAT(3X,6H WG2A,6F10.3)	DIGT 150
WRITE(6,1042) (V2A(I,K),I=1,ISECT)	DIGT 151
1042 FORMAT(3X,6H V2A,6F10.3)	DIGT 152
WRITE(6,1043) (ALF2A(I,K),I=1,ISECT)	DIGT 153
1043 FORMAT(3X,6H ALF2A,6F10.3)	DIGT 154
WRITE(6,1044) (SI(I,K),I=1,ISECT)	DIGT 155
1044 FORMAT(3X,6H SI,6F10.3)	DIGT 156
WRITE(6,1045) L,CPS(K),GAMS(K)	DIGT 157
1045 FORMAT(9X,1HL,15,9X,3F,CPS,F10.3,9X,5HGAMMA,F10.5)	DIGT 158
WRITE(6,1046) (PTP(I,L),I=1,ISECT)	DIGT 159
1046 FORMAT(3X,6H PTP,6F10.3)	DIGT 160
WRITE(6,1047) (PT0(I,L),I=1,ISECT)	DIGT 161
1047 FORMAT(3X,6H PT0,6F10.3)	DIGT 162
17 WRITE(6,1048) (TT0(I,L),I=1,ISECT)	DIGT 163
1048 FORMAT(3X,6H TT0,6F10.1)	DIGT 164
18 CONTINUE	DIGT 165
IF(SRFLAG) WRITE(6,20000)	*****
20000 FORMAT(1H1,45H AN EXIT HAS BEEN MADE FROM SUBROUTINE DIAGT )	*****
RETURN	DIGT 166
END	DIGT 167



# Listing of Code (continued)

```

SUBROUTINE INSTG
CINSTG
C INTERSTAGE OUTPUT
C NUMBER OF SECTORS IS THREE OR LESS,HUB AND CASING VALUES ARE
C CALCULATED AND PRINTED
C NUMBER OF SECTORS IS MORE THAN THREE,ONLY SECTOR PITCHLINE
C VALUES ARE PRINTED
C
REAL MFSTOP
LOGICAL PREVER,SHFLAG
COMMON SRFLAG
COMMON /SNTCP/G,AJ,PRPC,ICASE,PREVER,MFSTOP,JUMP,LOPIN,ISCASE,
1KN,GAMF,IP,SCRIT,PTRN,ISECT,KSTG,WOTOL,RHOTOL,PTOL,TRLOOP,LSTG,
2LBRC,IBRC,ICHOKE,ISORH,CHOKE,PTOP1(6,8),PTRS2(6,8),TRDIAG,SC,RC,
3DELPR,PASS,IPC,LOPC,ISS
C
COMMON /SINIT/H1(6,8),H2(6,8),DP0(6,8),DP1(6,8),DP1A(6,8),DP2(6,8),
1,DP2A(6,8),CSALF1(6,8),ALF1(6,8),CSHET2(6,8),BET2(6,8),RADSD(6,8),
2RADRD(6,8),ANN1(6,8),ANN2(6,8),ANN2A(6,8),ANN1A(6,8),U1A(6,8),
3U2(6,8),ANNO(6,8),PT0(6,8),TT0(6,8),ALPHA0(6,8),PTP(6,8)
C
COMMON /SINPUT/ RSL,TSL,PSL,GAMSI,
1PTPS,PTIN,TTIN,WAIR,FAIR,DELC,DELL,DELA,AACS,VCTD,STG,SECT,EXPN,
2EXPP,EXPRE, RPM,PAF,SLI,STGCH,FNDJOR,NAME(10),TITLE(10),PCNH(6),
3RV(6,8),GAM(6,8),DR(6,8),DT(6,8),RWG(6,8),ALPHAS(6,8),ALPHA1(6,8),
4ETARS(6,8),ETAS(6,8),CFS(6,8),ANNO(6,8),BETA1(6,8),BETA2(6,8),ETARINST
5R(6,8),ETAR(6,8),CFR(6,8),TFR(6,8),ANDOR(6,8),OMEGAS(6,8),AS0(6,8)
6,ASMP0(6,8),ACMN0(6,8),A1(6,8),A2(6,8),A3(6,8),A4(6,8),A5(6,8),A6(
7,OMEGAR(6,8),BSIA(6,8),BSMPIA(6,8),BSMNIA(6,8),B1(6,8),B2(6,8)
8,B3(6,8),B4(6,8),B5(6,8),B6(6,8),SESTHI(8),RERTHI(8)
C
REAL M0
COMMON /SSTA01/CP0(8),
18),VU0(6,8),VZ0(6,8),RHOS0(6,8),PS1(6,8),WGT1(8),TA1(8),WG1(6,8),
2DPDH1(6,8),SI(6,8), CP1(8),PHI1(6,8),TS1(6,8),V1(6,8)
3,RHOS1(6,8),ALF1E(6,8),VU1(6,8),VZ1(6,8),M0(6,8),WGT0(8),WG0(6,8)
C
REAL MR1A
COMMON /SSTA1A/VU1A(6,8),WG1A(6,8),WGT1A(8),VZ1A(6,8),
1PS1A(6,8),RU1A(6,8),R1A(6,8),RET1A(6,8),R1(6,8),TTR1A(6,8),PTR1A(6
2,8),MR1A(6,8),TS1A(6,8)
C
COMMON /SSTA2/V2(6,8),TTR2(6,8),PTR2(6,8),WG2(6,8),WGT2(8),TA2(8),
1PS2(6,8),PHI2(6,8)
C
REAL MR2,M2 ,MF2

```

```

INST 001
INST 002
INST 003
INST 004
INST 005
INST 006
INST 007
INST 008
INST 009
*****
*****
INST 011
INST 012
INST 013
INST 014
INST 015
INST 016
INST 017
INST 018
INST 019
INST 020
*****
INST 022
*****
INST 025
INST 026
INST 027
INST 028
INST 029
INST 030
INST 031
INST 032
INST 033
INST 034
*****
INST 036
INST 037
INST 038
INST 039
*****
INST 041
INST 042
INST 043
INST 044
INST 045

```

Listing of Code (continued)

```

COMMON /SFL0W2/TS2(6,8),CP2(8),R2(6,8),RHOS2(6,8),BET2E(6,8),RU2(6,8) INST 046
1,8),VU2(6,8),DPDR2(6,8),VZ2(6,8),MR2(6,8),MF2(6,8),M2(6,8) INST 047
C REAL M2A,MF2A INST 048
COMMON /SSTA2A/WG2A(6,8),WGT2A(8),VU2A(6,8),VZ2A(6,8),PS2A(6,8), INST 049
1ALF2A(6,8),TT2A(6,8),PT2A(6,8),TTBAR(8),PTBAR(8),STT0(8),SPT0(8), INST 050
2M2A(6,8),MF2A(6,8),CP2A(8),V2A(6,8),TS2A(6,8),TAS(8),PAS(8),GAMS(8) INST 051
3),CP0(8),DELHVD(6,8),HVBAR(8) ***** INST 052
C COMMON /SOVRAL/DELHT(6,8),DELHTI(6,8),DELHSI(6,8),DEHATI(6,8), INST 053
1ETATT(6,8),ETATS(6,8),ETATAT(6,8) INST 054
C COMMON STDP0(7),STFT0(7),STALF(7),STSI(7),STV0(7),STVU0(7), INST 055
1STVZ0(7),STTS0(7),STPS0(7),STDEN0(7),STM0(7),STDP1(7),STALFE(7), INST 056
2STDELA(7),STV1(7),STVU1(7),STVZ1(7),STTS1(7),STPS1(7),STDEN1(7), INST 057
3STM1(7),ZWIIINC(7), CPS(7),STDP1A(7), INST 058
4STPTR1(7),STBET1(7),STRI(7),STRIA(7),STHUA(7),STMR1A(7),STU1A(7), INST 059
5STDP2(7),STHET2(7),SOBETA(7),SR2(7),SRU2(7),SMR2(7),SU2(7),RX(7), INST 060
6STDELH(7),STPSI(7),SETATT(7),SETATS(7),SETAAT(7),RZWINC(7), INST 061
7 CFR(7),STPT2A(7),STTT2A(7),STV2A(7),STVU2A(7), ***** INST 062
8STALF2(7),STMF2A(7),STTTR1(7),STVZ2A(7),STTS2A(7),STPS2A(7),STDEN2 ***** INST 063
9(7),STM2A(7),STTT0(7),LJ,JJ,K,STWG0(7),STWG1(7),STWG1A(7),STWG2(7) ***** INST 064
9,STWG2A(7),SFL00,SFL01,SFL01A,SFL02,SFL02A,STPS1A(7),STTS1A(7), ***** INST 065
9STPTR2(7),STTTR2(7),STPS2(7),STTS2(7) ***** INST 066
C IF(SHFLAG) WRITE(6,10000) ***** INST 067
10000 FORMAT(44H AN ENTRY HAS BEEN MADE IN SUBROUTINE INSTG ) ***** INST 068
C 1 DO 9 K=1,KSTG ***** INST 069
SFL00 =0.0 ***** INST 070
SFL01 =0.0 ***** INST 071
SFL01A=0.0 ***** INST 072
SFL02 =0.0 ***** INST 073
SFL02A=0.0 ***** INST 074
E1=(GAMS(K)-1.)/GAMS(K) INST 075
E2=GAM(1,K)/(GAM(1,K)-1.) INST 076
E3=GAM(2,K)/(GAM(2,K)-1.) INST 077
E4=GAM(3,K)/(GAM(3,K)-1.) INST 078
E5=GAM(4,K)/(GAM(4,K)-1.) INST 079
E6=GAM(5,K)/(GAM(5,K)-1.) INST 080
C RELOCATE PITCHLINE VALUES INST 081
J=ISECT+1 INST 082
4 DO 5 I=1,ISECT INST 083
KS=J-I+1 INST 084
STWG0(KS)=WG0(KS-1,K) ***** INST 085
SFL00 =SFL00 +STWG0(KS) ***** INST 086
STTT0(KS)=TTT(KS-1,K) INST 087

```

# Listing of Code (continued)

STDP0(KS)=PP0(KS-1,K)	INST 042
STPT0(KS)=PTP(KS-1,K)	INST 043
STALF(KS)=ALPHA0(KS-1,K)*57.2958	INST 044
STSI(KS)=SI(KS-1,K)*57.2958	INST 045
STV0(KS)=V0(KS-1,K)	INST 046
STVU0(KS)=VU0(KS-1,K)	INST 047
STVZ0(KS)=VZ0(KS-1,K)	INST 048
STTS0(KS)=TS0(KS-1,K)	INST 049
STPS0(KS)=PS0(KS-1,K)	INST 050
STDEN0(KS)=1+*.STPS0(KS)/(STTS0(KS)*RV(1,K))	*****
STM0(KS)=M0(KS-1,K)	INST 052
STWG1(KS)=WG1(KS-1,K)	*****
SFL01=SFL01+STWG1(KS)	*****
STOP1(KS)=OP1(KS-1,K)	INST 053
STALF1(KS)=ALF1E(KS-1,K)*57.2958	INST 054
STDELA(KS)=(ALPHA0(KS-1,K)+ALF1E(KS-1,K))*57.2958	INST 055
STV1(KS)=V1(KS-1,K)	INST 056
STVU1(KS)=VU1(KS-1,K)	INST 057
STVZ1(KS)=VZ1(KS-1,K)	INST 058
STTS1(KS)=TS1(KS-1,K)	INST 059
STPS1(KS)=PS1(KS-1,K)	INST 100
STDEN1(KS)=HHOS1(KS-1,K)	INST 101
STM1(KS)=V1(KS-1,K)/(SQRT(GAM(2,K)*G*RV(2,K)*TS1(KS-1,K)))	*****
ZS=-2.*ALF1E(KS-1,K)-1.570796	INST 103
ZWI=INC(KS)=COS(ZS)*(SIN(ALPHA0(KS-1,K))*COS(ALF1E(KS-1,K))	INST 104
1-1,K)))/(COS(ALPHA0(KS-1,K))*SIN(ALF1E(KS-1,K)))+1.)	INST 105
CPS(KS)=1.-(STVU(KS)/STV1(KS))*2	INST 106
STWG1A(KS)=WG1A(KS-1,K)	*****
SFL01A=SFL01A+STWG1A(KS)	*****
STOP1A(KS)=OP1A(KS-1,K)	INST 107
STPTR1(KS)=PTR1A(KS-1,K)	INST 108
STTR1(KS)=TTR1A(KS-1,K)	INST 109
STBET1(KS)=HET1A(KS-1,K)*57.2958	INST 110
STH1(KS)=R1(KS-1,K)*57.2958	INST 111
STR1A(KS)=R1A(KS-1,K)	INST 112
STRU1A(KS)=RU1A(KS-1,K)	INST 113
STMW1A(KS)=MW1A(KS-1,K)	INST 114
STU1A(KS)=U1A(KS-1,K)	INST 115
STPS1A(KS)=PS1A(KS-1,K)	*****
STTS1A(KS)=TS1A(KS-1,K)	*****
STWG2(KS)=WG2(KS-1,K)	*****
SFL02=SFL02+STWG2(KS)	*****
STOP2(KS)=OP2(KS-1,K)	INST 116
STHET2(KS)=HET2E(KS-1,K)*57.2958	INST 117
SDHETA(KS)=(HET1A(KS-1,K)+HET2E(KS-1,K))*57.2958	INST 118
SR2(KS)=R2(KS-1,K)	INST 119
SRU2(KS)=RU2(KS-1,K)	INST 120

# Listing of Code (continued)

	SU2(KS)=U2(KS-1,K)	INST 121
	STPTH2(KS)=P(R2(KS-1,K)	INST 122
	STTH2(KS)=TTH2(KS-1,K)	*****
	RX(KS)=1.-(1.-(PS1(KS-1,K)/PTP(KS-1,K))*E1)/(1.-(PS2(KS-1,K)/	INST 123
	1PTP(KS-1,K))*E1)	INST 124
	STDELH(KS)=DELHT(KS-1,K)	INST 125
	STPS1(KS)=2.*G*AJ*DELHT(KS-1,K)/(U1A(KS-1,K)*U1A(KS-1,K)	INST 126
	1+U2(KS-1,K)*U2(KS-1,K))	INST 127
	SETATT(KS)=ETATT(KS-1,K)	INST 128
	SETATS(KS)=ETATS(KS-1,K)	INST 129
	SETAAT(KS)=ETATAT(KS-1,K)	INST 130
	ZR = -2.*HET2E(KS-1,K) -1.570796	INST 131
	RZWINC(KS)=COS( ZR )*(SIN(BET1A(KS-1,K))*COS(BET2E(KS-	INST 132
	11,K))/(COS(BET1A(KS-1,K))*SIN(BET2E(KS-1,K)))+1.)	INST 133
	CPR(KS)=1.-(STRIA(KS)/SH2(KS))*2	INST 134
	STPS2(KS)=PS2(KS-1,K)	*****
	STTS2(KS)=TS2(KS-1,K)	*****
	STWG2A(KS)=WG2A(KS-1,K)	*****
	SFL02A=SFL02A+STWG2A(KS)	*****
	STPT2A(KS)=PT2A(KS-1,K)	*****
	STTT2A(KS)=TT2A(KS-1,K)	*****
	STV2A(KS)=V2A(KS-1,K)	*****
	STVU2A(KS)=VU2A(KS-1,K)	INST 139
	STALF2(KS)=ALF2A(KS-1,K)*57.2958	*****
	STMF2A(KS)=MF2A(KS-1,K)	*****
	STVZ2A(KS)=VZ2A(KS-1,K)	*****
	STPS2A(KS)=PS2A(KS-1,K)	*****
	STTS2A(KS)=TS2A(KS-1,K)	*****
	STM2A(KS)=M2A(KS-1,K)	*****
	STOEN2(KS)=144.*STPS2A(KS)/(STTS2A(KS)*RV(5,K))	INST 146
5	CONTINUE	INST 147
	IF (ISECT-3)3,3,6	INST 148
C	CALCULATE HUB VALUES	INST 149
3	LJ=1	INST 150
	JJ=ISECT*2	INST 151
	I=1	INST 152
	L=1	*****
	STDP0(L)=DR(1,K)	*****
	R1=CP0(I,K)/DR(1,K)	*****
	STDP1(L)=DR(2,K)	INST 156
	R2=CP1(I,K)/DR(2,K)	*****
	STDP1A(L)=DR(3,K)	INST 158
	R3=CP1A(I,K)/DR(3,K)	INST 159
	STDP2(L)=DR(4,K)	*****
	R4=CP2(I,K)/DR(4,K)	INST 161
	TALF=SIN(ALF1(I,K))*R3/COS(ALF1(I,K))	

# Listing of Code (continued)

C	R5=CP2A(I,K)/DW(5,K)	INST 162
	STATION 0 STATOR INLET	INST 163
10	STT0(L)=TT0(I,K)	INST 164
	STPT0(L)=PTP(I,K)	INST 165
	STVZ0(L)=VZ0(I,K)	INST 166
	STVU0(L)=VU0(I,K)*R1	INST 167
	STV0(L)=SQRT(VZ0(I,K)*VZ0(I,K)+STVU0(L)*STVU0(L))	INST 168
	STTS0(L)=TT0(I,K)-STV0(L)*STV0(L)/(2.*G*AJ*CP0(K))	INST 169
	STPS0(L)=PS0(I,K)*(STTS0(L)/TS0(I,K))*E2	INST 170
	STDEN0(L)=144.*STPS0(L)/(RV(1,K)*STTS0(L))	*****
	STALF(L)=ATAN2(STVU0(L),STVZ0(L))*57.2958	INST 172
	STSI(L)=STALF(L)-ATAN2(SIN(RADSD(I,K))*R1,COS(RADSD(I,K)))	INST 173
	1*57.2958	INST 174
	AS0H=SQRT(GAM(1,K)*G*HV(1,K)*STTS0(L))	*****
	STM0(L)=STV0(L)/AS0H	INST 176
C	STATION 1 STATOR EXIT	INST 177
	STVZ1(L)=VZ1(I,K)	INST 178
	STVU1(L)=VU1(I,K)*R2	INST 179
	STV1(L)=SQRT(VZ1(I,K)*VZ1(I,K)+STVU1(L)*STVU1(L))	INST 180
	STTS1(L)=TT0(I,K)-STV1(L)*STV1(L)/(2.*G*AJ*CP1(K))	INST 181
	STPS1(L)=PS1(I,K)*(STTS1(L)/TS1(I,K))*E3	INST 182
	STDEN1(L)=144.*STPS1(L)/STTS1(L)/RV(2,K)	*****
	STALFE(L)=ATAN2(STVU1(L),STVZ1(L))*57.2958	INST 184
	STDELA(L)=STALF(L)+STALFE(L)	INST 185
	AS1H=SQRT(GAM(2,K)*G*HV(2,K)*STTS1(L))	*****
	STM1(L)=STV1(L)/AS1H	INST 187
	ZS=-2.*STALFE(L)/57.2958-1.570796	INST 188
	Z=INC(L)=COS(ZS)*(STVU0(L)*STVZ1(L)/(STVZ0(L)*STVU1(L))+1.)	INST 189
	CPS(L)=1.-(STV0(L)/STV1(L))*2	INST 190
C	STATION 1A ROTOR INLET	INST 191
	VU1AH=VU1A(I,K)*R3	INST 192
	STRU1A(L)=VU1AH-U1A(I,K)/R3	INST 193
	STBET1(L)=ATAN2(STRU1A(L),VZ1A(I,K))*57.2958	INST 194
	T=TALF-(TALF/R3-SIN(RADRD(I,K))/COS(RADRD(I,K)))/R3	INST 195
	STRI(L)=STBET1(L)-ATAN2(T.1.)*57.2958	INST 196
	STR1A(L)=SQRT(STRU1A(L)*STRU1A(L)+VZ1A(I,K)*VZ1A(I,K))	INST 197
	V1A1AH=VZ1A(I,K)*VZ1A(I,K)+VU1AH*VU1AH	INST 198
	DELTSH=(V1(I,K)*V1(I,K)-V1A1AH)/(2.*G*AJ*CP1A(K))	INST 199
	TS1AH=TS1(I,K)+DELTSH	INST 200
	STTS1A(L)=TS1AH	*****
	STM1A(L)=STR1A(L)/SQRT(GAM(3,K)*G*HV(3,K)*TS1AH)	*****
	TTRSH=1.+STM1A(L)*STM1A(L)*(GAM(3,K)-1.)/2.	INST 202
	STTHR1(L)=TS1AH*TTRSH	INST 203
	IF (RI(I,K))2*2*7	INST 204
2	EXPRI=EXPN	INST 205
	GO TO 11	INST 206
7	EXPRI=EXPP	INST 207

# Listing of Code (continued)

11	PTRSH=(1.+(TTTSH-1.)*ELTARR(I,K)*COS(RI(I,K))*EXPRI)**E4	INST 208
	PS1AH=PS1(I,K)*(1.+DELTSH/TS1(I,K))*E4	INST 209
	STPS1A(L)=PS1AH	*****
	STPTR1(L)=PS1AH*PTRSH	INST 210
	STU1A(L)=U1A(I,K)/R3	INST 211
C	STATION 2 ROTOR EXIT	INST 212
	VU2H=VU2(I,K)*R4	INST 213
	SHU2(L)=VU2H+U2(I,K)/R4	INST 214
	STHET2(L)=ATAN2(SHU2(L),VZ2(I,K))*57.2958	INST 215
	SDBETA(L)=STHET1(L)+SBET2(L)	INST 216
	SR2(L)=SQRT(SHU2(L)*SHU2(L)+VZ2(I,K)*VZ2(I,K))	INST 217
	V2V2H=VZ2(I,K)*VZ2(I,K)+VU2H*VU2H	INST 218
	DELTSH=(V2(I,K)*V2(I,K)-V2V2H)/(2.*G*AJ*CP2(K))	INST 219
	TS2H=TS2(I,K)+DELTSH	INST 220
	STTS2(L)=TS2H	*****
	SMR2(L)=SR2(L)/SQRT(GAM(4,K)*G*RV(4,K)*TS2H)	INST 222
	SU2(L)=U2(I,K)/R4	INST 223
	PS2H=PS2(I,K)*(TS2H/TS2(I,K))*E4	*****
	STPS2(L)=PS2H	INST 224
	RX(L)=1.-(1.-(STPS1(L)/PTP(I,K))*E1)/(1.-(PS2H/PTP(I,K))*E1)	INST 225
	STDELH(L)=(STU1A(L)*VU1AH+SU2(L)*VU2H)*TFR(I,K)/(G*AJ)	INST 226
	STPSI(L)=2.*G*AJ*STDELH(L)/(STU1A(L)**2+SU2(L)**2)	INST 227
	SETATT(L)=STDELH(L)/DELHT1(I,K)	INST 228
	SETATS(L)=STDELH(L)/DELHST1(I,K)	INST 229
	SETAAT(L)=STDELH(L)/DELHAT1(I,K)	INST 230
	ZR=-2.*STHET2(L)/57.2958-1.570796	INST 231
	RZ*INC(L)=COS(ZR)*(STU1A(L)*VZ2(I,K)/(VZ1A(I,K)*SRU2(L))+1.)	INST 232
	CPH(L)=1.-(STH1A(L)/SH2(L))**2	*****
	STPT2A(L)=PT2A(I,K)	*****
	STTT2A(L)=TT2A(I,K)	*****
	STVZ2A(L)=VZ2A(I,K)	*****
	STVL2A(L)=VL2A(I,K)*R5	*****
	V2A2AH=STVU2A(L)**2+VZ2A(I,K)**2	*****
	STV2A(L)=SQRT(V2A2AH)	*****
	STALF2(L)=ATAN2(STVU2A(L),VZ2A(I,K))*57.2958	INST 240
	DELTS2=(V2A(I,K)**2-V2A2AH)/(2.*G*AJ*CP2A(K))	*****
	STTS2A(L)=TS2A(I,K)+DELTS2	*****
	STPS2A(L)=PS2A(I,K)*(1.+DELTS2/TS2A(I,K))*E6	*****
	STDEN2(L)=144.*STPS2A(L)/(HV(5,K)*STTS2A(L))	*****
	STM2A(L)=STV2A(L)/SQRT(GAM(5,K)*G*RV(5,K)*STTS2A(L))	*****
	STMF2A(L)=STM2A(L)*COS(STALF2(L)/57.2958)	INST 246
	IF (L.GT.1) GO TO 8	INST 247
C	CALCULATE TJP VALUES	INST 248
	I=ISECT	INST 249
	L=ISECT+2	INST 250
	STDP0(L)=DT(I,K)	INST 251
	R1=DP0(I,K)/D1(I,K)	

# Listing of Code (continued)

STOP1(L)=DT(2,K)	INST 252
R2=CP1(I,K)/DT(2,K)	INST 253
STOP1A(L)=DT(3,K)	INST 254
R3=CP1A(I,K)/DT(3,K)	INST 255
STOP2(L)=DT(4,K)	INST 256
R4=CP2(I,K)/DT(4,K)	INST 257
TALF=SIN(ALF1(I,K))*R3/COS(ALF1(T,K))	INST 258
R5=CP2A(I,K)/DT(5,K)	INST 259
GO TO 10	INST 260
6 LJ=2	INST 261
JJ=ISECT+1	INST 262
8 CALL WOUT	INST 263
9 CONTINUE	INST 264
IF(SHFLAG) WRITE(6,20000)	*****
20000 FORMAT(45H AN EXIT HAS BEEN MADE FROM SUBROUTINE INSTG )	*****
RETURN	INST 265
END	INST 266

# Listing of Code (continued)

```

SUBROUTINE WOUT
C
REAL MFSTOP
LOGICAL PREVER,SRFLAG
COMMON /SRFLAG
COMMON /SNTCP/G,AJ,PRFC,ICASE,PRFVER,MFSTOP,JUMP,LOPIN,ISCASE,
1KN,GAMF,IP,SCRT,PTHK,ISECT,KSTG,WTOL,RHOTOL,PTOL,TRLOOP,LSTG,
2LHRC,IHRC,IHCKE,ISORH,CHCKE,PTOPSI(6,8),PTHS2(6,8),TRDIAG,SC,RC,
3DELPR,PASS,IPC,LOPC,ISS
C
COMMON /SINIT/H1(6,8),H2(6,8),DP0(6,8),DP1(6,8),DP1A(6,8),DP2(6,8),
1,DP2A(6,8),CSALF1(6,8),ALF1(6,8),CSHET2(6,8),BET2(6,8),RADSD(6,8),
2RADWD(6,8),ANN1(6,8),ANN2(6,8),ANN2A(6,8),ANN1A(6,8),U1A(6,8),
3U2(6,8),ANN0(6,8),PT0(6,8),TT0(6,8),ALPHA0(6,8),PTP(6,8)
C
COMMON /SINPUT/ RSL,TSL,PSL,GAMSI,
1PTPS,PTIN,TTIN,WAIR,FAIR,DELC,DELL,DELA,AACS,VCTD,STG,SECT,EXPN,
2EXPP,EXPRE, RPM,PAF,SLI,STGCH,FNDJOH,NAME(10),TITLE(10),PCNH(6),
3RV(6,8),GAM(6,8),DR(6,8),DT(6,8),RWG(6,8),ALPHAS(6,8),ALPHA1(6,8),
4ETAS(6,8),ETAS(6,8),CFS(6,8),ANNO(6,8),BETA1(6,8),BETA2(6,8),ETARWOUT
5R(6,8),ETAR(6,8),CFR(6,8),TFR(6,8),ANDOR(6,8),OMEGAS(6,8),AS0(6,8),
6,ASMP0(6,8),ACMNO(6,8),A1(6,8),A2(6,8),A3(6,8),A4(6,8),A5(6,8),A6(6,8),
76,8),OMEGAR(6,8),BSIA(6,8),RSMPIA(6,8),HCMNIA(6,8),B1(6,8),B2(6,8),
8,B3(6,8),B4(6,8),B5(6,8),B6(6,8),SESTHI(8),RETHI(8)
C
REAL M0
COMMON /SSTA01/CP0(8),
18),VU0(6,8),VZ0(6,8),RHOS0(6,8),PS1(6,8),WGT1(8),TA1(8),WG1(6,8),
2
3,RHOS1(6,8),ALF1E(6,8),VU1(6,8),VZ1(6,8),M0(6,8),WGT0(8),WG0(6,8)
C
REAL MR1A
COMMON /SSTA1A/VU1A(6,8),WG1A(6,8),WGT1A(8),VZ1A(6,8),
1PS1A(6,8),RU1A(6,8),R1A(6,8),RET1A(6,8),RI(6,8),TTR1A(6,8),PTR1A(6,8),
2,8),MR1A(6,8),TS1A(6,8)
C
COMMON /SSTA2/VZ2(6,8),TTR2(6,8),PTR2(6,8),WG2(6,8),WGT2(8),TA2(8),
1
PS2(6,8),PII2(6,8)
C
REAL MR2,M2,MF
COMMON /SFLOW2/TS2(6,8),CP2(8),R2(6,8),RHOS2(6,8),BET2E(6,8),RU2(6,8),
1,8),VU2(6,8),DPDR2(6,8),VZ2(6,8),MR2(6,8),MF2(6,8),M2(6,8)
C
REAL M2A,MF2A
COMMON /SSTA2A/WG2A(6,8),WGT2A(8),VU2A(6,8),VZ2A(6,8),PS2A(6,8),

```



Listing of Code (continued)

```

1ALF2A(6,8),TT2A(6,8),FT2A(6,8),TTBAR(8),PTBAR(8),STT0(8),SPT0(8), *****
2M2A(6,8),MF2A(6,8),CP2A(8),V2A(6,8),TS2A(6,8),TAS(8),PAS(8),GAMS(8)*****
3)CPO(8),DELHVD(6,8),HVBAR(8) *****
C *****
COMMON /SOVRAL/DELMT(6,8),DELMTI(6,8),CELHSI(6,8),DEHATI(6,8), *****
1ETATT(6,8),ETATS(6,8),ETATAT(6,8) *****
C *****
COMMON STCP0(7),STPT0(7),STALF(7),STSI(7),STV0(7),STVU0(7), WOUT n25
1STVZ0(7),STTS0(7),STPS0(7),STDEN0(7),STM0(7),STOP1(7),STALFE(7), WOUT n26
2STDELA(7),STV1(7),STVL1(7),STVZ1(7),STTS1(7),STPS1(7),STDEN1(7), WOUT n27
3STM1(7),ZWINC(7), CPS(7),STOP1A(7), WOUT n28
4STPTR1(7),STDET1(7),SIRI(7),STR1A(7),STRU1A(7),STMRI1A(7),STU1A(7), WOUT n29
5STDP2(7),STHET2(7),SDHETA(7),SR2(7),SRU2(7),SMR2(7),SU2(7),RX(7), WOUT n30
6STDELH(7),STPS1(7),SEIATT(7),SETATS(7),SETAAT(7),RZWINC(7), WOUT n31
7 CPR(7),STPT2A(7),STTT2A(7),STV2A(7),STVU2A(7),***** WOUT n32
8STALF2(7),STMF2A(7),STPTR1(7),STVZ2A(7),STTS2A(7),STPS2A(7),STDEN2*****
9(7),STM2A(7),STTT0(7),LJ,JJ,K,STWG0(7),STWG1(7),STWG1A(7),STWG2(7)*****
9,STWG2A(7),SFL00,SFL01,SFL01A,SFL02,SFLU2A,STPS1A(7),STTS1A(7), *****
9STPTR2(7),STTT2(7),STPS2(7),STTS2(7) *****
C WOUT n36
C PRINT OUT FOR INTERSTAGE DATA WOUT n37
IF(SHFLAG) WRITE(6,10000) *****
10000 FORMAT(44H AN ENTRY HAS BEEN MADE IN SUBROUTINE WOUT ) *****
8 WRITE(6,1000)NAME,TITLE,ICASE,ISCASE WOUT n38
1000 FORMAT(1H1,20X29HNASA TURBINE COMPUTER PROGRAM/6X10A6/6X10A6/30X WOUT n39
15HCASE 13,1H,13/24X23HINTER-STAGE PERFORMANCE//) WOUT n40
WRITE(6,1001)K,(STDP0(I),I=LJ,JJ) WOUT n41
1001 FORMAT(5X5HSTA 02X12HSTATOR INLET,10X5HSTAGE13,1H./4X6HDIAM 02X, WOUT n42
16F10.3) WOUT n43
WRITE(6,1002)(STTT0(I),I=LJ,JJ) WOUT n44
1002 FORMAT (10H TT 0,2X,6F10.1) WOUT n45
WRITE(6,1003)( STPT0(I),I=LJ,JJ) WOUT n46
1003 FORMAT (10H PT 0,2X,6F10.3) WOUT n47
WRITE(6,1004)( STALF(I),I=LJ,JJ) WOUT n48
1004 FORMAT (10H ALPHA 0,2X,6F10.3) WOUT n49
WRITE(6,1005)( STSI(I),I=LJ,JJ) WOUT n50
1005 FORMAT (10H I STATOR,2X,6F10.3) WOUT n51
WRITE(6,1006)( STV0(I),I=LJ,JJ) WOUT n52
1006 FORMAT (10H V 0,2X,6F10.3) WOUT n53
WRITE(6,1007)( STVU0(I),I=LJ,JJ) WOUT n54
1007 FORMAT (10H VU 0,2X,6F10.3) WOUT n55
WRITE(6,1008)( STVZ0(I),I=LJ,JJ) WOUT n56
1008 FORMAT (10H VZ 0,2X,6F10.3) WOUT n57
WRITE(6,1009)( STTS0(I),I=LJ,JJ) WOUT n58
1009 FORMAT (10H TS 0,2X,6F10.1) WOUT n59
WRITE(6,1010)( STPS0(I),I=LJ,JJ) WOUT n60
1010 FORMAT (10H PS 0,2X,6F10.3) WOUT n61

```

```

WRITE(6,1011)(STOENO(1),I=LJ,JJ)
1011 FORMAT (10H      DENS 0,2X,6F10.5)
WRITE(6,1012)(      STM0(1),I=LJ,JJ)
1012 FORMAT (10H      M 0,2X,6F10.5)
WRITE(6,1499)(      CP0(K),I=LJ,JJ)
1999 FORMAT(10H      CP 0,2X,6F10.5)
WRITE(6,2000)(RV(1,K),I=LJ,JJ)
2000 FORMAT (10H      HG 0,2X,6F10.3)
WRITE(6,2001)(GAM(1,K),I=LJ,JJ)
2001 FORMAT (10H      GAMG 0,2X,6F10.5)
WRITE(6,2002)(HWG(1,K),I=LJ,JJ)
2002 FORMAT (10H      HWG 0,2X,6F10.5)
IF(ISECT.LE.3)GO TO 11013
WRITE(6,2003)(      STWG0(1),I=LJ,JJ),SFL00
2003 FORMAT (10H      WG 0,2X,6F10.5,2X,11MTOTAL FLOW ,F10.5)
1013 WRITE(6,1013)(STOPI(1),I=LJ,JJ)
1013 FORMAT(/5X5HSTA 12X11HSTATOR EXIT,4X6HDIAM 12X,6F10.3)
WRITE(6,1014)(STALFE(1),I=LJ,JJ)
1014 FORMAT (10H      ALPHA 1,2X,6F10.3)
WRITE(6,1015)(STOELA(1),I=LJ,JJ)
1015 FORMAT (10H      DEL A,2X,6F10.3)
WRITE(6,1016)(      STV1(1),I=LJ,JJ)
1016 FORMAT (10H      V 1,2X,6F10.3)
WRITE(6,1017)(      STVU1(1),I=LJ,JJ)
1017 FORMAT (10H      VU 1,2X,6F10.3)
WRITE(6,1018)(      STVZ1(1),I=LJ,JJ)
1018 FORMAT (10H      VZ 1,2X,6F10.3)
WRITE(6,1019)(      STTS1(1),I=LJ,JJ)
1019 FORMAT (10H      TS 1,2X,6F10.1)
WRITE(6,1064)(      STPS1(1),I=LJ,JJ)
1064 FORMAT (10H      PS 1,2X,6F10.3)
WRITE(6,1020)(STDEN1(1),I=LJ,JJ)
1020 FORMAT (10H      DENS 1,2X,6F10.5)
WRITE(6,1021)(      STM1(1),I=LJ,JJ)
1021 FORMAT (10H      M 1,2X,6F10.5)
WRITE(6,1022)(ZW1INC(1),I=LJ,JJ)
1022 FORMAT (10H      ZW1 INC,2X,6F10.5)
WRITE(6,1026)(      CPS(1),I=LJ,JJ)
1026 FORMAT (10H      CP 5,2X,6F10.5)
WRITE(6,2999)(      CP1(K),I=LJ,JJ)
2999 FORMAT(10H      CP 1,2X,6F10.5)
WRITE(6,3000)(RV(2,K),I=LJ,JJ)
3000 FORMAT (10H      HG 1,2X,6F10.3)
WRITE(6,3001)(GAM(2,K),I=LJ,JJ)
3001 FORMAT (10H      GAMG 1,2X,6F10.5)
WRITE(6,3002)(HWG(2,K),I=LJ,JJ)
3002 FORMAT (10H      HWG 1,2X,6F10.5)

```

[illegible]

```

IF(ISECT.LE.3)GO TO 11000
WRITE(6,3003)( STWGI(I),I=LJ,JJ),SFL01
3003 FORMAT (10H      WG 1A,2X,6F10.5,2X,11HTOTAL FLOW ,F10.5)
1000 WRITE(6,1000)NAME, TITLE,ICASE,ISCASE
WRITE(6,1028)K,(STOPIA(I),I=LJ,JJ)
1028 FORMAT(4X6HSTA 1A2X11HROTOR INLET,10X5HSTAGE13,1H./3X7HDIAM 1A2X,
16F10.3)
WRITE(6,1027)(STPTR1(I),I=LJ,JJ)
1027 FORMAT (10H      PTR 1A,2X,6F10.3)
WRITE(6,1029)(STTTR1(I),I=LJ,JJ)
1029 FORMAT (10H      TTR 1A,2X,6F10.1)
WRITE(6,1030)(STHET1(I),I=LJ,JJ)
1030 FORMAT (10H      BETA 1A,2X,6F10.3)
WRITE(6,1031)( STRI(I),I=LJ,JJ)
1031 FORMAT (10H      I ROTOR,2X,6F10.3)
WRITE(6,1032)( STR1A(I),I=LJ,JJ)
1032 FORMAT (10H      R 1A,2X,6F10.3)
WRITE(6,1033)(STRU1A(I),I=LJ,JJ)
1033 FORMAT (10H      RU 1A,2X,6F10.3)
WRITE(6,1034)(STMRI1A(I),I=LJ,JJ)
1034 FORMAT (10H      MR 1A,2X,6F10.5)
WRITE(6,1035)( STUIA(I),I=LJ,JJ)
1035 FORMAT (10H      U 1A,2X,6F10.3)
WRITE (6,2035)(STPS1A(I),I=LJ,JJ)
2035 FORMAT (10H      PS 1A,2X,6F10.3)
WRITE (6,2036)(STTS1A(I),I=LJ,JJ)
2036 FORMAT (10H      TS 1A,2X,6F10.1)
WRITE(6,3999)(CP1A(K),I=LJ,JJ)
3999 FORMAT(10H      CP 1A,2X,6F10.5)
WRITE(6,4000)(RV(3,K),I=LJ,JJ)
4000 FORMAT (10H      RG 1A,2X,6F10.3)
WRITE(6,4001)(GAM(3,K),I=LJ,JJ)
4001 FORMAT (10H      GAMG 1A,2X,6F10.5)
WRITE (6,4002)(RWG(3,K),I=LJ,JJ)
4002 FORMAT (10H      RWG 1A,2X,6F10.5)
IF(ISECT.LE.3)GO TO 11037
WRITE(6,4003)(STWGI1(I),I=LJ,JJ),SFL01A
4003 FORMAT (10H      WG 1A,2X,6F10.5,2X,11HTOTAL FLOW ,F10.5)
1037 WRITE(6,1037)(STDP2(I),I=LJ,JJ)
1037 FORMAT(5X5HSTA 2X10HROTOR EXIT,4X6HDIAM 2X,6F10.3)
IF(ISECT.LE.3)GO TO 11036
WRITE (6,2037)(STPTR2(I),I=LJ,JJ)
2037 FORMAT (10H      PTR 2,2X,6F10.3)
WRITE (6,2038)(STTTR2(I),I=LJ,JJ)
2038 FORMAT (10H      TTR 2,2X,6F10.1)
1036 WRITE(6,1036)(STHET2(I),I=LJ,JJ)
1036 FORMAT (10H      BETA 2,2X,6F10.3)

```

```

WRITE(6,1033)(SUMETA(1),I=LJ,JJ)
1038 FORMAT (10H      DBETA,2X,6F10.3)
WRITE(6,1039)(      SR2(1),I=LJ,JJ)
1039 FORMAT (10H      R 2,2X,6F10.3)
WRITE(6,1040)(      SRU2(1),I=LJ,JJ)
1040 FORMAT (10H      RU 2,2X,6F10.3)
WRITE(6,1041)(      SMR2(1),I=LJ,JJ)
1041 FORMAT (10H      MR 2,2X,6F10.5)
WRITE(6,1042)(      SU2(1),I=LJ,JJ)
1042 FORMAT (10H      U 2,2X,6F10.3)
WRITE(6,1043)(      HX(1),I=LJ,JJ)
1043 FORMAT (10H      HX,2X,6F10.5)
WRITE(6,1044)(STDELH(1),I=LJ,JJ)
1044 FORMAT (10H      DELH,2X,6F10.3)
WRITE(6,1045)(      STPS1(1),I=LJ,JJ)
1045 FORMAT (10H      PS1 P,2X,6F10.5)
WRITE(6,1046)(SETATT(1),I=LJ,JJ)
1046 FORMAT (10H      ETA TT,2X,6F10.5)
WRITE(6,1047)(SETATS(1),I=LJ,JJ)
1047 FORMAT (10H      ETA TS,2X,6F10.5)
WRITE(6,1048)(SETAAT(1),I=LJ,JJ)
1048 FORMAT (10H      ETA AT,2X,6F10.5)
WRITE(6,1049)(RZWINC(1),I=LJ,JJ)
1049 FORMAT (10H      ZWI INC,2X,6F10.5)
WRITE(6,1065)(      CPH(1),I=LJ,JJ)
1065 FORMAT (10H      CP R,2X,6F10.5)
WRITE(6,2065)(      STPS2(1),I=LJ,JJ)
2065 FORMAT (10H      PS 2,2X,6F10.3)
WRITE(6,2066)(      STTS2(1),I=LJ,JJ)
2066 FORMAT (10H      TS 2,2X,6F10.1)
WRITE(6,4999)(      CP2(K),I=LJ,JJ)
4999 FORMAT(10H      CP 2,2X,6F10.5)
WRITE(6,5000)(RV(4,K),I=LJ,JJ)
5000 FORMAT (10H      RG 2,2X,6F10.3)
WRITE(6,5001)(GAM(4,K),I=LJ,JJ)
5001 FORMAT (10H      GAMG 2,2X,6F10.5)
WRITE(6,5002)(RWG(4,K),I=LJ,JJ)
5002 FORMAT (10H      RWG 2,2X,6F10.5)
IF(ISECT.LE.3)GO TO 11053
WRITE(6,5003)(      STWG2(1),I=LJ,JJ),5FLOP
5003 FORMAT (10H      WG 2,2X,6F10.5,2X,11HTOTAL FLOW ,F10.5)
11053 WRITE(6,1053)(      STPT2A(1),I=LJ,JJ)
1053 FORMAT (10H      PT 2A,2X,6F10.3)
WRITE(6,1054)(      STTT2A(1),I=LJ,JJ)
1054 FORMAT (10H      TT 2A,2X,6F10.1)
WRITE(6,1055)(      STV2A(1),I=LJ,JJ)
1055 FORMAT (10H      V 2A,2X,6F10.3)

```

[illegible]

Listing of Code (continued)

WRITE(6,1056) ( STVU2A(I),I=LJ,JJ)	*****
1056 FORMAT (10H VU 2A,2X,6F10.3)	WOUT 147
WRITE(6,1057) (STALF2(I),I=LJ,JJ)	WOUT 148
1057 FORMAT (10H ALPHA 2A,2X,6F10.3)	WOUT 149
WRITE(6,1058) ( STMF2A(I),I=LJ,JJ)	*****
1058 FORMAT (10H MF 2A,2X,6F10.5)	WOUT 151
WRITE(6,1059) ( STVZ2A(I),I=LJ,JJ)	*****
1059 FORMAT (10H VZ 2A,2X,6F10.3)	WOUT 153
WRITE(6,1060) ( STTS2A(I),I=LJ,JJ)	*****
1060 FORMAT (10H TS 2A,2X,6F10.1)	WOUT 155
WRITE(6,1061) ( STPS2A(I),I=LJ,JJ)	*****
1061 FORMAT (10H PS 2A,2X,6F10.3)	WOUT 157
WRITE(6,1062) (STDEN2(I),I=LJ,JJ)	WOUT 158
1062 FORMAT (10H DEN5 2A,2X,6F10.5)	WOUT 159
WRITE(6,1063) ( STM2A(I),I=LJ,JJ)	*****
1063 FORMAT (10H M 2A,2X,6F10.5)	WOUT 161
WRITE(6,5999) (CP2A(K),I=LJ,JJ)	*****
5999 FORMAT (10H CP 2A,2X,6F10.5)	*****
WRITE(6,6000) (RV(5,K),I=LJ,JJ)	*****
6000 FORMAT (10H RG 2A,2X,6F10.3)	*****
WRITE(6,6001) (GAM(5,K),I=LJ,JJ)	*****
6001 FORMAT (10H GAMG 2A,2X,6F10.5)	*****
WRITE(6,6002) (HWG(5,K),I=LJ,JJ)	*****
6002 FORMAT (10H HWG 2A,2X,6F10.5)	*****
IF (ISECT.LE.3) GO TO 21000	*****
WRITE(6,6003) (STWG2A(I),I=LJ,JJ),SFLO2A	*****
6003 FORMAT (10H WG 2A,2X,6F10.5,2X,11HTOTAL FLOW ,F10.5)	*****
21000 IF (SRFLAG) WRITE(6,20000)	*****
20000 FORMAT(1H1,45H AN EXI! HAS BEEN MADE FROM SUBROUTINE WOUT )	*****
RETURN	WOUT 162
END	WOUT 163

# Listing of Code (continued)

```

SUBROUTINE PHIM(EXI,ETA,TR,PR)
CPHIM LOGICAL PHEVER,SRFLAG
      COMMON SRFLAG
      IF(SRFLAG) WRITE(6,10000)
10000 FORMAT(44H AN ENTRY HAS BEEN MADE IN SUBROUTINE PHIM )
      A = EXI-.5
      B = -(EXI*(1.-ETA)/2.)
      C = ETA/2.
      X = (-B -SQRT(B**2 -4.*A*C))/(2.*A)
      TR = ETA/(ETA-X)
      PH = TR*EXI
      IF(SRFLAG) WRITE(6,20000)
20000 FORMAT(45H AN EXIT HAS BEEN MADE FROM SUBROUTINE PHIM )
      RETURN
      END

```

```

PHIM 001
PHIM 002
*****
*****
*****
*****
PHIM 003
PHIM 004
PHIM 005
PHIM 006
PHIM 007
PHIM 008
*****
*****
PHIM 009
PHIM 010

```

## CONTROL CARDS FOR WANL CDC-6600 COMPUTER

### B. Control Cards for Binary Deck Setup

	Example
JØB Card	JØB, 10.
Account Number Card	AS77987.
ID Card	ASD1097, TURBIN, 120, 7500, 01.
LØC Card	LØC, 75000.
LØAD Card	LØAD (INPUT)
EXECUTE Card	EXECUTE.
End-of-Record Card	7/8/9
End-of-Record Card	7/8/9
Binary Deck	Binary Cards
,	,
,	,
,	,
,	,
End-of-Record Card	7/8/9
End-of-Record Card	7/8/9
Data Deck	Data Cards
,	,
,	,
,	,
,	,
,	,
End-of-File Card	ENDJØB = 1.0 \$
	6/7/8/9

2-141

## 2.4 BLADE SURFACE VELOCITY CALCULATIONS\*

### 2.4.1 Background

As a part of the Westinghouse Astronuclear Laboratory analytical investigation of turbine erosion phenomena, calculations are made in the various areas of turbine flow. These procedures include the present calculation to determine the velocity distribution along the suction and pressure side of the turbine blades. Surface velocities from this calculation are then used as input to the AD-ROP code discussed in Section 2.6.

The purpose of this report is to show how the computer program was used in performing the calculation for the G.E. blade and to compare the results of this calculation with those by other methods. Comments on the use of this program extend the detailed account to include: the modifications for the CDC 6400 machine, the input and output for the G.E. blade calculation, and additional comment on the features of the program.

### 2.4.2 Calculation of G. E. Blade

Calculations were made on the 3rd stage stator blade, mean diameter section, for the G.E., 3 stage potassium turbine. This blade section, shown in Figure 2.4.2-1 is reproduced from Figure 11 of Reference 2.

#### Input

The input to the calculation is given by Table 2.4.2-1. Its format is identical to that in Reference 1. The input data are identified by the Figure 2.4.2-2 sketch and by the Description of Input in Reference 1. Note that all linear dimensions given by Table 2.4.2-1 and Figure 2.4.2-2 are ten times the actual blade size.

\*W. K. Fentress, Fellow Engineer, Development Engineering Department, Westinghouse Steam Divisions, Westinghouse Electric Corp., Lester, Pa.

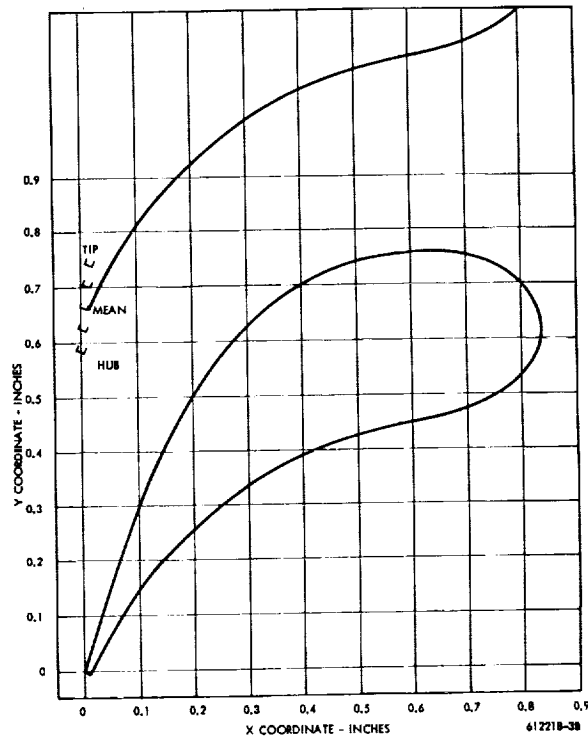


Figure 2.4.2-1 Third Stage Nozzle Mean Section

TABLE 2.4.2-1

#### INPUT

1	11	21	31	41	51	61	71
PITCH	CHORD	STGR	THETA1	THETA0	DTLR		
6.67	8.37	-6.19	28.2	-68.9	.0005		
RI	ALUT	ALLI	RO	ALUD	ALLO		
1.09	46.0	-37.3	.03	-72.9	-61.4		
6	11.6	2.6	.36				
HUB1	HUB0	HUB1	HUBP	HUBS	HUBT		
3.0	60	90	2.5	1.9	10		
ZU ARRAY							
	1.43	2.61	3.81	5.07	6.10	7.09	7.72
XSPU ARRAY							
	1.36	1.405	1.12	.39	-.78	-2.6	-4.17
ZL ARRAY							
	1.35	2.01	2.83	3.80	4.99	5.98	6.99
7.78							
XSPL ARRAY							
	5.33	5.11	4.95	4.69	4.10	3.43	2.49
1.39							
BLDATA	BLAKE	EPRT	STRE	SLCD	SLPT	ARPT	INTVELSUMVEL
1	0	1	1	0	1	1	1
W	WR		TOLER	ODA			BOO
1.6	.01		.0001	.63			3.2



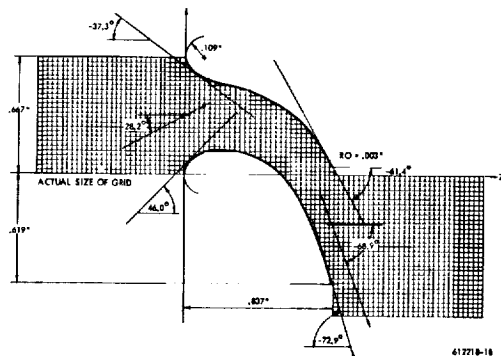


Figure 2.4.2-2 Geometric Data for the G. E. Blade

### Listing

The program is the same as listed in Reference 1 save for minor mechanical changes to allow for the use of the program on the CDC 6400 machine.

For the most part, these changes are in the format statements and in the indexing for the arrays listed in the Equivalence Statements; e.g., variables such as A(2500,4) were changed to equivalent statements involving single indices. The original program used a computer system-dependent plotting package which has been eliminated by deleting reference to subroutine PLOTMY.

### Output

A considerable amount of printout is generated by the program; for the present calculation only a small portion is pertinent. In Reference 1 the items of output are identified by item numbers 1 to 12. Items 4 and 5 are all that is necessary to construct the blade surface velocity curve, Figure 2.4.2-3. Output Item 4 gives the computed velocities at interior mesh points.

A sample of the latter is given in Table 2.4.2-2. The quantity IA refers to the axial coordinate index; thus at IA = 90 the free stream velocities across the exit plane of the blade section are given and at IA = 1 the inlet plane velocities are given. In the given problem the approximate average exit velocity is 0.4165 and the average inlet velocity is 0.170.

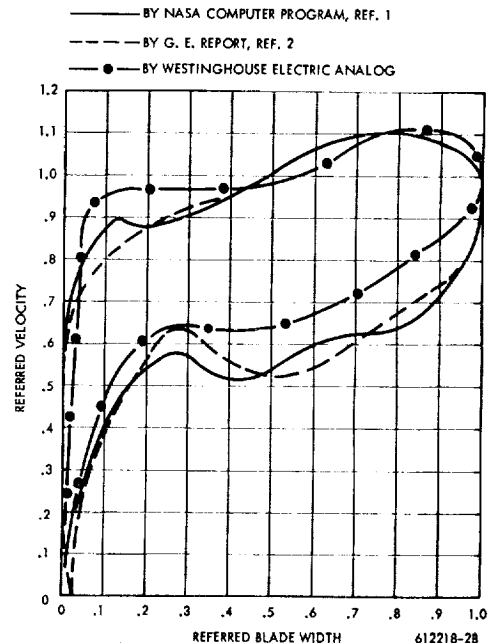


Figure 2.4.2-3 Surface Velocities Computed for the G. E. Blade

Item 5 gives the calculated surface velocities based on axial and tangential components. Thus, the referred velocity, with respect to the exit velocity is the ratio of the Item 5 surface velocity to 0.4165. Note that the value of velocity at the inlet and exit of the blade, corresponding to  $Z \approx 0$  and  $Z = 8.37$ , are taken as 0.170 and 0.4165 in constructing the velocity curve (Figure 2.4.2-3). The referred length, with respect to the axial length of the blade, is the ratio of  $Z$  to 8.37. A sample of Item 5 output is given in Table 2.4.2-3.

### 2.4.3 Discussion

The following discusses the use of the program and compares the calculation results with those by other methods.

### SAMPLE OF ITEM 4 OUTPUT

[illegible]

### Program

Machine time for the blade calculation was approximately 2 minutes with the CDC 6400 machine. This is in line with a tolerance of  $10^{-4}$  (TOLER), an assumed overrelaxation factor ( $\omega$ ) of 1.6, and 2006 mesh points. The tolerance is with respect to the maximum change in stream function in successive iterations, specified by the Item 8 printout as ERROR.

From the printout of ERROR it is evident that the number of iterations increases with decrease in tolerance (ERROR); e.g., 6, 30, 43 and 380 iterations for  $1. \times 10^{-2}$ ,  $1. \times 10^{-3}$ ,  $6. \times 10^{-4}$ , and  $1. \times 10^{-4}$  tolerance. Here there is a very large increase in the number of iterations between 6. and  $1. \times 10^{-4}$  tolerance, but this is consistent with the use of a factor ( $\omega$ ) of 1.6 in the calculation. It is shown by the following comparison, with other calculations for the same data, that the choice of the factor has a noticeable effect on the number of iterations, particularly in the region of close tolerance.

Note that  $(\omega) = 1.949$ , the optimum factor computed by subroutine SOR, requires less iterations at close tolerance, but generally requires a greater number of iterations at coarse tolerance. Thus the "optimum" factor is only optimum for a large number of iterations, i.e., for close tolerance.

$\times 10^{-4}$  It is probable that a tolerance of 5. to 1. is sufficiently close for most calculations based on the following check. Here calculations were made with  $10^{-2}$ ,  $10^{-3}$ ,  $10^{-4}$ , and  $10^{-5}$  tolerance and, while the velocity plot for  $10^{-2}$  tolerance was noticeably different in the region of the leading edge, there was very little change with respect to  $10^{-3}$  and  $10^{-5}$  and no visible change with respect to  $10^{-4}$  and  $10^{-5}$  tolerance.

Actually, several features of the program are not clearly explained by Reference 1.

### a) Solution of the Laplace Equation

Referring to Figures 4 and 5 of Reference 1: To solve the Laplace equation it is evident that the boundary conditions must be fully defined. Hence, as the boundary conditions are only defined, explicitly, along the upper and lower blade surface, it is probable that the stream function is specified along the other boundary surfaces by a process of interpolation based on: the stream function at points B, G, C and F,  $Q_{in}$  and  $Q_{out}$ , and the assumption (certainly in the first approximation) that the inlet and outlet stagnation streamline is straight.

Factor	Number of Iterations					
	$1. \times 10^{-2}$ Tolerance	$1. \times 10^{-3}$ Tolerance	$6. \times 10^{-4}$ Tolerance	$1. \times 10^{-4}$ Tolerance	$2. \times 10^{-5}$ Tolerance	$1. \times 10^{-5}$ Tolerance
1.949	45	105	106	157	199	213
1.90	24	75	88	---	---	---
1.80	12	40	86	---	---	---
1.70	7	30	46	---	---	---
1.60	6	30	43	380	718	---
1.50	6	30	43	---	---	---
1.40	5	31	44	---	---	---

TABLE 2.4.2-3

## SAMPLE OF ITEM 5 OUTPUT

SURFACE VELOCITIES BASED ON AXIAL COMPONENTS						
Z	UPPER SURFACE			LOWER SURFACE		
	VELOCITY	ANGLE (DEG)	WZ	VELOCITY	ANGLE (DEG)	WZ
-2.6921-010	0.0000+000	90.00	1.7583-003	0.0000+000	-90.00	-1.2521-002
2.7900-001	3.2218-001	48.08	2.1526-001	6.9851-002	-49.75	4.6670-002
3.5800-001	3.4315-001	37.34	2.7281-001	1.3147-001	-34.91	1.0950-001
8.3700-001	3.6507-001	27.42	3.2405-001	1.6791-001	-27.91	1.4965-001
1.1160+000	3.7321-001	18.52	3.5387-001	1.8830-001	-23.16	1.7412-001
1.3950+000	3.6616-001	11.95	3.5622-001	2.0514-001	-21.29	1.9206-001
1.6740+000	3.6858-001	7.29	3.6559-001	2.2354-001	-19.50	2.1156-001
1.9530+000	3.7183-001	2.92	3.7135-001	2.3912-001	-16.04	2.3040-001
2.2320+000	3.7490-001	-1.13	3.7483-001	2.3953-001	-12.04	2.3408-001
2.5110+000	3.7798-001	-4.81	3.7665-001	2.3421-001	-10.25	2.3072-001
2.7900+000	3.8208-001	-8.18	3.7617-001	2.2646-001	-10.73	2.2277-001
3.0690+000	3.8717-001	-11.57	3.7930-001	2.2082-001	-12.88	2.1562-001
3.3480+000	3.9607-001	-14.97	3.8263-001	2.1754-001	-15.59	2.1006-001
3.6270+000	4.0210-001	-18.35	3.8165-001	2.1758-001	-18.78	2.0676-001
3.9060+000	4.0934-001	-21.73	3.8025-001	2.1974-001	-22.32	2.0436-001
4.1850+000	4.2240-001	-25.57	3.8103-001	2.2646-001	-25.50	2.0583-001
4.4640+000	4.3070-001	-29.88	3.7365-001	2.3206-001	-28.18	2.0714-001
4.7430+000	4.4052-001	-34.48	3.6314-001	2.4144-001	-30.41	2.1039-001
5.0220+000	4.4678-001	-39.18	3.4431-001	2.4773-001	-32.22	2.1206-001
5.3010+000	4.5055-001	-43.84	3.2499-001	2.5375-001	-33.96	2.1326-001
5.5800+000	4.5271-001	-48.31	3.0109-001	2.5862-001	-35.83	2.1283-001
5.8590+000	4.5407-001	-52.50	2.7643-001	2.6161-001	-37.80	2.1023-001
6.1380+000	4.5300-001	-56.33	2.5118-001	2.6363-001	-40.01	2.0588-001
6.4170+000	4.5380-001	-59.62	2.2447-001	2.6534-001	-43.05	1.9844-001
6.6960+000	4.5361-001	-62.40	2.1118-001	2.6955-001	-46.74	1.8999-001
6.9750+000	4.5399-001	-64.75	1.9365-001	2.7787-001	-50.86	1.8177-001
7.2540+000	4.5320-001	-66.86	1.7613-001	2.9144-001	-54.70	1.7598-001
7.5330+000	4.5234-001	-69.05	1.6173-001	3.0919-001	-57.85	1.7333-001
7.8120+000	4.4295-001	-71.17	1.4298-001	3.1740-001	-60.47	1.6639-001
8.0910+000	4.2696-001	-72.44	1.2683-001	3.4152-001	-62.43	1.6907-001
8.3700+000	0.0000+000	-90.00	1.1023-001	0.0000+000	90.00	6.4755-002

## SURFACE VELOCITIES BASED ON TANGENTIAL COMPONENTS

UPPER SURFACE				LOWER SURFACE			
Z	VELOCITY	ANGLE (DEG)	WZ	Z	VELOCITY	ANGLE (DEG)	WZ
-2.6921-010	1.5396-001	90.00	1.5396-001	3.3200-002	8.2697-002	-75.82	4.0178-002
3.3200-002	2.3852-001	75.82	2.2932-001	1.3965-001	4.8237-003	-60.68	4.2057-003
1.3965-001	2.8998-001	60.68	2.5283-001	3.5022-001	8.5141-002	-42.74	4.7785-002
3.4871-001	3.2046-001	44.59	2.2498-001	7.3531-001	1.5217-001	-29.23	7.4307-002
1.7758-001	3.5449-001	33.06	1.9339-001	1.3342-000	1.9768-001	-20.75	7.0033-002
1.3123-000	3.8710-001	13.60	9.1020-002	2.1824-000	2.5271-001	-12.22	4.3483-002
3.0690-000	4.0988-001	-11.57	-8.1419-002	3.4578-000	2.1587-001	-16.22	-4.0314-002
3.9447-000	4.2174-001	-22.23	-1.5954-001	4.1731-000	2.2115-001	-24.52	-3.1784-002
4.4880-000	4.4052-001	-30.27	-2.2203-001	4.6981-000	2.3675-001	-29.06	-1.1500-001
4.8891-000	4.4555-001	-36.94	-2.6778-001	5.1504-000	2.4942-001	-31.89	-1.3176-001
5.2107-000	4.4937-001	-42.34	-3.0268-001	5.5587-000	2.5649-001	-34.48	-1.4519-001
5.4813-000	4.5124-001	-46.76	-3.2670-001	5.9294-000	2.6221-001	-37.02	-1.5787-001
5.7163-000	4.5181-001	-50.40	-3.4611-001	6.2663-000	2.6407-001	-39.91	-1.6942-001
5.9251-000	4.5178-001	-53.44	-3.6288-001	6.5664-000	2.6684-001	-43.45	-1.8352-001
6.1138-000	4.5254-001	-56.01	-3.7522-001	6.8308-000	2.7265-001	-47.07	-1.9962-001
6.2862-000	4.5146-001	-58.15	-3.8348-001	7.0646-000	2.8178-001	-50.42	-2.1717-001
6.4461-000	4.5099-001	-59.94	-3.9032-001	7.2746-000	2.9323-001	-53.10	-2.3450-001
6.5958-000	4.5165-001	-61.45	-3.9675-001	7.4671-000	3.0367-001	-55.23	-2.4446-001
6.7369-000	4.5144-001	-62.77	-4.0139-001	7.6461-000	3.1523-001	-56.98	-2.6032-001
6.8708-000	4.5208-001	-63.92	-4.0603-001	7.8145-000	3.3101-001	-58.45	-2.8207-001
6.9984-000	4.5188-001	-64.93	-4.0431-001	7.9745-000	3.3509-001	-59.62	-2.8907-001
7.1206-000	4.5231-001	-65.84	-4.1270-001	8.1280-000	3.4303-001	-60.53	-2.9864-001
7.2378-000	4.5289-001	-66.73	-4.1803-001	8.2764-000	3.4797-001	-61.24	-3.0505-001
7.3502-000	4.5209-001	-67.60	-4.1799-001				
7.4577-000	4.5124-001	-68.45	-4.1471-001				
7.5608-000	4.4892-001	-69.27	-4.1586-001				
7.6598-000	4.4687-001	-70.05	-4.2006-001				
7.7547-000	4.4358-001	-70.78	-4.1885-001				
7.8460-000	4.3844-001	-71.38	-4.1549-001				
7.9347-000	4.3403-001	-71.84	-4.1242-001				
8.0213-000	4.2943-001	-72.21	-4.0889-001				
8.1061-000	4.2376-001	-72.48	-4.0411-001				
8.1898-000	4.1867-001	-72.68	-3.9970-001				
8.2726-000	4.1344-001	-72.82	-3.9499-001				
8.3549-000	4.1539-001	-72.89	-3.9702-001				
8.3700-000	3.8802-001	-90.00	-3.8802-001				

## b) Inlet Stagnation Point

Points B and G (Figure 2 of Reference 1) are at the inlet extremity with respect to the axial direction and, by the numerical treatment, the velocity is zero at both of these points. This does not consider that the location of the stagnation point depends on the angle of incidence and, with large incidence can deviate from point B by a notable amount. It appears that the effect of this approximation is to displace the upper and lower velocity curves in the region of the blade inlet, but without affecting the velocity curve downstream of the leading edge region.

The surface velocity plot, Figure 2.4.2-3, compares the calculation results for the G. E. blade with those by the G. E. report (Reference 2) and with those by the Westinghouse Electric analog. From the general agreement, it appears that the calculation is sufficiently accurate for its intended use in the boundary layer calculation.

## 2.4.4 Conclusions

The NASA computer program (Reference 1) specifies the blade surface velocity with sufficient accuracy for its intended use in the boundary layer calculation. This is shown by comparing the calculation results with those by two other methods of calculation (Figure 2.4.2.3).

## 2.4.5 References

1. A Computer Program for Calculating Velocities and Streamlines for Two-Dimensional, Incompressible Flow in Axial Blade Rows - Theodore Katsanis - NASA TN D-3762 January 1967.
2. Three Stage Potassium Test Turbine, Final Design, Vol. 1, Third Design - R. J. Rossbach, et al - NASA CR 72249.

## 2.5 COLLECTION OF CONDENSATE AND MOVEMENT OF CONDENSATE ON TURBINE SURFACES \*

### 2.5.1 Nomenclature for Section 2.5

A	Shear profile empirical constant
$A_1, A_3$	Blade geometric constants
a	Condensate fog particle deposition constant for blade concave surface
B	Shear profile empirical constant
b	Condensate fog particle deposition constant for blade nose
$C_D$	Fog particle drag coefficient
$C_f$	Wall friction drag coefficient, stator blade surface drag coefficient
d	Drop diameter, feet or microns
D	Turbine housing inside diameter, inches
E	Condensate particle collection efficiency
F	Indicates relationship between variables
F	Centrifugal force on liquid film on rotor blades - lb
$g_n$	A function of $K_{cn}$
G	Mass velocity of vapor, lb/hr-ft <sup>2</sup>

---

\* W. K. Fentress, Fellow Engineer, Development Engineering Dept., Steam Divisions, Westinghouse Electric Corp., Lester, Pa.; J. W. H. Chi, Fellow Engineer, Systems & Technology Dept., Astro-nuclear Laboratory, Westinghouse Electric Corp., Pittsburgh, Pa. 15236; W. D. Pouchot, Advisory Engineer, Systems & Technology Dept., Astro-nuclear Laboratory, Westinghouse Electric Corp., Pittsburgh, Pa. 15236.

$h$	Blade height, ft.	$R$	Gas Constant, ft/lb-°R
$K_{cc}$	Condensate fog particle inertial impaction parameter for collection on concave surface of blades	$Re$	Condensate particle Reynolds Number
$K_{cn}$	Condensate fog particle inertial impaction parameter for collection on nose of blades	$R_o$	Pipe or channel equivalent radius, ft or inches
$K_n$	Knudsen No. based on condensate fog particle radius	$S$	Pitch (spacing of blades around turbine periphery) of blades in a row, ft
$L$	Blade nose radius, ft	$T$	Absolute temperature, °R
$\dot{L}$	Mass velocity of collected condensate, lb/hr-ft <sup>2</sup>	$V_a$	Bulk flow axial flow velocity - ft/sec
$\ell_b$	Length of blade in radial direction, hub to tip	$U_L$	Mean longitudinal velocity of collected film, ft/sec
$\dot{m}_L$	Mass flow rate per unit of casing periphery or per blade, slugs/sec-ft, or mass flow rate - slugs/sec	$U_v$	Bulk flow velocity relative to casing, ft/sec
$m$	Total turbine mass flow rate, lb/sec	$U_t$	Bulk flow tangential velocity - ft/sec
$N_b$	Number of blades	$U^*$	Friction velocity, ft/sec = $\sqrt{\tau_s/\rho}$
$N_{re,v}$	Vapor Reynolds No.	$U$	Liquid film velocity on stator or rotor blades
$P_{cc}$	Portion of condensate fog particles collected on concave surface of blades in a given row	$V_a$	Condensate particle axial flow velocity, ft/sec
$P_{cn}$	Portion of condensate fog particles collected on nose of blade in a given row	$V_r$	Bulk flow velocity relative to blades at inlet of blade row, ft/sec
$q_b$	Liquid from condensate fog particles collected by a representative blade in a blade row per unit of blade height, lb/sec/ft.	$V_t$	Condensate particle tangential velocity - ft/sec
$Q_p, Q_L$	Total liquid collected by a given blade row in the form of bulk flow condensate fog particles, lb/sec.	$W$	Width of blade row in axial direction from inlet to exit, ft
$Q_L +$	Dimensionless liquid film flow rate : $\frac{\delta U_L}{\nu}$	$W_L$	Liquid flow rate, lb/sec, slugs/sec
$r$	Average condensate fog particle radius, microns or ft	$x_v$	Average quality of vapor in a blade row
		$X$	Circumference of turbine casing or axial distance, or geometric coordinate - ft/in.
		$Y$	Geometric coordinate - ft
		$Y_\ell$	Average fraction of mixture flow as condensate fog particles

Z	Axial width of blade measured along blade surface - ft, in.
$\mathcal{G}$	Blade geometry parameter, ft
$\alpha_i$	Angle between normal to turbine axis and stator inlet velocity vector, degrees
$\delta$	Condensate film thickness, inches, mils, or feet
$\delta^+$	Film parameter = $U^*/U$
$\zeta$	Inlet width of concave surface capture curve - ft
$\lambda$	A density parameter, dimensionless
$\mu_v$	Viscosity of vapor, lb/ft-sec or (lb-sec)/ft <sup>2</sup>
$\mu_L, \mu$	Viscosity of liquid, lb/ft-sec or lb-sec/ft <sup>2</sup>
$\nu$	Kinematic viscosity, $\mu/\rho$ , ft <sup>2</sup> /sec
$\rho$	Mixture bulk flow density, lb/ft <sup>3</sup> or slugs/ft <sup>3</sup>
$\rho_L, \rho_L$	Working fluid density as a liquid, lb/ft <sup>3</sup> or slugs/ft <sup>3</sup>
$\rho_v, \rho_G$	Working fluid density as a vapor, lb/ft <sup>3</sup> or slugs/ft <sup>3</sup>
$\tau_s$	Wall friction drag per unit area, lb/ft <sup>2</sup>
$\sigma$	Surface tension, lb/ft
$\varphi, \varphi_1, \varphi_2$	Indicates relationship
$\psi$	Surface tension parameter
$\omega$	Rotor rotative speed - radius/sec

## 2.5.2 Deposition of Moisture on the Surface of Blades

### • Single Row Collection

When the moisture in the bulk flow is in the form of small spontaneously formed condensate

particles (as in steam or alkali metal vapor turbines), the mechanism of deposition of moisture on blade surfaces is considered to be that of inertial impaction based on the macroscopic application of the laws of motion. In this we have followed Gyarmathy<sup>(1)</sup>. While deposition by diffusion of particles (Brownian motion and/or eddy diffusion) is recognized as a possible factor, inertial impaction is thought to warrant first consideration. Even between inertial impaction calculations, as between Gyarmathy and Brun et al<sup>(2)</sup>, there is substantial difference in numerical values which we have been unable to resolve.

The inertial deposition of moisture is considered to be principally on the inlet edge (nose) of the blades and on the concave face of the blades. Therefore by definition the inertial deposition on a single row of blades may be written as:

$$Q_{\ell} = m Y_{\ell} (P_{cn} + P_{cc})$$

### • Deposition on the Inlet Edge of the Blades

The analysis considers the nose of the blade as a circular cylinder. Thus the impingement of moisture particles is specified by the path of the particles when acted upon by the potential flow about a circular cylinder.

The path and impingement of particles with respect to circular cylinders, based on two-dimensional trajectory calculations and suitable drag coefficients, is given in a number of reports. In addition to Gyarmathy<sup>(1)</sup> NACA Report 1215 by Brun, et al<sup>(2)</sup>, for example. In the Brun report the data are shown by a non-dimensional plot in terms of the conventional inertia parameter (K), a Reynolds Number parameter, and the collection efficiency. (Collection efficiency is the ratio of the width of the free stream capture stream tube, within which all particles strike the cylinder, to the diameter of the cylinder).

In symbolic terms the efficiency of collection may be written:

$$E = \frac{2L}{2L} = \varphi(K_{cn}) = \varphi(K, Re) = \varphi\left(\left(\frac{2\rho_L r^2 V_r}{9\mu_v 2L}\right), Re\right) \quad (1)$$

or in the Stokes Law region applicable to these miniature moisture drops:

$$E = \varphi\left(\left(\frac{24}{C_D Re}\right) \left(\frac{2\rho_L r^2 V_r}{9\mu_v 2L}\right)\right) \quad (2)$$

As the flow about the miniature moisture drops is often in the slip flow regime, it is necessary to correct this formulation for the reduction in drag due to slip flow. Correction is made by multiplying the continuum value of the inertia parameter by the ratio ( $C_{D,slip flow}/C_D$ ) where  $C_D$  is the conventional drag coefficient for continuum flow. This correction is specified by an empirical expression in terms of Knudsen Number. As shown in Figure 2.5.2-1,

$$\text{Gyarmathy's expression, } \frac{C_{D,slip flow}}{C_D} = \frac{1}{1 + 2.53 K_n}$$

is a simple approximation to the more complicated Emmons<sup>(3)</sup> expression. As shown also by this curve, the drag on 0.4 micron radius drops under Yankee turbine conditions is only 45% of the continuum drag. In fact, the drag on particles will only approach continuum values at approximately 15 microns or greater radius.

Making the slip flow correction to equation 2 and observing that in the Stokes flow regime that

$$\frac{24}{C_D Re} = 1, \text{ yields:}$$

$$E = \varphi\left(1 + 2.53 K_n\right) \left(\frac{2\rho_L r^2 V_r}{9\mu_v 2L}\right) \quad (3)$$

By use of the relationship of equation 3, as established in numerical terms by Gyarmathy or Brun et al, the collection efficiency for the nose sections of a turbine row can be calculated. Collection efficiencies have been calculated for the noses of the ninth stator blade row, 3/4 blade height position of the Yankee steam turbine, and are shown in Figure 2.5.2-2. As can be seen the data of Gyarmathy predicts higher collection efficiencies than that of Brun et al.

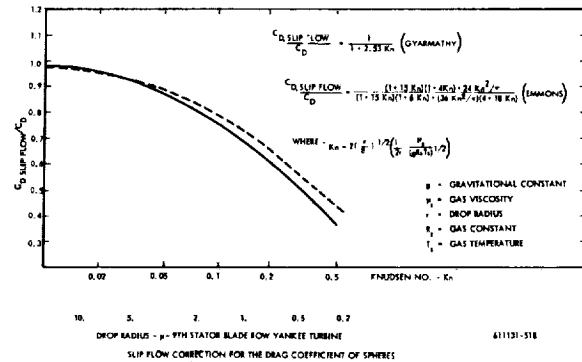


Figure 2.5.2-1 Knudsen Number Corrections

This difference cannot be explained by the fact that the Brun, et al, data account for the increase in Stokes law drag with Reynolds Number, as in this instance the fluid properties are nearly coincident with the Brun curve for zero Reynolds Number. Possibly, the difference could be explained by differences in trajectory calculation, but this calculation is not qualified in Gyarmathy's report.

The portion of the total number of condensate particles in the total flow which are collected by the noses of the blades of a given turbine row is given from simple geometric considerations, as indicated in Figure 2.5.2-3 as:

$$P_{cn} = \frac{2L'}{S \sin \alpha_i} = \frac{2LE}{S \sin \alpha_i} \quad (4)$$

Figure 2.5.2-3 also gives the calculated portion collected by the ninth stator noses of the Yankee turbine. It will be noted that the portion of the total drops collected by the noses of the blades of a row cannot exceed  $2L/S \sin \alpha_i$ .

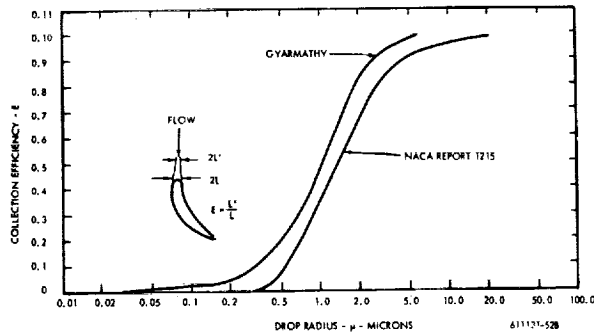


Figure 2.5.2-2 Collection Efficiency Ninth Stage Stator Nose Yankee Turbine

● Deposition of Moisture on the Concave Face of the Blade

Generally, the analysis is performed along the lines of Gyarmathy's (1) approach. The contour of the blade surface is approximated by a polynomial expression. The path of the vapor corresponds to the blade contour and the path of the particles, acted upon by the drag of the vapor, is calculated by trajectory equations. The drag on the particles is by Stokes law with correction for slip flow. By simplifying assumptions of constant vapor velocity with respect to the distance between blades and equal and constant moisture-particle axial velocity, the particle acceleration is described by a linear differential equation. By further assumptions as to boundary conditions, the integrated equation gives the width of the band at the blade inlet, within which all moisture particles impinged on the blade surface. Finally, the ratio of band width to the space between blades gives the amount of the collection with respect to the total moisture approaching the blades.

Thus, by the above assumptions, the collection of moisture is specified by closed form calculation. The detail derivation follows:

The concave surface of the blade is approximated by the third degree polynomial (see Figure 2.5.2-4)

$$F(x) = A_1 x + A_3 x^3 \quad (1)$$

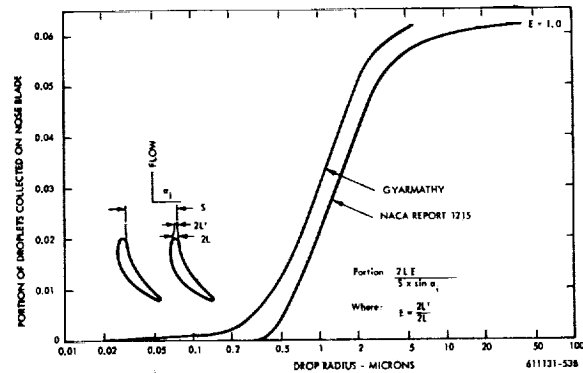


Figure 2.5.2-3 Portion Collected Ninth Stage Stator Nose Yankee Turbine

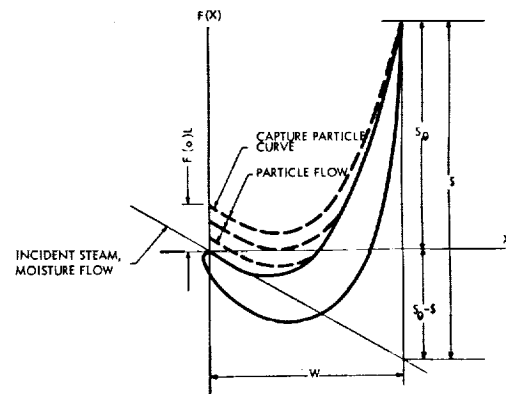


Figure 2.5.2-4 Collection of Moisture on the Concave Side of the Blade

The coefficients are specified by the inlet angle and the exit point as:

$$F'(0) = A_1 = (S_0 - \beta) / W \quad (2)$$

$$F(W) = S_0 - \beta + A_3 W^3 = S_0 ; A_3 = \beta / W^3 \quad (3)$$

Assume that the path of the steam is the same as the blade surface shape; then, the path and direction of the steam flow is:

$$F(x)_s = A_1 x + A_3 x^3 \quad (4)$$

$$F'(x)_s = A_1 + 3 A_3 x^2 \quad (5)$$



where constants  $A_1$  and  $A_3$  are as defined by equations 2 and 3, and the subscript  $s$  is for the vapor.

The path of the moisture particles is related to that of the vapor by the conventional trajectory equations:

$$\dot{V}_t = \frac{C_D R_e}{24} \frac{C_{D, \text{slip flow}}}{C_D} \frac{9 \mu_s}{2 r_L^2} (U_t - V_t) - \text{tangential} \quad (6)$$

$$\dot{V}_a = \frac{C_D R_e}{24} \frac{C_{D, \text{slip flow}}}{C_D} \frac{9 \mu_s}{2 r_L^2} (U_a - V_a) - \text{axial}$$

where  $U$  and  $V$  are the absolute vapor and particle velocity.

Assume that the vapor and particle axial velocity are equal and constant:

$$U_a = V_a = \text{const}$$

By this assumption the particle acceleration is described in equation 6, and noting that:

$$U_t = V_a F'(X)_s \quad (7)$$

$$V_t = V_a F'(X)_L \quad (8)$$

$$V_t = V_a^2 F''(X)_L \quad (9)$$

where subscripts  $v$  and  $L$  are for vapor and moisture particles. By substituting in equation 6:

$$W F''(X)_L = (1/K_c) (F'(X)_s - F'(X)_L) \quad (10)$$

where  $K_{cc}$ , the inertia parameter, is as follows:

$$K_c = \frac{24}{C_D R_e} \frac{C_D}{C_{D, \text{slip flow}}} \frac{2 r_L^2 V_a}{9 \mu_s W} \quad (11)$$

Substituting in equation 5 yields:

$$W F''(X)_L + (1/K_c) F'(X)_L = (1/K_c) (A_1 + 3 A_3 X^2) \quad (12)$$

This is the final differential equation of motion for the moisture particles.

Integrating equation 12 gives the following general solution:

$$F(X)_L = C_1 + C_2 e^{-X(W/K_c)} + A_3 X^3 - 3 A_3 W K_c X^2 - (A_1 + 6 A_3 W^2 K_c^2) X - W K_c (A_1 + 6 A_3 W^2 K_c^2) \quad (13)$$

Constants  $C_1$  and  $C_2$  are determined by the following boundary conditions:

1) the direction of flow of the vapor and moisture particles is the same at the blade inlet position; thus, by equation 5,  $F'(o)_L = F'(o) = A_1$ .

2) the end point position of the capture particle curve is coincident with the blade surface point at the trailing edge; thus by equation 3,  $F(W)_L = F(W) = S_\theta$ .

Solving for  $C_1$  and  $C_2$  and substituting in equation 13 gives the following equation for the capture particle curve:

$$F(X)_L = 6 A_3 W^3 K_c^3 (1 - e^{-1/K_c}) + A_3 (X^3 - W^3) - 3 A_3 K_c W (X^2 - W^2) + (A_1 + 6 A_3 K_c^2 W^2) (X - W) + S_\theta \quad (14)$$

The inlet width of the capture band is specified by the value of equation 14 for the inlet of blade as:

$$F(o)_L = 6 A_3 K_c^3 W^3 (1 - e^{-1/K_c}) - A_3 W^3 + 3 A_3 K_c W^3 - (A_1 + 6 A_3 K_c^2 W^2) W + S_\theta \quad (15)$$

Substituting for  $A_1$  and  $A_3$  (equations 2 and 3) in equations 14 and 15 gives the final equations for the capture particle curve and for the referred inlet width of the band.

$$F(X)_L / S = 6 K_c^3 (e^{-(1/K_c)} (X/W) - e^{-1/K_c}) + (X/W)^3 - 3 K_c (X/W)^2 + ((S_\theta/S) + 6 K_c^2 - 1) (X/W) + 3 K_c - 6 K_c^2 \quad (14a)$$

$$F(o)_L / S = 6 K_c^3 (1 - e^{-1/K_c}) - 6 K_c^2 + 3 K_c \quad (15a)$$

$$F(o)_L / S \approx 3 K_c : K_c < .03 \approx 3 K_c - 6 K_c^2 : K_c < .10 \quad (15b)$$

where the inertia parameter  $K_{cc}$  is:

$$K_c = \frac{24}{C_{D,R_e}} \frac{C_D}{C_{D, \text{slip flow}}} \frac{2 \rho_L r^2 V_a}{9 \mu_s W}$$

Note that the referred inlet width of the band is, in effect, the referred collection efficiency.

The above equations consider the blade surface shape as by a third degree polynomial. A similar development assuming the surface as by a second degree polynomial gives the following equation for the inlet referred width of the capture band:

$$F(o)_L / \xi = 2 K_c^2 (e^{-1/K_c} - 1) + 2 K_c \quad (16)$$

$$F(o)_L / \xi \approx 2 K_c : K_c < .05 \quad (16a)$$

where  $K_{cc}$  is as before.

Equations 15a and 16 are plotted and shown in figure 2.4.2-5.

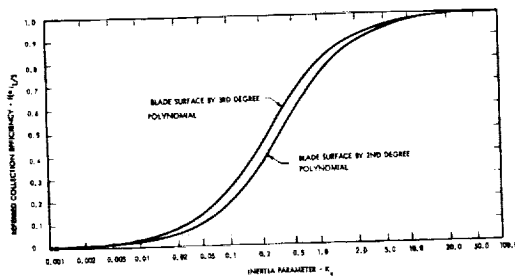


Figure 2.5.2-5 Referred Collection Efficiency on the Concave Side of the Blade

The calculation of collection drops on the concave side of the Yankee turbine ninth stator blade is illustrated by the following point calculation:

Moisture drop size: 0.4 micron radius =  $1.311 \times 10^{-6}$  ft radius

Fluid Properties:  $\rho_L = 1.935$  slugs/ft<sup>3</sup>,  $\mu_v = 2.4 \times 10^{-7}$  lb-sec/ft<sup>2</sup>,  $V_a = 456$  ft/sec

Blade geometry:  $W = 0.715$  ft,  $\xi = 0.566$  ft,  $S = 0.485$  ft

Inertia parameter:

$$K_c = \frac{24}{C_{D,R_e}} \frac{C_D}{C_{D, \text{slip flow}}} \frac{2 \rho_L r^2 V_a}{9 \mu_s W} = .00445$$

where:

$$\frac{24}{C_{D,R_e}} = 1, \text{ assuming Stokes' law drag}$$

$$\frac{C_D}{C_{D, \text{slip flow}}} = 1/.44 = 2.275 \quad (\text{Figure 2.5.2-1})$$

The blade surface shape in this instance is closely approximated by the average between a 2 and 3 degree polynomial. Hence, the referred efficiency is specified by the average curve value, or by the average of equations 15b and 16a:

$$F(o)_L / \xi = 2.5 K_c = .0111$$

The inlet width of the capture curve

$$\xi = (F(o)_L / \xi) \xi = .00629 \text{ f}$$

The portion of drops collected with respect to the total number approaching the blade is the ratio of the band width to the blade pitch.

$$\text{Portion} = \xi / S = .013$$

Calculation results for the Yankee steam turbine are shown in figure 2.5.2-6. This figure gives the portion of moisture collected as a function of drop size. As shown by the curve sketch, the portion collected is specified by the inlet width of the band ( $\xi$ ), within which all particles impinge on the blade with respect to the blade pitch. The band width cannot exceed the space between blades (pitch minus inlet edge blockage) which accounts for the break in the curve at 93.5 percent. Collection by Gyarmathy's data is 20 percent less in the range  $< 0.4$  micron drop radius. The difference is due to the fact that Gyarmathy specifies the blade shape by a quadratic expression compared to a higher order curve fit which, in this instance, better matches the blade.

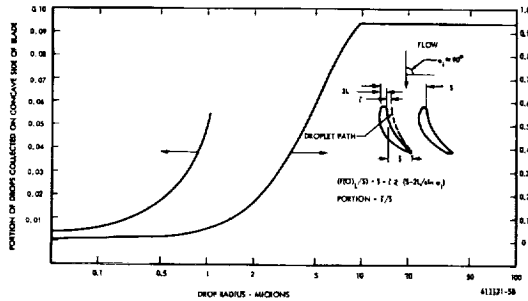


Figure 2.5.2-6 Portion Collected; Concave Side, Ninth Stator Yankee Turbine

### • Simplified Model of Single Row Collection

The general collection analysis does not give a completely closed form result.

The foregoing analysis has been recast by approximations to give a closed form result which may be more useful in making observations about turbine moisture collection.

Following Section 2.5.2.1 the expression for inertial deposition on a single row of turbine blades is:

$$Q_\ell = m Y_\ell (P_{cn} + P_{cc}) \quad (1)$$

where

$$P_{cn} = \frac{2L}{5 \sin a_i} \varphi_1 (K_{cn}) = \frac{2L}{5 \sin a_i} \varphi_1 (1 + 2.53 Kn) \left( \frac{2e_g r^2 v_r}{9 \mu_v 2L} \right) \quad (2)$$

$$P_{cc} = \frac{g}{5} \varphi_2 (K_{cc}) = \frac{g}{5} \varphi_2 (1 + 2.53 Kn) \left( \frac{2e_g r^2 v_r}{9 \mu_v W_r} \right) \quad (3)$$

Equation 1 may be written, using continuity of flow, for collection of condensate fog particles on a single blade as

$$q_b = \frac{Q_\ell}{N_b \ell b} = e S V_a Y_\ell (P_{cn} + P_{cc}) \quad (4)$$

and since

$$e Y_\ell = e_v \left( \frac{1 - x_v}{x_v} \right) \quad (5)$$

then

$$q_b = e_v S V_a \left( \frac{1 - x_v}{x_v} \right) (P_{cn} + P_{cc}) \quad (6)$$

From numerical examinations of concave surface collection it can be observed that for the range of condensate particle sizes likely to be encountered in turbines (for concave surface collection),

$$\varphi_2 (K_{cc}) \sim a K_{cc} \quad (7)$$

where  $a$  is the order of the polynomial expression needed to adequately describe the boundary of a tangential cross section of the concave surface of a particular blade in rectangular coordinates.

It can also be observed from numerical examination of the blade nose collection that, if the particle radius is between 0.4 and 2 microns in large steam turbines, a good approximation for nose collection is

$$\varphi_1 (K_{cn}) \sim b K_{cn} \quad (8)$$

where  $b$  is a constant.

Substitution of Eq. 8 in Eq. 2 and Eq. 7 in Eq. 3 with further substitution of these results in Eq. 6 and simplifying and rearranging gives

$$q_b \approx \frac{e_g \bar{r} v_r (1 + 2.53 K_n)}{9} \left( \frac{2e_g \bar{r} v_r}{\mu_v} \right) \left( \frac{1 - x_v}{x_v} \right) \left[ b + a \frac{g}{W_r} \sin^2 a_i \right] \quad (9)$$

One of the more interesting observations which can be made from Eq. 9 is that the amount of moisture collected ( $q_b$ ) per unit of blade height is independent of blade size for geometrically similar blade tangential cross sections.\* This says that between two turbine blade rows of equal height and geometrically similar tangential cross sections, the row with the smallest blade chords will collect the most total moisture when operating under the same working fluid conditions. If the smaller row has a chord one-half that of the larger, the moisture collected by the larger will be one-half that collected by the smaller, i.e., the same collection per blade but half as many blades in the larger row for geometrically similar tangential cross sections.

\*The cross section in a plane with one direction generally in the turbine axial direction and the other direction normal to corresponding diameters at the blade row inlet and exit stations.

The foregoing conclusion offers a definitive experimental way to check the basic premise that the dominant mechanism of collection is by inertial impaction rather than by eddy or molecular diffusion. Deposition by diffusion is proportional to the surface area, and the surface areas of the two hypothetical blade rows are equal.

A corollary to the Eq. 9 observations is that, other things being equal, big turbines could collect proportionately less moisture than small turbines and the amount of damaging impact liquid per unit of exposed rotor blade surface will reduce with an increase in turbine size.

The Knudsen number  $K_n$  in Eq. 9 is defined by

$$K_n = \frac{0.6275 \mu_v}{r \rho_v \sqrt{g_c R T}} \quad (10)$$

With  $\mu_v$  in lb/ft-sec,  $r$  in microns,  $\rho_v$  in lb/ft<sup>3</sup>, and  $T$  in °R, Eq. 2 becomes

$$K_n = \frac{5.35 \times 10^3 \mu_v}{\rho_v r \sqrt{T}} \quad (11)$$

Substituting Eq. 11 into Eq. 9, using the same set of units as for Eq. 11, yields

$$q_b = 2.36 \times 10^{-12} \rho_v \bar{r} V_r \left( 1 + \frac{1.354 \times 10^4 \mu_v}{\rho_v \bar{r} \sqrt{T}} \right) \left( \frac{\rho_v \bar{r} V_r}{\mu_v} \right) \left( \frac{1 - x_v}{x_v} \right) \left( b + a \frac{g}{W_r} \sin^2 \alpha_i \right) \quad (12)$$

where  $q_b$  is in lb/ft-sec and  $V_r$  is in ft/sec.

Let  $N_b$  = number of blades per row, and  $h$  = blade height in feet; then, the total amount collected per row is given by

$$Q_L = 2.36 \times 10^{-12} \rho_v \bar{r} V_r h N_b \left( 1 + \frac{1.35 \times 10^4 \mu_v}{\rho_v \bar{r} \sqrt{T}} \right) \left( \frac{\rho_v \bar{r} V_r}{\mu_v} \right) \left( \frac{1 - x_v}{x_v} \right) \left[ b + a \left( \frac{g}{W_r} \right) \sin^2 \alpha_i \right] \quad (13)$$

The constant  $a$  in Eq. 13 was taken to be 2.5. The constant  $b$  was evaluated from Gyarmathy's calculations<sup>(1)</sup>, from which it was determined that

$$g_n = \phi (K_{cn}) = \frac{b}{2 K_{cn}} \quad (14)$$

where  $b$  is approximately equal to unity.\* For some Westinghouse-type turbine geometries,  $g/W_r = 1.0$  for stators, and  $g/W_r = 1.25$  for rotors.

Substituting these values into Eq. 13 for stators:

$$Q_L = 2.36 \times 10^{-12} \rho_v \bar{r} V_r h N_b \rho_v \left( 1 + \frac{1.354 \times 10^4 \mu_v}{\rho_v \bar{r} \sqrt{T}} \right) \left( \frac{\rho_v \bar{r} V_r}{\mu_v} \right) \left( \frac{1 - x_v}{x_v} \right) (1 + 2.5 \sin^2 \alpha_i) \quad (15)$$

and for rotors:

$$Q_L = 2.36 \times 10^{-12} \rho_v \bar{r} V_r h N_b \rho_v \left( 1 + \frac{1.354 \times 10^4 \mu_v}{\rho_v \bar{r} \sqrt{T}} \right) \left( \frac{\rho_v \bar{r} V_r}{\mu_v} \right) \left( \frac{1 - x_v}{x_v} \right) (1 + 3.125 \sin^2 \alpha_i) \quad (16)$$

#### • Comparison of Experimental and Calculated Moisture Collection

A. Smith of Parsons Company has published the results of water extraction tests on a scale model of a Parsons steam turbine.<sup>(4)</sup> These tests were run on a four-stage machine with the water extraction between the third and fourth stages. The theoretical amount of moisture present at the exit of the third stage was varied by changing the amount of superheat in the vapor at the turbine inlet. Smith's data are shown as X's in Figure 2.5.2-7. This is a plot of theoretical moisture against the portion of the theoretical moisture collected. Superimposed on this figure is a curve representing theoretical calculations of the portion of moisture which would be collected by the Yankee steam turbine ninth stage stator if the turbine were operated to provide the varying amounts of theoretical moisture. In addition, the conditions and geometry are also adjusted to make the Wilson Point (at some location ahead of the ninth stator) occur at a value of  $\{1/P\} dp/dt$  of pressure and  $dp/dt$  is the rate of change of this pressure with time at the Wilson Point.

\* The numerical value of  $b$  will be different from that for other turbines and operating conditions.

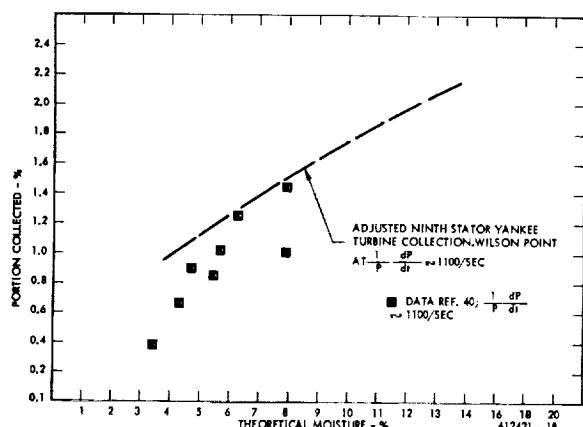


Figure 2.5.2-7 Calculated and Experimental Turbine Moisture Collection

The only "real" point on the calculated curves is that marked at 13.5% theoretical moisture, (1) considering the actual operation conditions and geometry of the Yankee turbine. If a line is drawn from this point through Smith's data, there is apparently excellent agreement. However, the calculations are for collection on a single turbine row, whereas Smith's data represent collection on a varying number of turbine rows and fractions thereof. That is, the Wilson Point in Smith's turbine is moving toward the front end of the turbine as the amount of theoretical moisture available at the third stage exit rises. Therefore, the collecting surface area subject to the condensing region is increasing. The moisture collected at the drain port between third and fourth stages probably represents that collected on less than one row for 3% theoretical moisture and on up to two or more rows for 8% theoretical moisture. This explains why the slope of the data points is substantially greater than the slope of the calculated lines. If the drain ports in Smith's experimental turbine are catching nearly all of the moisture collected on the blades and if the blade sections, spacing, and amount of turning of the experimental turbine rows are quite similar to that of the ninth stator of the Yankee turbine, then the theories of condensate spontaneous nucleation and deposition (taken together) somewhat over-estimate the actual amounts of moisture being collected in steam turbines. However, in the absence of definite knowledge on these points, no change in the present steam models of spontaneous nucleation and collection is indicated.

### 2.5.3 Movement of Moisture on Blade Surfaces

#### ● Movement on Rotor and Stator Blades

The movement of collected moisture over the blade surfaces is not a critical part of the overall erosion model with respect to numerical precision. The main value of the analysis is in pointing out certain variables which may be neglected and in the added qualitative understanding of one of the sequences of events leading to turbine blade erosion. A most important conclusion which can be drawn from the analysis is that the carryover of collected moisture from stage to stage will be negligible in a well-drained turbine because the flow of liquid on the rotor blades is essentially radial. The liquid is therefore slung from the tip against the outer casing and can be efficiently collected by suitable drain slots. Another conclusion is that the liquid flow on the stators is essentially along the vapor streamlines.

In this analysis, it is assumed that the collected moisture forms a continuous film controlled by the laws of viscous flow. Generally, the thickness and velocity of the moisture film are based on the force balance between the viscous shear of the film, vapor stream friction, and centrifugal force. The force on such a film from the radial pressure gradients in the turbines examined is small compared to the other forces mentioned. It is also assumed that the moisture collects only on the concave side of the blades for purposes of numerical calculation. (Collection on the convex sides through the action of secondary flows is neglected.) This is a conservative assumption since it places a higher liquid load per unit of surface on the blade than is probably actually present. Since different procedures are involved for the stator and rotor blade calculations, the discussion is by separate topics.

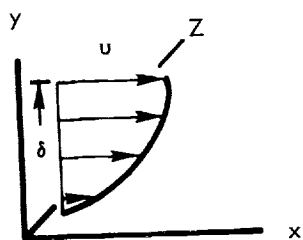
#### ● Rotor Blade Moisture Transport Model & Results

The main equation, based on the Navier-Stokes equations, relates the centrifugal force to the viscous shear of the film. This assumes that the flow is in the radial direction and is only acted

upon by the centrifugal force. The error in this assumption is shown by calculating the axial force on the film (due to steam friction) and the axial film velocity for the ninth stator of the Yankee turbine.

Assuming 2 percent moisture collection, the axial velocity is 0.88 fps compared to 6.5 fps velocity in the radial direction, corresponding to a 7.8 degree angle of flow with respect to the radial direction. Assuming the flow is in the radial direction only and disregarding the low order terms, the Navier-Stokes equations reduce to:

$$F = -\mu \frac{\partial^2 u}{\partial y^2}$$



611131-56B

where the body force F is the centrifugal force.

Integration with boundary conditions as specified by a parabolic velocity distribution gives:

$$\frac{F y^2}{2} - F \delta y = -\mu u \quad (1)$$

The mass flow and velocity are specified by continuity as:

$$\begin{aligned} d\dot{m}_L &= \rho_L Z u dy \\ u &= \frac{1}{\rho_L Z} \frac{d\dot{m}_L}{dy} L \end{aligned} \quad (2)$$

Combining (1) and (2) and integrating force gives:

$$\frac{F \delta^3}{3} = \frac{\mu}{\rho_L Z} \dot{m}_L$$

Substituting for the centrifugal force:  $\rho_L \omega^2 r$  gives the final expression for  $\delta$  at the tip of the blade:

$$\delta = \left( \frac{3 \mu_L \dot{m}_L}{Z \rho_L^2 r \omega^2} \right)^{1/3} \quad (3)$$

$$\bar{u} = \frac{\dot{m}_L}{\rho_L Z \delta} = \left( \frac{\dot{m}_L^2 r \omega^2}{3 \rho_L Z^2 \mu_L} \right)^{1/3} \quad (4)$$

This assumes that the flow is uniformly distributed over the surface of the blade.

The calculation also assumes a parabolic velocity distribution with film thickness. The latter assumption is for calculation purposes and could be improved upon by detailed investigation of the amount and distribution of moisture. As to the width of the film, the film thickness and mass average velocity at the tip of the blade are inversely proportional to the 1/3 power and 2/3 power of the film width respectively; thus, the film thickness and mass average velocity would be 1.26 and 1.59 times the calculated values, for full width, if the film extended over half the width of the blade. In the case of radial distributions, with a triangular distribution of film thickness along the height of the blade, the centrifugal force F would be roughly 0.58, the film thickness 1.2, and the velocity 0.83 times the calculated values for constant radial thickness. As to the moisture flow ( $\dot{m}_L$ ), the film thickness and velocity are directly proportional to the 1/3 power and 2/3 power of the flow.

TABLE 2.5.3-1

#### YANKEE TURBINE, EIGHTH ROTOR LIQUID FLOW

$\epsilon$	$\dot{m}_L \times 10^4$ $\frac{p-v}{f}$	$\delta \times 10^{-5}$ $\frac{f}{f}$	$\bar{u}$ fps	$Re_L$
0.005	0.215	1.59	2.58	7.65
0.010	0.43	2.02	4.11	15.3
0.020	0.86	2.52	6.49	30.6
0.050	2.15	3.44	12.0	76.5
0.100	4.30	4.31	18.9	153.0

Using the expressions just developed, parametric calculations for the eighth rotor of the Yankee steam turbine were carried out. The results

are shown in Table 2.5.3-1. The parameter varied is the fraction ( $\epsilon$ ) of equilibrium moisture collected since this quantity depends upon inputs from the rest of the model. Note that the film velocity ( $\bar{u}$ ) is the mass average at the tip of the blade.

#### ● Stator Blade Moisture Transport Model & Results

The main equation, based on the viscosity expression, relates the viscous shear to the axial force due to the steam friction drag and the impingement of the moisture particles. It is assumed that there is a linear velocity distribution with film thickness and that the flow per unit blade height (at the 3/4 section) is the average unit flow along the height of the blade. This assumption could be improved upon by detailed investigation of the radial distribution. The viscous shear in the liquid film is given by:

$$\tau = \mu_L \frac{\partial u}{\partial y}$$

assuming a linear velocity distribution:

$$\tau = \mu_L \frac{u_{\max}}{\delta} = \frac{2\mu_L \bar{u}}{\delta} \quad (5)$$

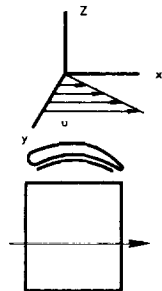
where  $\delta$  and  $\bar{u}$  are the film thickness and mass average velocity. The flow of liquid is by continuity:

$$\dot{m}_L = \rho_L Z \delta \bar{u}$$

and

$$\frac{\dot{m}_L}{\bar{u}} = \frac{\dot{m}_L}{\rho_L Z \delta} \quad (6)$$

at the blade exit position assuming that the flow is evenly distributed over the distance Z (see sketch that follows).



Combining (5) and (6) gives

$$\delta = \left( \frac{2 \dot{m}_L \mu_L}{\rho_L Z \tau} \right)^{1/2} \quad (7)$$

The viscous shear on the film is due to the drag of the vapor and the force of the impinging drops, i.e.,

$$\tau = C_f \rho_S \frac{V_S^2}{2} + \frac{\dot{m}_L}{Z X} V_S \quad (8)$$

where the boundary layer friction coefficient ( $C_f$ ) in the region of the trailing edge is specified as:

$$C_f = 2 \times 0.123 \times 10^{-0.678 H \left( \frac{\sqrt{\theta} \rho}{\mu} \right)^{-0.268}} \quad (\text{Schlichting}) \quad (9)$$

where  $\theta$  and  $H$  are boundary layer parameters.

Equations (7) and (8) may be combined to give:

$$\delta = \left( \frac{2 \dot{m}_L \mu_L}{\rho_L Z} \frac{1}{\tau + \frac{\dot{m}_L V_S}{X Z}} \right)^{1/2} \quad (10)$$

The film Reynolds Number is by definition:

$$Re_L = \bar{u} \delta \rho_L / \mu_L \quad (11)$$

Note that the axial force by the drag of the vapor is specified by the wall shearing stress of the boundary layer. The axial force due to the momentum of the impinging drops depends on the amount of the collection: for 1/2, 2, and 10 percent collection, the momentum force is roughly 5, 20, and 100 percent of the vapor drag force ( $\tau$ ).

As the amount of moisture collected depends on inputs from the other parts of the program, calculated film properties are, with respect to the amount of equilibrium moisture collected, designated as  $\epsilon$ . Results for the Yankee steam turbine ninth stator are given in Table 2.4.3-2, following. As shown, the film thickness and velocity are roughly proportional to the square root of  $\epsilon$ , when  $\epsilon$  is less than 0.05. The velocity ( $\bar{u}$ ) is the mass average value at the trailing edge of the blade.

TABLE 2.5.3-2  
YANKEE STEAM TURBINE, NINTH STATOR  
LIQUID FLOW

$\epsilon$	$h_L \times 10^4$ $p-x/f$	$\delta \times 10^5$ $f$	$\bar{u}$ $f_{ps}$	$Re_L$
0.005	0.63	2.58	0.404	1.55
0.010	1.26	3.56	0.585	3.1
0.020	2.53	4.81	0.869	6.23
0.050	6.30	6.75	1.54	15.5
0.100	12.6	8.22	2.54	31.0

From limited data (Gardner<sup>(5)</sup>, Baker<sup>(6)</sup>) it appears that there are ripples on the surface of the film when the film Reynolds Number ( $Re_L$ ) is greater than 4, corresponding to  $\epsilon$  greater than roughly 1 percent. These ripples probably affect the size of the drops from the blades as discussed in Section 2.7 under atomization.

#### 2.5.4 Collection on Turbine Casing\*

##### • Background

In conventional (steam) wet vapor turbine designs, the moisture leaving the turbine vanes and collecting on the turbine casing is removed by slots in the casing. The design of alkali metal vapor turbines might be considerably simplified if slots were unnecessary. However, if an appreciable amount of condensate collects on the turbine casing and is not removed, casing and rotor blade seal strip erosion may result. A rudimentary examination of casing flows for the cesium and potassium turbines design of NAS 5-250\* is reported in the following paragraphs.

##### • Condensate Collection on the Turbine Casing

It is expected that essentially all of the liquid collected on the turbine blades ends up on the turbine casing because of the centrifugal action of the turbine rotors. The drops formed departing the rotor blade tips impinge on the turbine casing. Along the turbine stages, a liquid film builds up on the turbine casing. The impingement of liquid drops

on the condensate film probably causes splashing and some removal of the liquid from the film. However, the net amount of condensate collected on the casing cannot be easily estimated; therefore, it is assumed that all of the condensate impinging on the turbine casing is collected. The amount of fog particles collected per turbine blade per unit blade height can be estimated by use of equations 15 and 16 of Section 2.5.2, and it is assumed that this same amount impinges and collects on the turbine housing.

The calculation of the amount of moisture collected per stage required an iteration procedure. The total condensed moisture was used to initiate the calculations. From these values, the average moisture content was calculated, from which the term  $(1 - x_v)/x_v$  was calculated. The condensate collected was then calculated from equation 15 or 16. The amount collected was then subtracted from the total condensate to yield the moisture content of the vapor. The calculations converged rapidly, however. The results of the calculations for the six-stage potassium turbine and the two-stage cesium turbine are presented in Tables 2.5.4-1 and 2.5.4-2 respectively.

TABLE 2.5.4-1  
MOISTURE COLLECTION ON TURBINE HOUSING  
SIX-STAGE POTASSIUM TURBINE

Row Number	Net Collection Efficiency (%)	Effective Moisture	$Q_{v, Net}$ (lb/sec)	Cumulative Condensate Collected (lb/sec)
3R	0.12	0.0005	$3.6 \times 10^{-6}$	$3.6 \times 10^{-6}$
4S	0.83	0.040	0.0019	0.0019
4R	1.55	0.088	0.0078	0.0097
5S	1.60	0.107	0.0098	0.0195
5R	1.76	0.119	0.0121	0.0316
6S	1.90	0.127	0.0139	0.0555
6R	0.78	0.136	0.0061	0.0616

Final percentage of total moisture collected is 7.8%

TABLE 2.5.4-2  
MOISTURE COLLECTION ON TURBINE HOUSING  
TWO-STAGE CESIUM TURBINE

Row Number	Net Collection Efficiency (%)	Effective Moisture	$Q_{v, Net}$ (lb/sec)	Cumulative Condensate Collected (lb/sec)
1S	0.04	0.011	$9.1 \times 10^{-5}$	$9.1 \times 10^{-5}$
1R	0.55	0.059	$3.3 \times 10^{-4}$	$4.2 \times 10^{-4}$
2S	0.62	0.122	0.0011	0.0015
2R	0.34	0.153	0.0016	0.0031

Final percentage of total moisture collected is 0.106%

\*See Section 1.2.3 for additional detail on the turbines.



The last two columns of the tables give, respectively, the total condensate collected on each row and the cumulative condensate collected on the turbine housing. It is seen that, for the six-stage potassium turbine, 7.8 percent of the total moisture content eventually collected on the turbine housing. In comparison, the percentage of the total moisture collected on the cesium turbine housing is 0.106 percent. The significantly smaller amount of moisture collected on the cesium turbine housing is due to the fact that fewer stages are required for the cesium turbine.

The estimated moisture collection may be conservative since it was assumed that impingement of liquid droplets on the condensate film and the resulting splashing does not cause a net removal of the condensate; consequently, the actual collection may be less than that indicated by the calculated results.

#### ● Stability of Condensate Collected on the Turbine Casing

In addition to the possibility of condensate removal by splashing, there is also the possibility that under the given hydrodynamic conditions the liquid film may be unstable and the condensate may be removed by shear forces at the vapor-liquid interface. In an attempt to resolve this question, the mode(s) of two-phase flow expected under the given conditions are related to the two-phase flow map of Baker.<sup>(38)</sup> Baker presents a map showing regions of various modes of two-phase flow as functions of two-phase flow parameters. Baker's map is reproduced in Figure 2.5.4-1. The map consists of a plot of the logarithm of  $G/\lambda$  versus the logarithm of  $L\lambda\psi/G$ , where  $G$  and  $L$  are the vapor and liquid mass velocities, respectively. Here,  $\lambda$  is a density parameter defined as

$$\lambda = \left[ \left( \frac{\rho_G}{0.075} \right) \left( \frac{\rho_L}{62.3} \right) \right]$$

and  $\psi$  is a surface tension parameter defined by

$$\psi = \frac{73}{\sigma_L} \left[ \mu_L \left( \frac{62.3}{\rho_L} \right)^2 \right]^{1/3}$$

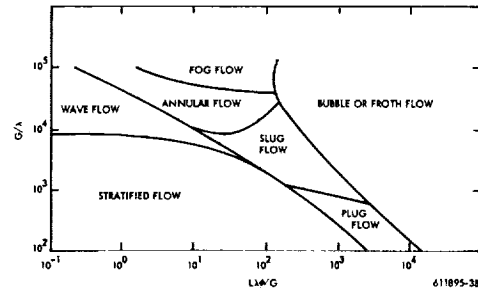


Figure 2.5.4-1 Baker's Map of Two-Phase Flow

Calculations for the various stages of the two turbines give values of  $G/\lambda$  on the order of  $10^3$  and values of  $L\lambda\psi/G$  less than  $10^{-2}$ . As can be seen, these values are out of the range from Baker's map. An "eyeball" extrapolation of the map would place the flow in the wave flow regime. Such an extrapolation is, of course, not trustworthy. In wave flow, it is expected that some of the wave crests would be carried away into the vapor. If annular flow prevails, substantial removal of liquid from the casing film is expected. If fog flow is present, then all of the liquid film would be entrained in the vapor as fog. About the best that can be concluded at this time is that some dispersion of the casing liquid is indicated.

#### ● Condensate Film Thicknesses on the Turbine Housings

The condensate film thicknesses on the turbine housings were estimated by the theory of Wrobel and McManus.<sup>(7)</sup> These investigators analyzed the film depth and wave height in annular two-phase flow and derived an equation relating the film depth to the film flow rate and the gas Reynolds number. The results checked reasonably well with the limited available data. The complete equation of Wrobel and McManus is

$$\frac{\delta}{R_o} \left( 1 + \frac{2R_o}{R_o} - \frac{3\nu_L}{\nu_v} \frac{Q_L^+}{N_{re,v}} \right) \left[ \ln \left( 2.95 \frac{(R_o/\delta) - 1}{1 - 10/\delta} \right) \right]^{-1} N_{re,v} = \frac{\nu_L}{\nu_v} \left( \frac{\rho_L}{\rho_v} \right)^{1/2} \frac{B}{A} (24)^{1/2} \left( Q_L^{+2} + 2A Q_L^+ \right)^{1/2} \quad (12)$$

where  $Q_L^+$  is the dimensionless liquid flow rate given by

$$Q_L^+ = \frac{\delta U_L}{\nu} \quad \text{and} \quad \delta^+ = \frac{U^*}{\nu}$$

where  $Q_L^+$  is the dimensionless liquid flow rate given by with  $U^*$  the friction velocity  $\sqrt{\tau_s/\rho}$ .

The constants A and B in Eq. (12) depend on the shear profile assumed. For a constant shear profile, A = 265 and B = 17.9.

From continuity,

$$W_L = \pi D e_L \delta U_L \quad (13)$$

where  $U_L$  is the mean film velocity, and D is the local turbine casing inside diameter. From Eq. (13)

$$\delta U_L = \frac{W_L}{\pi D e_L} \quad (14)$$

whence

$$Q_L^+ = \frac{\delta U_L}{\nu} = \frac{W_L}{\pi D \mu_L} \quad (15)$$

with

$$\delta^+ = 10 + 28 \left( \frac{e_v}{e_L} \right)^{1/2} \left( \frac{\nu_v}{\nu_L} \right)$$

The condensate flow rates are based on the turbine casing inside diameter. Parametric curves for the film height are presented in Figures 2.5.4-2 and 3. Estimates on the depth of liquid film on the potassium and cesium turbines of NAS 5-250 are given in Tables 2.5.4-3 and 4.

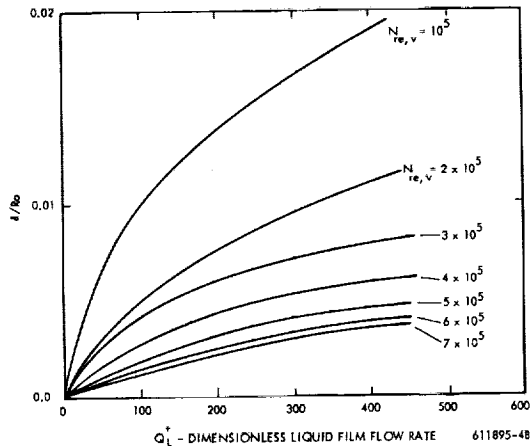


Figure 2.5.4-2 Effect of Condensate Film Reynold's Number on Film Thickness

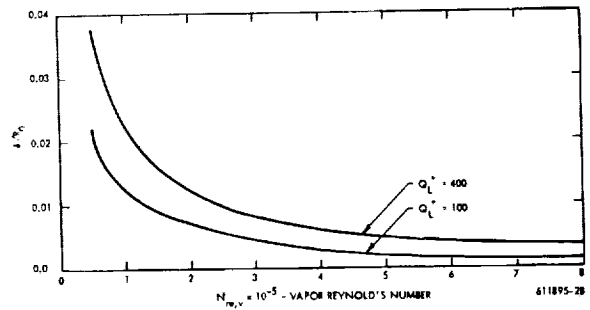


Figure 2.5.4-3 Effect of Vapor Reynold's Number on Film Thickness

TABLE 2.5.4-3

ESTIMATED CONDENSATE FILM DEPTH ON TURBINE HOUSING SIX-STAGE POTASSIUM TURBINE

Blade Row Exit	Cumulative Condensate Flow Rate (pps)	$Q^+$	$N_{re,v} \times 10^{-5}$	$e/r_o \times 10^4$	$\delta$ (mils)
3R	$3.6 \times 10^{-6}$	0.028	5.12	0.071	0.006
4S	$1.89 \times 10^{-3}$	14.3	5.04	1.28	0.122
4R	$9.71 \times 10^{-3}$	71.5	4.94	2.84	0.317
5S	0.0195	133	4.95	3.69	0.496
5R	0.0316	197	4.89	4.38	0.712
6S	0.0555	326	4.86	5.70	1.07
6R	0.0616	358	4.83	5.66	1.28

TABLE 2.5.4-4

ESTIMATED CONDENSATE FILM DEPTH ON TURBINE HOUSING TWO-STAGE CESIUM TURBINE

Blade Row Exit	Cumulative Condensate Flow Rate (pps)	$Q^+$	$N_{re,v} \times 10^{-6}$	$e/r_o \times 10^5$	$\delta$ (mils)
1S	$9.1 \times 10^{-5}$	0.981	1.17	3.22	0.0126
1R	$4.2 \times 10^{-4}$	3.77	1.26	4.19	0.0259
2S	0.0015	11.6	1.31	5.77	0.0649
2R	0.0031	20.2	1.35	6.48	0.129

● Average Drop Size Sheared From Casing Liquid

It is anticipated that the condensate film flowing over the casing will at least in part be atomized. Since this is presumably a random process, some of the drops will have relatively short time-of-flight available before impinging on the rotor blades. These drops can be relatively large and the resulting erosion on the rotor blades might be severe.

The average droplet size was estimated on the basis of the sheet atomization mechanism as given in Section 2.7. The equation derived for the average droplet size is

$$\bar{d} = 17.0 \left[ \frac{\dot{m}_L \mu_L}{\rho_L \left( \tau_s + \frac{\dot{m}_L U}{X} \right)} \right]^{1/4} \left( \frac{\mu_L}{\tau_s} \sqrt{\frac{\sigma}{\rho_L}} \right)^{1/3}$$

For the turbine casing, the momentum term is negligible compared to the wall friction term, and the equation reduces to

$$\bar{d} = 17 \left( \frac{\dot{m}_L \mu_L}{\rho_L \tau_s} \right)^{1/4} \left( \frac{\mu_L}{\tau_s} \sqrt{\frac{\sigma}{\rho_L}} \right)^{1/3}$$

where  $\bar{d}$  is in microns. The wall friction drag per unit area,  $\tau_s$ , was calculated from the Wrobel and McManus equation for the wall friction drag coefficient  $C_f$ , or

$$C_f \approx 0.33 \left[ \ln \left( \frac{3 R_0}{\delta (1 - 10/\delta)} \right) \right]^{-2}$$

To calculate the average droplet size, the condensate flow rates  $\dot{m}_L$  were based on the housing inside diameters. The results are presented in Table 2.5.4-5.

These average droplet sizes are significantly larger than the average droplet size entering the rotor blades from the stators of either turbine. In the case of the potassium turbine, the drops are certainly large enough to cause physical impact erosion damage. Therefore, periodic moisture removal similar to that in steam turbines is indicated for the potassium turbine if erosion is to be minimized.

TABLE 2.5. 4-5

MEAN DROPLET SIZES FROM SHEET ATOMIZATION OF CONDENSATE ON THE POTASSIUM AND CESIUM TURBINE HOUSINGS

Turbine Housing at Blade Row Exit	$\bar{d}$ (microns)
6K - 3R	4.48
6K - 4S	75.3
6K - 4R	149.
6K - 5S	235.
6K - 5R	331.
6K - 6S	455.
6K - 6R	667.
2Cs - 1S	5.38
2Cs - 1R	5.06
2Cs - 2S	17.4
2Cs - 2R	40.7

2.5.5 References

1. Gyarmathy, G., "The Bases for a Theory of the Wet Steam Turbine," Juris-Verlag, Zurich, 1962.
2. Brun, R. J., W. Lewis, P. J. Perkins, and J. S. Serafini, NACA Report 1215, 1955.
3. Emmons, H. W., Fundamentals of Gas Dynamics, Vol. III, Sect. H., Princeton University Press, Princeton, N. J., 1958.
4. Smith, A., "The Influence of Moisture on the Efficiency of a One-Third Scale Model Low Pressure Steam Turbine," Institution of Mechanical Engineers, Thermodynamics and Fluid Mechanics Convention, Paper 10, Liverpool (Gr. Brit.), April 13-15, 1966.
5. Gardner, G. C., "Events Leading to Erosion in the Steam Turbine," Proc. Inst. Mech. Engrg., 178, Pt I, No. 23, pp. 593 to 623, 1963-1964.
6. Baker, O., "Simultaneous Flow of Oil and Gas," The Oil Gas Jour., July 26, 1954.

7. Wrobel, J. R., and H. N. McManus Jr., "An Analytic Study of Film Depth, Wave Height, and Pressure Drop in Annular Two-Phase Flow," Development in Mechanics, Vol. I, Proceedings of the 7th Midwest Mechanics Conference, Sept. 6-8, 1961, Plenum Press, Inc., New York, 1961.
8. Baker, O., "Simultaneous Flow of Oil and Gas," The Oil Gas Jour., July 26, 1954.

## 2.6 TRANSPORT OF ATOMIZED DROPS BETWEEN STATORS AND ROTORS (ADROP CODE)\*

### 2.6.1 Background

This section describes the detailed aspects of the tubular blade erosion model which deals with the transport of potentially damaging liquid in the axial space between stator exit planes and rotor inlet planes.

The source of most of the potentially damaging moisture in steam and alkali metal turbines is the process of condensation in the bulk vapor by spontaneous nucleation. The condensate particles are generally less than a micron in diameter, so that if the turbine is well designed and orderly flow prevails, most of the moisture will follow the vapor streamlines and will exit from the turbine without interacting with the blades. A small fraction of the condensate fog will, however, tend to collect on blade surfaces because of the curvature of the flow passages and the rotation of the moving blades.

\* T. C. Varljen, Supervisor, Systems & Technology, Astronuclear Laboratory, Westinghouse Electric Corporation, Pittsburgh, Pa. 15236

These impacts by themselves cause negligible damage because of the small size of the particles involved. The moisture collected in this fashion on stator passage walls is carried along axially by the drag forces of the vapor stream toward the downstream end of the stator. The liquid is then torn away from the stator trailing edge in a primary atomization process. A wide spectrum of drop sizes is produced, with some diameters approaching the stator trailing-edge thickness. Most of the observed impact erosion damage is caused by drops formed in this manner.

Condensation directly on blade surfaces and boiler carry-over are other sources of moisture which may be considered. These would tend to dominate in mercury vapor machines, for instance, where condensation in the bulk vapor is theoretically negligible.

The work presented here is concerned with the motion of the moisture, regardless of its origin, after the conclusion of primary atomization. The analytical basis of the transport model will be discussed and a digital computer code package called ADROP will be described. This code is written in FORTRAN IV and was developed to unify the various numerical procedures involved in this phase of the overall turbine blade erosion model.

### 2.6.2 Analytical Model of Atomized Drop Transport

The central problem is the solution of the equation of motion of a drop of liquid in the space between the stator from which it was discharged and the rotor inlet plane. Mechanical erosion rates tend to be drop-size and velocity dependent. The upper limit of drop sizes which will impact the rotor blades is largely determined by the vapor wake characteristics immediately downstream of the stators.

The primary drops are caught up in the decaying wake. Some of these will simply be accelerated to some fraction of the local vapor velocity and will ultimately impact upon the rotors. Drops at the upper end of the size spectrum produced by primary

atomization will be unstable with respect to the applied aerodynamic forces and will fragment prior to impact. The latter process will be termed "secondary atomization." Drops traveling along streamlines near the edge of the stator wakes are subject to the greatest aerodynamic forces, while drops moving along the wake axis, essentially in the trough of the velocity defect, will experience the least amount of disruption. The largest, and hence potentially the most damaging, drops which reach the rotors will be those which move on streamlines near the wake centerline.

The study of the motion of atomized condensate has been undertaken on several levels. First, relatively simple closed form solutions of the equation of motion were obtained for certain special cases. A completely general dimensionless formulation of the equation of motion was also obtained and solved numerically. Finally, a detailed calculational procedure was developed to provide special solutions.

#### • The Bulk Flow Impact Velocity

A closed form solution to the drop motion problem has been derived for the special case of a drop moving along the wake-edge under bulk flow conditions. The aerodynamic force on a detached drop is given by:

$$F_d = 1/2 C_D \rho_v V_r^2 A_d \quad (1)$$

where  $A_d$  is the drop cross-sectional area and  $V_r$  is the relative velocity of the drop with respect to the local vapor stream velocity. That is  $V_r = U - V_d$ . If the drop remains intact, its equation of motion will be:

$$F_d = \frac{\pi}{6} D_d^3 \rho_v \frac{dV_d}{dt}$$

or:

$$\frac{dV_d}{dt} = \frac{3}{4} \frac{C_D}{D_d} \frac{\rho_v}{\rho_L} (U - V_d)^2 \quad (2)$$

Two assumptions were made to get a closed-form solution to the above. First, the local vapor velocity was assumed to be constant and equal to the bulk flow velocity at the stator exit plane ( $U = U_o$ ), and second, the following form of the drag coefficient was assumed:

$$C_D = a Re^b = a \left[ \frac{(U_o - V_d) \rho_v D_d}{\mu_v} \right]^b \quad (3)$$

Unfortunately the drag coefficient cannot (as far as we know) be represented by a single general relationship  $aRe^b$  over the Reynolds Number range of interest. According to Lambiris and Combs<sup>(1)</sup>, for the distorted drops:

$$C_D = 27 Re^{-0.84} \quad 0 \leq Re \leq 80 \quad (4a)$$

$$C_D = .271 Re^{.217} \quad 80 < Re \leq 10^4 \quad (4b)$$

$$C_D = 2 \quad 10^4 < Re \quad (4c)$$

The data which the above relations fit is shown graphically in Figure 2.6-1. Experimental data from References (1) and (2) are shown. The solution to the equation of motion, relating distance traveled and drop terminal velocity, covering cases (4a) and (4b), was found to be

$$x = \frac{4}{3} \left( \frac{D_d}{C_{D0}} \right) \left( \frac{\rho_L}{\rho_v} \right)^{\frac{1}{b(b+1)}} \left\{ 1 + \left[ \frac{V_d}{U_o} (b+1) - 1 \right] \left( 1 - \frac{V_d}{U_o} \right)^{-(b+1)} \right\} \quad (5)$$

For the case of a constant drag coefficient (case 4c for instance) the following solution was obtained:

$$x = \frac{4}{3} \left( \frac{D_d}{C_{D0}} \right) \left( \frac{\rho_L}{\rho_v} \right) \left\{ \frac{V_d/U_o}{1 - V_d/U_o} + \ln \left( 1 - \frac{V_d}{U_o} \right) \right\} \quad (6)$$

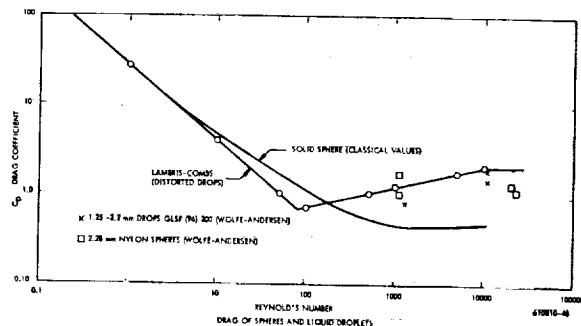


Figure 2.6-1 Drag of Spheres and Liquid Drops

Note that  $C_{D0}$  is associated with  $Re_o$ , the bulk flow Reynolds Number. Three distinct closed form solutions have therefore been obtained corresponding to the three Reynolds Number ranges used to represent the drag coefficient. A convenient dimensionless representation of these solutions is shown in Figure 2.6-2. The drop terminal-to-free-stream velocity ratio is plotted as a function of the parameter group  $\left(\frac{x}{D_d}\right) \left(\frac{\rho_v}{\rho_L}\right) C_{D0}$ . If the local Reynolds Number of a drop stays completely within one of the Reynolds Number ranges throughout its trajectory, the appropriate general trajectory curve will be followed. Otherwise, the curves form an envelope covering the behavior of cases where the Reynolds Number drops from one range to the next.

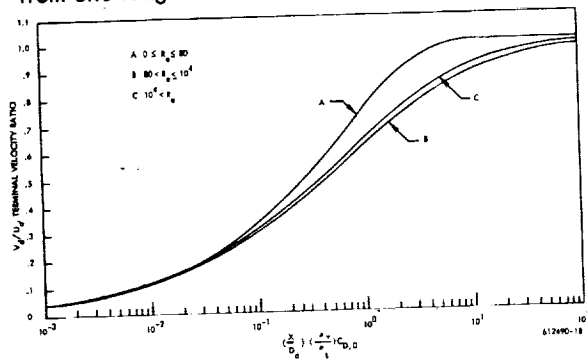


Figure 2.6-2 Analytic Solutions for the Bulk Flow Drop Impact Velocity

### • General Dimensionless Formulation

For the general case of motion with a variable field (i.e., within a stator wake for instance) a closed form solution does not seem possible because of the complexity of the resulting equation of motion. It has been noted that from the point of view of the erosion model the most important path of drop motion is near the axis of the stator wake.

Leiblein and Roudebush<sup>(3)</sup> have correlated the variation of wake trough velocity with downstream distance with the following expression:

$$U_{\min} = U_o \left( 1 - .13 \sqrt{\frac{x}{c}} + .025 \right) \quad (7)$$

The above is based on a limited amount of data for blade cascades with essentially zero trailing-edge thicknesses.

The basic equation of motion, now written for the wake axis streamline is then:

$$\frac{dV_d}{dt} = V_d \frac{dV_d}{dx} = \frac{3}{4} \left( \frac{\rho_v}{\rho_L} \right) \frac{1}{D_d} f \left[ \left( U_{\min} - V_d \right) \frac{\rho_v D_d}{\mu_v} \right] \left( U_{\min} - V_d \right)^2 \quad (8)$$

when the drag coefficient is represented functionally by:

$$C_d = f \left[ \left( U_{\min} - V_d \right) \frac{\rho_v D_d}{\mu_v} \right]$$

Now abbreviating eq (8) so that  $U_{\min} = U_o g(\epsilon)$ , where  $\epsilon = x/c$ , leads to

$$\left( \frac{V_d}{U_o} \right) \frac{dV_d/U_o}{d\epsilon} = K_d f \left[ \left[ g(\epsilon) - V_d/U_o \right] Re_o \right] \left[ g(\epsilon) - V_d/U_o \right]^2 \quad (9)$$

with  $K_d$  as the inertial parameter:

$$K_d = \frac{3}{4} \left( \frac{\rho_v}{\rho_L} \right) \left( \frac{C}{D_d} \right)$$

The above has been solved numerically for the velocity ratio as a function of referred distance along the wake axis ( $x/c$ ) with  $K_d$  and  $Re_o$  as parameters. Figure 2.6-3 shows a few of the solutions which have been obtained.

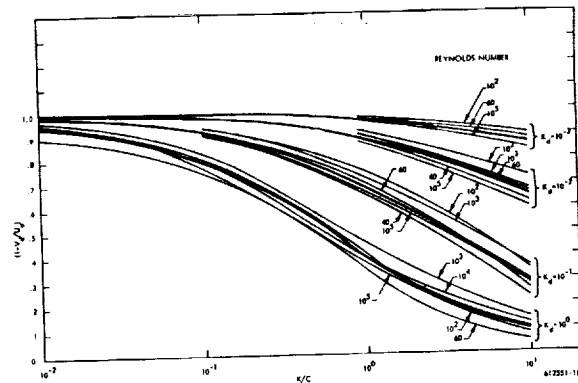


Figure 2.6-3 General Solutions for the Terminal Velocity of Drops Traveling along Stator Wake Axis Streamlines

These solutions by themselves are instructive guides to the overall relations between the parameters. It is conceivable that a least squares analysis of the various relations could be used to produce a "universal solution" curve of the form:

$$\frac{V_d}{U_o} = \left(\frac{x}{c}\right)^{n_1} K_d^{n_2} Re_o^{n_3} \quad (10)$$

From the point of view of turbine erosion, however, knowledge of the ultimate impact velocity is not sufficient and must be complemented by a secondary atomization study. It is for this reason that the detailed computer model was developed.

### 2.6.3 Computer Model of Atomized Drop Transport

The scope of the ADROP code package is as follows:

- Estimation of stator blade boundary-layer characteristics
- Generation of the local velocity field within the vapor wake downstream of stator blades
- Numerical integration of the equation of motion of drops traveling along various wake streamlines and the estimation of secondary atomization effects.
- Solution of drop impact velocity triangles to provide information on the magnitude of the normal component of impact velocity and the physical location of erosion.

#### • Stator Blade Boundary Layer Characteristics

The vapor wake downstream of stator blades is assumed to be controlled primarily by the viscous dissipation of the boundary layer at the trailing-edge of the blades. The boundary layer properties required include the momentum thickness, displacement thickness, full thickness, and the form factor. The local momentum thickness of the boundary layer<sup>(4)</sup> is found by integrating a form of Truckenbrodt's equation:

$$\frac{\theta}{s_o} = \left(\frac{U}{U_o}\right)^{-3} \left(\frac{C_f}{2}\right)^{\frac{n+1}{n}} \int_0^{s/s_o} \left(\frac{U}{U_o}\right)^{3+2/n} d\left(\frac{s}{s_o}\right)^{n/(n+1)} \quad (11)$$

where the exponent  $n$  is taken to be six, corresponding to large Reynolds numbers, and the friction factor is specified by the empirical expression for flat plate, turbulent flow:

$$C_f = .074/Re^{0.2} \quad (12)$$

In this statement of the Truckenbrodt equation it was assumed that the boundary layer is turbulent along the entire blade length. This is a useful approximation and does not have an appreciable effect on the results at the trailing edge. The shape factor may be obtained as shown in

$$L = -.23 + .0076 \left(\frac{n}{n+1}\right) + .0304 \ln Re + \ln \left(\frac{U}{U_o}\right) + .0076 \left(\frac{n}{n+1}\right) \ln \xi - \frac{1.0608}{\xi} \int_0^{\xi} \ln \left(\frac{U}{U_o}\right) d\xi \quad (13)$$

where:

$$\xi = \left[ \left(\frac{C_f}{2}\right)^{\frac{n+1}{n}} \int_0^{s/s_o} \left(\frac{U}{U_o}\right)^{3+2/n} d\left(\frac{s}{s_o}\right)^{n/(n+1)} \right]^4$$

As before laminar terms do not appear in the equations and the integrations are performed to the inlet edge of the blade, rather than to the laminar-turbulent transition point. The form factor  $H$  is related to the shape factor by:

$$L = \int_{E_o}^E \frac{1}{H-1} \frac{dE}{E} \quad (14)$$

where  $E$  and  $H$  are related empirically by:

$$E = \frac{1.269 H}{H - .379} \quad (15)$$

The lower limit of integration,  $E_o$ , is taken as 1.74 to make  $L = \text{zero}$  correspond to the case of the flat plate with zero pressure gradient, i.e.,  $H = 1.4$ . The empirical form (eq. 15) is in good agreement with experimental data below  $H = 1.7$  (Ref. 6). For larger values of  $H$  the correlation breaks down so that the equation is supplemented by a table of experimental data for use when  $1.6 < H < 2.6$ .

The remaining local boundary layer characteristics may be found after Schlichting<sup>(6)</sup> by applying the general power-law velocity-distribution where:

$$\frac{u}{U} = \frac{y}{\delta}^{1/n} \quad (16)$$

so that:

$$n = \frac{2}{H-1} \quad (17)$$

and

$$\frac{\delta^*}{\delta} = \frac{1}{1+n} \quad (18)$$

$$\delta^* = \theta H \quad (19)$$

### • The Generation of Stator Wake Velocity Profiles

The objective is to obtain a two-dimensional representation of the vapor velocity field between a stator exit plane and the inlet plane of the following rotor. Most of the work which has been done in this area has been oriented toward evaluating overall loss coefficients. There has apparently been very little interest in the fine structure of wakes per se. The work of Lieblein and Roudebush<sup>(3)</sup> comes closest to satisfying the requirements of the transport model in this respect. The analysis just cited deals with the low-speed wake characteristics of two-dimensional cascade and isolated airfoil sections. Strictly speaking, the conditions present in axial flow turbines are not quite the same as those assumed in the analysis.

The approach taken by Lieblein and Roudebush is to assume that the wake is formed by the merging of the boundary layers on the upper and lower blade surfaces at the trailing edge. The wake is eventually re-energized by a mixing process between the wake and the free-stream flow. The variation of certain wake properties with downstream distance is then predicted from both empirical and theoretical considerations.

A qualitative picture of the velocity profiles normal to the wake trough is shown in Figure 2.6-4. Note that the inclination of the wake centerline to the turbine axis is a slowly varying function of axial distance. Similarly, the wake minimum velocity increases and the wake-edge velocity or free-stream velocity decreases slightly with distance as a result of momentum transfer as the wake re-energizes.

The wake model appears to be particularly good where the ratio of blade trailing-edge thickness to chord length approaches zero and at a nominal distance downstream of the trailing edge. It is clear that very complex flow patterns will exist immediately downstream of blades of finite trailing-edge thickness. In fact, separate vortex flow may exist in many cases. The characteristics of the wake near the trailing edge are very important from the erosion point of view and directly affect the question of the upper size limit of drops reaching the rotor plane.

The atomized drops from the stator are shed into this region of complex flow. There is probably a sheltered region immediately downstream of the blade with components of flow both transverse and axial. Steam turbine observations indicate that the drops will migrate rather slowly deep in the wake, and at some point downstream are suddenly caught up and accelerated. Because of the uncertainty in this process a "dead-space" correction of about four trailing edge thicknesses has been arbitrarily introduced. The integration of the drop equation of motion is therefore begun at the edge of the dead space rather than at the blade trailing-edge.

The variation of wake trough velocity has previously been given (eq. 7 above). No consistent quantitative model for the actual shape of the transverse profile has been advanced. Provided the minimum and wake-edge velocities are reasonably correct, a half-sine curve fit to the two known points should yield consistent results for the transverse velocity profile. This method does not, however, account for the observed asymmetry in the wake. At the trailing edge the effective total boundary layer thickness is the sum:

$$\delta_{te} = \delta_{p, te} + \delta_{s, te} \quad (20)$$

The remaining trailing edge properties may be obtained from:

$$\delta_{te}^* = \delta_{p, te} + \delta_{s, te} \quad (21)$$

$$\theta_{te} = \theta_{p, te} + \theta_{s, te} \quad (22)$$

$$H_{te} = \delta_{te}^* / \theta_{te} \quad (23)$$

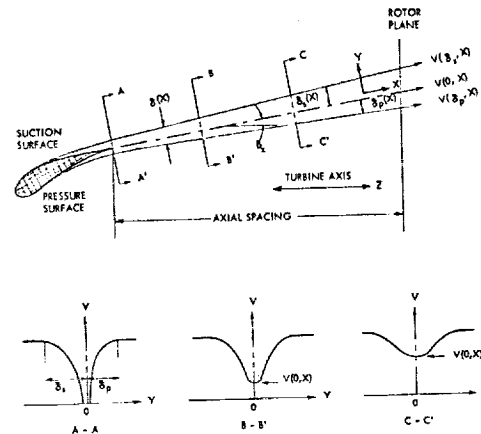


Figure 2.6-4 Qualitative Representation of Vapor Wake Development Downstream of a Stator Blade Section



The variation of the wake form factor was fitted in (6) by:

$$H_x = \frac{\sqrt{1 - 40xc}}{\sqrt{1 - 40xc} - \left(\frac{H_{te} - 1}{H_{te}}\right)} \quad (24)$$

The wake momentum thickness parameters,  $\hat{\theta}$ , and the flow angle simultaneously satisfy:

$$\frac{1 - \hat{\theta}_x (1 + H_x) - \frac{1}{2 \cos^2 \beta_x}}{(1 - \hat{\theta}_x H_x)^2} = \text{constant} = k_1 \quad (25)$$

$$\frac{1 - \hat{\theta}_x (1 - H_x)}{(1 - \hat{\theta}_x H_x)^2} \tan \beta_x = \text{constant} = \sqrt{K_2} \quad (26)$$

where:

$$\hat{\theta}_x = \left(\frac{\theta}{c}\right)_x \frac{\sigma}{\cos \beta_x} \quad (27)$$

Equations (25) and (26) may be solved by simultaneous iteration for  $\hat{\theta}_x$  and  $\beta_x$ . The constants are evaluated in terms of the trailing edge condition,  $H_{te}$ ,  $\theta_{te}$  and  $\beta_{te}$ . The wake-edge velocity may then be found from:

$$V(\delta/2, x) \cos \beta_x (1 - \hat{\theta}_x H_x) = \text{constant} = k_3 \quad (28)$$

The ratio  $V_{min,x}/V(\delta/2, x)$  is specified by the trough velocity equation(7) so that by applying (28) the trough velocity is obtained. Using a half-sine fit the transverse velocity profile is then:

$$\frac{V(y, x)}{V(\delta/2, x)} = \frac{1}{2} \left[ \left(1 + \frac{V_{min,x}}{V(\delta/2, x)}\right) - \left(1 - \frac{V_{min,x}}{V(\delta/2, x)}\right) \cos \frac{\pi y}{\delta/2} \right] \quad (29)$$

Transverse wake position is specified by the ratio  $y/(\delta/2)$ , which is unity at the wake edge and zero at the centerline.

The latter positions are generally the most interesting. It is assumed that if a drop starts out on a particular streamline  $y/(\delta/2)$ , it continues in this relative position until it impacts.

#### ● Drop Acceleration and Secondary Atomization\*

The drop size spectrum from primary atomization may be estimated using the method given in Section 2.7. The empirical Nukiyama-Tanasawa distribution function is applied and from these re-

sults a suitable group of drop sizes may be chosen for the drop transport analysis. The general drop equation of motion (eq. 2) may be solved for the drop terminal velocity as a function of drop size and wake position, with the local vapor velocity within the wake obtained following the procedure outlined above.

The conditions for subsequent drop fragmentation or secondary atomization may be correlated in terms of a critical Weber Number. This subject has been given much attention in the atomization literature in recent years; however, a consistent guide to its formulation remains to be found.\*\* Much of the empirical work has been done with steam or air streams and correlations suitable for use with liquid metal systems remain to be substantiated. Gardner<sup>(7)</sup>, for instance, recognized two regimes for the critical Weber Number in steam systems. For cases where drops were introduced into a relatively slow-moving stream, which was gradually accelerated, he recommends a "steady-flow" critical Weber Number of 22. For the case of abrupt acceleration he recommends a "shock" critical Weber Number of 13. Other authors (Nicholson<sup>(8)</sup> for instance) have reported an even wider range of critical Weber numbers. In lieu of more definitive data we have tentatively adopted Gardner's results with the following rationale. The Weber Number is defined by:

$$We = \frac{\rho_v V_r^2 D_d}{\sigma_L} \quad (30)$$

and is essentially the ratio of the local dynamic force to the surface tension. In the low pressure end of steam turbines the drop relative velocity, hence drop Weber Number, increases gradually to a maximum and then decreases with downstream travel. The conditions fit the "steady-flow" Weber Number

\* A comparison of calculated values of drop velocity for the Yankee turbine and experimental values from a CERL steam cascade is given in Appendix 2.6 to this section.

\*\* A more detailed discussion of this subject is undertaken in Section 2.7.

criterion of 22. In small alkali metal turbines the onset of acceleration is quite abrupt, with the peak Weber Number occurring initially. This situation suggests use of the "shock" critical Weber Number for these systems.

As far as the trajectory model is concerned, therefore, secondary atomization is assumed to begin when a certain fixed Weber Number is exceeded anywhere along the trajectory of a drop. The disruption process takes a finite amount of time and it is usually important to know whether the distance between blade rows is sufficient to insure complete atomization of all unstable drops. From basic considerations it can be shown (9) that the disruption time shows the following dependence:

$$t \propto \frac{D_d}{V_r} \sqrt{\frac{\rho_L}{\rho_v}} \quad (31)$$

From the data of Wolfe and Anderson<sup>(2)</sup> the time to the start of disruption was estimated to be:

$$t = 1.1 \frac{D_d}{V_r} \sqrt{\frac{\rho_L}{\rho_v}} \quad (32)$$

and the elapsed time to complete breakup was:

$$t' = 2.8 \frac{D_d}{V_r} \sqrt{\frac{\rho_L}{\rho_v}} \quad (33)$$

In the trajectory model reported here, when the local drop Weber Number exceeds the critical value at some time  $t$ , the disruption time  $t'$  is computed. Disruption is assumed to be completed at that point on the trajectory where time  $t + t'$  has elapsed. Presumably for drops with maximum Weber Numbers close to critical the drop may revert to a more stable condition prior to time  $t + t'$ . However, the uncertainty in the magnitude of the critical Weber Number precludes the use of such a refinement at this time.

When a primary drop disintegrates, a spectrum of secondary drop sizes may be expected, just as in the case of primary atomization. The mass mean diameter  $D'_d$  of the secondary drops is evaluated from the Wolfe-Anderson expression:

$$D'_d = \left\{ \frac{136 \mu_L \sigma^{3/2} D_d^{1/2}}{2 \rho_v V_r^4 \sqrt{\rho_L C_D}} \right\}^{1/3} \quad (34)$$

where all the quantities are evaluated for conditions at time  $t$ , that is, at the point where the critical Weber Number is first exceeded.

When the above analysis is concluded for a given turbine stage, an upper limit for the size of impacting drops will be obtained. The original primary drop distribution will be modified such that the "tail" extending beyond the maximum stable drop size will be removed. The fraction of the total spray volume represented by the tail represents the new secondary drop distribution which is now added to the original distribution. The mechanics of these calculations are discussed in Section 2.7. Comparison of calculated secondary drop distributions obtained using equation 34 with actual measurements in a large steam turbine are in poor agreement.

#### • Impact Velocity and the Geometry of Impact

The geometry conventions employed in this discussion are shown in Figure 2.6-5. Consider the inlet region of a rotor section at some fixed blade height. The pitch,  $S$ , tangential blade speed  $U_1$ , and the rotor inlet blade angle are thus fixed. The velocity  $V_d$  is the terminal drop velocity which is obtained from the solution of the equation of motion discussed previously. The direction of  $V_d$  is essentially that of the stator jet velocity; however, its magnitude depends on drop size. The drop velocity relative to the rotor is given by:

$$W_d = \sqrt{U_1^2 + V_d^2 - 2U_1 V_d \sin \alpha} \quad (35)$$

The "shadow angle"  $\alpha_d$  satisfies:

$$\cos \alpha_d = \frac{U_1 - V_d \sin \alpha}{W_d} \quad (36)$$

Depending on the angle of the blades and the angle of incidence of the drops, there will be generally a blade region which will be shadowed and free of damaging impacts. To estimate the extent of unshadowed blade surface, a first approximation is to consider the "impaction length"  $\Delta L$  defined along the tangent to the blade centerline at its nose. The actual impaction zone is the convex surface cut by the tangent line. A relation for  $\Delta L$  in terms of the blade spacing  $S$  and angles  $\alpha_i$  and  $\alpha_d$  is:

$$\Delta L \approx S \frac{\sin \alpha_d}{\sin(\alpha_i + \alpha_d)} \quad (37)$$

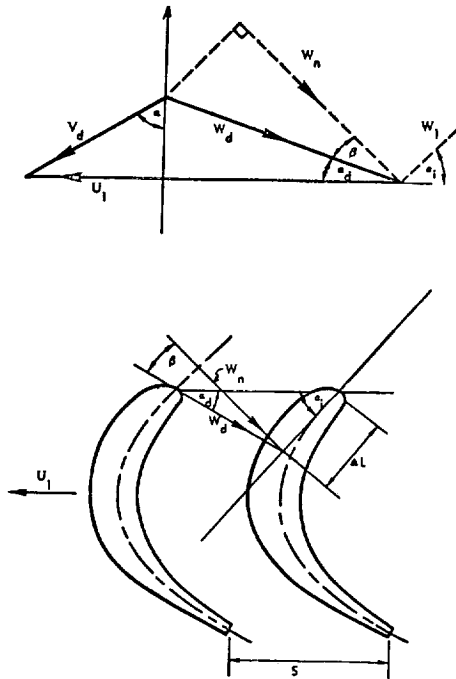


Figure 2.6-5 Drop Impingement Geometry

If the angles  $\alpha_d$  and  $\alpha_i$  are acute, the approximation is relatively good. Otherwise, scale drawings of the blades must be used.

The treatment employed by the overall erosion model to estimate material removal holds that it is the normal component of the component of the impacting drop velocity which is most directly related to the extent of damage. This component is obtained by noting that the angle  $\beta$  included between  $W_d$  and  $W_n$  is  $\pi/2 - \alpha_d - \alpha_i$ . Therefore:

$$W_n = W_d \cos \beta = W_d \sin(\alpha_d + \alpha_i) \quad (38)$$

Drops at the upper end of the size spectrum will have the smallest arrival velocity. In the limit, for very small  $V_d$ ,  $|W_d| \rightarrow |U_1|$  and the impact region is essentially confined to the blade nose. Such a situation is very unlikely since the unbroken drops below the secondary atomization limit are accelerated to an appreciable fraction of the free stream velocity.

At the other extreme some of the smallest drops will arrive at essentially free stream velocity so that  $|W_d| \rightarrow 0$ . The normal velocity  $W_n$  will be largest when  $V_d = 0$  and will decrease linearly to zero when  $V_d$  reaches the free stream value. For some value of drop terminal velocity the vectors  $W_n$  and  $W_d$  will coincide. Beyond this point, in the direction of higher terminal velocities and smaller drop diameters, the impact length concept breaks down. The significant impact area is the nose since  $W_d$  is normal to the nose at some point. The cross-over point is represented analytically by the condition  $\beta = 0$ . It follows then that:

$$\alpha_{do} = \frac{\pi}{2} - \alpha_i \quad (39)$$

$$V_{do} = \frac{U_1}{\sin(\cot \alpha_{do} - 1)} \quad (40)$$

$$W_{do} = V_{do} \frac{\sin \alpha}{\sin \alpha_{do}} \quad (41)$$

Therefore, when  $V_d > V_{do}$  the relative velocity  $W_d$  will exceed  $W_n$  and should be considered as far as potential damage is concerned. Note that increasing the blade speed has the effect of increasing  $V_{do}$ , thus decreasing the tendency of the damage to be confined to the nose area.

#### 2.6.4 Description of the ADROP Code Package

The ADROP code is designed to examine in detail the transport of atomized condensate from the stator exit plane to the rotor inlet plane in wet vapor axial flow turbines. The code facilitates parameter surveys and can be used to systematically test the implications of various assumptions made in the model. The computational model as outlined in the previous section is far from definitive, in fact it represents a first cut at a comprehensive explanation of observed phenomena.

A single stage and blade height position is examined at one time, however, as many problems as necessary may be run consecutively. Temperature-dependent working fluid properties are computed by an auxiliary subroutine, with a present capacity of eight materials: lithium, sodium, potassium, rubidium, cesium, mercury, NaK-78, and water. For a given stage, geometry, and bulk flow condition, a range of drop sizes are introduced into the vapor

stream at various wake positions. Terminal velocities are obtained for all drops. If the flow conditions are such that a drop satisfies the condition of aerodynamic instability, the approximate location of disruption is noted and the mass mean diameter of secondary drops is estimated.

The program source language is FORTRAN IV. The code is oriented toward the CDC machines 3600, 6400, and 6600; however, compatibility with equivalent IBM equipment can be achieved with a minimum of effort. On the CDC 6600 system operated by the Westinghouse Tele-Computer Center the field length required by the code, associated system routines, and storage areas is 18,000 words decimal. Calculations and output are in cgs units, with inputs in common engineering units. Options are available to control the quantity of printed output and the sequence of calculations. A source language listing of each item in the code package may be found in Appendix B to this section.

- The Main Program

Input functions, initialization, and option selection are handled by the main program. Data is input using the format-free NAMELIST feature. For each individual problem the input consists of a title card, and a sequence of cards defining quantities in the NAMELIST DRP. The 80-column card image of the title card is used to identify the output listing. Variables in the DRP list are /DRP/KOP, TR, VFREE, GDAT, XS, VS, XP, VP, PD, SD, PDS, SDS, PTH, STH, XQ, DIAM.

It should be emphasized that only those numbers required to do a particular problem configuration need to be input. Data is transferred from one problem to the next. Thus, the first problem in a series might have a complete input set, while subsequent problems might only require one or two input numbers. The input list variables involved are defined in Table 2.6-1. Blade surface velocity plots may be obtained in several ways. Our usual practice has been to employ the code of Reference 14 to generate this data.

Material properties required for the working fluid in question are the density of vapor and liquid, the viscosity of vapor and liquid and the surface tension of the liquid. These are obtained by calling subroutine PROPM. The data is then stored in common block/PRP/ for later use. Table 2.6-2 lists the important common blocks used for intersubroutine communication. A specific sample problem will be discussed in Section 2.6 to illustrate the input and output formats.

- Subroutine TRUCK

The calculation of the boundary layer properties along blade surface is handled in a code devised by W. K. Fentress. The code has been recast into subroutine form and incorporated into the ADROP system. The input surface velocity tables, which may contain as few as four points each is expanded into a 40-point table using parabolic spline interpolation (subroutine SPLINT). The Truckenbrodt boundary layer equation and the shape factor equation are then integrated by the trapezoidal method.

TABLE 2.6-1

## ADROP INPUT NAMELIST DEFINITIONS

<u>Name</u>	<u>Definition</u>	<u>Name</u>	<u>Definition</u>
KOP(1)	Working fluid sentinel (see definition of JFLUID on page 42)	XQ	Bulk vapor quality at stator exit.
KOP(2)	Number of stator blades	GDAT(1)	Stator exit flow angle (angle $\alpha$ in Figure 5)
KOP(3)	Number of rotor blades	GDAT(2)	Inlet rotor blade angle (angle $\alpha_i$ in Figure 5)
KOP(4)	Shaft RPM	GDAT(3)	Trailing-edge multiplier used to define the dead-space.
KOP(5)	Boundary-layer calculation option (subroutine TRUCK) $\leq 3$ calculation is deleted. Otherwise KOP(5) specifies the number of referred position-velocity pairs to be input.	GDAT(4)	Critical Weber Number
KOP(6)	TRUCK IO sentinel. If KOP(6) $> 0$ detailed boundary layer results will be printed.	GDAT(5)	Stator exit section diameter (inches)
KOP(7)	TRAX option sentinel. If KOP(7) $\leq 0$ trajectory calculations will be deleted. A value greater than zero sets the trajectory print interval.	GDAT(6)	Rotor inlet section diameter (inches)
KOP(8)	IMPAX option. If KOP(8) $\geq 0$ the drop impact geometry will be examined.	GDAT(7)	Axial space between stator exit and rotor inlet planes (inches)
KOP(9)	Wake option. If KOP(9) $\geq 0$ full wake treatment will be used. Otherwise the approximate treatment is specified.	GDAT(8)	Stator trailing-edge thickness (inches)
KOP(10)	Debug option = 0 option ignored >0 data will be printed out during each wake iteration = 2 trajectory data will be printed for each trial integration step.	GDAT(9)	Stator chord length (inches)
TR	Bulk vapor temperature at stator exit ( $^{\circ}\text{R}$ )	GDAT(10)	Pressure surface length (inches)
V FREE	Stator exit jet velocity (feet/sec.)	GDAT(11)	Suction surface length (inches)
		DIAM	Array of nine drop diameters (microns)
		XS, XP	Arrays of referred positions in suction and pressure sides
		VS, VP	Arrays of referred surface velocities on suction and pressure sides.
		PD, SD	Pressure and suction side boundary layer thicknesses (cm)
		PDS, SDS	Pressure and suction side displacement thicknesses (cm)
		PTH, STH	Pressure and suction side momentum thicknesses (cm)

TABLE 2.6-2  
COMMON BLOCK LAYOUT IN PROGRAM  
ADROP

BLOCK DEFINITIONS

/PRP/MAT,TEMP, RHOV, RHOL, SIGL, VISL, VISV  
/TBG/CHORD, PITCH, BTE, PD , SD, PDS, SDS, PTH, STH, VZERO  
/GEO/NSTAT, NROTR, RPM, ALPHA, ALPHI, F DEAD, WDC, DSTAT, DROTR, AXSP, STE,  
SCHD, SPARC, SSARC  
/CST/JOB(10), JMAT(10), PI, RD, NYD, DIAM(10)  
/BUG/IBUG  
/ICON/H, HMAX, HMIN, RELB, ABS B  
/TRX/ . . .

BLOCK REFERENCES

	<u>MAIN</u>	<u>TRUCK</u>	<u>TRAX</u>	<u>DERIV</u>	<u>IMPAX</u>	<u>WAKE</u>	<u>ICEAD</u>
PRP	X	X	X	X			
TBG	X	X	X	X		X	
GEO	X		X	X			
CST	X	X	X	X	X		
BUG	X			X		X	
ICON			X	X			X
TRX			X	X			

### Calling Sequence

Call TRUCK (M, SS, SP, XXS, XVS, XXP, XVP, IØ) where:

- M is the number of surface velocity points to be input for each surface.
- SS is the length of the suction surface.
- SP is the length of the pressure surface.
- XXS is the array of M suction surface referred position points.
- XVS is the array of referred surface velocities corresponding to each value of XXS.
- XXP, XVP are the position and velocity arrays for the pressure side
- IØ is the output listing control sentinel. If IØ > 0 a listing of boundary layer properties along the blade will be obtained.

Output quantities required for subsequent calculations in other subroutines are placed in common block/TBG/. These are PD, SD, PDS, SDS, PTH, STH, which are the pressure and suction side trailing edge values of boundary layer, displacement and momentum thicknesses. No assumptions are made internally concerning units. The unit of length used for the surface lengths SS and SP, however, should be the same as that used in the thermophysical properties. In the context of the ADROP code the units are cgs.

Probable flow separation is indicated if the shape factor (Eq. 13 above)  $L(\xi) < -0.18$  at any point. This condition is identified by a diagnostic message. If this situation occurs, the integer IØ is set to -10 before control returns to the main program. This is used to prevent the subsequent trajectory calculations from starting. Data for the next problem is then read in so that the failure of one problem will not interrupt the entire sequence.

Output listings which may be obtained are:

- The input surface velocity tables
- Boundary layer properties at each surface position (optional)
- Summary of the trailing-edge boundary layer values.

A listing of the subroutine is given in Appendix B to this section. Note that common blocks PRP/, TBG/ and EST/ are required by the subroutine.

### ● Subroutine WAKE

The function of this subroutine is to provide the local vapor velocity at a specified position within a stator blade wake. Common block/TBG/ is used to transmit the numerical values of the stator chord, exit pitch, jet velocity, and the boundary layer displacement and momentum thicknesses at the stator trailing-edge. The calling sequence for the subroutine is:

CALL WAKE (NS, XX, YD, VXY, BX)

where:

- XX is the distance from the trailing edge along the wake centerline where the vapor velocity is required
- YD is the transverse position  $y/(\delta/2)$  within the wake. It is necessary that  $0 \leq YD \leq 1$
- VXY is the output local vapor velocity
- BX is the local wake angle in radians, i.e., the inclination of the wake centerline to the turbine axis.

NS is used as a control sentinel which is set prior to the first WAKE CALL. If NS = 0 when WAKE is called, the constants defined by Equations 25, 26 and 28 are evaluated using trailing edge boundary layer data. WAKE changes NS to unity so that on subsequent calls the initialization section of the subroutine is skipped. If boundary layer data is not available, useful approximate solutions may be obtained assuming a constant free stream velocity and flow angle downstream of the stator. In this case the user must preset NS = 1. Only two values of YD may be used; YD = 0 or YD = 1 in this situation.

The simultaneous iterative solution of equations 25, 26 and 28 is accomplished with the assistance of the auxiliary subroutine VERGE. If convergence of the iterative process has not been accomplished after 20 attempts, there is usually something wrong with the input data. The process is suspended and a diagnostic printed out. The sentinel NS is set to 10 and control returned to the calling routine. It is recommended that NS be tested after each return so that appropriate action may be taken in the event of an iteration failure.

It is required that the unit of length used in the data in common block/TBG/be consistent with those employed in the input arguments XX and VXY.

#### ● Subroutine TRAX

TRAX is the control subroutine for the integration of the drop equation of motion. A fourth-order Adams predictor-corrector method is used in auxiliary subroutine ICEAD to perform the actual numerical integration. TRAX initializes ICEAD for each trajectory and stores final results. These results are eventually listed in a problem summary. Normally thirty trajectories are computed for each problem, i.e., one for each combination of the three wake positions ( $Y/(\delta/2) = 0, 0.35, \text{ and } 1$ ) and the ten input drop diameters. If the approximate wake treatment is used, the two limiting wake positions ( $Y/(\delta/2) = 0, \text{ and } 1$ ) are used so that twenty trajectories are computed.

The summary printout lists, for each drop diameter and wake positions, the time-of-flight, terminal drop velocity, initial and final relative velocities, the maximum Weber Number, and the final flow angle. A secondary atomization summary is also given. For each drop that satisfies the disruption criteria the summary lists the time-to-complete disruption, mass-mean diameter of secondary drops produced, drop velocity when the critical Weber Number is reached, and the referred distances to disruption. The absolute disruption distance is the total path length from the stator trailing edge to the estimated point of complete disruption. The first referred quantity gives the distance in drop diameters. The second gives the ratio of the absolute disruption distance to the total path length available between the stator and rotor planes. The distances are used to indicate whether there is sufficient space for the unstable primary drops to completely disintegrate before impact.

The input argument  $I\phi$  controls the print interval for the printout of values along the trajectory. If  $I\phi \leq 0$  the printout is deleted. The print interval is computed by:

$$ZP = (AXSP - XDEAD)/(I\phi - 1)$$

The effective total axial distance is the axial blade space minus the dead space. An input value of 11, for instance, will yield 11 sets of values spaced at intervals of one-tenth the total distance. The actual printing is done by subroutine DERIV.

#### ● Subroutine DERIV

This subroutine is used in conjunction with the integration scheme ICEAD to provide derivatives, intermediate printouts, and secondary atomization calculations. Three entry points DERIV, STEP and FAIL are employed. These satisfy the requirements of ICEAD. For each trail integration step ICEAD will call DERIV to obtain the derivatives associated with the simultaneous differential equations at that point. Certain error criteria are checked and if a given time step produces satisfactory results ENTRY STEP is called (the logic employed by ICEAD will be discussed below). When a trial integration fails, the step size (in the time variable) is halved. The process continues until an integration step yields satis-



factory results or a fixed lower step size limit is reached. In the latter event ICEAD calls FAIL which takes appropriate action.

Common blocks used in the subroutine are listed in Table 2.6-2. The calling sequence is as follows:

CALL DERIV (T, Y, DY, IRET)

where:

- |      |   |
|------|---|
| T    | is the present value of the time variable   |
| Y    | is a two-word array containing the present values of drop velocity, Y (1), and distance along the wake axis, Y (2).             |
| DY   | is a two word array containing the derivatives of Y (1) and Y (2).  |
| IRET | is a return sentinel. During the integration process IRET remains zero. When the integration is completed IRET is set to unity. |

A debug option (see main program for definition of KOP (10) is provided so that present values of distance, time and velocity are listed for each trial time step. After each successful integration STEP is entered and if a print interval has elapsed, the present values of time, distance along the wake axis, distance along the turbine axis, absolute and relative drop velocity, local Weber and Reynolds Numbers, and the time step used are printed.

Subroutine WAKE is called after each time step to get the local vapor velocity. If the wake iteration fails, diagnostics are printed and IRET is set to unity. This eventually returns control to subroutine TRAX so that the next trajectory may be started. The terminal flow angle is set to -1 if the wake calculation fails. Failure of the integration is indicated by inserting a value of -1 in the final velocity array.

#### ● Subroutine IMPAX

The geometry of drop impingement is evaluated with subroutine IMPAX. The range of possible absolute drop impact velocities is bounded by zero

and the stator exit jet velocity. Actually, the secondary atomization limit prevents the larger and slower moving drops from reaching the rotor. In any case the subroutine runs through all possible impact velocities and computes the drop velocity relative to the rotor, the normal component of impact velocity, and the impact length (these are defined as  $W_d$ ,  $W_n$ , and  $\Delta L$  in Figure 2.6-5).

Calling Sequence

Call IMPAX (NB, BDIA, RPM, AL, AI, VZERO)

where:

- |       |   |
|-------|---|
| NB    | is the number of rotor blades   |
| BDIA  | is the inlet diameter at the blade height in question   |
| RPM   | is the rotor RPM  |
| AL    | is the stator exit flow angle with respect to the turbine axis.   |
| AI    | is the actual rotor inlet blade angle (see $\alpha_i$ in Figure 2.6-5) with respect to the rotor inlet plane. |
| VZERO | is the stator jet velocity.   |

It was pointed out previously that the impact length approximation is only useful when impacts on the convex blade surface occur. When the conditions expressed by equations (39), (40) and (41) occur, nose impacts are important and the listed values of  $\Delta L$  will be set to:

$$\Delta L_{\max} = S \cos \alpha_i$$

#### ● Auxiliary Subroutines

Four general purpose subroutines are included in the code package. These were developed in the context of the overall turbine erosion model; however, they represent valuable tools which can be used in many other circumstances. Each is described fully in a separate report so that an abbreviated discussion is presented here.

### ● Subroutine SPLINT

This subroutine is designed to perform interpolation and differentiation using the parabolic spline. The spline is generated by a closed form expression, and an important characteristic of the method is that the first derivatives of the array of interpolated results are continuous. Unequal tabular intervals may be employed and a special search scheme has been devised to permit the independent variable to be either monotonically increasing or decreasing. A useful by-product of this method of interpolation is that an estimate of the local derivative (of the interpolated curve) may be readily obtained. The closed-form solutions used are due to Mintz and Jordan.

The subroutine has two entry points called SPLINT and DYDX, the former for interpolation and the latter for differentiation. The calling sequences are:

CALL SPLINT (XT, YT, NT, XI, YI, NI, JX, JY)

CALL DYDX (XT, YT, HT, XI, DY, NI, JX, JY)

where:

XT	is the name of the independent variable array
YT	is the name of the dependent variable array
NT	is the number of input (XT, YT) pairs. It is required that $NT \geq 4$ .
XI	is the name of the array of input interpolation arguments
YI	is the name of the output array of interpolated values
DY	is the name of the output array of first derivatives
JX, JY	are integers representing the storage increments in arrays XT and YT (standard values: $JX = JY = 1$ ).

The set (XT, YT) is the table in which the interpolation is to be done. Dummy dimensions are used for all arrays so that the storage space required is set by the calling program. XI, YI and DY are listed as arrays; however, they may represent single values.

### ● Subroutine VERGE

VERGE is designed to accelerate the convergence of iterative processes. Many equations encountered in the numerical solution of engineering problems do not permit explicit solution for certain variables; these must be solved by iterative techniques. A good example is the simultaneous set of equations (25), (26), and (28) employed in the stator wake treatment discussed above. The scheme utilized by VERGE accelerates the rate of convergence if the iteration converges and induces convergence if the basic iteration process tends to diverge. The subroutine is based on the convergence algorithm of Wegstein<sup>(12)</sup>. The general class of problems which is of interest is that which may be written in the form:  $x = f(x)$ . The right-hand side is typically a complicated transcendental relation or perhaps the result of a lengthy numerical operation.

### ● Calling Sequence

Call VERGE (XI, FØX, IK)

where:

XI	is the present value of the iterated variable. User must supply an initial guess, and at each pass through VERGE XI will be modified to induce convergence.
FØX	is the value of the function $F(XI)$ for the present XI
IK	is an iteration counter. User must preset IK for the first iteration. It is updated by VERGE and set negative when the convergence test is met. Normally IK is preset to zero. The user should test present values of IK as they are returned from VERGE to detect convergence.

- Convergence Criteria

It is necessary to insure that machine underflows will not result. If one is searching for a root near the origin, very small numbers (in absolute value) will be encountered during the iteration. Convergence is assumed if either of the following conditions is satisfied.

$$\begin{aligned} |f(x_n) - x_n| &< \text{EPS} \\ |x_n| &< \text{ETA} \end{aligned}$$

where EPS and ETA are quantities defined in a DATA statement and may be modified by the user to fit special situations. In the subroutine version described here they have been given the values  $1 \times 10^{-10}$  and  $1 \times 10^{-30}$ , respectively. Non-convergence is not detected explicitly. The user should check the present value of the iteration counter IK against some upper limit appropriate for the particular problem at hand. For the wake parameter iteration in subroutine WAKE it has been found that if convergence is not reached after 20 iterations, the input data is usually at fault.

- Subroutine ICEAD

This subroutine is a general purpose scheme for solving systems of ordinary differential equations. A fourth-order Adams predictor-corrector method is used with automatic error control. It is based on ICEADAMS, an ALGOL-5000 procedure by Geil and Wei<sup>(13)</sup> which was translated into FORTRAN by the author and modified for this application.

- Calling Sequence and Required Common Block

```
CALL ICEAD (N, T, XI, IRET)
COMMON/ICON/H, HMAX, HMIN,
REL, ABSB
```

where:

N is the number of dependent variables.  
(simultaneous differential equations)

T is input as the initial value of the independent variable

XI input as the vector (one-dimensional array) of initial values of each of the N dependent variables.

IRET output integer return sentinel which must be zero initially: When the subroutine detects a non-zero value of IRET, control is returned to the calling program. May be used to indicate that the integration is completed—either successfully or otherwise.

H is input as the suggested initial step-size. Will thereafter contain the present step size selected by ICEAD.

HMAX is the maximum acceptable step size.

HMIN is the minimum acceptable step size.

RELB is the maximum acceptable relative error (the ratio of the absolute difference between the predictor and corrector for each independent variable).

ABSB is the maximum acceptable absolute error. (If RELB is exceeded but the absolute difference between the predictor and corrector values is smaller than ABSB, ICEAD will accept the integration step as successful. ABSB is used to guard against exceeding the machine accuracy limits.

- General Use of the Subroutine

The analytical basis of the subroutine is given in Reference 13 which describes the ALGOL version. Certain mechanical aspects have been changed due to language incompatibilities; however, the basic numerical steps are identical in the two versions.

The common block ICON was incorporated to permit optional user control of the error bounds in the auxiliary subroutines. The FORTRAN version described here has been dimensioned to permit the solution of up to ten simultaneous differential equations. The user is required to provide three auxiliary subroutines with the names DERIV, STEP, and FAIL. It is usually convenient to use one subroutine with three entry points to perform the appropriate functions.

- Subroutine DERIV (T, X, DX, IRET)

The argument list consists of:

T	the present value of the independent variable (input)
X	vector of values of the dependent variables (input)
DX	vector of derivatives of array x (output)
IRET	return sentinel

The calling program provides ICEAD with a set of initial values for the independent and dependent variables. ICEAD will then determine trial step sizes and will call DERIV to calculate required derivatives based on present values of each dependent variable and associated derivatives. Note the initial values for the derivatives can be defined if necessary in DERIV. IRET is normally not used in DERIV. It may be set non-zero if an anomalous condition is encountered. If ICEAD detects a non-zero value at any time, control is returned to the calling program.

- Subroutine STEP (T, X, DX, IRET)

STEP is called by ICEAD after each successful integration step. The argument list is the same as for DERIV so that STEP may be defined alternately as an entry point in DERIV. A printout section may be provided here to list results at pre-determined increments of any of the variables. A test for the termination of integration must be included in STEP. The user may simply call EXIT or STEP, or set IRET > 0. Control will then pass to the routine which originally called ICEAD. Normally,

the last integration step will over-run the integration limit. This can be avoided by adjusting the step size limit HMAX just before the integration limit is reached to force termination at the desired point.

- Subroutine FAIL (T, X, DX, IRET)

FAIL is called by ICEAD when the integration step size has been reduced below HMIN. ICEAD will strive to select the largest step size available. Trial steps are taken at one-half and twice the present step size and the error criteria checked. If the criteria cannot be satisfied for any H such that  $HMAX > H > HMIN$ , FAIL is called. In FAIL the user may wish to print some diagnostic comments. It is necessary then to call EXIT, STOP, or set IRET > 0 and RETURN.

- Subroutine PROPM

This subroutine was designed to generate comprehensive thermophysical properties of various power system working fluids. It provides a central data source, with a consistent set of units, to support computerized design and analysis efforts. The basic system of units is metric; however, a conversion subroutine is supplied to communicate in engineering units. The user supplies a temperature and specifies a material and a property, and gets the required property value back.

All properties are taken along a saturation line and are assumed to be functions of temperature only. Most of the properties are described by equations obtained from least square fits. In a few cases this was not feasible and spline interpolation (subroutine SPLINT) is used on tabular data. In general the empirical fits are more desirable. They offer a speed advantage and require far less storage space than tabular data.

Eight working fluids are represented in the data compilation. Four of these, potassium, cesium, water, and mercury, have received the most attention since they have been required in various phases of turbine erosion analysis under the subject contract. The remaining fluids, lithium, sodium, rubidium, and NaK-78, have been given a cursory treatment and were included for the sake of completeness. No attempt at evaluation was made at this time. The

primary source of the potassium and cesium data is the work of Ewing, et. al. (14, 15) and Achener<sup>(16)</sup>. Water data was obtained from the recently completed ASME steam tables<sup>(17)</sup>. The mercury data was required for an erosion-oriented analysis of the Sunflower turbine series so that for the sake of compatibility at TRW data compilation<sup>(18)</sup> was used.

#### Calling Sequence

Call PROPM (XM, TK, JPROP, JFLUID)

Call PROPE (XE, TR, JPROP, JFLUID)

where

XM is the output property value in metric units.

XE is the output property value in engineering units.

TK is the input temperature in degrees Kelvin.

TR is the input temperature in degrees Rankine.

JPROP specifies a particular property according to the following table:

JPROP	Property	PROPM Units	PROPE Units
1	Liquid density	g/cm <sup>3</sup>	lbm/ft <sup>3</sup>
2	Vapor density	g/cm <sup>3</sup>	lbm/ft <sup>3</sup>
3	Liquid viscosity	g/sec-cm (poise)	lbm/ft-sec
4	Vapor viscosity	g/sec-cm	lbm/ft-sec
5	Liquid thermal conductivity	W/cm-°K	Btu/sec-ft-°R
6	Vapor thermal conductivity	W/cm-°K	Btu/sec-ft-°R
7	Liquid specific heat	joule/g-°K	Btu/lbm-°R
8	Vapor specific heat	joule/g-°K	Btu/lbm-°R
9	Surface tension	dyn/cm	lb/ft
10	Not Used	---	---
11	Liquid sonic velocity	cm/sec	ft/sec
12	Vapor sonic velocity	cm/sec	ft/sec
13	Vapor pressure	bars	psia
14	Latent heat of vaporization	joule/g	Btu/lbm
15	Liquid electrical resistivity	ohm-cm	ohm-in.

The rationale of the metric system chosen is that it almost completely eliminates the use of conversion factors. The unnecessary distinction between heat and energy units has not been made. JFLUID

specifies a particular working fluid according to the following convention:

JFLUID	MATERIAL
1	Lithium
2	Sodium
3	Potassium
4	Rubidium
5	Cesium
6	Mercury
7	NaK-78
8	Water

#### 2.6.5 The Solution of an Illustrative Problem

The sample problem chosen is an analysis of drop transport in a steam test rig used by Rocketdyne in a NASA-sponsored experimental program under Contract NAS 7-391. This program involves the examination of drop formation in a system using six stator blade shapes and a variety of flow conditions. Blade shape 1-A and the conditions designated as test 114A were chosen for the illustrative problem.

The series of input cards required for this problem are shown in Table 2.6-3. Input for a subsequent problem test 114B, is also given to show how the code makes use of data carried from one problem to the next. Only those values which are different from the previous case need to be specified.

The code-produced summary of input data is given in Table 2.6-4. Working fluid properties evaluated at the input temperature and quality are also tabulated. If a boundary layer calculation is required the listing shown in Table 2.6-5 will appear. This is a tabulation of the input blade surface velocity arrays and the blade Reynolds numbers, based on exit conditions and the surface lengths, for both pressure and suction sides. A sample of the detailed boundary layer result listing is given in Table 2.6-6. Since this output is optional, a summary of the boundary layer results evaluated at the blade trailing edge will always appear and is shown in Table 2.6-7.

A sample of the detailed results obtained from the drop trajectory calculations is shown in Table 2.6-8. Such a listing will appear for each possible combination of drop size and wake position.

ROCKETDYNE BLADE 1-A      TIP SECTION      TEST 114A

ROCKETDYNE BLADE 1-A      TIP SECTION      TEST 114B

TABLE 2.6-4

INPUT DATA		ROCKETDYNE BLADE 1-A		TIP SECTION	TEST 114A					
OPTIONS	KOP =	8	29	0	11	1	12	-R	0	0
BULK FLUID TEMPERATURE (DFG R)	=			601.50	FUEL-STARFAM VELOCITY (FPS)	=			1170.00	
RULK FLOW QUALITY	=			.9960	EXIT FLOW ANGLE (DFG)	=			48.80	
INLET ROTOW BLADE ANGLE (DFG)	=			0.00	DEAN-SPACE MULTIPLIER	=			6.70	
CRITICAL WFER NUMBER	=			22.00	EXIT STATOR DIAMETER (IN)	=			5.9419	
INLET HATOR DIAMETER (IN)	=			0.0000	AETAL INTER-ROW SPACE (IN)	=			1.0000	
STATOR TE THICKNESS (IN)	=			.0075	STATOR CHORD (IN)	=			1.2000	
PRESSURE SURF. LENGTH (IN)	=			1.4120	SUCTION SURF. LENGTH (IN)	=			1.1420	

2-180

TABLE 2.6-5

## BOUNDARY LAYER INPUT DATA SUMMARY

TWO-D BOUNDARY LAYER CALCULATION			ROCKETDYNE BLADE 1-A		TIP SECTION	TEST 114A
FLUID = WATER	RES =	1.354E+05	REP =	1.676E+05		
INPUT POSITION AND SURFACE VELOCITY ARRAYS						
SUCTION	X	V	PRESSURE	X	V	
	0.0000	.4080		0.0000	.1800	
	.1000	.8400		.1000	.4200	
	.2000	.8940		.2000	.5400	
	.3000	.9640		.3000	.5670	
	.4000	1.0600		.4000	.5650	
	.5000	1.0920		.5000	.6100	
	.6000	1.1000		.6000	.6300	
	.7000	1.0990		.7000	.6620	
	.8000	1.0900		.8000	.7280	
	.9000	1.0760		.9000	.8140	
	1.0000	1.0000		1.0000	1.0000	

TABLE 2.6-6

## DETAILED BOUNDARY LAYER RESULT PRINTOUT

TWO-D BOUNDARY LAYER CALCULATION			ROCKETDYNE BLADE 1-A		TIP SECTION	TEST 114A		
SUCTION SURFACE								
REFERRED DISTANCE	REFERRED VELOCITY	REFERRED MOM THIC	SHAPE FACTOR	FORM FACTOR	EXPONENT N	MOMENTUM THICKNESS	DISPL. THICKNESS	FULL THICKNESS
.025000	.551162	.000000	0.000000	1.400000	5.000000	.000244	.000342	.002171
.050000	.707050	.000159	-.049004	1.488689	4.092581	.000463	.000449	.003447
.075000	.767162	.000214	-.064414	1.520642	3.842889	.000721	.000945	.004474
.100000	.840000	.000270	-.072400	1.540074	3.703193	.001124	.001266	.005471
.125000	.880409	.000342	-.083054	1.578128	3.489439	.000492	.001545	.006070
.150000	.891875	.000437	-.096479	1.624942	3.280298	.001268	.002041	.006444
.175000	.891703	.000543	-.102153	1.647349	3.089522	.001474	.002497	.006412
.200000	.898000	.000634	-.095873	1.621864	3.216136	.001834	.002881	.007249
.225000	.913234	.000700	-.083212	1.575511	3.475170	.002032	.003201	.007424
.250000	.928625	.000762	-.074711	1.547734	3.651405	.002211	.003422	.007917
.275000	.945203	.000817	-.067341	1.528299	3.785735	.002371	.003624	.007740
.300000	.964000	.000863	-.059012	1.511317	3.911465	.002504	.003785	.007840
.325000	.987191	.000895	-.050444	1.490957	4.073480	.002594	.003870	.007934
.350000	1.014125	.000916	-.041444	1.472337	4.234264	.002657	.003912	.007977
.375000	1.039797	.000939	-.036187	1.462630	4.328439	.002725	.003944	.007970
.400000	1.060000	.000974	-.036424	1.462305	4.326164	.002832	.004141	.007966
.425000	1.073062	.001031	-.040895	1.470844	4.247472	.002949	.004397	.007964
.450000	1.081500	.001096	-.045048	1.481080	4.157237	.003174	.004704	.007964
.475000	1.087187	.001167	-.050257	1.490127	4.088579	.003385	.005044	.007960
.500000	1.092000	.001239	-.052879	1.495811	4.031797	.003594	.005377	.007964
.525000	1.095898	.001313	-.054402	1.499624	4.003010	.003809	.005644	.007964
.550000	1.098862	.001391	-.056444	1.503620	3.949407	.004036	.005944	.007964
.575000	1.099195	.001472	-.058104	1.507347	3.901051	.004270	.006237	.007964
.600000	1.100000	.001554	-.059074	1.509485	3.925432	.004504	.006492	.007964
.625000	1.100470	.001635	-.059485	1.510540	3.916067	.004743	.006744	.007964
.650000	1.100462	.001718	-.060090	1.511704	3.908444	.004984	.007035	.007964
.675000	1.100023	.001803	-.060415	1.512861	3.899496	.005231	.007314	.007964
.700000	1.099000	.001891	-.061174	1.514090	3.890347	.005484	.007603	.007964
.725000	1.097430	.001980	-.061849	1.515604	3.878430	.005744	.007895	.007964
.750000	1.095312	.002073	-.062444	1.517465	3.864947	.006012	.008187	.007964
.775000	1.092789	.002167	-.063479	1.519452	3.850210	.006287	.008479	.007964
.800000	1.089800	.002264	-.064427	1.521377	3.835995	.006567	.008771	.007964
.825000	1.086305	.002354	-.064122	1.520682	3.841116	.006829	.009063	.007964
.850000	1.087187	.002440	-.063284	1.518791	3.855114	.007077	.009355	.007964
.875000	1.083077	.002540	-.064288	1.521062	3.873414	.007344	.009647	.007964
.900000	1.076000	.002675	-.069234	1.532866	3.753336	.007740	.010144	.007964
.925000	1.062812	.002855	-.078149	1.544500	3.581019	.008280	.010644	.007964
.950000	1.045750	.003075	-.089014	1.599321	3.337108	.008910	.011444	.007964
.975000	1.024412	.003345	-.106234	1.655031	3.053292	.009703	.012444	.007964
1.000000	1.000000	.003678	-.121704	1.741637	2.696737	.010668	.013444	.007964

In the given sample problem 30 such sets will be generated. At each time point listed the drop position on the wake axis, along the turbine axis, the drop velocity, drop relative velocity, local drop Reynolds number, local drop Weber Number, and the present integration time step are tabulated. Table 2.6-9 shows the summary of trajectory results which appears at the conclusion of each problem. For each diameter and wake position the following items are given:

- TFLIGHT** This is the time-of-flight (seconds) of the drop along the trajectory.
- VDFINAL** This is the terminal velocity of the drop (cm/sec) at the rotor inlet plane.
- VRELI** This is the initial relative velocity of the drop (cm/sec) when it leaves the trailing edge dead band.
- VRELF** This is the final relative velocity of the drop (cm/sec).
- WEDM** This is the maximum local drop Weber Number which occurred along the trajectory.
- ALPHA** This is the terminal inclination of the velocity vector VDFINAL, with respect to the turbine axis, at the rotor inlet plane.

A secondary atomization data summary then appears as shown in Table 2.6-10. For each drop diameter-wake position combination where the critical Weber Number has been exceeded the following quantities are listed:

- TDIS** is the time (Equation 33) required to complete disruption.
- DSTC** is the mass mean diameter (cm) of secondary drops formed.
- /DIS** is the relative drop velocity at the point at which the critical Weber Number was exceeded.
- XDC** is the distance along the path from the trailing edge to the point of complete disruption divided by the drop diameter.

**XDIS** is the path length to the point of complete disruption, divided by the total possible path. A value greater than or equal to unity implies there is insufficient time for the drop to shatter prior to impact.

The sample problem used did not involve an examination of the impact geometry since the test rig did not incorporate a stator section downstream of the nozzle examined. The results of another problem are included here (Table 2.6-11) to illustrate the output form of the impact geometry summary. These data are taken from an analysis of drop transport in the last stage of the Sunflower mercury turbine. The nomenclature used on the printout corresponds with that used in Figure 2.6-5 and in the defining Equations 35 through 41.

#### 2.6.6 Summary

A model describing the transport of atomized condensate in wet vapor turbines has been assembled. The basic problem which is considered is the trajectories of drops of liquid in the space between the rotor, where it is discharged, and the rotor inlet plane. Relatively simple closed-form solutions for the drop equation of motion have been obtained for certain special cases. A detailed calculational procedure was developed to provide specific solutions to the problem in a more general context.

The drop transport code package (ADROP) has been described in detail. The scope of the numerical treatment is as follows:

- a) Estimation of stator blade boundary-layer characteristics.
- b) Generation of the local velocity field within the vapor wake downstream of stator blades.
- c) Numerical integration of the equation of motion of drops traveling along various wake streamlines and the estimation of secondary atomization effects.
- d) Solution of drop impact velocity triangles to provide information on the magnitude of the normal component of impact velocity and the physical location of erosion.



TABLE 2.6-7

TRAILING EDGE BOUNDARY LAYER DATA  
SUMMARY

TRAILING EDGE BOUNDARY LAYER DATA	ROCKETDYNE BLADE 1-A	TIP SECTION	TEST 114A
	PRESSURE SIDE	SUCTION SIDE	
MOMENTUM THICKNESS (CM)	.00359	.01067	
DISPLACEMENT THICKNESS (CM)	.00474	.01854	
FULL THICKNESS (CM)	.03448	.06868	

TABLE 2.6-8

## PRINTOUT OF DETAILED TRAJECTORY RESULTS

DROP TRAJECTORY STUDY      ROCKETDYNE BLADE 1-A      TIP SECTION      TEST 114A

DROP DIAMETER = 170.00 MICRONS      WAKE Y/D = 0.00

TIME	X=WAKE	Z=WAKE	VDROP	VREL	WED	RED	H
4.20117E-04	7.62314E-02	2.74186E-02	9.15721E+00	1.49087E+04	8.36201E+00	3.42150E+02	A.2012E-06
7.99951E-04	7.62542E-01	2.51401E-01	1.94434E+03	2.44865E+04	2.25572E+01	5.45550E+02	A.2012E-06
1.05420E-03	1.33584E+00	4.77421E-01	3.03727E+03	2.57673E+04	2.49787E+01	5.74085E+02	A.2012E-06
1.24023E-03	1.07833E+00	7.07063E-01	3.81378E+03	2.60419E+04	2.56126E+01	5.81311E+02	A.2012E-06
1.39526E-03	2.63302E+00	9.41040E-01	4.58013E+03	2.61132E+04	2.56539E+01	5.81742E+02	A.2012E-06
1.52549E-03	3.26859E+00	1.16774E+00	5.17108E+03	2.60120E+04	2.56554E+01	5.79537E+02	A.2012E-06
1.64331E-03	3.90908E+00	1.39440E+00	5.69972E+03	2.58534E+04	2.51454E+01	5.76004E+02	A.2012E-06
1.75493E-03	4.57289E+00	1.63337E+00	6.19297E+03	2.56598E+04	2.47707E+01	5.71690E+02	A.2012E-06
1.85415E-03	5.20879E+00	1.86037E+00	6.62401E+03	2.54611E+04	2.43886E+01	5.67264E+02	A.2012E-06
1.94717E-03	5.84347E+00	2.08492E+00	7.02104E+03	2.52575E+04	2.40002E+01	5.62726E+02	A.2012E-06
2.04019E-03	6.41473E+00	2.32653E+00	7.41086E+03	2.50411E+04	2.35907E+01	5.57907E+02	A.2012E-06
2.11915E-03	7.11204E+00	2.54002E+00	7.73586E+03	2.48497E+04	2.32314E+01	5.53442E+02	1.0000E-08

TABLE 2.6-9

## SUMMARY OF TRAJECTORY RESULTS

DROP TRAJECTORY STUDY      ROCKETDYNE BLADE 1-A      TIP SECTION      TEST 114A

## SUMMARY OF RESULTS

TIME	Y/D	FLIGHT	VDFINAL	VRFL1	VRFL2	WED	ALPHA
170.00	0.00	2.1192E-03	7.7358E+03	1.4917E+04	2.4850E+04	2.5677E+01	A.9078E+01
150.00	0.00	2.0269E-03	8.0671E+03	1.4917E+04	2.4533E+04	2.2314E+01	A.9078E+01
140.00	0.00	1.9779E-03	8.2224E+03	1.4917E+04	2.4343E+04	2.0674E+01	A.9078E+01
130.00	0.00	1.9268E-03	8.4141E+03	1.4917E+04	2.4171E+04	1.9631E+01	A.9078E+01
120.00	0.00	1.8732E-03	8.6244E+03	1.4917E+04	2.3961E+04	1.7390E+01	A.9078E+01
100.00	0.00	1.7573E-03	9.1172E+03	1.4917E+04	2.3448E+04	1.6174E+01	A.9078E+01
90.00	0.00	1.6940E-03	9.4117E+03	1.4917E+04	2.3174E+04	1.2590E+01	A.9078E+01
70.00	0.00	1.5531E-03	1.0138E+04	1.4917E+04	2.2448E+04	3.1765E+00	A.9078E+01
50.00	0.00	1.3851E-03	1.1164E+04	1.4917E+04	2.1422E+04	6.4460E+00	A.9078E+01
190.50	0.00	2.2071E-03	7.4407E+03	1.4917E+04	2.4125E+04	2.3140E+01	A.9078E+01
170.00	.35	1.8375E-03	8.0958E+03	2.0573E+04	2.5112E+04	2.4066E+01	A.9078E+01
150.00	.35	1.7581E-03	8.4204E+03	2.0573E+04	2.4288E+04	2.4460E+01	A.9078E+01
140.00	.35	1.7160E-03	8.6036E+03	2.0573E+04	2.4005E+04	2.2872E+01	A.9078E+01
130.00	.35	1.6720E-03	8.8436E+03	2.0573E+04	2.4505E+04	2.0904E+01	A.9078E+01
120.00	.35	1.6250E-03	9.0224E+03	2.0573E+04	2.4385E+04	1.9123E+01	A.9078E+01
100.00	.35	1.5261E-03	9.5171E+03	2.0573E+04	2.3871E+04	1.5617E+01	A.9078E+01
90.00	.35	1.4717E-03	9.8432E+03	2.0573E+04	2.3565E+04	1.3015E+01	A.9078E+01
70.00	.35	1.3505E-03	1.0590E+04	2.0573E+04	2.2809E+04	1.0526E+01	A.9078E+01
50.00	.35	1.2060E-03	1.1467E+04	2.0573E+04	2.1741E+04	7.2292E+00	A.9078E+01
190.50	.35	1.9132E-03	7.8087E+03	2.0573E+04	2.5600E+04	3.1799E+01	A.9078E+01
170.00	1.00	1.3950E-03	9.0961E+03	3.5635E+04	2.6507E+04	6.4674E+01	A.9078E+01
150.00	1.00	1.3356E-03	9.4582E+03	3.5635E+04	2.6141E+04	4.1291E+01	A.9078E+01
140.00	1.00	1.3040E-03	9.6622E+03	3.5635E+04	2.5937E+04	3.8484E+01	A.9078E+01
130.00	1.00	1.2711E-03	9.8848E+03	3.5635E+04	2.5714E+04	3.5884E+01	A.9078E+01
120.00	1.00	1.2366E-03	1.0129E+04	3.5635E+04	2.5470E+04	3.2994E+01	A.9078E+01
100.00	1.00	1.1619E-03	1.0701E+04	3.5635E+04	2.4897E+04	2.7303E+01	A.9078E+01
90.00	1.00	1.1211E-03	1.1042E+04	3.5635E+04	2.4557E+04	2.4518E+01	A.9078E+01
70.00	1.00	1.0305E-03	1.1882E+04	3.5635E+04	2.3771E+04	1.4064E+01	A.9078E+01
50.00	1.00	9.2230E-04	1.3065E+04	3.5635E+04	2.2634E+04	1.3707E+01	A.9078E+01
190.50	1.00	1.4517E-03	8.7757E+03	3.5635E+04	2.6823E+04	5.2612E+01	A.9078E+01

TABLE 2.6-10

## SECONDARY ATOMIZATION SUMMARY

DROP TRAJECTORY STUDY

ROCKETDYNE HLADF 1-A TIP SECTION

TEST 114A

## SECONDARY ATOMIZATION SUMMARY

DIAM	YD	TUIS	DSEC	VDIS	XDC	XDIS
170.00	0.00	1.6612E-04	1.8155E-03	2.4188E+04	5.8397E+01	1.3957E-01
150.00	0.00	1.3770E-04	1.6396E-03	2.5747E+04	1.3544E+02	2.8563E-01
190.00	0.00	1.9674E-04	1.9474E-03	2.2885E+04	3.8937E+01	1.0424E-01
170.00	.35	1.6610E-04	1.8152E-03	2.4191E+04	2.8254E+01	6.7524E-02
150.00	.35	1.3755E-04	1.6373E-03	2.5774E+04	5.0742E+01	1.0701E-01
140.00	.35	1.2414E-04	1.5496E-03	2.6655E+04	8.3975E+01	1.6529E-01
190.50	.35	1.9649E-04	1.9443E-03	2.2915E+04	1.9361E+01	5.1853E-02
170.00	1.00	1.1383E-04	1.0419E-03	3.5298E+04	9.3325E+00	2.2305E-02
150.00	1.00	1.0054E-04	1.0654E-03	3.5264E+04	1.0090E+01	2.1274E-02
140.00	1.00	9.3887E-05	1.0470E-03	3.5244E+04	1.0039E+01	1.9754E-02
130.00	1.00	8.7238E-05	1.0478E-03	3.5221E+04	1.1099E+01	2.0284E-02
120.00	1.00	8.0587E-05	1.0380E-03	3.5195E+04	1.1130E+01	1.8777E-02
100.00	1.00	6.7283E-05	1.0162E-03	3.5129E+04	1.2644E+01	1.7833E-02
90.00	1.00	6.0628E-05	1.0040E-03	3.5086E+04	1.2944E+01	1.6406E-02
190.50	1.00	1.2745E-04	1.0964E-03	3.5327E+04	8.7118E+00	2.3332E-02

TABLE 2.6-11

## IMPACT GEOMETRY DATA SUMMARY

SUNFLOWER TURBINE STAGE 3 MEAN SECTION WEC = 13

SECTION DIAMETER (CM) =	4.5720	WHEEL RPM	=	40000.0
WHEEL SPEED (CM/SEC) =	9575.57	ALPHA	=	73.50
BLADE PITCH (CM) =	.1818	ALPHA1	=	28.70
MAX DELTA L (CM) =	.1595	ALPHADO (DEG)	=	61.30
VDROPO (CM/SEC) =	6453.60	WD = WN (CM/SEC)	=	7054.51
VZFRO (CM/SEC) =	21781.01			

VD	WD	WN	ALPHAD	BETA	IMPACT LENGTH
0.00	9575.57	4598.42	0.00	61.30	0.00000
1090.00	8536.08	4368.07	2.08	59.22	.01289
2180.00	7510.91	4137.73	4.73	56.57	.02721
3270.00	6506.85	3907.38	8.21	53.09	.04321
4360.00	5535.41	3677.04	12.93	48.37	.06123
5450.00	4617.19	3446.69	19.59	41.71	.08165
6540.00	3791.10	3216.35	29.34	31.96	.10500
7630.00	3130.92	2986.00	43.80	17.50	.13195
8720.00	2758.44	2755.66	63.87	-2.57	.15948
9810.00	2791.34	2525.31	86.52	-25.22	.15948
10900.00	3217.20	2294.97	105.79	-44.49	.15948
11990.00	3909.64	2064.62	119.42	-58.12	.15948
13080.00	4753.58	1834.28	128.60	-67.30	.15948
14170.00	5681.89	1603.93	134.90	-73.60	.15948
15260.00	6659.39	1373.59	139.40	-78.10	.15948
16350.00	7667.28	1143.24	142.72	-81.42	.15948
17440.00	8695.01	912.90	145.27	-83.97	.15948
18530.00	9736.29	682.56	147.28	-85.98	.15948
19620.00	10787.20	452.21	148.90	-87.60	.15948
20710.00	11845.18	221.87	150.23	-88.93	.15948
21781.01	12889.92	0.00	151.32	-90.02	.15948

The model represents a first cut at a comprehensive explanation of observed phenomena. Unfortunately, the kinds of experimental data required to verify and improve the model simply do not exist. Key areas of uncertainty are the critical Weber Number estimates and wake behavior immediately downstream of stator trailing edges. The criterion for disruption should reflect the abruptness of the onset of accelerating forces and should be sufficiently general to permit its use with dissimilar working fluids. These deficiencies in the model, however, do not negate its usefulness in most circumstances. When a series of similar turbine designs is being considered, the model will give an excellent estimate of the relative erosion potential of the competing designs. The key effect of axial stator-rotor spacing can certainly be examined and with the use of a conservative critical Weber Number estimate these results can be expressed directly as a design limit. Another important factor which can be examined on a parametric basis is the effect of shaft rpm (hence, tip speed) on the erosion potential.

#### 2.6.7 Nomenclature

$a, b, n_1, n_2, n_3$  Empirical constants

$A_d$  Drop cross-sectional area

$C$  Stator blade chord length

$C_d$  Drop drag coefficient

$C_f$  Friction factor

$D_d, D'_d$  Primary and secondary drop diameters

$E$  Defined by Equation 15

$F_d$  Aerodynamic force on a drop

$f, g$  Functional relationship

$H$  Form factor

$K_d$  Inertial parameter group

$L$  Shape factor

$Re$  Reynolds Number

$S$  Blade pitch

$t, t', t''$  Time, time-to-disruption, time-to-complete disruption

$U, U_o, U_{min}$  Local vapor velocity, wake-edge, and wake axis vapor velocities

$U_t$  Tangential blade speed

$V_d$  Absolute drop velocity

$V_r$  Relative velocity between drop and vapor stream

$W_e$  Drop Weber Number

$W_d$  Drop terminal velocity relative to the rotor blade.

$W_n$  Drop terminal velocity normal to the stator blade.

$X$  Distance along the wake axis

$Y$  Distance normal to the wake axis

$Z$  Distance along the turbine axis

$\alpha$  Stator exit flow angles

$\alpha_i, \alpha_d$  Velocity triangle angles defined in Figure 2.6-5.

$\beta$  Local wake angle

$\Delta L$  Impact length

$\xi$  Defined in Equation 13

$\epsilon$  Normalized distance ( $x/\delta$ ) along the wake axis

$\delta, \delta^*$  Wake full thickness, displacement thickness

$\rho_v, \rho_L$  Vapor and liquid density

$\sigma_L$  Surface tension

$\theta, \hat{\theta}$  Wake momentum thickness and thickness parameter

$\mu_v$  Vapor viscosity

## 2.6.8 References

1. Lambiris, S. and L. P. Combs, "Steady-State Combustion Measurements in a LOX/RP-1 Rocket Chamber and Related Spray Burning Analysis," Detonation and Two-Phase Flow, Academic Press, p. 283, 1962.
2. Wolfe, H. E. and W. H. Anderson, "Kinetics, Mechanism and Resultant Drop Sizes of the Aerodynamic Breakup of Liquids," Report 6395-04-185P, Aerojet-General Corp., April 1964.
3. Lieblein, S. and W. H. Roudebush, "Low-Speed Wake Characteristics of Two-Dimensional Cascade and Isolated Airfoil Sections," NACA-TN-3771, October 1956.
4. Truckenbrodt, E., "A Method of Quadrature for Calculation of the Laminar and Turbulent Boundary Layer in Plane and Rotationally Symmetrical Flow," NACA-TM-1379, 1955.
5. Speidel, L., "Untersuchungen über die Stromungsverluste in Ebenen Schaufelgittern," VDI-Forschungsheft 464, 1957.
6. Schlichting, H., Boundary Layer Theory, Chapter XXII, McGraw-Hill, New York, 1960.
7. Gardner, G. C., "Events Leading to Erosion in the Steam Turbine," Proc. Inst. Mech. Engrs. Vol. 78, No. 23, pp 593-623, 1963-64.
8. Nicholson, J. E., "Drop Breakup by Air-stream Impact," Paper presented at the 2nd Rain Erosion Conference, Meersburg, Germany, August 1967.
9. Clark, B. J. "Breakup of a Liquid Jet in a Transverse Flow of Gas," NASA-TN-D-2424, August 1964.
10. Katsanis, T., "A Computer Program for Calculating Velocities and Streamlines for Two-Dimensional, Incompressible Flow in Axial Blade Rows," NASA-TN-D-3762, January 1967.
11. Mintz, M. D. and Jordan, D. P., "A Progressive Interpolation Scheme for Hand and Digital Computer Analysis of Tabulated Data," UCRL-7681, February 1964.
12. Wegstein, J. H., "Accelerating Convergence of Iterative Processes," Comm. of the ACM, Volume 1, No. 6, June 1958.
13. Geil, E. and Wei, D. P., "ICEADAMS-A Computer Package for Solving Systems of Ordinary Differential Equations," Report 65-IC4-COMP-R2, Westinghouse Research Laboratories, February 1965.
14. Ewing, C. E., et al., "High Temperature Properties of Potassium," NRL 6233, September 1965.
15. Ewing, C. E., et al., "High Temperature Properties of Cesium," NRL 6246, September 1965.
16. Achener, P. Y., et al., "Thermophysical and Heat Transfer Properties of Alkali Metals," AGN-8195, Volume 1, April 1968.
17. Thermodynamic and Transport Properties of Steam, American Society of Mechanical Engineers, New York, 1967.
18. Ross, D. P., "Thermodynamic Properties of Mercury," TRW Technical Memorandum (TM-777), June 1957.

## APPENDIX 2.6A

### CALCULATED AND EXPERIMENTAL ATOMIZED DROP VELOCITIES IN LAST STAGE OF CENTRAL STATION STEAM TURBINES

There are several aspects to the acceleration of the drops discharged from wet turbine stators. The first is the acceleration of the primary drops immediately after formation and up to the time of disruption. The second is the continued acceleration of the liquid as secondary drops. A third is where will the drops hit on the rotor blades?

Limited experimental information on primary and secondary drop accelerations under turbine-like conditions is available from steam cascade tests reported by the Central Electricity Research Laboratories (CERL) of the United Kingdom.\* These experiments were conducted on a stator cascade simulating the last row of stators in large central station steam turbines and using system conditions appropriate to such last stator rows.

The CERL results are compared to calculated values for the Yankee Atomic Plant steam turbine last stage at the mean diameter. Complete geometric data on the CERL cascade blades is not given in the referenced material.\*\* However, such dimensions as are supplied are within 20 percent of the mean diameter section values for the Yankee last stage, and the nozzle exit angles are nearly identical. Figure 2.6A-1 compares the CERL observed velocities for various sizes of primary drops at a location 0.74 in. downstream of the stators to those calculated for the Yankee steam turbine. Figure 2.6A-2 compares the CERL observed velocities of 150 micron diameter secondary drops at various downstream distances with calculated curves for 100 micron and 200 micron diameter secondary drops for the Yankee turbine. In both cases, the observed velocities are on the average higher than the calculated velocities.

\* Hays, L.G., Turbine Erosion Research in Great Britain, NASA Jet Propulsion Laboratory, C.I.T. Tech Memo, No. 33-271.

\*\* Christie, D.G., Experimental Investigation of Internal Flow in Turbines, Jet Propulsion Laboratory, C.I.T. Tech. Memo 33-354, Sect. 12, June 15, 1967.

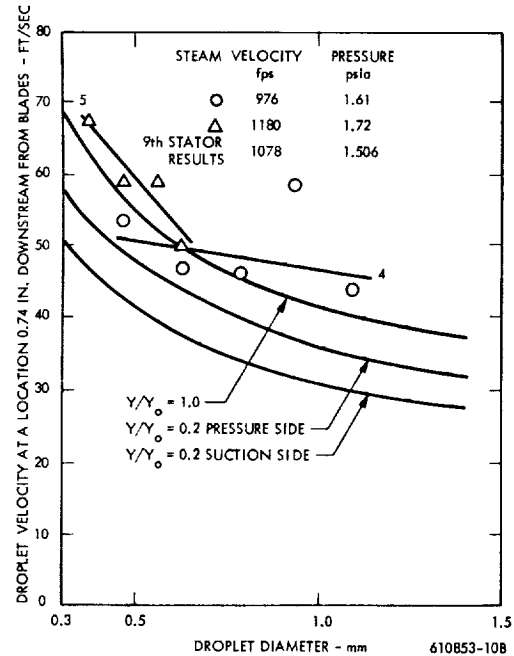


Figure 2.6A-1 Drop Velocity

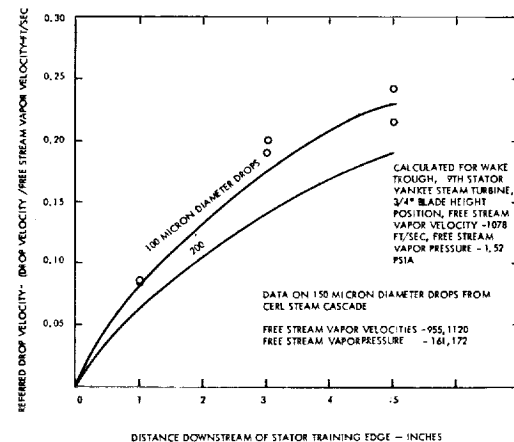


Figure 2.6A-2 Secondary Drop Velocity

Figure 2.6A-3 compares two sets of predicted values for drop impingement locations on last stage rotor blades aft of the nose of the rotor blade for various-size secondary drops. The solid line is that predicted by CERL on the basis of their stator experiments as applied to a hypothetical turbine at full load. The points are predicted values for impact on the last rotor blades of the Yankee Turbine at the mean diameter, using the Yankee calculated values.

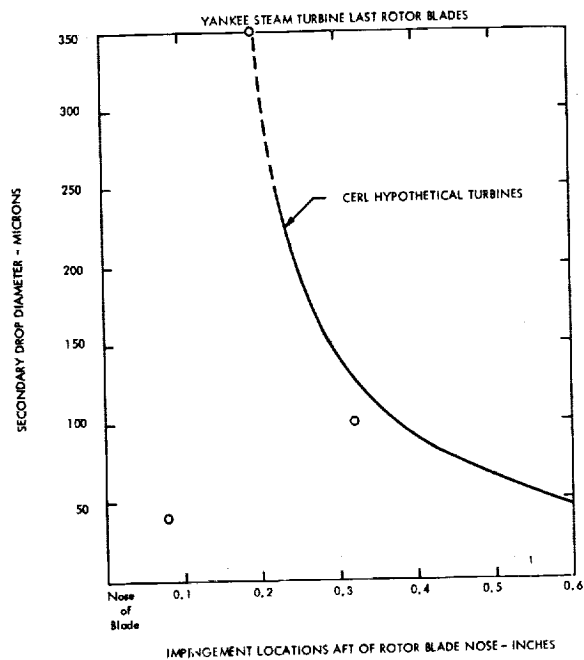


Figure 2.6A-3 Rotor Blade Impingement Locations

# APPENDIX 2.6B

## ADROP CODE SOURCE PROGRAM LISTING

### B.1 ADROP Main Program Listing

```

JOB,17.
ASR0440.
ASD1197,VARLJFN,67,20000,01.
C
      PROGRAM ADROP(INPUT,OUTPUT,TAPE5=INPUT,TAPE6=OUTPUT)
C
      TRANSPORT OF ATOMIZED CONDENSATE IN WET VAPOR TURBINES
C
      COMMON /PRP/MAT,TEMP,RHOV,RHOL,SIGL,VISL,VISV
1       /TRG/CHORD,PITCH,BTE,PD,SD,PDS,SDS,PTH,STH,VZERO
2       /GEN/NSTAT,NROTR,PPM,ALPHA,ALPHI,FDEAD,WDC,DSTAT,OROTR,
3       AXSP,STE,SCHD,SPARC,SSARC
4       /CST/JOB(10),JMAT(10),PI,RD,NYD,DIAM(10)
5       /BUG/IRUG
C
C
      DIMENSION GDAT(14),TOAT(14),XS(50),VS(50),XP(50),VP(50),KOP(10)
      EQUIVALENCE (ALPHA,TDAT)
      DATA PI,RD,KOP,GDAT/ 3.14159265,.0174533,10*0,14*0. /
      DATA JMAT / 7HLITHIUM,6HSODIUM,7HPOTASS.,8IRUBIDIUM,6HCESIUM,
1 7HMERCURY,6HNAK-78,6HWATER /
      DATA XS,VS,XP,VP,PD,SD,PDS,SDS,PTH,STH /206*0./, X0/1./
      NAMELIST/DRP/KOP,TR,VFREE,GDAT,XS,VS,XP,VP,PD,SD,PDS,SDS,PTH,STH
1, X0,DIAM
100  READ(5,10) JOB
      READ(5,DRP)
      IF (KOP(1)).EQ.0) STOP
      MAT = KOP(1) $ NSTAT = KOP(2) $ NROTR = KOP(3) $ MS = KOP(5)
      RPM = KOP(4) $ INK = KOP(6) $ NYD = KOP(9) $ IBUG=KOP(10)
      WRITE(6,14) JOB,KOP
C
C
      CONVERSION OF INPUT UNITS TO CGS
C
      TEMP = TR/1.8
      VZERO = VFREE*30.48
      ALPHA = GDAT(1) $ ALPHI = GDAT(2)
      FDEAD = GDAT(3) $ WDC = GDAT(4)
      DO 110 I=5,11
110  TOAT(I) = GDAT(I)*2.54
      CHORD = SCHD $ PITCH = PI*DSTAT/NSTAT $ BTE = ALPHA
      IF (MS.LE.0.AND.KOP(7).LT.0) GO TO 200
      WRITE(6,16) TR,VFREE,X0, (GDAT(L),L=1,7)
      WRITE(6,19) (GDAT(L),L=8,11)
C
C
      GENERATE FLUID PROPERTIES AT STATOR EXIT CONDITIONS
C
      CALL PROPM(RHOV,TEMP,2,MAT)
      CALL PROPM(RHOL,TEMP,1,MAT)
      CALL PROPM(VISV,TEMP,4,MAT)
      CALL PROPM(VISL,TEMP,3,MAT)
      VI = 1./RHOL
      CALL PROPM(SIGL,TEMP,9,MAT)
      VV = 1./RHOV
      VM = X0*VV+(1.-X0)*VI
      RHOV = 1./VM

```

```

C
C CHECK FOR PROPERTY ERROR SIGNAL
C
WRITE(6,12) JMAT(MAT),TEMP,RHOV,RHOL,VISV,VISL,SIGL
IF (RHOV*RHOL*VISV*VISL*SIGL.LE.0.) GO TO 400
C
C CALCULATE TRAILING EDGE BOUNDARY LAYER DATA
C
IF (MS.LE.0) GO TO 150
CALL TRUCK(MS,SSARC,SPARC,XS,VS,XP,VP,IOK)
IF (IOK.EQ.10) GO TO 200
C
C EXAMINE BALLISTICS OF ATOMIZED DROPS
C
150 IF (KOP(7).LT.0) GO TO 200
CALL TRAX(KOP(7))
C
C EXAMINE DROP IMPACT GEOMETRY
C
200 IF (KOP(8).LT.0) GO TO 400
CALL IMPAX(NROTR,DROTR,RPM,ALPHA,ALPHI,VZERO)
400 CONTINUE
GO TO 100
CALL EXIT
10 FORMAT(10A8)
12 FORMAT(1X, A8,23HWORKING FLUID AT T(K) = F7.1 / 10X,13HRHOV (G/CC)
1 = E14.4 / 10X,13RHOL (G/CC) = E14.4 / 10X,13HVISV (P) = E14.4 /
2 10X,13HVISL (P) = E14.4 / 10X,13HSIGL DYN/CM = E14.4 )
14 FORMAT(1H1,11H INPUT DATA,6X,10A8//17H OPTIONS KOP = 1018 //)
14 FORMAT(6X,32HBULK FLUID TEMPERATURE (DEG R) = F10.2,
1 9X,32HVEFF-STREAM VELOCITY (FPS) = F10.2/
2 6X,32HBULK FLUID QUALITY = F10.4,
3 8X,32HEXIT FLOW ANGLE (DEG) = F10.2/
4 6X,32HINLET ROTOR BLADE ANGLE (DEG) = F10.2,
5 8X,32HDEAD-SPACE MULTIPLIER = F10.2/
6 6X,32HCRITICAL WEBER NUMBER = F10.2,
7 8X,32HEXIT STATOR DIAMETER (IN) = F10.4/
8 6X,32HINLET ROTOR DIAMETER (IN) = F10.4,
9 8X,32HAXIAL INTER-ROW SPACE (IN) = F10.4 )
18 FORMAT(6X,32HSTATOR TF THICKNESS (IN) = F10.4,
1 9X,32HSTATOR CHORD (IN) = F10.4/
2 6X,32HPRESSURE SURF. LENGTH (IN) = F10.4,
3 8X,32HSUCTION SURF. LENGTH (IN) = F10.4 //)
END

```

## Appendix B.2 Subroutine TRUCK Listing

```

C
C SUBROUTINE TRUCK(M,SS,SP,XXS,XVS,XXP,XVP,I3)
C
C TWO DIMENSIONAL BOUNDARY-LAYER CALCULATION MARCH 1968
C REVISED VERSION OF CODE OF WNL-TME-1689
C
COMMON /PRP/MAT,TEMP,RHOV,RHOL,SIGL,VISL,VISV
1 /TAG/CHORD,PITCH,BTE,PD,SD,PDS,SDS,PTH,STH,VZERO
4 /CST/JOR(10),JMAT(10),PI,RO,NYO,DIAM(10)
DIMENSION XXS(2),XVS(2),XXP(2),XVP(2),XS(51),VS(51),TS(51),ZS(51),
1 FS(51),O(31),E(31),HS(51),EXN(51),TSIN(51),DSIN(51),DFSIN(51)
DATA(D=-.1803, -.1902, -.18, -.177, -.172, -.165,
1-.1555, -.145, -.130, -.123, -.1145, -.103, -.090,
2 -.075473, -.054770, -.030020, .0, .037065, .083859, .144673,
3.226930, .345038, .425548, .530005, .639995, .789418, 1.013354,
41.174106, 1.414472, 1.854390, 2.303073),
5(F= 2.6, 2.5, 2.4, 2.3, 2.2, 2.1, 2.0, 1.9, 1.8, 1.75, 1.70, 1.65,
61.60, 1.55, 1.50, 1.45, 1.40, 1.35, 1.30, 1.25, 1.20, 1.15, 1.125,
71.10, 1.08, 1.06, 1.04, 1.03, 1.02, 1.01, 1.005)

```



```

C      COMPUTE BLADE REYNOLDS NUMBER AND LIST INPUT
C
RES = RHOV*VZERO*SS/VISV      $ REP = RES*SP/SS
RE = RES                      $ S = SS
XS(1) = XXS(1) = XXP(1) = VS(1) = 0.
WRITE(6,102) JOB
WRITE(6,103) JMAT(MAT),RES,REP
WRITE(6,104) (XXS(I),XVS(I),XXP(I),XVP(I),I=1,M)
ISUR = 1      $ IDELT = 40      $ DELTA = 1./IDELT
II = IDELT+1      $ MI = II-2
DO 5 J=2,II
  XS(J)=XS(J-1)+DELTA
  XS(II) = VS(II) = 1.
CALL SPLINT(XXS,XVS,M,XS(2),VS(2),MI,1,1)
10  SUMS1 = FS(2) = 0.
  DO 16 I=2,II
    SUMS1=SUMS1+(XS(I)-XS(I-1))*(VS(I)**3.33+VS(I-1)**3.33)/2.0
    AS=((0.074/(RE**0.2))/2.0)**1.166
    BS=0.0304*(ALOG(RE))-0.23651
    TS(I)=(AS*SUMS1)**0.8571/VS(I)**3
    ZS(I)=(AS*SUMS1)**4
    IF(I-2)14,14,15
14  SUMS2=(BS+ALOG(VS(I))+0.00651*ALOG(ZS(I))-FS(2))*ZS(I)/1.0608
    GO TO 25
15  SUMS2=SUMS2+(ZS(I)-ZS(I-1))*(ALOG(VS(I))+ALOG(VS(I-1)))/2.0
    FS(I)=BS+ALOG(VS(I))+0.00651*ALOG(ZS(I))-1.0608*SUMS2/ZS(I)
    IF (FS(I).GT.(-.18)) GO TO 25
    XI=I      $ IO = 10
    POSITN = S*(.02*XI-.02)
    WRITE(6,111)I,POSITN,FS(I),TSIN(I-1),DSIN(I-1),DFSIN(I-1)
    GO TO 17
25  CALL SPLINT(D,E,31,FS(I),HS(I),1,1,1)
    EXN(I) = 2./(HS(I)-1.)
    TSIN(I) = TS(I)*S
    DSIN(I)=TSIN(I)*HS(I)
16  DFSIN(I) = DSIN(I)*(EXN(I)+1.)
17  IF (ISUR.GT.1) GO TO 50
    ISUR = 2      $ RE = REP      $ S = SP
    IF (IO.LE.0) GO TO 40
    WRITE(6,102) JOB
    WRITE(6,105)
    WRITE(6,106)
    WRITE(6,107) (XS(I),VS(I),TS(I),FS(I),HS(I),EXN(I),TSIN(I),
1  DSIN(I),DFSIN(I),I=2,II)
40  CALL SPLINT(XXP,XVP,M,XS(2),VS(2),MI,1,1)
    SO = DFSIN(II)
    STH = TSIN(II)
    SOS = DSIN(II)
    GO TO 10
50  IF (IO.LE.0) GO TO 70
    WRITE(6,102) JOB
    WRITE(6,109)
    WRITE(6,106)
    WRITE(6,107) (XS(I),VS(I),TS(I),FS(I),HS(I),EXN(I),TSIN(I),
1  DSIN(I),DFSIN(I),I=2,II)
    PO = DFSIN(II)
    POS = DSIN(II)
    PTH = TSIN(II)
70  RETURN
C
C
102  FORMAT(1H1,2X,32HTWO-D BOUNDARY LAYER CALCULATION,6X,10A8 / 1
103  FORMAT(9H FLUID = A8, 6X, 5HRES = E12.3, 6X, 5HREP =
1  F12.3///43H INPUT POSITION AND SURFACE VELOCITY ARRAYS//9H SUCTION
?N,11X,1HX,9X,1HV,10X,8HPRESSURE,11X,1HX,9X,1HW//)
104  FORMAT(F20.4,F10.4,F30.4,F10.4)
105  FORMAT(10X,15HSUCTION SURFACE )

```

```

106 FORMAT(/2X8HREFERRED, 4X8HREFERRED, 4X8HREFERRED, 6X5HSHAPE, 7X4HFO
1R4, 6X8HEXONENT, 4X8HMOMENTUM, 5X6HDISPL., 7X4HFULL, /2X8HDISTANCE, 4
2X9HVELOCITY, 4X9HMM THIC, 5X6HFACTOR, 6X6HFACTOR, 8X1HN, 8X9HTHICKNES
3S, 3X9HTHICKNESS, 3X9HTHICKNESS )
107 FORMAT (2XF8.6, 4XF8.6, 4XF8.6, 3XF9.6, 4XF8.6, 4XF8.6, 4XF8.6, 4XF
18.6, 4XF8.6)
109 FORMAT(10X, 16HPRESSURE SURFACE )
111 FORMAT(1H0, 1X, 60H****FLOW SEPARATION***SHAPE FACTOR .LT.-0.18
1 //1X, 2H1= E12.5, 2X, 10HSURF.POSN=E12.5, 5H1
2IN.), 2X, 11HSHAPE FAC= E12.5, 2X, 16HACT.MOM.TK(I-1)= E12.5, 4H(IN)
3 /1X, 17HACT.DISP.TK(I-1)= E12.5, 4H(IN), 2X, 14HNDRY.TK(I-1)= E12.
45, 4H(IN), 36H*****CONTINUING CALCULATION*****
END

```

### Appendix B.3 Subroutine WAKE Listing

```

SUBROUTINE WAKE(NS, XX, YD, VXY, BX)
COMMON /T8G/ CHORD, PITCH, RTE, PD, SD, PDS, SDS, PTH, STH, VZ
COMMON /BUG/ IBUG
C
C GENERATION OF STATOR WAKE VELOCITY
C
DATA (RD = .0174533), (PI = 3.1415926)
IF (NS) 200, 90, 100
100 SOLID = CHORD/PITCH
CORX = COS(RD*RTE) $ TABX = TAN(RD*RTE)
DSTE = (PDS+SDS)/CHORD $ DTE = (PD+SD)/CHORD
THTE = (PTH+STH)/CHORD $ HTE = DSTE/THTE
CHTE = THTE*SOLID/CORX $ OLDTE = CHTE
RA = 1.- CHTE*(1.+HTE)
RB = (1.- CHTE*HTE)**2
CK1 = (BA-1.)/(2.*CORX*CORX) )/BB
CK2 = (TABX*BA/BB)**2
CK3 = (CORX-SOLID*THTE*HTE)
NS = 1
100 X = XX/CHORD
AA = SQRT(1.+40.*X)
HX = AA/(AA-(HTE-1.)/HTE)
DO 115 LL=1,5
KNT = 2-LL
110 AA = (1.-OLDT*(1.+HX))**2
AB = 1.-OLDT*HX
FOX = (1.-CK1*AB*AB-(CK2*AB**4+AA)/(2.*AA))/(1.+HX)
IF (IBUG.EQ.2) WRITE(6,6) LL, KNT, XX, OLDTE, FOX
CALL VERGE(OLDTE, FOX, KNT)
IF (KNT.GE.20) GO TO 160
IF (KNT.GE.1) 110, 120
160 IF (ABS((OLDTE-FOX)/OLDTE).LE..001) GO TO 120
115 CONTINUE
WRITE(6,5) KNT, XX, CHTE, OLDTE
NS = 10
GO TO 150
120 CHTX = OLDTE
RX = ATAN (TABX*AB*AB/BB*RA/(1.-OLDTE*(1.+HX)))
THX = CHTX*COS(BX)/SOLID
VX = CK3/(COS(BX)-SOLID*THX*HX)
VMIN = 1.-.13/SQRT(X+.025)
YD = ABS(YD)
VXY = VX*VZ*.5*((1.+VMIN)-(1.-VMIN)*COS(PI*YD))

```

```

150 RETURN
200 HX = HTE*RD
    VXY = V7
    IF (YD.NE.0.) GO TO 150
    VXY = VZ*(1.-.13/SORT(XX/CHORD+.025))
    GO TO 150
5  F7EMAT(1H0,39H *** NON-CONVERGENCE IN WAKE, ITERATION, 16, 6H XX
  I= F6.4,7H CHTF = E12.5, 7H OLOT = E12.5 )
6  F7EMAT(2I10,3E20.5)
    END

```

#### Appendix B.4 Subroutine TRAX Listing

```

C  SUBROUTINE TRAX(10)
C  CALCULATION OF THE TRAJECTORIES OF ATOMIZED DROPS
C
COMMON /PRP/MAT,TEMP,RHOV,RHOL,SIGL,VISL,VISV
1  /TBG/CHORD,PITCH,BTE,PD,SD,POS,SOS,PTH,STH,VZERO
2  /GEN/NSSTAT,NROTR,RPM,ALPHA,ALPHI,FDEAD,WDC,DSTAT,DROTR,
3  AXSP,STE,SCHD,SPARC,SSARC
4  /CST/JO8(10),JMAT(10),PI,RO,NYO,DIAM(10)
COMMON/ICON/H,HMAX,HMIN,RELR,ABSR
COMMON/TRX/ ZP,ZPR,DPD,WDP,DPP,TRIG,YY,DD,KCRIT,I,J, TOF(10,3),
IVREL(10,3),VRELF(10,3),WFDM(10,3),TP2(10,3),VCX(10,3),XDC(10,3),
2  REX(10,3),VDF(10,3),DP2(10,3),XDIS(10,3),NS
DIMENSION YD(3),Y(50)
DATA HMIN,RELR,ABSR /3*1.E-8/
DATA (YD = 0.,.35,1.),
1  (DIAM = 1.,2.,5.,10.,20.,50.,100.,200.,500.)
DIAM(10) = AMIN1(STE*1.E4,1000.)
DO 80 I=1,300
80 TOF(I) = 0.
HI = AXSP/50.
XDEAD = FDEAD*STE
NE = 0
IF (NYO) 85,90,92
85 NYO = 2 $ NE = -1
YD(1) = 0.
YD(2) = 1.
GO TO 95
90 NYO = 3
92 WRITE(6,35) JO8,PTH,STH,POS,SOS,PD,SD
95 ZP = 10.
IF (10.GT.1) ZP = (AXSP-XDEAD)/(10-1.)
NS = NE
DO 500 J=1,NYO
DO 500 I=1,10
ZPR = I = 0.
Y(1) = 1.
Y(2) = XDEAD $ YY = YD(J)
TRFT = KCRIT = 0 $ H = HMAX = HI
DD = DIAM(I)*1.E-4 $ TRIG = 0.
DPD = RHOV*DD/VISV
WDP = RHOV*DD/SIGL
DPP = .75*RHOV/(RHOL*DD)
XDIS(I,J) = 100.
CALL WAKE(NS,Y(2),YD(J),VXY,RX)
IF (NS.NE.10) GO TO 100
REX(I,J) = -1.
GO TO 500

```

```

100 VREL(I,J) = VXY
    WEDM(I,J) = 0.
    CALL ICEAD(2,T,Y,IREF)
500 CONTINUE
    WRITE(6,5) JOB
    WRITE(6,20)
    WRITE(6,25) ((DIAM(I),YD(J),TOF(I,J),VDF(I,J),VREL(I,J),
1 VREL(I,J),WEDM(I,J),REX(I,J),I=1,10),J=1,NYD)
    WRITE(6,5) JOB
    WRITE(6,30)
    DO 520 J=1,NYD
    DO 520 I=1,10
    IF (TP2(I,J).EQ.0) GO TO 520
    WRITE(6,26) DIAM(I),YD(J),TP2(I,J),DP2(I,J),VCX(I,J),XDC(I,J),
1 XDIS(I,J)
520 CONTINUE
    RETURN
5 FORMAT(23H1 DROP TRAJECTORY STUDY,6X,10A8 //)
20 FORMAT(19H SUMMARY OF RESULTS //6X,4HDIAM,6X,2HYD,7X,7HTFLIGHT,
1 7X,7HVDFINAL,9X,5HVRELI,9X,5HVRELF,10X,4HWEDM,9X,5HALPHA //)
25 FORMAT(2X,2F8.2,6E14.4)
26 FORMAT(2X,2F8.2,6E14.4,F14.2)
30 FORMAT(30H SECONDARY ATOMIZATION SUMMARY // 6X,4HDIAM,6X,2HYD,
1 10X,4HTDIS,10X,4HDFEC,10X,4HVDIS,11X,3HXDC,10X,4HXDIS //)
35 FORMAT(11H1,35HTRAILING EDGE BOUNDARY LAYER DATA ,10A8 // 40X,13HP
1PTSSURE SIDE,17X,12HSUCTION SIDE // 30H MOMENTUM THICKNESS (CM)
2 F23.5,F29.5 / 30H DISPLACEMENT THICKNESS (CM) F23.5,F29.5 /
3 30H FULL THICKNESS (CM) F23.5,F29.5 )
END

```

#### Appendix B.5 Subroutine DERIV Listing

```

C
C SUBROUTINE DERIV(T,Y,DY,IREF)
C
C DERIVATIVE CALCULATION
C
COMMON /PRP/MAT,TEMP,RHOV,RHOL,SIGL,VISL,VISV
1 /TAG/CHORD,PITCH,RTF,PD,SD,PDS,SDS,PTH,STH,VZERO
2 /GEO/NSTAT,NROTR,RPM,ALPHA,ALPHI,FDEAD,WDC,DSTAT,DROTR,
3 AXSP,STF,SCHD,SPARC,SSARC
4 /CST/JOB(10),JMAT(10),PI,RO,NYD,DIAM(10)
5 /BUG/IRUG
COMMON/ICON/H,HMAX,HMIN,RELR,ARSR
COMMON/TRX/ ZP,ZPR,DPD,WDP,DPP,TRIG,YY,DD,<CRIT,I,J, TOF(10,3),
1VREL(10,3),VREL(10,3),WEDM(10,3),TP2(10,3),VCX(10,3),XDC(10,3),
2 3FX(10,3),VDF(10,3),DP2(10,3),XDIS(10,3),NS
DIMENSION Y(50),DY(50)
DATA KA,KR,LINES,TLAST,WED,Z /0,0,70,1.E10,0.,0./
KA = KA+1
CALL WAKE(NS,Y(2),YY,VXY,RX)
IF (NS.EQ.10) GO TO 480
Y(1) = AMAX1(1.E-6,AMIN1(Y(1),VXY))
VREL = VXY-Y(1)
RED = VREL*DPD
CO = 2.

```

```

      IF (RED.GT.0. .AND. RED.LT.80.)      CD = 27./RED**.84
      IF (RED.GE.80. .AND. RED.LE.1.E4)    CD = .271*RED**.217
      DY(1) = DPP*VREL*VREL*CD
      DY(2) = Y(1)
      IF (1BUG) WRITE(6,20) KA,KB,T,Y(1),Y(2),DY(1),DY(2),VXY,H,RED,
1 WED,Z,ZP,ZPR,TRIG
      IF (KA.GT.500. .AND. KB.LT.2) GO TO 380
      RETURN
C
C      SUCCESSFUL INTEGRATION STEP
C
      ENTRY STEP
C
      KP = KB+1
      Z = Y(2)*COS(BX) $ X = Y(2) $ VD = Y(1)
      WED = VREL*VREL*WDP
      IF (WED.GT.WEDM(1,J)) WEDM(1,J) = WED
342 IF (WED.GE.WDC .OR. KCRIT.NE.0) GO TO 400
344 IF (Z.GE.AXSP) GO TO 450
      IF (VD.NE.0.) TLAST = (AXSP-Z)/VD
      IF (TLAST.LT.H) H=HMAX=AMAX1(HMIN,1.001*TLAST)
      IF (Z.LT.ZPR. .OR. ZP.EQ.1.) RETURN
C
C      DETAILED PRINT SECTION
C
      ZPR = Z+ZP
      IF (LINES.LT.40) GO TO 364
      WRITE(6,5) JNR
      DD = DD*1.E4
      WRITE(6,6) DD,YY
      WRITE(6,15)
      LINES = 4
364 WRITE(6,10) T,X,Z,VD,VREL,WED,RED,H
      LINES = LINES+1
      RETURN
C
C      DROP DISRUPTION DETECTED
C
400 IF (TRIG.EQ.0. .AND. KCRIT.EQ.0) GO TO 410
      IF (T.LT.TRIG) GO TO 344
      XD(1,J) = X
      XD(1,J) = X/DD
      TRIG = 10. $ KCRIT = 0
      GO TO 344
410 VDX(1,J) = VREL
      TPP = TP2(1,J) = 2.8*DD/VREL*SQRT(RHOL/RHOV)
      TRIG = T+TPP
      DP2(1,J) = (136.*VISI*SIGL**1.5*DD**.5/(CD**.5*RHOV*RHOV*RHOL**.5
1 *VREL**4.))**.5*(1./3.)
      KCRIT = 1
      GO TO 344
C
C      END-OF-TRAJECTORY
C
450 IF (ZP.NE.10.) WRITE(6,10) T,X,Z,VD,VREL,WED,RED,H
      KA = KB = 0 $ TPET = 1
      LINES = 70
      TLAST = 1.E10
      TDF(1,J) = T
      VDF(1,J) = VREL
      VDF(1,J) = VD
      BFX(1,J) = BX/RD
      XD(1,J) = XD(1,J)/X
      RETURN

```

```

C
C WAKE CALCULATION ERROR
480 RFX(I,J) = -1.
    KA = KB = 0      $ IRET = 1
    TLAST = 1.E10
    RETURN
C
C ENTRY FAIL
C
C NON-CONVERGENCE IN INTEGRATION
C
380 KJ = KD+1
    VDF(I,J) = VRELF(I,J) = -1.
    KA = KB = 0      $ IRET = 1
    TLAST = 1.E10
    RETURN
5  FORMAT(23H) DROP TRAJECTORY STUDY,6X,10A8 //)
6  FORMAT(17H DROP DIAMETER = F8.2, 8H MICRONS,12X,10HWAKE Y/D =,
1F4.2 //)
10 FORMAT(7E14,5,E12.4)
15  FORMAT(10X,4HTIME,8X,6HX-WAKE,8X,6HZ-WAKE,9X,5HVDROP,10X,4HVRFL,
1 11X,3HWED,11X,3HREFD,11X,1HH //)
20  FORMAT(219/(8E15.5))
    END

```

## Appendix B.6 Subroutine IMPAX Listing

```

C
C SUBROUTINE IMPAX(NB,RDIA,RPM,AL,AT,VZERO)
C
C CALCULATION OF DROPLET IMPINGEMENT GEOMETRY
C
COMMON/CST/JOB(10),JMAT(10),PI,RD,NYD
DIMENSION VD(40),WD(40),WN(40),DLS(40),ASD(40),BETA(40)
JV = 21
KX = VZERO/100.      $ KX = KX+1
VJ(1) = 0.           $ AV = 5.*KX
DO 19 K=2,21
19 VJ(K) = VD(K-1)+AV
VJ(21) = VZERO
C
C I/O ANGLES IN DEGREES, USE RADIANS INTERNALLY
C
SAL = SIN(AL*RD)
SAI = SIN(AT*RD)
PB = PI*BDIA
UB = PB*RPM/60.
S = PB/FLOAT(NB)
ADD = 90.-AT
VDD = UB/(SAL*(1.+1./TAN(RD*ADD)))
WDD = VDD*SAL/SIN(RD*ADD)
DLO = S*COS(AT*RD)
DO 60 J=1,JV
WJ(J) = UB*UB+VD(J)*VD(J)-2.*UB*VD(J)*SAL
WJ(J) = SQRT(WJ(J))
AD = ACOSF ((UB-VD(J)*SAL)/WJ(J))
WN(J) = WJ(J)*SIN(AD+AT*RD)
WN(J) = AMAX1(WN(J),0.)
ASD(J) = AD/RD
BETA(J) = 90.-AT-ASD(J)
DOM = SIN(AD+AT*RD)
IF (ABS(DOM).LT.1.E-10) GO TO 58
DLS(J) = ABS(S*SIN(AD)/DOM)
IF (DLS(J).GT.DLO) DLS(J) = DLO
GO TO 60
58 DLS(J) = DLO

```

```

60 CONTINUE
WRITE(6,12) (JOB(K),K=1,10),RDIA,RPM,UB,AL,S,AL
WRITE(6,16) DLO,ADO,VDC,WDO,VZERO
WRITE(6,14)
WRITE(6,10) (VD(K),WD(K),WN(K),ASD(K),BETA(K),DLS(K),K=1,JV)
RETURN
10 FORMAT(5F12.2,F15.5)
12 FORMAT(1H1, 10X,10A8 // 6X,23HSECTION DIAMETER (CM) = F10.4,10X,
1 23HWHEEL RPM = F10.1 / 6X,23HWHEEL SPEED (CM/SEC) =
2 F10.2,10X,23HALPHA = F10.2 /6X,23HBLADE PITCH (CM
3) = F10.4,10X,23HALPHAT = F10.2 )
14 FORMAT(10X,2HVD,10X,2HWD,10X,2HWN,8X,6HALPHAD,8X,4HBETA,5X,
1 14HIMPACT LENGTH /)
16 FORMAT( 6X,23HMAX DELTA L (CM) = F10.4,10X,23HALPHADD (DEG
1) = F10.2/6X,23HVDRQPD (CM/SEC) = F10.2, 10X,23HWD =
2WN (CM/SEC) = F10.2/6X,23HVZERO (CM/SEC) = F10.2//)
END

```

### Appendix B.7 Subroutine SPLINT Listing

```

C
C      SUBROUTINE SPLINT(XT,YT,NT,XI,YI,NI,JX,JY)
C
C      XT IS THE FWA OF TABULATED INDEPENDENT VARIABLE ARRAY
C      YT IS THE FWA OF TABULATED DEPENDENT VARIABLE ARRAY
C      NT IS THE NUMBER OF (XT,YT) PAIRS
C      XI IS THE FWA OF INTERPOLATION ARGUMENTS
C      YI IS THE FWA OF INTERPOLATED VALUES
C      NI IS THE NUMBER OF INTERPOLATION ARGUMENTS (XI-YI PAIRS)
C      JX AND JY SPECIFY THE STORAGE INCREMENTS IN ARRAYS XT AND YT
C
C      DIMENSION XT(2),YT(2),XI(2),YI(2)
C      DATA (KX=1),(KY=1),(NN=1)
C
C      IT = 1
C      KX = JX
C      KY = JY
C      NV = NI
C      ICF = 1
C      ICR = 0
C      NA = (NT-1)*KX+1
C      IF (XT(NA).GT.XT(1)) GO TO 10
C      ICF = 0
C      ICR = 1
C10  NTT = NT - 1
C      DO 90 I=1,NN
C      X = XI(I)
C      CA = CB = 1.
C      DCA = DCB = 0.
C      DO 20 J=2,NTT
C      L = J*ICF+(NT+1-J)*ICB
C      NA = (I-1)*KX+1
C      IF (XT(NA).GE.X) GO TO 30
C20  CONTINUE
C      L = (NT-1)*ICF+ICB
C      CA = ICB
C      CB = ICF
C      GO TO 60
C30  IF (J.GT.2) GO TO 50
C      L = 3*ICF+(NT-2)*ICB
C      CA = ICF
C      CB = ICB
C50  L = (L-2)*ICF+(L-1)*ICB

```

```

60 NA = (L-1)*KX+1
   X1 = XT(NA)
   NA = (L-1)*KY+1
   Y1 = YT(NA)
   NA = L*KX+1
   X2 = XT(NA)
   NA = L*KY+1
   Y2 = YT(NA)
   NA = (L+1)*KX+1
   X3 = XT(NA)
   NA = (L+1)*KY+1
   Y3 = YT(NA)
   NA = (L+2)*KX+1
   X4 = XT(NA)
   NA = (L+2)*KY+1
   Y4 = YT(NA)

   D1 = (X1-X2)*(X1-X3)
   D2 = -(X1-X2)*(X2-X3)
   D3 = (X1-X3)*(X2-X3)
   D4 = (X2-X3)*(X2-X4)

   A1 = (X-X2)*(X-X3)/D1
   A2 = (X-X1)*(X-X3)/D2
   A3 = (X-X1)*(X-X2)/D3
   A4 = (X-X3)*(X-X4)/D4
   A5 = (X-X2)*(X-X4)/D5
   A6 = (X-X2)*(X-X3)/D6
   IF ((CA.EQ.0.).OR.(CB.EQ.0.)) GO TO 64
   DCA = X2-X3
   DCB = -DCA
   CA = (X-X3)/DCA
   CB = (X-X2)/DCB
64 PA = Y1*A1+Y2*A2+Y3*A3
   PB = Y2*A4+Y3*A5+Y4*A6
   IF (IT.EQ.2) GO TO 70
   YI(I) = CA*PA+CB*PB
   GO TO 60
70 A1 = Y1*((X-X2)+(X-X3))/D1
   A2 = Y2*((X-X1)+(X-X3))/D2
   A3 = Y3*((X-X1)+(X-X2))/D3
   A4 = Y2*((X-X3)+(X-X4))/D4
   A5 = Y3*((X-X2)+(X-X4))/D5
   A6 = Y4*((X-X2)+(X-X3))/D6
   YI(I) = CA*(A1+A2+A3)+PA*DCA+CB*(A4+A5+A6)+PB*DCB
90 CONTINUE
   RETURN
C
C ENTRY DYDX
C YI IS THE DERIVATIVE OF THE TABULATED DATA AT XI
C
IT = 2
GO TO 8
END

```



## Appendix B.8 Subroutine VERGE Listing

```

C      SUBROUTINE VERGE(XI,FOX,IK)
C
C      ACCELERATED CONVERGENCE OF ITERATIVE PROCESSES
C      T.C.VARLJEN  WANL 4/15/68
C
      DIMENSION QD(5)
      DATA EPS,ETA,QD / 1.E-12,1.E-30,0.,.3,.55,-1.,5. /
      IK = IK+1
      IF (IK.GT.1) GO TO 20
      K = IABS(IK-2)
      IK = 1
      ZB = XI
      XI = QD(K)*ZB+(1.-QD(K))*FOX
      GO TO 50
20  IF (ABS(FOX-XI).LT.EPS) GO TO 30
      ZC = (FOX*ZB-XA*XI)/(FOX+ZB-XA-XI)
      ZB = XI
      XI = ZC
      IF (ABS(ZB).GT.ETA) GO TO 50
30  IK = -IK
50  XA = FOX
      RETURN
      END

```

## Appendix B.9 Subroutine ICEAD Listing

```

C      SUBROUTINE ICEAD(N,T,XI,IREF)
C      COMMON/ICON/H,HMAX,HMIN,PELR,ABSR
C      DIMENSION XI(2),F(10),X(10,5),DY(10,5),XP(10),C(10,4)
C
C      N = NO. OF EQUATIONS
C      T = INDEPENDENT VARIABLE---SET IT=INITIAL T
C      H = STEP SIZE---SET IT=INITIAL H
C      HMAX = MAXIMUM STEP SIZE ACCEPTABLE
C      HMIN = MINIMUM STEP SIZE ACCEPTABLE
C      PELR = MAXIMUM ACCEPTABLE RELATIVE ERROR
C      ABSR = MAXIMUM ACCEPTABLE ABSOLUTE ERROR
C
C      INITIALIZATION
C
      RELT = 14.2*PELR  $  ARST = 14.2*ABSR
      FACT = RELR/ABSR  $  RB = RELT/200.
      CA = 1./6.        $  CR = 1./24.
      IREF = 0          $  H = 2.*H
      DO 100 I=1,N
100  X(I,1) = XI(I)
C
C      RUNGE-KUTTA STARTING METHOD
C
110  IA = IR = 2
120  DO 140 J=IA,IA
      CALL DERIV(T,X(I,J-1),DY(I,J-1),IREF)
      IF (IREF) RETURN
      DO 130 I=1,N
      C(I,1) = H*DY(I,J-1)
130  X(I,J) = X(I,J-1)+.5*C(I,1)
      TEMP = T+.5*H
      CALL DERIV(TEMP,X(I,J),DY(I,J),IREF)
      IF (IREF) RETURN
      DO 140 I=1,N
      C(I,2) = H*DY(I,J)

```

```

140 X(I,J) = X(I,J-1)*.5*C(I,2)
    CALL DERIV(TEMP,X(I,J),DY(I,J),IRET)
    IF (IRET) RETURN
    DO 150 I=1,N
    C(I,3) = H*DY(I,J)
150 X(I,J) = X(I,J-1)+C(I,3)
    T = T+H
    CALL DERIV(T,X(I,J),DY(I,J),IRET)
    IF (IRET) RETURN
    DO 160 I=1,N
    C(I,4) = H*DY(I,J)
160 X(I,J) = X(I,J-1)+C(I,3)+2.*C(I,2)+C(I,1)+C(I,4)
    IF (IB.NE.2) GO TO 170
170 DO 180 I=1,N
180 XP(I) = X(I,2)
    T = T+H * H = .5*H
    IF (H.LT.HMIN) CALL FAT( T,X,DY,IRET)
    IF (IRET) RETURN
    IR = 3
    GO TO 120
190 IF (IB.NE.3) GO TO 255
    J = 3
    DO 200 I=1,N
    E(I) = ABS(XP(I)-X(I,J))
    IF (E(I).GE.ABS(X(I,J))*RFLT) GO TO 220
    F(I) = E(I)/ABS(X(I,J))
    GO TO 250
220 IF (F(I).GE.ABST) GO TO 230
    E(I) = E(I)*FACT
    GO TO 250
230 T = T+H
    IF (J.NE.4) GO TO 170
    DO 240 K=1,N
240 X(K,1) = X(K,4)
    GO TO 110
250 CONTINUE
    IF (J.EQ.4) GO TO 310
    IA = IB = 4
    GO TO 120

C
C SEND STARTING VALUES TO STEP
C
255 T = T-3.*H
    DO 260 J=2,4
    T = T+H
260 CALL STEP(T,X(I,J),DY(I,J),IRET)
    IF (IRET) RETURN

C
C BEGIN ICF-ADAMS METHOD
C
280 CALL DERIV(T,X(I,4),DY(I,4),IRET)
    IF (IRET) RETURN
    DO 290 I=1,N
290 XP(I) = X(I,4)+CHORD(.55.*DY(I,4)-.49.*DY(I,3)+.37.*DY(I,2)-.2.*
    DY(I,1))
    T = T+H
    CALL DERIV(T,XP,DY(I,5),IRET)
    IF (IRET) RETURN
    DO 300 I=1,N
300 X(I,5) = X(I,4)+CHORD(.9.*DY(I,5)+.19.*DY(I,4)-.5.*DY(I,3)+.21.*
    DY(I,2))
    J = 5
    GO TO 250
310 DO 320 I=1,N
    X(I,4) = X(I,5)
    DO 320 J=2,5
320 DY(I,J-1) = DY(I,J)
    CALL STEP(T,X(I,4),DY(I,4),IRET)
    IF (IRET) RETURN
    DO 330 I=1,N
    IF (E(I).GT.WB) GO TO 280
330 CONTINUE
    IF (2.*H.GT.HMAX) GO TO 280
    DO 340 I=1,N
340 X(I,1) = X(I,4)
    H = 4.*H
    GO TO 110
    RETURN
END

```

## Appendix B.10 Subroutine PROPM Listing

```

C
C SUBROUTINE PROPM(XX,TK,JPROP,JFLUID)
C
C   COMPUTATION OF SAT LIQUID AND VAPOR PROPERTIES OF WORKING FLUIDS
C
C   JFLUID MATERIAL          JFLUID MATERIAL
C   1 LITHIUM              5 CESIUM
C   2 SODIUM               6 MERCURY
C   3 POTASSIUM            7 NAK-78
C   4 RUBIDIUM            8 WATER
C
C   THIS VERSION ASSUMES INPUT TEMP IN DEGREES KELVIN
C
C STEAM DATA TABULATIONS
C
C DIMENSION TH2(12),PSH2(12),VLH2(12),VGH2(12),CLH2(12),CVH2(12),
1 HLH2(12)
C DATA TH2/.01,10.,30.,50.,80.,120.,150.,200.,250.,300.,350.,374./,
2 PSH2/.006112,.012271,.04242,.12335,.47358,1.9854,4.7597,15.55,
3 VLH2/ 1.00021,1.0004,1.0044,1.0121,1.029,1.0603,1.0906,1.1565,
4 1.2512,1.4036,1.741,2.8 /,
5 VGH2/ 276146.,106422.,32929.,12045.,3408.,891.71,392.57,127.19,
6 50.756,21.643,8.805,3.47/,
7 CLH2/ 4.2174,4.1928,4.1787,4.1812,4.1965,4.2446,4.31,4.4966,
8 4.8667,5.7619,10.1047,1400.5 /
9 DATA CVH2 / 1.8542,1.8595,1.8745,1.8986,1.9616,2.1196,2.3144,
10 2.8429,3.7722,5.8631,17.1505,3513.7 /,
11 HLH2 / 2500.9994,2477.01,2430.34,2382.7,2308.1,2202.3,2114.8,
12 1947.6,1715.2,1404.,893.,114./,ITEM/0/
C TKTOP(0)= 1.8*R-459.67
C IF (ITEM.EQ.1) GO TO 10
C DO 20 I=1,12
C   PSH2(I) = ALOG(PSH2(I))
C   VGH2(I) = ALOG(VGH2(I))
C   HLH2(I) = ALOG(HLH2(I))
20 IFM=1
C T = TK
C JF = JFLUID
C JP = JPROP
C IF(T.LT.250..OR.T.GT.3000.) GO TO 410
C
C GO TO APPROPRIATE PROPERTY SECTION
C
C IF (JF.LT.1.OR.JF.GT.8.OR.JP.LT.1.OR.JP.GT.15) GO TO 400
C GO TO (1001,1002,1003,1004,1005,1006,1007,1008,1009,400,1011
1 1012,1013,1014,1015), JP
C
C SAT LIQUID DENSITY (G/CM3)
C
1001 GO TO (111,112,113,114,115,116,117,118), JF
111 T = 3173.15-T
X = .124+5.306E-3*SQRT(T)+4.135E-5*T
GO TO 500
112 T = T-273.15
X = .9501-2.2976E-4*T-1.46E-8*T+5.638E-12*T*T+T
GO TO 500
113 X=.983578E-1-2.244534E-4*T-1.274617E-8*T*T
GO TO 500
114 X=1.575802-3.074245E-4*T+3.837297E-8*T*T
GO TO 500
115 X=1.985607-4.549765E-4*T-8.955005E-8*T*T
GO TO 500
116 X=1.438176E1-2.861764E-3*T+3.763475E-7*T*T
GO TO 500

```

RL NA  
 R3L  
 R4L  
 R5L  
 R6L

```

117 X=0.3800519589F-1-2.3937338810E-4*T+3.5881034579E-9*T*T      R7L
G) TO 500
118 T = T-273.15
CALL SPLINT(TH2,VLH2,12,T,X,1,1,1)
X = 1./X
G) TO 500

C
C SAT VAPOR DENSITY (G/CM3)
C
1192 G) TO (121,122,123,124,125,126,400,128), JF
121 X=EXP(4.324234E-1-1.560572E4/T-1.124864E6/T**2)      R1G
G) TO 500
122 X=EXP(1.000785-1.012916E4/T-5.75469F5/T**2)      R2G
G) TO 500
123 X=EXP(8.135742E-1-8.24115E3/T-4.269861E5/T**2)      R3G
G) TO 500
124 X=EXP(4.677273F-1-6.10964E3/T-9.252185E5/T**2)      R4G
G) TO 500
125 X=EXP(1.757963-7.371427E3/T-1.931032E5/T**2)      R5G
G) TO 500
126 X=EXP(3.263496-4.55902E3/T-6.07443E5/T**2)      R6G
G) TO 500
128 T = T-273.18
CALL SPLINT(TH2,VGH2,12,T,X,1,1,1)
X = 1./EXP(X)
G) TO 500

C
C SAT LIQUID VISCOSITY (G/SEC-CM)
C
1003 G) TO (131,132,133,134,135,136,137,138), JF
131 X = 1.E-3*10.**((5.41921-155.991/T-1.61506*ALOG10(T)))
G) TO 500
132 X = .01*10.**((.5108+220.65/T-.4925*ALOG10(T)))      VL NA
G) TO 500
133 X=-4.390586E-4+2.028652/T-5.410948E2/T**2+1.646804E5/T**3      V3L
G) TO 500
134 X = 1.E-3*10.**((62.2374/T-.78639*ALOG10(T)+2.4459))      VL RB
G) TO 500
135 X = 1.E-3*10.**((104.013/T-.59011*ALOG10(T)+1.8781))      VL CS
G) TO 500
136 X=8.036587E-3-3.198539/T+2.791399E3/T**2-3.544087E5/T**3      V6L
G) TO 500
137 X=3.187261E-4*8.019051E-1/T+2.142332E2/T**2+2.596542E4/T**3      V7L
G) TO 500
138 X = 241.4E-6*10.**((247.8/(T-140.)))      VL H2O
G) TO 500

C
C SAT VAPOR VISCOSITY (G/SEC-CM)
C
1004 G) TO (141,142,143,144,145,146,400,148), JF
141 X=3.673815E-5+1.167182E-7*T-1.135025E-11*T*T      V1G
G) TO 500
142 X = .004134*(.03427+9.176F-6*TKTOF(T))      VG NA
G) TO 500
143 X=3.870094E-5+1.982508E-7*T-4.528330E-11*T*T      V3G
G) TO 500
144 X=P.619203E-5+2.027719F-7*T-3.327784E-11*T*T      V4G
G) TO 500
145 X=9.520004E-5+2.222279E-7*T-4.270371F-11*T*T      V5G
G) TO 500
146 X=7.143205E-5+6.300290E-7*T+3.373475F-10*T*T      V6G
G) TO 500
148 X = 1.E-6*(80.4+.407*(T-273.15))
G) TO 500

```

```

C
C      SAT LIQUID THERMAL CONDUCTIVITY (W/CM-K)
C
1005 GJ TO (151,152,153,154,155,156,157,158), JF
151 T = TKTOP(T)
X = .49998+2.7992E-4*T+2.2565E-8*T*T-2.4606E-11*T*T*T
GJ TO 300 T1L
152 T = TKTOP(T)
X = .01731*(54.306-.01878*T+2.0914E-6*T*T)
GJ TO 500 TL NA
153 T = TKTOP(T)
X = .96689-4.7904E-4*T+1.3778E-7*T*T-2.4884E-11*T*T*T
GJ TO 300 T3L
154 T = TKTOP(T)
X = .49609-8.5289E-5*T-2.8444E-8*T*T+3.4248E-12*T*T*T
GJ TO 300 T4L
155 X = 1.65E-6*SQR(T)
GJ TO 500
156 X = .14648093+50.8368/T-8.20005E4/T**2 +3.26295E7/T**3
-4.43661E9/T**4
GJ TO 500 T6L
157 X = 1.384235E-1+2.05547E2/T-1.062331E5/T**2+1.60138E7/T**3
GJ TO 500 T7L
158 T = T/273.15
X = .01*(-922.47+2839.5*T-1800.7*T*T+525.77*T*T*T-73.44*T**4)
GJ TO 500 TCL H2O
300 X = X*.7087
GJ TO 500

C
C      SAT VAPOR THERMAL CONDUCTIVITY(W/CM-K)
C
1006 GJ TO (161,162,163,164,165,166,400,168), JF
161 X = 1.211242E-4+5.135221E-7*T-5.902087E-11*T*T
GJ TO 500 T1G
162 T = TKTOP(T)
X = .0173*(1.639E-3+.3977E-4*T-.9697E-8*T*T)
GJ TO 500 TG NA
163 X = 3.033189E-5 +1.400357E-7*T -3.133830E-11*T**2
GJ TO 500 T3G
164 X = 3.970684E-5+6.325412E-8*T -9.535292E-12*T**2
GJ TO 500 T4G
165 X = 2.245009E-5+4.234143E-8*T-6.469024E-12*T*T
GJ TO 500 T5G
166 X = 2.749046E-6+1.175486E-7*T-2.454670E-11*T**2
GJ TO 500 T6G
168 T = T-273.15
X = 1.E-5*(17.6+.0587*T+1.04E-4*T*T-4.51E-8*T*T*T)
GJ TO 500 TCG H2O

C
C      SAT LIQUID SPECIFIC HEAT (W-SEC/G-K)
C
1007 GJ TO (171,172,173,174,175,176,177,178), JF
171 T = T-273.15
X = 4.194*(1.0577-1.2152E-4*T+5.3477E-8*T*T)
GJ TO 500
172 T = T-273.18
X = 4.187*(0.34324-1.3868E-4*T+1.1044E-7*T*T)
GJ TO 500 CL NA
173 X = 9.512849E-1-4.860081E-4*T+3.122763E-7*T*T
GJ TO 500 C3L
174 T = TKTOP(T)
X = 4.187*(.09915-3.106E-5*T+1.299E-8*T*T)
GJ TO 500 C4L
175 T = TKTOP(T)
X = 4.187*(.08543-9.605E-5*T+5.985E-8*T*T)
GJ TO 500 C5L
176 X = 1.519435E-1-5.970309E-5*T+5.301029E-8*T*T
GJ TO 500 C6L
177 T = T-273.18
X = 4.187*(.232-8.82E-5*T+8.2E-8*T*T)
GJ TO 500 CL NAK

```

```

GO TO 500
178 T = T-273.15
CALL SPLINT(TH2,CLH2,12,T,X,1,1,1)
GO TO 500

C
C SAT VAPOR SPECIFIC HEAT (W-SEC/G-K)
C
1004 GO TO (181,182,183,184,185,186,400,188), JF
181 X=3.96477-1.321868E4/T+7.253337E7/T**2-5.82616E10/T**3 C1G
GO TO 500
182 X = 4.187*(.21508+6.054*EXP(-20708./T)) CG NA
GO TO 500
183 X=-6.711841E-1+4.044715E3/T-3.393891E6/T**2+8.493131E8/T**3 C3G
GO TO 500
184 X=-1.733578E-2+8.663483E2/T-4.075597E5/T**2 C4G
GO TO 500
185 X=-1.354922E-2+5.228561E2/T-2.32491E5/T**2 C5G
GO TO 500
186 X=1.376087E-1+1.637431E-5*T+1.697121E-8*T*T C6G
GO TO 500
188 T = T-273.15
CALL SPLINT(TH2,CLH2,12,T,X,1,1,1)
GO TO 500

C
C SAT LIQUID SURFACE TENSION (DYN/CM)
C
1000 GO TO (191,192,193,194,195,196,197,198), JF
191 X=4.544948E2-1.356226E-1*T+1.615487E-6*T*T ST1
GO TO 500
192 X = 206.7-.1*(T-273.18) ST NA
GO TO 500
193 X = 115.51-.0653*(T-273.18) ST K
GO TO 500
194 X=1.347296E2-5.606006E-2*T-1.513351E-5*T*T ST4
GO TO 500
195 T = TKINF(T) ST5
X=76.4-.03*(T-83.)
GO TO 500
196 X = 678.-.357*T ST HG
GO TO 500
197 X=1.201687E2-3.890232E-2*T ST7
GO TO 500
198 X = 53.9-.216*(T-373.15) ST H2O
GO TO 500

C
C LIQUID SONIC VELOCITY (CM/SEC)
C
1011 GO TO (212,213,214,215,216,217,218), JF
212 X = 2.526F5-52.4*(T-370.78) SVL NA
GO TO 500
213 X = 1.869E5-53.*(T-373.18) SVL K
GO TO 500
214 X = 1.26E5-40.*(T-273.18) SVL RB
GO TO 500
215 X = 9.67E4-30.*(T-273.18) SVL CS
GO TO 500
216 X = 1.4608E5-45.75*(T-273.18) SVL HG
GO TO 500
217 X = 207000.-54.3*(T-273.18) SVL NAK
GO TO 500
218 X = 1.437E5+640.*(T-288.18) SVL H2O
GO TO 500

C
C SAT VAPOR SONIC VELOCITY (CM/SEC)
C
1012 GO TO (221,222,223,224,225,400,400,400), JF
221 X=7.650211E4+35.0503*T-2.883303E-3*T*T SV1
GO TO 500
222 X=4.710855E4+1.3694E1*T-5.391655E6/T SV2
GO TO 500
223 X=2.134288E4+2.836652E1*T-5.800705E-3*T*T SV3
GO TO 500
224 X=1.554827E4+1.626642E1*T-2.611827E-3*T*T SV4
GO TO 500
225 X=1.277488E4+1.217007E1*T-1.763269E-3*T*T SV5
GO TO 500

```

```

C
C      VAPOR PRESSURE (BARS)
C
1013 GO TO (231,232,233,234,235,236,237,238), JF
231 X = 1.01325*10.**(-2.1974-6499.1/T+1.939*ALOG10(T))
    GO TO 500
232 X = 1.013*EXP(6.6808-5544.41/T-.61344*ALOG(T))
    GO TO 500
233 X=EXP(9.191863-9.030992E3/T-4.33038E5/T**2)
    GO TO 500
234 T = T*1.8
    X=0.06895*10.**(5.20071-6994.68/T)
    GO TO 500
235 X=EXP(8.636035-7.715273E3/T-3.846408E5/T**2)
    GO TO 500
236 T = T*1.8
    X = .0013332*10.**(10.57757-5954.55/T-.8*ALOG10(T))
    GO TO 500
237 X = 1.013*(EXP(4.114-4367./T))
    GO TO 500
238 T = T-273.15
    CALL SPLINT(TH2,PSH2,12,T,X,1,1,1)
    X = EXP(X)
    GO TO 500

```

```

VP NA
VP3
VP4
VP5
VP HG
VP NAK

```

```

C
C      LATENT HEAT OF VAPORIZATION (J/GM)
C
1014 GO TO (241,242,243,400,245,400,400,248), JF
241 T = T/3173.
    X = 4.184*6061.2*(1.-T)**.3725
    GO TO 500
242 X=4.178649E3+2.829841E-1*T-4.765964E-4*T*T
    GO TO 500
243 X=2.269079E3-1.318445E-1*T-2.003039E-4*T*T
    GO TO 500
245 X=6.950302E2-6.543721E-2*T-5.902942E-5*T*T
    GO TO 500
248 T = T-273.15
    CALL SPLINT(TH2,HLH2,12,T,X,1,1,1)
    X = EXP(X)
    GO TO 500

```

```

LV2
LV3
LV5

```

```

C
C      SAT LIQUID ELECTRICAL RESISTIVITY (OHM-CM)
C
1015 GO TO (251,252,253,254,255,400,257,400), JF
251 T = TKTOP(T)
    X=2.54E-6 *(10.186+2.9187E-3*T+6.8168E-7*T*T+1.1545E-10*T*T*T)
    GO TO 500
252 T = TKTOP(T)
    X=2.54E-6 *(2.1729+7.6248E-3*T+5.8313E-7*T*T+1.1260E-9*T*T*T)
    GO TO 500
253 T = TKTOP(T)
    X=2.54E-6 *(2.6978+1.4055E-2*T-2.0398E-6*T*T+3.5792E-9*T*T*T)
    GO TO 500
254 T = TKTOP(T)
    X=2.54E-6 *(6.3519+2.0871E-2*T+5.1071E-6*T*T+6.2079E-9*T*T*T)
    GO TO 500
255 T = TKTOP(T)
    X=2.54E-6 *(10.9086+3.3902E-2*T-1.6701E-5*T*T+1.0964E-8*T*T*T)
    GO TO 500
257 T = TKTOP(T)
    X=2.54E-6 *(12.8180+1.2679E-2*T-3.6501E-7*T*T+2.852E-9*T*T*T)
    GO TO 500

```

```

PS1
RS2
RS3
RS4
RS5
RS7

```

```

C
C
400 WRITE (6,5) JP,JF
    X = -1.
500 XX = X
501 RETURN
410 WRITE (6,4) T
    X = -1.
    GO TO 501

```

```

C
C
5 FORMAT(//72H *** ERROR IN SUBROUTINE PROP -- ILLEGAL FLUID OR PROP
1ERTY CODE USED *** // 5X, 7HJPROP = I6,6X, 8HJFLUID = I6 //)
4 FORMAT(//63H *** ERROR IN SUBROUTINE PROP -- OUT OF BOUNDS TEMPERA
1TURE *** // 6X, 11HT(KELVIN) = E20.5 //)
END

```

## 2.7 ATOMIZATION OF COLLECTED CONDENSATE\*

### 2.7.1 Background

As has been frequently stated, it is that fraction of the condensate which has been collected by the various turbine surfaces and then discharged in the form of macroscopic diameter drops which is capable of causing erosion damage. In wet vapor turbines two locations of particular interest are: (1) atomization of liquid torn from that flowing along the turbine housing, and (2) atomization of liquid from the vicinity of the trailing edges of stator vanes. In both instances the liquid can be carried into the path of rotor blades moving with high velocities relative to the liquid. Impact of liquid at high velocities on surfaces can cause erosion damage providing the liquid drops are of sufficient girth to drive the threshold velocity to cause damage below the impact velocity.

In considering casing liquid atomization the Westinghouse erosion model assumes that drops are produced by the same general mechanism as that of the primary stage of atomization of the liquid torn from stators. This assumption allows the same equations to be used for predicting casing liquid atomized drop diameters for rotor impingement investigation as are used in predicting the primary atomization drop diameters from stator discharged liquid. Such a casing liquid calculation has been previously reported. To our knowledge there is no experimental data by which to check this assumption. A substantial discussion of the general nature of the casing liquid flows is provided in Spies, Baughman, and Blake.<sup>(1)</sup>

Visual observations in steam turbines<sup>(1,2)</sup> reveal that the liquid collected on the stators is torn from the vicinity of the trailing edges of the stator vanes. Initially this liquid is in the form of a distribution of sizes of fairly large drops. This stage of the atomization process is called primary atomization. These large primary drops are caught up in

the decaying wakes downstream of the stators and accelerated by the vapor stream. Most of the primary drops are unstable under the aerodynamic conditions prevailing during this acceleration. Providing there is sufficient distance (time of flight) between stator and rotor, these unstable drops are broken down into smaller stable drops. This stage of the atomization process is called secondary atomization. Completion of the secondary atomization process gives a relatively stable population of drops composed of a residual of primary drops which were small enough to be stable plus the secondary drops formed from shattered primary drops. In well designed turbines, it is this stabilized population of drops which impinge upon the rotor blades and can cause erosion damage. The discussion which follows is concerned with the various stages of atomization of stator discharged liquid.

### 2.7.2 Stator Atomization Model

#### a) General Description

To calculate the erosion by liquid of damaging form, it is necessary to know the size, relative velocity and number and location of impacts on the rotor blades as a relation of time. There are at least four different mechanisms of primary atomization and two for secondary atomization which have been observed under conditions related to those in turbine stators. To trace the history of all these possible processes would be a formidable, if not impossible task. Because of this, the approach taken in the Westinghouse model involves substantial simplification through gross description of droplet classes based in large part on empirical correlating relations commonly used in describing gas-atomized liquid sprays.

Furthermore, almost all the empirical observations used in preparing the numerical detail of the atomization model were taken from reference material where the tests reported were made using steam vapor or air atomization of water drops. Nonetheless, it is felt that observations on steam or air atomization of water drops, particularly observations in actual turbines or turbine-like cascades, are applicable to a broader spectrum of turbine

---

\* W. D. Pouchot, Advisory Engineer, Systems & Technology Section, Westinghouse Astronuclear Laboratory, Large, Pa.



working fluids (such as the liquid metals) of low liquid-viscosity and substantial surface tension.\*

# • Nomenclature

In dimensional equations the units used are:

Mass-slugs, Force-pounds, Length-feet,  
Time-seconds

a	Constant in Nukiyama-Tanasawa distribution functions
a	Stator blade trailing edge thickness
b	Constant in Nukiyama-Tanasawa distribution function
D	Drop diameter
D <sub>m</sub>	Most common drop diameter in terms of spray volume
D <sub>3-0</sub>	Mass mean drop diameter
D <sub>3σ</sub>	The drop approximately three standard deviations larger than the mean drop
D <sub>max</sub>	Maximum drop diameter
K	A constant
L	Length along surface of stator blade from nose to trailing edge
M <sub>a</sub>	Mach No. based on free stream conditions
$\dot{m}_l$	Collected liquid mass flow rate per unit casing periphery or blade height

\* Wettability of the liquid with respect to surface does not seem to be an important factor. Experiments reported in reference (4) seem to indicate that under the impress of aerodynamic forces liquids tend to become non-wetting. This is reasonable since the ground state of a liquid mass in the absence of external forces such as gravity, is a sphere and perturbations from aerodynamic sources would tend to allow films and rivulets to "ball up".

N	Number of drops
n	Exponent in Nukiyama-Tanasawa distribution function
p	Gamma function argument
Re <sub>D</sub>	Reynolds Number based on drop diameter
S <sub>b</sub>	Tanasawa's stability number (Heinze's viscosity number) - $\mu_l / \sqrt{\rho_l \sigma a}$
U <sub>r</sub>	Relative velocity between vapor and drop
u	Gamma function argument
U <sub>s</sub>	Bulk stream (free stream) velocity
V	Spray Volume
V <sub>x</sub>	Volume of spray between gamma function parameter (a) and parameter (x)
V <sub>tot</sub>	Total volume of spray
W <sub>e</sub>	Weber number - $\rho_v U_r^2 D / \sigma$ or $\rho_v U_s^2 D / \sigma$
X	Stator blade chord length
x	Gamma function parameter
$\rho_v$	Vapor density
$\rho_l$	Liquid density
$\sigma$	Liquid surface tension
$\tau_s$	Wall friction force per unit area on bulk flow
$\mu_v$	Vapor viscosity
$\mu$	Liquid viscosity

● Definition of Model

The model of atomization is defined in terms of the empirical Nukiyama-Tanasawa distribution function plus several characteristic drop diameters.

The distribution function is used in both a number of drops form and in volumetric form. These functions are:

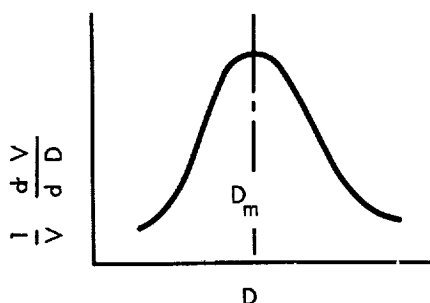
$$\frac{dN}{dD} = a D^2 e^{-bD^n} \quad (1a)$$

$$\frac{dV}{dD} = \frac{\pi a}{6} D^5 e^{-bD^n} \quad (1b)$$

The characteristic diameters used are:

1)  $D_m$  = most common diameter drop

$D = D_m$  when the second derivative of Eq. 1b equals zero or  $\frac{d^2V}{dD^2} = 0$ . This corresponds to the peak of the familiar distribution curve as:



2)  $D_{3-0}$  - Mass mean diameter drop

$$D_{3-0} = \left[ \frac{6}{\pi} \frac{\sum_0^\infty \Delta V}{\sum_0^\infty \Delta N} \right]^{1/3}$$

3)  $D_{3\sigma}$  - The drop approximately three standard deviations larger than the mean drop

$D_{3\sigma}$  is the drop for which

$$\frac{\sum_0^{\infty \sim x} \Delta V}{\sum_0^\infty \Delta V} = 0.997$$

$$\text{where } x = \frac{5}{n} \left( \frac{D}{D_m} \right)^n$$

4)  $D_{\max}$  - Defined maximum drop diameter

$D_{\max}$  is the drop for which

$$\frac{\sum_0^{x \rightarrow \infty} \Delta V}{\sum_0^\infty \Delta V} = K$$

The Nukiyama-Tanasawa distribution function is often used by experimentalists in reporting data on gas atomized liquid sprays. It is a monomodal function and the constants, "a, b and n" of the expression can be determined from a knowledge of the number of volume fractions of the spray of any two drop diameters. Conversely the spray can be characterized by a value of "n" and a characteristic drop diameter such as the mass mean or surface mean drop diameter.

From the point of view of the analyst, these various relationships between characteristic drop diameters and the constants of the Nukiyama-Tanasawa expressions may be found by such means as writing an appropriate computer program or by use of Pearson's tables of the incomplete gamma function<sup>(3)</sup>.

In connection with use of the reference (3) material, it may be shown that:

$$b = \frac{5}{n} \left( \frac{1}{D_m} \right)^n$$

Hence the exponential coefficient

$$(b d^n) = \frac{5}{n} \left( \frac{D}{D_m} \right)^n$$

If  $\frac{5}{n} \left( \frac{D}{D_m} \right)^n = x$ , equation (1b) may then be put in the form:

$$\frac{dV}{dx} = \frac{\pi a}{30} \left( \frac{n}{5} \right) \left( \frac{6-n}{n} \right) D_m^6 \left( x \frac{6-n}{n} \right) e^{-x} \quad (2)$$

If the additional substitution  $\frac{6-n}{n} = p$  is made,

$$\frac{dV}{dx} = \frac{\pi a}{30} \left( \frac{n}{5} \right)^p D_m^6 (x^p e^{-x}) \quad (3)$$

In integral form equation (3) may be written,

$$V_x = \frac{\pi a}{30} \left( \frac{n}{5} \right)^p D_m^6 \int_0^x x^p e^{-x} dx \quad (4)$$

When  $x = \infty$ ,  $V_x = V_{tot}$  (the total volume of the spray)

and therefore by definition:

$$\frac{V_x}{V_{tot}} = \frac{\int_0^x x^p e^{-x} dx}{\int_0^\infty x^p e^{-x} dx} \quad (5)$$

This is the ratio of the spray volume contained in all drops smaller than

$$D = \left( \frac{nx}{5} \right)^{\frac{1}{n}} (D_m)$$

to the total volume of the spray.

There is nothing fundamental in these previous substitutions and rearrangement of the Nukiyama-Tanasawa equation. They are for the purpose of putting the equation on a form for easy use with the tables of Reference (3).

The complete gamma function for the argument  $p$  is written  $\Gamma(p+1)$ . It can be defined by:

$$\Gamma(p+1) = \int_0^\infty e^{-x} x^p dx$$

The incomplete gamma function is defined after Pearson(3) to be:

$$\Gamma_x(p+1) = \int_0^x e^{-x} x^p dx$$

Hence equation (5) may be given as:

$$\frac{V_x}{V_{tot}} = \frac{\Gamma_x(p+1)}{\Gamma(p+1)} = I(x-p) \quad (6)$$

Pearson(3) has constructed tables of this ratio in the form:

$$\frac{V_x}{V_{tot}} = I(u, p)$$

where

$$u = \frac{x}{\sqrt{p+1}}$$

In terms of the spray parameters of interest,  $p$  and  $u$  are:

$$p = \frac{6-n}{n}$$

$$u = \left( \frac{D}{D_m} \right)^n \frac{5}{\sqrt{6n}}$$

Some numerical values for the ratios  $D_{3\sigma}/D_{3-\sigma}$  and  $D_{3\sigma}/D_m$  calculated in this way are given as a function of  $n$  in Table 2.7-1.

TABLE 2.7-1  
RELATIONSHIPS OF  $D_{3\sigma}$ ,  $D_{3-\sigma}$ ,  $D_m$ , AND  $n$

$n$	$D_{3\sigma}/D_{3-\sigma}$	$D_{3\sigma}/D_m$
0.25	28.70	15.5
0.50	8.14	5.61
1.0	3.84	2.99
2.0	2.40	1.99
3.0	2.01	1.69

#### b) Primary Atomization

Mechanisms of primary atomization as observed in an actual turbine<sup>(5)</sup> and in turbine-like stationary cascades<sup>(4,5)</sup> are: (1) stripping of liquid or sheets from liquid puddles, (2) stripping or tip bursting of oscillating pendant drops attached to the stator trailing edge, (3) eye-dropper tearing of individual drops from the stator trailing edge, and (4) direct formation of individual drops on the convex surface of a stator by some mechanism giving results similar to a drop of water on a hot stove.

The observations reported are qualitative. Quantitative information on the relative volumes of liquid involved in each of the processes is not available. It seems reasonable that the tearing of masses or sheets of liquid from stators involves a more important part of the total liquid available than the other observed mechanisms of detachment. On this basis, a sheet atomization model is the logical tool for estimation of primary drop sizes.

The model chosen is the classical one of a sheet of liquid ruffled under the impress of aerodynamic forces, the ripples developing into ligaments, and the ligaments in turn collapsing into drops. Using this model an expression for the most common drop diameter,  $D_m$ , has been developed. It is

$$D_m = 17 \left[ \frac{\dot{m}_l \mu_l}{\rho_l \left( \tau_s + \frac{\dot{m}_l U_s}{X} \right)} \right]^{1/4} \left[ \frac{\mu_l}{\tau_s} \sqrt{\frac{\sigma}{\rho_l}} \right]^{1/3} \quad (7)$$

The complete primary distribution is then obtained by applying the Nukiyama-Tanasawa distribution function assuming that  $n = 1$ . Given  $n$  and  $D_m$ , the ratio  $V_x/V_{tot}$  at any value of  $D$ , can be obtained through the use of Pearson's<sup>(3)</sup> tables by calculation of Pearson's arguments  $p$  and  $u$  as a function of  $D$ .

Typical values calculated for the ninth stator of the Yankee steam turbine are given in Appendix A to this Section 2.7, along with the derivation of the expression for  $D_m$  (equation 6).

A comparison between calculated values for the Yankee steam turbine and a small amount of experimental data on stator primary atomization obtained by Hays<sup>(5)</sup> from the British CEGB is also given in Appendix A to the Section 2.7. This data comparison cannot be said to confirm the model of primary atomization proposed here, because of the small number of drops sampled experimentally, but the comparison is encouraging.

### c) Secondary Atomization

To distinguish between those primary drops which are stable from origin to rotor impact and primary drops which undergo secondary atomization, a parametric time history analysis of the drops in the stator wake is carried out as previously discussed in Section 2.6. It is assumed that the primary drops become entrained by a given wake streamline and the liquid represented remains with that streamline until rotor impact. The criteria for disruption of a primary drop is taken as the exceeding of a critical drop Weber Number at some point along the path between detachment from the stator to impact with the rotor. This assumes that there is time for the drop to disrupt, after the critical Weber Number has been exceeded, before it impacts the turbine rotor. This time period for disruption is covered in Section 2.6. All primary drops which experience a Weber Number greater than the critical are presumed to disrupt to smaller stable secondary drops.

Primary drops which experience local Weber Numbers in the wake which are less than the critical Weber Number are assumed stable and retain their primary configuration. The maximum size drop which will impact the rotor is the primary drop which just experiences but does not exceed the critical Weber Number anywhere between origin and impact with the rotor.

This model uses Weber Number criteria because under local conditions at the time of breakup of the primary drops it is believed that the ratio of the dynamic pressure force to surface tension force is the single most important criteria as to whether a drop is stable or not. Unfortunately, Weber Number alone is not completely sufficient to allow a prediction of maximum drop diameters in sprays even when the local conditions at disruption are known with reasonable accuracy. For this reason, Westinghouse has varied the numerical value of the Weber Number which has been used in analysis of turbines from turbine to turbine.

For small turbines of the space type, 1" chord, 1"-2" high blades, the critical Weber Number used has been 13. For the large low pressure ends of central station steam turbines the value used has been Weber Number = 22. The rationale is due to Gardner<sup>(6)</sup> who apparently drew on the work of Heinze. According to Spies et al<sup>(1)</sup>, Heinze shows that for a "non-viscous" fluid (the turbine working fluids are considered "non-viscous") that the critical value of Weber Number is 13 for shock exposure of a drop to aerodynamic forces and this critical Weber Number increases to 22 for a steadily falling drop. This latter case is that of graduated application of aerodynamic forces to the drop. From trajectory calculations on both large and small turbines, it appears that the application of aerodynamic forces to the primary drops is quite abrupt or shock-like in the small space type turbine and quite gradual in the large central station steam turbine low pressure end. The selection of Weber Number = 13 for the small turbines and Weber Number = 22 are commensurate with the trajectory observations.

Since these values were selected, a considerable amount of actual observation in large steam turbines<sup>(2)</sup> and in a small steam turbine<sup>(1)</sup> built to simulate a space potassium turbine have become available. These data clearly show that from a conceptual point of view the simplified two valued scheme of this model is inadequate. However, in a numerical sense the selection of Weber Number = 13 for the small space turbines examined is a good average value based on an analysis of the results of Spies et al<sup>(1)</sup> as given in Appendix "B" of this section 2.7. For a typical design such as the NASA-GE 3 stage potassium test turbine the procedure of Weber Number = 13 may err in estimating the maximum size drop impinging on the rotor blades of that turbine by 30 microns. The maximum size drop is about 100 microns in diameter.

Spies et al<sup>(1)</sup> give three empirical expressions which affect a good correlation of their data. These are\*

$$We = 65 (M_a)^{1.16} \quad (i)$$

$$We = \frac{K}{s_b^{2/3}} \left( \frac{\mu}{\mu_v} \right) \left( \frac{\mu_v U_s}{\sigma} \right)^{7/6} \left( \frac{L}{a} \right)^{1/6} \quad (ii)$$

where  $K = 0.31$  for the data of Smith<sup>(7)</sup>

$$Re_D = 18 \quad (iii)$$

The first of these (i) is due to Smith<sup>(7)</sup>. It also correlates his data as does the second expression (ii). Both the first and second expressions badly overestimate the maximum size drops in large central station turbines low pressure ends as reported by Christie and Hayward<sup>(2)</sup>. The writer has not evaluated the third expression (iii). As a general comment, all three expressions lack a model as a basis for understanding the phenomena the expressions purport to correlate. They, therefore, pose a high risk when applied to situations other than those exact ones from which they were obtained.

The selection of critical Weber Number = 22 for the low pressure ends of large central station steam turbines seems to be overly conservative in terms of steam stationary cascade tests as reported by Christie and Hayward<sup>(2)</sup> but not necessarily for actual turbines as reported by the same reference<sup>(2)</sup>.

#### d) Final Drop Size Distribution

##### • Conceptual Approach

Conceptually the drop size distribution resulting from the completion of the secondary atomization process is the sum of the primary drops

\*All values are calculated using bulk flow (free stream) conditions not local wake conditions.

which escaped disruption plus the families of secondary drops formed from the disrupted primary drops.

The residual primary drops are those from the primary distribution which did not experience a greater than critical Weber Number.

The mass mean drop diameter ( $D_{3-0}$ ) of the sum of the families of the secondary drops is assumed to be given by a semi-empirical expression developed by Wolfe and Anderson<sup>(8)</sup>. This is:

$$D_{3-0} = \left[ \frac{136 \mu_f \sigma^{3/2} D_m^{1/2}}{\rho_v^2 \rho_f^{1/2} U_r^4} \right]^{1/3}$$

where  $D_m$  is the most common drop of the initial primary distribution.

The distribution function for the sum of the families of secondary drops is then taken as that of the Nukiyama-Tanasawa function for  $n = 1$  and the appropriate Wolfe and Anderson  $D_{3-0}$ .

Addition of this secondary distribution to the residual of the primary distribution gives the final drop size distribution impacting the turbine rotor blades.

This is the way in which the final drop size distribution used in calculating the erosion values for the Yankee steam turbine was obtained. A comparison of this distribution in dimensionless form with various test observations from the literature which have become available since the Yankee analysis was performed, reveals a rather striking lack of similarity between calculation and observation as shown in Figure 2.7-1. This may explain why the calculated erosion of the Yankee ninth rotor blades was lower than that actually observed in service.

### • An Empirical Approach

Since the conceptual approach just outlined yielded a drop distribution much askew compared to actual experimental observations, a more fully empirical approach was tried in connection with the Bayshore No. 2 turbine evaluation. This approach was to apply an average of the observed distributions shown in Figure 2.7-1 to the calculated maximum drop diameter.

Reservations about this approach must also be expressed. For example, the observational curves shown in Figure 2.7-1 correspond to Nukiyama-Tanasawa "n" values in the range of 2 to 3\*. This is far higher than characteristic values reported in the literature of gas atomized liquid sprays. Here a value of "n" much different from one is uncommon<sup>(9)</sup> and when values differ from one they are likely to be less than one.

A part of the difficulty may be in the interpretation of what experimentalists mean when they report a value of  $n = 1$  in the Nukiyama-Tanasawa expression effects a good correlation of their data. For example, turn to Figure 2.7-2. This is a plot of some data presented by Spies, Baughman, and Blake<sup>(1)</sup>. The open circles are the data. The solid line and dashed line are the Nukiyama-Tanasawa expression plotted with  $n = 1$  and  $n = 3$  respectively. It will be noted that the shape of distribution curves as given by the circles is very similar to the shape of other experimental results curves as shown in Figure 2.7-1.

Spies et al conclude in their report that a Nukiyama-Tanasawa distribution with  $n = 1$  affects a satisfactory correlation of their data. As can be seen in Figure 2.7-2 it does on the average affect a better correlation than  $n = 3$ . However, Spies et al report the maximum drop diameter observed for this particular set of test conditions to be 180 microns. An  $n = 1$  correlation implies at least 2 percent by number of drops with a diameter greater than 180 microns. This 2 percent number fraction represents a considerably larger volume fraction than number fraction because of the D-cubed effect. It seems

\*This is on the writer's terms; not necessarily on the terms of the experimentalist as is discussed shortly.

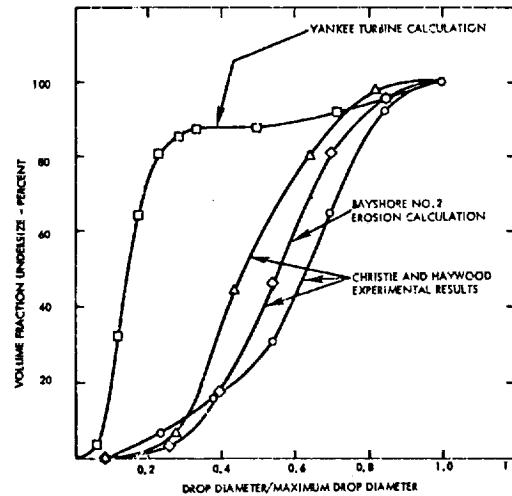


Figure 2.7-1 Drop Distribution Functions

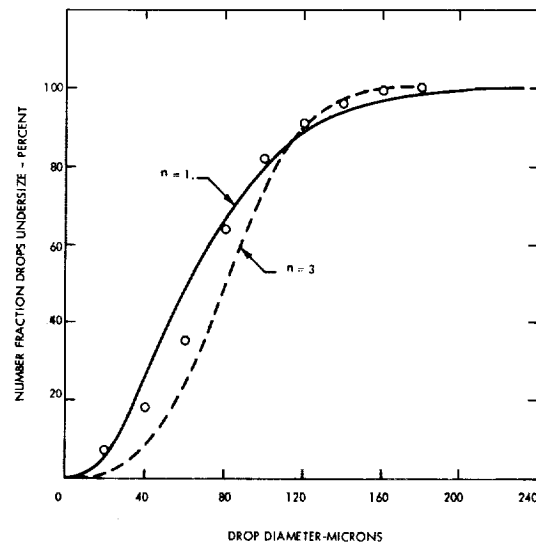


Figure 2.7-2 Distribution of Drop Sizes in a Small Steam Turbine after Spies, Baughman, and Blake

quite possible that the  $n = 1$  selection of Spies et al is in fact more nearly correct than the actual data points. It seems quite possible that they might have observed some (say) 240 micron diameter drops if their observations had covered 10,000 drops and not hundreds of drops.

This possible inaccuracy in distribution information is compounded in the empirical approach used in the Bayshore No. 2 turbine erosion examination by a "tail wagging the dog phenomena". A tabulation from reference (2) is reproduced as Table 2.7-2 following:

TABLE 2.7-2

TABULATION FROM REFERENCE 2

Size Range of Drop Diameters (microns)	Total No. of Droplets per Second in Each Size Range at Given Load		
	(Load 100%)	(Load 60%)	(Load 40%)
50 to 150	384	1160	1283
150 to 250	322	414	744
250 to 350	16	54	125
350 to 450	0	4	10

The most drops are reported in the 40 percent load column. The number is 2162. A plot of this 40 percent load tabulation is given as "Original Data" in Figure 2.7-3. If one 500 micron drop is added to this original 2162 drops, the distribution function shifts markedly (in the direction  $n = 1$ ) as shown by the curve "Original Data Plus One" of Figure 2.7-3.

The significance of the shift with respect to predicting erosion in turbines is marked in numerical evaluation using the empirical atomization model as applied to Bayshore No. 2. The model assumes that some particular characteristic diameter drop of the distribution of drops can be predicted either empirically or theoretically as a function of turbine flow and geometry for particular sets of turbine flow and geometry variables. Then the model assumes this particular characteristic diameter can be generalized to a complete particular distribution of drops by applying an empirical distribution function to the particular characteristic diameter drop.

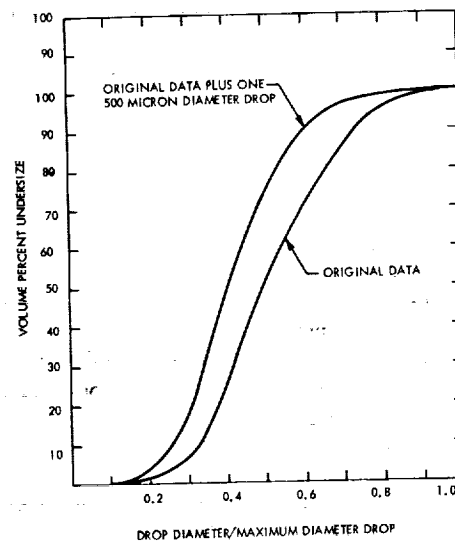


Figure 2.7-3 Manipulation of Experimental Drop Size Distribution

The foregoing are all reasonable assumptions. Unfortunately at this time the characteristic diameter drop on which there is substantial experimental data in turbines is the maximum diameter drop of the spray. While the general approach to the model is not limited to the use of the maximum diameter drop as the characteristic diameter drop, the weight of experimental evidence on maximum diameter drops has made them a logical if unfortunate choice.

Referring back to Figure 2.7-3, the actual change in total volume of the spray caused by adding one 500 micron drop is only 1.2 percent. However, if in reconstructing a distribution of drops based on a particular independently calculated maximum diameter drop, the distribution function marked "Original Data" is used, 30 percent of the volume of the spray will be predicted to be in drops greater than 0.6 the diameter at the maximum diameter drop; whereas if the distribution function marked "Original Data Plus One" is applied, only 10 percent of the volume of the spray will be predicted to be in drops greater than 0.6 the diameter of the maximum diameter drop. That is as little as 1 percent change in the experimental measurement



with respect to volume (or one part in two thousand with respect to number of drops) can shift the prediction of amount of moisture contained in damaged drop diameters\* by as much as 300 percent using this empirical procedure.

### 2.7.3 Conclusions

Means of assessing the drop sizes and distribution of liquid discharged from turbine stators have been presented. The numerical procedures suggested for predicting primary atomization drop sizes and the maximum diameter drop in the final distribution of drops impinging on turbine rotor blades have an apparent accuracy of  $\pm 30$  percent as compared to limited experimental information.

Two means of assessing the distribution of drops below the maximum drop diameter in the final distribution of drops impinging on the turbine rotor blades have been investigated.

The first of these methods which was of a semi-theoretical nature, when applied to the Yankee steam turbine low pressure end, yielded a calculated drop size distribution very different from those observed in an English steam turbine.

The second of the methods for assessing the distribution of drops in an empirical approach using an average of the observed distributions in the English steam turbine applied to a calculated maximum drop diameter. (Maximum Drop diameter Weber No. Criterion 13 for small turbines, 22 for large turbines as applied to stator wake trough conditions.) The second method is preferred although it can yield quite large inaccuracies in results with very small errors in determination of maximum drop diameter.

---

\*The 0.6 of maximum diameter was picked by example and does not imply that only drops greater than this can cause erosion damage.

## APPENDIX 2.7A

### PRIMARY ATOMIZATION EXPRESSIONS

Mechanisms of primary atomization reported are: (1) stripping of masses of liquid or sheets from liquid puddles, (2) stripping or tip bursting of oscillating pendant drops attached to the stator trailing edge, and (3) eye-dropper-like tearing of individual drops on the convex surface of the stator by some mechanism, giving results similar to a drop of water on a hot stove.

Unfortunately, none of the referenced work gives quantitative information on the relative volumes of liquid involved in the observed processes. It seems reasonable that the tearing of masses or sheets of liquid from the stators involves a more important part of the total liquid available than the other observed mechanisms of detachment. The sheet atomization model is on this basis the logical tool for estimation of average primary drop sizes. As available information is insufficient for definitive conclusions, the pendant modes may be more important than assumed.

#### NOMENCLATURE PRIMARY ATOMIZATION

<u>Symbol</u>	<u>Definition</u>		
a	Spray distribution constant	$\dot{m}_L$	Mass flow rate per unit of stator edge length (lb/sec/ft)/g
b	Spray distribution constant	n	Spray distribution constant
B	Ligament diameter	N	Number of drops
$C_f$	Stator wall friction drag coefficient	u	Gamma function parameter
d	Drop size	$U_s$	Bulk steam velocity
$\bar{d}$	An average drop size	V	Volume rate of spray formation
g	Gravitational constant	$V_{tot}$	Total volume rate of spray formation
H	Stator boundary layer form factor	X	Stator chord length
		x	Gamma function parameter
		z	Drop size
		$\beta$	Drag coefficient
		$\delta$	Stator liquid film thickness
		$\theta$	Stator boundary layer form factor
		$\lambda$	Wave length of ripples in liquid film
		$\lambda_B$	Wave length of varicosities in ligaments
		$\langle \bar{\lambda} \rangle$	Most probable wave length
		$\rho_L$	Density of liquid
		$\rho_s$	Density of vapor (bulk)
		$\sigma_L$	Liquid surface tension
		$\tau_s$	Stator wall friction drag per unit area
		$\mu_L$	Liquid viscosity
		$\mu_s$	Vapor viscosity

## SHEET ATOMIZATION

Based on actual turbine observations such as those reported by Hays<sup>(5)</sup>, the flow of collected moisture over stator vane surfaces is far from uniform. The flow gathers in rivulets or puddles which feed separated atomization sites.

In an actual turbine, the location of the atomization points is probably influenced by surface and vapor flow irregularities. However, even with a perfectly uniform surface, a distribution of attachment points can be expected. Under such uniform surface conditions it is to be expected that the fluid would initially start to collect in the wake of the stator trailing edge as a roll of liquid with a cross-sectional diameter of approximately the width ( $W$ ) of the trailing edge. As is well known, such a slender cylinder of liquid is unstable in the presence of surface tension forces and develops varicosities along its length. The pitch of these varicosities would then determine the atomization sites. The pitch (or length) of the varicosities would not be uniform but would have a distribution of pitches. Numerically as given by Green<sup>(10)</sup> after Rayleigh, the minimum pitch of a cylindrical instability is  $\pi W$  and the most probable pitch is  $4.5 W$ . Other pitches than those, of course, have a statistical probability of existence<sup>(11)</sup>.

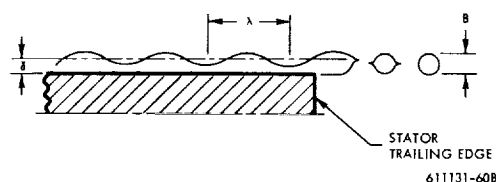
If the distance between the atomization sites becomes fairly large, the local liquid flow rates at the site will be many times that of a uniformly distributed flow. This high local flow rate results in a thickening of the local liquid boundary layer and an opportunity for the development of sufficient liquid boundary layer momentum with ripples to give sheet type atomization rather than pendant atomization. This sheet type atomization is analogous to the stage 3-type of whirling cup atomization which takes place at high rates of liquid feed to cup or disc atomizers<sup>(10)</sup>. In this example of the whirling disc atomizer, the flow rate on a uniform basis is high enough to produce sheet atomization. Such sheet atomization could obviously also take place from wet turbine stators on a uniform or nearly uniform film basis if the liquid flow rate is high enough. In the case of the Yankee Atomic turbine low pressure end, sufficient collection of moisture on the ninth (and wettest) stator to produce uniform film sheet atomiza-

tion does not seem likely. Sheet type atomization is probably a result of local flow rates greater than average.

### Average Droplet Size from Sheet Atomization

Schematically, the process of sheet atomization is assumed to be as follows:

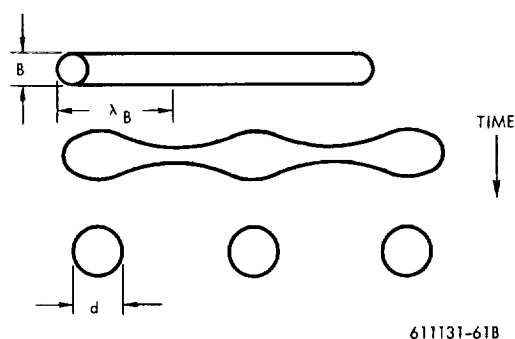
- 1) The liquid film of average depth ( $\delta$ ) flowing towards the stator trailing edge (as a result of air drag forces) develops ripples of wave length ( $\lambda$ ).



- 2) This rippled film is then blown from the trailing edge of the stator and collapses into ligaments of cross-sectional diameter  $B$  strung out parallel to the trailing edge. The cross-sectional area of the ligament is approximately equal to the product of the average film thickness times the ripple wave length or

$$B = \sqrt{\frac{4}{\pi} \delta \lambda} \quad (1)$$

- 3) The ligament so formed in turn develops instabilities of wave length ( $\lambda_B$ ) along its length and collapses into drops of diameter ( $d$ ).



The volume of the drop being approximately equal to a cylindrical section of diameter B of length  $\lambda_B$  or:

$$\frac{\pi}{6} d^3 = \frac{\pi}{4} B^2 \lambda_B$$

$$d = (3/2 B^2 \lambda_B)^{1/3} \quad (2)$$

As previously quoted from Green<sup>(10)</sup>, the most probable value of  $\lambda_B$  is:

$$\lambda_B = 4.5 B$$

$$d = \frac{3 B}{\sqrt[3]{4}} \quad (3)$$

Substituting for B from equation 1 into equation 3 gives:

$$d = 2.14 \sqrt{\delta \lambda} \quad (4)$$

The average liquid boundary layer thickness at the trailing edge of turbine stators is given by\*:

$$\delta = \left[ \frac{2 \dot{m}_L \mu_L}{\rho_L \left( \tau_s + \frac{\dot{m}_L}{X} U_s \right)} \right]^{1/2} \quad (5)$$

$$\tau_s = \frac{C_f \rho_s}{2} U_s^2$$

$$C_f = (2) (.123) (10^{-.678 H_s}) \left( \frac{U_s \theta \rho_s}{\mu_s} \right)^{-0.268}$$

\*See Section 2.5

An analysis by Jefferys of wind-generated gravity waves has been developed by Mayer<sup>(12)</sup> to predict the most probable capillary wave length in a windblown sheet. Mayer's expression gives:

$$\bar{\lambda} = 9 \pi \sqrt[3]{16} \left( \frac{\mu_L \sqrt{\sigma_L / \rho_L}}{\beta \rho_s U_s^2} \right) \quad (6)$$

Considering the expression  $\beta/2 \rho_s U_s^2$  as the effective drag force per unit area of film,<sup>s</sup> it may be written in terms of the boundary layer calculations (neglecting fog particle impact momentum) as:

$$\beta \rho_s U_s^2 = C_f \rho_s U_s^2 = 2 \tau_s$$

$$\text{or } \bar{\lambda} = 9 \pi \sqrt[3]{16} \left( \frac{\mu_L \sqrt{\sigma_L / \rho_L}}{2 \tau_s} \right)^{2/3} \quad (7)$$

Substituting in equation 4 from equations 6 and 7 results in an expression for an "average" drop size:

$$\bar{d} = 17.0 \left( \frac{\dot{m}_L \mu_L}{\rho_L \left( \tau_s + \frac{\dot{m}_L}{X} U_s \right)} \right)^{1/4} \left( \frac{\mu_L}{\tau_s} \sqrt{\frac{\sigma_L}{\rho_L}} \right)^{1/3} \quad (8)$$

In Figure 2.7A-1 "average" drop sizes from equation 8 are presented. It may be noted that the drop size predicted by equation 8 appears to become independent of flow rate at the higher values of flow rate examined. This suggests that a simplified expression such as equation 9 will be adequate for predicting the "average" drop size in many instances.

$$\bar{d} = 17.0 \left( \frac{\mu_L X}{\rho_L U_s} \right)^{1/4} \left( \frac{\mu_L}{\tau_s} \sqrt{\frac{\sigma_L}{\rho_L}} \right)^{1/3} \quad (9)$$

Numerical evaluation of equation 9, inserting the same values for the independent variables, as used in evaluating equation 8 gives:

$$\bar{d} = 630 \text{ microns.}$$

Examining equation 9, it will be seen that the average drop size predicted varies slowly with most of the variables except  $U_s$ . Setting  $\tau_s : U_s^2$  gives the variation with respect to  $U_s$  as:

$$d : : U_s^{-.92}$$

### Sheet Atomization Drop Size Distribution

There is a distribution of drop sizes resulting from sheet atomization (in fact from almost any atomization process). There is the distribution of sites (inflow rates) along the trailing edge, the distribution of atomization wave lengths ( $\lambda$ ) in the direction of flow, and the distribution of cylindrical wave lengths ( $\lambda_B$ ) producing the final primary drops. A distribution function could be developed from the Rayleigh<sup>(11)</sup> cylindrical instability function and the Jefferys-Mayer<sup>(12)</sup> capillary wave length function. However, an overall empirical distribution function due to Nukiyama-Tanasawa is easier to use:

$$\frac{dN}{dz} = a z^2 e^{-b z^n} \quad (10)$$

Quoting from Putnam<sup>(9)</sup>, "Two Japanese investigators, S. Nukiyama and Y. Tanasawa, obtained extensive data on drop sizes in sprays by air atomization, and sought to correlate these data ---". Their investigations indicated that a value of 2 for the exponent of (z) effected a good correlation of the experimental data in every case, and that exponent (n) varied but little from unity.

While other investigators, including the writer, have found that the value of the exponent (n) may fall as low as 1/4, a numerical case can be made for the Yankee turbine to consider this exponent as having a value of unity. An exponent of the

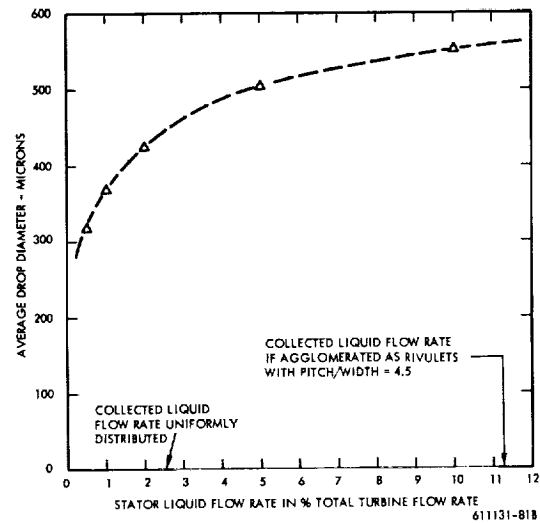


Figure 2.7A-1 Average Drop Size, Primary Atomization

order of unity is required to get a reasonable fit between an upper size limit on drops (order of 1500 to 2000 microns) resulting from the size of the trailing edge thickness and an unspecified kind of average drop size of the order of 500-600 microns.

Using  $n = 1$  and writing equation 10 in terms of volume rather than number of drops gives:

$$\frac{dV}{dz} = \frac{\pi a}{6} z^5 e^{-bz} \quad (11)$$

This equation contains two undetermined constants, (a) and (b). Constant (a) may be determined from the total volume of the spray using the continuity relationship once constant (b) has been found. In connection with constant (b), it may be observed that if a value of the "average" drop size corresponding to the most probable flow rate of figure 2.7A-1 is selected, the rate of change of

volume of spray produced is a maximum with respect to this average drop size ( $z_{av}$ ) or,

$$\frac{dV}{dz} = \left( \frac{dV}{dz} \right)_{\max.}$$

and

$$\frac{d^2V}{dz^2} = 0 = \frac{\pi a}{6} (e^{-bz}) z^4 (5 - zb)$$

or

$$b = 5/z_m$$

where

$$z_m \text{ is } z_{av} \text{ at } \left( \frac{dV}{dz} \right)_{\max.} \quad (12)$$

Substituting from equation 12 in equation 11 gives:

$$\frac{dV}{dz} = \frac{\pi a}{6} z^5 e^{-5z/z_m} \frac{z}{z_m} \quad (12a)$$

If the substitution,  $x = 5z/z_m$  is made in equation 12a, it becomes:

$$dV = \frac{\pi a}{6} \left( \frac{z_m}{5} \right)^6 x^5 e^{-x} dx \quad (13)$$

$$V_x = \frac{\pi a}{6} \left( \frac{z_m}{5} \right)^6 \int_0^x x^5 e^{-x} dx = \frac{\pi a}{6} \left( \frac{z_m}{5} \right)^6 \Gamma_x$$

$$\frac{V_x}{V_{\text{tot}}} = I(u, 5)$$

$$u = x / \sqrt{6} = \frac{5z}{z_m \sqrt{6}} \quad (13a)$$

and  $I(u, 5)$  is a form of the incomplete gamma function, as tabulated in Reference 3. The ratio of cumulative liquid volume to total liquid volume of spray is given as a function of drop size in table 2.7A-1 for the ninth stator of the Yankee turbine.

A small amount of data on stator primary atomization, obtained from the British CEGB, has been reported by Hays<sup>(5)</sup>. This information is reproduced in table 2.7A-2 for conditions which more or less bracket the conditions at the ninth stator of the Yankee Turbine. This data cannot be said to confirm the model of primary atomization used here because of the low number of drops sampled. A comparison between tables 2.7A-1 and 2.7A-2 is encouraging, however.

TABLE 2.7A-1

SPRAY LIQUID VOLUME DISTRIBUTION VERSUS DROP SIZE

Drop Size (z) (microns)	$V_z/V_{\text{tot}}$
100	0.0004
175	0.007
250	0.0356
350	0.12
525 = $z_m$	0.38
750	0.72
1050	0.93
1575	0.997

TABLE 2.7A-2

DATA ON STATOR PRIMARY ATOMIZATION

Static Pressure (psia)	Bulk Steam Velocity (ft/sec)	No. of Drops	Max. Size (microns)	Min. Size (microns)
1.61	976	5	1080	460
1.72	1180	4	620	360

## APPENDIX 2.7B

### ANALYSIS OF CONTRACT NAS 7-391 RESULTS \*

A series of erosion-related experiments have been performed by the Rocketdyne Division of North American Rockwell, sponsored by NAS 7-391. These experiments employ a series of stator blade shapes and test conditions designed to simulate space turbine environments. The working fluid used is steam. A particular objective of the program is to observe the detachment of collected liquid from trailing edge surfaces and to estimate the ultimate limiting size of atomized drops as a function of the various test conditions.

A drop transport analysis has been completed on a series of eleven tests performed by Rocketdyne. The analysis was performed with the ADROP computer code (Section 2.6). Blade shape I-A \*\* was chosen for these studies. This blade is similar to that used in the last stage of the General Electric three-stage potassium test turbine, differing only in the pitch. Rocketdyne is using a stator block containing six different blade shapes and apparently could not exactly reproduce the pitch of the G. E. blades in this configuration. The mean line pitch of the Rocketdyne blade I-A is 0.616 inch while the pitch of the G. E. blade is 0.641 inch.

The test conditions employed in this study are presented in Table 2.7B-1<sup>(1)</sup>. The tip section of the blade shape used is shown in Figure 2.7B-1. The blade surface velocities in the stator flow passage were evaluated using the two-dimensional flow analysis code of Reference(13). Figure 2.7B-2 summarizes the surface velocity results. The velocities are normalized by the exit free stream velocity. These velocities are plotted against normalized surface position, which is the ratio of the distance from the blade leading edge taken along the surface to the total surface length.

\*T. C. Varljen, Supervisor, Systems and Technology, Astronuclear Laboratory, Westinghouse Electric Corporation, Pittsburgh, Pa., 15236

\*\*Rocketdyne Dwg. N-01828-A

The surface velocities obtained for the tip section were then used to evaluate the boundary layer properties at the blade trailing edge. The properties of interest are the momentum thicknesses ( $\Theta_s$  and  $\Theta_p$ ), the displacement thicknesses ( $\delta^*$  and  $\delta_p^*$ ), and the full thicknesses ( $\delta_s$  and  $\delta_p$ ) on both the suction and pressure sides of the blade. These are summarized in Table 2.7B-2.

Trajectory calculations were performed for a series of drop sizes ranging downward from the thickness of the stator trailing edge (190 microns). An axial distance of one inch was arbitrarily chosen between the stator exit plane and the inlet plane of a hypothetical rotor row. This distance is sufficient to observe secondary atomization effects. Figure 2.7B-3 shows the variation of the maximum Weber Number observed with drop diameter for the eleven test conditions chosen. These were obtained from trajectories along the streamline coinciding with the stator wake axis. Note that these maxima occur at different locations downstream of the trailing edge; in no case did the maximum Weber Number occur at the start of the trajectory.

The WANL turbine blade erosion model has tentatively employed fixed Weber Number criteria to predict the onset of secondary atomization. These are obtained from Gardner's work (6) which indicates that, in steam systems, the critical Weber Number is about 22 when drops are slowly accelerated and is about 13 when the acceleration is abrupt. Results obtained by Rocketdyne<sup>(1)</sup> in the tests examined are shown in Figure 2.7B-3. In each case the limiting drop size observed has been plotted. It is evident that a disruption criteria based on Weber Number alone, is inappropriate. The use of a fixed critical Weber Number may perhaps be justified for very rough estimates or for qualitative descriptions, but it lacks the precision required in detailed erosion studies.

TABLE 2.7B-1  
ROCKETDYNE TEST CONDITIONS USED IN  
THE STUDY

Blade Shape	Test Series No.	Test Conditions							Inlet Quality, Percent	Stream Flow, lb/sec	Pressure at 2nd Stage Inlet, psia	2nd Stage Spouting Velocity, ft/sec
		Inlet Pressure, psia				Outlet Pressure, psia						
		10	15	20	23	3	7	10				
1	114A	X				X			99.5	.119	4.5	1170
	B	X				X			99.5		7.8	540
	C	X					X		99.6	.175	10.8	525
	D	X				X			99.6		8.5	780
	F	X				X			99.4		6.0	1450
	113G		X			X			98.6	.233	7.4	1680
	H		X			X			99.3		9.4	960
	I		X				X		99.4		11.5	660
	J			X		X			99.3	.270	11.8	800
	K			X	X				99.4		9.8	1150
	L			X	X				99.4		8.2	1875

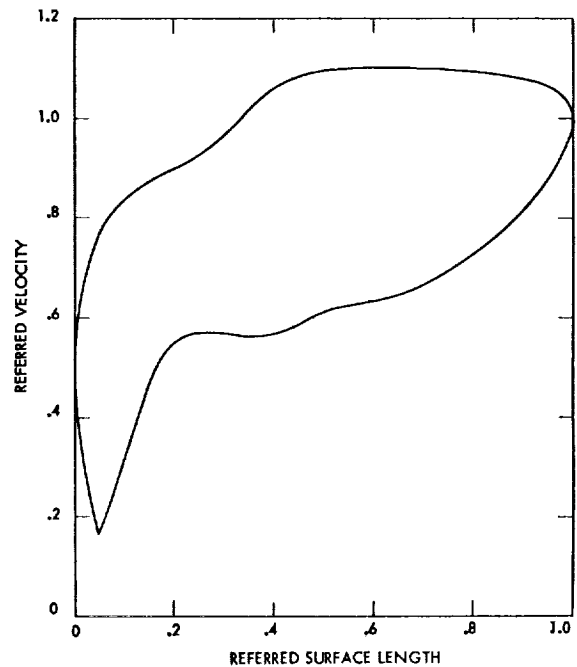
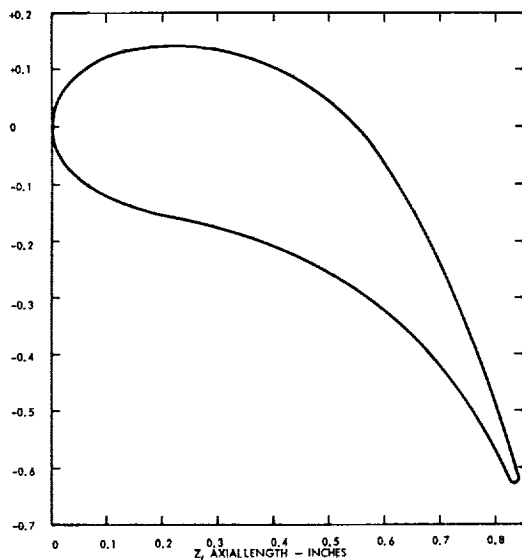


Figure 2.7B-2 Surface Velocities Computed for the Top Section of Rocketdyne Blade Shape 1-A



**Figure 2.78-1 Profile of Stator Blade 1-A**

TABLE 2.7B-2  
TRAILING EDGE BOUNDARY LAYER DATA  
OBTAINED FOR THE ROCKETDYNE TEST  
SERIES

Test	$U_a$ (ft/sec)	$n_{\text{exit}}$ (psia)	$T$ (°K)	$X$ (%)	$\theta_a$ (cm)	$\theta_o$ (cm)	$\delta_a^*$ (cm)	$\delta_o^*$ (cm)	$i_a$ (cm)	$i_o$ (cm)	$\Delta L$ (Microns)
	$(ft/sec)$	$(psia)$		(%)	(cm)						$W_{a13}$ $W_{a27}$
11A4	1170	3	601.30	98.6	.0067	.00359	.01838	.00474	.06868	.03468	92
11A8	540	7	636.85	96.3	.01073	.00362	.01874	.00477	.06896	.03463	187
11A4	525	10	653.21	98.8	.01021	.00344	.01746	.00452	.06664	.03383	155
11A0	780	7	653.85	97.7	.01000	.00337	.01697	.00442	.06568	.03283	102
11A7	1450	3	601.50	94.8	.01014	.00342	.01729	.00448	.06632	.03138	67
11G6	1680	3	601.50	93.3	.00918	.00331	.01654	.00433	.06480	.03227	48
11H4	960	7	636.85	96.7	.00957	.00323	.01601	.00421	.06363	.03177	71
11H3	600	10	653.21	97.9	.00973	.00328	.01636	.00429	.06441	.03217	105
11J1	840	10	653.21	97.6	.00936	.00315	.01536	.00411	.06259	.03174	176
11K3	1150	7	636.85	95.1	.00920	.00310	.01521	.00406	.06181	.03084	52
11L5	735	3	601.85	92.2	.00960	.00323	.01607	.00422	.06378	.03184	29.5



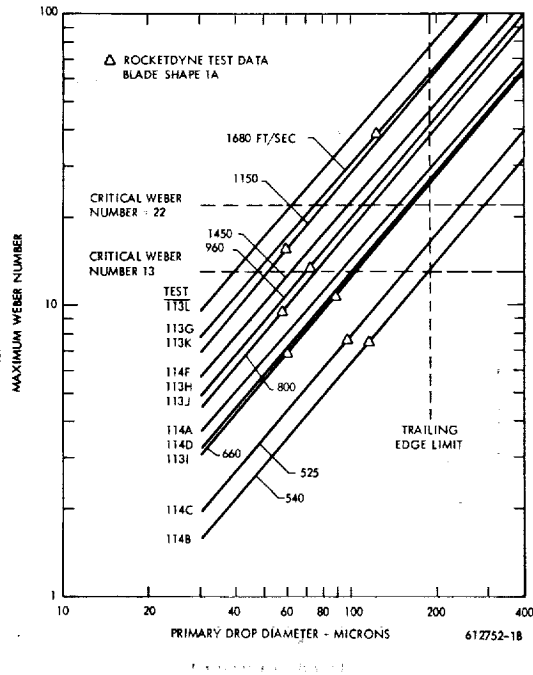


Figure 2.7B-3 Predicted Variation of Maximum Primary Drop Weber Numbers for the Rocketdyne Test Series with Blade Shape 1-A

Trajectory results are presented in more detail in Figures 2.7B-4 (Test 114A), 2.7B-5 (Test 114 B), 2.7B-6 (Test 114 F) and 2.7B-7 (Test 113L). These show the variation of drop velocity and Weber Number with total distance downstream of the stator trailing edge and along the wake axis streamline. In all cases a "dead-band" of four trailing edge thicknesses has been used to cover uncertainties in the local wake velocity in this region.

A brief examination was also made of trajectories associated with the hub section of blade 1-A. The small difference in pitch between the two sections made very little difference in the Weber Number and velocity result.

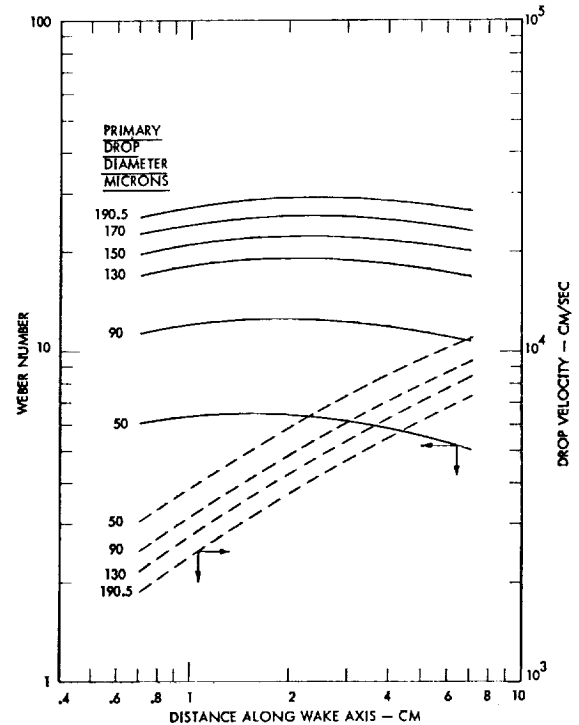


Figure 2.7B-4 Variation of Drop Weber Number and Velocity with Distance along the Wake Axis Predicted for Rocketdyne Test 114A

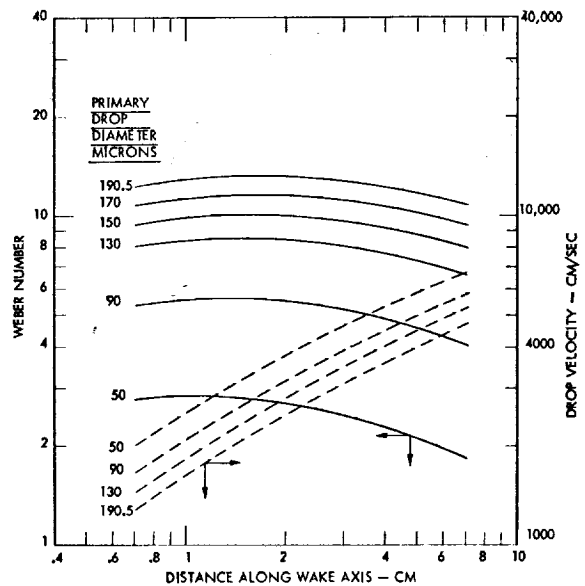


Figure 2.7B-5 Variation of Drop Weber Number and Velocity with Distance along the Wake Axis Predicted for Rocketdyne Test 114B

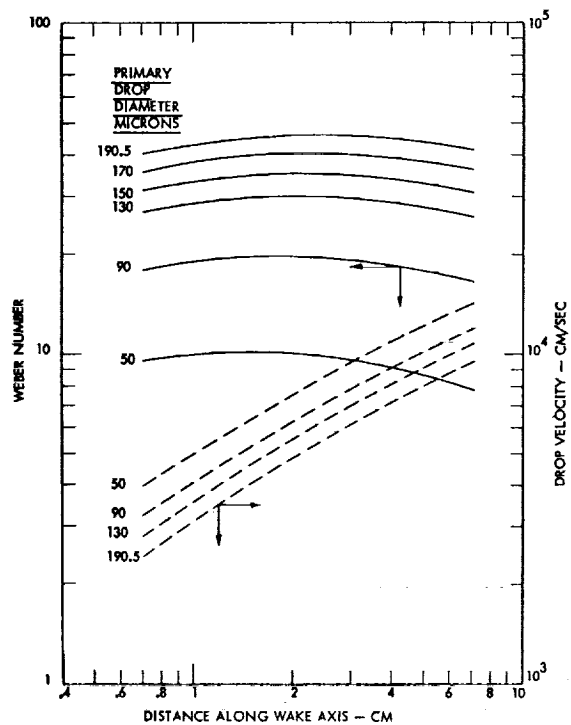


Figure 2.7B-6 Variation of Drop Weber Number and Velocity with Distance along the Wake Axis Predicted for Rocketdyne Test 114F

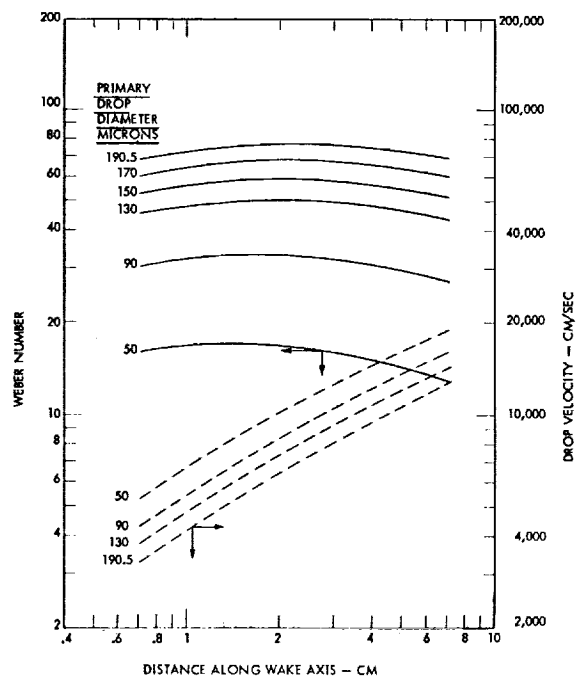


Figure 2.7B-7 Variation of Drop Weber Number and Velocity with Distance along the Wake Axis Predicted for Rocketdyne Test 113L

## APPENDIX 2.7C

### REFERENCES

1. Spies, R., J. R. Baughman, and J.E.T. Blake, "Investigation of Variables in Turbine Erosion, Influence of Aerodynamic and Geometric Parameters," Rocketdyne Division of North American Rockwell Corporation Report R-7650, December 1968, NASA Contract NAS7-391.
2. Christie, D. G., and G. W. Hayward, "Observation of Events Leading to the Formation of Water Drops which Cause Turbine Blade Erosion," Phil. Trans. Roy. Soc. London, Series A, No. 1110, Vol. 260, pg 183-192, 28 July 1966.
3. Pearson, Karl, ed., "Tables of the Incomplete  $\gamma$ -Function," Cambridge University Press, 1957.
4. Degner, V. R., Quarterly Status Letter No. 3, Contract NAS 7-391, "Investigation of Variables in Turbine Erosion," North American Aviation Inc., Rocketdyne Division Report 66RC5335.
5. Hays, L. G., "Turbine Erosion Research in Great Britain," NASA, Jet Propulsion Laboratory, Cal. Inst. Tech., Tech. Memo No. 33-271.
6. Gardner, G. C., "Events Leading to Erosion in Steam Turbines," Proc. Inst. Mech. Engrs. Vol. 178, Part 1: No. 23, pg. 593 to 623, 1963-1964.
7. Smith, A., R. P. Kent, and R.L. Armstrong, "Erosion of Steam Turbine Blade Shield Materials," ASTM Special Technical Publication No. 408, March 1967.
8. Wolfe, H. E. and W. H. Anderson, "Kinetics, Mechanism and Resultant Droplet Sizes of the Aerodynamic Breakup of Liquids," Aerojet-General Corp. Report 0395-04-185P, April, 1964.
9. Putnam, A. A. et al, "Injection and Combustion of Liquid Fuels," Battelle Memorial Institute, WADC Technical Report 56-344, May 1957.
10. Green, H. L., "Atomization of Liquids," In Hermans - Chapter VII, Interscience Publishers, Inc., New York, 1953.
11. Strutt, J. W. (Baron Rayleigh), "The Theory of Sound," p. 361, Dover Publ., New York, N. Y., 1945.
12. Mayer, E., "Theory of Liquid Atomization in High Velocity Gas Streams," ARS Jour. p. 1783 to 1785, December 1961.
13. Katsanis, T., "A Computer Program for Calculating Velocities and Streamlines for Two-Dimensional, Incompressible Flow in Axial Blade Rows," NASA TND-3762, January 1967.



# Section-3

## FOREWORD TO SECTION 3

Thanks are due to Messrs. E. A. Eaton and D. Pearson of the British Central Electricity Generating Board (CEGB) for not only personal discussions but also the reference use of a number of CEGB Marchwood Engineering Laboratories reports which have been of paramount value to this study. Acknowledgements are also due to R. I. Shrager and L. B. Godio, who collaborated on the mathematical formulations and computer programs involved in section 3.2 of this report.

## ABSTRACT

This report volume is concerned with those processes of the WANL turbine blade erosion model shown on this page that can directly cause the loss of metal from turbine blades: mechanical removal by drop impingement and dissolution into impinged liquid.

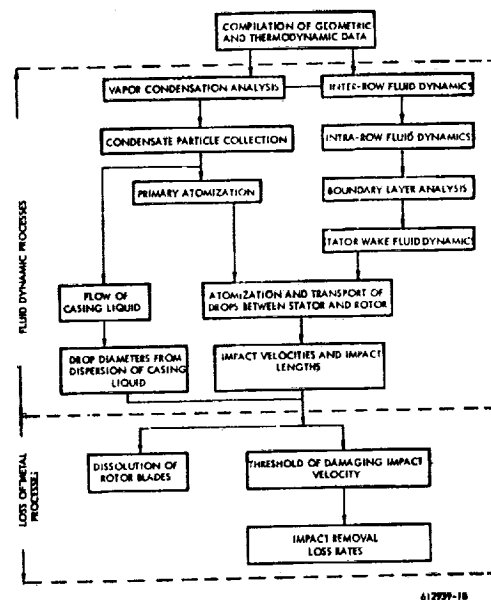
The literature on impingement erosion is examined with a view to deducing empiric, or analytic, relationships between erosion rate and the various external variables such as impact velocity, angle of impingement, size of impacting drops, impacting fluid properties, strength of materials, and rate-time variation.

In Section 3.1 the difficulties inherent in the interpretation of erosion test data are discussed and a rationalized approach is described.

One of the major difficulties in the correlation of test data is the variation of erosion rate during a test. In Section 3.2 an analytic model is proposed to explain the variation.

Sections 3.1 and 3.2 are mainly concerned with the mechanical aspects of erosion of metals by the impingement of liquid drops as influenced by external conditions such as impact velocity, etc. Sections 3.1 and 3.2 are not directly concerned with the erosion resistance of specific materials - except in passing - with the relationship between erosion resistance and other material properties.

Sections 3.3 and 3.4, on the other hand, attempt to use the observations of Sections 3.1 and 3.2, plus added information relevant to metal dissolution by liquid metals, to establish specific numerical relationships of erosion resistance of metals in terms of external variables and properties of materials. Section 3.3 deals with the mechanical aspects of metal loss through drop impingement, assuming no chemical interaction. Section 3.4 deals with the chemical aspect of metal loss by dissolution of the metal into the liquid of impinged drops, assuming that there is no mechanical interaction.



WANL Turbine Blade Erosion Model

## SECTION 3

### TURBINE BLADE EROSION MODEL

#### 3.1 SURVEY OF CLUES TO THE RELATIONSHIPS BETWEEN EROSION RATE AND IMPINGEMENT CONDITIONS\*

##### 3.1.1 General Considerations Relating to the Interpretation and Correlation of Test Data

###### 3.1.1.1 Independent Variables

The purpose of this section is to determine whether the impingement erosion test data in the literature can be made to yield generalized relationships, by which erosion can be predicted under arbitrary operating conditions. If the erosion could be expressed in terms of an empirical or semi-empirical equation, it would be a function of the operating variables and would contain constants which are properties of the materials of the target and of the impinging liquid.

The independent variables, or operating conditions, are as follows:

- a) Area of target subjected to impingement
- b) Shape of target
- c) Size of impinging liquid drops or slugs
- d) Shape of impinging liquid drops or slugs
- e) Rate of impingement of liquid on target
- f) Impact velocity between liquid and target
- g) Angle of impact between liquid and target surface
- h) Physical properties of liquid such as:
  - 1) density,
  - 2) viscosity,
  - 3) compressibility, or acoustic velocity.

i) Physical properties of target. While the significant properties are still unknown, the following may be listed as possibilities:

- 1) hardness or other strength property
- 2) strain energy to rupture or other energy property
- 3) elongation or other ductility property
- 4) endurance limit and fatigue S-N relationship
- 5) elasticity or acoustic velocity.
- j) Surface conditions of target, such as:
  - 1) roughness
  - 2) work hardening or other surface effects due to previous preparation or erosion
  - 3) presence of surface films of liquid.
- k) Microstructure and orientation of surface layers.

In this section of the report, primary emphasis is given to the velocity and the angle of impact, and the size and shape of impacting drops. Section 3.2 includes some discussions of the fatigue properties and surface conditions of the target.

###### 3.1.1.2 Dependent Variables

One of the greatest difficulties in the interpretation and correlation of erosion test data lies not in the multiplicity of the independent variables but in the identification of the dependent variable or variables, referred to as "the erosion". An approach must be found to characterize the erosion. Figure 3.1 (A) represents a typical weight loss versus time curve. (The axes are deliberately labeled erosion and duration since these quantities will be discussed more fully later.) This curve is characteristic of much of the data found in the literature; the various stages of the curve and possible explanations for them are discussed in Section 3.2 of this report.

---

\* F. J. Heymann, Senior Engineer, Development Engineering Department, Westinghouse Steam Divisions, Westinghouse Electric Corp., Lester, Pa.

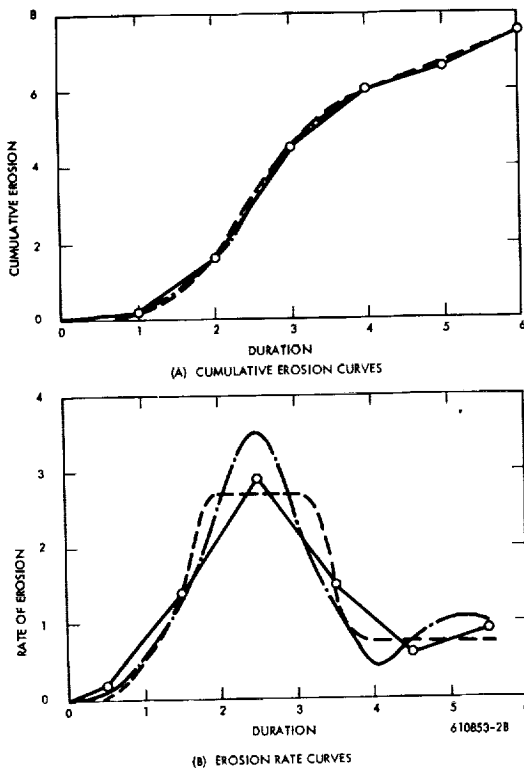


Figure 3.1-1 Various Interpretations of Same Hypothetical Erosion Data Points

A relatively well defined experimental plot is subject to a variety of interpretations. The circles in Figure 3.1 (A) represent hypothetical row data points. A conservative method of drawing the curve is to joint the experimental points by straight lines, as shown. Reference 1,\* for instance, shows curves in this form. An erosion rate curve can then be constructed by plotting the slopes of these line segments versus the time corresponding to their mid-points. This is shown by the circles and solid lines in Figure 3.1-1 (B). Reference 2 presents its data in this form. This approach requires no decisions, but is not accurate unless the data points are close together.

\* References cited are listed in a later section.

To draw in a smoothed curve, a decision must be made as to how smooth this curve should be. If the erosion rate rises from zero during an incubation period to a constant maximum value, and subsequently declines to a secondary constant value, a curve will be drawn such as the dashed one in Figure 3.1-1 (A), whose counterpart in Figure 3.1-1 (B) is also shown dashed. If the erosion rate reaches a rather steep peak value and then goes into a series of fluctuations, then the dash-dotted lines in Figures 3.1-1 (A) and (B) may result. This does not exhaust the possible variations, but serves to show how this decision can have a considerable effect on the shape of the erosion curve presented, particularly if data are presented in the form of erosion rate curves. (Graphical differentiation of empirical data with all its uncertainties is notoriously unreliable.)

The decision concerning what the erosion curves should be is closely related to the question of just how these curves should be quantitatively characterized, i.e., just what are the dependent variables that should correlate with the operating conditions. The objective of this empirical approach is to predict the amount of erosion expected after a given time, or at least the time required to reach some critical degree of erosion.

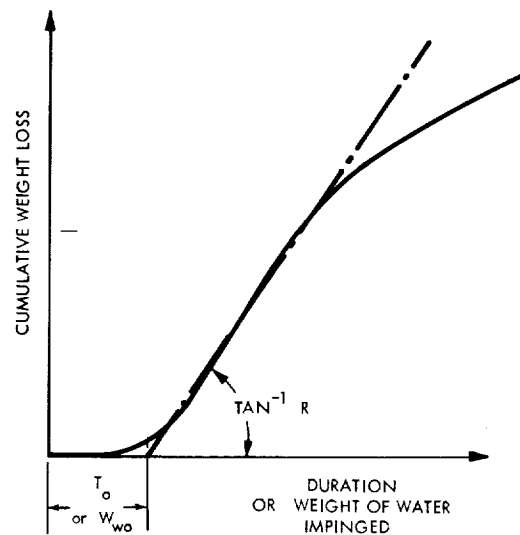
The parallel study reported in Section 3.2 concerns the possibility of predicting the form of the erosion versus time curve analytically, on the basis of assumed material removal mechanisms. This has not yet advanced to the stage where it can be of help in the present study. Therefore, the view adopted is the most widely held and is practical enough for present purposes. Namely, the first stage in erosion shows little or no weight loss and represents plastic deformation of the surface and initiation of fatigue cracks. This stage merges into the second stage wherein the rate of weight loss is at a maximum and approximately uniform over a period of time. This, in turn, merges into a later stage or stages wherein the erosion rate diminishes and may or may not tend toward another uniform value. Whatever the precise cause or causes of this decrease in erosion rate may be, it is usually associated with rather general and severe damage to the surface, which through geometrical effects alone



may result in an effective alteration of the impingement conditions. Thus, the best parameters to describe the progress of erosion in a relatively simple and yet significant manner are:

- a) A quantity representative of the duration of the initial (incubation) stage, denoted by  $T_0$  in Figure 3.1-2.
- b) A quantity representative of the rate of erosion during the second stage, denoted by  $R$  in Figure 3.1-2. This is the most significant quantity, and most of the following sections deal with it.
- c) Of additional interest would be some quantity representative of the degree of damage at the end of the second stage. This would help to establish whether this transition is really a geometric effect, and whether the first two stages do really cover the permissible degree of erosion in a practical application. However, very little information on this is available.

There are test data to which the foregoing generalizations and conclusions do not seem to apply, but for most of the usable data they do seem valid, and our correlation attempts are based on this type of curve. Eventually, however, the deviations from this type of curve must also be understood and accounted for. It is important to remember that more than one mechanism of material removal may be active. The above-described behavior applies to those conditions under which a fatigue mechanism predominates. This is valid for most of the material and impact velocity combinations for which test data are available and probably to most turbine operating conditions. If, however, impact velocities are increased, then material removal due to individual impacts will also occur. At sufficiently high speeds the rate of material removal by this process may be sufficiently high so that there is not enough time for fatigue failures to occur. The shape of the erosion-time curve, the significant dependent quantities, and their functional relationships to such independent variables as drop size and impact velocity can all be expected to change during this transition from one predominant mechanism to another. Test data at relatively high velocities (around 2000 ft/sec) are being generated but are not yet available. Steam turbine blades will soon be operating in this velocity range also.



611131-308

Figure 3.1-2 Definition of Incubation Period,  $T_0$ , and "Steady-State" Erosion Rate,  $R$

### 3.1.1.3 Correlation Problems

Returning now to an assumed characteristic curve, another difficulty will be demonstrated. Figure 3.1-3 shows three hypothetical but typical erosion-time curves from a given test series. Curves A, B, and C might have been obtained for three different materials under the same operating conditions, or for the same material at three different impact velocities or with three different drop or jet sizes. One may then try to compare these curves, or to determine from each, a number that represents the erosion to be correlated with material properties or with operating parameters. With insufficient thought given to the problem, the temptation might be to select a convenient point in time (say  $T = 3$  on Figure 3.1-3) and compare either the cumulative erosion, or with more sophistication, the slope of the erosion-time curve at that point. This has been done by many authors. It should be evident from the earlier discussions, however, that

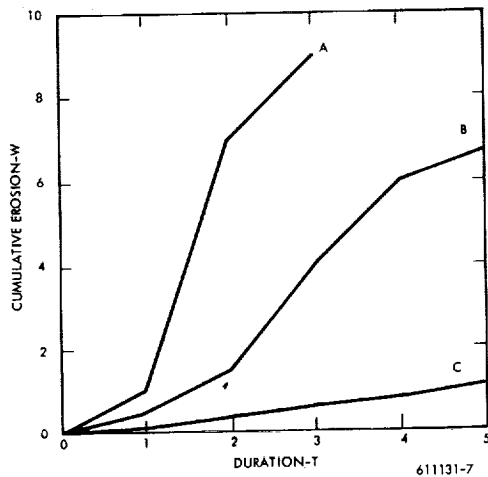


Figure 3.1-3 Hypothetical Erosion Curves

this procedure is entirely invalid. It can result in spurious comparisons between erosion rates corresponding to completely different stages of the erosion process. Thus, in Figure 3.1-3 at time  $T = 3$ , Curve B is in the probably significant second stage; Curve A has already broken and is into the third stage; Curve C may well still be in the incubation period.

For a valid comparison there are two desiderata. At least one, preferably both should be fulfilled. They are:

- The measured slopes, or erosion rates, should be, as nearly as possible, average or effective values representative of the second stages of the erosion-time curves.
- The measured slopes should be, as nearly as possible, the averages or effective values over the same range of cumulative erosion, i. e., associated with the same degree of damage done to the surface.

The first desideratum can be fulfilled only if the end of the second stage is clearly seen; if the test duration is not long enough for this to occur, then the second rule must suffice, and one must endeavor to choose the erosion interval over which the slope is measured in such a way that the first stage, or incubation period is excluded. In Figure 3.1-3, this is simply not possible for Curve C; when one examines the available test data, the choice is often reduced to one between doubtful comparisons or no comparisons at all.

#### 3.1.1.4 Rationalized Parameters

It was pointed out earlier that the axes in Figure 3.1-1 have been labeled vaguely as erosion and duration. Direct comparison between different test data is often complicated by the fact that the erosion may be given in terms of weight loss, or volume loss, and the duration in terms of time, or number of impacts (for wheel-and-jet apparatus), or in other ways. The target areas involved and the quantity of water impinging on it will differ not merely between different test series, but may also vary within a given test series as a consequence of varying one of the other independent parameters.

Thus, for instance, if in a wheel-and-jet apparatus the jet diameter is changed, this will effectively alter the area of the target subjected to impact and the quantity of water involved in each impact, and if the impact velocity is changed by changing the speed of rotation this also alters the weight of water impacting per unit time.

To permit valid comparisons and correlations, it is essential to express the erosion and the duration in a rationalized form which will compensate for these test variations.

Since the undesirable aspect of erosion is the loss of volume and the change of geometry - and this change of geometry in turn affects the rate of erosion - volume loss rather than weight loss should be considered. The rationalized erosion parameter is volume loss per unit area, sometimes referred to in the literature as mean depth of penetration (MDP).

The appropriate rationalized duration parameter is not quite so obvious. One could make a case for selecting the number of impacts per unit area. At present, however, preference is given to the volume of liquid impinged per unit area. This is attractive because results expressed in this way will show directly the effect of subdividing a given quantity of impinging liquid into particles of different sizes or shapes, and because it makes the rationalized erosion rate ( $E$ ) a non-dimensional quantity, as follows:

$$E = \frac{\text{Volume of material lost per unit area per time}}{\text{Volume of liquid impinged per unit area per unit time}}$$

The rationalized incubation time parameter corresponding to the above is the cumulative volume of liquid impinged per unit area at time  $T_o$  as defined by Figure 3.1-2.

For some correlations, where neither the target material nor the impinging liquid is changed, the rationalized erosion rate can be satisfactorily represented in terms of weight of material lost and weight of water impinged.

### 3.1.2 Dependence on Impingement Angle

Only recently have investigators shown serious concern with the impingement angle. The consensus appears to be that the normal component of the impingement velocity is primarily responsible for the damage, with the tangential component playing a secondary role.

Thus, according to Fyall and King<sup>(3,4)</sup> for initially smooth surfaces the normal impact velocity can be used successfully for correlations valid during the initiation and earlier stages of erosion, but that when the surface has been roughened by erosion, the tangential component also becomes significant because the true local impact angles can become more normal to the absolute velocity. No quantitative estimate is made for the latter effect.

Langbein and Hoff<sup>(5,6)</sup> state that the normal component governs the erosion; they show loci of equal average erosion rates plotted on a field of

absolute velocity versus inclination angle and state that these correspond to loci of constant normal velocity component ( $V_n = V \cos \theta$ ).

Pearson<sup>(7,8)</sup> has proposed the following correlation equation to represent the erosion rate  $E$  in terms of the impingement velocity  $V$ , and inclination angle  $\theta$  measured from the normal direction (expressed in our terminology):

$$E = K (V \cos \theta - V_c)^n / \cos \theta \quad (1)$$

in which  $K$ ,  $V_c$ , and  $n$  are to be regarded as constants of the target material. (Actually, at least some of these constants must also be functions of the impinging liquid properties, drop sizes, etc.)

Pearson justifies introducing the  $1/\cos \theta$  term by presenting the data reproduced here as Figures 3.1-4 and 3.1-5. (These are direct copies of Pearson's figures except that our terminology has been submitted and his curves, drawn through the points, have been omitted.) It appears that  $E \cos \theta$  (Figure 3.1-4) correlates somewhat better with  $V \cos \theta$  than does simply  $E$  with  $V \cos \theta$ . This improvement is hardly dramatic, however, and the  $1/\cos \theta$  correction should be regarded as tentative and subject to analytical or further experimental verification.

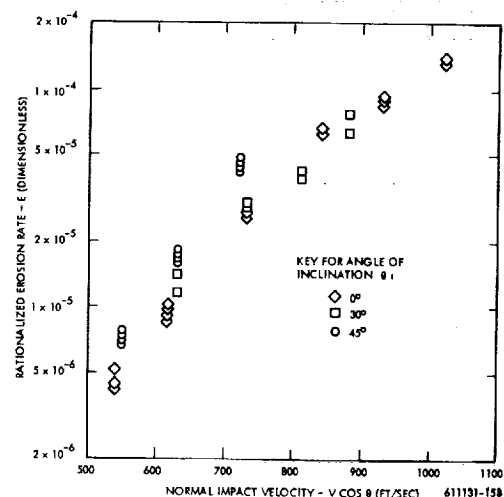


Figure 3.1-4 Rationalized Erosion Rate versus Normal Impact Velocity

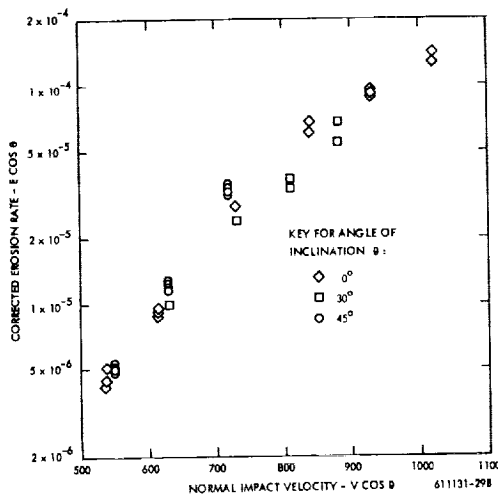


Figure 3.1-5 Corrected Erosion Rate ( $E \cos \theta$ ) versus Normal Impact Velocity (From Figure 5 of Reference 11)

For 12 percent chromium stainless steel, Pearson obtains values of approximately 400 ft/sec for  $V_c$ , and  $n = 2.6$  for use in Equation 1. Ratios of erosion rate at angle  $\theta$  to that at normal incidence ( $E_\theta/E_0$ ), based on this relationship, have been plotted in Figure 3.1-6 for three different velocities. Some independent support for this formulation may be provided by data points also shown in Figure 3.1-6, which were deduced from erosion-time curves given by Busch and Hoff<sup>(9)</sup>; these were obtained in a supersonic rain erosion facility, with target cones of different angles, but of the same base diameter. The material was pure aluminum; the absolute impact velocity was Mach 1.2, or approximately 1320 ft/sec.

In this situation the area exposed to erosion changes with the angle, but the total amount of impinging water remains the same. Thus, no area correction is necessary if the slopes of the erosion-

time curves are compared; on the other hand, it is necessary for a rational comparison of incubation times.

Note that the erosion rate at  $\theta = 10$  degrees is actually somewhat higher than that at  $\theta = 0$  degrees; if this is actually so, it would support an observation by Brunton<sup>(10)</sup> that the damage in single-impact tests could be greater at slight angles of inclination than with normal impact. (Note that at 1300 ft/sec on aluminum, single-impact damage occurs.) On the other hand, this may be an apparent effect only, and due to scatter or some other experimental variable. The curves in Reference 9 do not show actual data points.

The critical velocity  $V_c$  for aluminum would certainly be far lower than that for 13 percent chrome steel - perhaps on the order of 100 ft/sec. If one computes  $E_\theta/E_0$  from Pearson's equation with  $V = 1300$  ft/sec and  $V_c = 100$  ft/sec,  $n$  remaining 2.6, one obtains Curve E, which fits the data points reasonably well. Is this a confirmation of Pearson's equation, or is it merely fortuitous? The former can be true only if the assumptions of  $V_c = 100$  ft/sec and  $n = 2.6$  are indeed correct. (Differences in the values of  $K$  cancel out.)

In a previous progress report,<sup>(11)</sup> it was suggested that the data of Reference 9 could also be represented by the simple relationship  $E_\theta/E_0 = \cos^2 \theta$ , which is shown as Curve A in Figure 3.1-6. This simple angle-dependence does not fit any of Pearson's results presented in Figures 3.1-4 and 3.1-5, and should be rejected.

The physical meaning of Pearson's equation is: erosion is, in the first instance, a function of the normal component of the impact velocity, and additional erosion due to a tangential component is accounted for by the  $1/\cos \theta$  multiplier. Such a relation could not have been deduced from the data of Reference 9 alone, since the absolute velocity was held constant and the normal velocity component varied. Thus, there was no way of knowing whether the change in erosion with the angle was to be

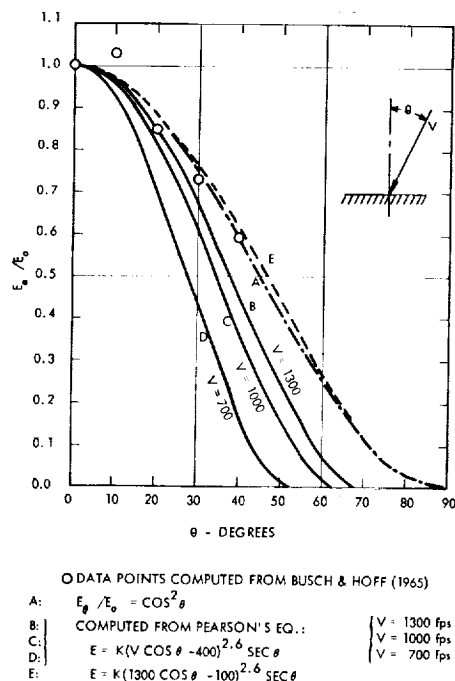


Figure 3.1-6 Comparison of Erosion versus Angle Curves

attributed to a function of the angle alone or to a combination of the changes in the angle and the normal velocity. A reliable formulation for the angle effect can be obtained only if a reliable formulation for the velocity effect is simultaneously determined, i.e., from test programs in which velocities and angles are varied independently. This is what Pearson has tried. Pending further testing of the generality of his equation, it is the best information available.

One set of data somewhat at variance with the foregoing was reported by Bradenberger and DeHaller<sup>(1)</sup>. They tested one material in a relatively low-speed, wheel-and-jet apparatus at various combinations of specimen velocity ( $u$ ) and jet velocity ( $v$ ). The jet velocity in a wheel-and-jet apparatus is in a direction perpendicular to the

specimen velocity and the absolute impact velocity is given by  $w = \sqrt{u^2 + v^2}$ . If the specimen were round as in a number of similar investigations, then  $w$  would also be the effective normal impact velocity. In this case, however, the specimens were rectangular and thus the velocity  $w$  is inclined at an angle,  $\theta = \tan^{-1}(v/u)$ , from the normal to the specimen surface. For a given value of  $u$ , a wide variance of results was obtained for different values of  $v$ . The authors claimed that these differences were far too great to be accounted for by the resulting differences in the absolute velocity  $w$ .

They speculated that cavitation may have been induced by the flow geometry but rejected this as a likely explanation because the location of the maximum damage was not consistent with this. They finally concluded that the tangential velocity,  $v$ , had some pronounced independent effect, not presently explainable, on the erosion measured. This conclusion has been introduced at some length because it has been quoted by subsequent authors, and because examination of the actual data simply does not bear it out, as will be shown below.

Table 3.1-1 lists best estimates of the mean erosion rates, for the weight loss interval of 0.05 to 0.5 gm, from Figures 4 and 6 of Reference 1. The normal, tangential, and absolute velocities are also listed, as well as the angles and the corrected erosion rates based on Pearson's hypothesis for angle effect discussed above. Figure 3.1-7 (a) shows the data points plotted versus the normal impact velocity  $u$ , with the  $1/\cos \theta$  angle correction. Figure 3.1-7 (b) shows the same data (without angle correction) plotted versus the absolute velocity  $w$ .

TABLE 3.1-1

EROSION RATE  $E$  FOR DIFFERENT SPECIMEN VELOCITIES  $u$  AND JET VELOCITIES  $v$

(From Reference 1)

$v$ m/sec	$u$ m/sec	$w$ m/sec	$\theta$ deg	$E$ gm/10 <sup>6</sup> impacts	$E'$ $E \cos \theta$ - gm/10 <sup>6</sup> impacts
52	20	55.7	21	1.05	0.98
52	15	54.2	16	0.86	0.83
52	10	53.0	11	0.67	0.66
52	5	52.3	6	0.64	0.64
42	20	46.5	25	0.32	0.29
42	15	44.5	20	0.26	0.245
31	20	36.9	33	0.122	0.102
31	15	34.4	26	0.075	0.067

NOTE: The jet diameter was 6 mm and the target material low carbon steel.

The following observations can be made:

- a) When plotted against  $u$ , there is a different curve for each value of  $v$ . A correction based on Pearson's assumption ( $E_{v,\theta} = E_{v,0}/\cos \theta$ ) did not suffice to bring them into one line.
- b) When the data are plotted against the absolute velocity  $w$ , they fall quite well into one curve.

These observations not only contradict the conclusion reached by the authors of Reference 1, but also seem to provide evidence contradicting the angle effect theory proposed by Pearson (Equation 1). A possible conclusion drawn from all of the observations is that in this case there is no angle effect, or none of the commonly expected nature, as a result of the jet velocity. This is conceivable when it is considered that the direction of the tangential component of the impact velocity is also the direction in which the impacting mass of liquid is of infinite length.

### 3.1.3 Dependence on Drop Size and Shape

#### 3.1.3.1 Review of Available Data

Despite the fact that the maximum impact stress is generally a function of the material properties and impact velocity and should be independent of the size of the impacting drops, there is ample evidence that both the size and the shape of the impacting liquid masses do affect the erosion measured. Here again, the quantitative data in the literature from which generalized relationships could be deduced is meager.

A frequently cited test is that of Honegger<sup>(2)</sup> in which he compared the erosion produced in a wheel-and-jet type apparatus by impact with one 1.5 mm water jet, with that produced by nine 0.5 mm jets, arranged as shown in Figure 3.1-8. The results are described as follows: "The splitting up of the jet is accompanied by a considerable reduction of the erosion, the numerical value of the reduction largely depends upon the speed, and for tests under consideration it varies from 1 to 5 for high speeds and 1 to 10 for low speeds." The test was

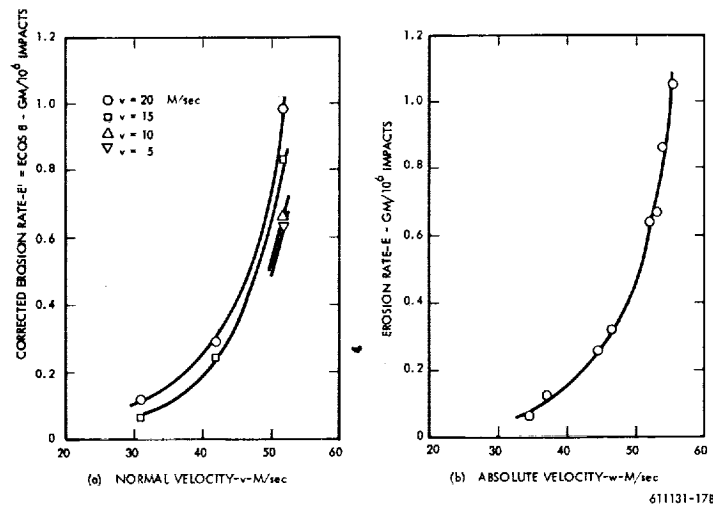
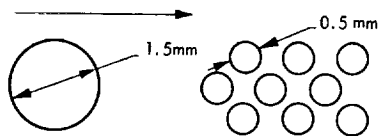


Figure 3.1-7 Erosion versus Velocities



THE ARROW SHOWS THE DIRECTION OF MOTION OF THE SPECIMEN.  
LEFT: A SINGLE NOZZLE, RIGHT: NINE NOZZLES

610853-8B

Figure 3.1-8 Arrangement of Nozzles for Water-Jet Tests

contrived to fulfill the requirements of a rationalized erosion measurement. Both the target area subjected to erosion and the volume of impinging water were the same for both configurations. Yet, upon reflection, one must conclude that this was not a valid test of the drop size effect, at least not if Figure 3.1-8 accurately portrays the nine-jet arrangement. This is because only the first three jets would impact on a dry surface; a liquid layer from these would almost certainly still be present to cushion the effect of the next three impacts, and similarly so for the last three. Thus, no quantitative conclusions should be drawn from these results, but the qualitative findings are of interest.

Some systematic tests with differing jet diameters were reported by Brandenberger and DeHaller. (1) The weight-loss versus number of impact time curves are reported in Figure 3.1-9a. The jet diameters varied from 4 mm to 12 mm, and attention should be given to the apparent anomaly presented by the 6 mm and 8 mm curves; this gives rise to the suspicion that these curves may have been accidentally mislabeled. This possibility will be discussed below.

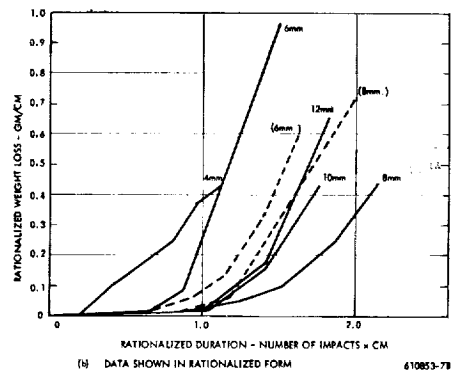
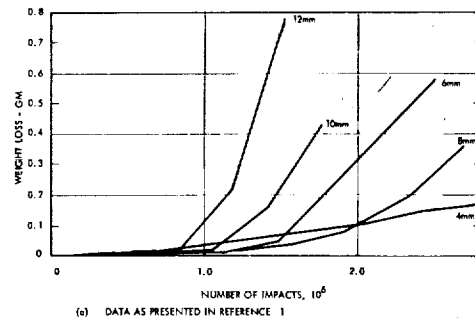
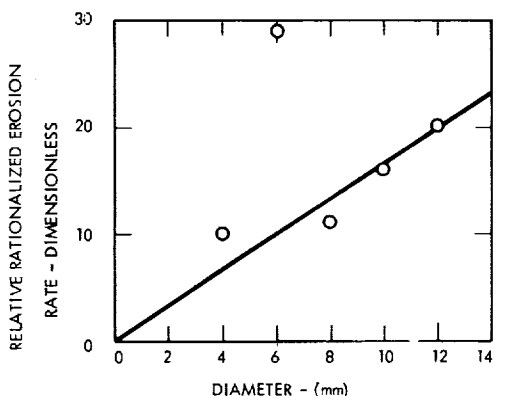


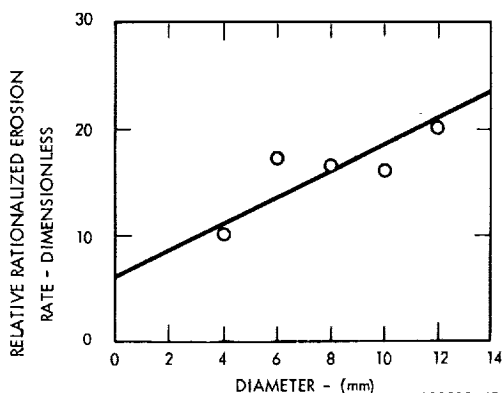
Figure 3.1-9 Erosion versus Jet Size (Adapted from Reference 1)

The first step in evaluating these data must be to express them in rationalized form (as discussed in Paragraph 3.1.1 of this report). Figure 3.1-9b is a replot of the data in terms of rationalized coordinates. The solid lines represent the original curves as labeled, and again there seems to be an apparent anomaly between the 6 mm and 8 mm curves. If the original curves were mislabeled, then the true rationalized 6 mm and 8 mm curves would appear as shown by the dotted lines in Figure 3.1-9b. In that case, the 6 mm through 12 mm curves would all come very nearly on top of one another, with the 4 mm curve the only discrepancy.

Relative values of the slopes of these erosion-time curves have been measured for the damage interval of 0.15 to 0.4 in Figure 3.1-9b, and these have been plotted in Figure 3.1-10. Figure 3.1-10a represents the data with the original curves of Figure 9 as labeled, and Figure 3.1-10b with the 6 mm and 8 mm curves of Figure 9 reversed. In neither case can any curve be established through these points with any degree of confidence. In Figure 3.1-10a, as shown, a proportionality between erosion rate and diameter could be supported, provided the 6 mm data point is rejected. In Figure 3.1-10b a straight-line relationship, not passing through the origin, has been shown, but the most that can be said, on the basis of the data points alone, is that they would support some relatively weak function of jet diameter.



(a) DATA WITH 6mm & 8mm CURVES AS LABELED



(b) DATA WITH 6mm & 8mm CURVES REVERSED

Figure 3.1-10 Erosion Rate versus Jet Diameter

Recently Pearson<sup>(8)</sup> has conducted systematic tests with different drop sizes in his wheel-and-spray type of apparatus. Figure 3.1-11 is a reproduction of Figure 1 of Reference 12, with our terminology. As in all of Pearson's results, the erosion rate given is an angle-corrected rationalized value of the maximum slope measured on the weight-loss versus time curve. It represents mass loss per unit area divided by mass of water impacting per unit area. This impingement angle correction used by Pearson was described in Paragraph 3.1.2. While Figure 3.1-11 shows an anomaly in the crossing of the 920 microns and 1050 microns lines, it seems to confirm that the relative effect of drop size diminishes at high drop sizes and high velocities, i.e., as one gets away from what may be considered the threshold conditions.

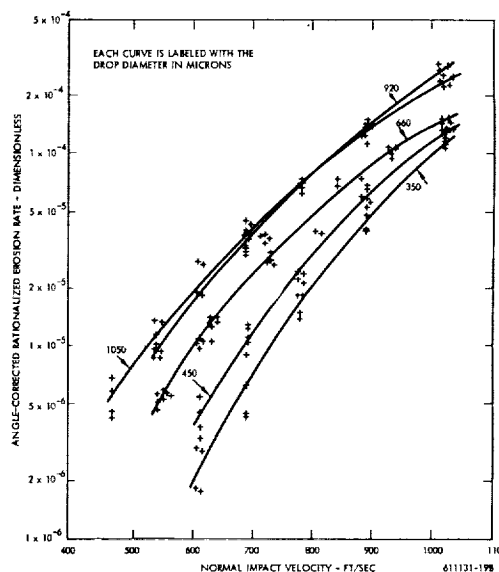


Figure 3.1-11 Effect of Drop Size on Erosion Rate

A cross-plot of the data on Figure 3.1-11 is shown in Figure 3.1-12; here as in Figure 3.1-10 it is difficult to justify a purely empirical curve other than a straight line to represent the erosion rate



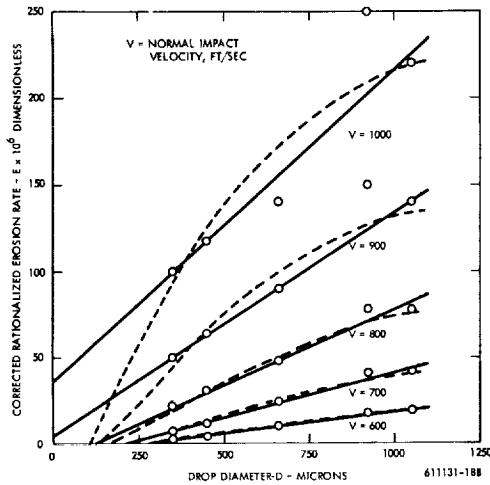


Figure 3.1-12 Effect of Drop Size on Erosion Rate  
Data Cross-Plotted from Figure 3.1-11  
(Dotted Lines are Based on  
Correlation of Figure 3.1-13.)

versus drop diameter relationship in the absence of any rational basis for some other type of curve. The extrapolation of the solid straight lines to their intercepts on the coordinate axes is, however, questionable. The dotted lines are based on a correlation to be developed below. (Reference 12 does not attempt to present any analytical or empirical equation for the drop size effect.)

It is assumed that the drop size effect can be represented by a factor of the form

$$\left(1 = G/V^2 D\right)$$

where G represents a critical or threshold combination of velocity and drop diameter, such that, for  $V^2 D \leq G$  no significant erosion occurs. Even if the hypothesis is not completely accepted, the attempt to use the above factor to correlate data on drop-size effect may be justifiable. The data of Reference 2 is for the same material as that of Reference 1, in which a critical velocity  $V_c$  of 390 ft/sec was found when testing with a drop size D of 660 microns. Thus,  $G = 390^2 \times 660 \approx 1.0 \times 10^8$ , and the above-mentioned factor, which shall be denoted as the critical factor, or  $K_c$ , takes on the value

$$K_c = \left(1 - 10^8 / V^2 D\right) \quad (2)$$

for this set of data.

Table 3.1-2 lists  $K_c$  for a number of combinations of V and D, and also the values of the erosion rate E taken from the curves (not the original data points) drawn in Figure 3.1-11. These values are the same ones plotted in Figure 3.1-12.

If  $K_c$  were a simple correction factor to be added to an equation such as Equation 1, then one would expect that  $E/K_c$  would become a function of velocity only. This is not the case, as can be seen in the fifth column of Table 3.1-2.

TABLE 3.1-2

DROP SIZE CORRELATION ATTEMPTS FOR  
DATA OF FIGURE 3.1-11

V (ft/sec)	D (μ)	$K_c =$ $1 - \frac{10^8}{V^2 D}$	$E \times 10^6$ (From Figure 11)	$\frac{E \times 10^6}{K_c}$	$K_c V$
600	350	0.205	2.0	9.75	123
	450	0.383	3.8	9.90	230
	660	0.578	10.0	17.3	347
	920	0.694	17.0	24.5	416
	1050	0.735	19.0	25.9	441
700	350	0.419	7.0	16.7	293
	450	0.547	10.7	19.6	383
	660	0.690	24.0	34.8	483
	920	0.778	38.0	48.9	545
	1050	0.801	41.0	51.1	561
800	350	0.554	20.5	37.0	443
	450	0.642	30	46.7	513
	660	0.763	47	61.6	610
	920	0.830	78	94.0	664
	1050	0.851	78	91.6	680
900	350	0.646	49	75.8	581
	450	0.725	64	88.3	652
	660	0.813	88	108.0	732
	920	0.886	146	171.0	780
	1050	0.882	138	157.0	793
1000	350	0.714	100	140.0	714
	450	0.778	116	149.0	778
	660	0.848	140	155.0	848
	920	0.891	250	280.0	891
	1050	0.905	220	243.0	905

Another and really more rational way of regarding  $K_c$ , since it is a criterion of the deviation both of drop size and velocity from a threshold or critical value, is to argue that the erosion rate  $E$  should be a function of  $K_c V$ , rather than of  $(V - V_c)$  as proposed by Equation 1. Here,  $V$  is understood to mean the normal component of impact velocity. The values of  $K_c V$  are listed in the last column of Table 3.1-2, and Figure 3.1-13 shows that when  $E$  is plotted versus  $K_c V$ , good correlation results.

Another valid approach would be to retain the form of Equation 1, and accept from the factor  $(1 - G/V^2 D)$  merely the consequence that for a given drop diameter  $D$  the critical velocity is given by  $V_{cd} = \sqrt{G/D}$ . That, in fact, was the reasoning which led to taking the value of  $G = 10^8$ . This suggests plotting  $E$  versus  $(V - V_{cd})$  with  $V_{cd}$  in this instance being given by  $V_{cd} = \sqrt{10^8/D}$ . The values of  $V_{cd}$  are listed in Table 3.1-3, and the points corresponding to those of Table 3.1-2 are plotted in Figure 3.1-14. Again the correlation seems good, though careful examination of the points suggests that the scatter is more systematic with drop size than that in Figure 3.1-13. No formal attempt at curve-fitting has been made for either Figure 3.1-13 or Figure 3.1-14; therefore, no statistical data can be given to substantiate or disprove the feeling that the former provides the better correlation. A hand-fitted curve from Figure 3.1-13, together with values of  $D$  from Table 3.1-3, have been used to generate the dotted lines shown in Figure 3.1-12.

The results discussed above should be regarded with caution until similar approaches can be tested against other sets of data. Some validating evidence is afforded by curves of the dependence of the critical velocity  $V_c$  (below which no erosion takes place) on the jet diameter  $D$  (in g. wheel-and-jet apparatus) presented by Vater. (13) He presented two curves, valid for materials of corrosion fatigue endurance limit of 2000 and 2200 kg/cm<sup>2</sup>, which have been approximately averaged and reproduced here as the solid line in Figure 3.1-15. According to the above hypothesis, this relationship should be represented by  $V_c^2 D = G = \text{constant}$ , if the jet diameter can be regarded as analogous to drop diameter. The dotted line in Figure 3.1-15 shows such a relationship and follows very closely the experimental curve.

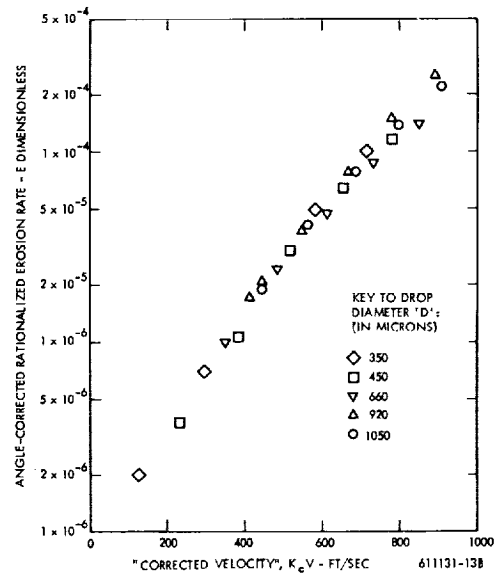


Figure 3.1-13 Correlation of Data of Figure 3.1-11 by Use of "Critical Factor"  
 $K_c \equiv (1 - 10^8/V^2 D)$

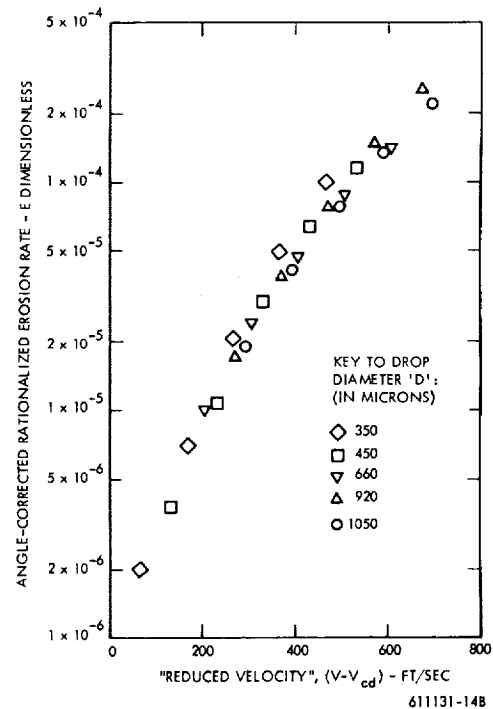
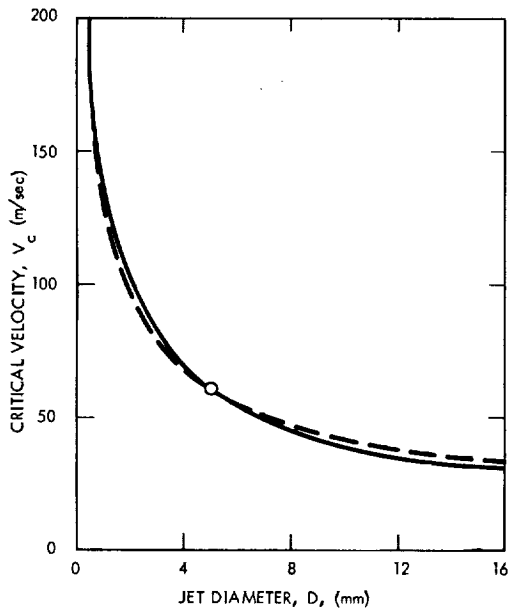


Figure 3.1-14 Correlation of Data of Figure 3.1-11 by Use of "Critical Velocity"  
 $V_{cd} \equiv \sqrt{10^8/D}$

TABLE 3. 1-3  
CRITICAL VALUES OF  $V_{cd}$  AND  $D_c$  BASED  
ON  $(V^2 D)_c = 10^8$

$D$ ( $\mu$ ):	350	450	660	920	1050
$V_{cd}$ (ft/sec):	535	471	396	330	308
$V$ (ft/sec):	600	700	800	900	1000
$D_c$ ( $\mu$ ):	276	204	156	123	100



SOLID LINE: CURVE FROM REF. (13)  
DOTTED LINE:  $V_c^2 D = \text{CONSTANT}$

Figure 3.1-15 Critical Velocity  
versus Jet Diameter

### 3. 1. 3. 2 Physical Reasons for Drop Size Effect

Consider the question as to why there should be a drop size effect at all. The maximum pressure developed under the impinging drop is generally held to be on the order of the water hammer pressure,  $\rho CV$ , where  $V$  is the impact velocity,  $\rho$  is the density of the liquid and  $C$  is the pressure wave velocity. This magnitude may be modified by factors which depend on the drop shape (e.g., Engel<sup>(14)</sup>); although Bowden and Field<sup>(15)</sup> hold that the maximum value of  $\rho CV$  holds for spherical drops as well as flat-ended drops, and on the relative acoustic impedance of the target and drop materials (e.g., Vater<sup>(13)</sup>). None of these is explicitly a function of drop size.

It is now known, however, what the true criterion of erosion damage is. While some general correlations have been made between the  $\rho CV$  value corresponding to the critical velocity and the endurance limit, it has also been shown<sup>(16)</sup> that surface deformation can occur at  $\rho CV$  values far below the yield point.

When erosion does take place, there is no certainty that the rate of erosion is strictly a function of impact pressure levels. Thiruvengadam<sup>(17)</sup> has proposed that in cavitation damage the energy available from the collapsing bubbles is a criterion of the volume rate of material removal, so that the impact energy of impinging drops might be of interest.

The question to be asked is: What properties of the impacts, or of their effect on the target surface, vary when one reduces the size of droplets into which a given amount of water, impinging on a given target area in unit time, is subdivided?

The total impact area (as distinguished from target area) actually increases, since the number of drops increases as  $D^{-3}$  and the impact area per drop decreases as  $D^2$  when the drop diameter  $D$  is reduced.

In other words, each target area element will be subjected to a greater number of stress pulses per unit time, if one can assume that the contact area of the impact bears a fixed relationship to the projected area of the drop. If this were a significant criterion, then the erosion would be expected to increase with decreasing drop size, which contradicts all experience.

However, another consequence of the increased impact area is that the total kinetic energy (which remains constant) of the impinging water is spread out over a greater area, and therefore the energy flux per unit area is reduced. A hypothesis based on this fact, led to the suggestion that the factor  $K_c$  (see Equation 2) represents the drop size effect.

Another factor which is of very likely significance is the duration of the pressure pulse on impact. Whatever precise reasoning is used to predict this duration (e.g., as in Reference 15), it is clear that for geometrically similar drops it must be proportional to drop diameter. Thus, the impulse per unit area is smaller in the impact of a smaller drop, and perhaps this is of consequence. Certainly the duration (microseconds) of the impact pressures are short enough so that strain rate effects, in those materials that exhibit them, may become significant. The smaller the drop, the higher the effective strain rate, therefore, the higher the effective yield point. The higher the effective yield point, the smaller the strain induced by the given applied stress which is determined by the impact pressure.

Finally, the impact areas may well be small enough where a size effect of the material itself becomes important. Particularly in the impact of a spherical drop (or sideways against a cylindrical jet), the impact area at the moment of peak pressure will be a small fraction of the projected area of the drop or jet. Size effects have been found in the values of endurance limits of notched specimens; this has been explained by Peterson<sup>(18)</sup> in the argument that for fatigue failure to occur, the endurance limit must be exceeded not merely at a point or line but across a dimension which is on the order of 0.002 to 0.003 inch, and may bear some relation to the grain size of the material. Since erosion damage, in the velocity domain now under consideration, is primarily

a fatigue process and failure has been shown to occur initially by intergranular cracking, e.g., Marriott and Rowden<sup>(19)</sup>, a similar size effect is very possible.

A physical or phenomenological picture of this kind of effect may be formed with reference to a fatigue model proposed by Weibull.<sup>(20)</sup> He points out that the fatigue process consists of two stages: crack initiation and crack propagation. A crack will initiate at a point in the material with a high damage factor,  $k$ , which can be regarded roughly as the ratio of the nominal applied stress magnified locally by stress raisers such as scratches or inclusions to the idealized strength of the material diminished locally by dislocations or other imperfections. The higher the local value of  $k$ , the smaller is the number of stress cycles  $N_0$  which are required to initiate a fracture at that point. Since the  $k$  values are dependent on local aberrations they vary statistically, and hence,  $N_0$  is a random variable with large scatter. Once a crack has been initiated, it raises the  $k$ -field in the vicinity so that adjacent points are brought more rapidly to the crack-initiation stage, and the crack thereby propagates.

As the drop size increases so does the surface area over which the impact pressure (assumed independent of drop size) extends, and so does (by elastic analysis) the depth to which a given stress level extends below the surface. Thus, the stress gradient into the material is reduced and the  $k$ -field under the surface is increased. Thus, not only is there a greater chance of initiating a sub-surface crack, by virtue of the fact that a greater volume is highly stressed, but the higher value of the  $k$ -field will result in more rapid and deeper crack propagation. In fact, if the depth of the stress field is less than some value characteristic of the grain size, it is unlikely that the cracks would ever propagate around the grain and no erosion would take place. This would establish the threshold drop size.

It is noteworthy that size effects have been found in other material removal processes: Backer, et al,<sup>(21)</sup> discovered a large increase in the shear energy required to remove a unit volume of material

as the chip size (or depth of cut) decreases in turning, micro-milling and grinding operations; the depth of cut in these tests ranged from about 0.010 inch down to  $2 \times 10^{-5}$  inch. It is thought that, as the affected depth of material is reduced, the theoretical strength of the material is approached. These findings have been considered by Finnie<sup>(22)</sup> to be of relevance to erosion by solid particle impingement.

### 3.1.3.3 Effect of Drop Shape

The effect of the drop shape poses two questions; one is difficult to answer at the present, the other is relatively easy, at least qualitatively.

The first is the effect of the shape of the front surface of the drop that contacts the target. Some authors have stated that this shape affects the maximum contact pressure; others stated that it does not. In either case, however, the time rate of the pressure rise and fall and the variation in size of the actual contact area will definitely be affected. Both of these (and the interaction between them) will affect the damage produced, if the strain rate effect and material size effect are significant. Also, the shape of the front of the drop will affect the radial outflow velocity over the target surface after impact (see Bowden and Brunton<sup>(23)</sup> and Engel<sup>(14)</sup>), and this, in turn, is of importance at impact velocities high enough to cause single-impact damage. Complete theories or experimental data relating this geometry to the damage are lacking.

The second question is that of the tail surface of the drop, or its length perpendicular to the contact plane. Bowden's group and also DeCorso<sup>(24)</sup> have shown in single-impact tests that the length of the impinging mass of water is of significance. The duration of the high (water hammer) pressure is governed essentially by the time it takes pressure-release waves to move inward from the boundaries of the contact area and meet, or, in the case of an extremely short mass of liquid, the time it takes for the pressure wave to be reflected from its back end as a release wave and return to the contact face. Thereafter, the contact pressure is only the stagnation pressure  $\rho V^2/2$ , and the mass of liquid arriving then is relatively harmless.

Thus, the effective mass of an impinging drop or mass of liquid may be hypothesized to be approximately that mass through which the pressure release waves must travel before the water-hammer pressure is completely relieved at the contact face.

A test result with some bearing on this was given by Brandenberger and de Haller<sup>(11)</sup>. An elongated jet cross section was used in a wheel-and-jet apparatus and when impacted by the specimens on its broad side resulted in far more rapid erosion than when impacted on its narrow side. Quantitative conclusions cannot be drawn, because in the latter case the second stage of erosion was not reached, so that a reliable comparison of erosion rates is not possible; and further because the actual dimensions of the jet cross section are not given (although the proportions are suggested by a sketch), the size effect and the shape effect cannot be distinguished. Additional experiments of this type might be of value in helping to establish the significant criteria of a drop's damage potential, even though drop shapes may be of fairly uniform shape.

### 3.1.4 Dependence on Impact Velocity

#### 3.1.4.1 Some Simple Empirical Equations for Velocity Dependence

The literature contains a considerable body of data relating erosion to velocity, but the usefulness of much of these data is limited by the considerations discussed in Section 3.1.1.

There are various functional forms to which one can attempt to fit such data; the most obvious ones are discussed below. Here,  $E$  = erosion rate and  $V$  = velocity:

$$E = a V^n \quad (3)$$

This represents a simple power relationship, and implies that some erosion will take place no matter how low the velocity. Usually, however, it is thought that there is a critical or threshold velocity,  $V_c$ , below which erosion is absent for all practical purposes. An obvious type of relationship to reflect this is

$$E = a (V - V_c)^n \quad (4)$$

$$= a_1 \left( \frac{V}{V_c} - 1 \right)^n \quad (4a)$$

This implies that erosion is proportional to a power of the velocity in excess of the critical or threshold velocity  $V_c$ . Pearson's equation is of that type. It has been used by a number of authors to express their results.

Another type of relationship involving a critical velocity is

$$E = a V^n - b \quad (5)$$

which implies  $V_c = (b/a)^{1/n}$

and can be rewritten

$$E = \left[ a_1 \left( \frac{V}{V_c} \right)^n - 1 \right] \quad (5a)$$

Clearly both Equations (4) and (5) have the property that

$$\text{when } \left( \frac{V}{V_c} \right)^n \gg 1, E \rightarrow a_1 \left( \frac{V}{V_c} \right)^n \quad (6)$$

and when  $V/V_c \rightarrow 1, E \rightarrow 0$

### 3.1.4.2 Some Physical Considerations Relating to Velocity Effect

#### 3.1.4.2.1 Analogy with Fatigue S-N Data

Which among equations (3), (4) and (5) is a more logical choice depends to some extent on what physical reasoning--if any--is used to account for the influence of velocity. One physical argument can lead to yet another type of relationship: Vater<sup>(13,25)</sup> noted that since erosion is a fatigue phenomenon, and the applied stress is proportional to (or at least a function of) velocity, the relation between velocity and erosion lends itself to a treatment analogous to the relation between stress and cycles to failure in fatigue. He presented curves in

which velocity is plotted versus the number of impacts to obtain a given weight loss (Figure 3.1-16a), or versus the reciprocal of the weight loss obtained after a given number of impacts (Figure 3.1-16b). (The latter is, however, once more an example of doubtful comparisons, since after a given number of impacts, different stages of the erosion-time curve may have been reached.)

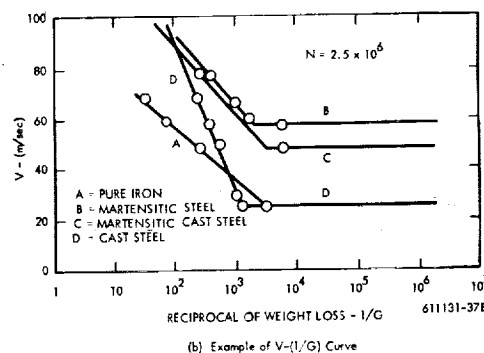
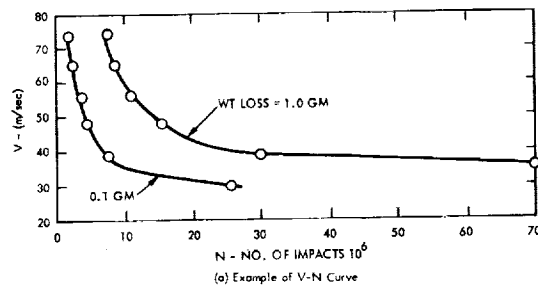


Figure 3.1-16 Erosion-Velocity Relationships Plotted in the Manner of Fatigue Data

Some caution should be exercised in making direct analogies between S-N fatigue curves and velocity versus erosion curves. If erosion takes place as a steady-state process and the mean size of erosion fragments is independent of  $V$ , then the volume rate of erosion  $E$  would be proportional to  $1/N$ , where  $N$  is the mean number of impacts required to generate a loose erosion fragment. In turn,  $N$  could be assumed to be related to the impact stress and hence to the velocity  $V$  in a manner similar to the relation between cycles to failure and stress in conventional fatigue tests.

If these assumptions are correct, a  $V - (1/E)$  curve should exhibit similar characteristics to a S-N fatigue curve. If erosion is not a steady-state process, then the number of impacts to obtain a given cumulative volume loss (as plotted in Figure 3.1-16a) should be a valid analogy, provided that there are no variations in the initial target surface conditions which could affect the life-times of the original surface layer elements. (It might be pointed out that one implication of the erosion-rate-time model proposed in Section 3.2 is that the erosion process during the period of maximum erosion rate is generally not a steady-state process; rather this peak in the rate-time curve can occur as a result of a deluge of erosion fragments being loosened at about the most probable value of the number of impacts to failure, as measured from the time the impingement attack was initiated. It is only because of scatter in the sizes and the impacts-to-failure of the erosion fragments that there is a tendency towards a steady-state value.)

Fatigue S-N data are often depicted as an approximately straight line on a semi-log plot for intermediate values of  $N$ , as follows:

$$S = S_0 - b \log N$$

with a leveling off to  $S = S_y$  at low values of  $N$ , and a transition to  $S = S_E$  at high values of  $N$  where

$S$  = stress corresponding to  $N$  cycles

$S_0$  = intercept of straight line on stress axis ( $S_0 > S_y$ )

$S_y$  = yield stress

$S_E$  = endurance limit

Consequently, one might expect some analogous relationship such as

$$V = a - b \log \left( \frac{1}{E} \right)$$

or, in a form which is equivalent but more consistent with the previous types of equations listed,

$$E = a e^{nV} \quad (7)$$

where  $e$  is the base of the logarithm chosen. This equation does not predict a critical velocity and must be combined with the separate condition that there is a transition to  $E \rightarrow 0$  at some value  $V = V_c$ .

This relation, even for conventional fatigue data, is valid only within a limited range. A number of more complicated equations have been proposed for representing S-N data over the full range of values; these are surveyed on pages 174-178 of Reference 26. Such equations would predict a critical velocity. It does not seem profitable to attempt to use these, partly because of the computational difficulty involved and partly because one of the previously mentioned assumptions inherent in this direct analogy is almost certainly unjustified; that is, the assumption that the mean erosion fragment size is independent of impact velocity. Since a higher velocity generates a greater impact pressure in turn producing a larger stress-field in the target, i.e., a greater volume of material is highly stressed, it seems very likely that the mean fragment size increases with velocity. A velocity relationship could be postulated from this fact alone, as will be shown below.

#### 3.1.4.2.2 Approach Based on Size of Stress-Field Under Impact

The approach will be demonstrated with reference to a two-dimensional model, which would apply to the wheel-and-jet type of apparatus: It is assumed that the contact pressure between the jet whose side impinges against the target, or vice versa, and the target surface can be reasonably represented by a belt of uniform pressure over the surface of a semi-infinite solid; furthermore that the effective width "2a" of this belt is a function of jet size and shape and is independent of impact velocity.

(This assumption seems more reasonable than a Hertzian contact stress distribution which would imply that the liquid behaves as an elastic solid on impact.) This corresponds to Case No. 11 on page 322 of Roark<sup>(27)</sup> where formulae are given for the compressive and shear stresses anywhere within the solid. Since the shear stress is surely a better criterion for failure than the compressive stress, consider the locus of a constant value of shear stress,  $S$ , as a function of the contact pressure,  $p$ , and the semi-width of the pressure belt,  $a$ . The formula given by Roark is

$$\begin{aligned} S &= 0.318 p \sin \alpha \\ &= (1/\pi) p \sin \alpha \end{aligned} \quad (8)$$

where  $\alpha$  is the angle subtended, at the point in question, by the boundaries of the pressure belt on the surface. It can easily be shown that the locus defined by Equation (8) consists of two circular arcs of radius,  $r$ , where

$$\frac{r}{a} = \frac{1}{\pi} \frac{p}{S},$$

whose centers lie a distance  $d$ , respectively, below and above the solid surface, where

$$\frac{d}{a} = \sqrt{\left(\frac{r}{a}\right)^2 - 1}$$

This is shown in Figure 3.1-17. The region stressed to values greater than  $S$  lies between the two arcs. Figure 3.1-18 shows these loci for a number of values of  $p/S$ ; the highest value of the shear stress is of course  $S = p/\pi$ , and its region reduces to a semi-circular locus of radius,  $r = a$ .

Figure 3.1-18 can be regarded in two ways. It can represent the loci of various shear stresses in a given stress field, if the contact pressure  $p$  is assumed to be a fixed quantity. On the other hand, assuming the shear stress  $S$  to be the independent fixed quantity, then the lines on Figure 3.1-18 represent the spreading of the boundaries of the region bounded by that stress, as the contact pressure  $p$  is increased. It is the latter point of view which we adopt for our argument.

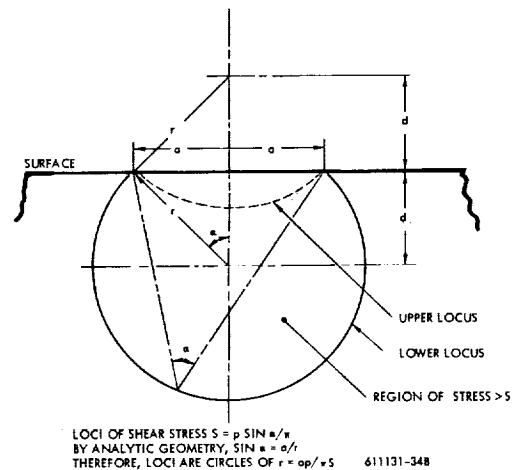


Figure 3.1-17 Loci of Constant Shear Stress  $S$  in Semi-Infinite Solid with Belt of Uniform Pressure  $P$

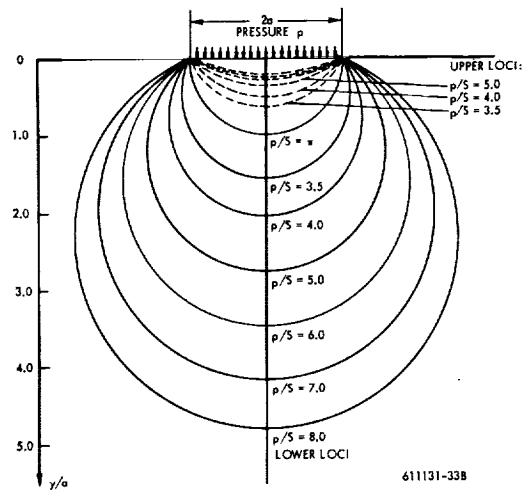


Figure 3.1-18 Upper and Lower Loci for Various Values of Pressure/Shear Stress Ratios



For the purpose of this argument it is assumed that if a reference stress  $S$  is selected exceeding an appropriate critical value or endurance limit, then the reference time (or number of impacts) required for fracture to have occurred all around the locus of  $S$  is independent of the length of that locus, since a greater length represents a proportionately greater number of crack initiation points. At this fixed reference time, all of the material between the original surface and the lower locus will have been lost. Therefore, a lower limit to the change in the erosion rate with contact pressure, and hence with velocity, is provided by the change in the area,  $A_S$ , which lies between the original surface and the lower locus of a given value of  $S$ , as  $p$  is increased.

The non-dimensionalized area  $A_S/a^2$  has been computed as a function of  $p/S$  and is plotted on log-log scales in Figure 3.1-19, which therefore should represent an approach to a velocity-erosion rate relationship. Note that the slope begins at a high value and gradually approaches the value of 2.

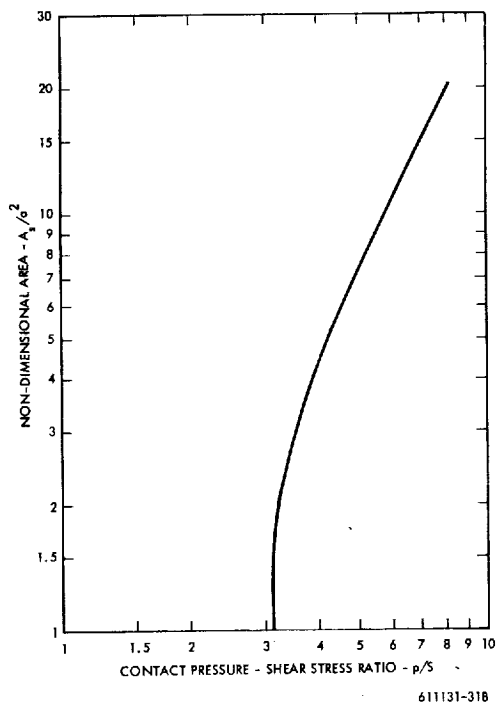


Figure 3.1-19 Area Between Surface and Lower Stress Locus

One should not, of course, take this model so literally as to infer from it that fracture actually occurs by cracks following along these loci. Moreover, it clearly gives a lower limit to the erosion rate because it ignores the fact that earlier fractures will occur above the reference stress locus because of the higher stresses there, thus altering the geometry and causing the locus of  $S$  to progress further down into the solid. In particular, this model predicts that when the pressure reaches  $p = \pi S$ , the erosion jumps from zero to a value corresponding to an area,  $A_S/a^2 = \pi/2 = 1.57$ .

In actuality, if the "reference stress"  $S$  is chosen to be above the endurance limit  $S_e$  so that the reference time is not infinite, then for all values of  $p$ , such that  $p > \pi S_e$ , there will still exist stresses high enough to cause material loss, though not within the same reference time. The model does show, however, that some quantitative conclusions may be drawn from a fatigue point of view, without any reference to specific  $S$ - $N$  relationships. It also serves to emphasize that the extent of the stress field under the impact must be taken into account in any analytical approach to predicting the erosion-velocity relationship, whether that approach is based on stress or energy concepts.

### 3.1.4.2.3 Energy Considerations

An energy approach was described in pages 167-174 of Reference 11, that sought to predict effects both of velocity and drop size on the erosion. It was based on the assumption that the volume of material removed per unit area per impact, is proportional to, or a function of, the impact energy per unit area in excess of some energy threshold per unit area characteristic of the material surface. This resulted in the following relationship, expressed in non-dimensional terms:

$$E = f \left\{ k_2 \left[ \frac{\frac{1}{2} \rho_L V^2}{S_o} \right] \left[ 1 - \frac{e_o}{k_3 \left( \frac{1}{2} \rho_L V^2 D \right)} \right] \right\} \quad (9)$$

where

- $E$  = rationalized erosion rate  
 $\left( \frac{\text{volume of eroded material}}{\text{volume of impinged liquid}} \right)$   
 $V$  = impact velocity  
 $D$  = characteristic dimension of droplet  
 $\rho_L$  = density of liquid  
 $k_2$  = ratio of "effective" volume to total volume of drop  
 $k_3$  = ratio of "effective volume" to "effective impact area" times drop dimension  
 $s_o$  = characteristic strength or elastic modulus of material  
 $e_o$  = "threshold energy" per unit area of material surface  
 $f$  = functional relationship or factor of proportionality

In a simplified form, and to bring out the "threshold conditions" implicit in it, Equation 9 can be rewritten as:

$$E = f_1 \left[ V^2 \left( 1 - \frac{G}{V^2 D} \right) \right] \quad (9a)$$

where  $G$  represents a "critical value" such that if  $V^2 D < G$  no erosion takes place. (The relationship is of the type of Equation 5.) This critical value has proved quite successful, in one or two instances, of correlating drop-size effect data, as was shown in the previous section. In particular, it was shown that the data of Pearson in Reference 12 correlated well in the form

$$E = f_2 \left[ V \left( 1 - \frac{G}{V^2 D} \right) \right] \quad (10)$$

However, the difference between Equations (9a) and (10) indicates that the energy threshold concept - at least in its present form - is still deficient.

A number of authors recently have sought to predict both erosion strength and erosion attack severity in terms of energy concepts (e.g., Thiruvengadam<sup>(17,28,29,30)</sup>, Hoff, et al,<sup>(6)</sup>; Shalnev, et al<sup>(31)</sup>) there are problems to be solved. The energy balance involved in a droplet impact is complex and has not yet been examined in sufficient depth. Part of the kinetic energy of the impinging drop will remain as the kinetic energy of the radial outflow velocities; part will be dissipated in the shock or pressure waves passing through the drop, and part in the shearing associated with the change of direction of the liquid flow; part will be dissipated in the target material; here too, the energy dissipation associated with stress waves should be examined as well as the quasi-static plastic strain hysteresis energy associated with each impact stress cycle. The picture is further complicated by the rather large amount of energy that will be stored temporarily as elastic strain energy in the target and will reappear in one of the previously-mentioned forms.

The energy dissipated in the target material is that energy associated with fracture, and therefore, with erosion. But it is not correct to assume that the volume of material removed is proportional to that energy. Two reasons account for this: One is that (at least in the case of larger drops at moderate velocities) erosion fragments produced by the random linking-up of fatigue-like cracks (see Reference 19) are not likely to be deformed to the fracture point throughout their volume; therefore, the accumulated plastic strain energy may be more related to the surface area of the fragment than to its volume, or at the least, be non-uniformly distributed within the volume. The other is that in fracture due to the repeated stressing, the total energy input increases greatly with the number of cycles to failure. This is evident in McAdams' results for impact fatigue tests,<sup>(32)</sup> and has been documented for a large collection of fatigue data by Halford<sup>(33)</sup>. Even if one postulates that the damaging energy is the same in all cases and the excess hysteresis energy is dissipated through non-damaging processes, the fact remains that all of the dissipated energy is supplied by the impinging droplets and even if the energy absorption by the target

material is known, that in itself will not establish the erosion rate. The crudest broad conclusion one can draw from the above is that the erosion is likely to vary with the velocity to a power higher than 2, since the impinging energy is proportional to velocity squared, and the total energy to failure decreases with increasing velocity (i.e., with increasing stress and decreasing number of impacts to failure).

#### 3.1.4.2.4 Relation Between Impact Pressure and Velocity

A final note of relevance to this subject concerns the relationship between the impact velocity and the contact pressure generated.

Let us first review one-dimensional approximations, and then discuss the three-dimensional effects introduced in the impact of a rounded drop or jet.

When a body has its velocity changed by means of an impact, a shock (or pressure, or stress) wave emanates from the initial impact interface and propagates into the body, progressively imparting the change of velocity to each particle "layer" through which the wave presses. The applicable pressure relationship is

$$p = \rho CV \quad (11)$$

where

- $p$  = pressure rise across shock wave
- $\rho$  = density of unshocked material
- $C$  = velocity of propagation of shock wave
- $V$  = change in particle velocity across shock wave.

If we consider the low speed impact of a liquid against a rigid target, then the above takes the form of the well known "water hammer" equation:

$$p = \rho_o C_o V_i \quad (11a)$$

where

- $\rho_o$  = density of undisturbed liquid
- $V_i$  = impact velocity
- $C_o$  = acoustic velocity of the liquid.

When target elasticity must be taken into account, then one may write two simultaneous equations (11), for the liquid and for the target material respectively: the pressures must be equal for both, and the two particle velocity changes must add up to the impact velocity. This leads to an equation sometimes attributed to deHaller:

$$p = \frac{\rho_o C_o V_i}{1 + \frac{\rho_o C_o}{\rho_T C_T}} \quad (12)$$

where

- $\rho_T$  = density of undisturbed target material
- $C_T$  = stress wave velocity or acoustic velocity in the target.

Note that equations (12) and (11a), besides being one-dimensional approximations, both assume fixed values of the propagation velocities  $C_o$  and  $C_T$ . This makes them quite inaccurate for high-speed impact calculations, because the propagation velocity of a shock wave itself depends strongly on the shock pressure (or the particle velocity change across the shock).

Various studies have shown that for many materials, both liquid and solid, the relationship between shock velocity,  $C$ , and particle velocity change across the shock,  $V$ , is a nearly linear one and can be approximated by

$$C = C_o + kV \quad (13)$$

where  $C_o$  is the acoustic velocity in the material and  $k$  is a constant for the particular material.

Heymann<sup>(34)</sup> gave a non-rigorous explanation of this relationship, demonstrating that for water  $k \cong 2$  (in the range  $0 \leq V \leq 1.2 C_o$ ), and derived the following equations for one-dimensional impact between a liquid and a target.

If the target is rigid,  $V = V_i$ , and substitution of (13) into (11) gives

$$P = \rho_o C_o V_i (1 + k M_o) \quad (14a)$$

where

$$M_o = V_i / C_o = \text{"Impact Mach Number"}$$

and

$k_o$  is the "shock velocity constant" for liquid, as defined by equation (13).

If the target is elastic, but its shock velocity is assumed constant, it is not correct simply to substitute equation (13) into equation (12), although the error is generally less than 20 percent. The exact expression, derived in Reference 34, can be written in dimensionless form as:

$$\frac{P}{\rho_o C_o V_i} = u (1 + k_o M_o u) \quad (14b)$$

where

$$u \equiv \left[ \left( \frac{1+x}{2 k_o M_o} \right)^2 + \frac{x}{k_o M_o} \right]^{\frac{1}{2}} - \left[ \frac{1+x}{2 k_o M_o} \right]$$

and

$$X \equiv \rho_T C_T / \rho_o C_o$$

( $u$  is the ratio of particle velocity change in the liquid to impact velocity, and  $x$  is the acoustic impedance ratio between target and liquid.)

The assumption of a constant shock velocity  $C_T$  in the target can be justified when  $x \ll 1$ , which is generally true for metallic targets. In that case,

the ratio of particle velocity change in the target to its acoustic velocity is so small that the difference between the true stress wave velocity and the acoustic velocity is negligible.

Curves of  $P / \rho_o C_o V_i$  versus  $M_o$ , for several values of  $x$ , are given in Figure 3. 1-20. These curves apply to  $k = 2$ , as for water.

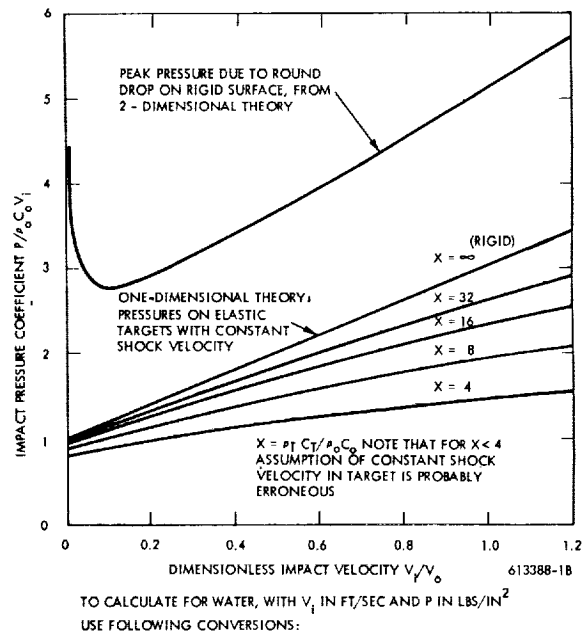


Figure 3.1-20 Impact Pressure Versus Velocity

When  $x \gg 1$ , as say in the impact between water and an elastomeric target, then the greater particle velocity change will occur in the target. Such a case can be treated by exchanging the meanings of the subscripts (e.g.,  $\rho_o$ ,  $C_o$ ,  $k_o$  now refer to the target material), provided  $k$  for the target material is known or determined.

Unfortunately, values of  $k$  are not easily found in the literature. The following is a partial list:

Material	$C_o$ (km/sec)	$k$	Source
Water	1.5	2.0	Heymann, Ref. 34 (Deduced from Cole, R. H: "Underwater Explosions", Princeton Univ. Press, 1948)
Sodium	2.563	1.242	Rice, M. H.; J. Phys. Chem. Solids, 26, 1965 pp. 483-492
Potassium	1.930	1.188	
Lithium	4.589	1.154	
Rubidium	1.232	1.184	Jones, A. H., et al: J. Appl. Phys., 37, 1966, pp. 3493-3499
Gold	3.0	1.56	
Tungsten	4.0	1.28	
"Forsteel 77"	3.9	1.355	Ruoff, A. L.; J. Appl. Phys., 38, 1967, pp. 4976-4980
K Br	2.33	1.546	
Cs I	1.66	1.41	
Sodium	2.706	1.22	

Equations 14a and 14b still apply strictly only to one-dimensional impact (i.e., two semi-infinite bodies colliding). An exact analysis of a liquid sphere impacting against a plane surface has not yet been achieved. However, a qualitative picture of the sequence of events, based on various contributions relevant to this problem, has been given by Heymann. (35) (75) According to this picture, the impact pressure at the first instant of contact is equal to the one-dimensional pressure. As the contact area grows, the pressure distribution becomes more and more non-uniform. The pressure at the expanding boundary of the contact area increases, while the pressure at the center of the contact area decreases, from the one-dimensional value.

A "critical condition" is reached when the shock front expands faster than the contact boundary, and lateral "jetting" outflow begins. Soon thereafter, the contact pressures may be assumed to decrease everywhere.

Heymann (35) also presented an approximate two-dimensional analysis for the impact of a round liquid body onto a rigid plane, which permits the calculation of the pressure at the boundary of the contact area, from the moment of initial contact until the "critical condition" is reached. The numerical results support the previously described qualitative picture. The peak impact pressure is that at the critical condition, and if this "critical pressure"  $p_c$  is plotted in nondimensional terms,  $p_c / \rho_o C_o V_i$  against nondimensional impact velocity  $M_o$ , for water, one finds that the lowest value of  $p_c / \rho_o C_o V_i$  is about 2.8, at  $M_o \approx 0.1$ ; at higher and lower values of  $M_o$  the value of  $p_c / \rho_o C_o V_i$  increases rapidly. Thus, the simple one-dimensional water hammer equation (11a) underestimates the peak pressure by at least a factor of about 3. The curve applicable to water is shown on Figure 3. 1-20. Similar results are obtained for sodium and potassium.

These results are true only for impact on a rigid plane; the analysis has not yet been extended to an elastic target, on which the peak pressures presumably are smaller. The results did show, however, that the pressure at the contact boundary rises only slowly during the first half of the growth of the contact zone, so that one may conclude that a considerable portion of the eventual contact area is subjected to little more than the one-dimensional pressure. This conclusion may perhaps be extended to elastic targets as well. It could well be that this pressure is more significant in determining target material response than the more localized and fleeting "critical pressures", but this should not be assumed without further evidence. In any case, it would be desirable to have analytical results for the contact pressures developed by impacting rounded drops on elastic targets, on rough targets, on film-covered targets, and at oblique angles. This still remains to be accomplished.

### 3.1.4.3 Empirical Data from the Literature Search

#### 3.1.4.3.1 Preliminary Remarks

In attempting to fit a simple equation to experimental data, equations like (3), (4), (5) or (7) would be selected. Equation (4) would form a straight line on log-log paper if plotted versus  $(V - V_c)$ , but one does not know  $V_c$  ahead of time. Equation (7) would form a straight line on semi-log paper, with  $V$  along the linear scale.

Figure 3.1-21 shows examples of these various relationships on a log-log plot. The upper portion represents equations of types (4) and (5) with  $V/V_c$  plotted against  $E$ , and the lower portion equations of types (3) and (7) with  $V$  plotted against  $E$ . For consistency, the constants,  $a$ , have been chosen so that all curves pass through the point  $E = 1$ ,  $V$  or  $V/V_c = 2$ . A plot of this kind may be of help in deciding what type of relationship to try to fit to experimental data points when these are plotted on a log-log graph. A corresponding plot of these families of curves could be constructed on semi-log paper, with  $E$  as the log coordinate; in that case the equations of type (7) would plot as straight lines.

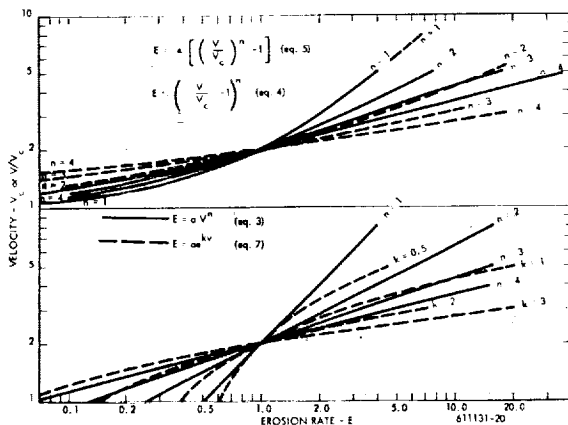


Figure 3.1-21 Families of Hypothetical Erosion Versus Velocity Curves, According to Equations (3) through (7)

A number of problems arise when attempting to establish an equation of these types for experimental data, either by plotting the data points on log or semi-log paper, or directly by numerical methods.

One of the problems is that much of the data is obtained at velocities not much greater than the critical velocity (seldom at more than  $V/V_c = 2$ ). Therefore, one is probably examining that portion of the curve in which a transition is taking place, or in which even in a log-log plot, the curvature is greatest. Consequently, small errors in the data points, or small differences in the manner in which a smooth curve is fitted to them, will have a great effect on the values of the exponent  $n$  and the critical velocity deduced.

This difficulty is compounded because the scatter in erosion data is inevitably great, that in many of the test series no more than three velocities have been investigated, and that the ratio of the highest to the lowest of these is often small, about 1.5. This covers a very short span of the velocity axis on log-log paper. In short, a problem exists in which:

- In the velocity range investigated the true relationship will not appear as a straight line.
- There are too few data points and these cover too short a velocity range to allow a curved line to be fitted with the necessary accuracy.

If testing could be done at much higher velocities, then in theory the influence of  $V_c$  on the apparent exponent, i.e., the slope of the curve on a log-log plot, would be reduced and a more accurate determination could be made of  $n$ . In practice, however, at velocities much above  $V/V_c = 2$  one gets into the region of single-impact damage, whose velocity dependence may not be the same as that for fatigue damage, and so, one may well be in another transition region.

#### 3.1.4.3.2 Examination of the Better Test Data

One of the earliest comprehensive sets of test data at various velocities was given by Honegger<sup>(2)</sup>. His conclusion was that while the behavior of the various materials differs considerably, the rate of erosion may be generally expressed as:

$$E \propto (V-125)^2 \quad (15)$$

where  $V$  is the impact velocity in m/sec. The

above relationship was evidently deduced from his Figure 7, on which was plotted the specific loss in weight (weight loss per impact, hence a measure of erosion rate  $E$ ) after 215,000 impacts, versus velocity. This type of comparison is not valid.

Also, the equation fits a mean curve drawn through the band of experimental curves; but some individual curves suggest exponents that are much higher. Thus, the curve for Specimen No. 26 is well described by  $E \propto (V-110)^{3.3}$ .

For a more valid basis of comparison, the rate-time curves presented for various materials and for the speeds of 175, 200, and 225 m/sec should be reviewed. From these, one can deduce characteristic erosion rates which fulfill the criteria specified in Section 3.1.1 of this report. This has been done as an approximation and the results are plotted on log-log coordinates in Figure 3.1-22. Their shape is not

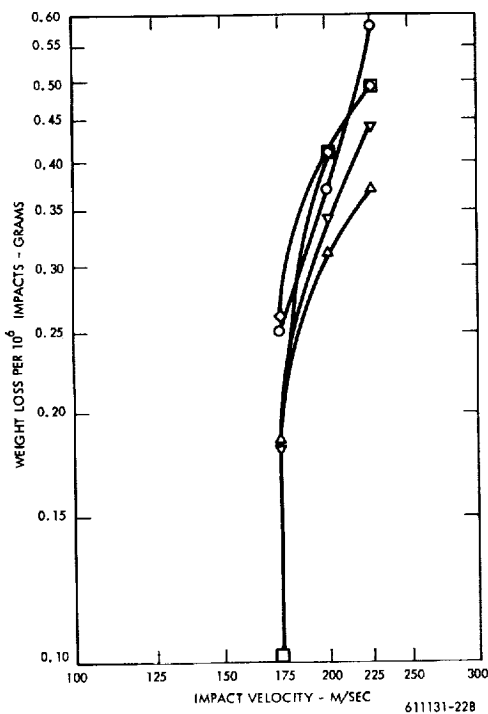


Figure 3.1-22 Erosion versus Velocity Curves, Computed from Data in Reference 2

unlike what is predicted by Figure 3.1-19, at velocities close to the threshold value, but it would be unwise to fit any empirical equation to these data.

An interesting set of results on one material was reported by Brandenberger & DeHaller<sup>(1)</sup>, which was discussed in Section 3.1.2 with reference to the angle-effect. The rationalized erosion rates deduced from Reference 1 were plotted in Figure 3.1-7, and the data points of Figure 3.1-7b have been replotted on semi-log coordinates on Figure 3.1-23. They fall into a straight line, giving some support to the simple fatigue model of velocity dependence represented by equations of type 3.1-7. It should be pointed out, however, that the determination of the best values of  $E$ , from the irregular slopes of the very small graphs shown in Reference 1, involved a certain amount of judgment and some extrapolation for the  $u = 31$  m/sec data. In preliminary attempts, with fewer pretensions to accuracy, the results were such as to fit equations of types 3.1-4 or 3.1-5 better than type 3.1-7.

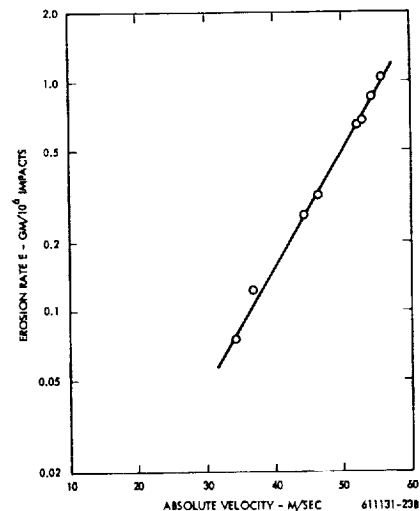


Figure 3.1-23 The Data of Figure 3.1-7b Plotted on Semi-Log Paper

The following equations have been fitted to the data of Reference 1 during these several attempts:

$$\begin{aligned}
 E &\propto (V-20)^{3.5} \\
 E &\propto (V-25)^{2.6} \\
 E &\propto \frac{V^4}{31} - 1.0 \\
 E &\propto e^{0.126V} \\
 E &\propto V^6
 \end{aligned}
 \tag{16}$$

And yet these data are among the better in the literature, in that the velocity range covered was almost 2:1 and there were 8 data points in that range. This, again, demonstrates the (near) futility of applying a purely empirical approach and hoping to deduce therefrom some useful generalizations.

Another set of data covering an even larger velocity range was given by Hobbs in his discussion to a paper by Leith and Thompson<sup>(36)</sup>, although no information was given on the material tested. The data were plotted on linear coordinates, labeled rate of weight loss, mg/sec, and impact velocity, ft/sec. From the units in which the erosion rate is given, one must infer that these data are not rationalized; therefore, the erosion rates should be divided by a factor proportional to the corresponding velocities to put them on a rationalized basis, i. e., on the basis of equal rates of impinging water. The actual data points from Hobbs' graph, and the values of  $E$  computed therefrom, are given in Table 3. 1-4. The values of  $E$  have been plotted on log-log scales in Figure 3. 1-24, both against actual velocity  $V$  (Curve "a"), and also against  $(V-V_c)$  with  $V$  taken as 270 ft/sec (Curve "b"). Smoothly fitted curves are drawn as solid lines, and straight-line approximations as broken lines. These latter suggest that the results can be represented over a certain range by

$$\begin{aligned}
 E &\propto V^{4.4}, \text{ or by} \\
 E &\propto (V-270)^{2.4}
 \end{aligned}
 \tag{17}$$

TABLE 3. 1-4

DATA OF HOBBS IN REFERENCE 36

V ft/sec	Erosion Rate, R gm/sec	Rationalized Rate, $E_r$ ( $2 \times 10^3 R/V$ )	Reduced Velocity ( $V-270$ ) ft/sec
270	0	0	0
330	0.02	0.122	60
385	0.03	0.156	115
440	0.06	0.272	170
495	0.11	0.444	225
570	0.32	1.12	300
620	0.40	1.29	350
680	0.85	2.50	410
735	1.01	2.75	465
775	1.28	3.30	505
825	1.58	3.83	555

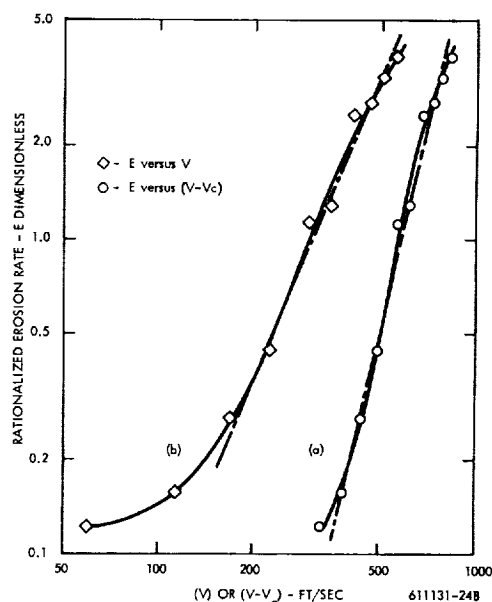


Figure 3. 1-24 Data of Hobbs in Reference 36, Plotted both versus  $V$ , (Curve "a"), and versus  $(V-270)$ , (Curve "b")



The latter may result in less scatter, but is valid over a more restricted range. The same data are shown plotted on semi-log coordinates in Figure 3.1-25. A straight line fits the data well in the lower velocity range, but a distinct breakaway from it occurs at about 700 ft/sec. Thus, these results, too, provide no evidence pointing toward any particular simple type of empirical formulation.

The most comprehensive body of test data recently made available is that of Pearson (8, 10, 12). These data have already been discussed in relation to angle effects in Section 3.1.2 and drop size effects in Section 3.1.3; in the latter section there was success in collapsing the data for different drop sizes into a single curve by two different methods as shown in Figures 3.1-13 and 3.1-14. No actual curves were drawn in those figures so as not to obscure the data points themselves. Curves fitted by hand to these points are shown in Figure 3.1-26. Curve (a) represents Figure 3.1-13 and Curve (b) Figure 3.1-14. The same curves, transposed onto log-log coordinates, are shown in Figure 3.1-27, and straight lines (dot-dashed) are shown which coincide with the curves

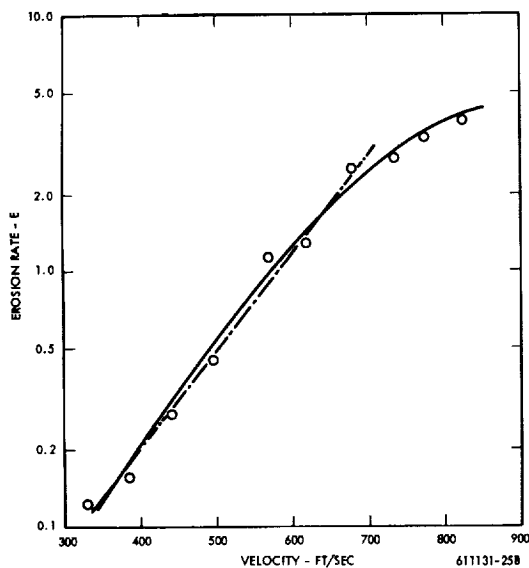


Figure 3.1-25 Data of Figure 3.1-24a on Semi-Log Paper

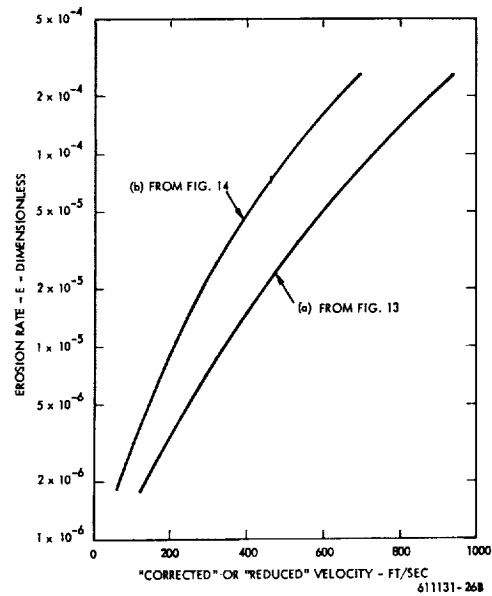


Figure 3.1-26 Curves Based on the Data Points of Figures 3-1-13 and 14. Original Data from Reference 12

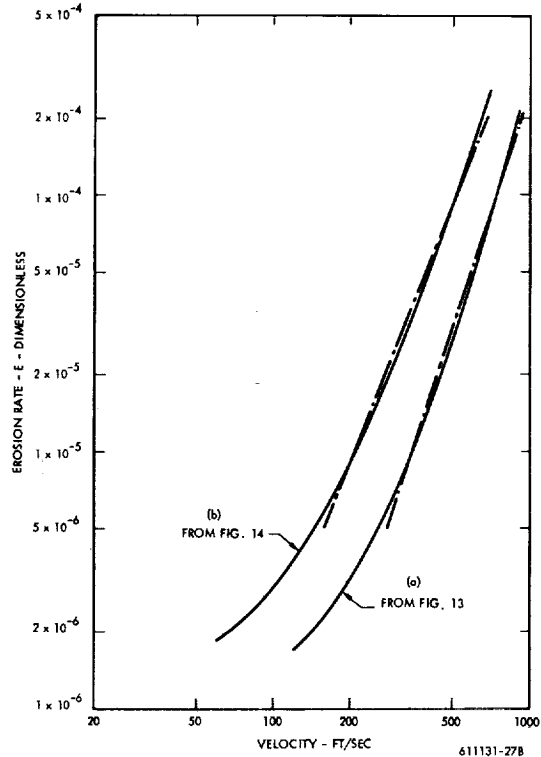


Figure 3.1-27 Curves of Figure 3.1-26 on Log-Log Plot

themselves at the values  $E = 10^{-5}$  and  $E = 10^{-4}$ . They are reasonably valid approximations for the range from  $E = 5 \times 10^{-6}$  to  $E = 2 \times 10^{-4}$ . These lines represent relationships as follows:

$$\begin{aligned} \text{Curve (a): } E &\propto (K_c V)^{3.05} \\ \text{Curve (b): } E &\propto (V - V_{cd}) \end{aligned} \quad (18)$$

where  $K_c$  and  $V_{cd}$  have been defined in Section 3.1.3 and in Figures 3.1-13 and 3.1-14.

Note that the latter has an exponent fairly close to the expression deduced by Pearson<sup>(10)</sup> for a single drop size:

$$E \propto (V - 390)^{2.6} \quad (19)$$

Note also that the general appearance of the curves of Figure 3.1-27 is similar to those of Figure 3.1-24 (except for the curvature at the highest velocities), and that the general appearance of those in Figure 3.1-26 is not unlike that of Figure 3.1-25. In particular, Curve 3.1-26a could reasonably be approximated by a straight line below about 600 ft/sec with a breakaway above that. (It must be remembered, however, that in Figure 3.1-25 the horizontal scale is actual velocity, whereas in Figure 3.1-26a it is a "corrected velocity" which is not a linear function of the actual velocity.)

### 3.1.4.3.3 Conclusions

About the only conclusion which seems justifiable, at this stage, is that even the best available erosion-versus-velocity data do not follow exactly any law such as represented by equations of types 3.1-3 through 3.1-7, but can, over limited ranges, be approximated by any of them. Equations of type 3.1-4 have seemed intuitively to be the most rational and have been adopted by many authors,

including Honegger (see Equation 3.1-15), Pearson (Equation 3.1-19), and Fyall, et al<sup>(3)</sup> who present the following equation for the erosion rate of "perspex":

$$\text{Weight Loss Rate} \propto (V - 208)^{3.37}$$

This, however, refers to the velocity of a target within a given rainfall. Thus the rate of water impingement increases linearly with velocity and the rationalized erosion rate would be given by

$$E \propto (V - 208)^{2.37} \quad (20)$$

The preceding comparison of various equations of the form of equation (3.1-4) suggests that when data can be represented in this manner, the value of the exponent will be not too far from 2.5.

Comparison of Figures 3.1-23 through 27 suggests that equations of the form of equation (3.1-7) tend to fit better in the lower velocity region (although there must also be transition to the critical velocity), whereas equations of the form of equation (4) fit best in the intermediate velocity region.

If a direct power law of the form of equation (3.1-3) is used to represent the results, the exponents tend to range from 4 to 6; though for brittle materials, such as glass, exponents as high as 13 have been quoted by Langbein<sup>(5)</sup>.

In no case does it appear justifiable to use any of these curve-fitting equations for the purpose of extrapolating out of the test range.

## 3.1.5 Dependent Parameters Other Than Rate

### 3.1.5.1 The Incubation Period

All of the correlations discussed in the previous three sections have related to the slope of the second-stage or steady-state region of the erosion

versus time curve, and minor attention has been given to the incubation-period or first-stage of erosion, which may be defined as the duration to the intercept of the steady-state or second-stage erosion line when that is extended to cross the zero-erosion axis. A proper understanding of the effect of velocity, and the other variables discussed, must eventually predict their effect on the incubation period as well as on the subsequent erosion rate, since the incubation period may under some conditions be a substantial portion of the effective life of the component being eroded. Figure 3.1-2 defined the incubation period as the term is used in this section and by the authors cited herein.

Pearson (8, 10, 12) has plotted incubation periods for different velocity drop sizes and impingement angles, and has found more scatter in these data than in the corresponding erosion rate data.

Figure 3.1-28 reproduces this data for different drop sizes in Reference 12, including the average curve drawn by Pearson, because "the amount of scatter . . . obscures the effect of drop diameter." It is nevertheless instructive to draw the best curves for each drop size separately, as is done in Figure 3.1-29, from the data points in Figure 3.1-28. From these points one can see a trend for the curvature of the lines to increase with decreasing drop size; this one would expect if the critical velocity increases with decreasing drop size, since near the critical velocity  $W_0$  would tend to infinity. In particular, the 350 micron curve seems consistent with the prediction from Table 3.1-3 that the critical velocity for this drop size is 535 ft/sec.

The simplified fatigue analogy which led to Equation (7) also implies that the incubation period should be proportional, or analogous, to the number of cycles to obtain fatigue failure. Some evidence supporting this has been given by Ripken, et al, 1965(37). For one material, Ripken has measured the number of impacts corresponding to the incubation period as previously defined, and the resulting impact stress assumed to be given by  $1/2 CV$ . He super-imposed these points on a standard S-N fatigue

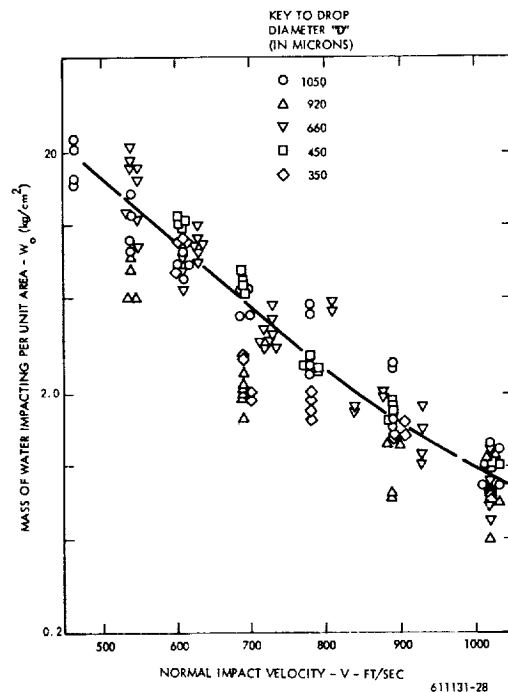


Figure 3.1-28 Rationalized Incubation Periods at Various Drop Diameters and Velocities (Copy of Figure 7 of Reference 12)

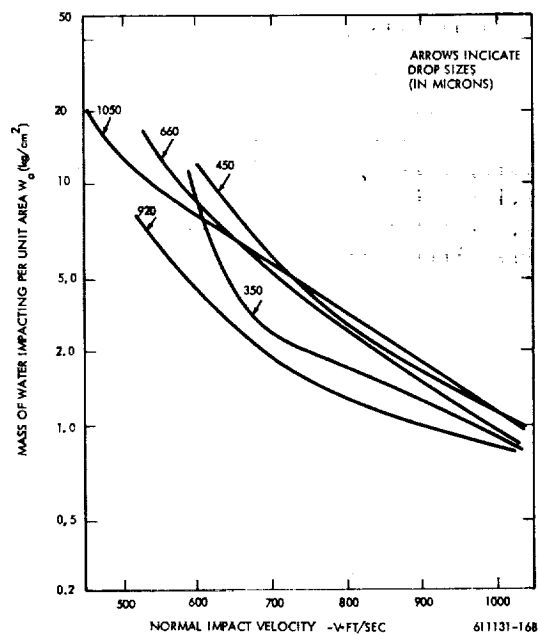


Figure 3.1-29 Individual Curves for Different Drop Sizes, Based on Data Points of Figure 3.1-28.

so-called incubation time. The data on incubation times are too sparse and exhibit too much scatter to allow any conclusions beyond the very broad and obvious one that as the impingement conditions (velocity and drop size) decline toward the threshold value, the incubation time increases.

The erosion rate-time model to be developed, in Section 3.2 of this report, implies that both the incubation time and the maximum erosion rate are strongly influenced by the statistical variations in the sizes and lifetimes of the erosion fragments formed. These, in turn, are influenced by the scatter in drop sizes and velocities as well as the scatter inherent in fatigue properties themselves. Consequently, it is suggested that future correlations should be attempted on the basis of the time required to attain specified damage levels rather than on the arbitrarily-defined incubation and rate parameters.

The view that erosion is a form of fatigue leads directly to a number of corollaries:

a) There is little likelihood of finding one specific independently measurable material property which will predict erosion resistance, since none has been found to predict fatigue strength uniquely, and far more research has been done on fatigue than on erosion.

b) In fatigue, the relation between stress and endurance is determined by a test for each material, and cannot be stated in simple analytical form. Similarly, the relation between impact velocity and erosion very likely does not follow any universal law but must be established empirically, perhaps in graphic form, for each material.

c) In erosion, as in fatigue, the condition of the surface is likely to be of considerable importance.

d) Although erosion is the result of many failures, and some of the statistical scatter found in fatigue data may well average out in an erosion test, yet to obtain valid results (or results with calculable confidence limits) many more data points must be taken and many more replications must be run than have been done to date. Related to this is

the need, often emphasized in this report, to establish accurately the erosion versus exposure curve, and to carry out all tests to the same degree of cumulative erosion damage if one wants to draw any quantitative comparisons. The amount of testing required and the validity of results should be optimized by proper statistical design of the experiment. This has seldom been done in erosion testing.

A final suggestion to those generating erosion test data is that with the results they should give all the pertinent information--material identification and preparation, physical and mechanical properties, surface preparation, size and shape of specimen, area exposed to erosion, amount of water impinging, and if possible, the drop size or drop size distribution, impact velocity, etc., -- necessary for computing the rationalized erosion and duration parameters and making meaningful correlations between these and the impingement and material parameters.

### 3.2 THE VARIATION OF EROSION RATE WITH EXPOSURE TIME\*

#### 3.2.1 Observed Rate-Time Patterns

The latest literature on the resistance of materials to impingement and cavitation erosion is concerned that the rate of material loss is not uniform in time. While this has been noted for many years, some of its consequences have only lately been emphasized. Thus, as Thiruvengadam and Preiser<sup>(50)</sup> have pointed out, the comparison of test results can be very misleading if not based on corresponding phases of the rate-time curve; therefore, the rather common practice of the earlier literature, to test all specimens for the same length of time is subject to criticism. The authors of Reference 50 proposed that characteristic erosion-time curves could be described in terms of four zones: an incubation zone with no weight loss, an accumulation zone with loss rate increasing to a peak, an attenuation zone with decreasing loss rate, and finally, a

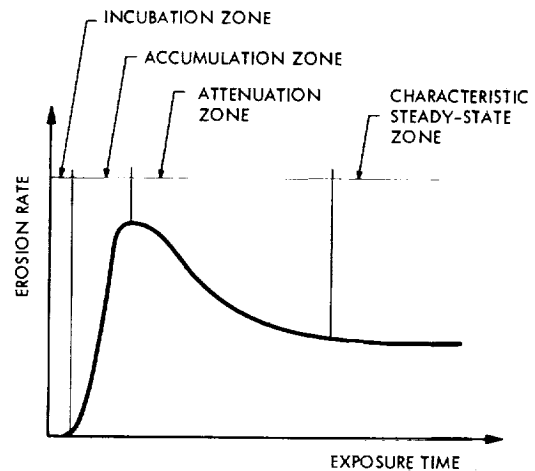
---

\* F. J. Heymann, Senior Engineer, Development Engineering Department, Westinghouse Steam Divisions, Westinghouse Electric Corp., Lester, Pa.

steady-state zone with constant loss rate, Figure 3.2-1. They do not attempt any detailed explanation of these zones, but suggest that the first three zones are influenced by the initial condition of the surface and that only the final zone is truly characteristic of the material itself and that it should be used for comparison or correlation purposes. This particular suggestion is disputed by Plesset and Devine<sup>(51)</sup>, who showed photographically that in a magnetostrictive oscillator the attenuation zone is associated with a cavitation cloud of much reduced intensity, attributed to hydrodynamic damping effects due to the heavily roughened specimen surface. Moreover, the authors of Reference 51 stated that the accumulation zone and the attenuation zone are connected by a period of essentially uniform high loss rate persisting for some time, rather than by the narrow peak described by Reference 50, and that there is no real indication of any final steady-state zone. (See Figure 3.2-2.) Similar observations have been made by a number of recent investigators.

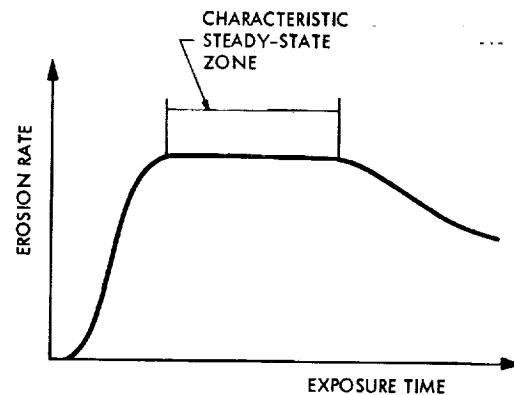
Thus, both Hobbs,<sup>(38)</sup> using a magnetostrictive oscillator cavitation test, and Pearson,<sup>(8,12)</sup> using a drop impingement erosion rig, have called the region of maximum erosion rate the "steady-state" period, and have based their correlations of erosion with material properties and test conditions (such as oscillation amplitude or impingement velocity) on this maximum loss rate. Both have associated the declining loss-rate of final period with heavy surface damage, as did Reference 51, and feel that it is not a practicable measure of the erosion resistance. This, for practical reasons, has also been the approach adopted in Section 3.1 of this report.

All of the previously mentioned results exhibited what may be called the conventional pattern or some minor variation thereof. (For an actual example, see Figure 3.2-3.) However, there are erosion results which do not follow this pattern at all. Thus, Lichtman, et al,<sup>(52)</sup> presented loss-time curves many of which exhibit no apparent incubation or acceleration stages, but rather begin with a maximum rate which declines thereafter (See Figure 3.2-4.) These results were obtained in a rotating disc cavitation device.



611131-3B

Figure 3.2-1 Characteristic Rate-Time Curve According to Thiruvengadam



611131-2B

Figure 3.2-2 Characteristic Rate-Time Curve According to Plesset, Hobbs, and Pearson

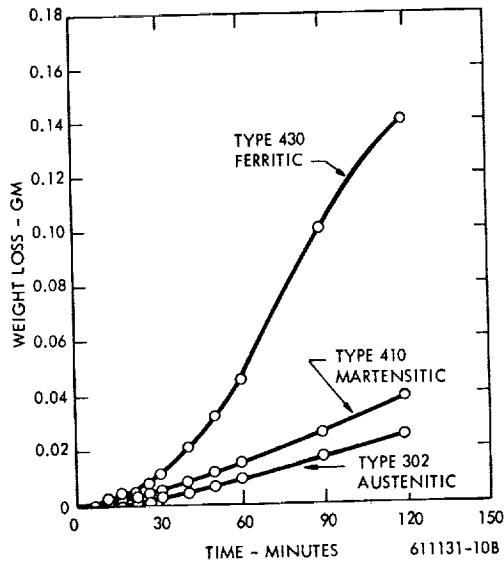


Figure 3.2-3 Typical Cumulative Erosion-Time Curves from Cavitation Tests, Adapted from Figure 7 of Reference 36. (Magnetostriction Device, in Distilled Water)

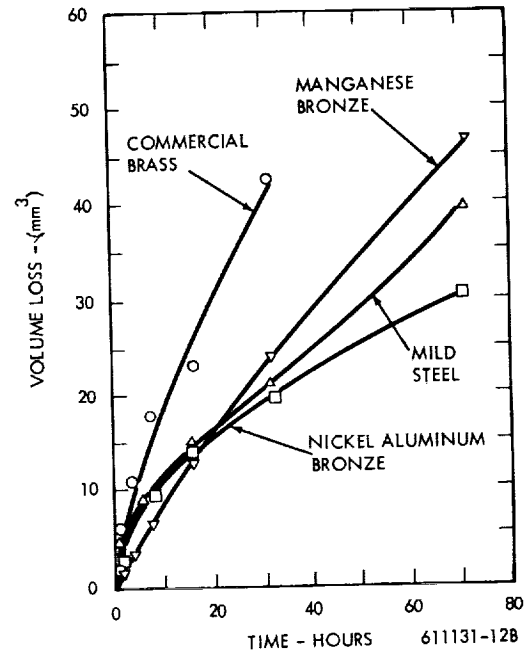


Figure 3.2-4 Cumulative Cavitation Erosion-Time Curves Which Begin at Maximum Rate, Adapted from Figure 24 of Reference 52. (Rotating Disc Device at 150 ft/sec)

Exactly the same type of result has been obtained in the spray impingement erosion test facility at the Westinghouse Steam Divisions Development Laboratory. Erosion rates invariably seem to begin at a maximum value and then decrease - rapidly at first, and then more gradually leading into or approaching a lower steady-state value. Figure 3.2-5 shows some characteristic erosion rate curves obtained by curve fitting through points obtained from several specimens for each material. One might suspect that incubation and acceleration stages lie in the region to the left of the curves as shown, and were simply missed because initial weight loss readings were generally not taken until after about two hours of exposure. To check this, the weight loss of one specimen - a titanium alloy of fairly good erosion resistance - was measured after five minutes of exposure and several more times during the first hour of testing. The result is shown in Figure 3.2-6 and suggests that the erosion rate does in fact begin at a maximum value, or, if there is an

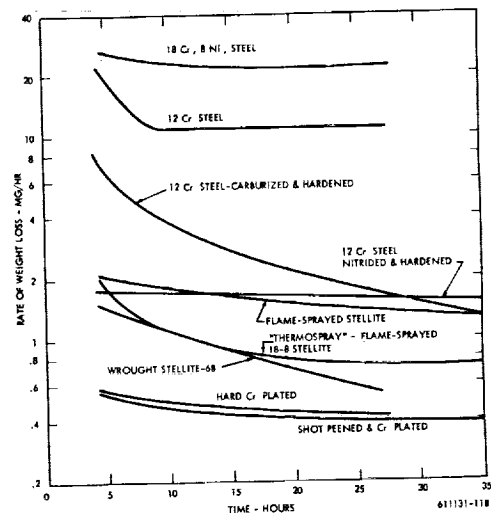


Figure 3.2-5 Typical Erosion Rate-Time Curve Obtained in Westinghouse Steam Division Spray Impingement Facility During 1956-1959

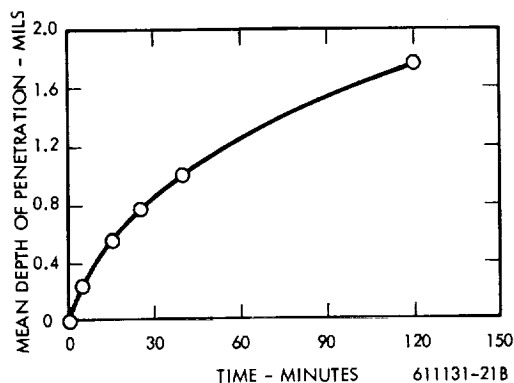


Figure 3.2-6 Early Loss Measurements for a Titanium (6% Al, 4% V) Alloy Tested in the Westinghouse Steam Division Facility)

incubation stage, it occurred within the first minute. The latter alternative is supported by the analytic model to be described. In all of the titanium specimens that were tested the erosion rate has continued to decrease for at least 30 hours. It may, however, be worth noting that Thiruvengadam(28) has shown the rotating disc to be the most intensive cavitation damage device, and that the Westinghouse test facility produces impingement of probably rather small droplets at a high velocity, probably exceeding 2000 ft/sec. Thus, single-impact damage may be occurring in both cases, contributing to the de-emphasis or lack of an incubation period.

The object of this section of the report is to show that a simple statistical model of the erosion process, which regards erosion as a multiplicity of fatigue failures, can predict characteristic rate-time curves of most observed types. Further, this section discusses some of the implications of this model in relation to the measurement and correlation problem.

### 3.2.2 Effect of Material Removal Mechanisms on Rate-Time Pattern

The spectrum of erosion mechanisms in a ductile material may be divided into several regimes as a function of impact intensity, or in the case of droplet impingement, as a function of impact velocity if drop size is held constant. These regimes merge one into the other; there are no sudden transitions between them.

For very low velocities below some first threshold value, no measurable damage or material loss will occur during any practical exposure time, or material loss is confined to isolated weak spots. Such threshold velocities, empirically deduced from test or operating experience or arbitrarily derived from the endurance limit of the material by some safety factor, have been used as design guides in some phases of steam turbine and condenser design. It is not fully established whether there actually is a velocity below which erosion will never occur: Honegger(2) doubted it; and Vater,(25) who suggested that the dependence of erosion on velocity could be regarded and plotted analogously to the dependence of fatigue life on applied stress, regarded the erosion process as one somewhat similar to corrosion fatigue (in which there is no endurance limit). He, therefore, stated that the threshold velocity has to be defined as that velocity below which no measurable weight loss occurred after some specified number of impacts. In any case, one might say that in this first regime the erosion, if any, corresponds to that in the incubation stage of the conventional rate-time pattern, i.e., it will be low, possibly gradually increasing with some random fluctuations, and will be highly influenced by the initial surface conditions and by the possibility of simultaneous corrosion as shown by Wheeler.(53)

As the velocity exceeds the first threshold, something akin to fatigue failure becomes the predominant failure mechanism. Metallurgical observations substantiating this, and descriptions of the probable sequence of events leading to failure and the formation of loose fragments, have been provided by many investigators including Vater,(25) von Schwartz, et al,(54) Brunton,(10) and Marriott and Rowden.(19)

Some investigators have found more plastic deformation in the surface than might be expected. Thus, Thomas<sup>(16)</sup> noted small plastic depressions in the surface during the early stages of exposure at velocities whose presumed impact pressures were less than the yield point of the material. Brandenberger and De Haller,<sup>(1)</sup> on the basis of extensive radiographic studies, concluded that fracture in erosion is neither like static fracture nor like fatigue fracture, but is accompanied by a degree of damage to the crystal structure which is intermediate between that associated with those failure modes. It must be remembered, though, that the stress-geometry condition - at least when the surface is still relatively smooth - is not of such a nature as to make static rupture easily possible: thus, the general regime of predominant fatigue or repeated-impact rupture will extend well into the velocity range where each drop could be expected to produce noticeable plastic deformation. As the velocity increases, the regions of plastic deformation presumably spread from the immediate vicinity of the fracture surface toward a general deformation of the eventually-produced erosion fragments. In this regime one may expect to find rate-time curves exhibiting the conventional pattern, i.e., an incubation stage related to the fact that a certain number of impacts are required before fatigue failures occur, an acceleration stage, possibly a steady-state stage, an attenuation stage, and possibly a final steady-state stage, though probably no generalizations should be made about the behavior when gross surface damage has set in. The possibility of relating these phases in the erosion rate-time curve more specifically to the fatigue properties of the material will be explored in the following sections of this report.

A second threshold velocity may be associated with that velocity at which the material loss due to single-impact damage process becomes significant. This is probably related to the visible damage threshold described by DeCorso and Kothmann,<sup>(24,43)</sup> above which a single impact leaves a distinct crater in a smooth material surface. This regime eventually must merge into the regime of hypervelocity impact. The exact determination of the second threshold velocity from the point of view of material removal is difficult, because in

single-impact experiments - such as those performed by DeCorso,<sup>(24)</sup> and also by Brunton,<sup>(10)</sup> Engel<sup>(39,40)</sup> and others - the actual amount of material removed from the surface could not be reliably established, although crater depths or crater profiles were measured. From two curves given in Reference 56, one can deduce that for hypervelocity impact of 1/16 inch diameter aluminum spheres on an aluminum surface, the ratio of target volume loss to crater volume is approximately 0.15 at a velocity of 7 km/sec (23,000 ft/sec), reducing to about 0.09 at 4 km/sec (13,000 ft/sec). One may cautiously infer from this that at the velocities of interest, say 1000-4000 ft/sec, the corresponding ratio will be very much smaller yet. (This inference should be valid qualitatively although the actual material removal mechanism in the hypervelocity regime is a liquid-like flow of the target material accompanied with some splashing out, whereas that in the regime of interest is related to the shear effect of radial outflow.) Of course, this must be balanced by the fact that such loss occurs with each impinging drop, whereas many repeated impacts over some finite area are required to generate one erosion fragment by the fatigue failure mechanism. For any quantitative estimate of the relative significance of the two mechanisms, more data are needed on each.

Qualitatively, one may say that as single-impact erosion becomes significant, the incubation period can no longer be a zero-weight loss period, but rather will begin by exhibiting an erosion rate corresponding to the single-impact erosion. This rate increases in time as additional fatigue-type erosion sets in. Fatigue in this instance probably corresponds more to low-cycle fatigue due to strain cycling than to high-cycle fatigue due to stress-cycling. The geometry of the eroded surface will now be affected by the heavy plastic deformation due to each drop as well as the breaking away of larger erosion fragments due to fatigue fractures. Eventually, as single-impact erosion becomes the predominant mechanism, one would expect to find little or no evidence of any incubation period, and the surface geometry should rapidly approach a steady-state condition, so that one might expect relatively little change of erosion rate with time.



### 3.2.3 An Analytic Model of the Erosion Rate-Time Relationship

#### 3.2.3.1 Qualitative Description of Proposed Model

As seen in the previous section, the conventional erosion-rate versus time pattern is that associated with a predominant fatigue mechanism for material removal. It is in this regime that most of the test data and the practical experience lie. As is well known, fatigue is intrinsically a statistical process exhibiting a considerable scatter, and this fact will be utilized in developing an analytical model for the erosion rate-time pattern applicable to this regime. The qualitative results have interesting implications with reference to the previously reviewed findings and to previously-attempted correlations between erosion and fatigue data. The approach to be described, though numerical in nature, can at this time predict no more than qualitative trends and should be considered as exploratory.

The basic reasoning of the model is as follows:

It is assumed that each small element of surface is subjected to an impact fatigue environment and that after a certain time (i.e., a certain number of impacts) it will be detached from the surface as an erosion fragment, due to sub-surface fatigue failure. The time-to-failure distribution function for these newly-exposed surfaces will probably not be the same as that for the original surface. Unlike the original surface the newly-exposed surfaces will have been subjected to some sub-surface stress condition even before being exposed to direct impingement, and the surface geometry will no longer be a plane but a series of pits. Further, it is assumed that when many such surface elements are considered, the individual times required for their removal would be described by some statistical distribution function, much as the number of cycles to failure of a large number of fatigue specimens (stressed to the same level) can be described by a distribution function. When erosion

fragments are removed and expose fresh surface to impingement attack, the time to remove elements of this new surface will likewise be described by a distribution function, and so on.

In the case of conventional fatigue specimens, the distribution occurs primarily as a result of the statistical nature of the fatigue process itself. In the case of erosion fragments it must ultimately reflect the variations in the concentration and the severity of impacts (i.e., droplet velocities and sizes), variations in the local surface geometry and properties, and variations in the size of fragments formed. At present, however, one arbitrary distribution curve is assumed to represent all of these sources of scatter.

Qualitatively, it can be seen that if these distributions had very little scatter or dispersion, i.e., if the lifetimes of all surface elements were about equal, then the erosion rate would be zero until that lifetime was reached; at this instant a very high rate would be exhibited while all of the original surface flaked off, to be followed by another interval of zero rate until the second layer flaked off, etc.

If, however, these distributions have a significant dispersion, one can predict that this will result in a rate-time curve which up to a first peak looks somewhat like the distribution curve, but in which subsequent peaks and valleys are attenuated and a steady-state rate is approached. An incubation period will exist if the dispersion is not excessive. One might think of the variation in the surface element lifetimes as dispersing the periodicity associated with one layer being removed after another.

The preliminary mathematical formulation and computer program considered one distribution function applicable to the original surface, and one other applicable to each of the subsequently exposed surfaces. Both were specified as normal distributions truncated and normalized over a finite time span. Thus the significant input parameters were the nominal mean lifetime ( $M_F$ ) and standard deviation ( $\sigma_F$ ) for the original surface, and the corresponding values ( $M_G$  and  $\sigma_G$ ) for the undersurfaces. Figure 3.2-7 shows some rate-time curves obtained by this program,

with the distribution parameters as indicated. Note that the attaining of a steady-state rate is hastened both by increasing the dispersion of the functions, and by specifying a shorter mean lifetime for the undersurfaces as compared to the original surface.

Fluctuations such as shown in Figure 3.2-7 have occasionally been observed, as illustrated by Figure 3.2-8 which shows rate-time curves computed from experimental cumulative erosion curves presented by Kent.<sup>(57)</sup> Moreover, fluctuations which would appear quite prominent in rate-time curves are not nearly as evident if the same data are plotted as cumulative erosion versus time - which is how the data are actually obtained. Therefore, it seems quite conceivable that in many cases such fluctuations would barely have been noted and would have been smoothed out of the raw data, or might have been lost entirely through the data points being too far apart in time.

The fluctuations, however, are by no means an inevitable consequence of this model if non-symmetrical distribution functions are used, as will be seen in the results obtained from the elaborated formulation of the model, described below.

### 3.2.3.2 Description and Results of Elaborated Model

In the elaborated analysis we have chosen to use log-normal distribution functions, since — as shown by References 58 and 59 — these provide a reasonable representation of fatigue life data. For added flexibility one can adopt a delayed log-normal, i.e., one which would appear as a normal distribution if the frequency of failures were plotted versus  $\log(t - T_0)$ , where  $T_0$  represents a delay time introduced to ensure that no failures occur prior to time  $t = T_0$ .

The distribution, when plotted on a  $\log_{10}$  scale, is then described by its mean ( $m$ ) and its standard deviation ( $\sigma$ ). But one must use the distribution as transformed onto arithmetic or real-time scales. An important point to note is that while in a symmetrical distribution the mean, median, and mode values coincide, that is not true for a skew distribution such as the log-normal. The real-time values

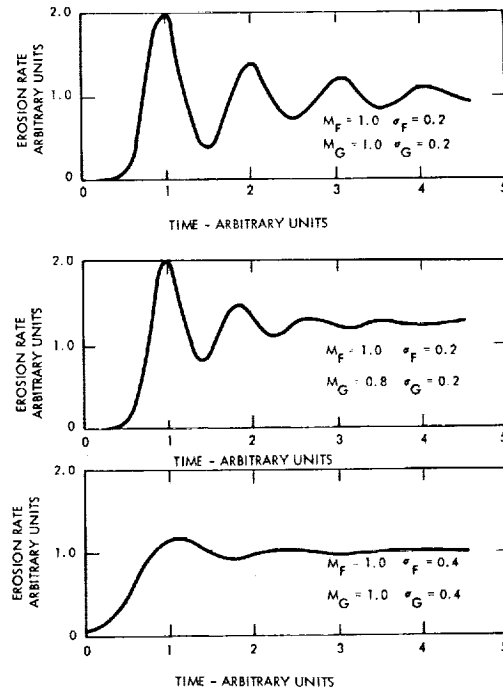


Figure 3.2-7 Typical Computed Erosion Rate-Time Curves from Preliminary Statistical Model, Using Normal Distribution Functions

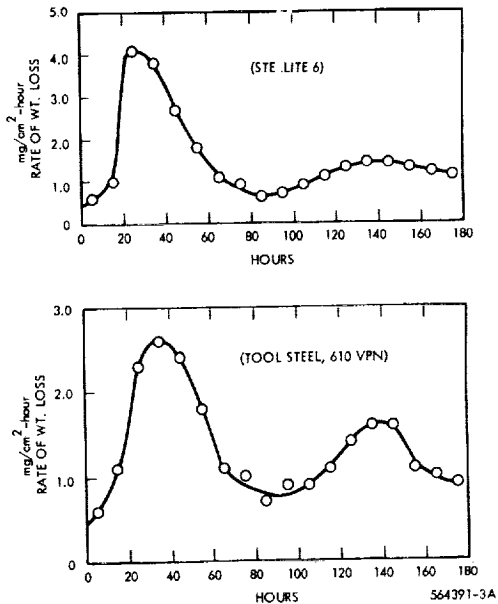


Figure 3.2-8 Experimental Erosion Rate-Time Curves, Computed from Cumulative Erosion Curves Given in Reference 32

corresponding to  $m$ , which is denoted by  $T_m = 10^m$ , establishes the median value of the log-normal distribution — i.e., that value of  $t$  at which half of the specimens (or surface elements) will have failed. This is the value generally used to establish a point of an engineering S-N curve. In the delayed log-normal, the median value is given by  $M = T_0 + T_m$ . The mode, or peak in the distribution curves, will occur at a time value less than  $M$ . The mean value, or arithmetic average of all life-times, will occur at a time value greater than  $M$ , or specifically at a time  $E = T_0 + T_m \times 10^{1.15\sigma^2}$ . For purposes of discussion, all distributions can be characterized by their values of  $T_0$ ,  $\sigma$ , and either  $M$  or  $E$ .

The elaborated model permits the specifying of a different distribution function for each level below the original surface, and of two different functions for the original surface: one for the unaffected surface, in which erosion takes place by the initiation of new pits, and one for the affected surface, which is that surrounding existing pits and in which erosion is presumed to take place by the lateral growth of these pits. The program computes the rate of erosion, the cumulative erosion, and the exposed area at each level, from which in turn, it can compute an average surface roughness at selected time points.

The number of variations which could be investigated with this program is unlimited, and all that can be demonstrated here are some of the important effects. The most significant of these is the effect of the dispersion parameter  $\sigma$ . References 49 and 59 suggest that in conventional fatigue tests,  $\sigma$ , on a  $\log_{10}$  scale, ranges approximately from 0.15 to 0.40, and for erosion fragment lifetimes even higher dispersions may be expected. Figure 3.2-9 shows computed erosion time curves for various values of  $\sigma$  from 0.15 to 0.80, with the median ( $M$ ) held constant; Figure 3.2-10 shows a corresponding set of curves with the mean ( $E$ ) held constant. In each case  $T_0 = 0$ , and the same distribution is assumed for all surfaces and levels. Since in such cases the eventual steady-state erosion rate must be proportional to the reciprocal of the mean lifetime, all curves in Figure 3.2-10 approach the same steady-state rate.

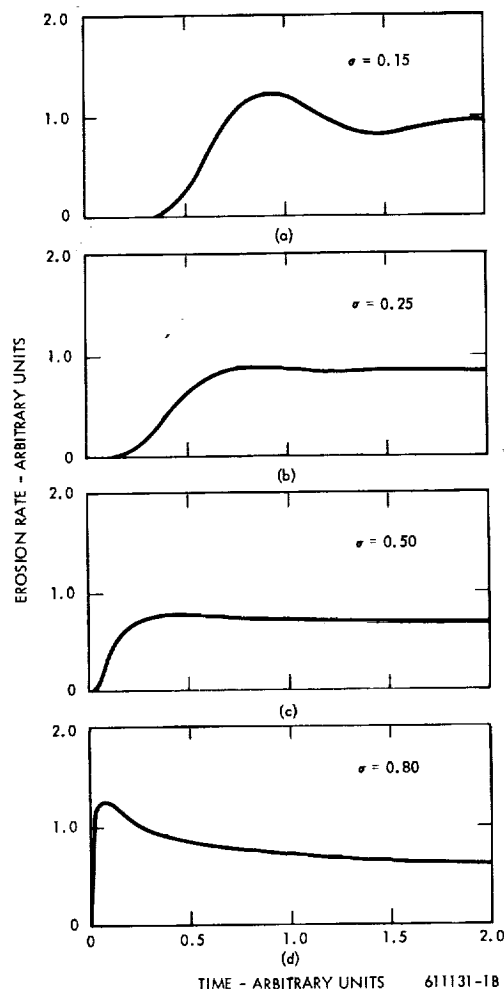


Figure 3.2-9 Computed Rate-Time Curves Based on Log-Normal Distributions, Showing Effect of Varying Dispersion,  $\sigma$ , with Median at Constant,  $M = 1.0$

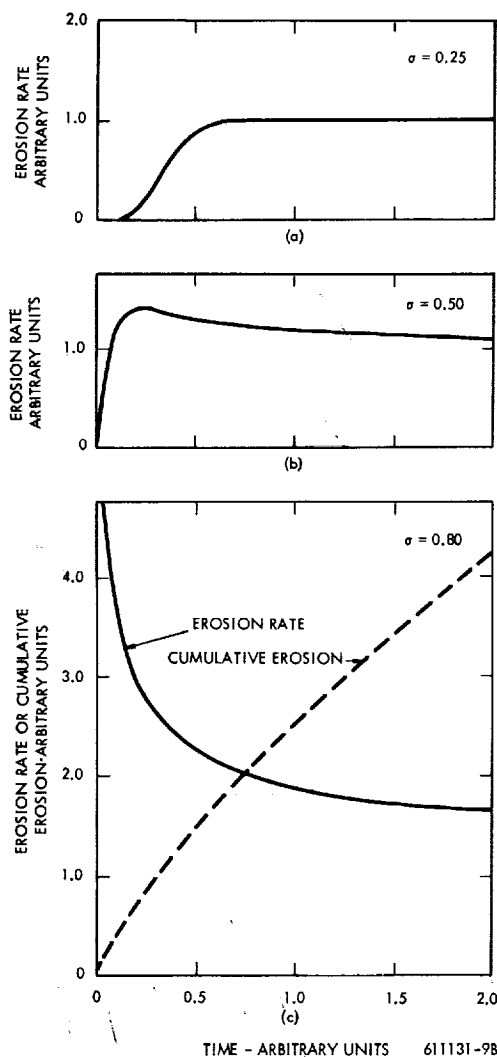


Figure 3.2-10 Computed Curves Based on Log-Normal Distributions, Showing Effect of Varying Dispersion,  $\sigma$ , with Mean at Constant,  $E = 1.0$

Two striking results appear from these curves: First, the maximum erosion rates vary considerably. Second, almost all of the experimentally-found rate-time patterns can be at least qualitatively generated by proper choice of the dispersion parameter  $\sigma$ . When  $\sigma$  is small, the curves exhibit damped fluctuations similar to those of Figure 3.2-7. When  $\sigma$  is increased, the fluctuations die out and the steady-state rate is attained quite quickly. When  $\sigma$  is further increased, a single peak appears in the curve, and at very high values of  $\sigma$  this peak may occur so early that the time resolution is just not fine enough to show the acceleration stage of the rate-time curve, and the curve therefore appears to begin at its maximum value. The same is probably true for experimental data like that of Figures 3.2-4, 5 and 6. It does not seem unreasonable to suppose that erosion due to very small droplets, where each impact stresses only a minute portion of the surface area, would be characterized by a high dispersion in the fragment lifetimes.

In many of the curves of Figures 3.2-9 and 10 the ratio of the erosion peak to the expected steady-state value is not as great as sometimes found in practice — but it should be recognized that at times values greater than the median, the surface has suffered heavy erosion damage and one may therefore expect that geometric effects, such as suggested by References 2, 8, and 51, may have set in by this time and have caused an additional diminution of the erosion rate and possibly suppression of further fluctuations. Certainly one would expect the results predicted by this analysis to be at least modified by the geometric effects. Thus, Figures 3.2-9 and 3.2-10 may correspond to experimental results of the type of Figures 3.2-1 and Figures 3.2-9 and 3.2-10 to results of the type of Figure 3.2-2. It is possible, however, that some appropriate combination of distribution functions for the different surfaces could result in a plateau such as in Figure 3.2-2, which then again would not correspond to a steady-state value.

Figure 3.2-11 shows an example of slowing down the loss rate from the unaffected surface as compared to that of all other surfaces — which are presumed to be more susceptible to erosion because of the irregular geometry. This case is identical to that of Figure 3.2-9 except that for the unaffected surface the median lifetime has been increased to 3.0. Note that the shape of the rate curve has been made more similar to that typified by Figure 3.2-1; the cumulative loss rate is also shown and is quite similar to typical curves such as Figure 3.2-3.

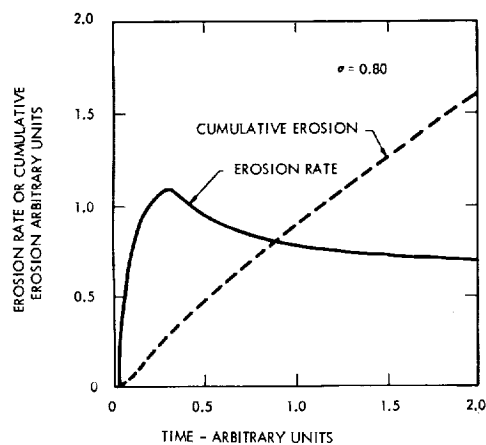


Figure 3.2-11 Effect of Higher Median Value for "Unaffected" Surface ( $M_u = 3.0$ ) than for Other Surfaces ( $M = 1.0$ ). (Compare with Figure 3.2-9. Note Difference in Vertical Scale)

Figure 3.2-12 shows surface profile curves, at various values of time  $T$ , for some of the previous cases. The ordinates indicate the surface level, with 0 representing the original surface. The abscissas represent the area not yet eroded away at each level. The difference in abscissa between adjacent levels represents the area exposed at the lower of the two levels. Note that in Figure 3.2-12, a case of low dispersion value ( $\sigma = 0.25$ ), the erosion is shallower and more evenly distributed than

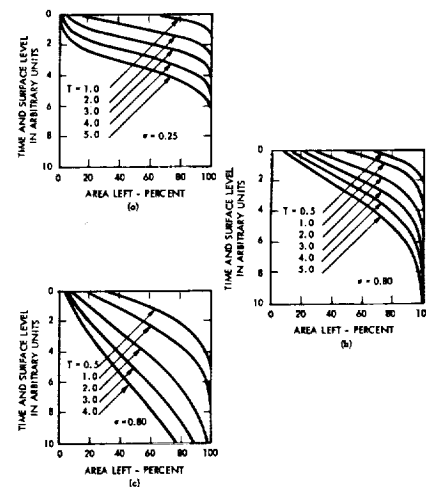


Figure 3.2-12 Examples of Computed "Surface Profile" Curves (Showing the Uneroded Area as a Function of Level Below the Original Surface, at Various Values of Time: (a) - Corresponding to Figure 3.2-9 (b) - Corresponding to Figure 3.2-11 (c) - Corresponding to Figure 3.2-10

in the other two cases which represent high dispersion values ( $\sigma = 0.8$ ). This suggests that the geometric effects which tend to reduce the erosion rate — i.e., those due to high roughness — are delayed in the former case; this may explain why the maximum erosion rate in such a case may persist for some time and give rise to rate curves typified by Figure 3.2-2. Figure 3.2-13 shows the computed surface roughness versus computed mean depth of penetration, for the same three cases, confirming the lower roughness associated with a lower dispersion value.

### 3.2.3.3 Discussion and Conclusions

Now to examine the implications of this model with respect to correlations of incubation times and erosion rates. Since the incubation time seems related to the fatigue nature of erosion, several investigators have attempted correlations reflecting this. Thus, Leith and Thompson<sup>(36)</sup> correlated the incubation times of several materials with the corrosion fatigue limit for  $10^7$  cycles of these materials.

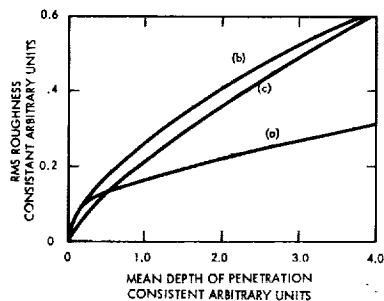


Figure 3.2-13 Computed rms Surface Roughness versus Mean Depth of Penetration (Cumulative Erosion) for Figure 3.2-12. The letters (a) (b) and (c) correspond to the Similarly-Designated Cases in Figure 3.2-12

Mathieson and Hobbs<sup>(60)</sup> made a similar correlation with the conventional endurance limit for several aluminum alloys. In both cases the results were reasonably consistent, but the approach is hardly logical since the incubation time in erosion surely should be related to a finite-lifetime to failure, rather than to a stress value at which no failure occurs. Thus, the success of these correlations depended on a second, implicit correlation between the finite fatigue lives at the test stress, and the endurance limits valid for the group of materials compared. Ripken, et al,<sup>(37)</sup> have used a more logical approach, and have correlated the number of impacts corresponding to the incubation time at a given impact velocity, with the number of cycles to failure in bending fatigue at an equivalent stress level. The stress level was assumed to be given by the waterhammer pressure ( $\rho CV$ ). The incubation period was defined by the intercept, on the time axis of the cumulative weight loss curve, of the straight line approximating the high erosion rate stage.

If the previously developed model is valid, this procedure is still not quite correct. The statistical model implies that the apparent incubation period depends not only on the mean lifetime of the erosion fragments but also on the scatter or dispersion in these lifetimes. The erosion-rate becomes non-zero when the first element fails, and continues

to increase until approximately the mode or most probable value of the lifetime is reached on the top surface. But it is the mean value — which may occur later yet if the distribution is skewed — which corresponds to the nominal lifetime at the appropriate stress as obtained from a conventional S-N fatigue curve. Whether either the median lifetime or the associated scatter in erosion fragments corresponds to that of full-scale bending or pull-type fatigue specimens is at present a moot question. However, the discrepancies in the correlations of Reference 37 are in the direction which the above argument would predict.

If one stipulates a steady-state erosion process, then the erosion rate would certainly be inversely proportional to the mean lifetime of erosion fragments (provided their size distribution remained constant). This is the basis from which one can draw the analogy between the  $(\text{loss rate})^{-1}$  versus impact velocity in erosion, and cycles to failure versus stress level in fatigue, as proposed by Reference 25. This appears to provide a rational basis for attempting to predict an erosion-speed relationship on the basis of known fatigue data for the material, although to our knowledge this attempt has not been made. But here, again, the statistical model suggests that the obvious approach is not quite correct. It implies that the maximum erosion rate — which many investigators have linearized and used in correlations, for good and valid practical reasons — does not necessarily represent a steady-state erosion process at all, but rather the deluge of erosion fragments from the top surface layer which takes place in the vicinity of the most probable fragment lifetime from the beginning of exposure. Thus again, the maximum instantaneous erosion rate is not merely a function of the average fatigue life of the surface elements but also of the scatter in lifetimes. Consequently, any external or internal effect which influences that scatter will influence the maximum erosion rate, even though it may not affect the eventual hypothetical steady-state rate.

Finally, what can this model contribute toward the resolution of the dispute referred to in Section 3.2.1. First, it implies that Reference 50 is correct in claiming that the erosion rates during the stages encompassing the first peak in the rate-time curve are not characteristic merely of the material under test, since the shape of this curve depends on the shape of distribution functions which, in turn, depends in part on characteristics of the test method such as the distribution of bubble or droplet sizes, etc. Secondly, it implies that while the erosion rate would, in the absence of other influences tend toward a steady-state value as postulated by Reference 50, this generally occurs only after most of the original surface has eroded away, by which time the surface damage will be so severe as to make the erosion conditions susceptible to geometry effects such as described in Reference 51. In short, the instantaneous erosion rate may never be characteristic of only the material, and for valid correlations it will become necessary to standardize the test method very carefully, or to use properly chosen cumulative erosion measurements, such as the time required to attain some specified value of the rationalized erosion (MDP) of practical significance.

### 3.2.4 Mathematical Formulation of Model

#### 3.2.4.1 First Simplified Formulation

Let any surface exposed to erosion be thought of as consisting of elementary areas (or volumes, if their thickness is considered) whose lifetimes under the erosion attack can be described by a normalized distribution function  $f(t)$ . Thus by definition

$$\int_0^{\infty} f(t) dt = 1.0 \quad (21)$$

and the distribution function for a specific area  $A$ , exposed to erosion from time  $t = 0$ , is therefore

$$F_A(t) = A f(t) \quad (22)$$

Since a surface element is lost from the surface when its lifetime is reached, Equation 22 can equally well be regarded as a loss rate function for the area  $A$ .

Equation 22 may be further generalized by stating that the loss rate from an area  $A_1$ , first exposed to erosion at time  $t = T_1$ , is thereafter given by

$$F_1(t) = A_1 f(t - T_1) \quad (23)$$

Let us now consider the original or top surface of a body exposed to erosion. One may take its area to be unity, and every portion of its area is simultaneously exposed to erosion at time  $t = 0$ . Thus  $f(t)$  adequately describes the loss rate from the top surface. As surface area is eroded, or lost from the top surface, an equal area is created or exposed at the second level located at distance  $h$  below the surface, where  $h$  is assumed as the thickness of erosion fragments. For convenience, the thickness  $h$  will also be assigned a numerical value of unity on some appropriate scale. In turn, the second level surface will be eroded to expose a third level surface and so on. But in computing the actual loss rates from all of the undersurfaces one must recognize that the lifetimes of surface elements must be measured from the time they were first exposed, and the total loss rate from all surface elements which were first exposed during a time increment  $dT$  at time  $T$  depends on the total area which was first exposed during that time interval.

Let  $Y(t)$  be the total rate of erosion, from all levels, at time  $t$ . This is what one desired to compute. But  $Y(t)$  is also equal to the rate at which new surface area is exposed, at all levels below the top surface, at time  $t$ . (Strictly speaking, it is proportional to it, but with  $h = 1.0$  it is numerically equal.)

Thus, the total surface area first exposed during increment  $dT$  at time  $T$ , is  $Y(T) dT$ , and the loss rate from this area at time  $t$  is, by Equation 23,

$$F_T(t) = f(t - T) Y(T) dT \quad (24)$$

The total loss rate at time  $t$ , from all undersurfaces, is composed of contributions from all undersurface areas first exposed during all time increments from  $T = 0$  to  $T = t$ , or

$$\int_0^t f(t - T) Y(T) dT$$

The total loss rate or erosion rate,  $Y(t)$ , is the sum of that from the top surface and that contributed by all undersurfaces, or

$$Y(t) = f(t) + \int_0^t f(t-T) Y(T) dT \quad (25)$$

The fact that the contributions from the undersurfaces and from the top surface form two distinct terms in Equation 25 makes it convenient to assign a different distribution function for the top surfaces as compared to all undersurfaces. This is desirable if one wants to reflect the fact that the tip surface has, in many ways, a different nature and history than the undersurfaces exposed as a result of erosion. Finally, one can state

$$Y(t) = f(t) + \int_0^t g(t-T) Y(T) dT \quad (26)$$

where

$f(t)$  = distribution function for top surface  
 $g(t)$  = distribution function for undersurfaces

It is worth noting that Equation 26 is a well-known integral equation having a convolution integral as its last term. A Laplace transformation yields

$$y(s) = f(s) + g(s) y(s)$$

By ordinary algebra

$$y(s) = f(s) / [1 - g(s)] \quad (27)$$

or

$$Y(t) = L^{-1} \left\{ f(s) / [1 - g(s)] \right\} \quad (28)$$

This solution may be useful if Equation 26 has Laplace transform and Equation 27 has an easy inverse transform. Ordinarily, numerical methods are required.

For the initial explorations Equation 26 was computer-programmed directly, using normal distributions for functions  $f(t)$  and  $g(t)$ , normalized over specified time spans rather than between the limits of plus and minus infinity as suggested by Equation 21.

### 3.2.4.2 Formulation of Elaborated Model

In further explorations of this approach, it is desirable not only to keep track of the area exposed at each level as a function of time, so that an average surface profile or surface roughness can be computed, but it also may be desirable to assign different distribution functions for all levels. An analytical continuity approach to this becomes very cumbersome, and since the final evaluation is in any case a numerical one by computer, it becomes advantageous to develop the model as a step-wise process in time, and to have the computer program compute the processes occurring in each time interval, one after the other. In a sense, the computer program becomes a digitalized analog of the physical process.

The crux of the approach is that the program maintains, and up-dates for each time interval, the array  $S_{L,J}$ , in which each value represents the surface area presently existing at level  $L$  and dating back to time interval  $J$  during which it was first exposed as a result of loss from the next-higher level. Thus the total surface area presently existing at level  $L$  would be given by

$$\sum_{J=1}^{N-1} S_{L,J}, \text{ where } N \text{ is the present time interval}$$

at which the evaluating is being done.

Let us now define a modified rate or quotient function  $q(t)$ , which represents the loss rate as a proportion of the remaining area at time  $t$ . In terms of the previously used distribution function  $f(t)$ , this is

$$q(t) = \frac{f(t)}{1.0 - \int_0^t f(t) dt} \quad (29)$$

For computation purposes the continuous function  $q(t)$  is replaced by a loss quotient  $Q_i$  representing the finite amount of loss during the  $i$ th time interval after the surface has first been exposed. This can be represented by

$$Q_i = q(i \Delta t) \Delta t$$



where  $\Delta t$  is the length of a time interval. The program computes and stores all values of  $Q_{L, J}$ , where the additional subscript  $L$  refers to the level; thus a different distribution function  $f(t)$  can be specified for each level.

The total erosion from all levels during time interval  $N$ ,  $Y_N$ , will then be composed of all contributions of the type

$$R_{L, J} = S_{L, J} Q_{L, N-J} \quad (30)$$

where  $R_{L, J}$  represents the loss rate from that area at level  $L$  which was first created during time interval  $J$ . The total erosion rate is therefore approximated by

$$Y_N = \sum_{L=L}^M h_L \sum_{J=1}^{N-1} R_{L, J} \quad (31)$$

$\Delta t$

where  $h_L$  = thickness of erosion fragments lost from the  $L^{\text{th}}$  level

$M$  = total number of levels considered

Using the  $R_{L, J}$  values computed from the  $S_{L, J}$  array which was valid for the beginning of the  $N^{\text{th}}$  time interval, one can readily compute the new values of  $S_{L, J}$  which are valid for the end of the  $N^{\text{th}}$  interval, i.e., for the beginning of the  $(N+1)^{\text{th}}$  interval:

$$[S_{L, J}]_{N+1} = [S_{L, J}]_N - [R_{L, J}]_N \quad (32a)$$

for all values of  $J < N$ , and

$$[S_{L, N}]_{N+1} = \left[ \sum_{J=1}^{N-1} R_{L-1, J} \right]_N \quad (32b)$$

for  $J = N$ .

The manner in which the cumulative erosion, surface profile and surface roughness can be computed from the above-mentioned quantities is straightforward.

The log-normal frequency distribution function as programmed is of the form

$$f(t) = \frac{1}{\sigma(t-T_0)\sqrt{2\pi}} \exp \left\{ -\frac{[\log_e (t-T_0)-m]^2}{2\sigma^2} \right\} \quad (33)$$

This function has the following properties:

The mean, or expected value, is

$$E = T_0 + e^m + (1/2)\sigma^2 \quad (34)$$

The median value is

$$M = T_0 + e^m \quad (35)$$

The mode, or most probable value, is

$$P = T_0 + e^{m-\sigma^2} \quad (36)$$

The input may be prescribed in terms of  $T_0$ ,  $m$ , and  $\sigma$  directly; the latter two may also be prescribed in terms of the equivalent logarithms to base 10, or in terms of the equivalent real-time quantities  $T_m = e^m$  and  $R = e^{\sigma}$ .

#### 3.2.4.3 Discrete Pit Formation and "Affected" Surface

In order to model the probable progress of erosion damage more faithfully, a further elaboration has been introduced for the top surface only. This is based on the observation that erosion tends to proceed by the formation and growth of discrete pits — which may extend to a considerable depth while the adjacent top surface is still intact — rather than by a randomly-distributed depth.

To approach this condition, the top surface is considered as consisting of two kinds of surface: affected areas and unaffected areas. Affected areas are defined as those areas of the top surface immediately surrounding existing erosion pits, whose resistance to erosion may be assumed to be influenced by this fact. Therefore, one distribution function,  $f_a(t)$ , is provided for the affected area, and another,  $f_u(t)$  for the unaffected area which is the remainder of the still existing top surface. (In general one would suppose that  $f_a$  is such as to result in more rapid erosion than  $f_u$ , but the program does not make this a requirement.) The actual amount of area considered as affected is computed as follows: Let  $w$  be a characteristic dimension of erosion fragments which must be prescribed in the

program input. Then the affected area  $A_a$  associated with a pit of surface area  $A_p$  is defined as the area of an annulus of width  $w$  surrounding a circle of area  $A_p$ . In other words, all of the potential erosion fragments bounding upon an existing pit are considered affected area. To carry this calculation through, it is necessary to know the number and size distribution of all pits. This is done as follows: During any time interval  $N$ , the loss from the existing unaffected surface, based on the  $f_u$  distribution function, is divided into an integral number of values  $A_0$  (where  $A_0$  is the area of a circle of diameter  $w$ ). Thus a known number of new pits — all of area  $A_0$  — are said to be initiated. For the subsequent time interval, the new pits are assigned their annulus of affected area. Further enlargement of each of this generation of pits takes place by erosion from the affected area surrounding it, requiring the transformation of additional surrounding area to maintain the previously specified relationship between affected area and pit area. Thus, the number and present size of each generation of pits, and extent of affected area surrounding them, can be established and updated.

The rate of loss from the affected areas is based on the  $f_a$  distribution function, but not in a simple manner. Let us for the moment talk in terms of the continuous functions, though the actual calculations are carried through in terms of step-wise loss quotients. Consider an area which existed as unaffected area until time  $T_T$ , at which time it becomes transformed into affected area. Up until  $T_T$  the loss from this area was governed by  $f_u$ ; henceforth, it is to be governed by  $f_a$ . Upon reflection it can be seen that our purpose would not be served in any realistic way by simply saying that at  $t = T_T$  the loss rate jumps from  $f_u(T_T)$  to  $f_a(T_T)$ , and henceforth is given by  $f_a(t)$ . (In an extreme case,  $f_a(t)$  may represent such rapid erosion that  $T_T$  is well beyond the mean or mode value and  $f_a(T_T)$  is already sensibly zero. Thus no further erosion, rather than more rapid erosion, would result from this switch.) A wholly rigorous approach would have to be based on cumulative fatigue damage theory, but a device which is adequate for our purpose is to require that the  $f_a$  distribution function be entered at an effective time  $T_E$ , such that the cumulative loss due to  $f_a$  at  $T_E$  is equal to the cumulative loss due to  $f_u$  at  $T_T$ , or

$$\int_0^{T_E} f_a(T) dT = \int_0^{T_T} f_u(T) dT \quad (37)$$

If  $T_E$  is defined by Equation 37, then the loss rate from the area under consideration, at any time  $t$  subsequent to  $t = T_T$ , is given by  $f_a(t - T_T + T_E)$ . This device will at least ensure that if a given area is transformed at any time  $T_T$  whatever, then 100 percent of it — no more and no less — will have been lost at time  $t = \infty$ , which is the minimum logical requirement of any realistic approach. For some types of distribution functions, it is possible to express  $T_E$  in terms of  $T_T$  and the function constants. Thus, for the simple case of (normalized) exponential functions, where

$$f_u(t) = p_u e^{-p_u t} \text{ and } f_a(t) = p_a e^{-p_a t}$$

It is easy to show that

$$T_E = T_T (p_a / p_u)$$

An analytical expression can also be obtained for the log-normal distribution, but in many other cases, including the normal distribution,  $T_E$  would have to be computed by trial-and-error procedures from the relationship of Equation 37.

A consequence of this approach is that not only must the total affected area associated with each generation of pits be known, but so must each generation of affected area, since the rate of loss from any portion of the affected area depends on when it had been transformed from the unaffected to affected status. The number of pertinent computations required during the  $N^{\text{th}}$  time interval is therefore  $N^2$ , and the number of memory locations required for the affected area array is  $M^2$ , where  $M$  is the maximum number of time intervals to be computed. This is a compelling argument for making  $M$  reasonably small (100 in our program), which makes for a rather coarser time grid than one would otherwise desire.

The details of the computation method would require too much space to present here, but are generally analogous to the method described for the undersurfaces by Equations 30 through 32.

It should be emphasized merely that the concept of erosion by discrete particles of specified size is applied only to the initiation of new pits in the unaffected surface, and that the loss rates from the second and lower layers do not concern themselves with whether the second layer surface was exposed as a result of loss from unaffected or affected surface. This distinction is only made for the loss rates from the top surface itself.

The program in its present form has provision for using either log-normal distributions (to represent fatigue damage), or exponential distributions (to represent single-impact damage).

### 3.3 HYDRODYNAMIC MODEL OF CORRELATION OF METAL REMOVAL RATES FROM REPETITIVE DROP IMPACT \*

#### 3.3.1 Background

This section establishes numerical relationships between materials properties and the external variables and drop impingement loss rates. This is done through the use of a hydrodynamic model of correlation of metal removal rates from repetitive drop impacts applied to empirical information. This empirical information is that on metal removal by water drops impacting on steam turbine blade materials made available by the Central Electricity Generating Board (CEGB) of the United Kingdom<sup>(61, 62)</sup>.

The CEGB results are from multiple impact tests. In these tests, samples of metals to be eroded are mounted around the rim of a wheel. Once each revolution of the wheel, each sample intersects a curtain of water drops of relatively uniform size at a known relative velocity. It seems likely that after a small number of impacts the water wets the sample and a film of water develops on the surface. In principle, this can change the maximum impact pressure and duration of impact from that resulting from the impact of a water drop on a dry surface.

Many have objected to this hypothesis on the basis that this is contrary to their experience with splashing water. They say splashing water does not form thin films, it runs from surfaces as drops or rivulets. However, this drop-rivulet behavior is probably true for contaminated surfaces. The contaminated surface is the type ordinarily seen, even if the contamination is only from fingerprints. In this connection it has been pointed out, to the author, by A. P. Fraas<sup>(63)</sup> that it is next to impossible to maintain dropwise-condensation in condensing water systems for useful lengths of times. The scrubbing action of the condensing water removes the surface contaminants and the process changes from drop-type condensation to film condensation. The scrubbing should be even more thorough in a repetitive drop impact situation. Therefore, observation of water runoff from casually prepared fresh surfaces is likely to be completely misleading as to the nature of this runoff after many impacts.

The basic approach used is that of dimensional analysis. The virtue of dimensionless analysis is its mathematical simplicity. The drawback is that its use to correlate data is valid only where it is reasonably sure the data exhibit similitude over the range of the data and the pertinent variables are known.

In the area of drop impact erosion there is very little in the way of established definitions, conventions, or theories by which conditions of similitude or selection of pertinent variables can be established. For this reason, the bulk of this section is concerned with establishing a reasonable presumption that the variables selected are the pertinent ones and that a condition of similitude exists between the correlated data.

#### 3.3.2 Review of Some Observations on Drop Impact Material Removal

##### 3.3.2.1 Single Impact Removal

As has been pointed out by several investigators<sup>(64, 65)</sup>, there are at least two mechanisms of material removal operative during single liquid impact on metal surfaces. The first of these is the loss of material as the direct result of a hammer blow of a liquid drop or jet on the solid surface. The

---

\* W. D. Pouchot, Advisory Engineer, Systems and Technology Dept., Astronuclear Laboratory, Westinghouse Electric Corp.

second is that small projections of metal are removed by the fluid squirting out of the region of liquid compression created and maintained momentarily by the liquid-solid impact. For the first of these mechanisms, at least for single impact damage, there is much evidence that the extent of the damage is directly proportional to the size of the drop or jet causing the damage <sup>(64, 66)</sup>. There is more limited evidence that the same is true for single-impact lateral outflow damage <sup>(65)</sup> as well. It may be concluded from experimental evidence, that the damage done by single liquid impacts on dry metal surfaces is proportionally the same for small and large drops. De Corso and Kothman <sup>(64)</sup> in reporting results of their single-impact tests conclude that larger jets require a lower impact velocity than smaller jets to cause visible damage. Their data were taken at velocities greatly above a visibility threshold. The data also have a large scatter. Extrapolation of this data back to a visible threshold is a very doubtful procedure. In at least one of these cases such extrapolation will lead to a conclusion opposite to the one drawn.

• A General Description After Hancox and Brunton<sup>(65)</sup>

With multiple impact metal removal as with single impact metal material removal, there is loss of material as a result of the lateral flow of liquid along the surface of the liquid compressed by the primary impact. Paraphrasing Hancox and Brunton, erosion of metals begins with a roughening of the surface due to the appearance of small surface depressions and tilted grains. The larger projections in the roughened surface are later sheared by the flow to give surface pits. The pits grow and erosion continues either by a ductile tearing action or by the propagation of brittle fractures from the bottom of the pits. The erosion of metals depends entirely on the initial formation of small regions of plastic deformation. If a metal surface can be kept smooth by preventing roughening due to depressions and grain boundaries, then erosive action due to outward flow cannot take place. It seems, however, that in plastically deforming materials a few areas can be deformed at stress levels considerably below the average flow stress. As soon as this happens, the

change in the shape of the surface leads to stress concentration at projections and depressions, the impact stresses increase, and ductile or brittle fracture brings about erosion. The final stage of erosion in metals is the growth of pits throughout the specimen -- a stage which is accompanied by appreciable weight loss. In metals prone to brittle fracture there is the formation of a network of cracks which fan out from the initial pits. With more ductile metal erosion proceeds by shear fractures in the metal around the pits.

The author interprets these preceding statements of Hancox and Brunton as saying that (1) the initial deformations which lead to erosion are caused by the primary impact of the drops working on weak spots in the surface, but (2) the major source of actual material removal is the secondary impacts from the outflow liquid working on the deformations produced by the primary impact.

• The Stages of Erosion as Defined by Pearson<sup>(67)</sup>

Usually there are several stages of erosion evidenced in multiple impact erosion tests carried out at constant liquid impingement rates, impinging drop diameter, and normal velocity of impingement. These are illustrated in Figure 3.3-1 and are as follows: (1) an incubation period during which the surface is deformed but there is no metal loss from the surface, (2) a period when surface metal loss rises rapidly to a maximum, (3) a period of maximum metal loss rate, and (4) a period when the metal loss rate falls toward or oscillates about an apparent steady-state value.

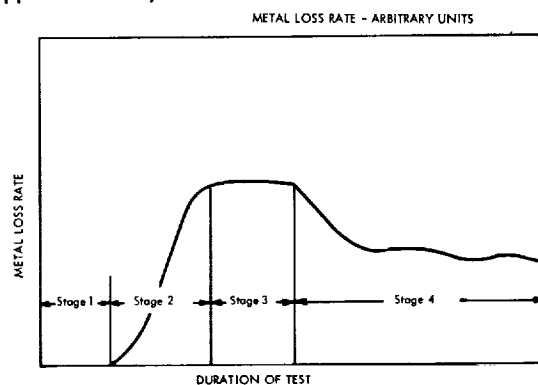


Figure 3.3-1 Model of Stages of Erosion After Pearson

### • CEGB Data

The most extensive tabulations from the CEGB on material removal from steam turbine blade metals by impinging water drops record only the incubation period (stage 1) and the maximum rate of erosion (stage 3). Pearson<sup>(67)</sup> of the CEGB has examined and reported on an extensive set of these experiments carried out using a 12 percent chrome stainless steel.

The stage 1 stainless steel data is shown in Figure 3.3-2. This is a plot of the measured amount of impacting water per unit area required to incubate erosion at various normal impact velocities using a succession of constant diameter drops of the diameters indicated in the figure.

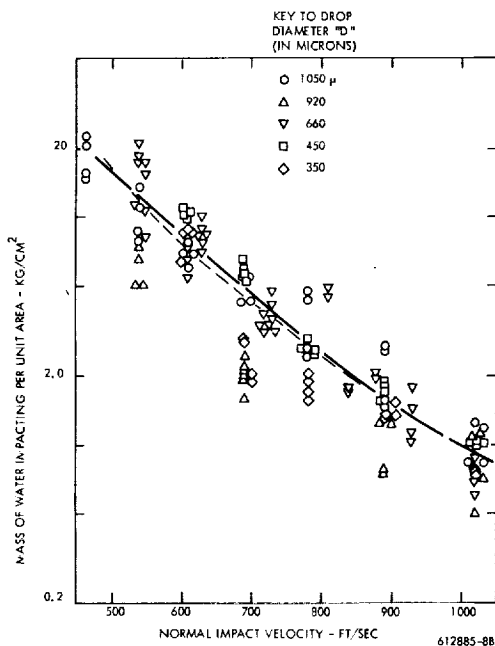


Figure 3.3-2 CEGB 12% Chrome Incubation (Stage 1) Data

The data scatter considerably. It has been noted by Heymann, in section 3.1, that there is no apparent trend to the data with respect to the diameter of drops impacted except at the lower limit of the test range of normal impact velocity.

For both jet impact and drop impact tests, if it is assumed that the duration of an individual impact is directly proportional to jet or drop diameter; the total impulse per unit area to which a particular surface location is subjected can be expressed as:

$$\sum p_i t_i :: p_i D N_i$$

It may also be noted that the mass of water impacted on a particular site per unit area has the same proportionality as  $\sum t_i$ :

for drops

$$m/A :: \frac{D^3 N_i}{D^2} :: D N_i$$

for cylindrical jets

$$m/A :: \frac{D^3 L N_i}{D L} :: D N_i$$

That is, the measurement of the mass of water impacted per unit area to incubate erosion is a direct measure of the total impulse per unit area to incubate erosion at constant impact pressure. Therefore, since the stainless steel data, as plotted in Figure 3.3-2, does not evidence any consistent trend with drop diameter over most of the test range of normal impact velocities, it suggests that the important parameter during stage 1 erosion is the total impulse per unit area and not the number of blows per unit area. This is interpreted to mean that the end of the incubation period is signaled by a buildup to a certain level of permanent strain and that it is unimportant whether this strain is occasioned by many little blows or a few big ones. This conclusion also seems consistent with the previously paraphrased Hancox and Brunton description of surface distortions during stage 1 of erosion.

The stage 3 stainless steel erosion data of Pearson<sup>(67)</sup> is shown in Figure 3.3-3.\* The marked separation of that data by drop diameter is quite apparent. Pearson found that the data could be correlated by an equation of the form:

$$\frac{m}{m_0} = (U \sin \theta - U_{cd})^n \operatorname{cosec} \theta$$

Heymann in Section 3.1 showed that for Pearson's data:

$$U_{cd} = \frac{1}{\sqrt{d}}$$

As stated by Pearson, since all the testing was carried out above the apparent threshold velocity,  $U_{cd}$  is only a convenient mathematical parameter and may not represent an absolute lower limit on normal impact velocity to cause erosion.

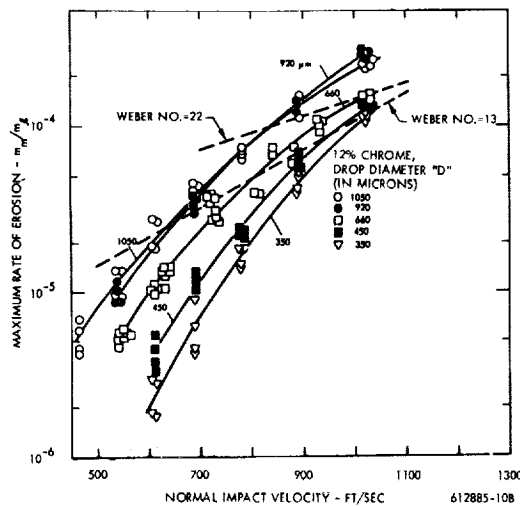


Figure 3.3-3 Stage 3 Erosion of 12% Chrome Steel (CEGB Data)

\* The Weber No. lines will be discussed later.

In correlating the CEGB data on a hydrodynamic basis, it is important that there be similarity of eroded surface at corresponding points in the erosion cycle. This is what the CEGB found. Quoting from Reference 61, "In general, the topographical examination (of the eroded stainless steel) showed the following features:

- a) The average distance between adjacent peaks in the surface increases as the mass loss increases. This is probably associated with the intersection of widening pits which tends to eliminate, progressively, the narrowest of the escarpments remaining between them.
- b) Within the duration of the longest tests carried out, the average depth of the erosion pits continually increases.
- c) There is no observable topographical difference between specimens which have suffered the same mass loss produced by water droplets of the same size but different impact velocities.
- d) For corresponding positions on the curves of mass loss against mass of impacting water, the coarseness of the surface increases with drop size and the distance between adjacent erosion peaks is proportional to, and of the same order as, the droplet diameter."

### 3.3.3 Possible Reasons For Drop Size Effects

That Erosion Rates are drop diameter sensitive and that the erosion peaks and valleys are proportional to drop diameter has been noted by others (68, 69, 70), in addition to the CEGB. Various explanations of the drop diameter effect on erosion rates have been offered. Some of these are: (1) increase in local material fatigue limit as effective impact lengths become smaller with smaller drops as suggested by Heymann in Section 3.1, (2) smaller drops create more surface area per unit volume of material removed than do larger drops and it has been suggested that this means that more energy is required per volume of material removed with small drops than large drops (70), (3) smaller drops are

more easily deflected by gas forces before impact than larger drops and therefore do not hit with as high an actual normal impact velocity, (4) the impacting drops become unstable aerodynamically and start to break up before impact, and (5) the test samples retain a film of water which attenuates the blow from smaller drops more than that of larger drops.

### 3.3.3.1 Size Effects in Fatigue Failure

Size effects in fatigue failure as related to multiple-impact erosion have been discussed in Section 3.1. In this discussion Heymann concludes after Peterson that for fatigue failure to occur the endurance limit must be exceeded not merely at a point or line but across a dimension which is on the order of 50 to 75 microns. Heymann then goes on to point out that, for an impact of a spherical drop or sideways impact of a cylindrical jet the impacted cross-sectional length is only a fraction of the projected drop cross-sectional length during the time of peak pressure. Hence, for drops of small effective impact length (less than 50 to 75 microns), an apparent increased erosion resistance of the material would be observed.

Some measure of the ratio of this effective impact length for dry surfaces can be obtained by reference to the work of Hancox and Brunton (65). These investigators impacted jets of mercury on polymethyl methacrylate specimens. They found values of interface angle  $\beta$  where vigorous outflow begins (see nomenclature for definition of  $\beta$ ) as given in Table 3.3-1.

TABLE 3.3-1

VALUES OF THE INTERFACE ANGLE  $\beta$  FOR WHICH FLOW FIRST DEFORMS THE SURFACE

Jet Diameter (mm)	Velocity of Impact (m/s)	Angle
Mercury Jet 1	183	17° 15'
	169	16° 45'
	154	17° 0'
	152	16° 45'

Making the logical conclusion that there cannot be much release of impact pressure until there is substantial lateral liquid flow, the effective impact length must be on the order of 0.3 times the projected impacting jet diameter or larger. This value should also be a measure of the effective length ratio in drops impacted normal to a surface since the impact is axisymmetric. If this 0.3 value is applied to the drop diameters of the CEGB data (Figure 3.3-3), all effective length values are greater than 75 microns, some considerably so. It seems unlikely, that a material size effect is an adequate explanation of the evidenced drop size effect in terms of impacts on dry surfaces.

As seen by Table 3.3-1, Hancox and Brunton found that the angle  $\beta$  at which vigorous outflow began in their tests was about 17 degrees. They point out, from elementary considerations, that such outflow should have begun when the lateral velocity of impact of the jet on the solid surface fell below the compression wave velocity in the liquid. From geometric considerations, Hancox and Brunton find that the theoretical angle  $\beta$  is given by

$$\beta = \sin^{-1} \left( \frac{U_n}{C} \right)$$

where  $C$  is the compression wave velocity in the liquid, and  $U_n$  is the normal impact velocity.

As seen in Table 3.3-1, Hancox and Brunton found no such velocity dependence for  $\beta$ . In addition, the theoretical value of  $\beta$  is, in all cases, much less than the observed value. They attribute the observed delay in outflow to friction at the solid surface. (It should also be noted, however, that a jet is not necessarily a cylindrical object but may be varicose. In this case, the actual effective diameter of the jet might be considerably greater than the cylinder from which it originated. Hancox and Brunton's measurements may be misleading.) This is interpreted here to mean that vigorous outflow is delayed until the effective depth of compressed liquid is large enough for the dynamic forces to swamp the viscous forces.

A liquid film over the impact surface will give a lubricating effect such that lateral outflow (release of peak impact pressure) can begin much sooner than for a dry surface. In correlating the CEGB data, the assumption is made that such a film existed on the CEGB test pieces and that the angle  $\beta$  is a function of  $U_N/C$ .

Perhaps the most telling reason, however, for supposing that local material effects do not explain the drop diameter effect is that the dimensions of the peaks and valleys of the eroded surface are characteristically proportional to the drop size. It seems unlikely that such behavior would be observed if local material factors are a dominant influence. It seems likely that the area of impact of even smallest drops used by the CEGB is too great to bring local material strengthening factors into prominence.

### 3.3.3.2 Surface Area Effect

If the sizes of the peaks and valleys in an eroded surface are proportional to the diameter of the drops impinging, then more surface area is created per volume of metal removed with small drops than large drops. It has been argued that this greater surface to volume ratio of small versus large drops implies a greater energy requirement of small drops to remove the same volume of material as large drops. For this argument to be valid, erosion of metals would have to be a two-dimensional skin effect like atomization of liquid where the new surface is created by stretching the old surface and

$$E = \sigma(\Delta A)$$

All reported observations reviewed by this author clearly indicated that new surface is produced during erosion, not by stretching of old surface but by breakage of solid material. A stress level is, therefore, the appropriate strength of materials criterion. By the logic of dimensions then:

$$E = SV$$

or the energy of creation of new surface is proportional to the volume of material removed. The energy per unit volume removed is the same whether the removal is by many small pieces or a few big pieces.

### 3.3.3.3 Hydrodynamic Effects

In the CEGB tests, deflection of the smaller drops relative to the larger drops can almost certainly be ruled out. The CEGB could observe the impact of the drops and in fact had to make substantial modifications in the rig as originally designed to remove such deflections<sup>(71)</sup>.

However, the impinging drops might have been aerodynamically unstable. It takes a finite time for a drop to disrupt even when unstable. For a considerable portion of that time period, it is difficult to observe any marked distortions indicating that the drop is in the process of disruption<sup>(72)</sup>. Assuming that the velocity of the vapor at the radius of the target in the CEGB apparatus was the same as the target velocity, calculations of drop Weber Number during the CEGB tests have been carried out, using Gardner's<sup>(73)</sup> (or if you prefer Hinze's<sup>(74)</sup>) water drop instability range of Weber Number  $13 \longleftrightarrow 22$ . These lines are plotted on Figure 3.3-3. The author interprets this range as:  $We < 13$  - drops almost certainly stable,  $We > 22$  - drops almost certainly unstable. From this it would appear that for most, but not all, of Figure 3.3-3 the impacting drops were aerodynamically stable. The 1050 and 920 micron drops may have been breaking up before impact at the higher test velocities. This may explain the crossover anomaly in the data.

If the drop diameter effects evident in the CEGB data for stage 3 erosion are not numerically feasible, in terms of local materials effects or aerodynamic effects before impact, they must be caused by the hydrodynamics of the impact itself. These might be due to frictional effects within the drop (either from surface tension or viscosity of the liquid) or to films of liquid on the surface. Numerically, the impact pressure forces over the range of drop sizes and impact velocities of the CEGB data are so great that surface tension cannot be a factor. This is also true for the mercury jet impacts of Hancox and Brunton, even though the surface tension of mercury is considerably higher than that of water, because the acoustic impedance of mercury is also markedly higher than that of water.



If the observed drop diameter effect is solely a result of internal hydrodynamics in the impacting drop, a viscosity-like effect must be the cause. Superficially, one might say in this connection, that such is the cause. The surface to volume ratio increases with decreasing drop diameter and the flow of liquid out of the impingement zone will be impeded and the violence of outward flow reduced. Reduced outward flow violence then can be equated with less erosion. This kind of reasoning, however, implies a steady-state continuity of impinging flow and outward flow which need not and probably does not exist during the most damaging period of impact. Over the entire period of impact there must be continuity of flow into and out of the impact, but this does not have to be true instantaneously except at one instant during the entire process. If, because of viscous effects, the liquid cannot initially flow out of the impact as fast as it is flowing in, the maximum pressure of the impact will have to be prolonged until it can. Otherwise, overall continuity of flow will not be preserved. This means that if internal viscous effects are a major cause of the drop diameter effect, the period of maximum impact pressure will be longer for smaller drops than larger drops. Smaller drops should inflict a more severe impact than larger drops and therefore cause proportionally greater damage. Since this is obviously not the case, one is left with the hydrodynamic interaction of the impacting drop with a film of liquid as the most probable cause for the observed drop diameter effect.

An obvious effect of a water layer would be to cushion the impact between the drop and the metal surface. The effective cushioning from a given thickness of surface water will be greater for smaller drops than for larger drops. This is a possible reason that for equal amounts of impacting water, the finer the division of the water and the lower the impact damage. This is one aspect of the water film. Another and perhaps more important aspect is that such a water film will provide a lubricated surface for lateral flow or a path for dissipation of the impact as a compression wave moving radially away from the impact through the film. This aspect of a liquid film is most important since it allows a postulation that the duration of drop impact during the CEGB tests was a function of normal impact velocity even though the Hancox and Brunton

mercury jet single impact tests indicated no change in size of impact with change in normal impact velocity. The tests were carried out with dry surfaces and the results (even if taken at face value) are not applicable to a wet surface.

### 3.3.4 Correlation Model

It is assumed that because of the presence of the liquid film, the duration of the pressure pulse, liquid outflow, etc., correspond to the hypothetical model of Hancox and Brunton (65) as implied by their statement:

$$\beta = \sin^{-1} \left( \frac{U_n}{c} \right)$$

At the moment of impact between the water drop and liquid film, compression waves start into the film and the drop at or near the velocity of sound in the liquid. Initially, this compression wave is maintained at full liquid to liquid impact value by the crashing of successive segments of the drop on the surface at a rate in excess of the compression wave velocity. If during this period, the compression wave in the liquid film is reflected from on the solid surface, the average pressure exerted on the solid surface will be that of the full water hammer level. The pressure rise over the wave is equal to the water-to-water impact,  $1/2 \rho C U_n$ , to which must be added the change in momentum of the liquid following the wave at velocity  $U_n/2$ , causing an additional pressure rise at the solid surface of  $1/2 \rho C U_n$ .

Sometime later, the rate at which liquid crashes on the surface is reduced (because of the geometry of a sphere) to a level where a compression wave can outdistance the disturbance, reach a free surface, and be reflected back as a rarefaction wave. At this time, liquid outflow from the compressed region begins. The area of average maximum pressure then dwindles to nothing as the rarefaction wave progresses to the center of impact.

#### 3.3.4.1 Forces of Impingement

There are two force or pressure levels of concern. The first of these is the pressure level of the initial impact, and the second is the impingement pressures generated by the liquid squirting laterally from the impacted area.

The first of these is taken to be the water hammer pressure. (Throughout this section, it will be assumed that the impact velocity levels and the strength of the metal surfaces are such that the metal can be considered rigid with little loss in accuracy.):

$$p_1 = \rho_2 C U_n$$

Heymann has shown that the shock wave velocity,  $C$ , in water is to a first approximation, a simple function of  $C_o$ , the acoustic velocity in the uncompressed liquid, and the normal impact velocity,  $U_n$ , so that pressure,  $p_1$ , becomes, using Heymann's relation:

$$p_1 = \rho_2 C_o U_n \left(1 + 2 \frac{U_n}{C_o}\right)$$

The maximum secondary impingement pressures are similarly assumed to be the water hammer pressure from impingement on a rigid projection at maximum lateral velocity. These maximum lateral velocities have been experimentally observed to be approximately:

$$U_2 = \sqrt{2 U_n C}$$

or

$$p_2 = \rho_2 C_2 \sqrt{2 U_n C} = \rho_2 C_o \left(1 + \frac{2}{C_o} \sqrt{2 U_n C_o \left(1 + 2 \frac{U_n}{C_o}\right)}\right) \sqrt{2 U_n C_o \left(1 + 2 \frac{U_n}{C_o}\right)}$$

For water drops impacting with normal velocities in the range of the CEGB experiments, this reduces in numerical approximation to:

$$p_2 \sim 9.5 \rho_2 C_o U_n$$

That  $p_2$  is numerically first order linear in  $\rho_2 C_o U_n$  simplifies the correlation problem with the CEGB water drop data since it may be assumed that the dimensionless ratio,  $p_1/p_2$ , is nearly constant.

### 3.3.4.2 Impingement Process, Duration, Total Impulse, and Total Energy

Assuming the geometry of the situation as illustrated in Figure 3.3-4, at time  $t$  after impact,

$$U_n t = r - y$$

$$\text{or} \quad \frac{dy}{dt} = -U_n \quad (1)$$

Making use of the equation of a circle,  $\frac{dy}{dx} = -\frac{x}{y}$ , the rate of progression of the disturbance along the surface is

$$\frac{dx}{dt} = \frac{\sqrt{r^2 - x^2}}{x} U_n \quad (2)$$

At a time defined as  $t_\beta$ , the rate of progression of the disturbance will fall to the velocity of the compression wave in the liquid along this same surface, or

$$\left(\frac{dx}{dt}\right)_\beta = C = \frac{\sqrt{r^2 - x_\beta^2}}{x_\beta} U_n,$$

and

$$x_\beta = \frac{r}{\sqrt{\left(\frac{C}{U_n}\right)^2 + 1}} \quad (3)$$

In the regime of interest to turbines,

$$\left(\frac{C}{U_n}\right)^2 \gg 1,$$

or

$$x_\beta \approx r \frac{U_n}{C}$$

This model is identical to that of the hypothesis of Hancox and Brunton, since

$$\sin \beta = \frac{x_\beta}{r} = \frac{U_n}{C}$$

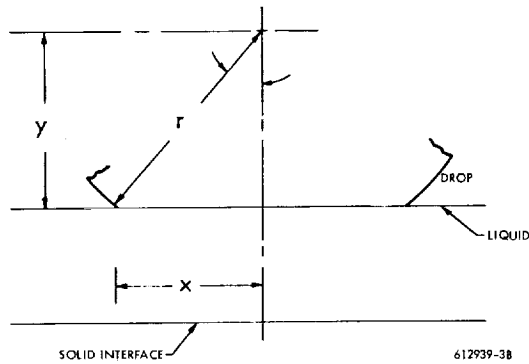


Figure 3.3-4 Configuration Diagram

Similarly, by integrating Equation 1 from zero to  $x_\beta$  and approximating,

$$t_\beta \approx \frac{r}{2} \left( \frac{U_n}{C} \right) \quad (4)$$

This  $t_\beta$  is the time at which liquid outflow begins, and the compressed zone covers the maximum area. The complete time of the pressure pulse  $t_\beta$  is the time  $t_\beta$  plus the time for the rarefaction wave to travel to the point of initial impact from its radius of origin  $x_\beta$ . Thus,

$$t_b = t_\beta + \frac{x_\beta}{C} \quad (5)$$

In approximate terms for  $\left( \frac{C}{U_n} \right)^2 \gg 1$ ,

$$t_b \approx \frac{3}{2} \frac{r U_n}{C^2} \quad (6)$$

The average area over which the pressure pulse acts during  $t_b$  is then, approximately,

$$A = \frac{7\pi}{18} r^2 \left( \frac{U_n}{C} \right)^2 \quad (7)$$

The total impulse exerted by single drop on the surface during the maximum pressure phase of impact is (neglecting the time to compress the liquid film) given by:

$$\begin{aligned} I_i &= \rho_l C U_n \sum A_i t_i = \rho_l C U_n \left( \frac{7\pi}{96} \right) D^3 \left( \frac{U_n^3}{C^4} \right) \\ &= \rho_l C \left( \frac{U_n}{C} \right)^4 \left( \frac{7\pi}{96} D^3 \right) \quad (8) \end{aligned}$$

The total impulse per unit of surface area in terms of total water impacted per unit of surface area in the form of drops of diameter  $D$  is then:

$$\frac{\sum I_i}{A} = \frac{7}{16} \frac{m_l}{A} U_n \left( \frac{U_n}{C} \right)^3 \quad (9)$$

By observation earlier in this section, the quantity of total impulse per unit area that a given material can endure should be a constant of the material, or the amount of water to cause incubation is:

$$\left( \frac{m_l}{A} \right) = \frac{\sum I_i / A}{\frac{7}{16} U_n \left( \frac{U_n}{C} \right)^3} \propto \frac{1}{U_n^4} \quad (10)$$

Referring to Figure 3.3-2, the dashed line shown is drawn for a  $(m_l/A) \propto 1/U_n^4$  dependence. The solid line is that drawn through the data by the original investigators.

The energy used in deforming a single drop, during this maximum pressure stage of impact, is the energy flux across the liquid solid interface required to maintain the compressive shock moving through the liquid or

$$E_i = C U_n^2 \sum A_i t_i = I_i U_n \quad (11)$$

Hence, the total energy available per unit area to cause erosion from deformation of impinging drops (neglecting the time to compress the liquid film) is:

$$\frac{E_l}{A} = \frac{7}{16} \frac{m_l}{A} \left( \frac{U_n}{C} \right)^3 U_n^2 \quad (12)$$

$$\text{or} \quad \frac{E}{A} \propto U_n^5$$

It has been observed by several investigators (76, 77) that the rate of erosion of metals changes approximately as the fifth power of the normal impact velocity.

### 3.3.4.3 Liquid Film Thickness During the CEGB Tests

As stated previously, it is assumed that the CEGB test pieces were covered with a water film. At each revolution of the test sample this film is replenished as it passes through the curtain of water drops. This water then drains from the test piece under the centrifugal force field, gradually thinning the film until the next collision with the water drops.

Assuming that the surface of the sample is smooth and plane, that the flow from the sample is viscous and only in the radial direction, neglecting the low order terms in the Navier-Stokes equation, neglecting all external forces except centrifugal force and specifying a parabolic velocity distribution of the liquid film, a straightforward derivation of an approximate average film thickness at the moment of impact of the drops results. (See Section 3.3.8.)

$$\delta = \sqrt{\frac{3 \mu D_s}{4 \pi \rho_l U_s}} \quad (13)$$

Calculated film thicknesses as a function of erosion sample velocity are shown in Figure 3.3-5. As can be seen, these calculated films are quite thin. It has been pointed out to the author by Professor D. E. Elliott, that the foregoing film thicknesses would, at best, apply only during the initial stage of an erosion test before the surface has become roughened. After the surfaces become roughened, the liquid film thickness will increase. This offers a possible explanation as to why the CEGB data show drop diameter segregation for stage 1 erosion not only at the lowest test velocities but over the entire range of test velocities for stage 3 erosion.

For correlation purposes, it is not necessary to know the absolute value of the film thickness so long as this thickness for a particular stage of erosion is the same multiple of the minimum thickness for all impinging drop diameters. This is apparently the case for the CEGB data since the characteristic size of the roughness, as previously quoted from Reference 61, is proportional to the drop diameter. If the film flow remains of a viscous character and follows the roughness of the surface, then the film thickness would be proportional to the square root

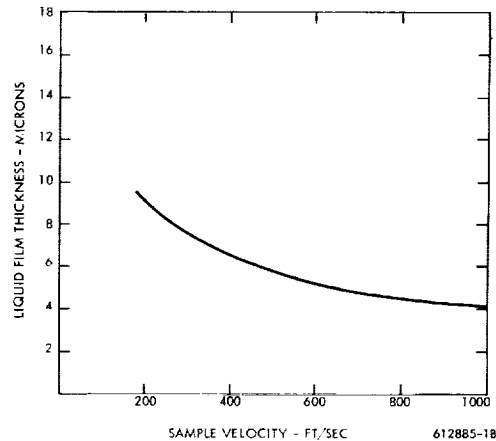


Figure 3.3-5 Calculated Film Thicknesses, CEGB Apparatus

of the path length. For geometrically similar roughness, the path length would be independent of the characteristic size so long as the characteristic size is much smaller than the total path length. This is not to say that the surface roughness level does not change from stage to stage, but rather that surface similitude with respect to impinging drop diameter prevails at any particular stage of erosion. Therefore, dimensional analysis based on minimum film thickness is a rational procedure so long as the stage of erosion is constant and the character of the film flow does not change.

The character of the film flow could change above and below the point where the pits or distortions of the surface retain water by capillarity. If the effective diameters of the pits are greater than some critical diameter, the pits would not retain water. If the effective pit diameters are less than this critical diameter, the pits would retain water. Equating surface tension forces and centrifugal forces, the order of the critical pit diameter should be:

$$D_c = 4 \sqrt{\frac{\sigma R}{\rho_l U_s^2}} \quad (14)$$

Characteristic numbers for the CEGB apparatus using Equation (13) are given in Table 3.3-2

TABLE 3.3-2  
CRITICAL PIT DIAMETERS FOR CAPILLARY  
WATER RETENTION

$U_s$ ft/sec	$D_c$ microns
328.	253
492.	169
656.	127
984.	84

According to the CEGB investigators (61), the distances between erosion peaks tend to be of the order of the drop diameters. Since almost all the CEGB test data is for velocities greater than 600 ft/sec, and the minimum drop diameter used was 350 microns, it is unlikely that capillary retention of water was much of a factor.

In conclusion then, excluding the data taken using the 900, 1050 micron diameter drops above about 600 ft/sec, as these may have been unstable under the aerodynamic forces present, the CEGB data can be taken as a set of fluid-dynamic similitudes for a particular stage of erosion.

#### 3.3.4.4 Impact Damage Threshold Velocity Correlation

It has been determined that the CEGB data may be expected to exhibit fluid-dynamic similitude for any particular stage of erosion. The film flow will be assumed to be always in the viscous flow regime. Its thickness for any particular stage of erosion may be assumed to be a simple multiple of a plane surface film thickness for any of the tests using stable drops. The unattenuated pressure of drop impact is numerically, to a good approximation, a simple multiple of the water hammer pressure for either the primary impact or secondary impacts from liquid squirting from the impact zone. It has also been found by Pearson (67) that the CEGB

data for the third stage of erosion exhibits an apparent threshold velocity for damage which can be used to correlate the erosion material rates above this threshold. As observed by Heymann this apparent threshold velocity varies inversely as the square root of the drop diameter.

On the basis of these foregoing considerations, it is reasonable to assume that for relatively non-viscous fluids such as water and potassium, the only variables of importance are: (1) the threshold water hammer pressure to cause damage ( $\rho_l C U_{cd}$ ), (2) some strength of material criterion ( $S$ ), (3) the liquid film thickness at threshold condition ( $\delta_{cd}$ ) over the uneroded surface, and (4) the diameter of the impinging drop ( $D$ ). These variables may be related by dimensional analysis to give:

$$\frac{\rho_l C U_{cd}}{S} = \varphi \left( \frac{\delta_{cd}}{D} \right)$$

Ignoring the relatively small change in shock wave velocity,  $C$ , with threshold normal impact velocity,  $U_{cd}$ , gives:

$$\frac{\rho_l C_o U_{cd}}{S} = \varphi \left( \frac{\delta_{cd}}{D} \right)$$

#### 3.3.4.5 Stage 3 Threshold Velocity Correlation

The summary of CEGB data (62) reports tests on three different materials where both the impinging drop diameter and normal impact velocity are varied. The materials are a Stellite 6, a 12 percent chrome steel, and a maraging steel.

From this information, it is possible to establish approximate relations between the dimensionless quantities of Equation (14), provided that a material strength criterion is selected. The criterion selected is the hardness of the material as measured in terms of the Vickers VPN. It is felt that none of the usual strength of materials quantities will be a universal criterion of the erosion strength of materials. From a cursory review of various available erosion test results, it is concluded that all suggested criteria

are fallible. Among these usual criteria, hardness appears to be one of the best. In addition, it has also been observed by the CEGB (61) that it provides a reasonably good indicator with respect to the CEGB data.

The averaged results of examining the CEGB data in terms of Equation (14) are shown in Figure 3.3-6. In Figure 3.3-6, the factor  $2.08(10^5)$  is used to convert the Vickers Hardness Number from metric to English units. The dimensions used are:  $\rho$  in slugs/ft<sup>3</sup>,  $C$  in ft/sec, VPN in kg/mm<sup>2</sup>,  $\delta$  in ft,  $D$  in ft, and  $U_{cd}$  in ft/sec. On an averaged basis there seems to be a clear separation between the materials. A data point by data point plot would somewhat obscure this separation, since the data scatter in the 12 percent chrome information (the only substantial body of data) is greater than the span between Stellite and the maraging steel. The separation by materials is hardly unexpected since it is well known that the erosion resistance of Stellite-like materials is almost always superior to that of other materials of similar physical property values. Similarly, the high hardness steels almost always show poorer erosion resistance than would be expected from a review of physical property values. It might be added that the vertical spread in Figure 3.3-6 is of the same order as that likely to be reported from a series of tests for the common strength of materials criteria for a single material.

#### 3.3.4.6 State 1 Threshold Velocity

Because during the incubation period the impacted surface is smooth and not pitted as in the third stage of erosion, the liquid film covering the surface is, by this model, thinner than during the third stage. This means that the threshold velocity to incubate damage will be lower than the threshold velocity necessary to continue damage.

That the threshold velocities to cause incubation are lower than those required to continue erosion is evidenced by the less marked segregation by drop diameter of the incubation period data (see Figure 3.3-2). However, as pointed out by Heymann, at normal impact velocities below 700 ft/sec such segregation with drop diameter is present. Unfortunately, the data do not extend to low enough velocity levels to make an empirical correlation of the data practical.

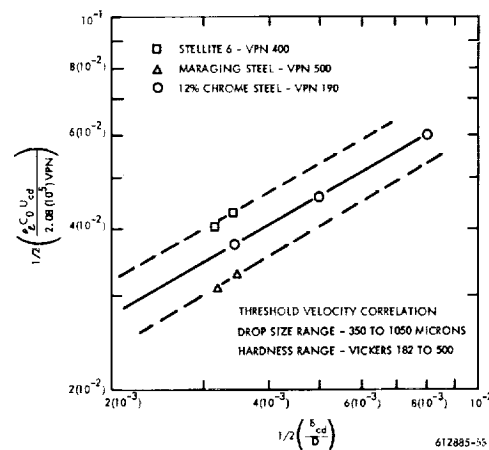


Figure 3.3-6 Threshold Velocity Correlation

Assuming that the basic rate controlling cause of damage and its mitigation by a liquid film does not change between the first and third stage of erosion, the correlation of Figure 3.3-6 can be used to estimate threshold velocities for incubation by accounting for the ratio in average film thicknesses between Stage 3 and Stage 1. To a first approximation, the ratio will be proportional to the square root of the ratio of the respective flow path lengths. From pictures in reference (61), it would appear that the flow path length during Stage 3 erosion is approximately three times the length of the original or incubation path length, or the film thicknesses in Stage 3 erosion are about 1.8 times the film thicknesses during the incubation period. On this basis, division of the calculated value of  $(\delta_{cd}/D)$  by 1.8 before entering Figure 3.3-6 provides an estimate of Stage 1 erosion threshold velocities where  $\delta_{cd}$  is calculated by Equation (13). In approximate terms, this yields a Stage 1 threshold velocity of about 70 percent of the Stage 3 threshold velocity.

### 3.3.4.7 Damage Rates Above the Threshold Velocity

It has been hypothesized by observers, that the ability of a material to resist erosion should be proportional to its ability to absorb the energy of impact above some threshold pressure level necessary to start erosion. Therefore, it will be assumed that the energy which must be absorbed by the impacted solid is proportional to the energy being expended in compression of the drops. Also, it will be assumed that the energy represented by that above the level necessary to produce a threshold pressure level  $P_{cd} = \rho_l C U_{cd}$  is that available to produce erosion damage.

The total compression energy has already been given in Equation (12). Subtracting the energy below the threshold and rearranging terms yields:

$$E = \frac{7}{16} m_l U_n^2 \left( \frac{U_n}{C} \right)^3 \left( 1 - \frac{U_{cd}}{U_n} \right) \quad (15)$$

By dimensional considerations, energy E must be equal to a product of volume of metal eroded,  $V_{mm}$ , and a material strength level, S, divided by an efficiency of removal. Further,  $V_m = \frac{m}{\rho}$ . Application of these relations to Equation (15) and rearranging of terms gives:

$$\frac{m_m}{m_l} = \frac{7}{16} \epsilon \frac{\rho_m U_n^2}{S} \left( \frac{U_n}{C} \right)^3 \left( 1 - \frac{U_{cd}}{U_n} \right) \quad (16)$$

Substitution for C in terms of  $C_o$  and U by use of Heymann's<sup>(75)</sup> relationship for water, introduction of the liquid density, and grouping of the variables in convenient dimensionless groups yields:

$$\frac{m_m}{m_l} = \frac{7}{8} \epsilon \left( \frac{\rho_m}{\rho_l} \right) \left( \frac{\rho_l U_n^2}{2 S} \right) \left( \frac{U_n}{C_o} \right)^2 \left( \frac{\frac{U_n}{C_o}}{\left[ 1 + \frac{2 U_n}{C_o} \right]^3} \right) \left( 1 - \frac{U_{cd}}{U_n} \right) \quad (17)$$

For the CEGB data on steels, the minimum test impact velocity is approximately 500 ft/sec. The maximum is approximately 1050 ft/sec. That is, the minimum value of  $U_n/C_o$  is slightly greater than 0.1 and the maximum is somewhat greater than 0.2. Values for the quantity

$$\frac{\frac{U_n/C_o}{\left( 1 + \frac{2 U_n}{C_o} \right)^3}}$$

are given in the following as a function of  $\frac{U_n}{C_o}$

$\frac{U_n}{C_o}$	$\frac{\frac{U_n/C_o}{\left( 1 + \frac{2 U_n}{C_o} \right)^3}}$
0.01	0.9 ( $10^{-2}$ )
0.05	3.8 ( $10^{-2}$ )
0.10	5.8 ( $10^{-2}$ )
0.15	6.8 ( $10^{-2}$ )
0.20	7.3 ( $10^{-2}$ )
0.30	7.3 ( $10^{-2}$ )
0.40	6.9 ( $10^{-2}$ )

It would seem, therefore, that for most of the CEGB data, Equation (17) might well be applied as

$$\frac{m_m}{m_l} \approx \left( \frac{\epsilon}{17} \right) \left( \frac{\rho_m}{\rho_l} \right) \left( \frac{\rho_l U_n^2}{2 S} \right) \left( \frac{U_n}{C_o} \right)^2 \left( 1 - \frac{U_{cd}}{U_n} \right) \quad (18)$$

It will be noted that the proportionality terms in Equation (18) relating the materials loss ratio to the impingement velocity are a function of both the liquid and material properties.

Equation (18) can be written as

$$\frac{m_m}{m_\ell} :: \left( \frac{U_n}{U_{cd}} \right)^4 \left( 1 - \frac{U_{cd}}{U_n} \right) \quad (19)$$

This analytic expression for the erosion rate is compared with the CEGB data in Figure 3.3-7. The data points shown are taken from the 600 micron drop curve of Figure 3.3-3 for which  $U_{cd}$  was established as 390 ft/sec. The dotted lines shown in Figure 3.3-7 represent Equation (19) with a suitably chosen constant of proportionality. Figure 3.3-7 then illustrates the excellent agreement of Equation (19) with the experimental 660 micron drop data.

#### 3.3.4.8 Summary of Model Equations and Empirical Constants

The correlating relations of the model in equation form for Stage 3 erosion under water impingement conditions at or near CEGB test velocities are:

$$\frac{m_m}{m_\ell} = \left( \frac{\epsilon}{17} \right) \left( \frac{\rho_m}{\rho_\ell} \right) \left( \frac{\rho_\ell U_n^2}{2 S} \right) \left( \frac{U_n}{C_o} \right)^2 \left( 1 - \frac{U_{cd}}{U_n} \right)$$

$$U_{cd} = K \left( \frac{S}{\rho_\ell C_o} \right) \left( \frac{\delta_{cd}}{D} \right)^n$$

where for the particular CEGB apparatus the correlating film thickness  $\delta$  is given by:

$$\delta = \sqrt{\frac{3 \mu D_s}{4 \pi \rho_\ell U_s}}$$

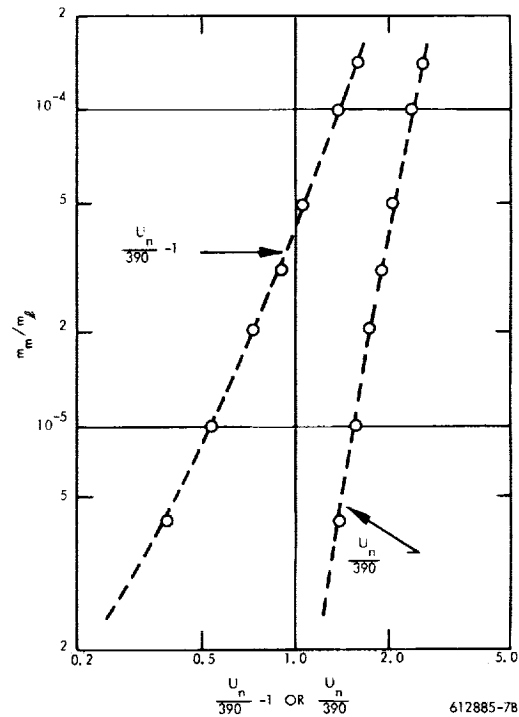


Figure 3.3-7 Correlation of CEGB Data by Means of Equation 19

Empirical coefficients for the maraging steel of VPN—500, the Stellite 6 of VPN—400, and the 12 percent chrome steel of VPN —190 are given below

Material	K	n	$\epsilon$	$(m_m/m_\ell)^*$
Maraging steel	1.14	0.57	0.46	26 ( $10^{-6}$ )
12% chrome steel	1.31	0.57	0.43	147 ( $10^{-6}$ )
Stellite 6	1.52	0.57	0.12	8 ( $10^{-6}$ )

\* At  $U_n = 1020$  ft/sec,  $D = 660$  microns



It will be noted that even though the hardness of the two steels varies by a factor of 2.5 and the erosion rate by 5.5 at 1020 ft/sec impact velocity, the empirical coefficients are about the same. The threshold velocity constants for Stellite are similar to those for the steels but the constant  $\epsilon$ , which is a measure of the effectiveness of the erosion process, is much lower. As is already known, Stellites are generally somewhat more erosion resistant in relation to surface hardness than are steels.

### 3.3.5 Temperature Effect In Drop Impingement Material Removal

In cavitation erosion tests there is a strong temperature effect on the measured erosion rates when materials and other conditions are held constant. A large amount of this effect can be ascribed to hydrodynamic causes (79).

Between cavitation erosion and impingement erosion there are often analogous effects. This is not to say that the detail causes are necessarily the same or that there is a quantitative correspondence, but in gross terms the two types of erosion exhibit a similar kind of behavior.

The possibility of a temperature linked hydrodynamic effect in drop impingement erosion sample testing in potassium has been investigated using the impingement correlation equations. The circumstances are analogous to a whirling arm drop impingement test using potassium drops of uniform size impinging on an erosion material sample mounted on the arm. The tests are such that the velocity of impact and the test temperature are the independent variables under investigation.

The behavior of the dependent variable, mass loss rate at temperature ( $T$ ), has been investigated in terms of the independent parameters  $T$  and  $U_n/U_{cd}(T_o)$ . The results are shown in Figure 3.3-8 where ratio  $m_m(T)/m_m(T_o)$  is on the y-axis, temperature is on the x-axis, and  $U_n/U_{cd}(T_o)$  is the parameter. The base temperature has been taken as 350°K.

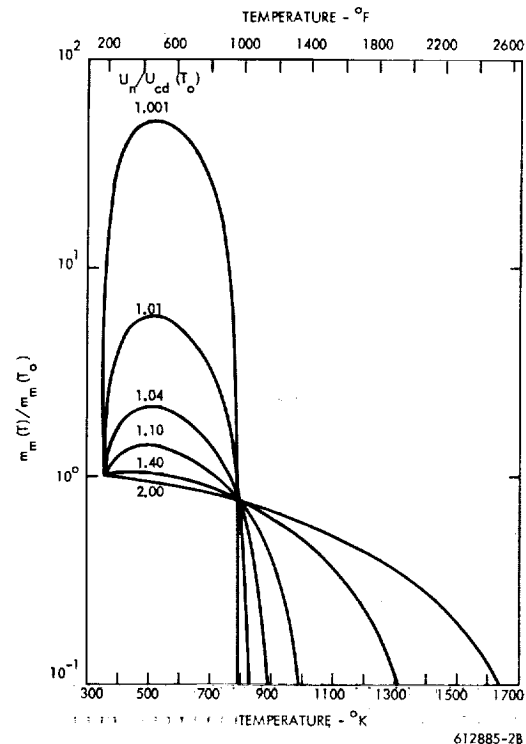


Figure 3.3-8 Referred Erosion Rates

As can be seen, there is a substantial change in the referred erosion rates with temperature. For low values of  $U_n/U_{cd}(T_o)$  there is a marked erosion peak at 400-500°F. A low value of  $U_n/U_{cd}(T_o)$  implies that at  $T_o$ , the reference temperature, the erosion conditions are only a little above a threshold condition to cause erosion. It is to be noted that: (1) the values plotted are referred values and that absolute values of material removal would be higher, the higher  $U_n/U_{cd}(T_o)$ ; and (2) the supposed conditions are for a whirling arm materials test and no conclusion relative to actual turbine blade erosion should be drawn. The situation leading to turbine blade erosion is more complex and involves variation in drop sizes, amount of liquid impinging, etc.

integrated and manipulated, subject to specification of a parabolic velocity distribution in the liquid film and continuity of flow, \* to give:

$$\frac{dm}{dt} = \frac{\rho U^2 \delta^3}{3R} \left( \frac{\rho \Delta Z}{\mu} \right) \quad (2)$$

At any time  $t$  after passing through the water curtain, the amount of liquid contained in a segment of length  $D$  and Width  $\Delta Z$  is

$$m = \rho \Delta Z \delta D, \quad (3)$$

and the rate of change of this mass is

$$\frac{dm}{dt} = \rho \Delta Z D \frac{d\delta}{dt} \quad (4)$$

Because this film is very thin it is reasonable to assume that  $\delta_f \sim \delta_o$  and on substituting Eq. (4) in Eq. (2) on the basis that  $\delta_f = \delta$  and integrating, the result is

$$\frac{\delta}{\delta_o} = \sqrt{\frac{3 \mu D R}{2 \rho U^2 \delta_o^2 \Delta t + 3 \mu R D}} \quad (5)$$

The time  $\Delta t$  between impacts or replenishing of the water film is given by

$$\Delta t = \frac{2 \pi R}{U}, \quad (6)$$

which upon substitution in Eq. (5) yields

$$\frac{\delta}{\delta_o} = \sqrt{\frac{3 \mu D}{4 \pi \rho U \delta_o^2 + 3 \mu D}} \quad (7)$$

When the film thickness after a complete circuit of the wheel is substantially less than its initial value, the term  $3 \mu D$  in the denominator of Eq. (7) may be neglected relative to the other term

$$4 \pi \rho U \delta_o^2, \text{ or } \delta \approx \sqrt{\frac{3 \mu D}{4 \pi \rho U}} \quad (8)$$

If the film thickness added at each pass through the water spray is of the same order as the final film thickness after a turn of the wheel, Eq. (8) is still a reasonable numerical approximation to Eq. (7) after enough revolutions that a steady state of operation is approached. This is illustrated by the following numerical example: the assumptions are (1) at the start of each revolution the initial film thickness is the residual film thickness plus an instantaneously deposited 4 microns (2) viscosity of water - 0.0114 poises, (3) density of water - 1 gm/cm<sup>3</sup>, (4) erosion sample velocity - 3(10<sup>4</sup>) cm/sec, and (5) erosion sample diameter - 2 cm.

The calculated residual film thicknesses as a relation of the number of revolutions after startup are given in the following table:

Revolution No.	Initial Film Thickness (cm)	Residual Film Thickness (cm)
1	4 (10 <sup>-4</sup> )	2.92 (10 <sup>-4</sup> )
2	6.92 (10 <sup>-4</sup> )	3.64 (10 <sup>-4</sup> )
3	7.64 (10 <sup>-4</sup> )	3.68 (10 <sup>-4</sup> )
4	7.68 (10 <sup>-4</sup> )	3.73 (10 <sup>-4</sup> )
5	7.73 (10 <sup>-4</sup> )	3.74 (10 <sup>-4</sup> )

Using Eq. (8), the value of residual film thickness is 4.25 (10<sup>-4</sup>) cm, not too different from the values in the table.

Thus, the thickness of water film impacted by the water drops is largely independent of the past history of the film and depends mainly on the liquid properties, the velocity of the sample (which is also the velocity of impact), and the size of the test sample.

\*Refer to Section 2.5.3 of WANL-TME-1977

### 3.4 TURBINE BLADE DISSOLUTION IN LIQUID METALS

#### 3.4.1 Background

##### 3.4.1.1 Discussion of Potassium Tests Involving Erosion

Table 3.4-1 lists some coupon and turbine tests where wet potassium vapor impinged on metal coupons or turbine surfaces. In all these tests there was some material removal.

In tests such as Nos. 1 and 5, where the oxygen content of the potassium is reported or suspected to have been high (high not defined quantitatively by authors), the rates of material or damage are substantial in 100 to 2000 hours for TZM material. It may be concluded that TZM is oxygen sensitive.

In tests such as Nos. 2, 3, 4, 7, 10, and 13, where the oxygen content of the potassium is reported to be low and impinging particle diameters are most probably submicronic, regardless of the theoretical moisture level or impact velocity or material tested, the loss rates observed were the order of 1 mil per 1000 hours or less. It may be concluded that where, because of the sub-micronic size of the impinging particles, impingement effects can be definitely assumed to be absent, material removal rates by material dissolution are quite low.

During the General Electric two-stage turbine tests, in tests such as Nos. 8 and 9, material losses were substantial for U-700 material. Calculated impinging drop velocities are of the order of 770 ft/sec and calculated impinging particle diameters are in the range of 30 to 100 microns. (Losses were massive during test No. 6, but for this test an estimate of the liquid particle diameters could not be made on the basis of the information examined and the particle diameters may have been very large.) Neither the impingement erosion model nor the dissolution model formulated hereafter would predict the substantial degree of material removal experienced during tests Nos. 8 and 9 on U-700 material. It may be concluded that there was a combined interaction of chemical (dissolution)

removal and mechanical (impingement erosion) removal taking place in the U-700 material. The Westinghouse erosion analysis model treats dissolution and mechanical removal as independent processes with no interaction. However, under identical conditions (and at the same time actually) as test No. 8, TZM inserts, test No. 11, did not show this interaction. This observation is a justification for the formulation of a non-interaction erosion model.

The General Electric three-stage turbine tests, tests No. 12, 13 and 14, resulted in substantial material removal from the three stage rotor blades and damage to erosion (coupons) inserts aft of the third stage. This material removal may have been caused by liquid or it may have been mechanical damage from some blade retainer clips or pieces of third stage shrouding which broke loose during the course of the tests. It is Westinghouse opinion that most of the damage was caused by these broken pieces. It must be added, however, that informed opinion of NASA and its contractors is divided with respect to the causes of this material removal and the significance of this test.

##### 3.4.1.2 Chemical Dissolution

The chemical dissolution of various materials into alkali and heavy liquid metals has been extensively investigated. Results, particularly with alkali metal systems, have been scattered. This scatter occurs because many difficulties arise when working with alkali liquid metals. Dissolution rates, besides varying with the standard parameters of temperature, material, flow rates, and temperature gradients, are also strongly influenced by alkali metal purity (small ppm concentrations of oxygen, carbon, or nitrogen contribute to increased corrosion), by dissimilar metal couples within the system, hot trap and getter efficiency, etc. Also, as experimental techniques and controls improve, the comparison of recent experimental results with earlier data further contributes to the problem.

TABLE 3.4-1  
EXPERIENCE ON MATERIAL REMOVAL BY  
LIQUID POTASSIUM

Agency	No. & Type of Test		Y %	V ft/sec	D Microns	Materials	Oxygen Content ppm	Test Duration hr.	Material Removal	Remarks	Ref.	
ORNL	1	Coupon	17	~2000	D < 1	TZM	Unknown, high	1000-2000	High	Material removal attributed to oxygen attack	80	
ORNL	2	Coupon	17	~2000	D < 1	TZM	Unknown, low	1000	Small		80	
ORNL	3	Coupon	17	~2000	D < 1	Cb-TZr	Unknown, low	3000	1-7 mils	Dissolution or corrosion attack	80	
ORNL	4	1 stage turbine	15	~2000	D < 1	TZM	Unknown, low	2700	Unknown	No visual damage	80	
Philco-Aeronautics	5	1 stage turbine	15	~2000	D < 1	TZM	Unknown, high	100	Several mils	Liquid jet cut groove in rotors Liquid collected in stator flow separation	80	
General Electric	6	2 stage turbine No. 1	10-15	~500	Large Unknown	U-700	Unknown	< 50	Massive	Liquid sprayed into turbine inlet to increase wetness	81	
General Electric	7	2 stage turbine No. 2	4-5	~500	D < 1	U-700	< 20 ppm	2000-3000	Nil	Rotor blades	80	
General Electric	8	2 stage turbine	4-5	> 700	30 < D < 100	U-700	< 20 ppm	2000-3000	8-10 mils	Erosion Inserts (coupon test)	Simul- taneous experi- ments during 2 stage turbine test.	80
General Electric	9	2 stage turbine No. 2	4-5	> 700	30 < D < 100	U-700	< 20 ppm	2000-3000	Some	Shrouds, clips		80
General Electric	10	2 stage turbine No. 2	4-5	< 700	D < 1	TZM	< 20 ppm	2000-3000	2.8 mils	Rotor blades	Simul- taneous experi- ments during 3 stage turbine test.	80
General Electric	11	2 stage turbine No. 2	4-5	> 700	30 > D > 100	TZM	< 20 ppm	2000-3000	Nil	Erosion Inserts (coupon test)		80
General Electric	12	3 stage turbine	8-12	~500	70 > D > 150	U-700 TZM, TZC	< 20 ppm	1300	20-40 mils	Leading edges 3rd stage rotor blades, not clearly liquid removal	Simul- taneous experi- ments during 3 stage turbine	82
General Electric	13	3 stage turbine	8-12	~500	D < 1	U-700 TZM, TZC	< 20 ppm	1300	1-2 mil rivulations	Rotor blades		82
General Electric	14	3 stage turbine	8-12	> 850	20 < D < 30	U-700 TZM, TZC	< 20 ppm	1300	Substantial	Erosion Inserts (coupon test) Not clearly liquid removal	82	

Y - Theoretical moisture content of bulk flow (reported values)  
V - Liquid impingement velocity (Westinghouse estimates)  
D - Liquid particle diameter (Westinghouse estimates)

Most liquid metal corrosion data, either from refluxing capsules, natural convection loops, or pumped loops, have been of a qualitative nature. General surface dissolution, grain boundary penetration, and general mass transfer have been noted. However, the vast number of variables involved in most systems has not permitted the mathematical approaches expressed by Epstein in Reference 83 or Gill in Reference 84 to be extended to these more complex systems. Thus, experience with materials and systems has been relied upon to designate the materials and their properties most compatible to the system in which they are to be incorporated.

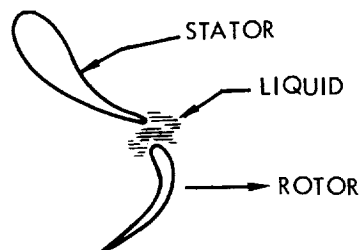
Within the last few years improved experimental techniques and equipment have permitted investigators to reduce some of the variables (especially oxygen contamination) to less influential levels. The quantitative data being generated today can, with due consideration of its source and system, be extrapolated to other similar systems for rough, predictive comparisons.

In this section the chemical dissolution of a turbine blade material into the thin stream of condensed potassium that flows radially outward along the blade is considered. Epstein's static

dissolution equation in Reference 4 was solved with dynamic dissolution parameters from Gill in Reference 84.

### 3.4.2 Analytical Model

To repeat, a fraction of the condensed moisture present in the wet vapor will be collected by the stator blades and will carry over to the subsequent rotor row in the form of atomized drops.

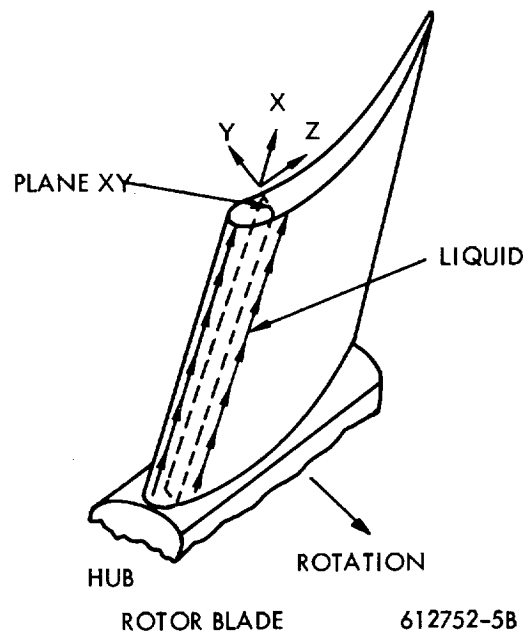


612752-4B

This liquid impacts the rotor blades along a relatively narrow portion of the leading edge of the convex surface and then flows in a nearly radial direction to discharge at the tips of the blades. It is assumed that the impacted moisture forms a continuous film and that the fluid impinges uniformly along the blade impaction zone. The concern of this analysis is the chemical dissolution of the blade material associated with the flow of this film.

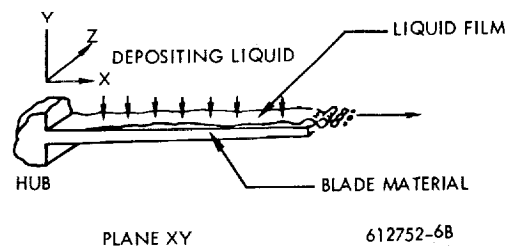
Because the film of liquid formed on the rotor blades is at most a few micrometers thick and is violently stirred by the incoming drops, it is assumed that the rate controlling step in the dissolution process is that of the rate of dissolution for the blade material into the liquid at the liquid-solid interface.

This is different than for dissolution of solids into liquids in pipe flow. In pipe flow, the rate controlling step is often the rate of diffusion of the dissolved solute across the solvent boundary layer into the bulk flow of solvent in the pipe.



612752-5B

For a turbine operating at some steady-state condition, rates of flow are a function only of position. Hence at any location (see drawing below)  $x, z$



612752-6B

measured from the hub and nose, respectively, of the rotor blade the rate flows of solute and solvent in the liquid film are time independent and the concentration,  $S$ , of solute in the solvent at location

$s, z$  is the ratio of the rate flow of solute to rate flow of solvent at this location or

$$S = \rho_l \frac{\dot{V}_m}{\dot{m}_l} \quad (1)$$

where  $\dot{V}_m$  is the rate flow of solute in the x direction per unit width of film (z direction) —  $\text{cm}^2/\text{sec}$   
 $\dot{m}_l$  is the rate of solvent in the x direction per unit width of film —  $\text{gm/sec/cm}$   
 $\rho_l$  is the solvent density —  $\text{gm/cm}^3$

According to Epstein (83), the rate of dissolution of a pure metal into a pure liquid solvent at the metal — liquid interface is given by:

$$S = S_o \left[ 1 - \exp \left( - \frac{\alpha A t}{V_l} \right) \right] \quad (2)$$

where  $A$  is the surface area in contact with the liquid —  $\text{cm}^2$   
 $S_o$  is the saturation solubility of material in the solvent — dimensionless  
 $S$  is the solute concentration in the solvent at time  $t$  — dimensionless  
 $V_l$  is the volume of liquid in contact with the metal for time  $t$  —  $\text{cm}^3$   
 $t$  is the contact time between liquid and metal along surface  $A$  — sec  
 $\alpha$  is the solution rate constant —  $\text{cm/sec}$

From Equation D-2 the following differential equations may be inferred:

$$\frac{dS}{dt} = \frac{\alpha}{V_l} (S_o - S) A \quad (3)$$

and since  $\frac{dS}{dV_l} = \frac{1}{V_l} \frac{dV_m}{dV_l}$

$$\frac{dV_m}{dt} = V_m = \alpha (S_o - S) A \quad (4)$$

In the case of the rotor blade film of unit width at location  $x$ , Eq. (4) may be written:

$$\dot{V}_m = \int_0^x \alpha (S_o - S) dx \quad (5)$$

By the assumption of uniform deposition of liquid along the rotor blade impaction zone:

$$\dot{m}_l = \dot{m}_a x \quad (6)$$

where  $\dot{m}_a$  is the rate of deposition per unit area per unit time —  $\text{gm/cm}^2/\text{sec}$ .

Substitutions from Eq. (5) and (6) into Eq. (1) yield, after some rearranging of terms:

$$S_x = \frac{\rho_l}{\dot{m}_a} \int_0^x \alpha (S_o - S) dx \quad (7)$$

Differentiation of Eq. (7) and rearrangement of terms gives:

$$\frac{dS}{dx} = \frac{\rho_l \alpha}{\dot{m}_a} \left( S_o - \left( 1 + \frac{\rho_l \alpha}{\dot{m}_a} \right) S \right) \quad (8)$$

Equation (8) is readily integrated to give:

$$S = \frac{\dot{m}_a}{\dot{m}_a + \rho_l \alpha} \left[ \frac{\rho_l \alpha}{\dot{m}_a} S_o - \frac{C}{x \left( 1 + \frac{\rho_l \alpha}{\dot{m}_a} \right)} \right] \quad (9)$$

where  $C$  is a constant of integration.

Now, it may be noted that when  $x = 0$  in Eq. (9) that  $S = -\infty$  unless  $C = 0$  (in which case  $S$  is indeterminate). However, a  $C$  taken equal to zero is the only reasonable physical interpretation, since the physical concentration  $S$  must fall with the limits:

$$0 \geq S \geq S_o$$

and the equation:

$$S = \frac{\dot{m}_a}{\dot{m}_a + \rho_l \alpha} \left[ \frac{\rho_l \alpha}{\dot{m}_a} S_o - \frac{(0)}{x \left( 1 + \frac{\rho_l \alpha}{\dot{m}_a} \right)} \right] \quad (10)$$

satisfies these limits as  $x \rightarrow 0$ .

Equation (9), therefore, reduces to:

$$S = \frac{\rho_l \alpha}{\dot{m}_a + \rho_l \alpha} S_o \quad (11)$$

It will be noted that the concentration  $S$  is not only time independent but is constant throughout the liquid flow zone along the rotor blades leading edge.

$S$  in terms of  $S_o$  from Equation (11) may be substituted into Equation (5) to give:

$$\dot{V}_m = \int_0^x \alpha S_o \left( \frac{\rho_l \alpha}{\dot{m}_a + \rho_l \alpha} \right) dx = \alpha S_o \left( \frac{\dot{m}_a}{\dot{m}_a + \rho_l \alpha} \right) x \quad (12)$$

The rate of material thickness removal,  $\delta_m$ , therefore is:

$$\dot{\delta}_m = \frac{\dot{V}_m}{x} = \alpha S_o \left( \frac{\dot{m}_a}{\dot{m}_a + \rho_l \alpha} \right) \quad (13)$$

This Eq. (13) presents a reasonable physical picture. If  $\dot{m}_a \gg \rho_l \alpha$ , this implies that  $S \rightarrow 0$  or the rate of material thickness removal is:

$$\dot{\delta}_m = \alpha (S_o - (0)) = \alpha S_o$$

The thickness removal rate is dissolution rate constant controlled and is independent of liquid flow rate.

If  $\dot{m}_a$  is low,  $\dot{m}_a \ll \rho_l \alpha$ , this implies that  $S \rightarrow S_o$  and

$$\dot{\delta}_m = S_o \frac{\dot{m}_a}{\rho_l \alpha}$$

The thickness removal rate is then directly proportional to the liquid flow rate and independent of the dissolution rate constant.

In between these extremes the thickness removal rate is affected by both dissolution rate constant and liquid flow rate.

The discussion so far has assumed a pure metal dissolving into a pure liquid. The latter assumption, pure liquid, is probably reasonable since turbine system operators go to some length to keep a pure liquid in the system. However, turbine blade materials are alloys composed of materials of differing solubility and probably chemical activity. In advanced high temperature Rankine cycle liquid metal systems, the turbine blade materials are likely to be refractory alloys such as TZM and TZC. These are molybdenum alloys with small amounts of titanium, carbon, and zirconium. The alloying materials such as Ti and Zr are more soluble than the base material and while present in concentrations of only 1 percent to 2 percent, tend to collect at the alloy grain boundaries where they may be more readily leached from the surface than if they were uniformly mixed. In addition, if there is preferential leaching at the grain boundaries, this may so weaken the material that a considerably greater amount of material may be lost than that which simply dissolved.

At the present time there are insufficient experimental results or theory to judge these factors adequately. Nonetheless, it seems worthwhile to delineate these areas of uncertainty by the application of multiplicative correction factors to Equation (13), as:

$$\dot{\delta}_s = k_1 \dot{\delta}_m = k_1 k a \alpha S_o \left( \frac{\dot{m}_a}{\dot{m}_a + \rho_\ell k a \alpha} \right) \quad (14)$$

where

- $a$  is the activity level of a readily dissolvable constituent of the alloy in the alloyed form relative to the constituents dissolvability in pure form
- $k$  is ratio of the effective surface area from which the constituent is dissolving to the total surface area of the alloy
- $k_1$  is the ratio of total alloy removal rate to dissolving constituent removal rate
- $\dot{\delta}_s$  is the thickness removal rate for the alloy surface as a whole

In the numerical example given hereafter, it has been assumed that

$$k = 1/k_1 \text{ and } a \sim 1.$$

Hence,

$$\dot{\delta}_s = \alpha S_o \frac{\dot{m}_a}{\dot{m}_a + \rho_\ell k a \alpha} \quad (15)$$

In addition, it has been assumed that  $k$  (the effective surface area ratio) is equal to the ratio of dissolving constituent volume to total alloy volume.

### 3.4.3 Analysis of Last Rotor of a Potassium Turbine Design

Using the previously derived equations, a numerical analysis of possible dissolution of metal from the last rotor blades of a potassium turbine design was performed. The numerical analysis was done by Westinghouse at the request of the AiResearch Manufacturing Company as a part of a study of Potassium Turbine-Alternator designs, for NASA Lewis Research

Center, under Contract NAS 3-10934, and has been previously reported in reference 85. It is repeated here to give the reader an idea of the numerical levels that result from application of the model to potassium turbine designs.

To our knowledge there are no experimental values of dissolution rate constant ( $\alpha$ ) available for TZM, TZC constituents dissolving into potassium. There are values for Fe dissolving in Na<sup>(83)</sup> and 304 SS dissolving in Li<sup>(84)</sup>. The values for 304 SS dissolving in Li are used. (See Figure 3.4-1.) The saturation solubilities of the various materials are taken to be:

Material	$S_o$
Mo	0.2 ppm
Zr	58 ppm
Ti	68 ppm

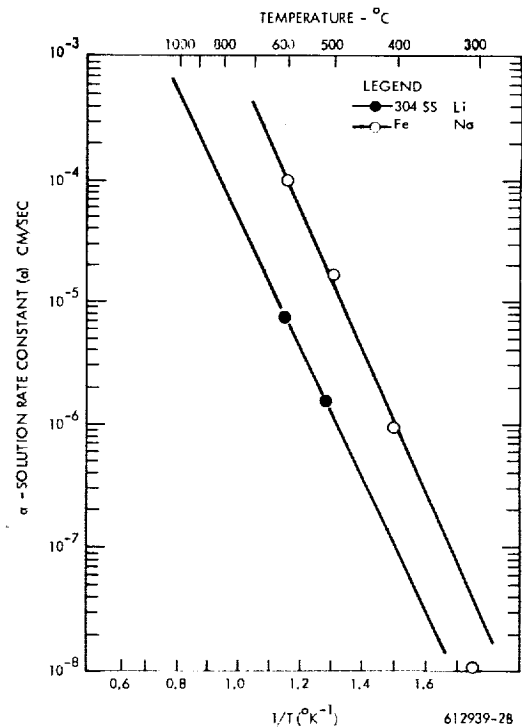


Figure 3.4-1 Temperature Dependence of  $\alpha$



The saturation solubilities of Zr and Ti are most uncertain (85) and may be as low as 10 ppm at analyzed rotor conditions. The values used are near the maximum values reported in the literature at the analyzed rotor temperature. The rotor blade material is assumed to be TZM of the following composition (86):

Constituent	Volume Fraction
Carbon	0.0009
Titanium	0.0110
Zirconium	0.0014
Molybdenum	0.9867

The fluid and geometric conditions along the leading portion of the convex surface of the rotor blades are taken to be as follows: (85)

#### Rotor Blade Conditions

Total liquid flow	17.8 gm/sec
No. of rotor blades	59
Liquid flow/blade	0.302 gm/sec
Blade height	4.03 cm
Temperature	670° C
Liquid density	0.685 gm/cc
Liquid film width	0.25 cm
Liquid film area	1. cm <sup>2</sup>

The information from Figure 3.4-1 and the previous three tables on material solubilities, the composition of TZM, and the rotor blade conditions were used to calculate material removal rates using Equation 15. The results of this calculation follow:

#### Rotor Blade Dissolution Results

$\dot{m}_a$ — liquid deposition rate/unit area	0.302 gm/cm <sup>2</sup> /sec
$a$ solution rate constant	$2(10^{-5})$ cm/sec
$k$ effective surface area ratio of Ti + Zr	0.012 dimensionless
$S_o$ average saturation solubility of Ti and Zr	$63(10^{-6})$ ppm
$\rho_l$ a $k$ dissolution factor	$1.65(10^{-7})$ gm/cm <sup>2</sup> /sec
$\delta_s$ material thickness	$1.26(10^{-8})$ mm/sec
Thickness removed in 2000 hr	0.0036 in.
Thickness removed in 20,000 hr	0.0356 in.

It will be noted from the tabulation of results that the liquid deposition rate,  $\dot{m}_a$ , is some 2 million times greater than the dissolution factor,  $\rho_l$  a  $k$ . Therefore, the material loss rate is independent of the rate of liquid flow and deposition. By this model of material removal by dissolution, the liquid flow rate will have to be reduced to about  $10^{-6}$  of the level used here to effect a substantial reduction in material loss rate. It will also be noted that the calculated removal of material in 20,000 hours is substantial in terms of a 4 cm (1.575 in.) high blade. Hopefully, the model and empirical coefficients used are overly conservative.

### 3.4.4 References

1. Brandenberger, E., and P. DeHaller, "Untersuchungen über Tropfenschlagerosion," Schweitzer Archiv-Annales Suisses, Vol. 10; n. 11, pp. 331 - 341, November 1944; and n. 12, pp. 379 - 386, December 1944.
2. Honegger, E., "Tests on Erosion Caused by Jets," The Brown Boveri Review, Vol. 14, n. 4, pp. 95 - 104, April 1927.
3. Fyall, A. A., R. B. King and R. N. C. Strain, "Rain Erosion Aspects of Aircraft and Guided Missiles," J. Roy Aero. Soc., Vol. 66, pp. 447 - 453, July 1962.
4. King, R. B., "Rain Erosion Testing at Supersonic Speeds Using Rocket-Propelled Vehicles," Paper presented at Rain Erosion Conference, Meersburg, Germany, May 1965.
5. Langbein, G., "The Dependence of Rain Erosion on the Velocity and the Angle of Incidence of Drops," Paper presented at Rain Erosion Conference, Meersburg, Germany, May 1965.
6. Hoff, G., G. Langbein and H. Rieger, "Investigations of Material Destruction due to Liquid Impact," Paper to be presented at ASTM Symposium on Erosion by Impingement and Cavitation, Atlantic City, June 1966.
7. Baker, D. W. C., K. H. Jolliffe and D. Pearson: "The Resistance of Materials to Impact Erosion Damage," Paper No. 13 at Discussion on the Deformation of Solids by the Impact of Liquids, The Royal Society, London, May 27, 1965. To be published in Phil. Trans. Roy. Soc., 1966.
8. Pearson, D., "Some Factors Influencing the Erosion of a Stainless Steel," Central Electricity Generating Board (of Gt. Britain), Report RD/M/N 100, June 1964.
9. Busch, H. and G. Hoff, "Rain Erosion in High-Speed Flight," Interavia, Vol. 20, pp. 675-676, May 1965.
10. Brunton, J. H., "Deformation of Solids by Impact of Liquids at High Speeds," Symposium on Erosion and Cavitation, ASTM STP-307, Am. Soc. Testing Mats., pp. 83 - 89, 1962.
11. "Second Quarterly Progress Report; October 1, 1965 through January 15, 1966; Basic Investigation of Turbine Erosion Phenomena; Contract NAS 7-390," WANL-PR (DD)-077, Westinghouse Astronuclear Laboratory, February 1966.
12. Pearson, D., "The Effect of Drop Size on the Erosion of a Stainless Steel," Central Electricity Generating Board (of Gt. Britain) Report RD/M/N 128, December 1964.
13. Vater, M., "Prüfung und Verhalten metallischer Werkstoffe gegen Tropfenschlag und Kavitation," Korrosion und Metallschutz, Vol. 20, n. 6, pp. 171 - 179, June 1944.
14. Engel, Olive G., "Waterdrop Collisions with Solid Surfaces," J. Research NBS, Vol. 54, Vol. 54, n. 5, pp. 281-298, May 1965.
15. Bowden, F. P., and J. E. Field, "The Brittle Fracture of Solids by Liquid Impact, by Solid Impact, and by Shock," Proc. Roy. Soc. A, Vol. 282, pp. 331-352, 1964.
16. Thomas, G. P., "Multiple Impact Experiments and Initial Stages of Deformation," Discussion on the Deformation of Solids by the Impact of Liquids, The Royal Society, London, 1955. (To be published, Phil. Trans. Roy. Soc., 1966).
17. Thiruvengadam, A., "A Unified Theory of Cavitation Damage," ASME Trans. (J. Basic Engrg), Vol. 85D, pp. 365-376, September 1963.
18. Peterson, R. E., "Application of Stress Concentration Factors in Design," Experimental Stress Analysis (Proc. SESA), Vol. 1, n. 1, pp. 118-127,

19. Marriott, J. B., and G. Rowden, "The Deformation of Steam Turbine Blade Materials by Liquid Impact," Discussion on the Deformation of Solids by the Impact of Liquids, The Royal Society, London, 1965. (To be published, Phil. Trans. Roy. Soc., 1966).
20. Weibull, W., "Basic Aspects of Fatigue," IUTAM Colloquium on Fatigue (Stockholm, 1955), Springer-Verlag, Berlin, pp. 289-298, 1956.
21. Backer, W. R., E. R. Marshall, and M. C. Shaw, "The Size Effect in Metal Cutting," Trans. ASME, Vol. 74, pp. 61-72, 1952.
22. Finnie, I., "The Mechanism of Erosion of Ductile Materials," Proc. 3rd National Congress Applied Mechanics, pp. 527-532, 1958.
23. Bowden, F. P., and J. H. Brunton, "The Deformation of Solids by Liquid Impact at Supersonic Speeds," Proc. Roy. Soc. A, Vol. 263, pp. 433-450, October 1961.
24. DeCorso, S. M., and R. E. Kothmann, "Erosion by Liquid Impact," Symposium on Erosion and Cavitation, ASTM STP-307, Am. Soc. Testing Mats., pp. 32-45, 1962.
25. Vater, M., "Das Verhalten metallischer Werkstoffe bei Beanspruchung durch Flüssigkeitsschlag," Z. VDI, Vol. 81, n. 45, pp. 1305-1311, November 6, 1937.
26. Weibull, W., "Fatigue Testing and Analysis of Results," Oxford, Pergamon Press, 1961. (Published for and on behalf of AGARD).
27. Roark, R. J., "Formulas for Stress and Strain," New York, McGraw-Hill, 4th Edition, 1965.
28. Thiruvengadam, A., "A Comparative Evaluation of Cavitation Damage Test Devices," ASME Symposium on Cavitation Facilities and Techniques, 1964, pp. 157-164. (Also Hydronautics, Inc., Tech. Rept. No. 233-2, November 1963).
29. Thiruvengadam, A., and S. Waring, "Mechanical Properties of Metals and their Cavitation Damage Resistance," Hydronautics, Inc. Tech. Rept. No. 233-5, Contract Nonr-3755(00)FBM, June 1964.
30. Thiruvengadam, A., "The Concept of Erosion Strength," Hydronautics, Inc. Technical Report 233-9, December 1965. (Also to be presented at ASTM Symposium on Erosion, Atlantic City, June 1966.)
31. Shalnev, K. K., J. J. Varga and G. Sebestyen, "Verification of Energy Parameter for Cavitation Damage," Paper to be presented at ASTM Symposium on Erosion by Impingement and Cavitation, Atlantic City, June 1966.
32. McAdam, J. D., Jr., "Endurance Properties of Steel: Their Relation to Other Physical Properties and to Chemical Composition," ASTM Proc., Vol. 23, pp. 56-105, 1923.
33. Halford, G. R., "The Energy Required for Fatigue," Journal of Materials, Vol. 1, No. 1, pp. 3-18, March 1966.
34. Heymann, F. J., "On the Shock Wave Velocity and Impact Pressure in High-Speed Liquid-Solid Impact," Trans. ASME, J. Basic Engrg., Vol. 90D, Sept. 1968, pp. 400-402.
35. Heymann, F. J., "High-Speed Impact Between a Liquid Drop and a Solid Surface," J. Appl. Phys., Vol. 40, Dec. 1969, pp. 5113-5122.
36. Leith, W. C., and A. L. Thompson, "Some Corrosion Effects in Accelerated Cavitation Damage," ASME Trans., (J. Basic Engrg.), Vol. 82D, pp. 795-807, 1960.
37. Ripken, J. F., et al, "A New Facility for Evaluation of Materials Subject to Erosion and Cavitation Damage," Univ. of Minn., St. Anthony Falls Hydro. Lab., Project Report No. 77, Contract Nonr 710(56), March 1965.

38. Hobbs, J. M., private communication. (See also L. Hays, "Turbine Research in Great Britain," Informal trip report in connection with NAS 7-390 and NAS 7-391. Jet Propulsion Laboratory, November 11, 1965.)
39. Engel, O. G., "Pits in Metals Caused by Collision with Liquid Drops and Soft Metal Spheres," J. Research NBS, Vol. 62, n. 6, pp. 229-246, June 1959.
40. Engel, O. G., "Pits in Metals Caused by Collision with Liquid Drops and Rigid Steel Spheres," Journal of Research, National Bureau of Standards, Vol. 64A, pp. 61-72, 1960.
41. Jenkins, D. C., J. D. Booker, and J. W. Sweed, "An Experimental Method for the Study of the Impact Between a Liquid Drop and a Surface Moving at High Speed," Ministry of Supply (Gt. Britain), R & M 3203; Obtainable from NASA as N62-10146.
42. Jenkins, D. C., and J. D. Booker, "The Impingement of Water Drops on a Surface Moving at High Speed," in "Aerodynamic Capture of Particles", Pergamon Press, pp. 97-103, 1960.
43. DeCorso, S. M., "Erosion Tests of Steam Turbine Blade Materials," Proc. ASTM, Vol. 64, pp. 782-796, 1964.
44. International Conference on Rain Erosion Problems. Held in Meersburg/Bodensee, Germany, May 1965. Proceedings in English to be published by the Royal Aircraft Establishment, edited by A. A. Fyall.
45. Discussion on the Deformation of Solids by the Impact of Liquids, held at the Royal Society, London, England, May 27, 1965. To be published in Phil. Trans. Roy. Soc., 1966.
46. Symposium on Erosion by Cavitation and Impingement. (To be held during ASTM Annual Meeting), Atlantic City, N. J., June 1966. Proceedings will probably be published in 1967 as a "Special Technical Publication" by ASTM.
47. Heymann, F. J., "On the Time Dependence of the Rate of Erosion due to Liquid Impact or Cavitation," Westinghouse Steam Division Report E-1448, June 1966. (Also Paper No. 136, ASTM Annual Meeting, Atlantic City, June 1966.)
48. Busch, H., G. Hoff, and G. Langbein, "General View on Rain Erosion Tests in Germany," Discussion on the Deformation of Solids by the Impact of Liquids, The Royal Society, London, 1965. (To be published, Phil. Trans., Roy. Soc., 1966).
49. Freudenthal, A. M., "Physical and Statistical Aspects of Cumulative Damage," IUTAM Colloquium on Fatigue (Stockholm, 1955), Springer-Verlag, Berlin, pp. 53-62, 1956.
50. Thiruvengadam, A., and H. S. Preiser, "On Testing Materials for Cavitation Damage Resistance," Technical Report 233-3, Hydronautics, Inc., December 1963.
51. Plesset, M. S., and R. E. Devine, "Effect of Exposure Time on Cavitation Damage," Paper No. 65-WA/FE-23, Am. Soc. Mechanical Engrs., 1965.
52. Lichtman, J. Z., D. H. Kallas, C. K. Chatten and E. P. Cochran, Jr., "Study of Corrosion and Cavitation-Erosion Damage," Transactions, Am. Soc. Mechanical Engrs., Vol. 80, pp. 1325-1341, 1958.
53. Wheeler, W. H., "Mechanism of Cavitation Erosion," Cavitation in Hydrodynamics, (National Physical Laboratory Symposium, Teddington, England, 1955), Philosophical Library, New York, 1957.
54. von Schwarz, M., W. Mantel and H. Steiner, "Tropfenschlaguntersuchungen zur Feststellung des Kavitationswiderstandes (hohlsog)," Zeitschrift fur Metallkunde, Vol. 33, pp. 236-244, 1941.
55. See 10.

56. Eichelberger, R. J., "Hypervelocity Impact," Behavior of Materials Under Dynamic Loading, Am. Soc. Mechanical Engrs., pp. 155-187, 1965.
57. Kent, R. P., "Some Aspects of Metallurgical Research and Development Applied to Large Steam Turbines," Parsons Journal, Vol. 10, pp. 285-295, Christmas 1964.
58. Roeloffs, R., and F. Garofalo, "A Review of Methods Employed in the Statistical Analysis of Fatigue Data," Proceedings, Am. Soc. Testing Mats., Vol. 56, pp. 1081-1090, 1956.
59. Epremian, E., and R. F. Mehl, "The Statistical Behavior of Fatigue Properties and the Influence of Metallurgical Factors," Symposium on Fatigue with Emphasis on Statistical Approach, ASTM STP-137, Am. Soc. Testing Mats., pp. 25-27, 1953.
60. Mathieson, R., and J. M. Hobbs, "Cavitation Erosion: Comparative Tests," Engineering, Vol. 188, pp. 136-137, January 22, 1960.
61. Baker, D. W. C., K. H. Jolliffe, and D. Pearson, "The Resistance of Materials to Impact Erosion," Phil. Trans. Roy. Soc. London, Series A, No. 1110, Vol. 260, pp. 193-204, 28 July 1966.
62. Pearson, D., "A Summary of the M. E. L. Experimental Data on Erosion," Marchwood Engineering Laboratories, CEGB, RDD/M/M18, Job. No. 30023, November 1964.
63. Fraas, A. P., loc. cit. Oak Ridge National Laboratories.
64. Engel, Olive G., "Mechanism of Rain Erosion; Part XIV, Pits in Metals Caused by Collision with Liquid Drops and Rigid Steel Spheres," WADC TR 53-192, U. S. National Bureau of Standards, May 1960.
65. Hancox, N. L. and J. H. Brunton, "The Erosion of Solids by the Repeated Impact of Liquid Drops," Phil. Trans. Roy. Soc. London, Series A, No. 1110, Vol. 260, pp. 121-140, 28 July 1966.
66. DeCorso, S. M., and R. E. Kothmann, "Erosion by Liquid Impact," Symposium on Erosion and Cavitation, ASTM STP-307, Am. Soc. Testing and Mats., pp. 32-45, 1962.
67. Pearson, D., "The Effect of Drop Size on the Erosion of a Stainless Steel," CEGB Report RD/M/N128, December 1964.
68. Honegger, E., "Tests on Erosion Caused by Jets," The Brown Boveri Review, Vol. 14, n. 4, pp. 95-104, April 1927.
69. Brandenberger, E., and P. DeHaller, "Untersuchungen über Tropfenschlagerosion," Schweitzer-Archiv-Annales Suisses, Vol. 10; n. 11, pp. 331-341, November 1944 and n. 12, pp. 379-386, December 1944.
70. Herbert, W., "Behavior of Iron and Hardened Steels Towards Drop Impact," Proc. Second Meersburg Conf. Rain Erosion and Allied Phenomena, August 16-18, 1967, Vol. I, Sect. 4.4.4, Published by RAE, Farnborough, England, Ed. by A. A. Fyall and R. B. King.
71. Pearson, D., "Turbine Blade Erosion Rig Research and Development Work Carried Out at Brighton," CEGB Report RD/M/N41, Job No. 43123, December 1962.
72. Wolfe, H. E. and W. H. Anderson, "Kinetics, Mechanism and Resultant Droplet Sizes of the Aerodynamic Breakup of Liquids," Report 0395-04-18SP, Aerojet-General Corp., April 1964.
73. Gardner, G. C., "Events Leading to Erosion in the Steam Turbine," Proc. Inst. Mech. Engrs., Vol. 178, Part I: No. 23, pp. 593-623, 1963-1964.
74. Hinze, J. O., "Fundamentals of the Hydrodynamic Mechanism of Splitting in Dispersion Processes," A. I. ChE. Journal, Vol. I, No. 3, P. 289 ff; September 1955.

75. Heymann, F. J., "A Survey of Clues to the Relationship between Erosion Rate and Impact Parameters, " Proceedings of the Second Meersburg Conference on Rain Erosion and Allied Phenomena, Vol. 2, pp. 655-682. (Issued by Royal Aircraft Establishment, Farborough, England, 1968.)
76. Hobbs, J. M., Discussion of Paper of Leith and Thompson, ASME Trans., (J. Basic Engrg.) Vol. 82D, pp. 795-807, 1960.
77. Thiruvengadam, A. and S. L. Rudy, "Experimental and Analytical Investigations of Multiple Liquid Impact Erosion, " Hydronautics, Inc. Tech. Report 719/1, June 1968 Contract NAS W-1608.
78. Elliott, D. E., Private Communication, 4 September 1968.
79. Thiruvengadam, A., S. L. Rudy and H. S. Preiser, "Cavitation Damage in Liquid Metals, " Hydronautics Inc., TR 607, Contract NAS 3-8506, April 1968.
80. Hays, Lance G. (Ed.), Summary of Turbine Erosion Meeting Held at Jet Propulsion Laboratory, Dec. 29-30, 1966, NASA, JPL Tech. Memo 33-354, June 15, 1967.
81. Schnetzer, E. (Ed.), "Two Stage Potassium Test Turbine, " Quarterly Progress Report No. 15, Period: Nov. 8, 1964 through Feb. 8, 1965, NASA-CR-54392, Contract NAS 5-1143.
82. Loc. cit., Potassium test turbine review meeting on October 15, 1968 at General Electric Co., Cincinnati, Ohio.
83. Epstein, L. F., "Static and Dynamic Corrosion and Mass Transfer in Liquid Metal Systems, " Chem. Engr. Prog. Symp. Series, Vol. 53, No. 20, p. 67 (1957).
84. Gill, W. N., et al, "Mass Transfer in Liquid-Lithium Systems, " A.I.Ch.E. Journal, Vol. 6, No. 1, p. 139 (1960).
85. Pouchot, W. D., "Technical Support for the Aerothermodynamic Design of the Potassium Turboalternator (KTA), " Westinghouse Astro-nuclear Laboratory, WANL-TME-1886, January 3, 1969, AiResearch Contract P711340 Final Report.
86. Climax Molybdenum Co., Spec No. CMX-WB-TZM-2, May 1964.

# SECTION 4

## LOW SPEED CASCADE TESTS \*

### ABSTRACT

Low speed cascade tests run on a turbine blade section, with various trailing edge thicknesses and shapes, investigated the downstream trailing edge wake. The blade section was modeled after a 3rd stator blade of the three stage potassium test turbine of NASA Contract NAS3-8520.

The wake velocity profiles were recorded by pressure traverse measurements at five different downstream positions. With these measurements, the mixing of the boundary layer and the vorticity associated with the trailing edge based drag of the wake were investigated. This investigation compared the traverse measurements with theoretical models for viscous and vortex flow.

### 4.1 BACKGROUND

Moisture erosion studies have been conducted by Westinghouse for the past four years under the sponsorship of NASA. These investigations have been largely analytical and have been performed on a number of liquid metal and steam turbines.

An important factor in each of these investigations has been the trailing edge wake downstream of the stator blade row. It is within the environment of this downstream wake that the moisture drops exist from the time of their discharge from the trailing edge to the time of their impingement on the downstream rotor. Hence, the properties of the wake, such as vorticity and velocity profile, have an important effect on the size and trajectory of the moisture drops.

The wake traverse tests investigated the effect of the trailing edge thickness and shape on the properties of the blade wake. The wake properties include the change in velocity profile with downstream distance and the nature of the wake flow. The latter property is influenced by whether the wake flow is predominantly viscous or vortex.

The wake flow associated with zero trailing edge thickness and the momentum mixing of the boundary layer should be viscous. On the other hand, the flow associated with large trailing edge thickness would be expected to resemble the separated vortex flow downstream of a circular cylinder.

---

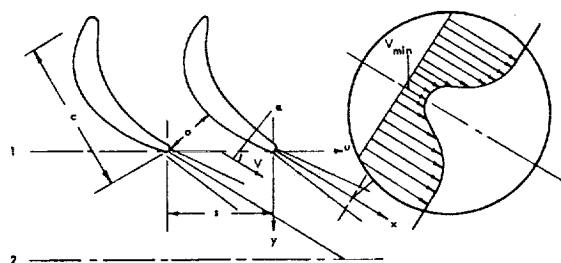
\* W. K. Fentress, Senior Engineer and K. A. Desai, Engineer, Development Engineering Dept., Westinghouse Steam Divisions, Lester, Pa.

Data on the wake profiles and the wake decay were supplied by the pressure traverse measurements. Information on the wake vorticity was obtained from the traverse measurements by comparing the downstream loss by test with the downstream loss by theoretical models. These models gave the theoretical downstream loss with viscous mixing and vortex flow. These comparisons indicated whether the downstream flow was largely viscous or vortex.

The tests were run on the third stage, stator blade section, of the three stage potassium test turbine of Contract NAS3-8520, with various trailing edge configurations. This blade was selected because of the association of the three-stage turbine with the NASA liquid metal program. Also, this blade was typical of those used in liquid metal and steam turbines.

A literature survey was conducted at the start of the program and a number of survey reports are listed in the reference section. However, not all of these reports are cited as references.

#### 4.2 SYMBOLS



$a^*$	critical velocity
$c$	projected chord length of blade
$C_D$	trailing edge drag coefficient based on the trailing edge thickness $T$ .
$CF$	energy loss coefficient, Eq. 2
$CF_D$	increase in loss coefficient due to trailing edge thickness at position 2; i.e., $CF_{2,T} - CF_2$
$CF_T$	loss coefficient, finite trailing edge thickness
$CF_1$	loss coefficient, zero trailing edge thickness, at position 1
$CF_2$	loss coefficient, zero trailing edge thickness, at position 2
$CF_{1,T}$	loss coefficient, finite trailing edge thickness, at position 1
$CF_{2,T}$	loss coefficient, finite trailing edge thickness, at position 2
$h$	blade height
$o$	throat dimension
$p_i$	inlet stagnation pressure
$p_s$	downstream static pressure
$p_t$	downstream stagnation pressure
$s$	blade pitch
$T$	trailing edge thickness, temperature. See Table 4.3-1.
$u$	distance from blade trailing edge in the tangential direction
$u/s$	referred distance from blade trailing edge in the tangential direction
$V$	downstream velocity
$V'$	downstream velocity based on isentropic expansion from the inlet stagnation condition
$V_r$	Referred downstream velocity, Eq. 1
$V_{r,min}$	minimum, referred velocity in core of wake
$\dot{w}$	flow rate
$x$	distance along streamline downstream of the trailing edge



- x/c referred distance along streamline downstream of the trailing edge
- y distance in axial direction downstream of the trailing edge, inches
- $\alpha$  flow angle with respect to the tangential direction
- $\alpha'$  blade exit angle, with respect to tangential direction, based on the average of the suction and pressure surface angle at the trailing edge
- $\gamma$  specific heat ratio, 1.4

#### Subscripts and Superscripts

- 1,2 downstream position at blade trailing edge, at position of uniform flow
- D drag
- i inlet stagnation
- s static
- t downstream stagnation
- T finite trailing edge thickness
- r referred
- min minimum
- ' isentropic, blade

### 4.3 TEST APPARATUS AND PROCEDURE

#### 4.3.1 Blade Description

The test blade is a 2 times full size model of the blade section from the three stage potassium test turbine of Contract NAS3-8520, e/4 blade height from the inner diameter position, third stator blade row.

There are nine separate configurations of the test blade which differ in trailing edge thickness and shape. These configurations consist of three different trailing edge thicknesses, 0.028 inch, 0.106 inch, and three different trailing edge shapes, round, square, and tapered (Table 4.3-1). The thin, round trailing edge configuration is an exact scale of the turbine blade section. The medium and thick trailing edge configurations

differ slightly in the trailing edge suction surface region, but the gauging dimension and blade pitch are the same in all blades. Due to the constant gauging with change in thickness, the blade exit angle,  $\alpha'$ , varies from 21 to 27 degrees.

Three sets of blades with thin, medium and thick trailing edge thickness were used. The blades had a round trailing edge shape and were changed from round to square and from square to tapered, by machining the trailing edge. Details of the trailing edge shapes are given in Table 4.3-1.

The calculated boundary layer properties at the trailing edge of the blade follow:

	MOMENTUM THICKNESS--INCHES	DISPLACEMENT THICKNESS--INCHES	FULL THICKNESS--INCHES	EXPONENT
PRESSURE SURFACE	0.00164	0.00207	0.0179	7.68
SUCTION SURFACE	0.00763	0.0120	0.0540	3.51

These boundary layer properties were calculated by the methods in Reference 2 and are for a blade Reynolds number of  $3.4 \times 10^5$ . The exponent is used in the velocity profile equation.

Trip wires of 0.018 inch diameter were installed on the suction and pressure side of the blade approximately 0.45 inch from the leading edge.

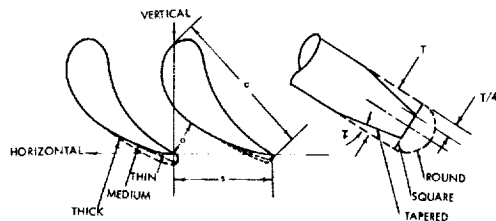
#### 4.3.2 Test Rig

The low speed cascade rig is illustrated in Figure 4.3-1. The cascade consisting of six blades was mounted between the circular end walls. The height of the test blade was set by the three inch space between the end walls.

The traversing probe was accessible to the region downstream of the blades by a slot in the end walls. This provided an approximate two inch travel in the axial direction and an approximate eight inch travel in the tangential, pitchwise direction.

TABLE 4.3-1

## TEST BLADE SPECIFICATIONS



	c in.	o in.	s in.	T in.	r deg.	h in.
Thin	2.14	.524	1.41	.028	4.5	3.0
Medium	2.20	.524	1.41	.106	12.4	3.0
Thick	2.24	.524	1.41	.160	18.4	3.0

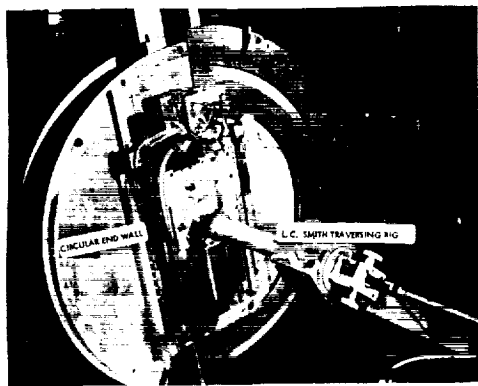


Figure 4.3-1 Cascade Test Rig

HORIZONTAL INCHES	VERTICAL (INCHES)		
	Thin	Medium	Thick
0.000	0.000	-0.035	-0.147
0.100	0.032	-0.142	-0.096
0.200	0.062	+0.001	-0.045
0.300	0.096	0.046	+0.008
0.400	0.130	0.093	0.062
0.500	0.168	0.141	0.116
0.600	0.208	0.190	0.172
0.700	0.252	0.242	0.229
0.800	0.300	0.295	0.287
0.900	0.350	0.350	0.346
1.000	0.406	0.406	0.406
1.100	0.472	0.472	0.472
1.200	0.552	0.552	0.552
1.292	0.650	0.650	0.650
1.370	0.750	0.750	0.750
1.426	0.850	0.850	0.850
1.470	0.950	0.950	0.950
1.495	1.050	1.050	1.050
1.506	1.150	1.150	1.150
1.510	1.250	1.250	1.250
1.504	1.350	1.350	1.350
1.484	1.450	1.450	1.450
1.440	1.550	1.550	1.550
1.350	1.638	1.638	1.638
1.250	1.674	1.674	1.674
1.150	1.656	1.656	1.656
1.050	1.582	1.582	1.582
0.994	1.500	1.500	1.500
0.948	1.400	1.400	1.400
0.922	1.300	1.300	1.300
0.902	1.200	1.200	1.200
0.882	1.100	1.100	1.100
0.855	1.000	1.000	1.000
0.824	0.900	0.900	0.900
0.780	0.800	0.800	0.800
0.726	0.700	0.700	0.700
0.664	0.600	0.600	0.600
0.592	0.500	0.500	0.500
0.500	0.388	0.388	0.388
0.400	0.288	0.288	0.288
0.300	0.206	0.206	0.206
0.200	0.138	0.138	0.138
0.100	0.082	0.082	0.082
0.012	0.026	0.026	0.026

While there are circular end walls at the end of the blade span, there is a slot in each of these end walls and there are no end walls at the ends of the cascade in the axial-tangential direction. Thus the flow is not confined along the boundaries of the jet.

#### 4.3.3 Instrumentation

A Kiel total pressure probe operated by the L. C. Smith traversing rig was used for traversing downstream of the cascade. The overall shield diameter of the probe was 1/16 inch. This probe measures the total pressure over a wide angle range and thus does not require point adjustment for yaw.

A total pressure cylindrical probe and thermocouple were located at the inlet to the cascade.

The probes were connected to pressure transducers. The electrical signals from the transducers and from the traversing rig were fed to the computerized data acquisition system.

#### 4.3.4 Data Logging and Calculation

The data logging system, which is capable of accepting up to 300 channels of analog signals, digitizes the information and records the data on computer magnetic tape. In addition, the Hewlett Packard 2116A computer was coupled to a teletype printer which gave a continuous printout of the wake velocity. This made it possible to continuously monitor the data as they were acquired.

The L. C. Smith traversing rig was adjusted for traverse readings in 0.005 inch steps, approximately 10 seconds per step. Thus, each downstream traverse across the 1.41 inch blade pitch consisted of approximately 282 points and required approximately 50 minutes time.

The data from the magnetic tape were fed to the CDC 6400 computer. Calculations were made to determine the point by point referred

velocity and the flow weight average loss coefficient by the following equations:

$$V_r = V_r(u, y) = V/V' = \left( \frac{1 - (P_s/P_t)^{(\gamma-1)/\gamma}}{1 - (P_s/P_t)^{(\gamma-1)/\gamma}} \right)^{1/2} \quad \text{Eq. 1}$$

$$CF = CF(\gamma) = \frac{\int_0^S (1 - V_r^2) d\dot{w}}{\int_0^S d\dot{w}} = \frac{\int_0^S V_r^2 P_t^{-1/2} ((P_s/P_t)^{2/\gamma} - (P_s/P_t)^{(\gamma+1)/\gamma})^{1/2} du}{\int_0^S P_t^{-1/2} ((P_s/P_t)^{2/\gamma} - (P_s/P_t)^{(\gamma+1)/\gamma})^{1/2} du} \quad \text{Eq. 2}$$

The computer output included Cal Comp plots of the referred velocity across the pitch of the blade.

#### 4.3.5 Checkout Procedure

A number of tests were run to determine the most suitable type of probe for the traverse tests and to establish the measurements. At the time it was not known how sharp the wake profile would be in the region of the trailing edge, how many points it would take to specify the profile, how the size of the probe would affect the measurements, or how quickly the profile would change with downstream distance.

Tests were performed with a number of probes: the 1/8 inch total-static cylindrical probe, 1/16 inch total-static Cobra probe, 1/16 inch total pressure pitot tube, and 1/8 inch total pressure Kiel probe. It was found that the Cobra probe and the Kiel probe gave a clear definition of the blade wake and gave wake profile plots that were nearly identical. However the Cobra probe required adjustment for yaw in each pitchwise traverse, particularly in the region of the trailing edge, while the Kiel probe required no adjustment. Also, the measured static pressure by the Cobra probe was particularly the same as atmospheric and gave essentially the same referred velocity except in the region 1/16 to 1/8 inch downstream of the trailing edge. Here the static pressure readings were erratic. It was therefore decided to use the

Kiel total pressure probe, consider the static pressure as atmospheric, and disregard the flow angle measurement.

In addition, tests were run to check on the downstream entrainment, the use of end walls, and the necessary number of blades for undisturbed flow in the center of the cascade. It was found that the six blade cascade was adequate. The wake profiles from the two center blades were practically identical and there was little change with respect to the wakes from the two center blades and the adjacent blades. This was true at all downstream positions. Measurements also were made at several blade span positions with similar results. Thus, it was not considered that the entrainment had an important effect on the flow in the center of the cascade or that it was necessary to have additional blades or end walls at the ends of the cascade in the axial-tangential direction. Further, it was feared that these end walls would restrict the downstream angle adjustment associated with the trailing edge thickness and invalidate the atmospheric pressure assumption.

Traverse measurements in the pitchwise direction were taken in 0.050 inch steps and in 0.005 inch steps. The 0.005 inch measurements gave much sharper profiles in the region of the blade trailing edge. As the traverse rig only provides for adjustment by factors of 10, and as it requires considerable time to make the adjustment, it was decided to take all the measurements in steps of 0.005 inch.

Finally, tests were run with and without the 0.018 inch trip wires. Although the wake profiles were apparently unaffected, it was decided to traverse with trip wires. This was to assure a turbulent boundary layer along the length of the blade as in turbine operation.

#### 4.3.6 Wake Traverse Tests

Traverse tests were run on eight trailing edge configurations at zero incidence. These configurations were with thin, medium, and thick trailing edge thickness and with round, square, and tapered trailing edge shape. In addition, incidence angle tests were run on two of these configurations at  $\pm 12$  degrees incidence and Reynolds number tests on one of the configurations at  $1.8 \times 10^5$  and  $4.24 \times 10^5$  blade Reynolds number. Table

4.3-2 gives a list of the tests and the test conditions are listed below:

Tests	$P_i - P_s$ (inches of water)	$V/a^*$	Reynolds No. ( $\times 10^5$ )
0° incidence	26.	0.33	3.4
$\pm 12^\circ$ incidence	26.	0.33	3.4
Reynolds No.	42.	0.41	4.2
	7.	0.17	1.8

The blade Reynolds number is based on the blade exit conditions and the projected chord length.

Traverse measurements were taken in 0.005 inch steps, across one blade pitch in the center of the cascade, and at five axial downstream positions. The order of tests on each of the three blade thicknesses was with round, square, and tapered trailing edge shape. Change in the original trailing edge shape, from round to square to tapered, was made by removing the blades from the cascade and machining the trailing edge. The blades were numbered and provided with positioning pins to provide for the same setting in each assembly.

Hot wire measurements of the downstream wake gave no indication of immediate results and were abandoned. It was felt that more could be gained by detailed analysis of the data.

## 4.4 RESULTS AND DISCUSSION

### 4.4.1 Theoretical Models of Flow

By comparing the traverse results with theoretical models of the downstream flow, it is possible to tell how nearly the various models conform to the actual process. Thus, it is shown whether the wake flow is associated with a viscous or a vortex process.

TABLE 4.3-2

## LIST OF TESTS

BLADE TRAILING EDGE THICKNESS (INCHES)	TRAILING EDGE THICKNESS PITCH T/S	BLADE TRAILING EDGE SHAPE	0° INCIDENCE ANGLE TESTS	+12° and -12° INCIDENCE ANGLE TESTS	REYNOLDS NUMBER TESTS
THIN	0.0198	ROUND	X		
0.028	0.0198	SQUARE	X	X	
MEDIUM	0.0751	ROUND	X		
0.106	0.0751	SQUARE	X		X
	0.0751	ROUND	X		
THICK	0.1134	SQUARE	X		
0.160	0.1134	ROUND	X	X	
	0.1134	TAPERED	X		

The following models were used in the comparison.

- 1) Lieblein Model - Eq. 3 of reference 6 gives the referred velocity in the core of the wake as:

$$V_{r, \min} = 1 - 0.13 (x/c + 0.025)^{-1/2}$$

As the empirical equation is based on theory and test results for airfoils with zero trailing edge thickness, it associates the downstream wake with the viscous mixing of the boundary layer. This model is of particular interest as it was used in the moisture erosion calculations.

- 2) Viscous Model - This model associates the downstream loss with the mixing of the viscous boundary layer and with the filling of the dead space downstream of the trailing edge. The equations are specified by continuity, momentum, and energy relations; see reference 12. The equations are with respect to the positions at the trailing edge and at the downstream point of uniform flow, assume incompressibility, and assume constant static pressure in the pitchwise direction at the trailing edge position. The exponent in the boundary layer equations was taken as 5.5, corresponding to the calculated average for the suction and pressure surface. The constant pressure

assumption implies no base drag at the trailing edge, i.e., that the trailing edge drag coefficient is zero.

- 3) Viscous Model with Trailing Edge Drag - This is the same as the viscous model, but without the constant static pressure assumption at the trailing edge position. The trailing edge drag coefficient would be expected to be approximately 0.41 for the round trailing blade as for a circular cylinder. The equations are the same as for the viscous model except for the addition of the  $C_D$  term in the axial momentum equation to allow for the base drag at the trailing edge, e.g., equation C3 of Reference 12:

$$g_{p,s,1} + \sin^2 \alpha_1 [1 - \delta^* - \delta_{te} - \theta^*] [\rho(v')^2]_1 = g_{p,s,2} + \sin^2 \alpha_2 [\rho v^2]_2$$

after the addition of the base drag term appears as:

$$[g_{p,s,1}]^{-1/2} [\rho(v')^2]_1 \delta_{te} C_D + \sin^2 \alpha [1 - \delta^* - \delta_{te} - \theta^*] [\rho(v')^2]_1 = g_{p,s,2} + \sin^2 \alpha_2 [\rho v^2]_2$$

where  $g$ ,  $\rho$ ,  $\delta^*$ ,  $\delta_{te}$ , and  $\theta^*$  are in the symbols of the reference report ( $\alpha$  is with respect to the tangential). Trailing edge drag implies vortex flow similar to the separated flow downstream of a circular cylinder.

#### 4.4.2 Test Results

Figure 4.4-1 gives the Cal Comp plots of the traverse results. Bear in mind that the traverse was made in the pitchwise direction rather than normal to the wake. Thus, the traverse curves are at an approximate angle of 21 degrees to the blade wake rather than 90 degrees. The pressure and suction side of the wake are to the left and right of the trough and, due to the angularity, the pressure side of the wake is farther downstream in the streamline direction. This probably accounts for the fact that the wake appears to be thicker on the pressure side than on the suction side of the trough.  $V_{r, \min}$  does not occur at exactly the same value of  $u/s$  because of the impracticality of aligning the traversing rig in the pitchwise direction with respect to the center of the wake. Finally, all of the Figure 4.4-1 curves are for  $3.4 \times 10^5$  Reynolds number.

Figure 4.4-2 compares the traverse results with the Lieblein model. This curve is a plot of the referred velocity at the core of the wake with downstream, streamline distance. While the cascade results for the thin trailing edge blade agree with the model, the discrepancy increases with trailing edge thickness; in particular, the thick trailing edge blade shows a slower rate of decay than specified by the Lieblein model. This is probably due to the increase in vorticity, with increase in trailing edge thickness, for which reason the wake does not attenuate as rapidly as with viscous flow. Also, the tapered trailing edge shape agrees better with theory in the medium thickness blade. Probably this is due to the lower effective thickness at which the boundary layer breaks away from the trailing edge. Allowing that the thin trailing edge is a direct scale of the turbine blade section, it appears that the Lieblein model gives a good account of the process.

The Figure 4.4-3 curves give the energy loss coefficient with respect to the downstream distance. These curves specify the loss coefficient at the trailing edge position and at the downstream point of uniform flow. The loss coefficients at the trailing edge and downstream positions are used in constructing Figure 4.4-4 and 5.

The Figure 4.4-4 and 5 curves compare the increase in downstream loss with respect to the downstream and trailing edge positions, and the increase in loss with trailing edge thickness, by test and theory. The theoretical curves are for the viscous model with trailing edge drag corresponding to  $C_D = 0$ , 0.20, and 0.41. Generally, the tapered trailing edge blades conform to the model with  $C_D$  of 0. to 0.1, the round trailing edge blade to the model with  $C_D$  of roughly 0.2, and the square trailing edge blade to the model with  $C_D$  of roughly 0.3. Note that all trailing edge shapes, including the square trailing edge, exhibit less drag than the equivalent drag of a circular cylinder with separated flow. This corresponds to approximately  $C_D = 0.41$ . Perhaps this is due to the reduction in effective thickness caused by the blanketing effect of the boundary layer beyond the end of the blade or, in the tapered blade, due to the lower effective thickness at the point where the boundary layer breaks away from the trailing edge. As the  $T/s$  for the 3 stage blade is 0.02, it appears that the model with  $C_D$  of 0.2 is in good agreement with the flow.

Traverse tests at high and low blade Reynolds numbers of  $4.2 \times 10^5$  and  $1.8 \times 10^5$  did not show any distinguishable difference compared to those at  $3.4 \times 10^5$  Reynolds numbers. Tests at higher and lower Reynolds numbers were limited by the capacity of the equipment and the accuracy of the instrumentation.

Also, tests at +12 and -12 degrees angle of incidence did not show any notable difference compared to those at zero incidence; see Figures 4.4-1 a, b, g, and i. This  $\pm 12$  degree incidence range is as large as that usually encountered in turbines.

Bear in mind that the magnitude of the theoretical trailing edge loss depends on the blade exit angle, increasing with  $\alpha'$ , e.g., CFD given by Figure 4.4-5 for  $\alpha' = 21$  degrees would be 12 percent greater for  $\alpha' = 30$  degrees at  $0 < T/s < 0.08$  and  $C_D = 0.2$ . It is probable that the test loss would correspond to this trend.

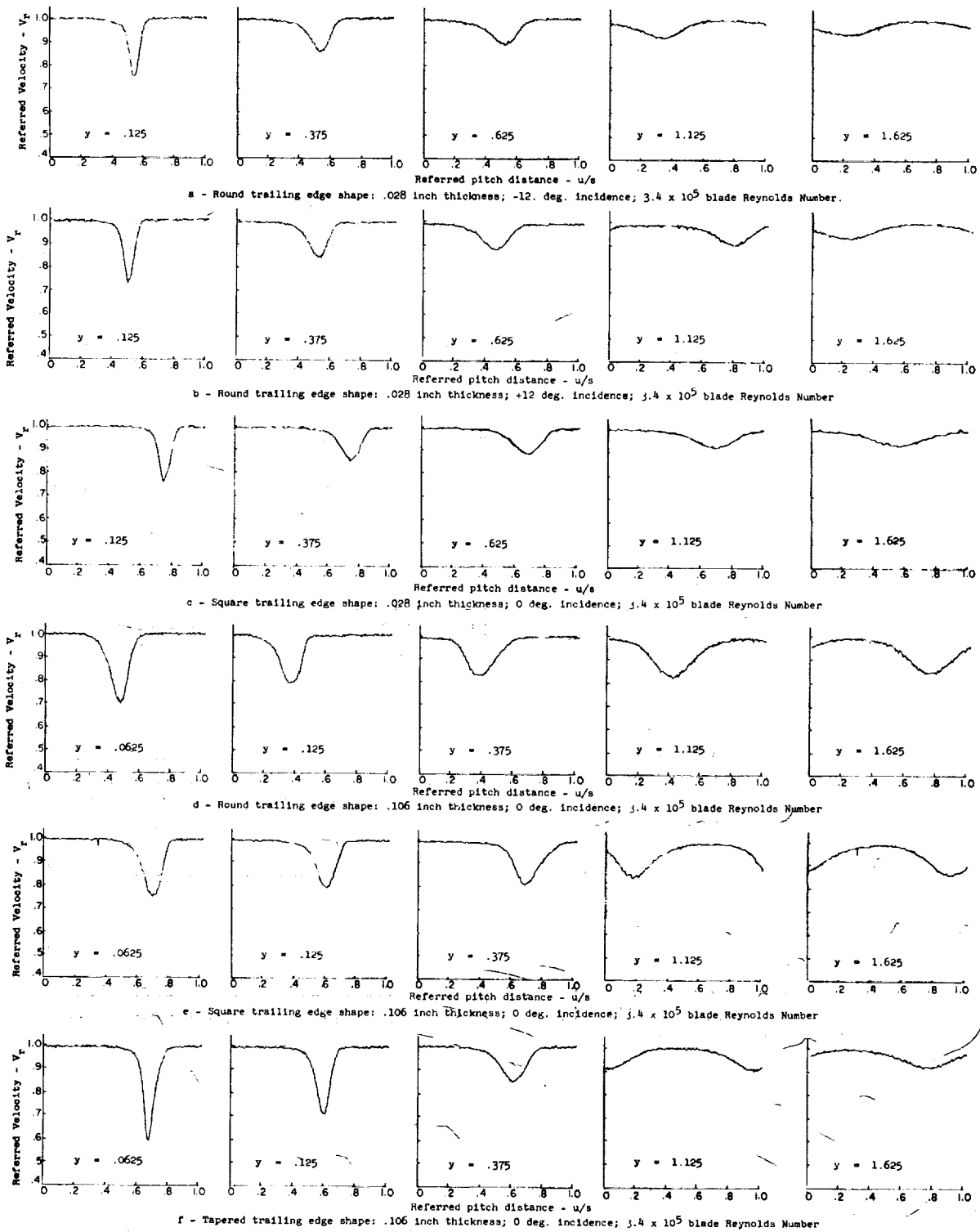


Figure 4.4-1 Wake Velocity Profiles  
at Various Downstream Positions

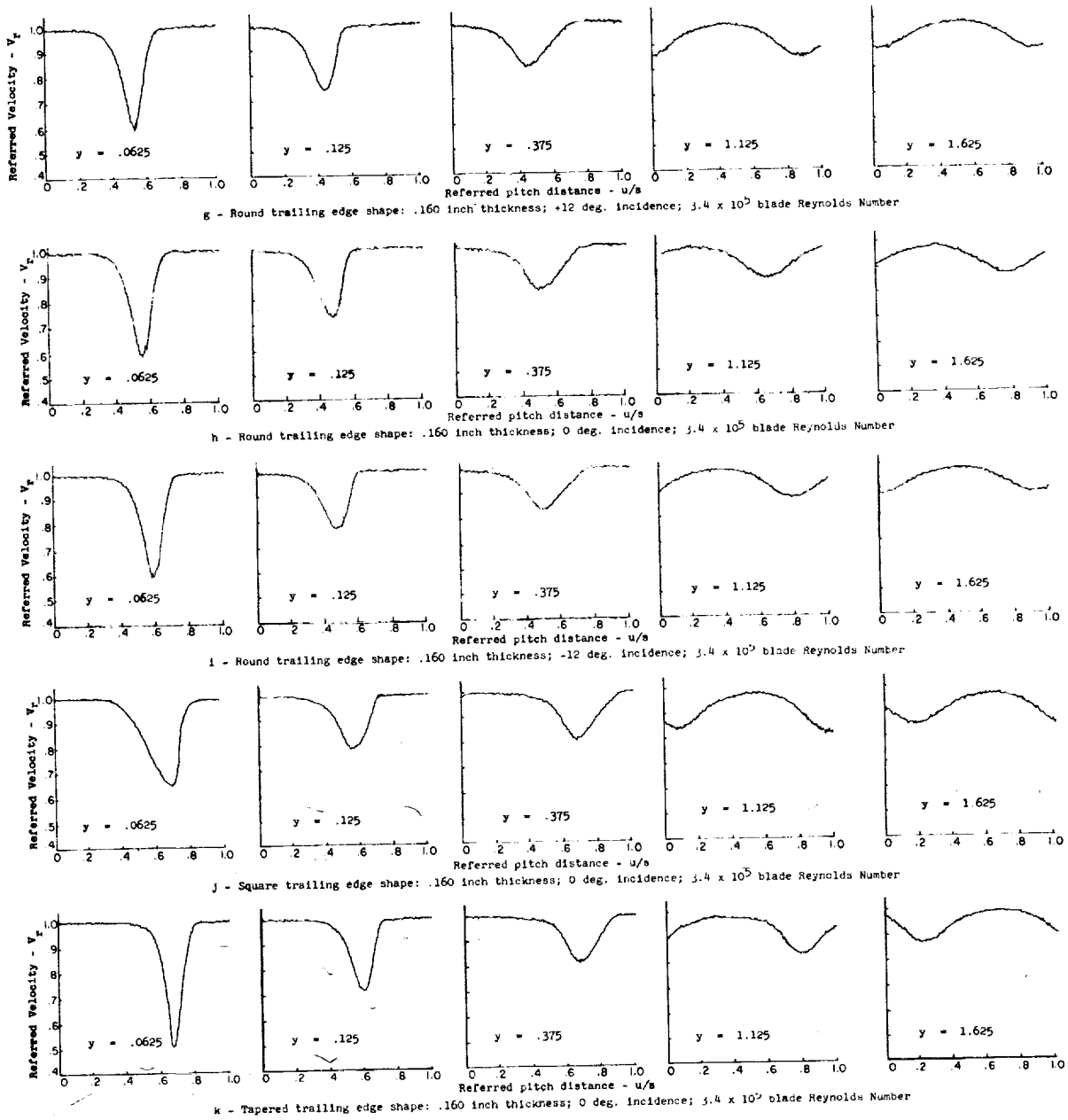


Figure 4.4-1 Wake Velocity Profiles  
at Various Downstream Positions



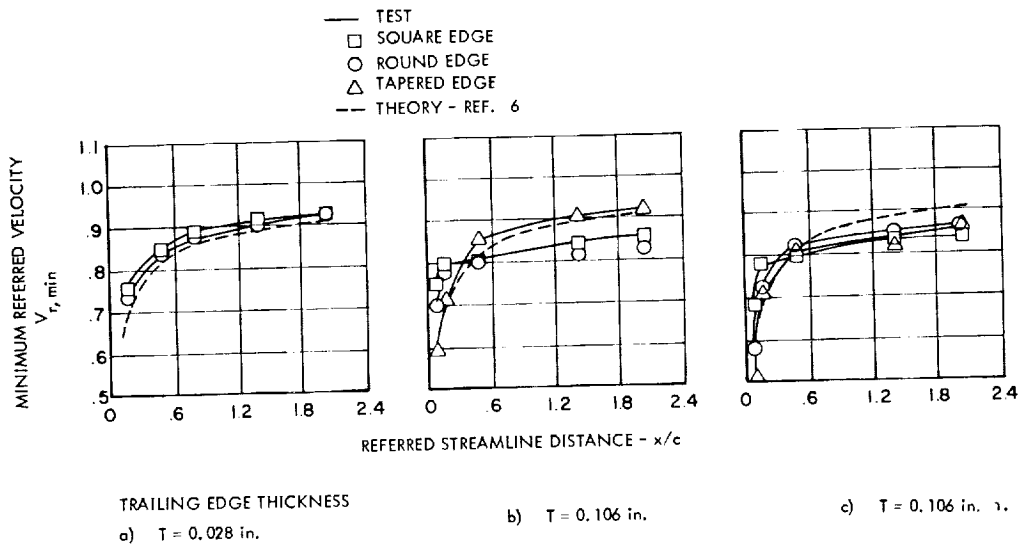


Figure 4.4-2 Change in Velocity in Core of Wake  
 with Downstream Distance 0 Deg. Incidence;  
 $3.4 \times 10^5$  Reynolds Number

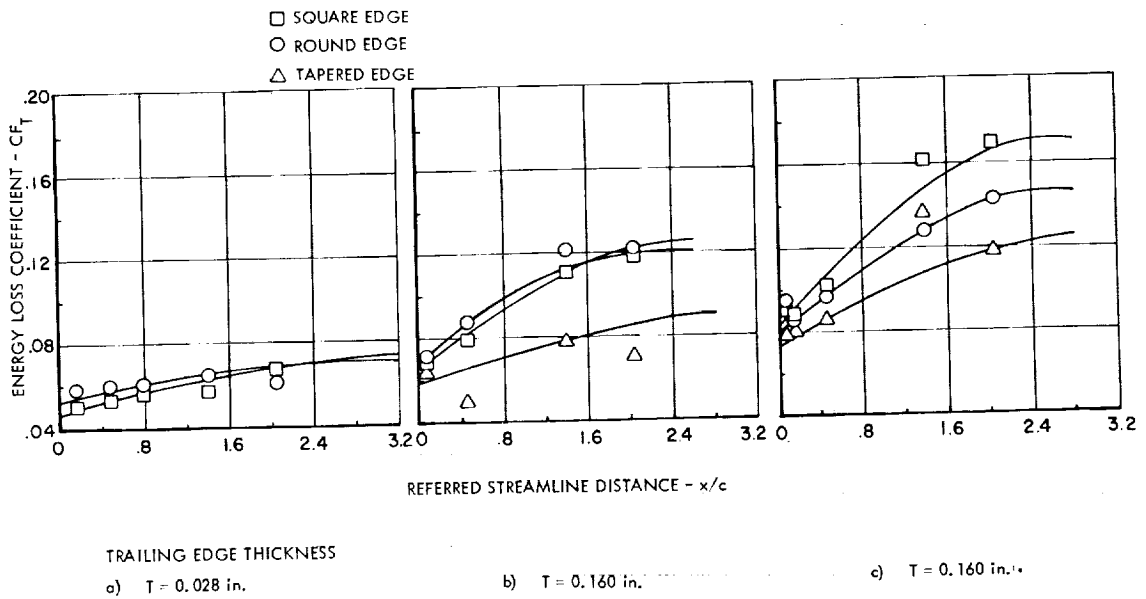


Figure 4.4-3 Increase in Wake Mixing Loss with  
 Downstream Distance; 0 Deg. Incidence;  
 $3.4 \times 10^5$  Reynolds Number

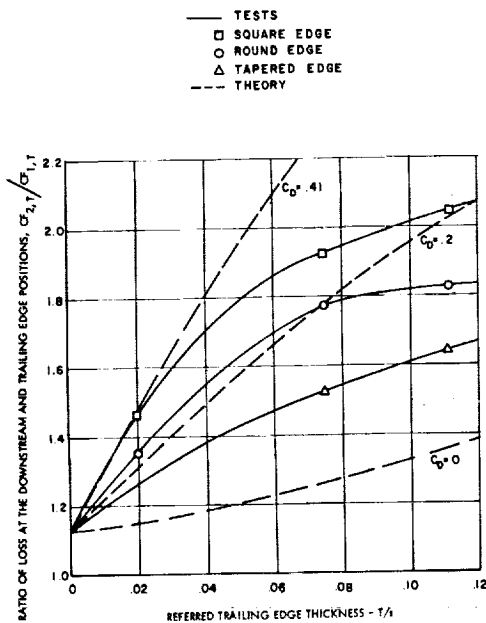


Figure 4-4 Increase in Wake Mixing Loss with Trailing Edge Thickness. 0 Deg. Incidence;  $3.4 \times 10^5$  Reynolds Number

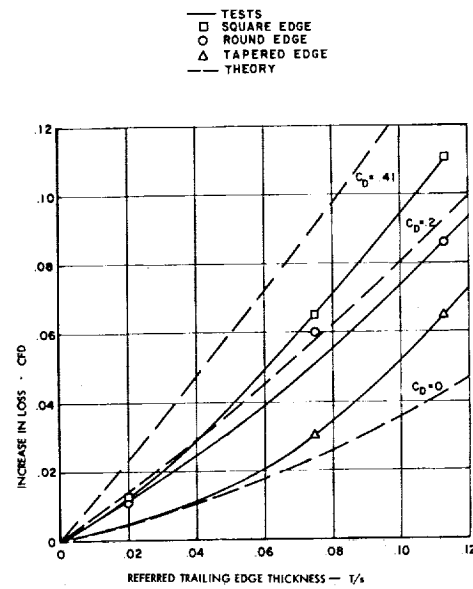


Figure 4-5 Increase in Loss Coefficient with Trailing Edge Thickness. 0 Deg. Incidence;  $3.4 \times 10^5$  Reynolds Number

#### 4.5 SUMMARY OF RESULTS

The Lieblein empirical equation gives a good account of the wake decay for the thin trailing edge configurations,  $T/s = 0.02$ . At large trailing edge thickness,  $T/s = 0.075$  and  $T/s = 0.113$ , the rate of decay is less than specified by the equation due to the increase in the vorticity. Generally, the tapered trailing edge more nearly agrees with the model due to the reduction in effective thickness.

From a more detailed analysis: The wake flow is associated with the viscous mixing of the boundary layers shed from the suction and pressure

side of the blade and with the vortex flow due to the base drag at the trailing edge of the blade. Generally, the base drag and vorticity increases with the trailing edge thickness and with the bluntness of the trailing edge. In the case of the round trailing edge, the wake flow is approximated by a theoretical model based on the momentum mixing of the boundary layer and a base drag corresponding to  $C_D = 0.2$ .

Blade Reynolds number in the range of  $1.8 \times 10^5$  to  $4.2 \times 10^5$  and blade incidence in the range of  $\pm 12$  degrees did not have a distinguishable effect on the properties of the wake.

#### 4.6 REFERENCES

1. Bearman P. W., "On Vortex Street Wakes," J. Fluid Mech. (1967), Vol. 28, part 4, pg. 625-641.
2. Fentress, W. K., "A Computer Program for Calculating the Boundary Layer Properties Along the Surface of Turbomachinery Blades," Astro-nuclear Laboratory, Westinghouse Electric Corporation, WANL-TME-1689, Nov. 1, 1967.
3. Heskestad, G. and Olberts, D. R., "Influence of Trailing-Edge Geometry on Hydraulic Turbine-Blade Vibration Resulting from Vortex Excitation," J. of Eng. for Power, Trans. ASME 82A, 1960, pg. 103-110.
4. Hoerner, S. F., "Fluid-Dynamic Drag," Published by Author, Midland Park, N. J., 1958.
5. Johnston, I. H., Dransfield, D. C., and Fullbrook, D. J., "Experiments Concerning the Effect of Trailing-Edge Thickness on Blade Loss and Turbine Stage Efficiency," ARC - R&M 3459, 1964.
6. Lieblein, S. and Roudebush, W. H., "Low-Speed Wake Characteristics of Two-Dimensional Cascade and Isolated Airfoil Sections," NACA TN 3771, 1956.
7. Markov, N. M., "Calculation of the Aerodynamic Characteristics of Turbine Blading," Translated and Published by Associated Technical Services, Glen Ridge, N. J., 1958.
8. Nash, J. F., "An Analysis of the Subsonic Flow Past Symmetrical Blunt-Trailing-Edge-Aerofoil Sections at Zero Incidence, in the Absence of a Vortex Street," ARC R&M 3436, 1966.
9. Reeman, J. and Simonis, E. A., "The Effect of Trailing Edge Thickness of Blade Loss," RAE TN 116, 1943. (NASA Sc. and Tech. Info. Fac. Accession no. X65 - 81166.)
10. Rossbach, R. J., Wesling, G. C. and Lemond, W. F., "Three Stage Potassium Test Turbine - Final Design - Vol. 1 - Fluid Design," NASA - CR - 72249.
11. Schlichting, H., "Boundary Layer Theory," Pergamon Press, New York, 1955.
12. Stewart, W. L., "Analysis of Two-Dimensional Compressible-Flow Loss Characteristics Downstream of Turbomachine Blade Rows in Terms of Basic Boundary-Layer Characteristics," NACA TN 3515, 1955.
13. Toebe, G. H. and Eagleson, P. S., "Hydro-elastic Vibrations of Flat Plates Related to Trailing Edge Geometry," J. of Basic Eng., Trans. ASME 83D, 1961, pg. 671 - 678.









